THÈSE POUR OBTENIR LE GRADE DE DOCTEUR DE L'UNIVERSITÉ DE MONTPELLIER

En Biologie Santé

École doctorale Sciences Chimiques et Biologiques pour la Santé

Unité de recherche Physiologie et Médecine Expérimentale du Cœur et des Muscles
INSERM U1046 – CNRS UMR 9214 – Université de Montpellier

Targeting the YAP1/TAZ signaling axis in GastroIntestinal Stromal Tumors (GIST)

Présentée par Irene PEZZATI
Le 1er Décembre 2025

Sous la direction de Prisca BOISGUÉRIN et Sébastien DESHAYES

Devant le jury composé de

Céline GONGORA, DR, IRCM-RTTI, INSERM, Université de Montpellier, France	Président du jury
Georg MELLITZER, CRCN, CRBS-NanoMedReg, INSERM, Université de Strasbourg, France	Rapporteur
Emilie ALLARD-VANNIER, Professeure, CBM-NMNS, UPR-CNRS, Université de Tours, France	Rapportrice
Frédéric CHIBON, DR, CRCT-ONCOSARC, INSERM, Université de Toulouse, France	Examinateur
Prisca BOISGUÉRIN, DR, PhyMedExp, CNRS, Université de Montpellier, France	Directrice de thèse
Sébastien DESHAYES, CRCN, PhyMedExp, CNRS, Université de Montpellier, France	Co-directeur de thèse

UNIVERSITÉ DE MONTPELLIER

THÈSE POUR OBTENIR LE GRADE DE DOCTEUR DE L'UNIVERSITÉ DE MONTPELLIER

En Biologie Santé

École doctorale Sciences Chimiques et Biologiques pour la Santé

Unité de recherche Physiologie et Médecine Expérimentale du Cœur et des Muscles
INSERM U1046 – CNRS UMR 9214 – Université de Montpellier

Targeting the YAP1/TAZ signaling axis in GastroIntestinal Stromal Tumors (GIST)

Présentée par Irene PEZZATI
Le 1er Décembre 2025

Sous la direction de Prisca BOISGUÉRIN et Sébastien DESHAYES

Devant le jury composé de

Céline GONGORA, DR, IRCM-RTTI, INSERM, Université de Montpellier, France	Président du jury
Georg MELLITZER, CRCN, CRBS-NanoMedReg, INSERM, Université de Strasbourg, France	Rapporteur
Emilie ALLARD-VANNIER, Professeure, CBM-NMNS, UPR-CNRS, Université de Tours, France	Rapportrice
Frédéric CHIBON, DR, CRCT-ONCOSARC, INSERM, Université de Toulouse, France	Examinateur
Prisca BOISGUÉRIN, DR, PhyMedExp, CNRS, Université de Montpellier, France	Directrice de thèse
Sébastien DESHAYES, CRCN, PhyMedExp, CNRS, Université de Montpellier, France	Co-directeur de thèse

UNIVERSITÉ DE MONTPELLIER

ABSTRACT

Targeting the YAP1/TAZ pathway in gastrointestinal stromal tumors (GIST)

Gastrointestinal stromal tumors (GIST) are the most common malignant mesenchymal neoplasms of the digestive tract. Up to 85% harbor gain-of-function mutations in *KIT* or *PDGFRA* genes encoding receptor tyrosine kinases. Most metastatic cases are treated with tyrosine kinase inhibitors, such as first-line Imatinib (IM). Despite the substantial clinical benefits, the emergence of secondary resistance, which is often caused by additional *KIT* mutations, remains a major challenge for *KIT*-mutant GIST patients. This highlights the importance of identifying new therapeutics.

This thesis explores the role of YAP1 (Yes-associated protein 1) and TAZ (Transcriptional co-activator with PDZ-binding motif), downstream effectors of the Hippo pathway, in GIST development and therapy response. Previous work from our team showed the involvement of these proteins in smooth muscle cell plasticity and suggested a link to IM resistance in *KIT*-dependent GIST. However, their specific functions in GIST were unclear.

First, we validated WRAP5, a tryptophan (W)- and arginine (R)-rich amphipathic peptide that self-assembles into nanoparticles in the presence of nucleic acids, as an efficient and non-toxic siRNA delivery system for GIST. Furthermore, WRAP5-based nanoparticles enabled robust and combinatorial silencing of multiple targets in the same cell by encapsulating up to three different siRNA.

We then used WRAP5-based nanoparticles loaded with siRNA against YAP1, TAZ, or with a combination of both in three IM-sensitive GIST cell lines. TAZ silencing strongly reduced cell proliferation and migration, whereas YAP1 knockdown had surprisingly limited effects, with only modest additive inhibition upon dual targeting. CYR61 (cysteine-rich angiogenic inducer 61) and CTGF (connective tissue growth factor) emerged as key downstream drivers, predominantly regulated by TAZ, with CYR61 downregulation particularly related to increased proliferation. Moreover, patient dataset analyses associated high *TAZ* or *CYR61* expression with shorter disease-free survival and higher metastatic potential, highlighting the central TAZ-CYR61 axis.

Finally, in IM-resistant GIST models, YAP1 and TAZ expressions were higher compared to sensitive counterparts. Furthermore, the study demonstrated the potential for the silencing of both proteins through the utilization of WRAP5:siRNA nanoparticles. Preliminary results revealed that these paralogs are subject to differential regulation by IM treatment, and that the combination of IM and siTAZ does not result in a synergistic antiproliferative effect.

In conclusion, this work identifies TAZ as a key regulator of GIST biology, reveals context-dependent functions for YAP1, and establishes WRAP5-mediated siRNA delivery as a promising tool to investigate their therapeutic potential, particularly in IM-resistant GIST.

Keywords: GIST, YAP1, TAZ, siRNA, WRAP5, Imatinib resistance

FRENCH SUMMARY

Cibler la voie YAP1/TAZ dans les tumeurs stromales gastro-intestinales (GIST)

Les tumeurs stromales gastro-intestinales (GIST) sont les néoplasmes mésenchymateux malins les plus fréquents du tube digestif. Jusqu'à 85% des cas présentent des mutations activatrices des gènes *KIT* ou *PDGFRA* codant des récepteurs tyrosine-kinases. La plupart des formes métastatiques sont traitées par des inhibiteurs de tyrosine-kinase tels que l'imatinib (IM) en première ligne. Malgré des bénéfices cliniques substantiels, l'apparition de résistances secondaires, souvent liées à des mutations supplémentaires chez *KIT*, reste un défi majeur pour les patients atteints de GIST mutés sur KIT. Cela souligne l'importance d'identifier de nouvelles cibles moléculaires.

Cette thèse explore le rôle de YAP1 (Yes-associated protein 1) et TAZ (Transcriptional co-activator with PDZ-binding motif), effecteurs en aval de la voie Hippo, dans le développement des GIST et leur réponse thérapeutique. Des travaux antérieurs de notre équipe ont montré l'implication de ces protéines dans la plasticité des cellules musculaires lisses et ont suggéré un lien avec la résistance à l'IM dans les GIST *KIT*-dépendants. Cependant, leurs fonctions spécifiques dans les GIST restaient indéterminées.

Nous avons d'abord validé WRAP5, un peptide amphipathique riche en tryptophane (W) et arginine (R) capable de s'auto-assembler en nanoparticules en présence d'acides nucléiques, comme système efficace et non toxique de délivrance de siARN dans les GIST. De plus, les nanoparticules à base de WRAP5 ont permis une inhibition robuste et combinée de plusieurs protéines dans la même cellule, grâce à l'encapsulation de trois siRNA différents.

Nous avons ensuite utilisé des nanoparticules à base de WRAP5 chargées de siARN dirigées contre YAP1, TAZ, ou contre les deux simultanément, dans trois lignées de GIST sensibles à l'IM. L'inhibition de TAZ a fortement réduit la prolifération et la migration cellulaires, tandis que l'inhibition de YAP1 a eu des effets limités, avec seulement un effet additif modéré en ciblant simultanément YAP1 et TAZ. CYR61 (cysteine-rich angiogenic inducer 61) et CTGF (connective tissue growth factor) sont apparus comme des médiateurs clés en aval, majoritairement régulés par TAZ. La diminution de CYR61 a été particulièrement associée à une prolifération cellulaire accrue. Par ailleurs, les données de patients analysées ont permis d'associer une forte expression de *TAZ* ou *CYR61* à une survie sans récidive plus courte et à un potentiel métastatique accru, mettant en évidence l'axe central TAZ-CYR61 et un rôle plus limité de YAP1.

Enfin, dans des modèles de GIST résistants à l'IM, les expressions de YAP1 et TAZ étaient plus élevées que dans les modèles sensibles. De plus, l'étude a montré que les deux protéines pouvaient être réduites grâce à l'utilisation de nanoparticules WRAP5:siARN. Des résultats préliminaires ont révélé que ces paralogues sont soumis à une régulation différentielle par le traitement à l'IM et que la combinaison de l'IM et du siTAZ n'entraîne pas d'effet antiprolifératif synergique.

En conclusion, ce travail identifie TAZ comme régulateur clé de la biologie des GIST, met en évidence une différence de fonction pour YAP1, et établit la délivrance de siARN par WRAP5 comme un outil prometteur pour évaluer le potentiel thérapeutique de ces protéines, en particulier dans les GIST résistants à l'IM.

Mots-clés : GIST, YAP1, TAZ, siARN, WRAP5, résistance à l'Imatinib

« Qui veut faire quelque chose trouve un moyen,
qui ne veut rien faire trouve une excuse. »

Proverbe arabe

« J'ai combattu le bon combat,
je suis allée jusqu'au bout de la course,
j'ai gardé la foi. »

2 Timothée 4:7

ACKNOWLEDGEMENTS / REMERCIEMENTS

Trois ans et deux mois, ça en fait des jours pour rencontrer du monde et pour impliquer des personnes de près ou de loin dans ce gros travail ! Il est venu le moment de faire le bilan de ces vagues de soutien qui m'ont permis d'aller jusqu'au bout. Pour les personnes qui liront cette page, sachez que l'ordre d'apparition n'est pas un indicateur d'appréciation 🤗

Je remercie tout d'abord Dr. **Georg Mellitzer** et Pr. **Emilie Allard-Vannier** pour avoir accepté de rapporter mes travaux de thèse. Je suis convaincue que vos expertises distinctes nous permettront d'avoir des discussions très riches. Ces remerciements vont aussi à Dr. **Céline Gongora** et Dr. **Frédéric Chibon**, pour avoir pris de votre temps pour examiner cette thèse de cancérologie, votre domaine d'expertise.

J'adresse également un grand merci sincère aux membres qui ont participé à mon CSI : Pr. **Christine Varon** et Dr. **Véronique Baldin**. Nos échanges durant ces deux réunions ont été très inspirants. Mon projet a pu évoluer avec un point de vue extérieur très apprécié. Vous m'avez beaucoup encouragée et félicitée. Chaque année, je suis ressortie pleine d'énergie pour la suite. Ce manuscrit est plein de résultats issus de ces comités, alors je vous en remercie.

Dear Dr. **César Serrano**, thank you so much for your involvement in the project. For over two years, you have always supported me from Barcelona with great passion and have been my expert mentor in GIST. This work is a small step forward in understanding this sarcoma, and for patients for whom it is still difficult to receive treatment. The plan to come to Barcelona did not work due to a lack of time and money, but I retain only positive memories of our exchanges, our meetings at conferences, and the time you took to support me.

Merci à toute l'**équipe 4** pour l'accueil et l'entraide. Tous les team building, les pique-niques, les repas nous auront bien fait marrer.

À mes directeurs de thèse,

Ce travail est une histoire de premières fois entre nous. Première fois que vous dirigiez une thèse ensemble, dans ce laboratoire, et dans un nouveau domaine, la cancérologie. Pour toutes ces nouveautés, il faut faire confiance. Je sais que vous m'avez accordée la vôtre dès le premier jour 🙏.

Sébastien, merci d'avoir initié le projet avant mon arrivée pour que je ne me perde pas au début. Tu as été d'une grande aide pour toute la partie expérimentale et nous faisions un binôme de paillasse, puisqu'à deux, on va plus vite et on est sûr que ça ne marche pas qu'entre nos mains 😉. Il y a trois ans, tu m'as dit de me préserver car je préparais un marathon. J'y suis à la fin de ce marathon, et bien entourée 💪🏻.

Prisca, ces quelques lignes ne saurait représenter à quel point je te remercie. On en a vécu des choses, toi et moi. Des messages sur des idées de manip ou des résultats à pas d'heure. Des trajets de trains bien trop longs sans batterie sur l'ordinateur, et des discussions sans fin sur nos anecdotes de vie. Tu as toujours été là pour me soutenir, dans le travail et dans la vie. Ces trois ans m'ont prouvé ce qu'est une mentore bienveillante en tant que directrice de thèse, et c'est rare 😇. Merci pour ta compréhension, pour m'avoir toujours fait voir le positif quand je voyais tout bien trop gris, pour ton calme quand je m'impatientais trop. Merci d'avoir cru en mon potentiel, même quand j'ai eu les plus grands doutes. Merci de n'avoir jamais reculé devant mes idées, même si beaucoup n'ont pu être abouties, et aussi, merci d'avoir financé mes congrès car ils ont été de très belles expériences.

Aux jeunes qui ont partagé mon bureau à CDP, entre rires, plaintes et sciences, merci.

À **Luigi**, sans qui ma thèse en 180 secondes n'aurait pas été si réaliste au vu de mon aversion pour le foot ! Et pour tous les débats, tu as laissé un vide quand tu es parti 😎.

À **Sanaa**, qui m'a toujours dit « ça va aller », et qui m'a toujours bien nourrie de gâteaux (miam les makrout) et de couscous salé/sucré 😋.

À **Kamilia**, que j'ai appris à connaître en évoluant durant ces deux dernières années. Gossip ou pas, à l'autre bout du labo, ou séparées durant des semaines, on trouvera toujours quelque chose à se raconter (de sciences évidemment). Merci pour ton empathie, pour ta bienveillance, tes questions farfelues sans queue ni tête qui parfois font beaucoup trop réfléchir, ta douceur et ta présence.

À **Thania**, à qui il a fallu une soirée au téléphone pour faire le choix de quitter Bordeaux pour Montpellier. J'espère que tu ne regrettes pas ! Arrivée en plein rush de cette dernière année chaotique pour moi, je te remercie d'avoir pu m'épauler au début de ta thèse. On en aura vécu des résultats bizarres entre gels déformés et cellules qui meurent de manière aléatoire.

À mes copains/copines de labo, merci 👬 👭.

À **Héloïse** pour les nombreuses pauses douceurs, tresses et papotages (j'en passe) 😊.

À **Elisa** pour nos moments à nous, même s'il n'y en a pas eu une pour rattraper l'autre 🤗. Je nous souhaite le bonheur pour la suite.

À **Mathieu**, pour ta force d'écoute, ta capacité à rassurer même quand ça ne fait qu'une semaine que tu côtoies la personne, et tes fabuleuses capacités d'organisateur et déménageur, t'es un as 👵.

À mes chipettes du lab 104.

Manon, merci de m'avoir fait découvrir le meilleur moyen de m'évader aka les bracelets de perles Blooming Beads.

Giulia, Zuly, la mia stella che si alza sempre più in alto. Grazie per esserci stata dal primo mese del tuo arrivo in Francia, di esserti data a fondo per sostenermi, in tutti gli ostacoli degli ultimi 2 anni e mezzo. In Francia o in Italia, io ci sono sempre 💙. E grazie al mio amico **Andrea**, non lo posso dimenticare 😏.

À mes amis de master, qui ont suivi mes aventures et mésaventures de loin toujours avec bienveillance et soutien : **Maureen** et **Rilès** 😀.

À mes amis du crosstraining.

Jeremy, on en aura passé du temps sur le tapis roulant après les séances pour se raconter nos vies, j'attends toujours notre apéro Brets 😂.

Amira, le destin nous a bien réunies finalement, deux domaines différents et pourtant tant en commun. Merci de m'avoir toujours fait voir le côté pragmatique pour ne pas être trop impactée émotionnellement ! Et force à nous, bientôt libérées 😈.

Mélissa, entre futures docteures, on s'est bien comprises, même si moi je ne sauve pas directement des vies 😇. À nos séances de cross training, qui nous ont même amenées à une compèt ! J'attends nos prochaines découvertes culinaires avec impatience 😋.

À mes amis de longue date, qui ont supporté mes plaintes et pas que pour cette thèse : **Mathieu**, **Marine**, **Margot**, **Cyanna** et **Yasmin**.

À **Nathalie**, ma force tranquille sur qui je peux m'appuyer peu importe la situation, à n'importe quelle heure. Ton soutien sans faille m'a permis d'accomplir bien plus que cette thèse. Je pense que Whatsapp a explosé au vu des heures de vocaux qu'il contient parlant de mon doctorat, des joies et des déceptions des manips, de toute mon organisation bien trop remplie. Merci pour ton écoute, merci pour ta patience, merci pour avoir été là depuis le début, merci d'avoir découvert Montpellier avec moi 😙.

À **Manon**, ma confidente, qui n'oublie jamais une étape de la plus insignifiante à la plus importe de ma vie. Merci pour ta présence, ton aide à trouver des solutions, ton amitié est précieuse 🫶.

À **Marine**, avec qui j'ai partagé mon stage de M2 et qui a suivi mes aventures de thèse entre Montpellier et Nîmes, merci d'être là 🧡

À ma sœur, ma moitié, mon appui le plus grand, celle qui me vend devant tous ces amis parce que bientôt BAC+8. Tu n'as pas tout tout compris à cette thèse je le sais, mais en tout cas je t'ai bien embêtée avec toutes mes histoires. Merci pour ne pas avoir besoin d'explication pour être là. Merci pour ton écoute, pour ta présence bien que loin de 350 km, merci d'être celle qui me raisonne en quelques mots quand j'ose baisser les bras et avoir des doutes. Merci car toi seule sait me rappeler ma valeur ❤️‍🩹.

Ai miei nonni, lontani ma sempre vicini al mio cuore, che mi hanno continuamente ripetuto di essere fieri di me. Grazie per il vostro sostegno infallibile, che porterò per sempre con me in tutte le tappe della vita. Grazie per avermi insegnato a vedere le piccole bellezze di ogni momento di questa tesi. La vostra forza di vita mi ha fatto crescere.

Ai miei genitori, grazie ai quali oggi sono qui, più forte che mai. Grazie per aver sostenuto tutte le mie scelte senza mai dubitare della mia riuscita. Grazie per il vostro grande amore, che mi ha fatto superare tutti gli ostacoli di questi ultimi tre anni. Queste trecento pagine sono dedicate a tutto ciò che avete fatto per i miei studi, al vostro sostegno e alla vostra pazienza. A voi devo tutto.

À mon Lucas, qui a osé prendre le train en cours de route de cette épreuve qu'a été ma thèse. Je te remercie de m'épauler chaque jour avec ton calme rationnel et rassurant. Merci de n'avoir jamais douté de moi durant cette année et demi, alors que je doutais constamment. Merci pour ton amour, ké an mwen, il me porte si fort.

Merci pour les roses, merci pour les larmes.

Merci pour toutes ces petites choses qui ont façonné ma thèse, grâce à elles, je suis qui je suis.

TABLE DES MATIÈRES

ABSTRACT **1**

FRENCH SUMMARY **2**

ACKNOWLEDGEMENTS / REMERCIEMENTS **4**

LIST OF FIGURES **15**

LIST OF TABLES **19**

LIST OF ABBREVIATIONS **21**

INTRODUCTION **25**

1. GASTROINTESTINAL STROMAL TUMORS: CLINICAL FEATURES AND BIOLOGY **26**

1.1. GIST PATHOLOGY 26

1.1.1. Definition *26*

1.1.2. Epidemiology *27*

1.1.3. Clinical presentation *27*

1.2. THE CELLULAR ORIGIN OF GIST 28

1.2.1. Interstitial cells of Cajal *29*

1.2.2. Smooth muscle cells *30*

1.3. DIAGNOSTIC APPROACH TO GIST 31

1.3.1. Diagnostic workflow *31*

1.3.2. Immunohistochemical markers *32*

1.3.3. Clinical risk stratification *33*

1.4. GENETIC CLASSIFICATION OF GIST 35

1.4.1. KIT-mutant GIST (75-80%) *36*

1.4.2. PDGFRA-mutant GIST (10-15%) *37*

1.4.3. "Wild type" GIST (10-15%) *38*

1.4.3.1. SDH-deficient WT GIST 38

1.4.3.2. SDH-competent WT GIST 39

1.5. DETAILS OF THE ACTIVATED SIGNALING PATHWAYS IN GIST 40

1.5.1. Receptor tyrosine kinase pathways: KIT and PDGFRA *40*

1.5.2. Metabolic and hypoxia-related pathways: SDH-deficient WT GIST *42*

1.5.3. Alternative pathways: SDH-competent WT GIST *43*

2. THERAPEUTIC STRATEGIES AND RESEARCH ADVANCES IN GIST **44**

2.1. STANDARD OF CARE FOR GIST PATIENTS 44
2.1.1. Surgical resection 44
2.1.2. First-line therapy: Imatinib mesylate (IM) 45
2.1.3. Second- and third-line TKI 47
2.1.3.1. Sunitinib (SU) 47
2.1.3.2. Regorafenib (RE) 47
2.1.4. Next-generation novel TKI 48
2.1.4.1. Ripretinib (RI) 48
2.1.4.2. Avapritinib (AVA) 48
2.2. MOLECULAR MECHANISM OF TKI RESISTANCE IN GIST 49
2.2.1. Disease progression: primary VS secondary resistance 49
2.2.2. Activation of alternative signaling pathways 51
2.3. CLINICAL EMERGING THERAPEUTIC STRATEGIES FOR ADVANCED GIST 53
2.3.1. TKI targeting RTK other than KIT and PDGFRA 54
2.3.2. PI3K/AKT pathway inhibitors 54
2.3.3. MAPK/ERK pathway inhibitors 55
2.3.4. Others clinical strategies 55
2.4. PRECLINICAL AND FUNDAMENTAL RESEARCH IN GIST 56
2.4.1. Experimental GIST models 56
2.4.1.1. GIST cell lines 56
2.4.1.2. Mouse models 58
2.4.2. Emerging molecular targets 59
2.4.2.1. Targeting KIT expression and upstream regulators 59
2.4.2.2. Adaptative stress responses and protein homeostasis 61
2.4.2.3. Disrupting compensatory signaling and cell cycle regulation 61
2.4.2.4. Toward a functional convergence: the YAP1/TAZ axis 62
3. YAP1 AND TAZ: CENTRAL EFFECTORS OF THE HIPPO PATHWAY AND THEIR ROLE IN CANCER 63
3.1. THE HIPPO SIGNALING PATHWAY: AN OVERVIEW 64
3.1.1. From Drosophila to Mammals 64
3.1.2. Regulation of the Hippo pathway 65
3.2. REGULATORY COMPLEXITY AND FUNCTIONAL SPECIFICITIES OF YAP1 AND TAZ 67
3.2.1. YAP1: structure, function and regulation 68
3.2.2. TAZ: paralog with distinct characteristics 70
3.2.3. Similarities and differences in transcription factor interactions 72
3.2.4. Transcriptional corepressors of YAP1 and TAZ 75

3.2.5. Evolving perspective on YAP1 and TAZ divergent functions *76*
3.3. FUNCTIONAL DIVERGENCE AND CONVERGENCE IN CANCER 77
3.3.1. YAP1 and/or TAZ in epithelial cancers *78*
3.3.2. YAP1 and/or TAZ in sarcomas *81*
3.4. YAP1 AND TAZ TRANSCRIPTIONAL TARGETS : DRIVERS OF TUMOR BEHAVIOR 83
3.4.1. CYR61 and CTGF: extracellular matrix remodeling and angiogenesis *83*
3.4.2. CD1: Cell cycle regulation and proliferation *84*
3.4.3. Survivin and MCL-1: apoptosis inhibition and cell survival *84*
3.4.4. AXL: Invasion, EMT, and drug resistance *85*
3.4.5. Additional targets supporting tumor adaptation *85*
3.5. THERAPEUTICS TARGETING OF YAP1 AND TAZ 86
3.5.1. Targeting YAP1/TAZ interaction with TEAD *87*
3.5.2. Indirect YAP1/TAZ targeting through TEAD palmitoylation inhibitors *88*
3.5.3. Targeting YAP1 and TAZ activity *90*
3.5.3.1. YAP1/TAZ regulatory factor inhibitors 90
3.5.3.2. Molecules reducing YAP1/TAZ activity 90
3.5.4. Perspective on drugs targeting YAP1 and TAZ activity *91*
4. SMALL INTERFERING RNA AS A THERAPEUTIC STRATEGY 92
4.1. OVERVIEW OF RNA INTERFERENCE 92
4.2. SIRNA MECHANISMS OF GENE SILENCING 94
4.3. CHALLENGES OF SIRNA-BASED THERAPY 96
4.3.1. Intracellular barriers limiting the conception of siRNA therapeutics *96*
4.3.1.1. Off-target effects and efficacy 96
4.3.1.2. Immune response and toxicity 96
4.3.1.3. Bio-stability 97
4.3.1.4. Cellular delivery and endosomal escape 98
4.3.2. Pharmacological challenges: absorption and distribution *98*
4.3.3. How to develop an optimal siRNA for efficient silencing without side effects *99*
4.4. SIRNA THERAPEUTICS AND THEIR CHALLENGES 100
4.4.1. Food and Drug Administration-approved siRNA drugs *100*
4.4.2. siRNA as cancer therapy *101*
4.4.3. Delivery challenges *103*
4.5. CELL-PENETRATING PEPTIDES FOR CELLULAR SIRNA DELIVERY 104
4.5.1. A brief presentation of cell-penetrating peptides *104*
4.5.2. Covalent CPP to deliver cargoes *106*

4.5.3. From non-covalent CPP to peptide-based nanoparticles 107

4.6. WRAP5 AS A DELIVERY TOOL FOR SIRNA-BASED GENE SILENCING 108

4.6.1. Characteristics of the WRAP family 108

4.6.2. The internalization mechanism of WRAP-based nanoparticles 110

4.6.3. WRAP5-based nanoparticles siRNA delivery 111

4.6.4. Optimizing to "smart" WRAP5 PBN for siRNA delivery 112

THESIS OBJECTIVES 114

RESULTS 117

CHAPTER 1: MULTI-SIRNA DELIVERY USING WRAP5-BASED NANOPARTICLES IN GIST CELLS 118

1. STRUCTURED SUMMARY 119

1.1. INTRODUCTION 119

1.2. METHODS 119

1.3. RESULTS 120

1.4. DISCUSSION 121

1.5. CONCLUSION AND PERSPECTIVES 121

2. PUBLISHED WORK "MULTIPROTEIN SILENCING USING WRAP-BASED NANOPARTICLES: A PROOF OF CONCEPT" 121

RESULTS 143

CHAPTER 2: STUDYING INDIVIDUAL ROLES OF YAP1 AND TAZ IN GIST TUMOR BIOLOGY 144

1. STRUCTURED SUMMARY 145

1.1. INTRODUCTION 145

1.2. METHODS 145

1.3. RESULTS 146

1.4. DISCUSSION 147

1.5. CONCLUSIONS AND PERSPECTIVES 148

2. SUBMITTED WORK "BREAKING THE REDUNDANCY: TAZ OUTPERFORMS YAP1 IN GIST PROGRESSION" 149

RESULTS 183

CHAPTER 3: YAP1 AND TAZ: PLAYING AROUND WITH IM RESISTANCE? 184

1. AIM OF THE STUDY 184

2. PRELIMINARY RESULTS 186

2.1. YAP1 AND TAZ HETEROGENEITY IN IM-SENSITIVE AND IM-RESISTANT GIST CELL LINES 186

2.2. YAP1 AND TAZ SILENCING IN GIST-T1/670 AND GIST-430/654 USING WRAP5:SIRNA NANOPARTICLES 190

2.3. IM TREATMENT IMPACT ON YAP1 AND TAZ PROTEIN EXPRESSION 192

2.4. COMBINED EFFECT OF TAZ SILENCING AND IM TREATMENT ON GIST CELL PROLIFERATION 195

3. DISCUSSION 196

DISCUSSION 201

1. WRAP5-BASED NANOPARTICLES AS PROMISING THERAPEUTIC TOOLS? 203

2. DISTINCT ROLES OF YAP1 AND TAZ IN GIST BIOLOGY 205

3. YAP1 AND TAZ IMPLICATIONS IN IM SENSITIVITY AND RESISTANCE 210

4. LIMITATIONS OF THIS STUDY AND FUTURE PERSPECTIVES 211

CONCLUSION 213

MATERIALS AND METHODS 216

1. USED CELL LINES AND CULTURE CONDITIONS 217

2. SCREENING PROTEIN EXPRESSION USING A GIST CLINICAL DATA SET 219

3. CHARACTERISTICS OF THE USED CELL-PENETRATING PEPTIDE 219

4. DESIGN OF THE USED SIRNA SEQUENCES AND THEIR CHARACTERISTICS 220

5. HOW TO FORMULATE AND CHARACTERIZE WRAP-BASED NANOPARTICLES 222

5.1. FORMULATION OF THE WRAP5:SIRNA NANOPARTICLES 222

5.2. CHARACTERIZATION OF THE WRAP5:SIRNA NANOPARTICLES BY DYNAMIC LIGHT SCATTERING 222

6. WRAP5:SIRNA EVALUATION IN CELLS 223

6.1. CELL TRANSFECTION OF WRAP5:SIRNA NANOPARTICLES 223

6.2. CELL TOXICITY MEASUREMENT BY LDH ASSAY 224

6.3. PROTEIN EXPRESSION EVALUATION BY WESTERN BLOT 225

6.4. RNA EXTRACTION AND QPCR 228

7. CONFOCAL MICROSCOPY 229

7.1. WRAP5-BASED NANOPARTICLES CELLULAR INTERNALIZATION 229

7.2. YAP1 AND TAZ LOCALIZATION BY IMMUNOFLUORESCENCE 230

8. ASSAYS FOR CELLULAR BIOLOGICAL ACTIVITIES 231

8.1. CLONOGENIC ASSAY 231

8.2. CELL PROLIFERATION 232

8.2.1. MTT assay using the CellTiter96® kit 232

8.2.2. Counting cells 233

8.3. WOUND HEALING ASSAY 233

9. IMPACT OF AN IM TREATMENT ON GIST-T1 CELLS 234

9.1. TIME-DEPENDENT EFFECT OF IM ON PROTEIN EXPRESSION IN GIST-T1 CELLS 234

9.2. DETERMINATION OF THE IM IC_{50} VALUE AFTER GIST-T1 CELL INCUBATION 235

10. STATISTICAL ANALYSES 235

11. EDITORIAL ASSISTANCE 236

12. ILLUSTRATION TOOLS 236

REFERENCES 237

APPENDICES 270

1. APPENDIX 1: OTHER PUBLICATION DURING THESIS 271

2. APPENDIX 2: SCIENTIFIC CONTRIBUTIONS RELATED TO THIS THESIS 284

2.1. PUBLICATIONS 284

2.2. ORAL PRESENTATIONS 284

2.3. POSTERS 285

2.4. ATTENDANCE AT CONFERENCES 286

3. APPENDIX 3: SUBSTANTIAL FRENCH SUMMARY 287

LIST OF FIGURES

INTRODUCTION

Figure 1: Typical anatomical locations and relative frequencies of GIST in older adults.

Figure 2: Schematic and immunofluorescence representation of the cellular origin of GIST.

Figure 3: Histological and immunohistochemical features relevant to the diagnosis of GIST.

Figure 4: Distribution of genetic subtypes in GIST.

Figure 5: Schematic representation of the KIT protein structure and the distribution of primary *KIT* mutations in GIST. The mutation frequency percentages refer to global GIST cases.

Figure 6: Schematic representation of the PDGFRA protein structure and the distribution of primary *PDGFRA* mutations in GIST. The mutation frequency percentages refer to global GIST cases.

Figure 7: Schematic representation of the mitochondrial Succinate Dehydrogenase (SDH) complex with the four subunits and the distribution of primary mutations in *SDH*-deficient WT GIST.

Figure 8: KIT and PDGFRA receptor signaling pathways in physiological and pathological contexts.

Figure 9: Representation of the oncogenic signaling in *SDH*-deficient WT GIST.

Figure 10: Mechanism of action of imatinib mesylate (IM) in the treatment of GIST.

Figure 11: Overview of approved targeted therapies for *KIT*- and *PDGFRA*-mutant GIST.

Figure 12: Mutational landscape and drug sensitivity profiles of *KIT*- and *PDGFRA*-mutant GIST.

Figure 13: Overview of the clinical course and molecular mechanisms of imatinib sensitivity and secondary resistance in GIST.

Figure 14: Overview of perturbated pathways of TKI resistance in *KIT*- and *PDGFRA*-mutant and Wild Type GIST.

Figure 15: Emerging therapies under investigation in advanced GIST targeting key signaling pathways.

Figure 16: Emerging molecular targets beyond KIT involved in current research.

Figure 17: Schematic representation of the conservation of the core Hippo signaling module between *Drosophila melanogaster* (left) and mammals (right).

Figure 18: Overview of the Hippo pathway and its regulation of YAP1 and TAZ activity.

Figure 19: Schematic representation of YAP1 3D structure and protein structure, highlighting key functional domains, known interactors, and post-translational modification sites.

Figure 20: Schematic representation of the TAZ 3D and protein structure, highlighting key functional domains, known interactors, and post-translational modification sites.

Figure 21: Diverse transcription factor interactions of YAP1 and TAZ.

Figure 22: Regulation of YAP1 and TAZ transcriptional activity by corepressors.

Figure 23: YAP1/TAZ functions in cancer cells. Adapted from Zanconato et al., 2016.

Figure 24: Overview of functional evidence of YAP1/TAZ's role in human cancers. Abbreviation : CSC: Cancer Stem cells. From Zanconato et al., 2016.

Figure 25: Transcriptional targets of YAP/TAZ and their roles in tumor progression.

Figure 26: Therapeutic strategies targeting YAP1/TAZ signaling in cancer.

Figure 27: Spatial visualization of the protein-protein interaction between YAP1/TAZ and TEAD.

Figure 28: Overview of RNA interference.

Figure 29: Molecular mechanism of siRNA-mediated gene silencing.

Figure 30: Challenges in siRNA therapeutics.

Figure 31: Examples of siRNA delivery systems

Figure 32: Overview of different Cell-Penetrating Peptides (CPP) (non-exhaustive examples).

Figure 33: WRAP-based nanoparticles characteristics.

Figure 34: Mechanism of WRAP:siRNA nanoparticles cellular internalization.

Figure 35: Overview of WRAP5 optimization to develop “smart” WRAP5 nanoparticles.

RESULTS

CHAPTER 1: Multi-siRNA delivery using WRAP5-based nanoparticles in GIST cells

Figure 1: Evaluation of the dose-dependent silencing of WRAP5:siRNA nanoparticles in U87 cells.

Figure 2: Evaluation of the dose-dependent silencing of WRAP5:[siCD1/siCDK4/siMCL-1] (14/3/3) nanoparticles.

Figure 3: WRAP5:siCOCK (14/3/3) nanoparticles affect cell proliferation on U87 cells depending on the incubation time.

Figure 4: Evaluation of WRAP5:[siCD1/siCDK4/siMCL-1] nanoparticles transfection in GIST-T1 cells.

Figure 5: Evaluation of WRAP5:[siCD1/siCDK4/siMCL-1] nanoparticles transfection in GIST-T1 cells.

Figure S1: Evaluation of the dose-dependent silencing of WRAP5:siRNA nanoparticles in U87 cells.

Figure S2: Graphical representations of the measured mean sizes of WRAP5:siRNA nanoparticles.

Figure S3: Evaluation of the dose-dependent silencing of WRAP5:siRNA nanoparticles in GIST-T1 cells.

Figure S4: Evaluation of the silencing of WRAP5:siRNA nanoparticles encapsulating different siCDK4 in GIST-T1 cells.

CHAPTER 2: Studying individual roles of YAP1 and TAZ in GIST tumor biology

Figure 1: Correlation of YAP1 and TAZ expression with the prognosis of GIST patients.

Figure 2: Evaluation of YAP1 or TAZ silencing in GIST-T1 cells with WRAP5:siRNA nanoparticles.

Figure 3: Specific targeting of YAP1 and TAZ, individually or simultaneously, using WRAP5:siRNA cocktails.

Figure 4: Immunofluorescence analysis of YAP1 and TAZ expression following siRNA-mediated silencing in GIST-T1 cells.

Figure 5: TAZ silencing reduced GIST-T1 cell migration and proliferation.

Figure 6: Evaluating TAZ silencing on different signaling pathways in GIST-T1 cells.

Figure 7: WRAP5:siRNA nanoparticles enabled selective silencing of YAP1 and TAZ across GIST cell lines, with conserved downstream regulation of CYR61 and CTGF.

Figure 8: CYR61 and CTGF are effectors of TAZ for cell proliferation control.

Figure S1: Characterization of WRAP5:siRNA nanoparticles by dynamic light scattering (DLS).

Figure S2: Evaluation of YAP1 or TAZ silencing in GIST-T1 cells with WRAP5:siRNA' nanoparticles.

Figure S3: Silencing YAP1 and TAZ protein expression using a single siRNA in GIST-T1 cells.

Figure S4 : YAP1 and TAZ protein expression in GIST-T1 cells.

Figure S5: Cell proliferation remains unaffected at 48 h post siRNA transfection.

Figure S6: Basal expression of YAP1, TAZ, KIT, pKIT in GIST cell lines.

Figure S7: Morphology of three different GIST cell lines.

Figure S8: Evaluation of CYR61 or CTGF silencing in GIST-T1 cells with WRAP5:siRNA nanoparticles.

CHAPTER 3: YAP1 and TAZ: playing around with IM resistance?

Figure 1: Analysis of protein expression in different GIST cell lines.

Figure 2: Representative images of GIST cell lines.

Figure 3: Specific YAP1/TAZ silencing, individually or simultaneously, using WRAP:siRNA nanoparticles in GIST-T1/670 and GIST-430/654.

Figure 4: Time-dependent IM impact on GIST-T1 cells.

Figure 5: Dose-response curves of GIST-T1 cells treated with IM for 72 hours following WRAP5:siRNA nanoparticles transfection with either control siRNA (siNEG) or siTAZ (60 nM).

DISCUSSION

Figure 1: WRAP5-based nanoparticles for siRNA therapeutic delivery system.

Figure 2: Pharmacologic and genetic strategies targeting YAP1/TAZ in *KIT*-independent and *KIT*-dependent GIST.

Figure 3: Proposed model of differential interactions of YAP1 and TAZ in GIST biology.

CONCLUSION

Figure 1: Summary of the main findings and perspectives of this thesis.

MATERIALS AND METHODS

Figure 1: Representative images of GIST cell lines.

Figure 2: Schematic representation of WRAP:siRNA nanoparticle formulation for the subsequent cell transfection.

Figure 3: Schematic representation of the LDH cytotoxicity assay.

Figure 4: Schematic representation of the MTT assay.

LIST OF TABLES

INTRODUCTION

Table 1: Risk assessment of primary GIST.

Table 2: GIST cell lines and their KIT mutations with TKI sensitivity.

Table 3: Roles of YAP1 and TAZ across selected human epithelial cancers (non-exhaustive list).

Table 4: Roles of YAP1 and TAZ across selected human sarcomas (non-exhaustive list).

Table 5: FDA-approved siRNA therapeutics.

Table 6: siRNA-based therapeutics investigated in oncology clinical trials (non-exhaustive list).

Table 7: Two main WRAP sequences (Konate et al., 2019).

RESULTS

CHAPTER 1: Multi-siRNA delivery using WRAP5-based nanoparticles in GIST cells

Table S1: Used siRNA sequences.

CHAPTER 2: Studying individual roles of YAP1 and TAZ in GIST tumor biology

Table S1: Used siRNA sequences.

Table S2: List of antibodies.

Table S3: Human gene-specific primers used for RT-qPCR.

CHAPTER 3: YAP1 and TAZ: playing around with IM resistance?

Table 1: GIST cell lines used in this study.

Table 2: Summary of YAP1 and TAZ profiles in relation to IM response in *KIT*-dependent GIST.

MATERIALS AND METHODS

Table 1: List of GIST cell lines available in the laboratory with their KIT mutations, sensitivity to TKI, and corresponding references.

Table 2: Biochemical characteristics of WRAP5.

Table 3: Used siRNA sequences.

Table 4: Experimental conditions for GIST cell transfection.

Table 5: List of antibodies for Western blot.

Table 6: Human gene-specific primers used for RT-qPCR.

Table 7: List of antibodies for Immunofluorescence.

LIST OF ABBREVIATIONS

A

[1]ACK1	Activated Cdc42-associated kinase 1
AGO2	Argonaute-2 protein
AMOT	Angiomotin family proteins
ANO1	Anoctamin-1
AP-1	Activator protein-1
ATP	Adenosine triphosphate
AVA	Avapritinib

B

BET	Bromodomain and extra-terminal domain
BRAF	V-Raf murine sarcoma viral oncogene homolog B
BRD4	Bromodomain-containing protein 4

C

CD1	Cyclin D1
CDK4	Cyclin-dependent 4
cDNA	complementary DNA
CML	Chronic Myeloid Leukemia
CPP	Cell-penetrating peptides
CSC	Cancer stem cells
CT	Computed tomography
ctDNA	Circulating tumor DNA
CTGF	Connective tissue growth factor
CYR61	Cysteine-rich angiogenic inducer 61

D

DPBS	Dulbecco's phosphate-buffered saline
DMEM	Dulbecco's modified eagle's medium
dsRNA	double-stranded RNA

E

ECM	Extracellular matrix
EGF	Epithelial growth factor
EMT	Epithelial-mesenchymal transition

[1] Gene names are written in italic uppercase letters, while protein names are written in non-italic uppercase letters.

ENS	Enteric nervous system
ERK	Extracellular signal-regulated kinases
ETV1	ETS translocation variant 1
E2F	helix-loop-helix transcription factors

F

FBS	Fetal bovine serum
FBXW7	F-box and WD repeat domain-containing 7
FDA	Food and drug administration
FGFR	Fibroblast growth factor receptor

G

GalNAC	N-acetylgalactosamine
GI	GastroIntestinal
GIST	Gastrointestinal stromal tumor(s)

H

HIF1α	Hypoxia-inducible factor 1α

I

ICC	Interstitial cells of Cajal
IGF	Insulin-like growth factor
IHC	Immunohistochemical
IM	Imatinib mesylate

J

JAK	Janus kinase
JM	Juxtamembrane

K

KRAS	Kirsten rat sarcoma virus

L

LATS1/2	Large tumor suppressor homolog 1/2

M

MCL-1	Induced myeloid leukemia cell differentiation
MEK/MAPK	Mitogen-activated protein kinase
MET	mesenchymal-epithelial transition factor receptor
MITF	Microphthalmia-associated transcription factor
mRNA	messenger RNA

miRNA	microRNA
MRTF	Myocardin-related transcription factor
MST1/2	Mammalian sterile 20-like 1/2
mOS	median overall survival
mPFS	median progression-free survival
mTOR	mechanistic Target Of Rapamycin

N

NF1	Neurofibromatosis type 1
NIH	National Institutes of Health

O

ORR	Overall rate response
OXPHOS	Oxidative phosphorylation

P

PBN	Peptide-based nanoparticle(s)
PCR	Polymerase chain reaction
PDGFRA	Platelet-Derived Growth Factor Receptor A
PDX	Patient-Derived Xenograft
PEG	polyethylene glycol
PET	Positron Emission Tomography
PI3K	Phosphatidylinositol 3-kinase
PLCγ	Phosphoinositide-specific Phospholipase C γ
PPARγ	Peroxisome proliferator-activated receptor γ
PPI	Protein-protein interaction

Q

qPCR	quantitative PCR

R

RAS	Rat sarcoma virus
RE	Regorafenib
RI	Ripretinib
RISC	RNA-induced silencing complex
RNAi	Ribonucleic acid interference
RTK	Receptor tyrosine kinase

S

SAV1	Salvador family WW domain containing protein 1

SCF	Stem cell factor
SDH	Succinate dehydrogenase
shRNA	short hairpin RNA
SH3BP2	adaptor molecule SH3-binding protein 2
siRNA	small interfering RNA
SMA	Smooth Muscle Actin
smRNA	small RNA
SMC	Smooth muscle cells
SOCS2	Suppressor of cytokine signaling 2
SPRY4	Sprouty RTK signaling antagonist 4
SRF	Serum response factor
STAT	Signal transducers and activators of transcription
SU	Sunitinib

T

TAD	Trans activation domain
TBS	Tris-buffered saline
TCA	Tricarboxylic acid
TEAD	TEA domain transcription factors
TF	Transcription Factor(s)
TGF-β	Transforming growth factor-β
TKI	Tyrosine Kinase Inhibitor(s)

V

VEGF	Vascular endothelial growth factor

W

W5	WRAP5
WRAP	W- and R- amphipathic peptide(s)
WT	Wild-type
WWTR1	WW domain containing transcription regulator 1

Y

YAP1	Yes-associated protein 1

INTRODUCTION

1. **Gastrointestinal Stromal Tumors: clinical features and biology**
2. **Therapeutic strategies and research advances in GIST**
3. **YAP1 and TAZ: central effectors of the Hippo Pathway and their role in cancer**
4. **Small interfering RNA as a therapeutic strategy**

1. Gastrointestinal Stromal Tumors: clinical features and biology

The gastrointestinal (GI) tract is affected by a large diversity of diseases, including benign disorders such as inflammatory and infectious conditions, as well as malignant tumors (Sbaraglia et al. 2021). More than 98% of digestive cancers are of epithelial origin, such as gastric cancer, colorectal cancer, and various adenocarcinomas arising from the mucosal lining. In contrast, mesenchymal tumors, from mesenchymal origin, account for less than 1-2% of GI malignancies (Corless et al. 2004; Miettinen and Lasota 2006). They represent a diverse group of lesions with distinct histopathological and clinical features. Among these, gastrointestinal stromal tumors (GIST) are the most prevalent, representing approximately 80% of all mesenchymal tumors in the GI tract (César Serrano et al. 2023). Over the past two decades, our understanding of GIST pathogenesis, risk stratification, and management has evolved rapidly, making GIST a paradigm for precision oncology in solid tumors (Blay et al. 2021; Casali et al. 2022; Miettinen and Lasota 2006; Sbaraglia et al. 2021). This chapter focuses on the clinical and biological characteristics of GIST.

1.1. GIST pathology

1.1.1. Definition

The term “gastrointestinal stromal tumor” was first introduced in 1983, as this subgroup of tumors could not be classified as either neurogenic- or smooth muscle-derived (Mazur and Clark 1983). Following the GIST workshop held at the National Institutes of Health (NIH) in April 2001, it was agreed that GIST should be defined as mesenchymal neoplasms of the GI tract that display the receptor tyrosine kinase (RTK) KIT (also known as CD117 or the stem cell factor receptor, SCFR) as an immunopositive marker, with sporadic exceptions (Fletcher et al. 2002). A mesenchymal neoplasm is a tumor that arises from the mesenchymal tissues, which are the embryonic connective tissues that develop into structures such as bone, cartilage, fat, muscle, blood vessels, and lymphatic tissue (Sbaraglia et al. 2021). This discovery enabled the accurate diagnosis and reclassification of many tumors that had previously been misdiagnosed (Bucher et al. 2004). GIST comprise a majority of tumors previously classified as GI leiomyomas, leiomyoblastomas, and leiomyosarcomas and include many tumors previously

considered neurofibromas, colorectal muscularis mucosae leiomyomas, and schwannomas (Miettinen and Lasota 2006).

Nowadays, GIST are the most common mesenchymal tumors of the GI tract (Miettinen and Lasota 2006). These tumors are characterized by their origin in non-epithelial and non-hematopoietic tissues. All GIST are regarded as having malignant potential, and none can be definitively classified as benign (Sbaraglia et al. 2021).

1.1.2. Epidemiology

Epidemiologically, GIST are rare, accounting for 1-2% of all GI neoplasms. Their incidence is estimated to be ~12 cases per million individuals per year worldwide, with differences between regions and over time (Blay et al. 2021; Cao et al. 2024; Casali et al. 2022). In France, approximately 15 people out of 1 million are affected by GIST, resulting in 800 to 900 new diagnoses annually (Landi et al. 2010). This figure is supported by multiple systematic reviews of population-based cohort studies, which report similar incidence rates across most Western countries (Khan et al. 2022; Monges et al. 2010; Sandvik et al. 2011; Søreide et al. 2016; Verschoor et al. 2018). Unfortunately, estimates are also complicated by the subsequent discovery of microGIST (defined as tumors measuring less than 1 cm in diameter) in up to 20% of patients after autopsy (Blay et al. 2021).

1.1.3. Clinical presentation

GIST develop most commonly in older adults, with a median age at diagnosis ranging from 55 years to 60 years, and exceptionally rarely in children during their second decade of life (1%). They show a slight male predominance (~53%) (Mucciarini et al. 2007). The majority of these tumors are located in the stomach (60-65%), called gastric GIST, and small intestine (20-35%), and less than 5% in rectum, esophagus, omentum, and mesentery (Blay et al. 2021; Bucher et al. 2004; Menge et al. 2018; Parab et al. 2019) (**Figure 1Erreur ! Référence non valide pour un signet.**).

Clinically, GIST may be discovered incidentally or present with symptoms, that depend on the size and location of the tumor, which complicates diagnosis. Small GIST measuring less than 2 cm in diameter are often referred to as miniGIST (1-2 cm) or microGIST (<1 cm). These tumors are usually asymptomatic and frequently detected incidentally during gastroduodenal endoscopy. For suspected GIST with a diameter less than 2 cm, the most common symptoms

include GI bleeding, abdominal pain, or, less commonly, intestinal obstruction. In many cases, these lesions are identified through endoscopic ultrasound, and a biopsy is subsequently recommended when feasible. About 18% of GIST cases are found incidentally, and there is an elevated risk of malignant transformation for tumors located outside the stomach (Blay et al. 2021; Bucher et al. 2004; Casali et al. 2022). In contrast, larger GIST (≥2 cm in diameter) are more inclined to become symptomatic. Clinical manifestations comprise GI bleeding, abdominal pain, early satiety, and palpable abdominal mass in advanced cases. Tumors located in the small intestine are subject to obstruction or perforation, while gastric GIST more often present with bleeding due to mucosal ulceration (Bucher et al. 2004). Compared to small lesions, these GIST carry a higher risk of malignant potential, and their diagnosis is frequently established through cross-sectional imaging (computed tomography (CT) or magnetic resonance imagining), followed by histological confirmation via biopsy when safe and feasible (Parab et al. 2019) (**Figure 1**).

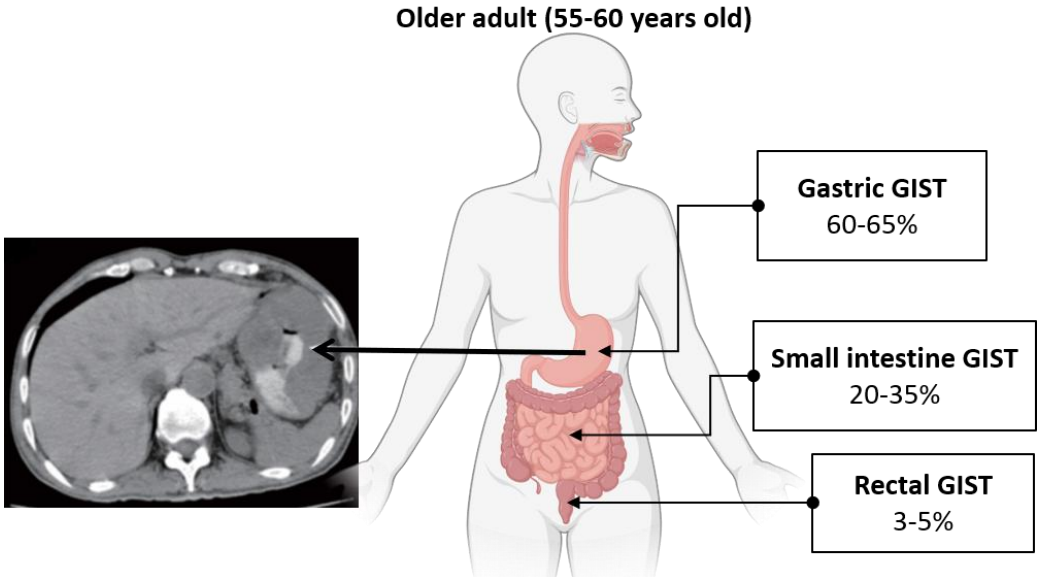

Figure 1: Typical anatomical locations and relative frequencies of GIST in older adults.
The computed tomography scan on the left shows a larger gastric GIST in a representative patient with bleeding and necrosis.
According to Blay et al., 2021 and Parab et al., 2019.

1.2. The cellular origin of GIST

The discovery of the cellular origin of GIST in the GI tract has been essential for understanding their pathogenesis and for developing targeted therapies. The GI tract wall is composed of several concentric layers that include a diverse cellular population, each contributing to specific physiological functions. These layers include the mucosa, submucosa, muscularis

propria, and serosa (Shen 2009). The mucosal lining is first composed of epithelial cells, which mediate absorption and secretion. Other types of cells can be found, including immune cells that provide immunological defense, fibroblasts that maintain the extracellular matrix (ECM), endothelial cells that form the microvasculature, neurons, and glial cells that constitute the enteric nervous system (ENS) (Bourret et al. 2017; Kurahashi et al. 2011; Neunlist et al. 2013). Among the cells residing within the muscular layers, two types are particularly relevant for understanding GIST development: interstitial cells of Cajal (ICC) and smooth muscle cells (SMC). Both cell types are critical for coordinating GI motility and share a common developmental origin.

1.2.1. Interstitial cells of Cajal

In the late 1990s, analyses of ultrastructure, immunohistochemistry, and biomolecular composition demonstrated that GIST arise from ICC or their mesenchymal (stem cell-like) precursors (Kindblom et al. 1998; Torihashi et al. 1999). ICC are specialized mesenchymal cells that form dense networks between and within the circular and longitudinal muscle layers of the GI tract (Maeda et al. 1992). They measure 30 µm in length and 3-6 µm in width. The primary function of these cells is to act as electrical pacemakers. They generate rhythmic depolarizations known as slow waves, which establish the basic electrical rhythm that coordinates GI tract contractions (Blair et al. 2012; Ward and Sanders 2001). ICC are characterized by the expression of *KIT* (encoding the RTK KIT) and feature long, thin

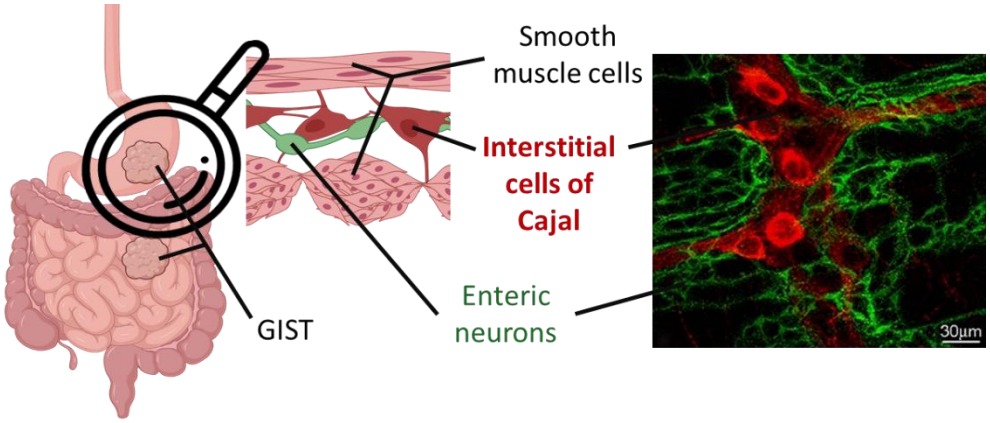

Figure 2: Schematic and immunofluorescence representation of the cellular origin of GIST.
The left panel illustrates the anatomical localization of GIST and the relationship between smooth muscle cells, interstitial cells of Cajal and enteric neurons according to Kondo et al., 2020. The right panel shows an immunofluorescence image highlighting interstitial cells of Cajal (red) and enteric neurons (green), as described by Huizinga et al., 2009.

projections that facilitate electrical coupling with neighboring cells. They regulate gut motility by linking SMC and the ENS (**Figure 2**) (Huizinga et al. 2009; Ward and Sanders 2001).

Subsequent studies have corroborated the cellular origin of GIST *in vivo* by highlighting the shared molecular and phenotypic features between GIST and ICC, particularly the universal expression of *KIT*, a gene that is critical for ICC development (Rubin et al. 2005; Sommer et al. 2003). KIT receptor became a hallmark for GIST diagnosis (see section 1.3.2). Moreover, GIST cells express high levels of ETS translocation variant 1 (ETV1), a transcription factor required for ICC development (Chi et al. 2010). This breakthrough resolved decades of diagnostic confusion as GIST were misclassified, and it is now widely accepted that GIST originate from ICC (Kondo et al. 2020; Min and Leabu 2006).

1.2.2. Smooth muscle cells

Although GIST are widely accepted to originate from ICC, the close developmental and functional interconnection between ICC and SMC highlights the importance of considering SMC features when addressing the cellular context of these tumors. SMC constitute the contractile machinery of the GI muscularis propria, producing the forces necessary for peristalsis and contractions. These cells are spindle-shaped, typically measuring 200-300 µm in length and 5-15 µm in width (Nakamura and Yamamoto 1988). SMC contain three key types of cytoplasmic filaments, which collectively support contractile function: thin actin filaments, thick myosin filaments, and intermediate filaments. The contraction of SMC is regulated by changes in intracellular calcium concentrations. While the slow waves generated by ICC set the underlying membrane potential oscillations, the action potentials and the contractions that follow in SMC only occur if the depolarization surpasses a threshold sufficient (Ward and Sanders 2001). A hallmark of SMC biology is its remarkable phenotypic plasticity. These cells can shift from a differentiated, contractile state to a dedifferentiated, proliferative, or migratory phenotype in response to environmental or inflammatory signals (Liu et al. 2015; Scirocco et al. 2016).

Importantly, both ICC and SMC are believed to arise from a common mesenchymal progenitor during embryonic development, a relationship supported by developmental biology studies and molecular profiling (Le Guen et al. 2015; Torihashi et al. 1999). As differentiation proceeds, these cells elongate and acquire the contractile machinery that defines mature SMC

(Gabella 2002). A subset of mesenchymal progenitors gives rise to ICC, which subsequently intercalate among the muscle layers to establish the pacemaker network (Wallace and Burns 2005).

1.3. Diagnostic approach to GIST

1.3.1. Diagnostic workflow

The diagnostic workflow for GIST begins with patient history and physical examination, as the tumors may be asymptomatic or be discovered incidentally (Bucher et al. 2004).

Imaging modalities like CT, magnetic resonance imaging, ultrasound, and positron emission tomography (PET) scans help identify the tumor, assess its size, vascularity, and detect possible metastases. However, imaging alone cannot reliably distinguish GIST from other tumors such as gastric cancers (Bucher et al. 2004; Mayo Foundation for Medical Education and Research 2025).

Endoscopic techniques contribute further to diagnosis. Upper endoscopy allows visualization of lesions in the esophagus, stomach, and proximal small intestine, though many GIST grow beneath the mucosa and may remain hidden. Endoscopic ultrasound offers better assessment of submucosal tumors and guides fine-needle aspiration or core biopsies. Nonetheless, these biopsies sometimes yield insufficient material or inconclusive results, requiring surgical resection for definitive diagnosis in some cases (American Cancer Society 2019; Mayo Foundation for Medical Education and Research 2025).

The definitive diagnosis of GIST relies on histopathological examination and immunohistochemistry. Moreover, molecular analysis is increasingly incorporated into the diagnostic workflow. Polymerase chain reaction (PCR)-based techniques or sequencing are employed to detect specific mutations in GIST, which not only confirm the diagnosis but also guide therapeutic decisions and predict response to targeted therapies (refer to section 1.4) (Bauer et al. 2021). In addition, the mitotic index (ratio dividing cells to total number of cells) is assessed on surgical or biopsy specimens, providing crucial prognostic information that contributes to risk stratification (César Serrano et al. 2023).

While biopsy and immunohistochemical (IHC) studies are essential for diagnosis, it is important to recognize that tissue sampling is not always feasible. Some GIST are inaccessible

for endoscopic or percutaneous biopsy due to their location or the risk of bleeding, and in certain cases, resection is performed without a preoperative histologic diagnosis if the imaging features and clinical context strongly suggest a GIST (Casali et al. 2022; Mayo Foundation for Medical Education and Research 2025).

1.3.2. Immunohistochemical markers

In medical diagnostics, the gold standard is the hematoxylin and eosin stain, which is the primary stain used in histology. In the GIST diagnosis, histological examination could revealed three main histological patterns: spindle cell (about 70%), epithelioid (about 20%), and mixed types (about 10%) (Blay et al. 2021) (**Figure 3A-C**). However, morphology alone is not sufficient for a conclusive diagnosis. IHC analysis is essential, as it helps distinguish GIST from other mesenchymal tumors.

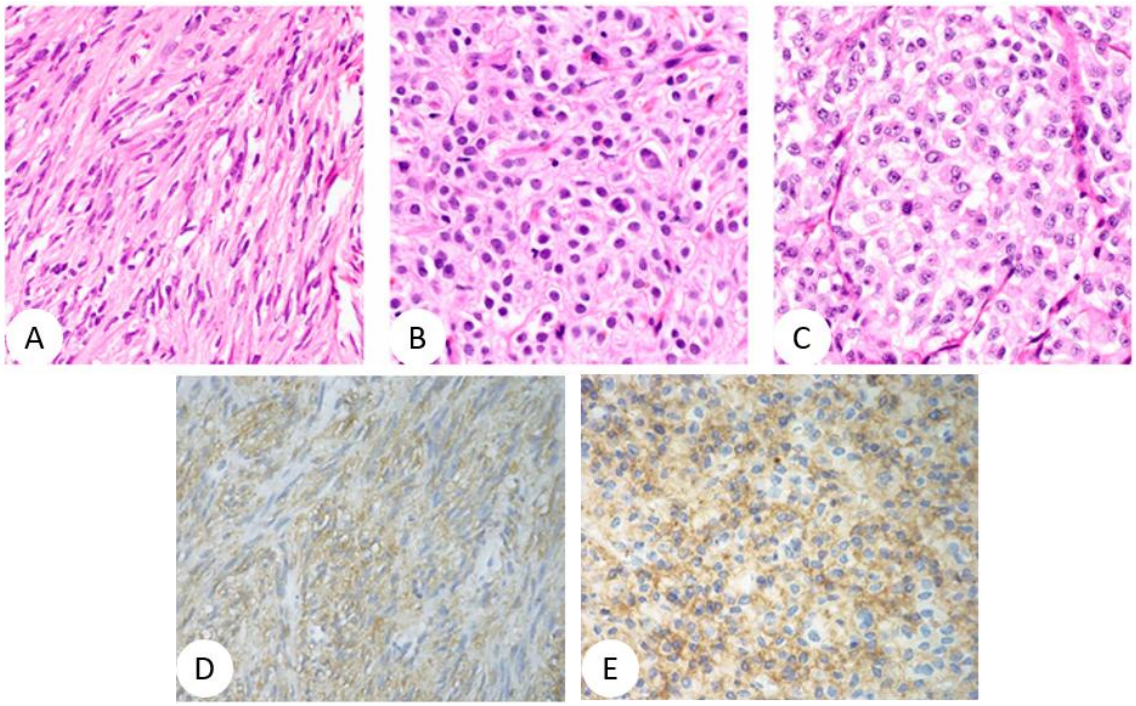

Figure 3: Histological and immunohistochemical features relevant to the diagnosis of GIST.
Hematoxylin and eosin staining of GIST samples: (**A**) Spindle-cell morphology in a *KIT*-mutant GIST; (**B**) Epithelioid morphology characteristic of a *PDGFRA*-mutant GIST; (**C**) Succinate dehydrogenase-deficient *KIT/PDGFRA* WT GIST also with epithelioid features.
Immunostaining of GIST samples: (**D**) Strong cytoplasmic KIT expression; (**E**) Diffuse membranous ANO1 localization.
All sections are displayed at ×200 magnification. Adapted from Blay et al., 2021, and Schaefer et al., 2022.

Before the identification of the expression of *KIT* in GIST, the transmembrane phosphoglycoprotein protein CD34, a hematopoietic progenitor cell antigen, was regarded as the optimal GIST marker (Miettinen et al. 1995). However, it could only identify 2/3 of GIST,

its lack of specificity was due to its immunoreactivity in fibroblastic and endothelial cell tumors (Bure et al. 2017; Miettinen et al. 2000; Robinson et al. 2000).

After the discovery of their origin from ICC, GIST characteristically express markers such as KIT and ANO1. This breakthrough was precipitated by studies that demonstrated a correlation between activating *KIT* mutations and tumorigenesis (Hirota et al. 1998). Expressed in approximately 95% of GIST, KIT protein staining typically shows cytoplasmic, membranous, or paranuclear (Golgi pattern) distribution (**Figure 3D**). While most GIST harbor *KIT* mutations (see section 1.4), *KIT* expression does not always correlate with mutation status (Hornick and Fletcher 2007; Hou et al. 2004; Tzen and Mau 2005). KIT protein remains the gold standard for diagnosis, though rare expression in non-GIST tumors (for example, in melanoma) requires additional tests, and healthy ICC and mastocytes are KIT-positive cells.

For KIT-negative cases (5-10%), another protein could be used as a marker: Anoctamin-1 (ANO1), also known as Transmembrane member 16A (TMEM16A), which is encoded by the *ANO1* gene (also known as *DOG1*) (Casali et al. 2022). Thanks to microarray analysis, it was identified in 2004 as a calcium-activated chloride channel highly expressed in GIST (West et al. 2004). Notably, the ANO1 protein shows superior sensitivity in gastric GIST (98%) and those with *PDGFRA* (platelet-derived growth factor receptor A, also known as *CD140a*) mutations (95%), often missed by KIT labeling. Its expression mirrors the ICC, and it is found at the cytoplasmic membrane of GIST cells (**Figure 3E**). Moreover, ANO1 is rarely expressed in non-GIST tumors and other neoplasms, making it a robust complement to KIT (Bae et al. 2017; Lee et al. 2010; Simon et al. 2013; Swalchick et al. 2015).

Together, KIT and ANO1 cover ~99% of GIST and are rarely expressed in non-GIST tumors. Additional markers are occasionally employed to exclude smooth muscle tumors (leiomyomas/leiomyosarcomas) or neural tumors (schwannomas), such as SMA (Smooth Muscle Actin), Desmin, or S100 (Tzen and Mau 2005).

1.3.3. Clinical risk stratification

Risk stratification is another tool used to obtain crucial prognostic information about primary GIST mainly from surgical or biopsy samples (without complications and metastasis status). This information is instrumental in guiding critical decisions regarding subsequent follow-up, and the selection of the most appropriate therapeutic intervention. The implementation of a

classification system is imperative, given the observed variability in the risk of recurrence and the manifestation of aggressive behavior. The most used system is the NIH Consensus Criteria, introduced in 2002 (Corless et al. 2004; Fletcher et al. 2002). Based on two primary pathological factors, tumor size and mitotic count, GIST are stratified into very low, low, intermediate, and high-risk categories. This discrimination can be done by endoscopic ultrasonography or resection (Demetri et al. 2007; Gao et al. 2024; Lu et al. 2023).

Physicians recently found that gastric GIST generally have a more favorable prognosis than non-gastric tumors of similar size and mitotic rate, leading to subsequent modifications to the NIH criteria. Tumor location and rupture status are now recognized as significant adverse prognostic factors. The Armed Forces Institute of Pathology classification further refined risk assessment by statistically distinguishing risk groups and the importance of anatomical site. This takes into consideration also the risk of metastasis or tumor-related death (Schaefer et al. 2022; César Serrano et al. 2023) (**Table 1**).

Table 1: Risk assessment of primary GIST.

Tumor parameters		**Risk of progressive disease (metastasis or tumor-related death)**			
Tumor Size (cm)	**Mitotic Rate (/50 HPFs)**	**Gastric GIST**	**Duodenal GIST**	**Jejunal/Ileal GIST**	**Rectal GIST**
≤ 2	**≤ 5**	0 (none)	0 (none)	0 (none)	0 (none)
> 2 to ≤ 5	**≤ 5**	1.9% (very low)	8.3% (low)	4.3% (low)	8.5% (low)
> 5 to ≤ 10	**≤ 5**	3.6% (low)	Insufficient data	25% (moderate)	57% (high)
> 10	**≤ 5**	12% (moderate)	34% (high)	52% (high)	57% (high)
≤ 2	**> 5**	† (none)	Insufficient data	† (high)	54% (high)
> 2 to ≤ 5	**> 5**	16% (moderate)	50% (high)	73% (high)	52% (high)
> 5 to ≤ 10	**> 5**	55% (high)	85% (high)	85% (high)	Insufficient data
> 10	**> 5**	86% (high)	86% (high)	90% (high)	71% (high)

Footnote: Table adapted from Blay et al., 2021 and Serrano, Martin-Broto, et al., 2023.
HPF: High-power field; Risk stratification: very low/low/moderate/high; † Small number of cases.

These risk stratification systems have been validated in multiple retrospective and prospective studies, demonstrating their utility in predicting recurrence and informing the use of adjuvant therapies, particularly for patients with intermediate- and high-risk disease. In clinical practice,

patients with very low- and low-risk GIST often require less intensive follow-up. Despite their limitations, these systems remain central to the prognostic evaluation and management of GIST (Lu et al. 2023; César Serrano et al. 2023).

1.4. Genetic classification of GIST

In one hand, GIST constitute a relatively homogenous group defined by their origin from ICC and shared histopathological characteristics. In the other hand, behind this morphological homogeneity lies significant molecular heterogeneity. GIST harbor diverse somatic, activating, and mutually exclusive mutations (Casali et al. 2022; Corless et al. 2004; Hirota et al. 1998). The recognition of GIST as a distinct pathological entity emerged in 1998 following the identification of gain-of-function mutations in *KIT*, a pivotal discovery that subsequently extended to *PDGFRA* mutations (Hirota et al. 1998). While *KIT*- and *PDGFRA*-mutant GIST represent the predominant molecular subtypes, recent advances have revealed additional molecularly defined groups (Casali et al. 2022; Schaefer et al. 2022) (**Figure 4)**. These molecular alterations not only drive tumorigenesis but also determine biological behavior, anatomical distribution, and sensitivity to targeted therapies (Blay et al. 2021; Schaefer et al.

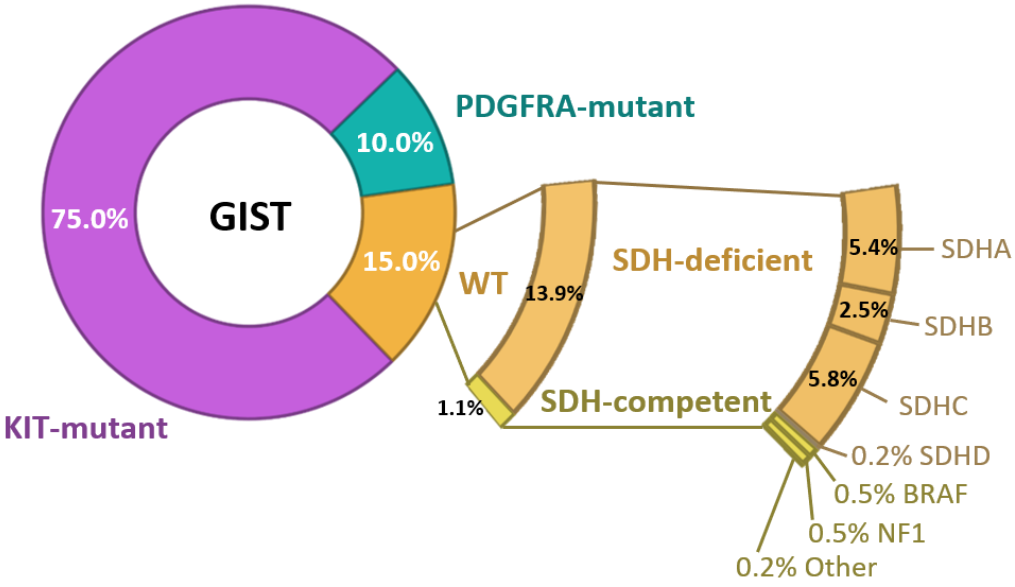

Figure 4: Distribution of genetic subtypes in GIST.
Each segment represents a distinct genetic category, with the proportion of each subtype shown as a percentage of the total cases. The chart highlights the relative frequency of key genetic alterations identified in GIST. Abbreviations: WT: Wild type / SDH: Succinate dehydrogenase; Adapted from Schaefer et al., 2022 and Rutkowski et al., 2022.

2022; Serrano and George 2020). This evolving molecular landscape underscores the shift from purely histopathological diagnosis towards an integrated molecular approach in the management of GIST.

1.4.1. KIT-mutant GIST (75-80%)

Today, it is widely accepted that GIST are mainly caused by oncogenic mutations in *KIT* (75-80% of cases) (Zhou et al. 2024). The glycosylated transmembrane KIT protein contains a N-terminal extracellular region comprising five immunoglobulin-like domains, a transmembrane region, and an intracellular tyrosine kinase domain at the C-terminus including an activation loop and an adenosine triphosphate (ATP)-binding pocket (Blay et al. 2021). Within the larger group of *KIT*-mutant GIST, different hotspots have been reported (**Figure 5**).

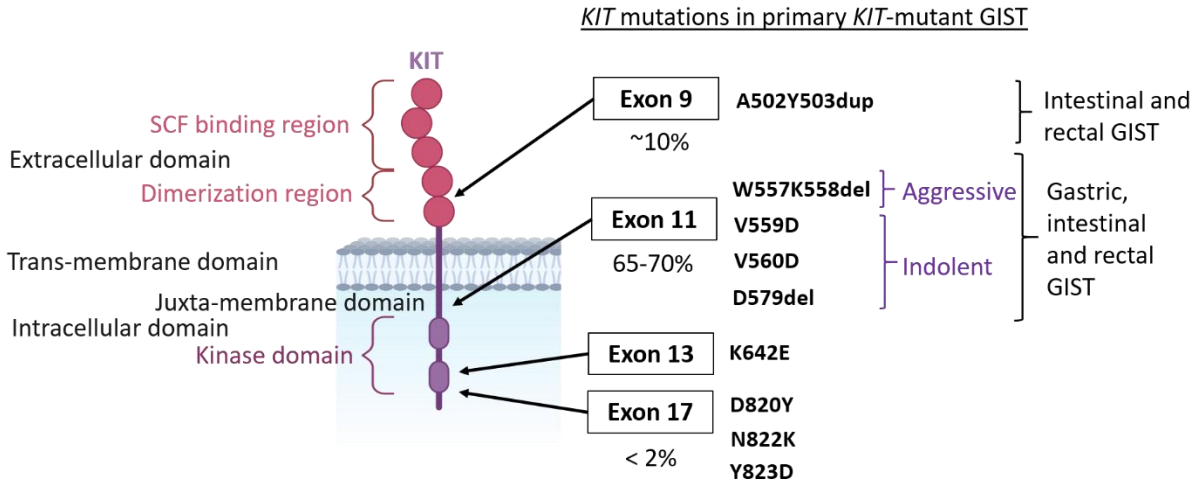

Figure 5: Schematic representation of the KIT protein structure and the distribution of primary *KIT* mutations in GIST. The mutation frequency percentages refer to global GIST cases.
Abbreviations: SCF: stem cell factor; Adapted from Cilloni et al., 2024, Blay et al., 2021 and Serrano & George, 2020.

Approximately 65 to 70% of the classified GIST harbor a *KIT* gene with primary mutations in exon 11, encoding for the intracellular juxtamembrane (JM) domain (Serrano and George 2020) (**Figure 5**). The frequency is well distributed throughout the GI tract (Blay et al. 2021). These mutations disrupt the JM domain's autoinhibitory function, resulting in constitutive, ligand-independent kinase activation and downstream signaling pathways (see section 1.5) (Blay et al. 2021; Serrano and George 2020). All the modifications revealed in-frame deletions (W557K558del and D579del), or missense changes (V559D and V560D). Deletions involving codons 557 and 558 of exon 11 are associated with aggressive clinical behavior and poorer

prognosis, while distal exon 11 duplications tend to confer a more indolent phenotype (Miettinen and Lasota 2006; Wu et al. 2019).

Within primary mutations in the *KIT* gene, approximately 10% of global GIST are found in exon 9, which is responsible for encoding the KIT extracellular protein domain (**Figure 5**). These mutations are more frequent in the small or large intestine involving duplication of codons 502-503 (A502Y503) (Blay et al. 2021; Zhou et al. 2024).

Primary mutations in the intracellular kinase domain are rare (**Figure 5**). Mutations in exon 13 (e.g., K642E) have been identified in the ATP-binding pocket. Also, mutations in exons 17 (e.g., D820Y), accounting for less than 2% of *KIT*-mutant GIST and coding for the activation loop, appeared and can influence both prognosis and response to treatment (Zhou et al. 2024).

1.4.2. PDGFRA-mutant GIST (10-15%)

In approximately 10 to 15% of all GIST cases, *PDGFRA* gene mutations are found leading to a constitutively active PDGFRA protein. The *PDGFRA* gene shares a high degree of similarity to the *KIT* gene, as both genes encode for a type III RTK. For both receptors, mutations disrupt the autoinhibitory regions (e.i. JM domain), resulting in ligand-independent activation (Cao et al. 2024; Serrano and George 2020) (**Figure 6**). Unlike *KIT*-mutant GIST, *PDGFRA*-mutant tumors often have variable or even absent KIT protein expression and generally follow a more indolent clinical course with a lower risk of malignancy (Corless et al. 2011). These tumors have mutually exclusive *PDGFRA* mutations without *KIT* mutations (Heinrich, Corless,

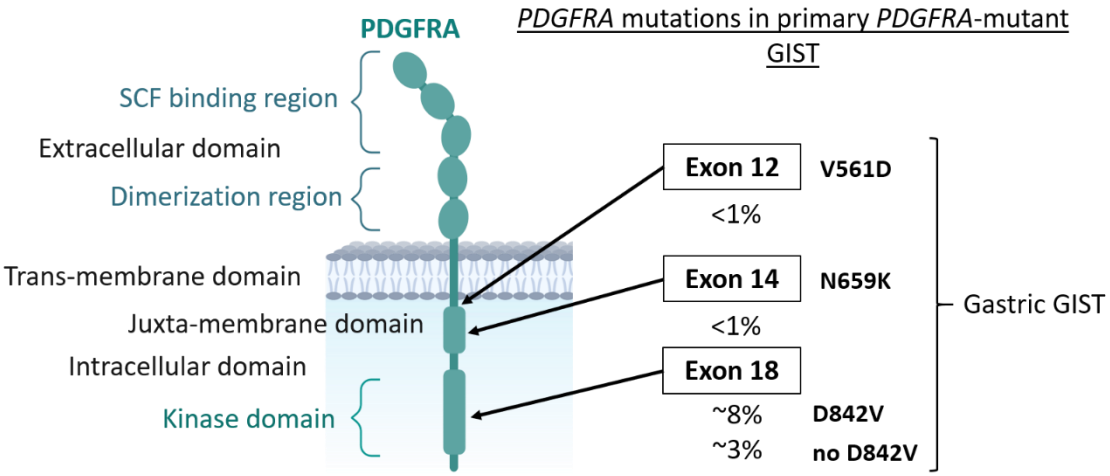

Figure 6: Schematic representation of the PDGFRA protein structure and the distribution of primary *PDGFRA* mutations in GIST. The mutation frequency percentages refer to global GIST cases.
Adapted from Corless et al., 2011 and Blay et al., 2021.

Duensing, et al. 2003). Multiple studies consistently report that over 85% to 90% of *PDGFRA*-mutant GIST are gastric in origin, making the stomach the hallmark site for these tumors (Kwon et al. 2009).

PDGFRA gene mutations occur predominantly in exon 18, especially the D842V substitution, which accounts for up to ~65% of *PDGFRA*-mutant GIST (~8% of global GIST) (Bauer et al. 2021; Blay et al. 2021) (**Figure 6**). The remaining mutations on exon 18 account for approximately 3% of all GIST (Serrano and George 2020). At a lower frequency (<2%), some mutations are found in exons 12 (e.g., V561D substitution) and in exon 14 (e.g., N659K) (Cao et al. 2024; Corless et al. 2011; Miettinen and Lasota 2006) (**Figure 6**). *PDGFRA*-mutant GIST display a strong predilection for the stomach (90%), where they typically present with an epithelioid morphology, although rare cases in the small intestine and duodenum have also been reported (Cao et al. 2024; Corless et al. 2011; Miettinen and Lasota 2006).

1.4.3. "Wild type" GIST (10-15%)

Approximately 10 to 15% of global GIST lack oncogenic *KIT* or *PDGFRA* mutations and these tumors are often called "wild type" (WT) GIST (Nannini et al. 2021). Here, the term "WT GIST" will be used to refer to GIST that are WT for both *KIT* and *PDGFRA* (i.e., *KIT*/*PDGFRA* WT GIST). They have their own morphology, anatomic localization, different than those for *KIT*/*PDGFRA*-mutant GIST (Schaefer et al. 2022).

1.4.3.1. SDH-deficient WT GIST

20 to 40% of WT GIST are mainly based on mitochondrial succinate dehydrogenase (SDH) IHC defect status, called *SDH*-deficient WT GIST (~8% of global GIST) (Rutkowski et al. 2022). SDH is also known as mitochondrial complex II and succinate-ubiquinone oxidoreductase. It is a highly conserved heterotetrameric enzyme complex composed of four protein subunits: SDHA, SDHB, SDHC, and SDHD (Ibrahim and Chopra 2020). It acts at the interphase of the tricarboxylic acid (TCA) cycle and for electron transport chain, where it provides electrons for oxidative phosphorylation (OXPHOS). SDHA and SDHB subunits take the main catalytic component of the complex in the mitochondrial matrix, while SDHC and SDHD are two integral inner membrane proteins (Esteban-Amo et al. 2024; Schipani et al. 2023) (**Figure 7**).

SDH-deficient WT GIST result in loss of SDH complex function, often due to *SDHx* subunit mutations or epigenetic silencing. Approximately 30% of *SDH*-deficient GIST harbor mutations

in *SDHA*, while mutations in *SDHB*, *SDHC*, or *SDHD* are found in 20–30% of cases. The remaining 50% lack *SDHx* mutations but exhibit hypermethylation of the *SDHC* promoter (Nannini et al. 2021; Schipani et al. 2023). *SDH*-deficient WT GIST are also syndromic GIST, meaning they are associated with Carney triad (GIST, pulmonary chondromas, and extra-adrenal paragangliomas, typically in young women) or Carney-Stratakis syndrome (an inherited disorder combining GIST with paragangliomas due to *SDH* gene mutations) (Rutkowski et al. 2022).

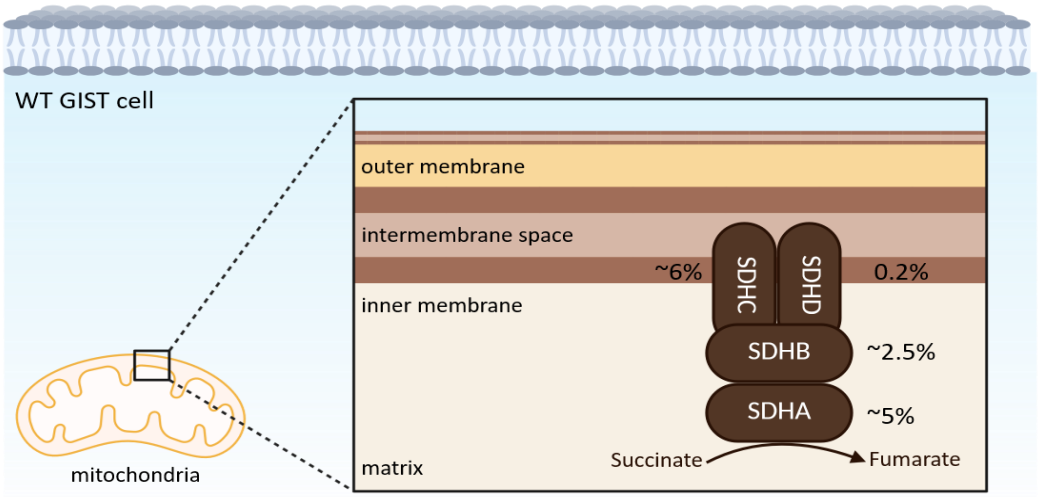

Figure 7: Schematic representation of the mitochondrial Succinate Dehydrogenase (SDH) complex with the four subunits and the distribution of primary mutations in *SDH*-deficient WT GIST.
The mutation frequency percentages refer to global GIST cases.
Adapted from Schipani et al., 2023 and Esteban-Amo et al., 2024.

These tumors predominantly occur in the stomach and affect adolescents (median age of 20-25 years) and young adults (70% female) who characteristically have multinodular gastric masses (Ibrahim and Chopra 2020). They represent over 90% of pediatric GIST.

1.4.3.2. SDH-competent WT GIST

The remaining WT GIST (~1% of global GIST) are classified as *SDH*-competent because they do not harbor mutations in SDH subunits. Among them, approximately 15% exhibit mutations in the RAS/RAF/MAPK pathway such as *NF1* (*Neurofibromatosis type-1*), *BRAF (V-Raf Murine Sarcoma Viral Oncogene Homolog B*), *RAS* (*Rat sarcoma virus)* or *KRAS* (*Kirsten RAt Sarcoma virus*) mutations. In details, *NF1*-associated GIST patients present multiple tumors in the small intestine and have spindle cell morphology. *BRAF*-mutant GIST patients harbor activating mutations in *BRAF*, most commonly the V600E mutation (Nishida et al. 2024). Rare cases of *KRAS*-mutant GIST patients (e.g., G12D, G13D mutations) have been reported (Mullen et al. 2023). The last 50% are classified as quadruple WT GIST, because they lack mutations in *KIT*,

PDGFRA, *SDH*, and RAS/RAF/MAPK pathway genes, representing a poorly understood group with unknown drivers (Mavroeidis et al. 2025; Schipani et al. 2023).

1.5. Details of the activated signaling pathways in GIST

The pathogenesis of GIST is driven by the activation of several key molecular pathways, all involved in tumor initiation, progression, and therapeutic response.

1.5.1. Receptor tyrosine kinase pathways: KIT and PDGFRA

KIT and PDGFRA proteins share a highly conserved structural topology: an extracellular ligand-binding domain, a JM region, and a split cytoplasmic kinase domain (Blay et al. 2021; Corless et al. 2011). Under physiological conditions, these receptors are activated by their specific ligands, called Stem Cell Factor (SCF) for KIT and PDGFA for PDGFRA. Ligand binding induces receptor dimerization and autophosphorylation of intracellular tyrosine residues. This ligand-dependent activation regulates downstream signaling pathways. However, gain-of-function mutations in the *KIT* and *PDGFRA* genes result in ligand-independent activation, leading to persistent oncogenic signaling (Zhou et al. 2024). Upon activation, whether physiological or oncogenic, KIT and PDGFRA proteins trigger downstream signaling cascades that involve the MAPK/ERK (Mitogen-Activated Protein Kinase/Extracellular Signal-Regulated Kinases), PI3K/AKT (Phosphatidylinositol 3-kinase/ Protein kinase B, also known as AKT), PLCγ (Phosphoinositide-specific phospholipase C γ), and JAK/STAT (Janus Kinase/Signal Transducers and Activators of Transcription) pathways (Cilloni et al. 2024) (**Figure 8**).

The autophosphorylation of specific tyrosine residues on KIT or PDGFRA is critical for the recruitment of adaptor proteins and the activation of many pathways, notably when oncogenic signaling is persistent. For example, KIT phosphorylation at positions Y703 or Y936 activates the MAPK/ERK pathway, which plays a pivotal role in transcriptional activation for cell proliferation, differentiation, anti-apoptosis, migration, survival, and treatment resistance. Phosphorylation at Y721 is linked to the PI3K/AKT pathway, promoting cell survival and proliferation, resistance to apoptosis and autophagy, and treatment resistance. KIT activation can also stimulate the PLCγ pathway, leading to the generation of IP_3 and DAG (Dystroglycan) and mediating cellular responses such as PKC (Protein Kinase C) activation for migration and anti-apoptosis.

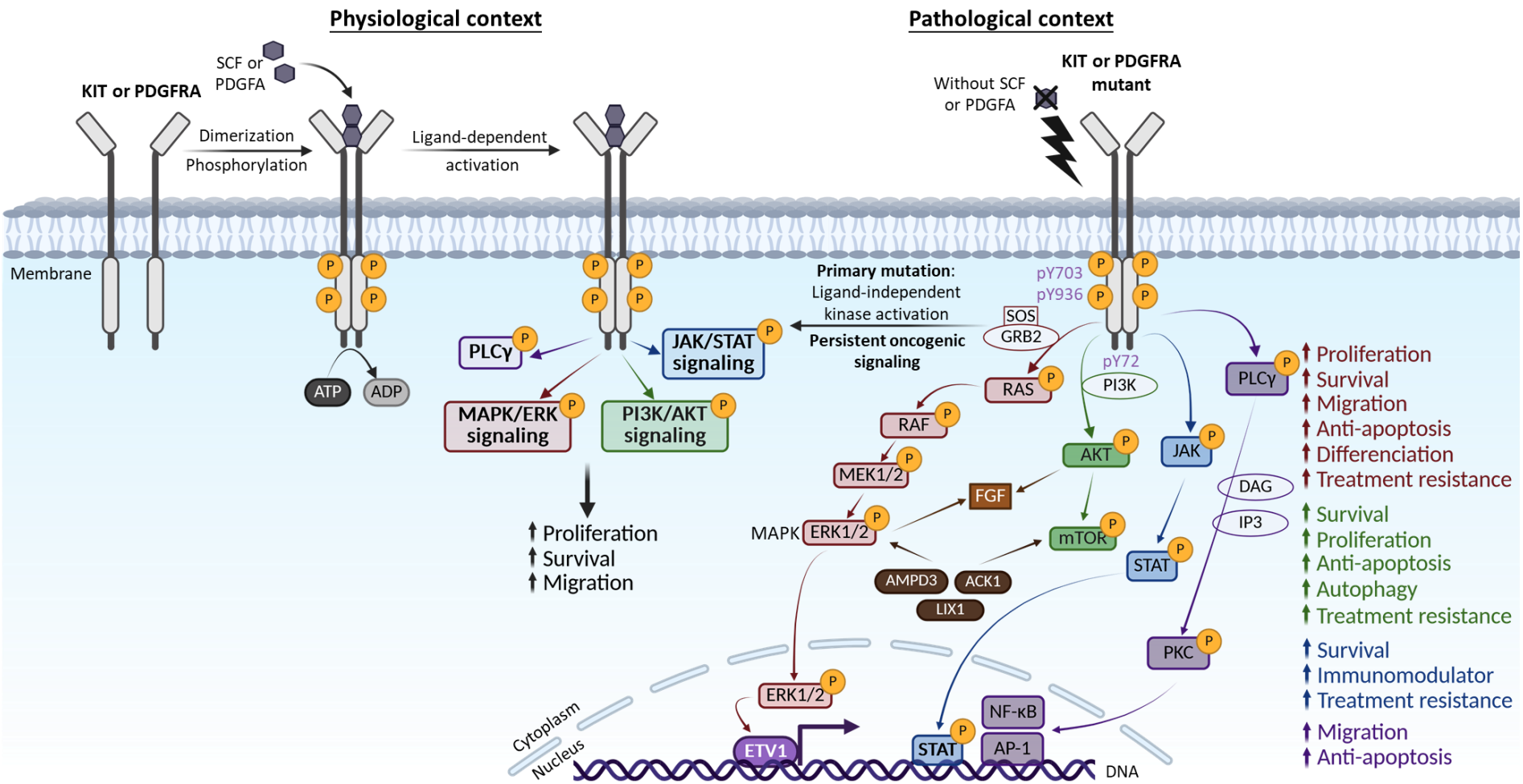

Figure 8: KIT and PDGFRA receptor signaling pathways in physiological and pathological contexts.
On the left, under physiological conditions, binding of stem cell factor (SCF) or PDGFA to KIT or PDGFRA, respectively, induces dimerization and phosphorylation, leading to the activation of downstream signaling cascades such as MAPK/ERK, PI3K/AKT, PLCγ, and JAK/STAT. These pathways regulate key cellular processes including proliferation, survival, and migration. On the right, in the pathological context, activating primary mutation in KIT or PDGFRA (represented by the lightning bolt) results in ligand-independent receptor activation and persistent oncogenic signaling, driving uncontrolled cell proliferation, survival, and resistance to treatment through aberrant activation of the same downstream pathways. The figure highlights the molecular mechanisms underlying KIT-driven tumorigenesis and the complexity of signaling networks involved.
Adapted from Corless et al., 2011; Blay et al., 2021; Zhou et al., 2024.

Additionally, KIT may also engage the JAK/STAT pathway through JAK-mediated phosphorylation of STAT proteins, leading to their translocation into the nucleus for transcriptional regulation of survival and others (Cilloni et al. 2024). Moreover, the complexity of KIT and PDGFRA signaling is maintained by crosstalk with other regulatory pathways.

For example, the MAPK/ERK and PI3K/AKT pathways interact with the FGF (fibroblast growth factor) signaling module, and feedback loops involving proteins such as AMPD3 (adenosine monophosphate deaminase 3), LIX1 (Limb expression 1), and ACK1 (Activated CDC42 kinase 1) modulate signal intensity and duration (Blay et al. 2021; He et al. 2023; Ruiz-Demoulin et al. 2023; Zhou et al. 2024). The resulting activation of KIT and PDGFRA, MAPK/ERK, and PI3K/AKT converges to the ETV1 signaling pathway (Blay et al. 2021). Finally, all these downstream signaling cascades promote tumor cell proliferation, survival, and resistance to apoptosis, autophagy (Bosbach et al. 2017; Duan et al. 2020; García-Valverde et al. 2020; He et al. 2023; Patel 2013).

1.5.2. Metabolic and hypoxia-related pathways: SDH-deficient WT GIST

The loss of function in the SDH enzyme complex in *SDH*-deficient WT GIST drastically affects the mitochondrial respiratory chain and the Krebs cycle. Mutations or epigenetic silencing of one SDHx subunit destabilizes the complex, leading to protein degradation and subsequent succinate accumulation (Ibrahim and Chopra 2020; Nannini et al. 2021) (**Figure 9**).

Elevated succinate inhibits α-ketoglutarate-dependent enzymes, including prolyl-hydroxylase (PHD), which normally tags hypoxia-inducible factor 1α (HIF1α) for degradation. In *SDH*-deficient WT GIST, HIF1α is stable, even under normal oxygen level conditions, and translocates to the nucleus, driving transcription of pro-angiogenic genes such as *VEGF (vascular endothelial growth factor)*, and *IGF1* or *IGF2* (*insulin-like growth factor-1 and 2*) (Schipani et al. 2023).

On the other hand, succinate inhibits ten-eleven translocation (TET) family of DNA hydroxylases, causing genome-wide hypermethylation, a hallmark of *SDH*-deficient tumors (Blay et al. 2021; Schipani et al. 2023). *BRAF*-mutant GIST patients harbor activating mutations in *BRAF*, most commonly the V600E mutation, leading to MAPK/ERK pathway activation (Nishida et al. 2024).

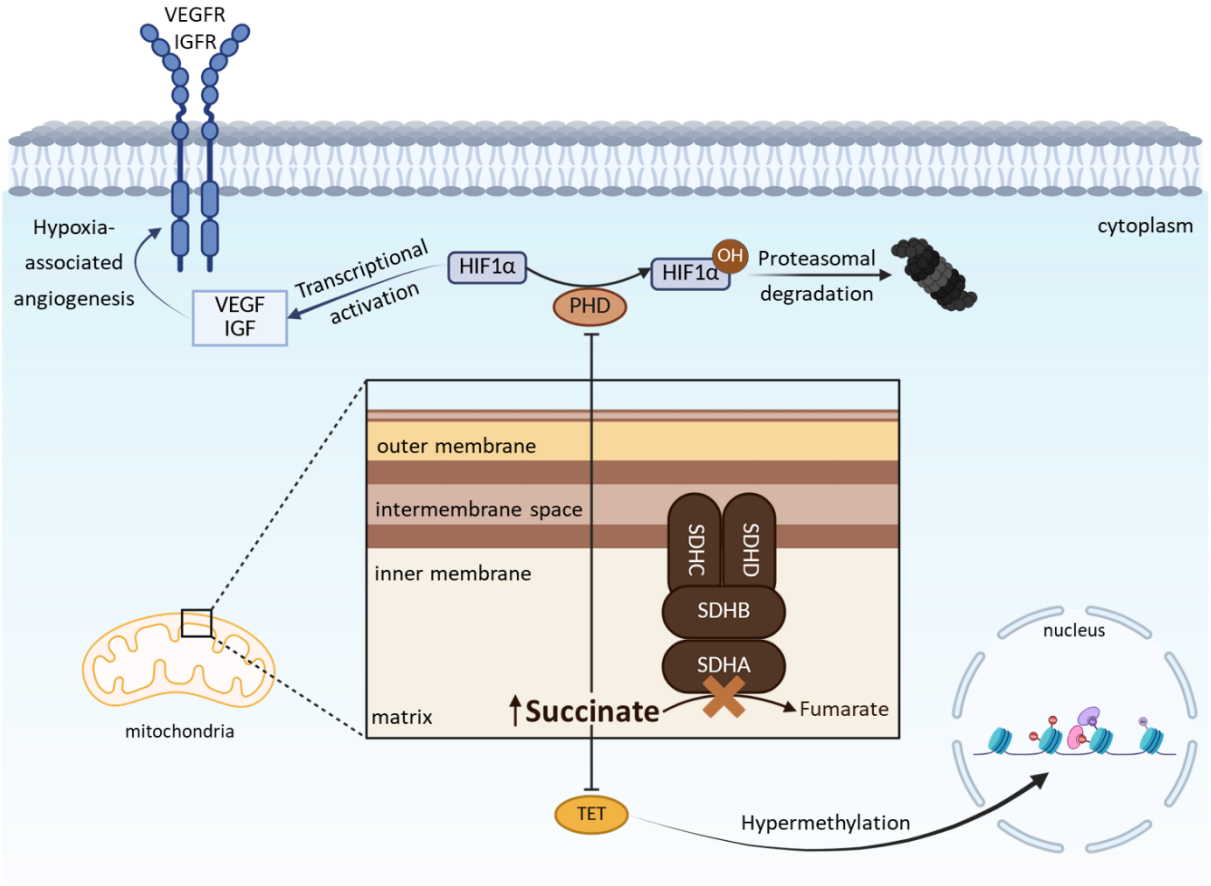

Figure 9: Representation of the oncogenic signaling in *SDH*-deficient WT GIST.
In the mitochondria, the SDH complex catalyzes the conversion of succinate to fumarate in the tricarboxylic acid cycle. Accumulation of succinate inhibits prolyl hydroxylase domain (PHD) enzymes, preventing hydroxylation and proteasomal degradation of HIF1α. Stabilized HIF1α translocates to the nucleus, promoting transcriptional activation of target genes such as *vascular endothelial growth factor (VEGF*) and *insulin-like growth factor (IGF*). On the other hand, genome-wide hypermethylation is caused by the inhibition of ten-eleven translocation (TET) family.
Adapted from Blay et al., 2021 and Scipani et al., 2023.

1.5.3. Alternative pathways: SDH-competent WT GIST

In the context of *SDH*-competent WT GIST, the MAPK/ERK downstream pathway has been shown to be activated in the presence of mutations in *NF1*, *BRAF*, and, less frequently, *RAS* (Corless et al. 2011; Kays et al. 2018). This observation underscores the heterogeneity of GIST and highlights the need for comprehensive genomic analysis to elucidate the underlying molecular mechanisms.

2. Therapeutic strategies and research advances in GIST

The management of GIST has evolved considerably over the past two decades, with therapeutic strategies now tailored to disease stage, risk stratification, and tumor molecular profile. Nevertheless, the probability of therapeutic resistance remains considerable, and research is still ongoing to find novel therapeutic targets.

2.1. Standard of care for GIST patients

The current standard of care for GIST patients reflects a multidisciplinary approach, combining surgery and molecular targeted therapies depending on localized or metastatic GIST. Each therapeutic choice plays a distinct role depending on tumor localization, mutational status, and the clinical course of the disease. In this context, therapeutic drugs may be administered either in the neoadjuvant context (to reduce tumor size and facilitate resection in anatomically challenging cases) or as adjuvant therapy (to prevent recurrence following complete surgical excision in high-risk patients) (Blay et al. 2021).

2.1.1. Surgical resection

Surgical resection is typically the main treatment for low-risk localized GIST. The goal is to achieve a complete removal of the tumor (R0 resection), as it is linked to a favorable survival prognosis (Blay et al. 2021; Casali et al. 2022). Minimally invasive approaches, such as laparoscopy or robotic surgery, are preferred for smaller tumors in favorable locations. The surgery is reserved for larger or anatomically complex lesions (> 2cm) to avoid tumor rupture, which increases relapse risk (Blay et al. 2021; César Serrano et al. 2023). For GIST with a high risk of recurrence after resection, surgery is not sufficient. For locally advanced and metastatic GIST, surgery is not first-line. Instead, adjuvant or neoadjuvant tyrosine kinase inhibitors (TKI) are used. In the second case, surgery may be considered later in select cases when the tumor is reduced (Blay et al. 2021; Casali et al. 2022; César Serrano et al. 2023). A preoperative biopsy is therefore not always necessary if the diagnosis is clear and the reduced tumor is resectable (César Serrano et al. 2023).

The 5-year survival rate after surgery is between 48% and 70% and prognosis depends on tumor size, location, mitotic rate, and mutation status (Schaefer et al. 2022).

2.1.2. First-line therapy: Imatinib mesylate (IM)

Imatinib mesylate (IM) (formerly STI-571 and commercialized as Gleevec) is a potent, selective inhibitor of several RTK, including KIT, PDGFRA, ABL1 and BCR-ABL. The efficacy of this drug marks a turning point in the treatment and management of metastatic GIST patients (Demetri et al. 2002; van Oosterom et al. 2001). Importantly, IM was initially discovered and developed for the treatment of chronic myeloid leukemia (CML), specifically targeting the constitutive activated BCR-ABL fusion protein, which is present in 95% of CML patients (Druker et al. 1996). IM was later extended to GIST due to its ability to inhibit also KIT and PDGFRA receptors (Demetri et al. 2002; Li and Raut 2019).

IM binds to the ATP-binding pocket of the KIT protein, thereby preventing ATP binding and KIT phosphorylation, resulting in the inactivation of downstream signaling pathways essential for tumor cell proliferation and survival (Demetri et al. 2002; Mol et al. 2004; Zhou et al. 2024) (**Figure 10**).

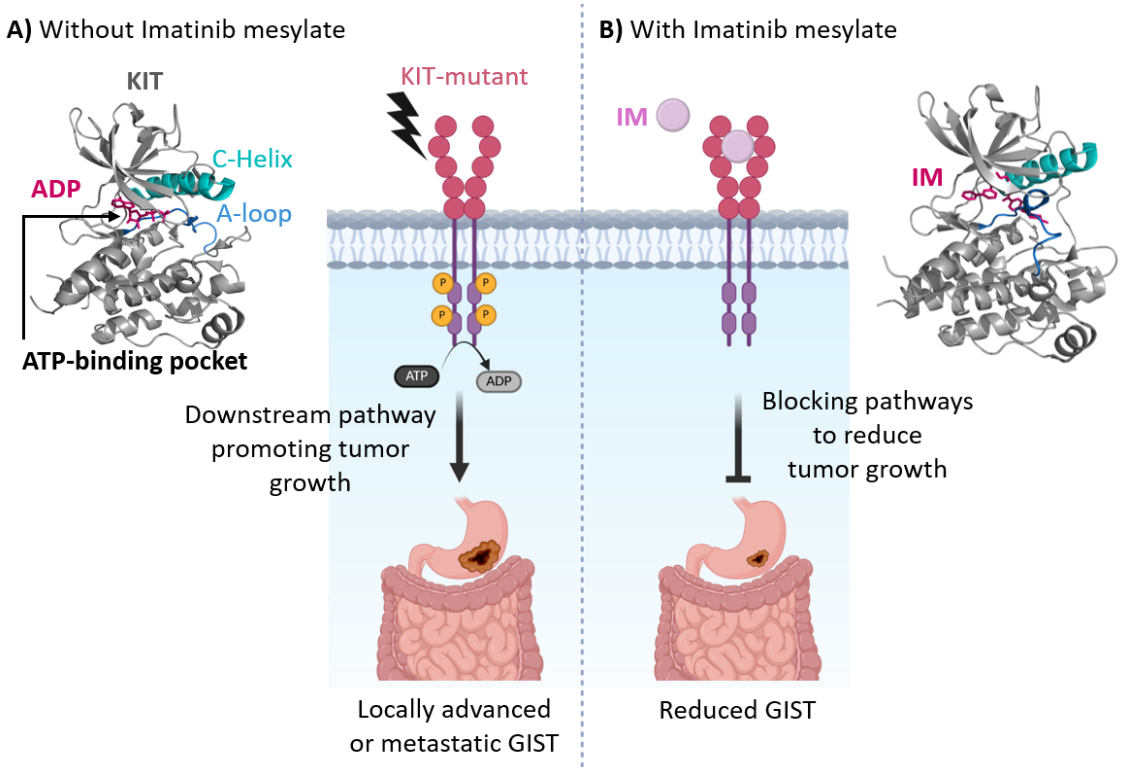

Figure 10: Mechanism of action of imatinib mesylate (IM) in the treatment of GIST.
A) Without IM, mutant KIT receptors are constitutively activated, leading to continuous ATP binding and phosphorylation of downstream signaling partners, which promotes tumor growth and progression of locally advanced or metastatic GIST. The lightning bolt represents the activation of the receptor.
B) With IM, the drug binds to the ATP-binding pocket of the KIT receptor, inhibiting its kinase activity and blocking downstream signaling pathways, resulting in reduced tumor growth.
Abbreviations: ADP: adenosine diphosphate; ATP: adenosine triphosphate; IM: imatinib mesylate; A-loop: activation-loop.
3D KIT structures (PDB code 1PKD for A and 1T46 for B) were obtained by PyMol. Adapted from Mol et al., 2004.

For high-risk resected GIST, adjuvant IM for at least 3 years is now recommended, based on the SSG XVIII trial and the guidelines from the European Society for Medical Oncology, the British Sarcoma Group, and the Japan Society of Clinical Oncology.

IM is the first-line treatment for patients with metastatic or inoperable GIST. First clinical trials (phase II) for neoadjuvant IM treatment in patients with advanced and metastatic GIST have reported a partial response with a median progression-free survival (mPFS) of 20.4 months and an overall response rate (ORR) of 51% (Blanke et al. 2008; Demetri et al. 2002) (**Figure 11**).

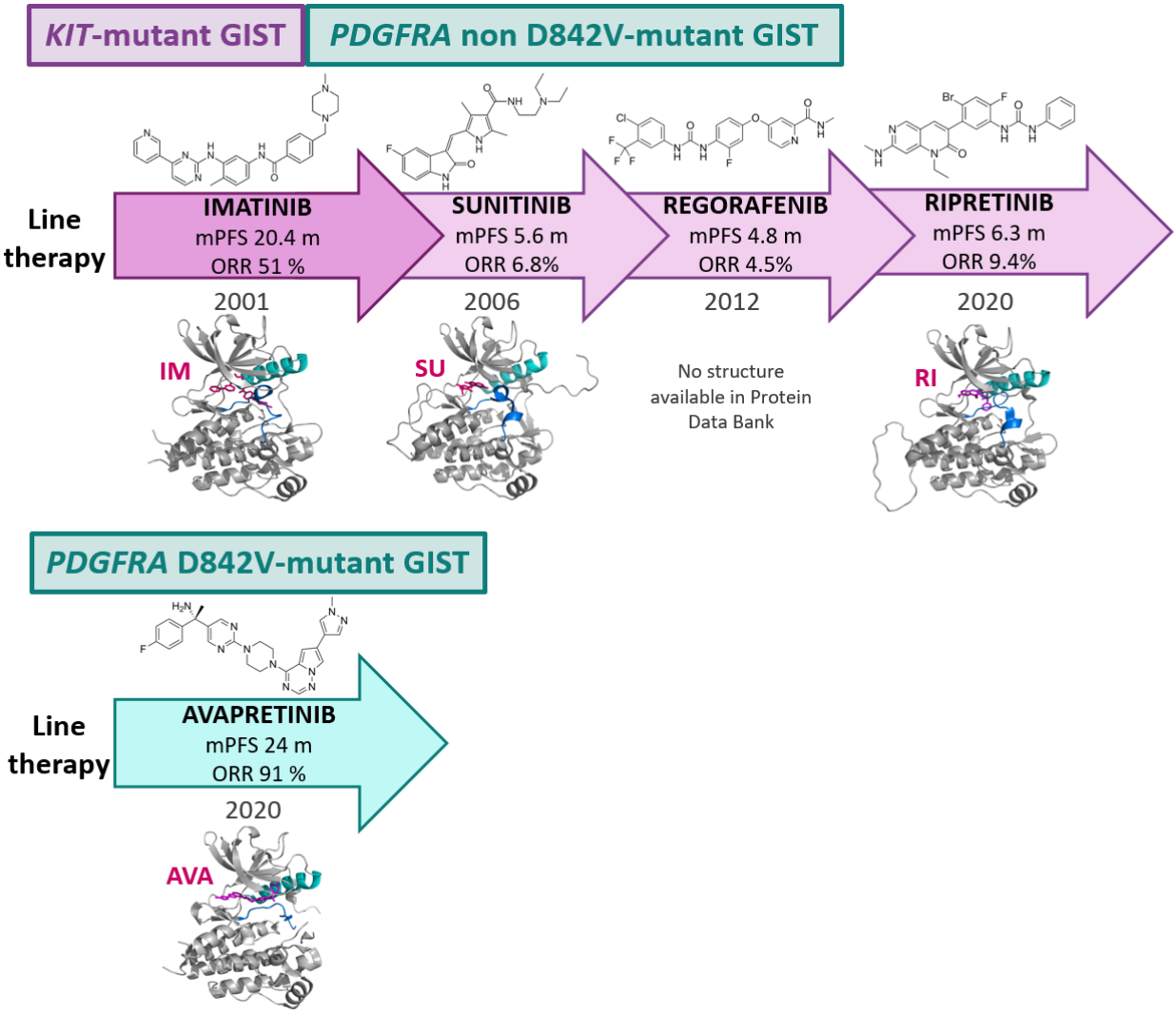

Figure 11: Overview of approved targeted therapies for *KIT*- and *PDGFRA*-mutant GIST.
For *KIT*-mutant GIST and *PDGFRA* non D842V-mutant GIST, imatinib (IM), sunitinib (SU), regorafenib (RE), and ripretinib (RI) are used sequentially as first, second, third, and fourth-line therapies, respectively. The median progression-free survival (mPFS, in months) and objective response rate (ORR, in %) for each agent are indicated. The molecular structures of the drugs and their binding modes to the kinase domain are depicted below each arrow. For *PDGFRA* D842V-mutant GIST, avapritinib (AVA) is the approved targeted therapy.
3D KIT structures (PDB code 1T46 for KIT+IM, 3G0E for KIT+SU, 6MOB for KIT + RI, 8PQG for PDGFRA+AVA) were obtained by PyMol. Adapted from Serrano & George, 2020; Gajiwala et al., 2009; Smith et al., 2019.

Long-term follow-up studies have shown that IM significantly improves survival, with median overall survival (mOS) exceeding 4 years (57 months) in advanced GIST, compared to less than 12 months before its discovery (Blanke et al. 2008). However, the therapeutic response to IM is strongly influenced by the tumor's mutational status (referred to section 2.2).

The recommended dose of IM for adult patients with unresectable or metastatic GIST is 400 mg once daily, taken orally (Blay et al. 2021). In patients harboring *KIT* exon 9 mutations, a higher dose of 800 mg daily (400 mg twice daily) may provide improved disease control, although at the expense of increased toxicity (Debiec-Rychter et al. 2006). Rare but serious complications can appear unless IM is generally well tolerated. Current guidelines recommend indefinite continuation of IM for advanced and metastatic GIST, as interruption often leads to disease progression (Casali et al. 2022). The hope remains that surgery will be possible after treatment.

2.1.3. Second- and third-line TKI

2.1.3.1. Sunitinib (SU)

Sunitinib (SU) (formerly SU11248) is the second-line TKI for patients with GIST who are refractory or intolerant to IM (Demetri et al. 2006). It is a multitarget TKI of the ATP-binding site, mainly of VEGFR-1 and -2, but also of KIT and PDFRA. It was first developed as a treatment for acute myeloid leukemia and advanced renal cell carcinoma (Bauer et al. 2021). In the phase III clinical trial (NCT00085618) leading to its approval as a second-line GIST therapy, SU, administrated at 37.5 mg daily, significantly improved mPFS compared to placebo (27.3 weeks vs 6.4 weeks) (Demetri et al. 2006). Now, SU mPFS is 5.6 months with an ORR of 6.8% (Demetri et al. 2012; Serrano and George 2020) (**Figure 11**). The maximum tolerated dose was determined to be 50 mg daily (Bauer et al. 2021). However, some *KIT* mutations are resistant to SU, in contrast with *PDGFRA* mutations (excluding D842V mutation) (referred to section 2.2). Finally, SU is used in *SDH*-deficient WT GIST due to intrinsic IM resistance (Blay et al. 2021).

2.1.3.2. Regorafenib (RE)

Regorafenib (RE) (formerly BAY 73-4506) is an oral, multitarget TKI approved as third-line therapy for advanced GIST after progression on IM and SU (Demetri et al. 2013). It inhibits KIT, PDGFRA, VEGFR, BRAF and other RTK. In the phase III GRID trial (NCT01271712), RE has a mPFS

of 4.8 months and an ORR of 4.5%, with most patients achieving stable disease and a small proportion partial responses (Demetri et al. 2013) (**Figure 11**). RE is administered on an intermittent schedule of 160 mg daily for 21 days, followed by a 7-day treatment break, in repeating 28-day cycles. Its toxicity profile is comparable to that of SU. As observed for SU, the efficacy of RE is mutation-dependent for *KIT* (see section 2.2). (Blay et al. 2021).

2.1.4. Next-generation novel TKI

2.1.4.1. Ripretinib (RI)

Ripretinib (RI) (formerly DCC-2618) is a novel, broad-spectrum TKI, approved for patients with advanced GIST, who have received at least three prior TKI treatments (Blay et al. 2021). RI targets both the switch pocket and activation loop of KIT and PDGFRA, effectively inhibiting a wide range of primary and secondary resistance mutations, including those in the activation loop that are poorly addressed by earlier TKI. RI is particularly used for patients with secondary mutations in *KIT*, since very few patients with *PDGFRA* mutations reach this last line of therapy (Bauer et al. 2021; Blay et al. 2021; Schaefer et al. 2022). The phase III clinical trial INVICTUS (NCT03353753) has demonstrated a mPFS of 6.3 months and an ORR of 9.4% in fourth-line therapy when a daily dose of 150 mg was administrated (Blay et al. 2020) (**Figure 11**). Thanks to its dual mechanism of action, RI overcomes resistance mechanisms associated with conformational changes in the kinase domain (Schaefer et al. 2022).

2.1.4.2. Avapritinib (AVA)

Avapritinib (AVA) (formerly BLU-285) is a next-generation TKI specifically developed to target the PDGFRA D842V mutation, which is highly resistant to IM and other earlier TKI (Bauer et al. 2021) (**Figure 12**). The relative phase I clinical trial NAVIGATOR (NCT02508532) has shown that AVA (300 mg) leads to a mPFS of 24 months and an ORR of 91% (Jones et al. 2021) (**Figure 11**). However, when compared with RE in the phase III trial VOYAGER (NCT03465722), no improvement was noticed in mPFS (Kang et al. 2021). Another breakthrough was achieved in VOYAGER trial. Circulating tumor DNA (ctDNA) sequencing efficiently detected *KIT*/*PDGFRA* mutations and prognosticated outcomes in patients with TKI-resistant GIST treated with AVA, highlighting its utility for disease monitoring and personalized therapeutic strategies (C. Serrano et al. 2023).

2.2. Molecular mechanism of TKI resistance in GIST

2.2.1. Disease progression: primary VS secondary resistance

Resistance to IM is classified into primary and secondary resistance, and it is a well-established clinical challenge in the management of advanced GIST (Serrano 2021; Serrano et al. 2019). A series of early mutations in *KIT* or *PDGFRA* (primary mutations) induces what is called primary resistance, defined by tumor progression during the initial IM treatment. About 10% of GIST display primary resistance to IM. It is often associated with specific tumors' genetic status (Serrano and Fletcher 2019) (**Figure 12**).

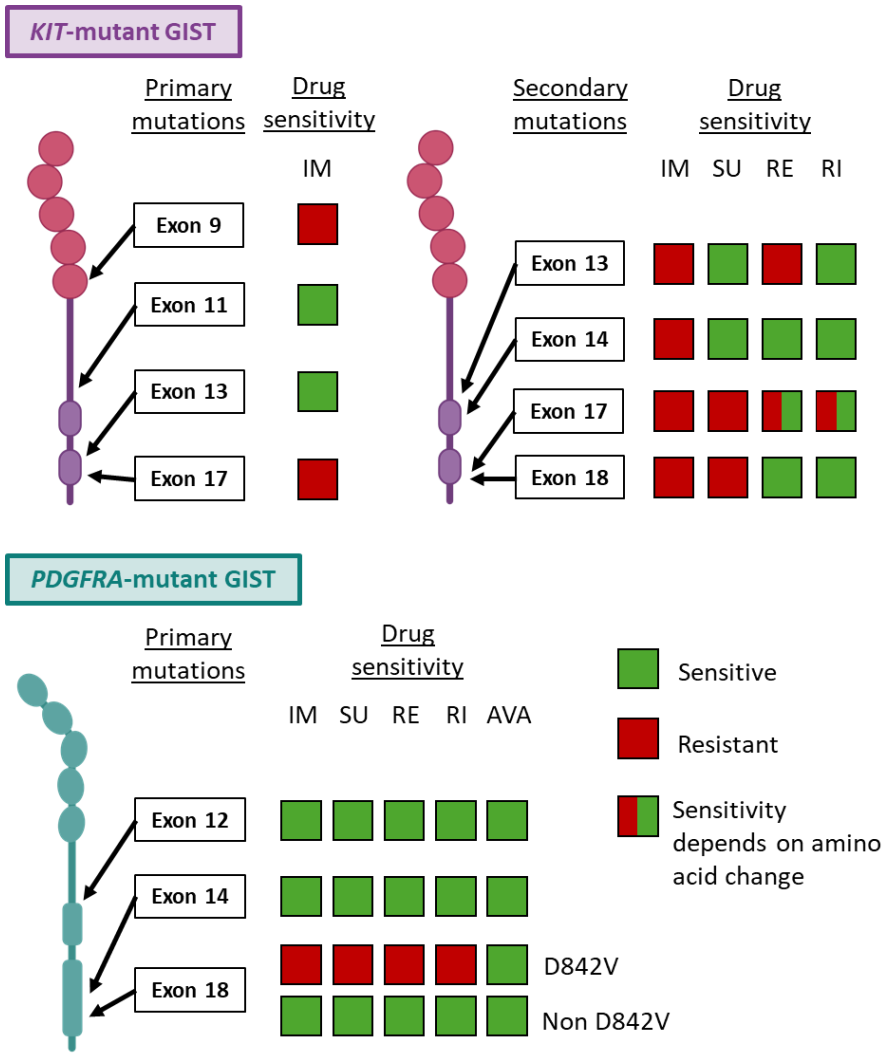

Figure 12: Mutational landscape and drug sensitivity profiles of *KIT*- and *PDGFRA*-mutant GIST.
The figure illustrates the correlation between specific mutations and response to tyrosine kinase inhibitors. Adapted from Serrano & Fletcher, 2019.

Patients with *KIT* exon 11 mutations exhibit the highest response rates to IM treatment (up to 83%) unlike *KIT* exon 9 mutations which are insensitive (48%), and *KIT* exon 17 mutations (e.g.,

D820Y, N822K, Y823D) which are frequently more resistant (Casali et al. 2022; Corless et al. 2004; Heinrich, Corless, Demetri, et al. 2003; Schaefer et al. 2022; Wu et al. 2019) (**Figure 12**). For patients whose tumors harbor a *KIT* exon 9 mutation, or for those who experience disease progression, an increased dose of 800 mg daily may be considered if tolerated (Debiec-Rychter et al. 2006).

Patients with *PDGFRA* mutations in exon 12 and 14, as well as certain deletions in exon 18, are sensitive to IM (Blay et al. 2021; Schaefer et al. 2022). It is the contrary for WT GIST and for tumors harboring the most common *PDGFRA* mutation in exon 18, D842V (Bauer et al. 2021; Neppala et al. 2019; Rutkowski et al. 2022; Serrano and George 2020) (**Figure 12**). Finally, rare cases *SDH*-competent WT GIST such as KRAS-mutant GIST patients (e.g., G12D, G13D mutations) have been reported to be primary resistant to IM (Mullen et al. 2023).

Secondary resistance typically develops after an initial period of response or disease stabilization during IM treatment (**Figure 13**).

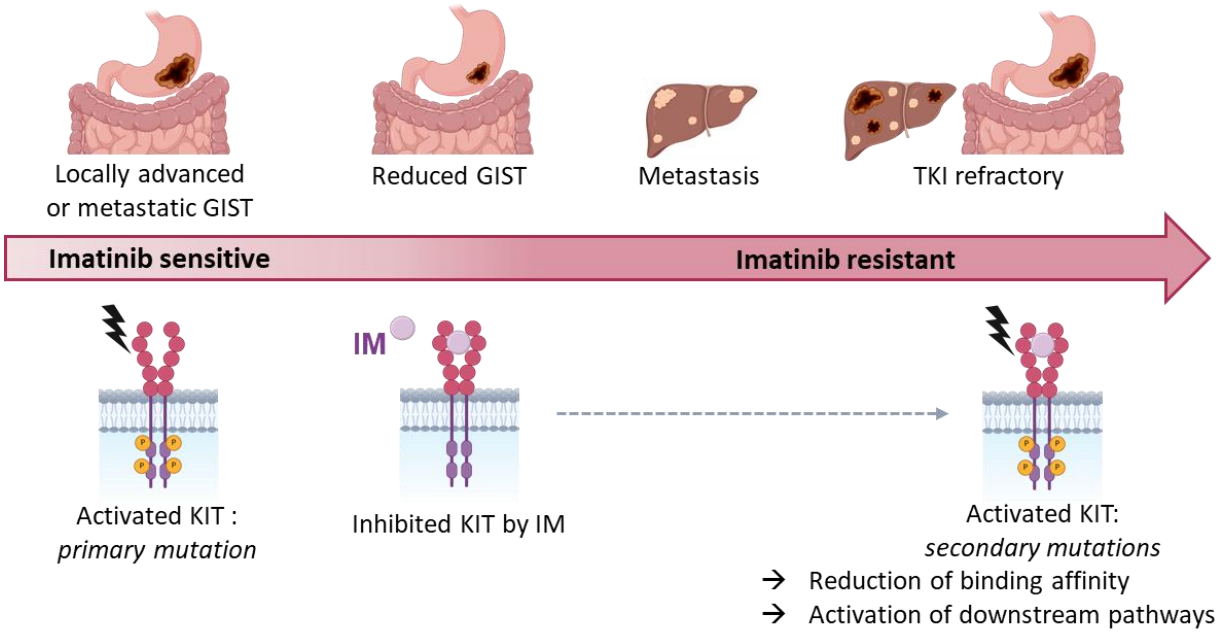

Figure 13: Overview of the clinical course and molecular mechanisms of imatinib sensitivity and secondary resistance in GIST.
The upper panel illustrates the progression from locally advanced or metastatic GIST to tumor reduction under imatinib treatment, followed by the development of metastasis and eventual resistance to tyrosine kinase inhibitors (TKI). The lower panel depicts the molecular basis: primary activating mutations in *KIT* lead to constitutive signaling and tumor growth, which is effectively inhibited by imatinib (IM) in sensitive cases. Over time, secondary mutations in *KIT* can arise, resulting in reduced drug binding affinity and reactivation of downstream signaling pathways, thereby conferring resistance to imatinib.
Adapted from Serrano & George, 2020.

This phenomenon is most documented for *KIT* mutants, as *PDGFRA* mutants are most often receptive to first-line TKI, excluding the more common D842V primary mutation, for which AVA has been specially adopted since 2020 (Serrano and George 2020). Secondary resistance is due to secondary mutations in *KIT* gene which reduce the binding affinity to TKI and activate downstream oncogenic pathways (Antonescu et al. 2005; Serrano and George 2020). These secondary mutations commonly occur in exons 13 and 14 (ATP-binding pocket) and exons 17 and 18 (activation loop) of *KIT* (Serrano et al. 2019) (**Figure 12**).

After IM failure, second- and third- line TKI are administrated but these therapies are also mutation-dependent. GIST patients with *KIT* secondary mutations on exons 13 and 14 have better outcome when treated with SU while patients with *KIT* mutations in exon 17 have better survival when treated with RE (Bauer et al. 2021; Schaefer et al. 2022; Serrano et al. 2019).

Despite resistance, these tumors often remain dependent on KIT signaling for survival, providing a rationale for switching to an alternative TKI (Blay et al. 2021). However, after personal discussions with clinicians during conferences (Occitanie GIST 2024 regional meeting and ESMO 2025 congress), it is possible in practice to administer standard of care TKI in certain cases, not knowing the mutational status of the tumor (especially when a biopsy cannot be performed), but also in the hope of slowing tumor progression.

2.2.2. Activation of alternative signaling pathways

Several interleaved molecular mechanisms have been identified as central to TKI resistance in *KIT*- and *PDGFRA*-mutant GIST or WT GIST. Most of this research has been carried out on *KIT* mutations, although theoretically it works the same way for the PDGFRA receptor (Serrano and George 2020). This section is illustrated in **Figure 14**, which summarizes the known perturbated pathways resulting in TKI resistance.

Firstly, overactivation of KIT and PDGFRA can appear in case of TKI resistance, leading to a high stabilized protein (Serrano and George 2020). As previously mentioned, secondary mutations in the *KIT* gene, which alter the kinase domain and reduce drug binding, are the main factors contributing to the emergence of secondary resistance. This results in the reactivation of the major KIT downstream pathways promoting tumor growth by increasing proliferation, survival and migration. This reactivation can also occur for PDGFRA-mutant receptor (Hu et al. 2022;

Serrano and George 2020). Several additional mutations in *retinoblastoma tumor suppressor 1* (*RB1*), *SWI/SNF-related matrix-associated actin-dependent regulator of chromatin subfamily B member 1 (SMARCB1)*, and *Myc-Associated factor X (MAX)* cause the reactivation of other signaling pathways such as JAK/STAT. In rare cases, resistance is associated with the activation of downstream pathways such as MAPK/ERK and PI3K/mTOR, independent of KIT and PDGFRA, demonstrating convergent evolution toward kinase-independent growth (Serrano and George 2020; Zhou et al. 2024).

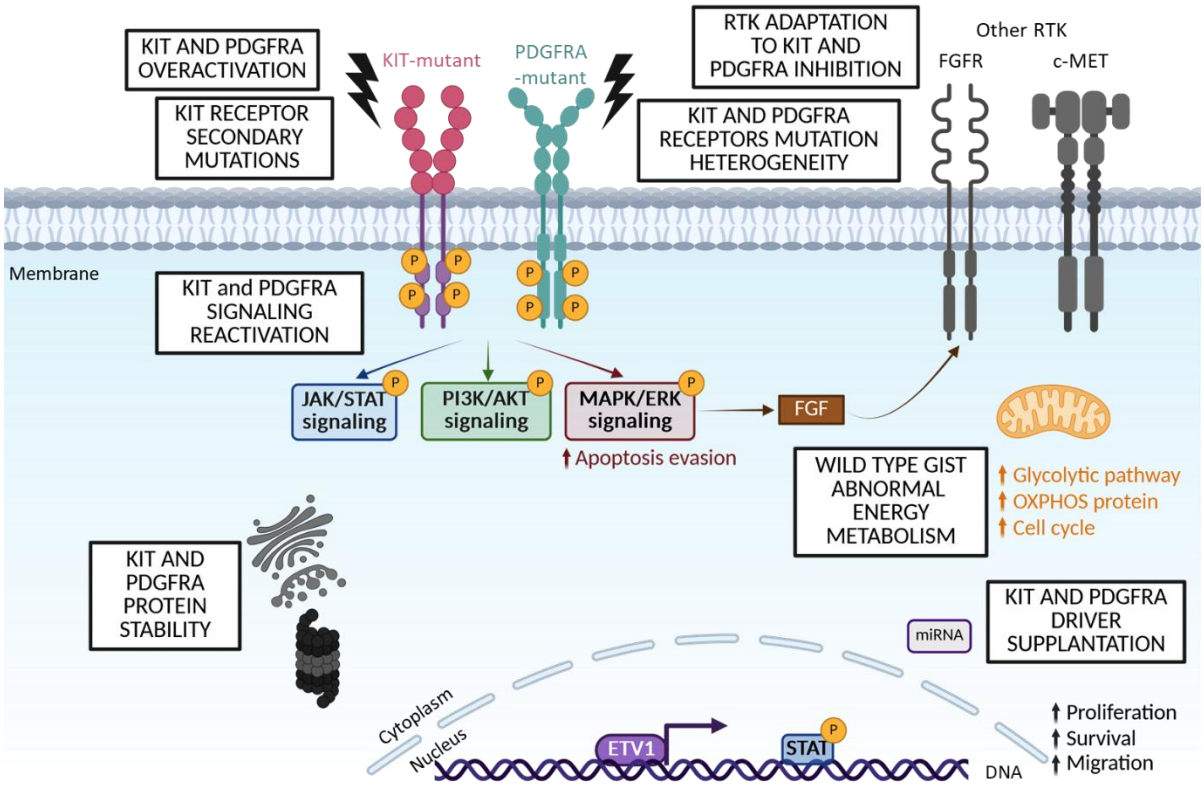

Figure 14: Overview of perturbated pathways of TKI resistance in *KIT*- and *PDGFRA*-mutant and Wild Type GIST. Resistance mechanisms include receptor overactivation, secondary mutations, receptor tyrosine kinase adaptation, and mutation heterogeneity. Downstream reactivation of KIT/PDGFRA signaling leads to JAK/STAT, PI3K/AKT, and MAPK/ERK pathways reactivation, promoting proliferation, survival, and apoptosis evasion. Additional mechanisms involve KIT/PDGFRA protein stability and driver supplantation while abnormal energy metabolism occurs in Wild-Type GIST.
Abbreviation: RTK: receptor-tyrosine kinase; OXPHOS: oxidative phosphorylation.
Adapted from Serrano & George, 2020; Hu et al., 2022.

GIST cells can adapt to KIT and PDGFRA inhibition by activating stress responses that induce cellular quiescence, involving regulators of the cell cycle and autophagy. The MAPK/ERK pathway through FGFR (fibroblast growth factor receptor) and MET (mesenchymal-epithelial transition factor receptor) signaling due to apoptosis evasion can also be reactivated (Corless et al. 2011; Hu et al. 2022; Serrano and George 2020). This mirrors the resistance mechanisms

observed in other kinase-driven malignancies, such as CML, in which feedback loops are disrupted upon kinase inhibition (Serrano and George 2020; Zhou et al. 2024). This mechanism can also involve the evolution of GIST toward reduced dependence on KIT or PDGFRA signaling, particularly after all lines of treatment. An exploratory analysis of the phase III INVICTUS trial for RI revealed genomic heterogeneity with subclones showing variable dependence on *KIT* (*KIT*-dependent vs *KIT*-independent) (Blay et al. 2020).

This phenomenon is further exacerbated by the presence of tumor heterogeneity, wherein multiple *KIT* and *PDGFRA* mutant subclones with differential sensitivities to TKI can coexist within a single tumor (Bauer et al. 2021; He et al. 2024).

MicroRNA-mediated regulation has also been implicated in resistance, with specific miRNAs modulating key signaling pathways and thereby contributing to TKI resistance (Zhou et al. 2024).

Moreover, WT GIST, are intrinsically resistant to current TKI, as their oncogenic drivers are not inhibited by these drugs. Metabolic plasticity, including enhanced glycolysis, increased OXPHOS activity, and a shift toward the pentose phosphate pathway, plays a role in the WT GIST resistance but also in some TKI-resistant *KIT*-mutant GIST (Hu et al. 2022). In short, abnormal energy metabolism is found in GIST with TKI resistance.

Personalized approaches, guided by molecular profiling and real-time resistance monitoring, are likely to be the key in developing more effective treatments for resistant GIST (Cao et al. 2024; Zhou et al. 2024).

2.3. Clinical emerging therapeutic strategies for advanced GIST

Overcoming therapeutic resistance remains the central challenge in the management of advanced GIST, whatever the type of mutation. Consequently, there is an urgent need to develop new therapeutic strategies, including combination approaches and alternative molecular targets, to improve patient outcomes and extend disease control. In the following sections, the principal categories of emerging therapeutic strategies currently under clinical investigation will be presented, with selected examples of investigational drugs and novel compounds used to illustrate key concepts. Due to the extensive scientific and clinical research currently underway, only a selection of new strategies will be presented (**Figure 15**).

2.3.1. TKI targeting RTK other than KIT and PDGFRA

One of the major resistance mechanisms in advanced GIST involves the reactivation of downstream signaling pathways, such as MAPK/ERK and PI3K/AKT (He et al. 2024). To circumvent this problem, a growing number of therapeutic strategies aim to inhibit alternative RTK beyond KIT and PDGFRA, including VEGFR, FGFR, MET, AXL, and RET (REarranged during Transfection) (He et al. 2024; Santoro and Carlomagno 2013; Serrano and Bauer 2022) (C. He et al., 2024; Santoro & Carlomagno, 2013). Among them, Crenolanib is undergoing late-phase clinical testing in the CRENOGIST trial (NCT02847429) (Serrano and George 2020). A broader list of ongoing clinical candidates targeting alternative RTK is provided in gray in **Figure 15**.

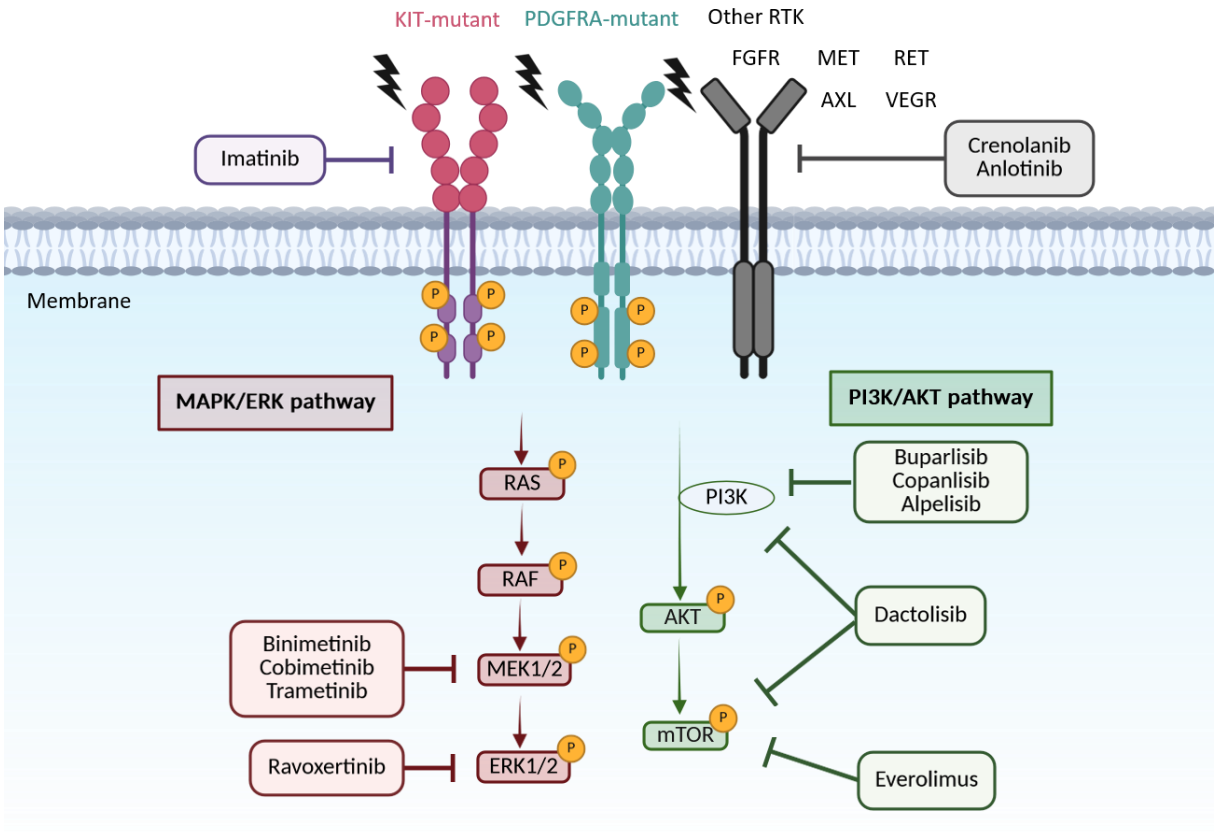

Figure 15: Emerging therapies under investigation in advanced GIST targeting key signaling pathways.
Schematic overview of other RTK (gray), the PI3K/AKT (red) and MAPK/ERK (green) pathways and inhibitors targeting different parts of these pathways in GIST, highlighting the central role of RTK activation and the emerging therapeutic strategies aimed at disrupting key nodes within the signaling cascade.
Abbreviation: RTK: Receptor Tyrosine Kinase; Adapted from Duan et al., 2020 and He et al., 2024.

2.3.2. PI3K/AKT pathway inhibitors

Constitutive activation of the PI3K/AKT pathway is a well-characterized feature of *KIT* and *PDGFRA*-mutant GIST and contributes to both tumor growth and therapeutic resistance.

Inhibition of this signaling cascade has demonstrated anti-proliferative and pro-apoptotic effects in preclinical models, supporting its relevance as a therapeutic target (Lindblad et al. 2015; Zhu et al. 2020).

Several strategies are currently under investigation to block key components of the PI3K/AKT/mTOR axis, either alone or in combination with IM. Although preclinical data supported PI3K/AKT inhibition in GIST, early-phase trials combining IM with either the pan-PI3K inhibitor Buparlisib (BKM120) or the isoform-specific Alpelisib (BYL719) (respectively NCT01468688 and NCT01735968) showed limited clinical activity and substantial toxicity, and were therefore not pursued further (Duan et al. 2020; Floris et al. 2013; Gelderblom et al. 2020; Pantaleo et al. 2022; Van Looy et al. 2014).

Additionally, Everolimus (RAD001), a rapamycin analog targeting mTOR, has shown synergistic effects with IM *in vitro* and has progressed to Phase I/II trials for resistant GIST (Schöffski et al. 2010). Despite promising preclinical results, the clinical development of these agents remains challenged by toxicity and limited efficacy (Duan et al. 2020). A broader overview of candidate molecules targeting this pathway is highlighted in green in **Figure 15**.

2.3.3. MAPK/ERK pathway inhibitors

The MAPK/ERK pathway plays a central role in mediating resistance to TKI in GIST, making it an attractive target for therapeutic intervention. Multiple levels of this cascade, including RAF, MEK (Mitogen-activated protein kinase), and ERK1/2, can be inhibited to disrupt downstream signaling (He et al. 2024). Among these strategies, MEK inhibitors such as Binimetinib (MEK162) in combination with IM have demonstrated promising tumor reduction in previously unresectable cases (NCT01991379) (Chi et al. 2022; Ran et al. 2015). Combinatorial strategies involving dual MEK and ERK inhibition are currently under evaluation to improve specificity while minimizing toxicity (He et al. 2024). Other examples are presented in red in **Figure 15**.

2.3.4. Others clinical strategies

In addition, a variety of alternative strategies are under clinical investigation in advanced GIST, including approaches targeting protein homeostasis, nuclear export, immune modulation, and cell cycle regulation (George et al. 2023; He et al. 2024; Kelly et al. 2021; Kurokawa et al. 2022; Serrano and George 2020). These efforts reflect a broader shift toward addressing tumor

heterogeneity and resistance through mechanisms beyond oncogenic signaling, often supported by emerging tools such as liquid biopsies and advanced preclinical models.

2.4. Preclinical and fundamental research in GIST

Preclinical and fundamental research efforts have played a pivotal role in shaping our understanding of GIST biology and therapeutic vulnerabilities. This section highlights key experimental models that have enabled mechanistic insights, as well as emerging molecular targets that may guide the development of future therapeutic strategies.

2.4.1. Experimental GIST models

For researchers and clinicians, the development of robust experimental models is essential to elucidate the molecular mechanisms underlying GIST development and their evolution toward drug resistance.

2.4.1.1. GIST cell lines

The most common GIST cell lines in fundamental research are divided into three categories: IM-sensitive *KIT*-mutant, IM-resistant *KIT*-mutant, and *KIT*-independent GIST cell lines.

IM-sensitive *KIT*-mutant cell lines include GIST-882, GIST-T1, GIST-430, GIST-48, GIST-62, and GIST-522, each with distinct mutation profiles, particularly in the *KIT* gene (Serrano et al. 2019; Zhou et al. 2024). All the well-defined mutation profiles and characteristics are listed in **Table 2**. For examples, GIST-T1 (primary mutation in KIT exon 11: Δ560–578) cells were established from a metastatic gastric tumor and exhibits strong expression of KIT, but are negative for DESMIN, S-100, and α-SMA (Taguchi et al. 2002). GIST-882 cells were derived from a primary IM-naive GIST and carry a homozygous exon 13 missense mutation (K642E) in KIT (Tuveson et al. 2001). The three IM-sensitive GIST cells used in this manuscript are the GIST-T1, the GIST-430 and the GIST-882. Some advances have enabled the establishment of new cell lines such as GK1C and GK3C, derived directly from patient tumor samples (Fukuda et al. 2013).

IM-resistant *KIT*-mutant cell lines include subclones of IM-sensitive *KIT*-mutant GIST cells with some secondary mutations in the *KIT* gene (**Table 2**). They have been obtained by chronic TKI treatment of GIST-T1 or GIST-430 cells, such as GIST-T1/670, GIST-T1/816, GIST-T1/820, GIST-T1/829, and GIST-430/654. All of these cell lines have different sensitivity to TKI (Serrano et

al. 2019). The two IM-resistant GIST cells used in this manuscript are the GIST-T1/670 and the GIST-430/654, having a secondary KIT mutation in exon 14: T670I and in exon 13: V564A, respectively.

Table 2: GIST cell lines and their KIT mutations with TKI sensitivity.

Cell lines	KIT mutations	Other TKI sensitivity	
		SU	**RI**
IM-sensitive *KIT*-mutant			
GIST-T1	Exon 11: V560-Y578del	S	S
GIST-882	Exon 13: K642E	S	S
GIST-430	Exon 11: V560-L576del	S	S
GIST-522	Exon 11: delEVQWK554-558	NR	NR
GIST-62	Exon 11: MYEVQWK552-558T	NR	NR
GIST-474	Exon 11	NR	NR
GIST-554	Exon 9: AY503-504ins	NR	NR
IM-resistant *KIT*-mutant			
GIST-T1/670	Exon 11 + Exon 14: T670I	S	S
GIST-T1/816	Exon 11 + Exon 17: D816E	R	S
GIST-T1/820	Exon 11 + Exon 17: D820A	R	S
GIST-T1/829	Exon 11 + Exon 11: A829P	R	R
GIST-430/654	Exon 11 + Exon 13: V564A	R	R
GIST-48	Exon 11: V560D / Exon 17: D820A	R	R
***KIT*-independent GIST**			
GIST48B	None	R	R
GIST226	None	R	R

Footnote: Abbreviations: TKI: tyrosine inhibitor kinase, S: sensitive, R: resistant, NR: not reported, del: deletion, ins: insertion

Adapted from Zhou et al., 2024; Serrano et al., 2019.

GIST48B and GIST226 represent models of *KIT*-independent GIST, IM-resistant, characterized by the loss of KIT expression. These cell lines have been instrumental in studying mechanisms of KIT signaling bypass, resistance to TKI, and the potential involvement of alternative oncogenic pathways, providing valuable tools for exploring therapeutic targets beyond KIT (Serrano et al. 2019).

The diversity of available GIST cell lines, including those derived from different genetic backgrounds and clinical presentations, is crucial for dissecting the heterogeneity of GIST and for preclinical evaluation of novel therapeutic strategies.

2.4.1.2. Mouse models

Mouse models of GIST are indispensable for *in vivo* studies, allowing the evaluation of tumor growth, metastasis, and therapeutic response in a physiologically relevant context.

Patient-derived xenografts (PDX) models represent a critical bridge between clinical samples and experimental research. These models are established by culturing (expanding) tumor cells directly extracted from patient specimens, which were engrafted into immunodeficient mice (Fukuda et al. 2013; García-Valverde et al. 2020; 2021; Na et al. 2017). Such PDX mouse retain the genetic mutations and phenotypic traits of the original tumors, including *KIT* mutations. It helps the study of tumor heterogeneity, metastatic potential, and drug sensitivity.

Additionally, genetically engineered mouse models have provided further insights into the molecular drivers of GIST. They harbor activating mutations in *KIT* or *PDGFRA* genes, recapitulating key features of human GIST, from dedifferentiation to tumor heterogeneity (Sano et al. 2023). Interesting studies on GIST have primarily used models such as $KIT^{V558\Delta}$/+ mice to analyze the constitutive activation of KIT (Sommer et al. 2003), or $KIT^{V558\Delta;T669I}$/+ mice to evaluate IM resistance and microcytic erythrocytosis (Bosbach et al. 2012; Deshpande et al. 2013). Functional studies using transgenic mice have also been conducted to identify novel therapeutic targets, notably Suppressor of Cytokine Signaling (SOCS2) which plays a potential regulatory role in oncogenic signaling and drug response in GIST (Zhang et al. 2025). Collectively, these diverse mouse models are a useful tool to study GIST pathogenesis, heterogeneity, and therapeutic resistance in a physiologically relevant context. However, the reproductive cycle for genetically engineered mice is lengthy, and the process is both costly and technically challenging.

Another more recent approach involves a chemically-induced GIST mouse model through the implantation of 3-methylcholanthrene-soaked sutures to recapitulate spontaneous GIST development (Zhao et al. 2025). This model, characterized by positive staining of KIT and ANO-1, is valuable for studying tumor initiation and progression in an immunocompetent context.

While the principles of the 3R (Replacement, Reduction, and Refinement) guide the ethical use of animals in research, the development of alternative models such as the cultivation of a wide variety of GI tissues *in vitro* from tissue-derived and pluripotent stem cell-derived sources has significantly improved. The discipline has been able to move away from the frequently nonphysiological, altered cell lines that have been employed in GI research for decades thanks to these systems, which are generally referred to as organoids (Merker et al. 2016). However, developing GIST organoids that accurately replicate the complexity of *in vivo* GIST remains a major challenge, and to our knowledge, no robust system has yet been achieved.

2.4.2. Emerging molecular targets

Over the past few years, efforts to find new ways to overcome or avoid TKI resistance in GIST have significantly expanded our understanding of this sarcoma's molecular complexity. Although most therapies have concentrated on directly targeting KIT and PDGFRA, growing interest makes it clear that many different signaling pathways and regulatory systems contribute to tumor growth and resistance to treatments. Scientists have started to identify novel targets across various cellular processes, including transcriptional regulation, compensatory signaling, and cell cycle control, regardless of TKI presence. This section outlines several mechanistic classes of emerging therapeutic strategies, illustrated by selected representative molecular targets in **Figure 16**. Research has been mainly focused on secondary resistance in *KIT*-mutants because this is where most of the resistance is found.

2.4.2.1. Targeting KIT expression and upstream regulators

Today, the standard of care for patients with advanced GIST is TKI, which directly inhibits KIT activity. However, over time, resistance appears to be mainly due to secondary mutations in *KIT* (Schaefer et al. 2022). To avoid this, recent research aims to modulate *KIT* gene expression by targeting upstream regulators to suppress the oncogenic signaling pathway (see **Figure 16**, orange highlighted molecules) (Ainsua-Enrich et al. 2015; Li et al. 2023; Serrano-Candelas et al. 2018).

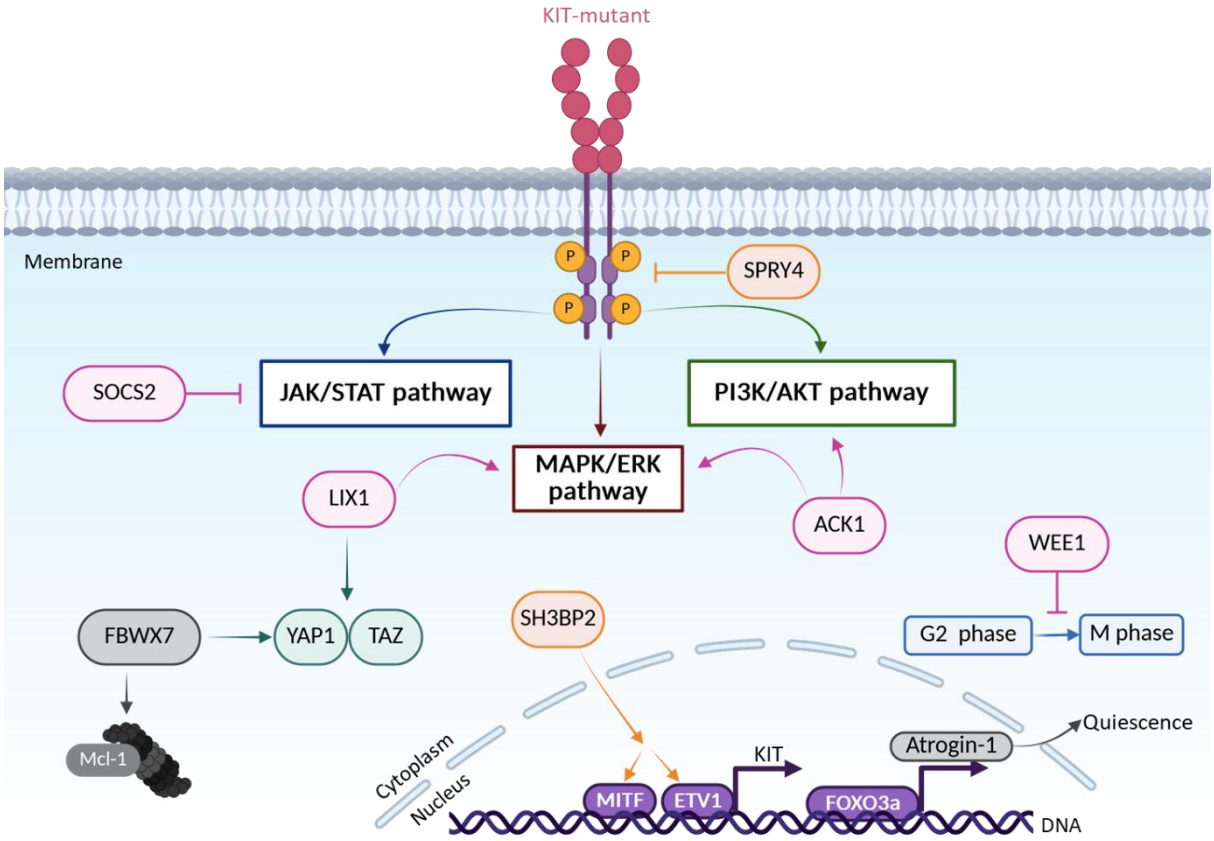

Figure 16: Emerging molecular targets beyond KIT involved in current research.
Schematic overview of *KIT*-dependent targets (orange), proteasome-related targets (gray), and modulators of downstream signaling pathways and cell cycle regulation target (pink). YAP1/TAZ axis is represented in green. Homemade figure.

Notably, the cytoplasmic adaptor molecule SH3-binding protein 2 (SH3BP2) has been identified to control *KIT* transcription via the regulation of ETV1 and Microphthalmia-associated Transcription Factor (MITF), both essential transcription factors for GIST cell survival (Proaño-Pérez et al. 2022; 2023). Silencing SH3BP2 results in downregulation of KIT expression, increasing apoptosis *in vitro* and reducing cell migration and tumor growth *in vivo* in both IM-sensitive and IM-resistant cells (Serrano-Candelas et al. 2018).

Similarly, Sprouty RTK Signaling Antagonist 4 (SPRY4) is highly expressed in GIST, and its expression is induced by KIT itself. SPRY4 associates with both WT and *KIT* with primary mutation, leading to reduced KIT protein levels without affecting its mRNA, and inhibits KIT activation as well as downstream signaling through the activation of PI3K/AKT and MAPK/ERK. This negative regulation enhances the sensitivity of primary *KIT*-mutant GIST cells to IM. In contrast, *KIT* mutants with secondary mutations remain unaffected by SPRY4 inhibition (Li et al. 2023).

2.4.2.2. Adaptative stress responses and protein homeostasis

GIST cells can survive under therapeutic stress by engaging adaptive programs, notably through the ubiquitin-proteasome system. Promising therapeutic targets have been identified as being linked to the proteasome, i.e. involved in proteostasis (see **Figure 16**, grey highlighted molecules).

One of these molecules is Atrogin-1 (encoded by *FBXO32* gene), an E3 ubiquitin ligase transcriptionally regulated by the KIT-FOXO3a axis. When GIST are treated with TKI (i.e. IM), Atrogin-1 enables tumor cells to escape apoptosis and enter a quiescent state, promoting resistance to TKI (García-Valverde et al. 2021).

Another protein identified in GIST is the F-box and WD repeat domain-containing 7 (FBXW7), part of the SCF-type E3 ubiquitin ligase complex (Koga et al. 2019). FBXW7 protein mediates the degradation of the anti-apoptotic protein MCL-1, thereby promoting apoptosis (Wu et al. 2024). High *FBXW7* gene expression correlates with improved outcomes in IM-treated patients, whereas its loss is associated with resistance and tumor progression (Wu et al. 2024). More recently, FBXW7 has been mechanistically linked to Yes-associated protein (YAP) for the regulation of GIST growth and metastasis (Wu, Yamashita, Matsumoto, et al. 2025). In addition, another study showed that targeting MCL-1 by the BCL-2 inhibitor, AT101, reduced GIST growth and induced apoptosis *in vitro* and *in vivo* (Wu, Yamashita, Lou, et al. 2025).

2.4.2.3. Disrupting compensatory signaling and cell cycle regulation

Several compensatory signaling pathways have been implicated in GIST resistance and tumor progression. The JAK/STAT and MAPK/ERK pathways can be reactivated upon KIT inhibition (see **Figure 16**, pink highlighted molecules and referred to section 2.2).

In this context, SOCS2, a negative regulator of JAK/STAT signaling, has been shown to inhibit *KIT*-mutant and enhance IM response. Its downregulation leads to increased tumorigenesis and therapeutic resistance (Zhang et al. 2025).

ACK1, also known as Tyrosine non-receptor kinase 2 (TNK2), is another example of a kinase that interacts with KIT and activates downstream PI3K/AKT and MAPK/ERK signaling pathways. Pharmacological or genetic inhibition of ACK1 reduces invasiveness and sensitizes both IM-sensitive and -resistant GIST models (He et al. 2023; Xu et al. 2017).

Additionally, cell cycle regulators are also included, such as the G2/M checkpoint kinase WEE1, which participates to cell survival and proliferation in GIST (Liu et al. 2020). Pharmacological inhibition of WEE1, using the small molecule inhibitor MK1775, enhances KIT degradation and potentiates the effects of TKI (Ye et al. 2021).

Among the molecular players implicated in the adaptation of GIST to KIT inhibition, LIX1 has recently emerged as a relevant candidate. Initially described as a regulator of mesenchymal progenitor cell fate through modulation of the Hippo pathway effector Yes-associated protein 1 (YAP1), LIX1 has progressively gained attention in the context of GIST biology (Guérin et al. 2020; McKey et al. 2016). Evidence from our research group has shown that LIX1 expression is upregulated in GIST cells after TKI exposure, whether in IM-sensitive or -resistant cells treated with IM or SU (Ruiz-Demoulin et al. 2023). This upregulation appears functionally relevant, since LIX1 promotes the early reactivation of the MAPK/ERK pathway following KIT inhibition. When LIX1 expression is experimentally silenced (shLIX1), this MAPK rebound is significantly impaired, leading to enhanced sensitivity to IM and increased cytotoxic effects (Ruiz-Demoulin et al. 2023). LIX1 contributes to GIST cell survival by sustaining mitochondrial function and regulating KIT protein level (Guérin et al. 2022). Mechanistically, LIX1 acts upstream of the Hippo pathway, through the regulation of the transcriptional co-activators YAP1 and the transcriptional co-activator with PDZ-binding motif (TAZ, encoded by *WWTR1*) (Guérin et al. 2020; Ruiz-Demoulin et al. 2023). This has led to the hypothesis that YAP1 and TAZ may represent key downstream mediators of LIX1 in GIST, and thus represent convergent therapeutic targets.

2.4.2.4. Toward a functional convergence: the YAP1/TAZ axis

In GIST, accumulating studies support a role for the Hippo pathway effectors YAP1 and TAZ in tumor progression and resistance to targeted therapy (see **Figure 16**, green highlighted molecules). Although they operate independently of KIT signaling, growing evidence suggests that they contribute to GIST tumorigenesis through parallel and possibly convergent mechanisms. For now, most of these studies focus on *in vitro* and *in vivo* research, with a lack of clinical data (especially for TAZ).

In *KIT*-independent GIST subtypes, Cyclin D1 (CD1, encoded by *CCND1*) overexpression and Hippo/YAP1 pathway activation have been found to drive the disease through the YAP1/CD1 signaling. It has been shown that CD1 inhibition had anti-proliferative and pro-apoptotic

effects, which were associated with Rb (retinoblastoma protein) activation and cyclin-dependent kinase inhibitor 1B (CDKN1B also known as p27) upregulation. In parallel, dysregulation of the Hippo pathway through increasing nuclear YAP1 activity drives tumor growth and progression, establishing Hippo through YAP1 signaling as a central oncogenic mechanism in this cell context (Chen et al. 2021; Ou et al. 2019). Pharmacological targeting of this pathway by proteasome inhibitor bortezomib has yielded encouraging preclinical results, with attention about the toxicity.

In *KIT*-dependent GIST, it has been recently found for the first time that YAP1 is an independent prognostic marker for recurrence in GIST patients (Wu, Yamashita, Matsumoto, et al. 2025). Subsequently, in GIST sensitive and resistant to IM, pharmacological inhibition by the BCL-2 inhibitor, AT101, of the YAP1/TAZ-CD1 axis has shown reduction in tumor growth and induction in apoptosis in preclinical GIST models (Wu, Yamashita, Lou, et al. 2025). Moreover, pharmacological inhibition of YAP1 and TAZ with verteporfin promotes ferroptotic cell death in both IM-sensitive and -resistant GIST cells, and its efficacy appears to be greater in aggressive tumor phenotypes (Delvaux et al. 2022; Vandenberghe et al. 2019). Despite these findings, the respective roles of YAP1 and TAZ in *KIT*-dependent GIST remain incompletely understood.

Together, these findings highlight a potential therapeutic axis involving YAP1 and/or TAZ, and downstream survival pathways that could be exploited to prevent resistance to TKI.

3. YAP1 and TAZ: central effectors of the Hippo Pathway and their role in cancer

Building on the emerging evidence implicating YAP1 and TAZ in GIST progression and therapeutic resistance, this section provides an overview of the Hippo signaling pathway, its role in cellular homeostasis, and the oncogenic functions of its downstream effectors across cancer types. Current efforts to therapeutically target YAP1 and TAZ are also discussed, considering their relevance to both *KIT*-dependent and -independent GIST subtypes. It is worth noting that a general introduction to the main features of YAP1/TAZ in the Hippo signaling pathway will be provided before a specific focus on YAP1 and TAZ, as well as their downstream pathways. Although the term “YAP” originally refers to a protein first identified

in 1994 as a binding partner of the tyrosine kinase YES (Sudol 1994), subsequent studies revealed the existence of two main isoforms generated by alternative splicing, initially named YAP1 (with one WW domain) and YAP2 (with two WW domains). Over time, the nomenclature has been refined, and the isoform with one WW domain is now designated YAP1-1γ in the Protein Data Bank, while the term YAP1 unambiguously refers to the isoform containing two WW domains (Reggiani et al. 2021). In this chapter, only the term "YAP1" will be used, as the current protein nomenclature. YAP1 represents the most extensively studied and functionally relevant isoform in the context of cancer and GIST biology (Shibata et al. 2018).

3.1. The Hippo signaling pathway: an overview

The Hippo signaling pathway is a highly evolutionary conserved signaling cascade regulating organ size, cell proliferation, apoptosis, and playing a crucial role in tissue homeostasis (Fu et al. 2022; Ma et al. 2019; Zhao, Tumaneng, et al. 2011).

3.1.1. From Drosophila to Mammals

This pathway was first discovered in *Drosophila melanogaster* through genetic screening experiments designed to identify mutations resulting in tissue overgrowth (Zhao, Tumaneng, et al. 2011). These mutations led to the identification of key tumor suppressor genes such as *Hippo (hpo)* (Harvey et al. 2003; Jia et al. 2003; Pantalacci et al. 2003; Udan et al. 2003; Wu et al. 2003), *Warts (wts)* (Justice et al. 1995; Xu et al. 1995), *Salvador (Sav)* (Kango-Singh et al. 2002; Tapon et al. 2002), *Mob as tumor suppressors (Mats)* (Lai et al. 2005), and *Yorkie* (*Yki*) (Huang et al. 2005), a downstream effector negatively regulated by this pathway. All these proteins act as part of a kinase cascade at the heart of the Hippo pathway. Loss-of-function mutations in *hpo* gene lead to dramatically enlarged organs due to uncontrolled cell proliferation and impaired apoptosis. Phenotypes made the flies appear unusually bulky, reminiscent of a hippopotamus, which gave its name to the Hippo pathway (Ma et al. 2019). The terminal effectors *Yki* and the transcriptional factors *Scalloped* were only later discovered as positive regulators of proliferation (Goulev et al. 2008).

The core components of the Hippo pathway are highly conserved in mammals. The mammalian orthologs of *Hpo, Sav, Wts, Mats*, and *Yki* are, respectively, *Mammalian sterile 20-like 1/2* (*MST1/2*), *Salvador Family WW Domain Containing Protein 1* (*SAV1*), *Large tumor*

suppressor homolog 1/2 (*LATS1/2*), *MOB kinase activator 1A/B* (*MOB1a/b*), and *YAP1/TAZ* (Y.-A. Chen et al. 2019; Yu et al. 2015). The transcriptional factors *Scalloped,* where YAP1 and TAZ mainly bind, are TEA Domain Transcription Factors (TEAD). The correspondence between the Hippo pathway in Drosophila and mammals is shown in **Figure 17.**

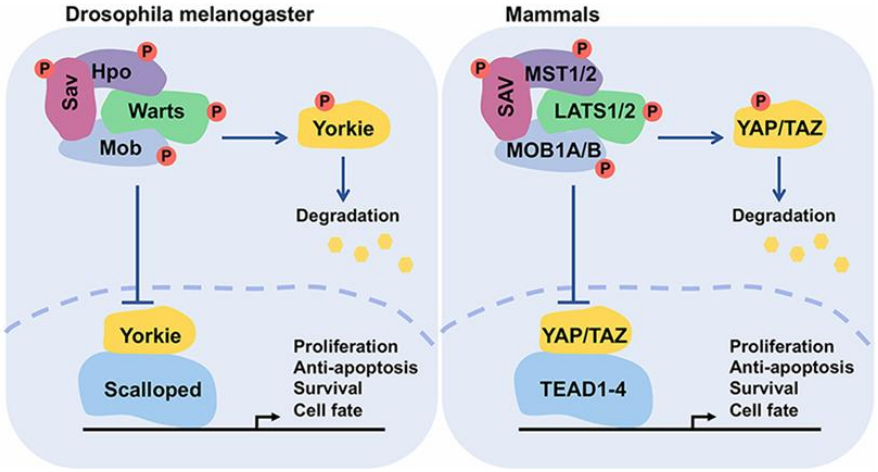

Figure 17: Schematic representation of the conservation of the core Hippo signaling module between *Drosophila melanogaster* (left) and mammals (right).

In *Drosophila*, the signaling complex composed of Salvador (Sav), Hippo (Hpo), Warts (Wts), and Mob as tumor suppressors (Mats) promotes the phosphorylation (P) of Yorkie (Yki), leading to its cytoplasmic retention and degradation. When unphosphorylated, Yki translocates into the nucleus and binds to the transcription factor Scalloped to activate target genes involved in cell proliferation, survival, anti-apoptosis, and cell fate determination.

In mammals, homologous components include Salvador family WW domain-containing protein 1 (SAV1), Mammalian sterile 20-like kinases 1/2 (MST1/2), Large tumor suppressor kinases 1/2 (LATS1/2), and MOB kinase activators 1A/B (MOB1A/B). This complex phosphorylates Yes-associated protein (YAP) and its paralog TAZ (transcriptional coactivator with PDZ-binding motif), resulting in their degradation. In the absence of phosphorylation, YAP/TAZ accumulate in the nucleus and interact with TEA domain family transcription factors 1–4 (TEAD1–4) to drive gene expression promoting proliferation, survival, and cell fate decisions.

From Chen et al., 2019.

3.1.2. Regulation of the Hippo pathway

The core function of the Hippo mammalian signaling as a central gatekeeper of tissue growth and organ size consists in the inhibition of the YAP1/TAZ activity by preventing their nuclear translocation (Yu et al. 2015) (**Figure 18"ON"**). This pathway can be conceptually divided into three interconnected modules:

1) The first comprises **upstream regulatory inputs** that tightly control Hippo activation or inhibition. The pathway is typically triggered by intra- or extra-cellular signals. Mechanical cues are crucial regulators and include cell-cell contact, high cell density, cytoskeletal tension, ECM stiffness. These factors act through proteins like Rho GTPases, AGRIN, and RAS-related proteins, which influence cytoskeletal organization and geometry (Fu et al. 2022; Ma et al.

2019). Thus, the activity of YAP1/TAZ is controlled through mechanotransduction, a tissue-level signaling process that relies on the exchange of physical forces between cells and the ECM. Moreover, cell polarity signals involve apical-basal polarity complexes and cell junction proteins such as α-Catenin, Angiomotin family proteins (AMOT), Zonula occludens (ZO) proteins (Fu et al. 2022; Meng et al. 2016). Cell density and cell contact signals include molecules like Annexin and E-cadherin (Fu et al. 2022; Ma et al. 2019). These proteins help maintain tissue architecture, thus promoting activation of the Hippo pathway under high-density conditions (Schroeder and Halder 2012). Soluble factors encompass a variety of hormones, growth factors, and inflammatory cytokines. These factors can activate G protein-coupled receptors (GPCR) or other signaling cascades (Heng et al. 2021; Meng et al. 2016). Stress signals such as hypoxia, energy stress, osmotic stress, and heat shock can also modulate YAP1 and TAZ activity (Fu et al. 2022; Ma et al. 2019; Yu et al. 2015).

2) The second module consists of the **Hippo core kinases** MST1/2 and LATS1/2. Interaction between SAV1 and MST1/2 results in the activation of MST, which then activates LATS1/2, with MOB1A/B providing assistance (Ma et al. 2019; Meng et al. 2016). Activated LATS1/2 subsequently phosphorylate YAP1 and TAZ, the principal effectors of the pathway, on specific serine residues (for details see section 3.2) (Piccolo et al. 2014).

3) The third module comprises the **transcriptional effectors** themselves, YAP1 and TAZ, but also their principal DNA-binding partners, TEAD family of transcription factors (TF) (Meng et al. 2016; Piccolo et al. 2014). Neither YAP1 nor TAZ have DNA-binding motifs, but they are able to interact with TF to induce transcription of target genes. Phosphorylation of YAP1 and TAZ prevents them from entering the nucleus and engaging with TEAD, thereby suppressing the transcriptional programs that drive cell proliferation and survival (Y.-A. Chen et al. 2019).

When the upstream signals are decreased or absent, such as in low-density conditions or when the ECM is soft, the Hippo pathway becomes inactive (**Figure 18 "OFF"**) (Y.-A. Chen et al. 2019). In this state, all the kinases are no longer phosphorylated, so that YAP1 and TAZ can translocate into the nucleus, where they bind mainly to TEAD and drive the expression of genes involved in cell growth, migration, survival, and tissue identity in numerous organs, including the digestive tract (LeBlanc et al. 2021; Messina et al. 2023; Piccolo et al. 2014; Seeneevassen et al. 2022). This shift in YAP1 and TAZ localization and activity is a key mechanism by which cells sense and respond to their environment, allowing for controlled

tissue regeneration and repair. However, persistent inactivation of the Hippo pathway can lead to unchecked cell proliferation and is associated with tumor development and other pathologies. This balance between activation and inactivation of the pathway is essential for maintaining proper tissue architecture and function (Ma et al. 2019; Piccolo et al. 2014; Zhao, Tumaneng, et al. 2011).

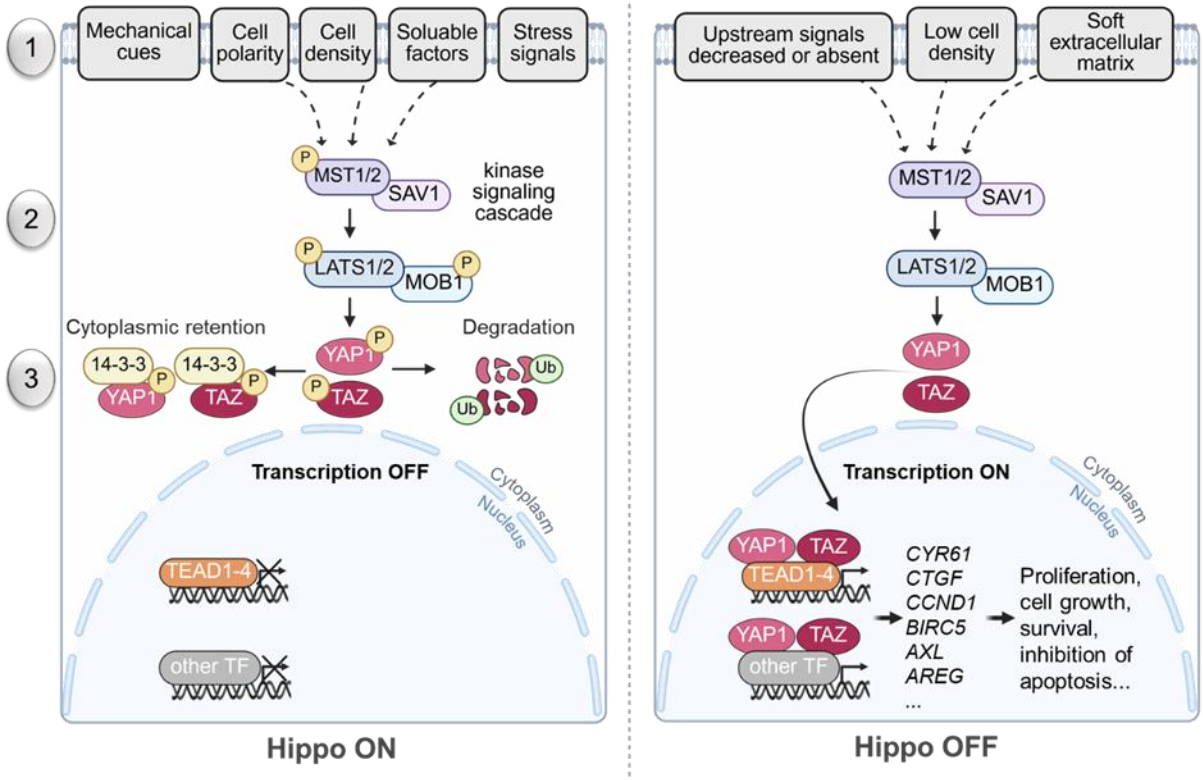

Figure 18: Overview of the Hippo pathway and its regulation of YAP1 and TAZ activity.
The Hippo pathway is divided in three modules : Upstream regulators (**1**), kinases (**2**) and effectors (**3**).
When the Hippo pathway is active (Hippo ON, left panel), MST1/2 in complex with SAV1 phosphorylates and activates LATS1/2 kinases, which in turn phosphorylate YAP1 and TAZ. This phosphorylation promotes their binding to 14-3-3 proteins, resulting in cytoplasmic sequestration and/or proteasomal degradation *via* ubiquitination. Consequently, YAP1/TAZ are excluded from the nucleus, preventing transcription of their target genes.
On the other hand, when the Hippo pathway is inactive (Hippo OFF, right panel), MST1/2 and LATS1/2 kinases are not phosphorylated, allowing YAP1 and TAZ to remain unphosphorylated and translocate into the nucleus. There, they associate mainly with TEAD transcription factors (TEAD1–4), as well as other transcription factors (TF), to promote the expression of genes involved in cell proliferation, survival, drug resistance, and inhibition of apoptosis.
Adapted from Chen et al., 2019; Hansen et al., 2015

3.2. Regulatory complexity and functional specificities of YAP1 and TAZ

The transcriptional coactivators YAP1 and TAZ have emerged as pivotal regulators of cell proliferation, survival, and tissue homeostasis (Piccolo et al. 2014). While often studied

together due to their functional redundancy, increasing evidence suggests differences in their protein domain features and biological roles (Reggiani et al. 2021).

3.2.1. YAP1: structure, function and regulation

YAP1 was first identified in 1994 as a binding partner of the non-RTK YES, located on chromosome 11, from which it derives its name (Sudol 1994). Although the theoretical molecular weight of YAP1 is approximately 55 kDa, it is commonly observed to migrate between 65 and 75 kDa on Western blots, likely due to post-translational modifications such as phosphorylation or isoform-specific differences (Reggiani et al. 2021). Initial studies recognized YAP1 as a modular protein capable of interacting with proto-oncogene tyrosine-protein kinase SRC Homology 3 (SH3) domain-containing proteins, implicating it in diverse signaling pathways (Sudol 1994; Zhao, Tumaneng, et al. 2011). Subsequent research established YAP1 as a transcriptional coactivator that does not bind DNA but exerts its function through interaction with various TF, most notably TEAD1-4 (Ferrigno et al. 2002; Strano et al. 2001; Yagi et al. 1999).

The 3D structure of YAP1 is presented in **Figure 19A**. Concerning protein domains, YAP1 harbors a TEAD-binding domain composed of two α-helices separated by a flexible loop, which facilitates high-affinity interaction with TEAD in N-terminal (**Figure 19B, blue**) (Reggiani et al. 2021; Wei et al. 2023). This interaction is essential for the activation of transcriptional programs that govern proliferation, survival, and tissue growth (LeBlanc et al. 2021; Zhao, Tumaneng, et al. 2011). Moreover, YAP1 contains a PxxΦP (proline/any amino acid/any amino acid/hydrophobic residue/proline) motif within this region that contributes to a distinct mode of TEAD heterodimers interaction (Reggiani et al. 2021).

Beyond this, YAP1 features two WW domains, allowing it to recognize proline-rich PPxY (proline/proline/any amino acid/tyrosine) motifs in interacting proteins (**Figure 19B, red**), thereby integrating diverse signaling input (Boopathy and Hong 2019; Reggiani et al. 2021).

Additionally, YAP1 contains the specific proline-rich region that mediates interaction with SH3 binding domain (**Figure 19B, yellow**) (Sudol 1994; Zhao et al. 2010). In C-terminal, YAP1 carries a PDZ-binding domain, which contributes to its subcellular localization and interaction with cytoskeletal and membrane-associated complexes (**Figure 19B, purple**) (Y.-A. Chen et al. 2019).

INTRODUCTION

YAP1 activity is tightly regulated by phosphorylation events that control its subcellular localization and stability. Among the multiple regulatory residues, serine 127 (S127) is phosphorylated by LATS1/2, promoting YAP1 binding to 14-3-3 proteins and its retention in the cytoplasm (**Figure 19B, green**).

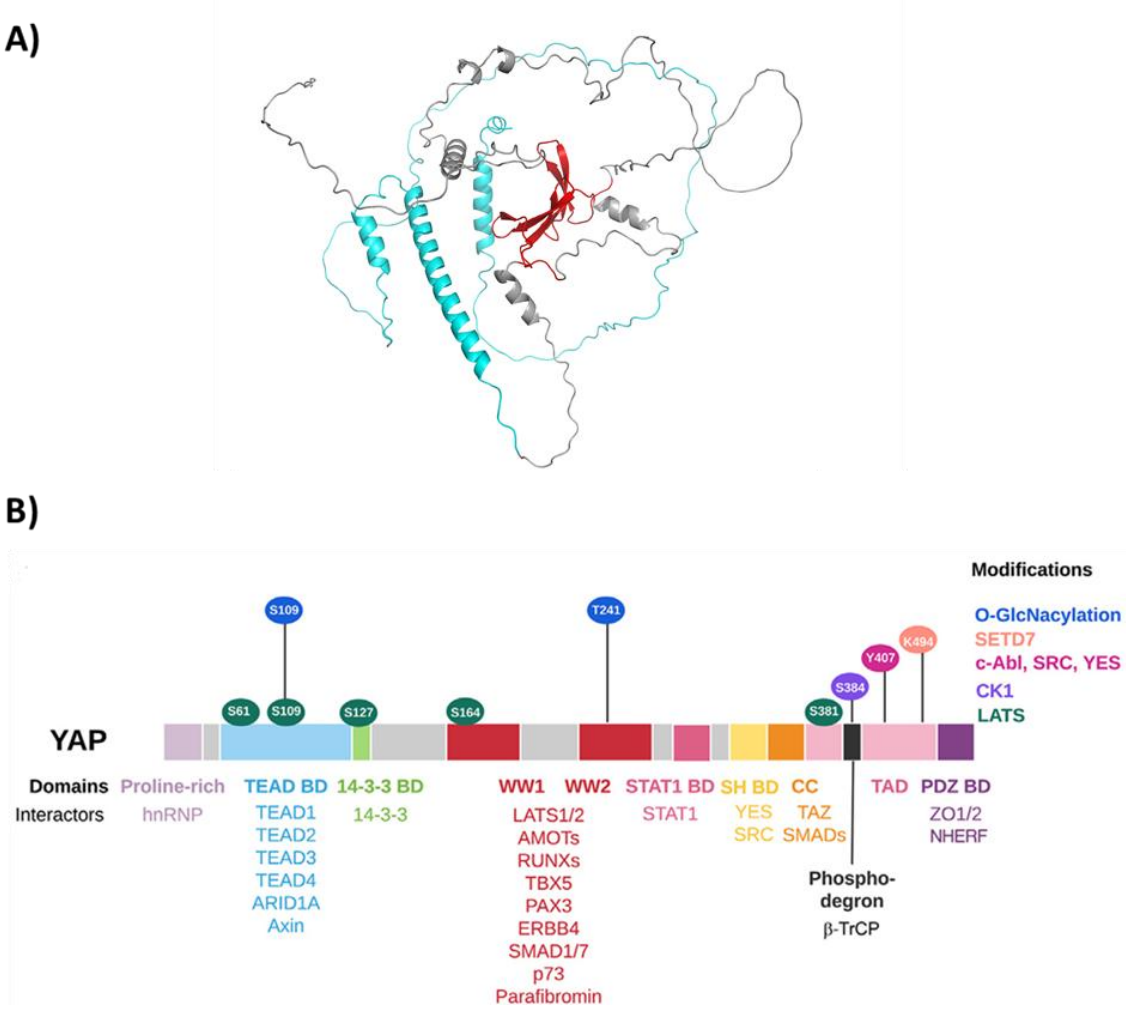

Figure 19: Schematic representation of YAP1 3D structure and protein structure, highlighting key functional domains, known interactors, and post-translational modification sites.
A) 3D YAP1 structure 3D (PDB code AF-P46937) was obtained by PyMol. WW domains are highlighted in red, the TEAD binding region is blue.
B) Colored boxes represent distinct protein domains: TEAD BD: TEA domain family member-binding domain (blue), 14-3-3 BD: 14-3-3 protein-binding domain (green), WW1 and WW2: WW domains (red), protein interaction modules recognizing proline-rich PPxY motifs, STAT1 BD: Signal Transducer and Activator of Transcription 1-binding domain (pink), SH BD: SH3 domain-binding motif (yellow), CC: Coiled-coil domain (orange), TAD: Transactivation domain (light pink), PDZ BD: PDZ-binding domain (purple). Phosphorylation sites and other post-translational modifications are indicated: O-GlcNAcylation (blue), SETD7 methylation (light orange), Tyrosine phosphorylation by c-Abl, SRC, YES kinases (magenta), CK1 phosphorylation (light purple), LATS kinase phosphorylation (green), which primes YAP1 for ubiquitin-mediated degradation via the β-TrCP ubiquitin ligase complex (black phospho-degron). Residues with specific phosphorylation marks (S61, S109, S127, etc.) are indicated by colored circles.
From Reggiani et al., 2021.

Phosphorylation at S381 in the trans activation domain (TAD) (**Figure 19B, pink**), in contrast, marks YAP1 for ubiquitin-mediated degradation *via* the proteasome (Piccolo et al. 2014; Seeneevassen et al. 2022; Zhao et al. 2010).

In addition to serine phosphorylation, YAP1 is subject to tyrosine phosphorylation by kinases, such as proto-oncogene tyrosine-protein kinase SRC and ABL, which increase its oncogenic potential, particularly in hematological malignancies and certain solid tumors (Guo et al. 2022; Messina et al. 2023). Other layers of post-translational regulation include ubiquitination, methylation, and O-GlcNAcylation, which control YAP1 localization, stability, and transcriptional output (Reggiani et al. 2021).

3.2.2. TAZ: paralog with distinct characteristics

TAZ was initially described in 2000 as a 14-3-3-binding phosphoprotein involved in cytoskeletal regulation and later identified as a transcriptional coactivator negatively regulated by the Hippo pathway (Kanai et al. 2000; Lei et al. 2008). The gene coding for TAZ is *WWTR1 (WW domain containing transcription regulator 1),* which is located on chromosome 3. Although the theoretical molecular weight of TAZ is approximately 44 kDa, it is frequently observed near 50-55 kDa in Western blot analyses, likely due to post-translational modifications or experimental conditions (Reggiani et al. 2021). Like YAP1, TAZ acts as a transcriptional coactivator downstream of the Hippo pathway and interacts with TEAD to regulate gene expression (Piccolo et al. 2014). Phylogenetically, TAZ is considered a vertebrate-specific paralog of YAP1, arising from a gene duplication event over 500 million years ago (Hilman and Gat 2011).

Notably, TAZ is 46% homologous to YAP1 with a similar domain organization and 3D structure (**Figure 20A**) (Reggiani et al. 2021). Similarities comprise the TEAD-binding domain near the N-terminal **Figure 20B, blue**), one WW domain (**Figure 20B, red**), a 14-3-3 binding domain (**Figure 20B, green**) and a PDZ-binding motif at its C-terminal (**Figure 20B, purple**) (Reggiani et al. 2021; Wei et al. 2023). TAZ is also subject to phosphorylation and additional regulatory modifications, including ubiquitination, methylation, and O-GlcNAcylation (Reggiani et al. 2021).

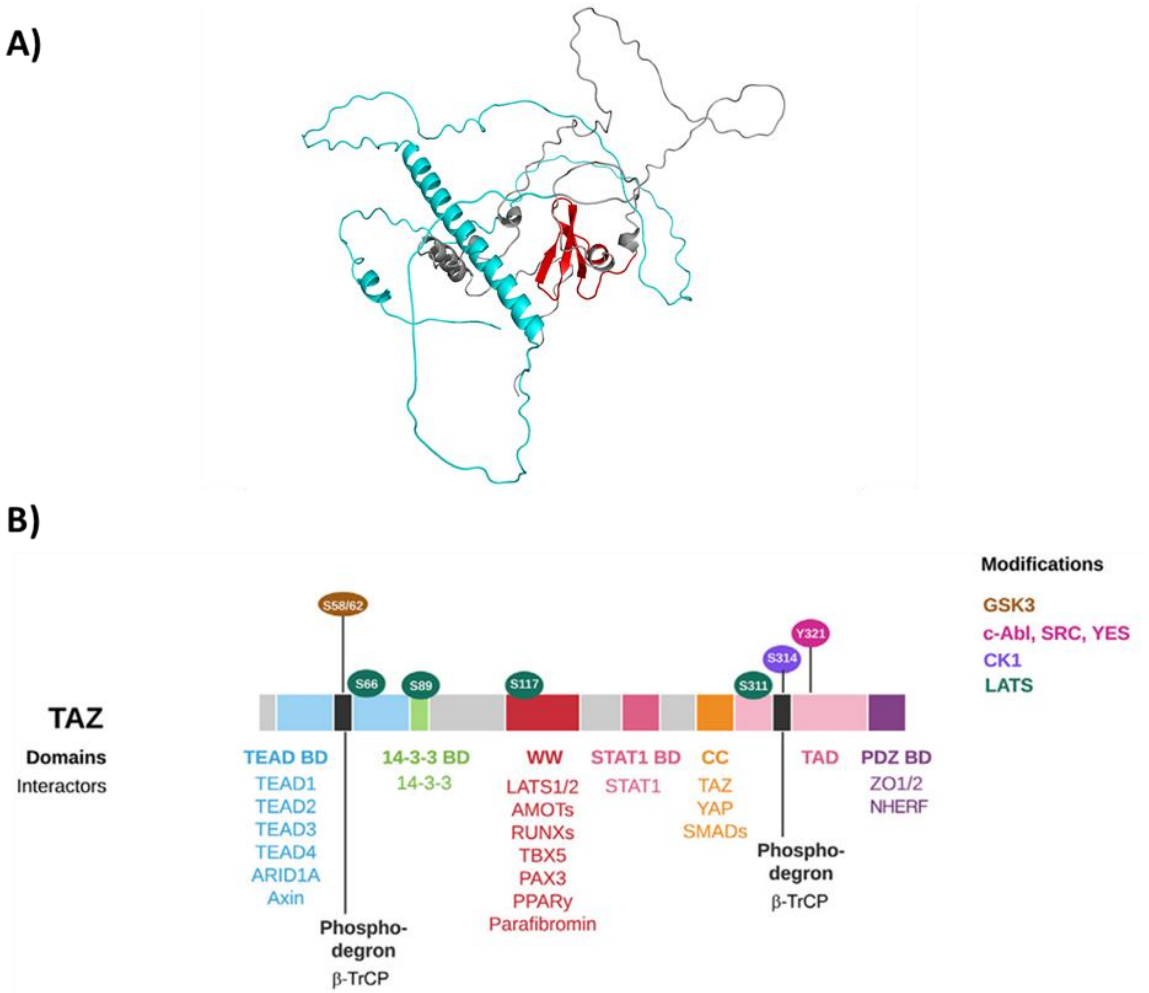

Figure 20: Schematic representation of the TAZ 3D and protein structure, highlighting key functional domains, known interactors, and post-translational modification sites.
A) 3D TAZ structure 3D (PDB code AF-Q9GZV5) was obtained by PyMol. WW domain and TEAD binding region are highlighted in red and in cyan, respectively.
B) Colored boxes represent distinct protein domains: TEAD BD: TEA domain family member-binding domain (blue), 14-3-3 BD: 14-3-3 protein-binding domain (green), WW: WW domains (red), protein interaction modules recognizing proline-rich PPxY motifs, STAT1 BD: Signal Transducer and Activator of Transcription 1-binding domain (pink), CC: Coiled-coil domain (orange), TAD: Transactivation domain (light pink), PDZ BD: PDZ-binding domain (purple). Phosphorylation sites and other post-translational modifications are indicated: GSK3 methylation (brown), Tyrosine phosphorylation by c-Abl, SRC, YES kinases (magenta), CK1 phosphorylation (light purple), LATS kinase phosphorylation (green), which primes TAZ for ubiquitin-mediated degradation via the β-TrCP ubiquitin ligase complex (black phospho-degrons). Residues with specific phosphorylation marks (S66, S89, S117, etc.) are indicated by colored circles.
From Reggiani et al., 2021.

However, TAZ differs notably from YAP1 in several levels. Firstly, the genomic architecture of the two proteins contributes to their isoform diversity: YAP1 is encoded by nine exons and undergoes extensive alternative splicing, whereas TAZ arises from a six-exon gene with more limited variability (Reggiani et al. 2021). TAZ is also tightly regulated at the post-translational level, particularly through phosphorylation. One of the key regulatory residues is serine 311 (S311), whose phosphorylation by LATS1/2 initiates a cascade involving casein kinase 1 (CK1)-

mediated phosphorylation at serine 314. This dual phosphorylation marks TAZ for recognition by the β-TrCP-containing SCF E3 ligase complex in the TAD, targeting it for ubiquitin-dependent proteasomal degradation (**Figure 20B, pink**) (Piccolo et al. 2014; Seeneevassen et al. 2022; Zhao et al. 2010). This process is facilitated by two phosphodegron motifs (**Figure 20B, black**), one in the TAD and the other in TEAD binding region, unique to TAZ and absent in YAP1 (Plouffe et al. 2018; Reggiani et al. 2021). As a result, TAZ is generally less stable than YAP1, with a half-life of less than two hours in non-cancerous cells (Piccolo et al. 2014). TAZ also lacks the conserved PxxΦP motif within TEAD region, resulting in a subtly different mode of TEAD engagement (Reggiani et al. 2021). Notably, TAZ can form not only heterodimers but also heterotetrameric complexes with TEAD, a feature that may influence its transcriptional dynamics (Kaan et al. 2017; Reggiani et al. 2021).

Compared to YAP1, which is largely regulated through nuclear-cytoplasmic shuttling, TAZ is predominantly controlled through targeted degradation, reflecting distinct layers of control that impact their respective roles in cancer biology (Piccolo et al. 2014; Seeneevassen et al. 2022).

3.2.3. Similarities and differences in transcription factor interactions

Another crucial aspect of YAP1 and TAZ function consists in their interactions with TF, which can overlap or be distinct, resulting in differential regulatory outcomes (Hong and Guan 2012; Lopez-Hernandez et al. 2021; Reggiani et al. 2021) (**Figure 21**).

The most prominent and evolutionary interaction is with the TEAD family, comprising TEAD1 to TEAD4 (**Figure 21A**). This interaction is central to the function of both coactivators (H. Zhang et al. 2009; Zhou et al. 2016). The YAP1/TAZ-TEAD complex modulates gene expression programs associated with cell growth, survival, and organ size control, and its oncogenic potential is well documented across a multitude of cancer types (Holden and Cunningham 2018; Zhou et al. 2016). Importantly, this core module is often reinforced by the recruitment of additional co-factors. The best-known are BRD4 (Bromodomain-containing protein 4), AP-1 (Activator protein-1), E2F (helix-loop-helix transcription factors), MRTF/SRF complex (Myocardin-related transcription factor/serum response factor), which lead to the transcription of YAP1 and TAZ target genes (Lopez-Hernandez et al. 2021; Reggiani et al. 2021; Zanconato et al. 2015; 2018).

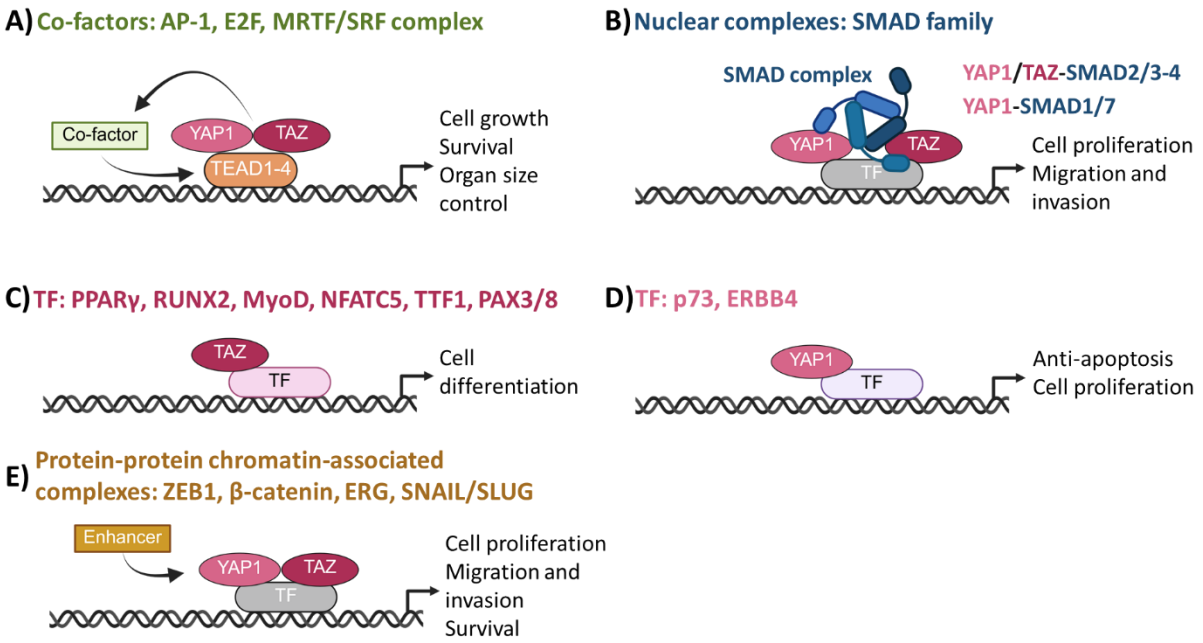

Figure 21: Diverse transcription factor interactions of YAP1 and TAZ.
YAP1 and TAZ exert their transcriptional functions through multiple modes of interaction with transcription factors (TF) and chromatin-associated complexes.
A) Both coactivators primarily act via binding TEAD family members (TEAD1–4), a central axis reinforced by additional co-factors such as BRD4, AP-1, E2F, and MRTF/SRF complexes, which enhance transcriptional output.
B) YAP1 and TAZ can also form complexes with SMAD family members. Both interact with SMAD2/3 and SMAD4 to modulate TGF-β signaling, whereas YAP1 uniquely associates with SMAD1/7, linking it to BMP pathways and negative regulation of TGF-β signaling.
C) TAZ specifically interacts with various lineage-specific TF including PPARγ, RUNX2, MyoD, NFATC5, TTF1, and PAX3/8, contributing to cell fate determination and differentiation processes.
D) YAP1 has unique partnerships with TFs such as p73, promoting pro-apoptotic transcriptional programs in response to cellular stress, and with ERBB4, linking Hippo signaling to receptor tyrosine kinase pathways.
E) YAP1 and TAZ also participate in chromatin-associated protein-protein complexes with factors such as ZEB1, β-catenin, ERG, and SNAIL/SLUG, enabling context-dependent enhancer recruitment and transcriptional integration independent of canonical DNA-binding motifs.
Adapted from Varellas et al., 2008; Hansen et al., 2015; Lopez-Hernandez et al., 2021.

This interaction model can be further explored, because YAP1 and TAZ can interact with cytosolic and nuclear partners that bind to TEAD or other different TF (**Figure 21B**). Among common partners, the SMAD family (an acronym from the fusion of *Caenorhabditis elegans Sma* genes and the *Drosophila Mad*, Mothers against decapentaplegic) stands out as a major actor of crosstalk between YAP1/TAZ and the TGF-β/BMP (transforming growth factor-beta/bone morphogenetic protein) signaling cascades, forming complexes predominantly in the nucleus, although interactions can also occur in the cytoplasm (Grannas et al. 2015; Hansen et al. 2015; Huang et al. 2016; Varelas et al. 2008; 2010). Both YAP1 and TAZ form complexes with activated SMAD2/3 and SMAD4, thereby modulating the nuclear translocation and transcriptional output of these effectors (Varelas et al. 2008; 2010). Interestingly, TAZ, but not YAP1, is upregulated in response to TGF-β signaling, suggesting

differential responsiveness to upstream cues (Varelas et al. 2008). Conversely, YAP1 has been shown to interact specifically with SMAD1 and with SMAD7, enhancing its repressive effects on TGF-β signaling (Aragón et al. 2012; Grannas et al. 2015; Huang et al. 2016). Despite these shared mechanisms, YAP1 and TAZ also display unique transcriptional partnerships that underscore their non-redundant roles.

TAZ, for example, engages in lineage-specific transcriptional networks (**Figure 21C**). Notably, it interacts with the nuclear peroxisome proliferator-activated receptor gamma (PPARγ), which is critical for adipogenesis and smooth muscle dedifferentiation. In this context, TAZ acts as a transcriptional repressor that inhibits PPARγ-driven gene expression regardless of ligand binding. Conversely, TAZ can function as a coactivator for RUNX2 (Runt-related transcription factor 2) to promote osteogenic differentiation and for MyoD (Myoblast determination protein 1) to help myogenic differentiation (Hong et al. 2005; Jeong et al. 2010). Furthermore, TAZ interacts with NFATC5 (Nuclear factor of activated T-cells 5) following phosphorylation by tyrosine-protein kinase ABL under hyperosmotic stress in renal medullary cells, repressing NFATC5-dependent transcription and linking TAZ activity to osmoadaptive gene expression (Hong and Guan 2012; Lopez-Hernandez et al. 2021; Reggiani et al. 2021). TAZ is also a coactivator of TTF1 (thyroid transcription factor 1) and PAX3/8 (paired box gene 3 and 8) (Di Palma et al. 2009; Murakami et al. 2006; Park et al. 2004).

YAP1, in turn, possesses its own unique set of interactions (**Figure 21D**). One particularly well-characterized partner is p73, a member of the p53 (tumor protein) family of TF. YAP1 enhances p73-driven transcription and apoptosis in response to DNA damage *via* its WW domain binding the PPxY motif of p73. This interaction confers a tumor-suppressive role to YAP1 in certain hematologic malignancies. Additionally, YAP1 forms a complex with the intracellular domain of ERBB4, a cleaved RTK of the EGFR (Epithelial growth factor receptor) family. The WW domain of YAP1 binds the PPxY motif of ERBB4, resulting in the co-activation of YAP1/ERBB4 target genes and bridging Hippo and EGFR signaling. (Hong and Guan 2012; Lopez-Hernandez et al. 2021; Strano et al. 2001).

In addition to direct TF partnerships, recent chromatin studies have revealed that YAP1 and TAZ may be recruited to transcriptional enhancers through cooperation with other factors such as AP-1, MRTF/SRF, or MYC. In some instances, such as ZEB1, β-catenin, ERG or SNAIL/SLUG, these factors may interact independently of their DNA binding motifs, suggesting

that protein-protein interactions and chromatin topology govern the selective association of YAP1/TAZ complexes (**Figure 21**) (Lopez-Hernandez et al. 2021).

To summarize, while both proteins share key binding partners and canonical mechanisms (TEAD, SMAD), different interactions such as those with p73 (YAP1) or PPARγ and NFATC5 (TAZ) highlight their distinct roles in cells. These differences likely arise from variations in expression patterns, post-translational modifications, and cofactor availability, ultimately contributing to divergent biological outcomes even within the same signaling context.

3.2.4. Transcriptional corepressors of YAP1 and TAZ

In addition to their well-established roles as transcriptional coactivators (alone or in combination with other factors) (Lopez-Hernandez et al. 2021; Reggiani et al. 2021; Zanconato et al. 2015; 2018), YAP1 and TAZ also interact with some transcriptional corepressors. These interactions modulate their activity and expand their regulatory potential (**Figure 22**).

The most common corepressor is VGLL4 (Vestigial Like Family Member 4), which acts as a natural antagonist by competing with YAP1 and TAZ for the binding to TEAD transcription factors. The outcome of this process is the prevention of the initiation of pro-proliferative gene expression, thereby acting as a physiological repressor on Hippo signaling (Jiao et al. 2014; Koontz et al. 2013; Zhang et al. 2014) (**Figure 22,** orange).

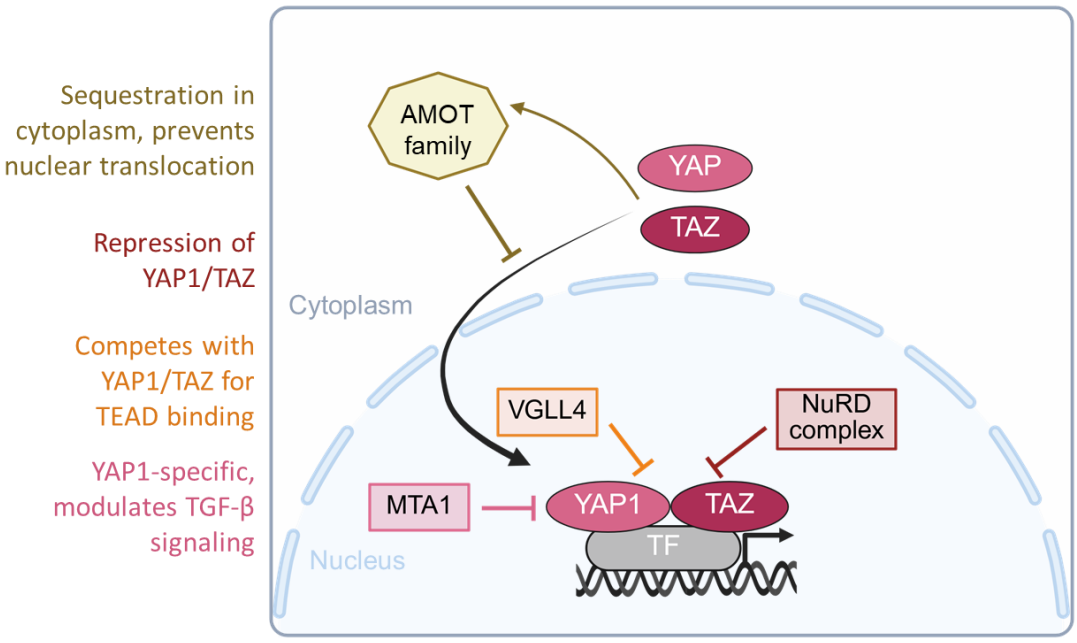

Figure 22: Regulation of YAP1 and TAZ transcriptional activity by corepressors.
The AMOT (Angiomotin) family sequesters YAP1 and TAZ in the cytoplasm, preventing their nuclear translocation and subsequent transcriptional activity. Within the nucleus, VGLL4 competes with YAP1 and TAZ for binding to TEAD transcription factors, thereby inhibiting pro-proliferative gene expression. Groucho/TLE and the NuRD complex can be recruited by YAP1 or TAZ to repress transcription, particularly in differentiation contexts. MTA1 acts as a YAP1-specific corepressor, modulating gene repression and impacting pathways such as TGF-β signaling. Together, these corepressors contribute to the context-dependent regulation of YAP1/TAZ activity in development, homeostasis, and oncogenesis.
Adapted from Hansen et al., 2015.

Moreover, the AMOT protein family can sequester YAP1 and TAZ in the cytoplasm, effectively preventing their nuclear translocation and subsequent transcriptional activity (Paramasivam et al. 2011; Zhao, Li, et al. 2011) (**Figure 22, yellow**).

Another corepressor is the NuRD (Nucleosome Remodeling and Deacetylase) complex, both of which can be recruited by YAP1 or TAZ to repress gene expression, particularly in differentiation contexts (Hillmer and Link 2019) (**Figure 22, red**).

Certain corepressors interact selectively with one paralog. For instance, the MTA1 (metastasis-associated protein 1) has been identified as a YAP1-specific corepressors, modulating gene repression and impacting processes such as TGF-β signaling and tumor progression (Aragón et al. 2012; Qiu et al. 2024) (**Figure 22, pink**). To the best of our knowledge, no corepressor has been described in the literature as being specific for TAZ.

These findings underscore the dual nature of YAP1 and TAZ as both transcriptional activators and repressors, with their functional output being dictated by the specific cofactors and corepressors they recruit. This complexity is highly relevant to their roles in development, tissue homeostasis, and oncogenesis. It also provides a nuanced framework for understanding their context-dependent actions in both physiological and pathological states (Zanconato et al. 2016).

3.2.5. Evolving perspective on YAP1 and TAZ divergent functions

Over the years, YAP1 and TAZ have often been described side by side, frequently treated as a single functional entity because of their similar structures and overlapping target genes (Cunningham and Hansen 2022). In many experimental systems, YAP1 and TAZ are still commonly described as interchangeable transcriptional coactivators within the Hippo pathway and are often analyzed together, or not distinguished at all (Cunningham and Hansen 2022; Luo et al. 2023; Plouffe et al. 2018; Shreberk-Shaked et al. 2020; Thrash and Pendergast 2023). Yet, recent findings increasingly point to significant differences between the two. As

previously discussed, YAP1 and TAZ differ not only in their protein domain architecture but also in the repertoire of transcriptional partners they engage with. Emerging studies reveal that YAP1 and TAZ are not simply interchangeable coactivators; instead, they exhibit distinct regulatory behavior, variable expression patterns across tissues, and context-specific roles that shape their functions in development, normal physiology, and disease (Piccolo et al. 2023; Reggiani et al. 2021). It underscores the need to assess their separate contributions in relevant cancer models, particularly in mesenchymal tumors such as sarcomas (Bae et al. 2016; C. Chen et al. 2019; Patterson et al. 2024; Zhang et al. 2013). This shift in understanding paves the way for a more precise focus at how each protein contributes to cancer, a topic explored further in the next section.

3.3. Functional divergence and convergence in cancer

The Cancer Genome Atlas has identified the Hippo pathway as one of the eight major signaling pathways most dysregulated in cancer (Sanchez-Vega et al. 2018). YAP1 and TAZ, the core effectors of the Hippo pathway, thus play a fundamental role in controlling organ size, tissue regeneration, and stem cell fate under physiological conditions (see section 3.1). When properly regulated, YAP1 and TAZ remain largely cytoplasmic and inactive, ensuring balanced cellular proliferation and apoptosis (Piccolo et al. 2014). However, perturbations of this pathway can lead to nuclear YAP1 and TAZ localization, shifting their function from physiological regulators to potent oncogenic drivers (Fu et al. 2022).

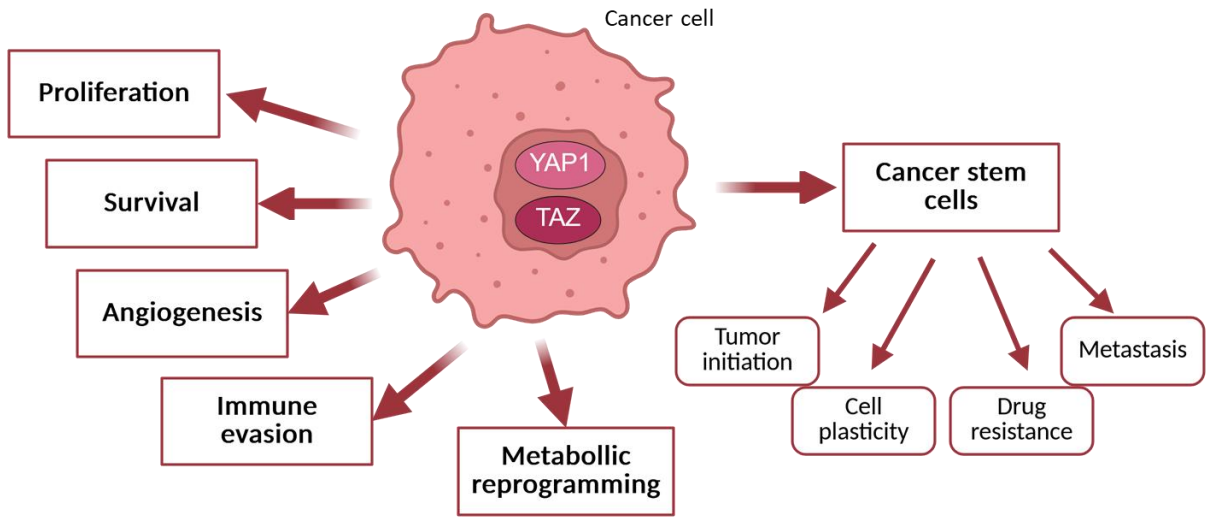

Figure 23: YAP1/TAZ functions in cancer cells. Adapted from Zanconato et al., 2016.

3.3.1. YAP1 and/or TAZ in epithelial cancers

YAP1 and TAZ are frequently co-activated and often collaborate to drive overlapping transcriptional programs that contribute to uncontrolled proliferation, aggressive phenotypes, therapy resistance, and metastatic dissemination in cancers (Guo et al. 2022; Piccolo et al. 2023; Plouffe et al. 2018; Wei et al. 2023) (**Figure 23**).

Carcinoma is a term used to describe a malignant neoplasm of epithelial origin or cancer of the internal or external lining of the body. Carcinomas, which are malignancies of epithelial tissue, account for 80% to 90% of all cancer cases. In the context of epithelial cancers, the role of YAP1 and TAZ has been largely studied (**Figure 24**).

In breast cancer, elevated YAP1 and TAZ activity has been strongly linked to poor differentiation, enrichment of cancer stem cell (CSC) signatures, and worse patient outcomes (Guo et al. 2022; Piccolo et al. 2023; Zanconato et al. 2016). Moreover, the activation of TAZ nuclear translocation is associated with the highly aggressive in triple-negative subtype of breast cancer (Díaz-Martín et al. 2015). Moreover, overexpression of YAP1 increases the metastatic potential of benign breast cancer cells, while loss of YAP1 delays tumor development and reduces metastasis in mouse models (Chen et al. 2014).

Gastric cancer has emerged as another cancer where YAP1 and TAZ play crucial and distinct roles. Both YAP1 and TAZ are frequently activated and contribute to cell proliferation, survival, epithelial-mesenchymal transition (EMT), and the maintenance of CSC-like properties (Seeneevassen et al. 2022; Tiffon et al. 2020). *Helicobacter pylori* infection has been shown to trigger EMT and stemness through TAZ activation, linking chronic inflammation to tumorigenesis (Molina-Castro et al. 2020; Tiffon et al. 2020). Importantly, pharmacological inhibition of YAP1/TAZ-TEAD transcriptional activity using compounds like verteporfin has demonstrated efficacy in suppressing the tumorigenic potential of gastric CSC, highlighting YAP1 and TAZ as promising therapeutic targets (Giraud et al. 2020).

Similarly, in colorectal cancer, YAP1 and TAZ are frequently co-upregulated, with high expression correlating with poor prognosis (Mouillet-Richard and Laurent-Puig 2020). However, YAP1 tends to play a more dominant role in sustaining tumor growth, partly through crosstalk with the Wnt/β-catenin signaling (Guo et al. 2022; Zanconato et al. 2016). Genetic

inhibition of YAP1 severely compromises tumor initiation *in vivo*, underscoring their collective importance in colorectal tumorigenesis (Cai et al. 2015; Gregorieff et al. 2015).

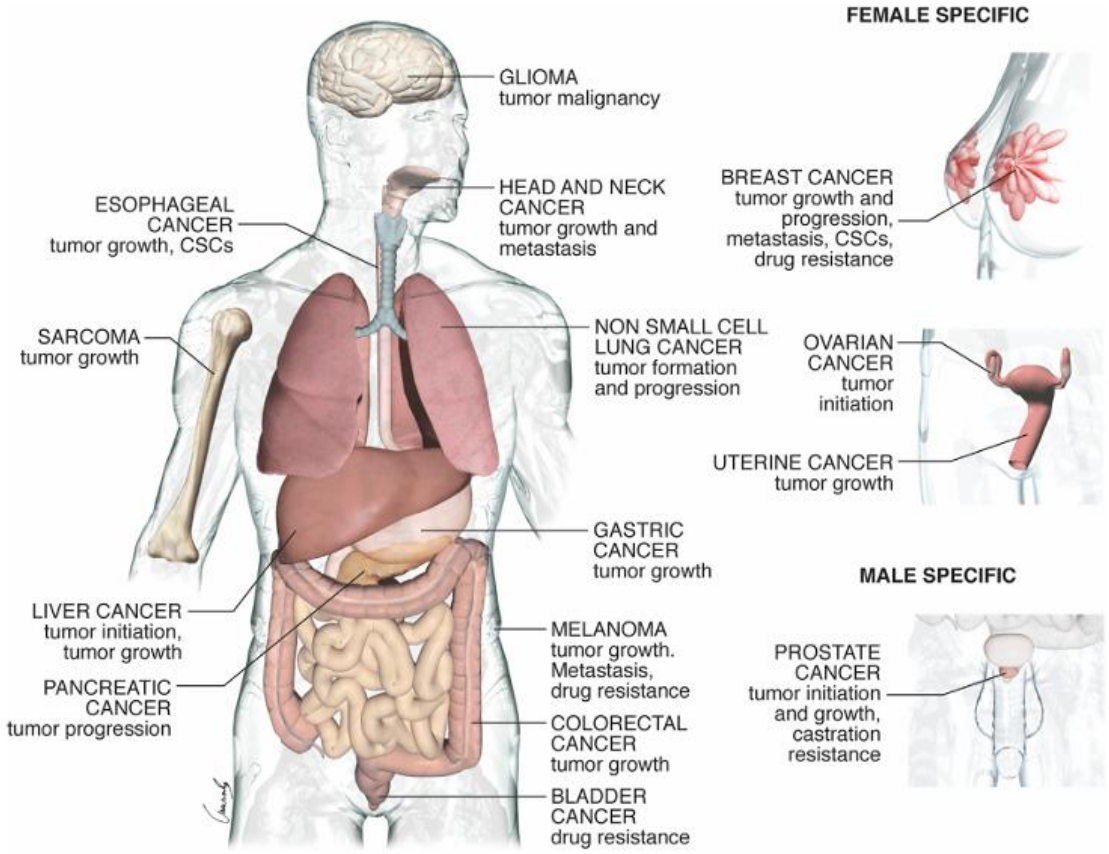

Figure 24: Overview of functional evidence of YAP1/TAZ's role in human cancers. Abbreviation : CSC: Cancer Stem cells. From Zanconato et al., 2016.

Beyond these examples, YAP1 and TAZ display similarly nuanced roles in a range of other epithelial cancers, including lung, liver, pancreatic, prostate, and skin cancers. While both effectors have been demonstrated to promote tumor progression and therapy resistance, the extent to which they contribute varies. The studies are not equivalent regarding to the two proteins. Sometimes, one factor may predominate, depending on the tumor type, the genetic background, or the microenvironmental cues present (Guo et al. 2022; Piccolo et al. 2023). An overview of these findings, based on those of human cancer models, is provided in **Table 3**.

Table 3: Roles of YAP1 and TAZ across selected human epithelial cancers (non-exhaustive list).

Epithelial cancer type	Patient data	Experimental functional studies
Breast cancer	Elevated YAP1 and TAZ expression lead to poor tumor differentiation, enrichment of cancer stem cells, bad clinical outcome, and metastatic potential. TAZ protein expression and nuclear localization is associated with poor outcome. Nuclear YAP is linked with invasive lobular breast cancer.	YAP1 and TAZ knockdown prevent tumorigenesis in mice. TAZ knockdown decreases tumor proliferation and development *in vitro* whereas overactivation lead to cancer stem cells properties. YAP1 knockdown reduces mammary tumor formation and metastasis *in vitro* and *in vivo*.
Gastric cancer	High YAP1 and TAZ protein expression in cancer tissues. Elevated YAP1 and TAZ expression is linked to poor tumor differentiation, shorter survival. Nuclear YAP1 correlates with bad prognosis. High TAZ protein expression induces pre-neoplastic lesions in cancer tissues.	YAP1/TAZ-TEAD inhibitors reduces tumor growth *in vitro*. YAP knockdown inhibits tumor growth and metastatic dissemination *in vitro* whereas YAP1 overexpression enhances tumor growth *in vivo*. TAZ silencing reduces EMT phenotype and inhibits invasion *in vitro.*
Colorectal cancer	High YAP1/TAZ levels predict poor prognosis. Upregulation of YAP1/TAZ mRNA and protein expression in cancer tissues.	YAP1 knockdown reduces tumor growth and metastatic potential *in vitro*. YAP1 and TAZ knockdown *in vivo* prevent tumor formation.
Non-small cell lung cancer	High YAP1/TAZ expression are correlated with bad outcome and shorter patient survival.	YAP1 overexpression promotes tumor progression *in vivo*. TAZ knockdown reduces tumor formation *in vivo*.
Hepatocellular carcinoma	High level of nuclear YAP1 is associated with poor prognosis.	YAP1 knockdown inhibits tumor development *in vitro* and *in vivo*.
Pancreatic adenocarcinoma	Overexpression of YAP1 leads to poor prognosis and nuclear localization.	YAP1 knockdown limited tumor initiation *in vivo*.
Prostate cancer	YAP1 nuclear expression is enriched in prostate cancer with recurrence.	YAP1 knockdown impairs growth *in vivo* whereas YAP1 overexpression promotes tumor formation.
Melanoma	Elevated YAP1 expression is found in a subset of cutaneous melanoma and YAP1/TAZ are nuclear.	YAP1/TAZ knockdown impairs the growth *in vitro* whereas metastatic dissemination is limited *in vivo.*

Footnote: Adapted from Piccolo et al., 2023; Zanconato et al., 2016; Guo et al., 2022.

3.3.2. YAP1 and/or TAZ in sarcomas

Beyond their prominent roles in epithelial cancers, the high expression of YAP1 and TAZ levels, as well as their context-dependent roles, has also been found in mesenchymal tumors, such as sarcomas, where lineage-specific transcriptional networks further shape their functions. Thousands of studies have presented widespread alterations in the Hippo pathway across various bone and soft tissue sarcomas (**Table 4**), implicating dysregulated YAP1/TAZ activity as a recurrent feature in these malignancies (Merritt et al. 2018; Salguero-Aranda et al. 2022).

Table 4: Roles of YAP1 and TAZ across selected human sarcomas (non-exhaustive list).

Sarcoma type	YAP1/TAZ alterations and effects
Osteosarcoma	High YAP1 expression is found in most cancer tissues and is related to proliferation, invasion, and cell differentiation.
Ewing sarcoma	YAP1 and TAZ activity is associated with poor prognosis. Reduction in metastases after YAP1/TAZ inhibition. YAP1 activation potentially cooperating with EWS-FLI1; promotes survival and growth.
Rhabdomyosarcoma	High nuclear YAP1 level is found in human samples. TAZ modulates myogenic differentiation.
Synovial sarcoma	Nuclear YAP1 detected; possible crosstalk with SS18-SSX fusion.
Angiosarcoma	Nuclear YAP1/TAZ associated to endothelial proliferation and aggressive behavior.
Other sarcomas (liposarcoma, leiomyosarcoma)	Variable YAP1/TAZ expression: further studies needed.
GIST	High YAP1 expression is associated with poor prognosis in cancer tissues. Nuclear YAP1 level drives tumor growth and progression. Inhibition of YAP1/TAZ reduces tumor growth, induces apoptosis or ferroptotic cell death *in vitro* and *in vivo*.

Footnote: Adapted from Isfort et al., 2019; Merritt et al., 2018 ; Salguero-Aranda et al., 2022 ; Wu et al., 2025.

In osteosarcoma (mesenchymal cells that exhibits osteoblastic differentiation), several investigations have highlighted elevated YAP1 and TAZ expression correlating with aggressive phenotypes, including increased cell proliferation, invasion, and metastatic potential (Kovar et al. 2020; Rothzerg et al. 2021). Predominant nuclear localization of these transcriptional coactivators has been associated with poorer prognosis and resistance to chemotherapy, suggesting they may serve as biomarkers and therapeutic targets in this disease context (Fullenkamp et al. 2016). Importantly, as in epithelial cancers, YAP1 and TAZ do not always act as a single unit, they can exert distinct roles. For instance, in osteosarcoma, the expression

level of YAP1 appears to be particularly elevated, and this elevated expression has been associated with tumor proliferation and invasion. In addition, YAP1 expression has been linked to cell differentiation processes, suggesting a dual role in oncogenesis and tissue-specific developmental pathways (Rothzerg et al. 2021; Zhang et al. 2013).

In Ewing sarcoma, another type of bone sarcoma, evidence indicates that YAP1 and TAZ are frequently activated and might cooperate with EWS-FLI1 (Ewing sarcoma breakpoint region 1-Frien Leukemia Integration 1 transcription factor) fusion-driven oncogenesis, contributing to cell survival and tumor growth. However, the precise molecular mechanisms underlying these interactions require further elucidation (Bierbaumer et al. 2021; Merritt et al. 2018; Salguero-Aranda et al. 2022).

Conversely, in rhabdomyosarcoma (mesenchymal cells that have failed to fully differentiate into myocytes of skeletal muscle), TAZ activity appears closely tied to the regulation of myogenic differentiation, underscoring its potential role in dictating lineage-specific transcriptional programs (Hebron et al. 2025).

In synovial sarcoma (tissue sarcoma), YAP1 nuclear localization has been documented, even if with variable prevalence among cohorts, raising questions about its role in modulating the transcriptional programs driven by SS18-SSX fusion proteins (Isfort et al. 2019). Likewise, in malignant peripheral nerve sheath tumors (MPNST), increased YAP1 activity has been observed, possibly linked to downstream effects of NF2 (Neurofibromatosis type II) loss or Hippo pathway disruption (Salguero-Aranda et al. 2022).

Other sarcoma subtypes, such as liposarcomas (Shrestha et al. 2019), leiomyosarcomas (Isfort et al. 2019), and angiosarcomas (Ha et al. 2018), have also shown variable levels of YAP1 and/or TAZ activation, though data remain more fragmentary.

These observations underline the relevance of Hippo pathway effectors as potential biomarkers and therapeutic targets across diverse sarcomas.

[*It should be noted here, that the role of YAP1 and/or TAZ in GIST has already been discussed separately (see section 2.4.2.4).*]

3.4. YAP1 and TAZ transcriptional targets : drivers of tumor behavior

As demonstrated in previous chapters, the overexpression and hyperactivation of YAP1 and TAZ play a critical role in the development of various cancers. Therefore, it is essential to explore the repertoire of their downstream transcriptional targets. The main downstream genes coding for TF that YAP1 and/or TAZ bind included *CYR61*, *CTGF*, *CCND1, BIRC5, AXL, AMOT, MCL-1* and many others (**Figure 25**).

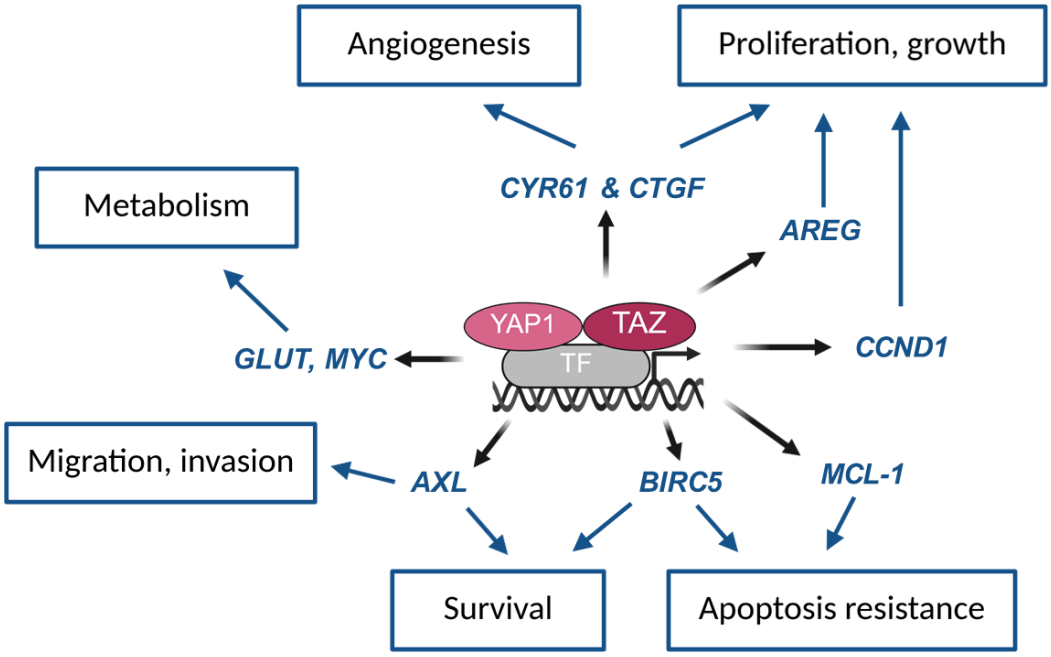

Figure 25: Transcriptional targets of YAP/TAZ and their roles in tumor progression.
Abbreviations: CYR61: cysteine-rich angiogenic inducer 61, CTGF: connective tissue growth factor, AREG: Amphiregulin, CCND1: Cyclin D1, MCL-1: Induced myeloid leukemia cell differentiation, BIRC5: Survivin, AXL: tyrosine-protein kinase receptor UFO.

3.4.1. CYR61 and CTGF: extracellular matrix remodeling and angiogenesis

Among the best-characterized transcriptional targets of YAP1 and TAZ are the matricellular proteins CYR61 (cysteine-rich angiogenic inducer 61, also known as CCN1) and CTGF (connective tissue growth factor, also known as CCN2). They are both members of the CCN family (acronym of the first family members discovered: CYR61, CTGF and NOV) of secreted factors (Boopathy and Hong 2019; Zhou et al. 2016).

CYR61 is a multifunctional protein capable of binding various integrins, particularly αvβ3. This protein also activate downstream pathways such as NF-κB and COX2 (cyclo-oxygenase-2) that promote cell migration and invasion (Boopathy and Hong 2019; Koo et al. 2020). In gastric

cancer, elevated CYR61 expression correlates with advanced disease stage, lymph node metastasis, and poor prognosis (Lin et al. 2005). In addition to promote cell motility, CYR61 contributes to tumor angiogenesis both by directly acting on endothelial cells and indirectly via VEGF regulation (Mo et al. 2002).

Similarly, CTGF plays a role in the deposition of ECM, fibroblast activation, and angiogenesis (Hiemer et al. 2014; Li et al. 2024). Its functions vary according to its integrin partners, highlighting its complex role in tumor progression and fibrotic responses. CTGF is also a target of TGF-β signaling, illustrating the convergence of multiple pathways towards common effectors that mediate tissue remodeling in physiological and pathological contexts (Ramazani et al. 2018). It is crucial in cellular processes such as proliferation, differentiation, motility, and adhesion. Notably, in gastric cancer cells, CTGF inhibition reduces invasive potential (Jiang et al. 2011).

3.4.2. CD1: Cell cycle regulation and proliferation

YAP1 and TAZ have been demonstrated to influence cell proliferation by regulating genes critical for cell cycle progression, including *CCND1*, which encodes CD1. CD1 is a key driver of the G1/S transition, binding to and activating cyclin-dependent kinases that phosphorylate retinoblastoma protein (Rb), thus allowing E2F-mediated transcription of S-phase genes (Qie and Diehl 2016). Elevated CD1 levels lead to uncontrolled proliferation and have been linked to greater invasiveness and therapeutic resistance in multiple cancers, including GIST and sarcomas (LeBlanc et al. 2021; Montalto and De Amicis 2020). While *CCND1* transcription is also regulated by other oncogenic signals such as β-catenin, MYC, and estrogen receptors (Qie and Diehl 2016), its induction by YAP1 and TAZ underlines the central role of Hippo pathway in coordinating proliferation with mechanical and biochemical stimuli (Mizuno et al. 2012; Shen et al. 2021).

3.4.3. Survivin and MCL-1: apoptosis inhibition and cell survival

Beyond promoting proliferation, YAP1 and TAZ enhance tumor cell survival through the transcriptional activation of anti-apoptotic genes like *BIRC5*, which encodes for Survivin (Hansen et al. 2015). Survivin is a member of the inhibitor of apoptosis family that suppress caspase activation and stabilize mitotic spindle formation during cell division (Wheatley and Altieri 2019). Its high expression is characteristic of many malignancies. Targeting *BIRC5* can

sensitize cancer cells to chemotherapy by restoring apoptotic pathways (Lim et al. 2015). The induction of *BIRC5* by YAP1/TAZ highlights the role of Hippo pathway dysregulation in conferring resistance to cell death (Rosenbluh et al. 2012).

Another example of apoptosis resistance is mediated by *MCL-1*, a member of the apoptosis regulation proteins BCL-2 family that localizes to the mitochondria and prevents cytochrome c release, thereby inhibiting the intrinsic apoptotic cascade (Perciavalle et al. 2012). Recent studies have identified MCL-1 as a direct transcriptional target of YAP1 and TAZ. In the case of metastatic uveal melanoma, combined MCL-1 and YAP1/TAZ inhibition could be used as a treatment (Glinkina et al. 2023).

3.4.4. AXL: Invasion, EMT, and drug resistance

Concerning invasion and metastasis, YAP1 and TAZ regulate genes such as *AXL* (encoding for tyrosine-protein kinase receptor UFO), involved in EMT, cell motility, and resistance to targeted therapies (Xu et al. 2011; Zhou et al. 2016). UFO has similar functions to KIT and PDGFRA, triggering downstream cascades including the PI3K/AKT, MAPK/ERK, NF-κB and JAK/STAT pathways (Goyette et al. 2018). These signaling events promote migration and invasion, as well as survival, EMT and proliferation.

3.4.5. Additional targets supporting tumor adaptation

YAP1 and TAZ have been shown to play a regulatory role in the expression of genes that facilitate the adaptation and survival of tumor cells under conditions of stress. The activation of the *AREG* (encoding for Amphiregulin) gene, which is part of the *EGF* family, by YAP1, stimulates EGFR signaling pathway, supporting cell growth, especially under EGF deprivation (J. Zhang et al. 2009; Zhou et al. 2016).

Metabolic reprogramming is another key feature, with targets like *GLUT1* increasing glucose uptake to fuel rapid proliferation (Lin and Xu 2017). Moreover, YAP1/TAZ can upregulate *MYC*, amplifying oncogenic transcriptional programs tied to metabolism and growth, though *MYC* alone cannot fully replicate YAP1/TAZ effects (Zhou et al. 2016).

Together, these diverse targets underline how YAP1 and TAZ enable tumor cells to thrive despite environmental or therapeutic challenges. Understanding the differential regulation of these genes and the distinct roles of YAP1 and TAZ across cancer types is thus essential for

developing more precise therapeutic interventions, a topic explored in detail in the following section on their transcriptional regulation.

3.5. Therapeutics targeting of YAP1 and TAZ

Building upon the transcriptional roles of YAP1 and TAZ, considerable efforts have been directed toward exploiting their oncogenic functions for therapeutic purposes. This section reviews current strategies aimed at modulating YAP1 and TAZ activity, highlighting the diversity of approaches and the remaining challenges. A summary of therapeutic strategies targeting YAP1 and TAZ is shown in **Figure 26**.

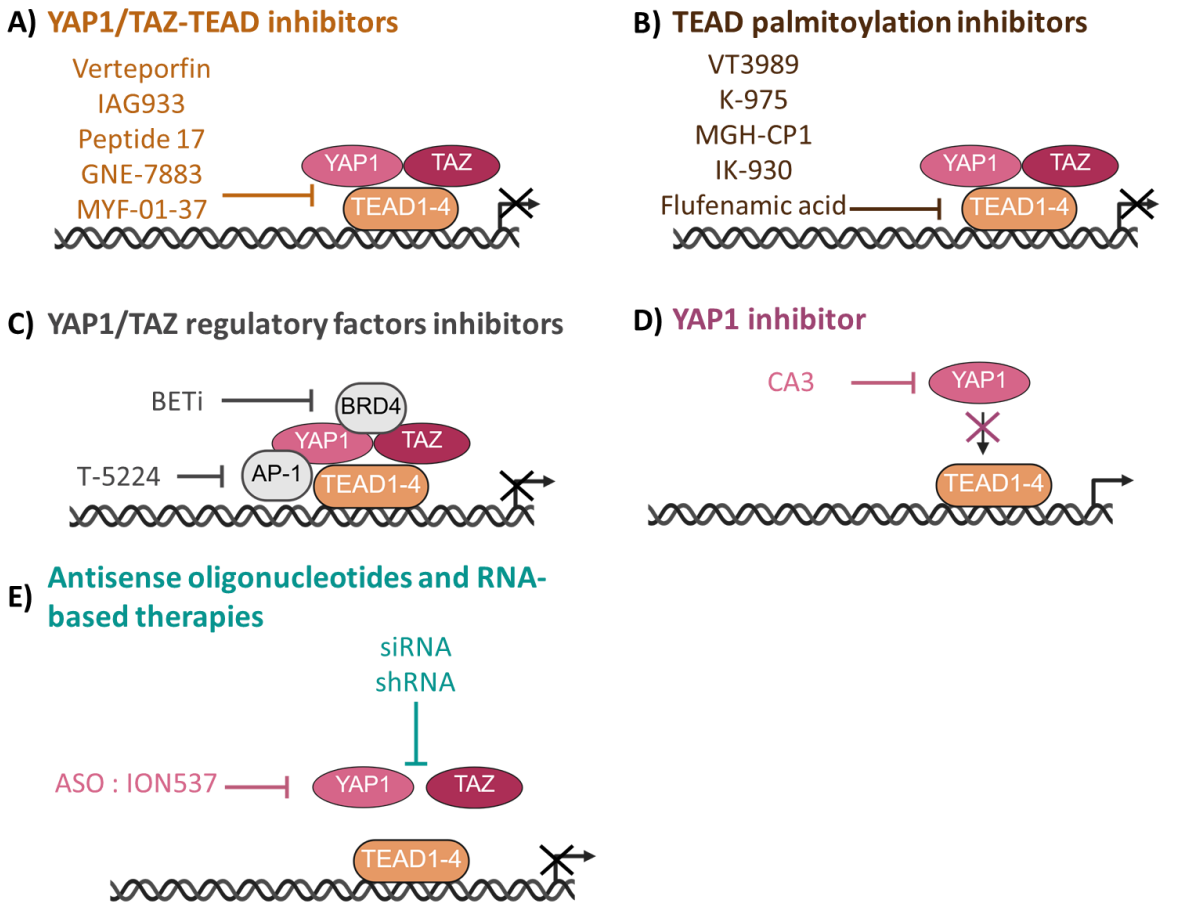

Figure 26: Therapeutic strategies targeting YAP1/TAZ signaling in cancer.
This figure summarizes various pharmacological approaches developed to inhibit YAP1/TAZ activity directly or indirectly. **A)** YAP1/TAZ–TEAD inhibitors, including Verteporfin, IAG933, Peptide 17, GNE-7883, and MYF-01-37, block the interaction between YAP1/TAZ and TEAD transcription factors. **B)** TEAD palmitoylation inhibitors such as VT3989, K-975, MGH-CP1, IK-930, and flufenamic acid interfere with TEAD function by preventing its palmitoylation. **C)** Inhibition of YAP1/TAZ regulatory factors involves BET inhibitors (BETi) targeting BRD4, which interacts with YAP/TAZ, and AP-1 inhibitors such as T-5224. **D)** Direct YAP1 inhibitors like CA3 specifically target YAP1 to reduce its transcriptional activity. **E)** Antisense oligonucleotides and RNA-based therapies, including siRNA, shRNA, and the antisense oligonucleotide ION537, aim to reduce YAP1/TAZ expression at the transcript level, offering a highly specific strategy for modulating Hippo pathway activity in cancer treatment.
Adapted from Piccolo et al., 2023.

Despite their well-established roles in cancer progression, YAP1 and TAZ remain difficult therapeutic targets. Both proteins lack intrinsic enzymatic activity and act primarily as transcriptional coactivators, exerting their oncogenic functions through protein-protein interactions, especially with TEAD (Piccolo et al. 2023; Zanconato et al. 2016). Unlike kinases or other classical drug targets, YAP1 and TAZ do not possess well-defined active sites suitable for conventional small-molecule binding (even if some exists). This structural feature significantly complicates direct pharmacological inhibition. To date, no drugs have been approved by the Food and Drug Administration (FDA) that directly inhibit YAP1 and/or TAZ (Baroja et al. 2024; Fu et al. 2022; Thrash and Pendergast 2023). Some of drugs are being tested in Phase 1 for advanced solid tumors, glioblastoma, and mesothelioma, but no molecules have yet moved on to Phase 2 (Thrash and Pendergast 2023).

3.5.1. Targeting YAP1/TAZ interaction with TEAD

One prominent line of research aims to directly inhibit the interaction between YAP1/TAZ and TEAD, given that this binding is essential for driving oncogenic transcriptional programs. Although YAP1 and TAZ themselves lack clear druggable pockets, structural studies have revealed a hydrophobic pocket within TEAD proteins that is critical for binding coactivators and for undergoing S-palmitoylation, a lipid modification essential for TEAD's stability and transcriptional activity (Barry et al. 2021; Noland et al. 2016) (**Figure 27**). This pocket has emerged as a promising pharmacological target.

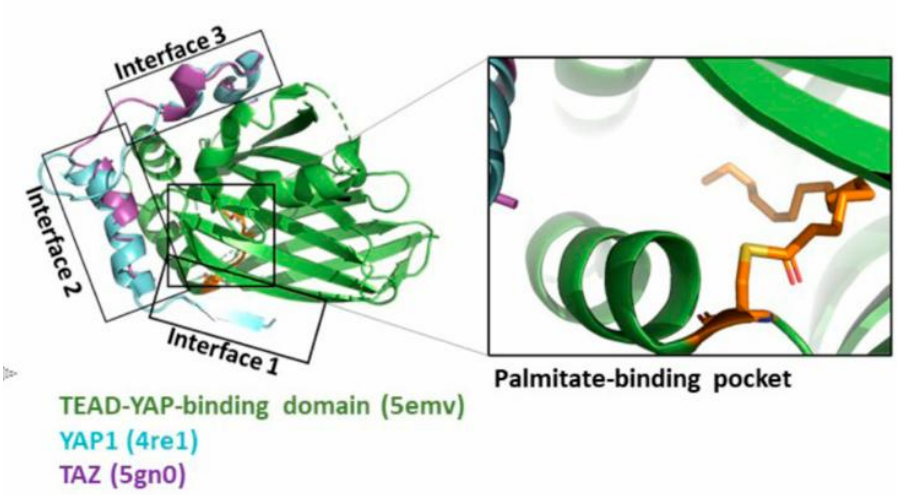

Figure 27: Spatial visualization of the protein-protein interaction between YAP1/TAZ and TEAD.
Interfaces 2 and 3 correspond to several drug pockets that can be inhibited by small and large molecules. Notably, the central lipophilic palmitate pocket (interface 1) seems the most targetable (PDB: 5emv, 4re1 and 5gn0).
From Barry et al., 2021

Among the first compounds identified to disrupt the YAP1/TAZ-TEAD complex was Verteporfin (Visudyne), a benzoporphyrin derivative initially approved by the FDA for photodynamic therapy in 2016 (Lv and Zhou 2023; Thrash and Pendergast 2023; Zanconato et al. 2016). This molecule binds covalently to cysteine residues within the TEAD hydrophobic pocket, thereby inhibiting the formation of the YAP1/TAZ-TEAD complex and suppressing oncogenic gene expression (Liu-Chittenden et al. 2012). This has led to its investigation in a Phase 1/2 clinical trial for EGFR-mutated glioblastoma (NCT04590664), underlining its translational potential (Liu-Chittenden et al. 2012). However, verteporfin's non-specific binding profile and poor pharmacokinetics, notably high toxicity, limit its application in the clinic (Lv and Zhou 2023).

Because these limitations, several new molecules (small molecules, peptides, etc.) have been optimized to target more selectively the YAP1/TAZ-TEAD interface (**Figure 26A**). IAG933 (YAP-TEAD-IN-3), developed by Novartis Pharmaceuticals, is an orally available drug that was designed to block the YAP1/TAZ-TEAD interface directly (Chapeau et al. 2024). It has been investigated in a Phase 1 clinical trial for mesothelioma since 2021 (NCT04857372) (Lv and Zhou 2023; Thrash and Pendergast 2023). MYF-01-37 is another compound identified as a covalent TEAD binder that effectively targets non-small cell lung cancer cells harboring EGFR mutations (Barry et al. 2021; Kurppa et al. 2020). Another innovative organic agent is GNE-7883, which functions as an allosteric pan-TEAD inhibitor. Instead of directly competing with YAP1/TAZ binding, GNE-7883 induces conformational changes in TEAD that impair its transcriptional activity across multiple isoforms, potentially enabling broader therapeutic effects (Hagenbeek et al. 2023).

Besides small molecules, a YAP-like peptide (17mer) occupying the interface 3 on TEAD was developed. This so-called Peptide 17**,** corresponding to the cyclic version of the YAP sequence from amino acid 84 to 100, is another YAP1-TEAD binding inhibitor (IC50 value ~3 µM) currently in preclinical studies in ovarian cancer (Zhou et al. 2015).

3.5.2. Indirect YAP1/TAZ targeting through TEAD palmitoylation inhibitors

Beyond direct disruption of protein-protein interactions, therapeutic strategies have increasingly focused on targeting TEAD palmitoylation (Baroja et al. 2024; Lv and Zhou 2023; Thrash and Pendergast 2023) (**Figure 26B**). By preventing this modification, these inhibitors

aim to destabilize TEAD proteins and reduce their capacity to support YAP1/TAZ-mediated transcription.

VT3989, an orally available small molecule developed by Vivace Therapeutics (Tang et al. 2021), has emerged in 2021 as a main example of this class and is currently undergoing Phase 1 clinical evaluation in mesothelioma (NCT04665206) (Lv and Zhou 2023; Thrash and Pendergast 2023). Similarly, K-975, another small molecule, has shown to be a strong and selective TEAD inhibitor with the potential to become an effective drug candidate for malignant pleural mesothelioma therapy (Kaneda et al. 2020). However, a recent study revealed that mesothelioma cells exhibited primary resistance to K-975 through the activation of the MYC signaling (Akao et al. 2025). Other molecules, such as MGH-CP1, a commercially available compound, have been primarily tested in preclinical studies, further validating the feasibility of this approach (Li et al. 2020). MGH-CP1 acts as an inhibitor of the auto-palmitoylation of TEAD2 and TEAD4 and has been shown to inhibit nasopharyngeal carcinoma cell migration, invasion, and cisplatin resistance (Lv and Zhou 2023). IK-930 is another noteworthy TEAD palmitoylation inhibitor developed in 2022 and is currently undergoing Phase 1 clinical evaluation for epithelioid hemangioendothelioma and mesothelioma (NCT05228015) (Lv and Zhou 2023; Thrash and Pendergast 2023). Finally, flufenamic acid, a commercially available compound (non-steroidal anti-inflammatory drug), has also been shown to interfere indirectly with the YAP1/TAZ-TEAD interaction by inhibiting TEAD palmitoylation, further underscoring the diversity of chemical approaches being explored to target this critical protein-protein interaction (Franklin et al. 2023; Thrash and Pendergast 2023).

Nevertheless, TEAD inhibition leads to transient inhibition of cell cycle progression without inducing cell death, undermining their potential therapeutic utilities. Consistently, combination of TEAD and AKT inhibitors exhibits strong synergy in inducing cancer cell death as reported recently (Sun et al. 2022). In addition, despite the encouraging potential of these inhibitors as a therapeutic intervention, the long-term safety of interfering with lipid modifications in transcription factors remains to be fully elucidated. Further clinical investigations are required to clarify their therapeutic window and ensure the optimal use of these inhibitors.

3.5.3. Targeting YAP1 and TAZ activity

3.5.3.1. YAP1/TAZ regulatory factor inhibitors

YAP1 and TAZ activity can be indirectly inhibited by targeting key cofactors that facilitate their transcriptional functions (**Figure 26C**). One notable example is BRD4, a member of the BET (bromodomain and extra-terminal domain) family. BRD4 interacts with YAP1/TAZ which is recruited to the chromatin to amplify YAP1/TAZ-driven gene expression (Piccolo et al. 2023; Zanconato et al. 2018). BRD4 recognizes acetylated histones and facilitates transcriptional elongation by recruiting additional transcription factors. Consequently, BET inhibitors such as the thienotriazolodiazepine JQ1, a competitive BRD4 inhibitor, have been shown to reduce MAPK/ERK and NF-κB pathways activity (Liu et al. 2021). A derivative of JQ1, Birabresib (OTX-015), is in clinical phase 1b (Lewin et al. 2018). Despite promising preclinical results, clinical trials using BET inhibitors across various cancers have yielded inconclusive outcomes, and none are yet approved specifically for targeting YAP1/TAZ activity (Piccolo et al. 2023; Shorstova et al. 2021).

Additionally, AP-1, a transcription factor complex also recruited by YAP1 and TAZ to chromatin, represents another indirect target. The benzophenone derivative T-5224, an AP-1 inhibitor, has demonstrated efficacy in head and neck cancers (Kamide et al. 2016). However, its anti-tumor effects have not been definitively linked to YAP1/TAZ inhibition to date (Piccolo et al. 2023; Zanconato et al. 2015).

3.5.3.2. Molecules reducing YAP1/TAZ activity

While verteporfin remains the most widely studied compound for inhibiting the interaction between YAP1 and TEAD, another small-molecule inhibitor, CA3, has also shown potential as a YAP1-targeting agent (**Figure 26D**). Unlike verteporfin, CA3 directly suppresses YAP1-driven transcriptional activity and has demonstrated antitumor effects in models of esophageal adenocarcinoma (Song et al. 2018), pancreatic cancer (Nimmakayala et al. 2022), and osteosarcoma (Morice et al. 2020).

An emerging and highly targeted approach to suppress YAP1 function involves nucleic acid-based therapies, particularly antisense oligonucleotides (**Figure 26E**). Developed by Ionis Pharmaceuticals in 2020, ION537 was specifically designed to bind YAP1 mRNA and reduce its expression at both transcript and protein levels (Macleod 2021). This strategy offered the

potential advantage of high specificity and even isoform-selective silencing, which could be crucial given the nuanced roles of YAP1 and TAZ across different tumor contexts. A Phase 1 trial evaluating ION537 in advanced solid tumors (NCT04659096) has been completed, although detailed results from this study have not yet been disclosed (Thrash and Pendergast 2023).

Another effective strategy to downregulate YAP1 and TAZ expression involves small interfering RNA (siRNA) therapies, which provide a more specific alternative to traditional small-molecule inhibitors (**Figure 26E**) (Fu et al. 2022). Preclinical studies have shown that YAP1/TAZ-targeted siRNA treatments can successfully suppress tumor progression in various animal models. For instance, angiopep-2 peptide modified cationic liposomes loaded with both doxorubicin and YAP1 siRNA effectively inhibited glioblastoma growth (Lihuang et al. 2021). Similarly, lipid-based nanoparticles delivering YAP1 siRNA have been shown to impede the development of hepatocellular carcinoma in murine models (Fitamant et al. 2015).

Additionally, short hairpin RNA (shRNA) is another widely used genetic tool to inhibit YAP1, as evidenced by studies where administration of adeno-associated virus vectors encoding shRNA against YAP1 attenuated bleomycin-induced pulmonary fibrosis (**Figure 26E**) (Y. Chen et al. 2019).

All these nucleic acid-based therapeutics represent a great breakthrough for the development of a Hippo-targeted drugs (Fu et al. 2022).

3.5.4. Perspective on drugs targeting YAP1 and TAZ activity

To date, while significant advances have been made and are still ongoing in exploring strategies to modulate YAP1 and TAZ, no drugs targeting either protein directly was approved by the FDA (Baroja et al. 2024). This absence of specific therapeutics highlights the necessity of further investigating YAP1 and TAZ as separate molecular targets, given their partially overlapping roles across different biological contexts, especially in diverse cancers and sarcomas (Seeneevassen et al. 2022; Wei et al. 2023). Developing tools capable of selectively silencing each factor represents a promising avenue for future research. In this regard, RNA interference and related gene-silencing technologies are emerging as attractive strategies to precisely inhibit YAP1 or TAZ activity, an approach discussed in the following section.

4. Small interfering RNA as a therapeutic strategy

This chapter addresses the therapeutic potential of RNA interference (RNAi) and the use of siRNA in the field of oncology. A comprehensive introduction to the molecular mechanisms of RNAi will be provided initially. This will be followed by an in-depth discussion of the properties and challenges associated with siRNA therapeutics. Subsequently, the focus will shift to advanced delivery systems, in order to use WRAP (W- and R- amphipathic peptides) as promising cell-penetrating peptides (CPP). These siRNA-loaded peptide-based nanoparticles show considerable potential in enabling effective gene silencing strategies against otherwise undruggable targets, such as YAP1 and TAZ.

4.1. Overview of RNA interference

RNA molecules play a variety of roles in cell biology, beyond their central role in the transfer of genetic information for protein production. In addition to messenger RNA (mRNA), cells produce a variety of non-coding RNA (ncRNA) that serve critical regulatory functions. Among these, small ncRNA are central to the process of RNAi (Esteller 2011).

RNAi is defined as a conserved cellular sequence-specific mechanism of post-transcriptional gene silencing that regulates gene expression in eukaryotic cells. Initially, it was discovered in 1998 as a naturally occurring defense mechanism against the invasion of foreign nucleic acids (such as viral genomes) and the control of gene expression (Fire et al. 1998). Small RNA (smRNA) molecules mediate sequence-specific silencing of gene expression by promoting degradation of target mRNA, which induces inhibition of its translation into protein (Fire et al. 1998; Xu et al. 2016). Multiple classes of smRNA participate in RNAi, each characterized by distinct origins, structures, and modes of action (**Figure 28**).

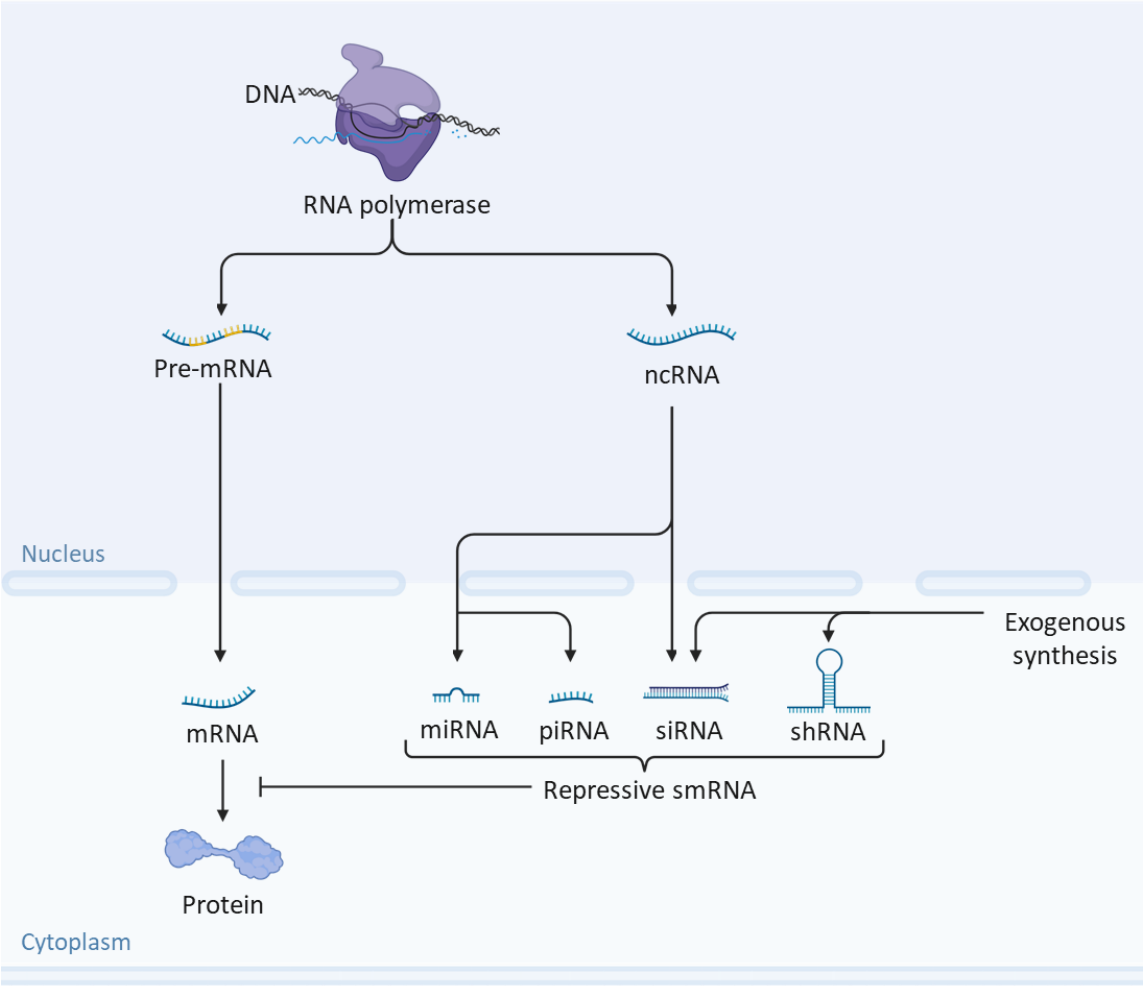

Figure 28: Overview of RNA interference.
RNA polymerase transcribes genomic DNA into either protein-coding pre-mRNA or non-coding RNA (ncRNA). Pre-mRNA is processed into mature mRNA, which is translated into proteins. ncRNA include several classes of regulatory RNA, among which small RNA mediate gene silencing. Endogenous microRNA (miRNA) bind target mRNA to repress translation. Piwi-interacting RNA (piRNA) are involved in the epigenetic and post-transcriptional silencing especially in germ line cells. Small interfering RNAs (siRNA) can originate from endogenous or exogenous sources and mediate sequence-specific mRNA cleavage. Short hairpin RNA (shRNA), typically synthesized exogenously and expressed from vectors, form hairpin structures that are processed intracellularly into siRNA-like duplexes capable of silencing gene expression. Together, miRNA, siRNA, and shRNA constitute repressive small RNA (smRNA) involved in post-transcriptional gene regulation. Inspired by Biorender template.

The three classes most studied in biomedical research are presented below:

- **MicroRNA** (**miRNA**) are endogenous non-coding RNA, approximately 21-23 nucleotides long, which regulate gene expression by binding to target mRNA and blocking their translation or promoting their degradation. miRNA play important roles in development, differentiation, and various diseases (Bartel 2004; Ha and Kim 2014).

- **Short hairpin RNA** (**shRNA**) are synthetic RNA molecules designed to fold into hairpin structures and mimic endogenous regulatory RNA. When expressed from plasmid or viral vectors, shRNA are processed inside cells into short RNA duplexes that guide the silencing of specific target mRNA. They are widely used in research for stable and long-term gene knockdown (McIntyre et al. 2011; Paddison and Hannon 2002).
- **Small interfering RNA (siRNA)** molecules are generated from internal genomic sources (transposons or repetitive sequences) and contribute as endogenous siRNA to gene regulation and protect against genomic instability. In contrast, exogenous siRNA originate from external sources such as viral infections or chemically synthesized double-stranded RNA molecules. Independent of their origin, siRNA molecules are always double-stranded RNA with a typical length of 21-23 nucleotides. siRNA guide precise cleavage of target mRNA through perfect or near-perfect sequence complementarity, leading to effective and specific gene silencing (Elbashir et al. 2001; Friedrich and Aigner 2022; Ozcan et al. 2015).

Although miRNA and shRNA hold significant biological and experimental relevance, siRNA have emerged as the most clinically advanced RNAi tool. siRNA are interesting therapeutic molecules due to their high specificity, programmable sequence design, and suitability for synthetic production and chemical modification. These features allow optimization of pharmacokinetic properties, stability, and therapeutic efficacy (Friedrich and Aigner 2022; Ranasinghe et al. 2023).

4.2. siRNA mechanisms of gene silencing

The mechanism of using siRNA to silence genes is based on a well-conserved post-transcriptional mechanism. Firstly, long double-stranded RNA (dsRNA) precursors expressed in cells are processed in the cytoplasm by the RNase III enzyme Dicer, which cleaves them into siRNA duplexes bearing characteristic two-nucleotide 3’ overhangs (**Figure 29A,B**) (Hu et al. 2020). When directly introduced into cells, synthetic siRNA bypass this processing step and are available for incorporation into downstream machinery (Ozcan et al. 2015).

Once delivered into the cytoplasm, the siRNA duplex (endo- or exogenous) is recognized by the RNA-induced silencing complex (RISC) (**Figure 29C**). Within RISC, the duplex is unwound by the Argonaute-2 protein (AGO2), a catalytic part of RISC, to form single-stranded siRNA (**Figure 29D**). The guide strand (antisense) is selectively retained, while the passenger strand (sense) is degraded (Elbashir et al. 2001; Friedrich and Aigner 2022; Hu et al. 2020).

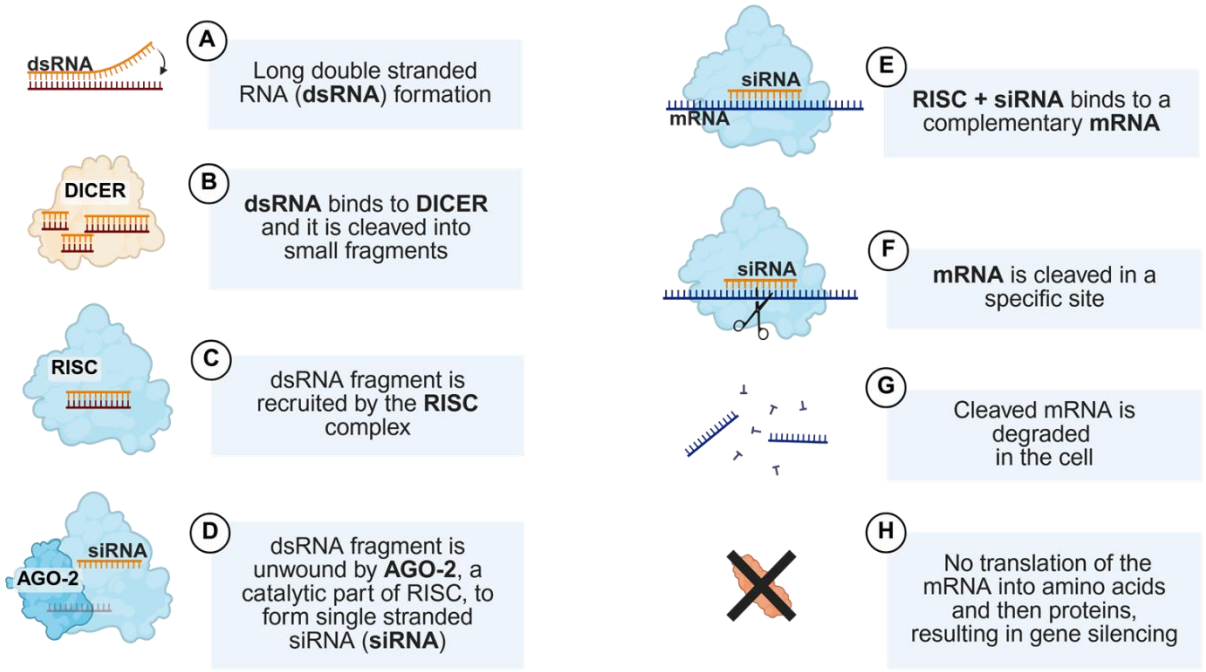

Figure 29: Molecular mechanism of siRNA-mediated gene silencing.
(**A**) Long double-stranded RNA (dsRNA) is generated either endogenously or introduced exogenously. (**B**) The dsRNA binds to the RNase III enzyme Dicer, which cleaves it into small interfering RNA (siRNA) duplexes of ~20–25 nucleotides with characteristic 3′ overhangs. (**C**) The resulting siRNA fragments are recruited by the RNA-induced silencing complex (RISC). (**D**) Within RISC, the siRNA duplex is unwound by the catalytic component Argonaute-2 (AGO-2), and the passenger strand is discarded while the guide strand remains bound. (**E**) The guide strand directs RISC to bind a complementary messenger RNA (mRNA) sequence through base pairing. (**F**) Ago2 cleaves the mRNA at a specific site within the paired region. (**G**) The cleaved mRNA fragments are degraded within the cell. (**H**) As a result, translation of the target mRNA into protein is prevented, leading to efficient gene silencing.
Scheme adapted from Biorender template.

The guide strand directs RISC to complementary target mRNA through sequence-specific base pairing. Upon perfect or near-perfect complementarity between the siRNA and the target mRNA, the latter is cleaved by the catalytic activity of Argonaute proteins within RISC. This leads to the rapid degradation of the mRNA fragments, which in turn prevents protein translation (Hu et al. 2020; Mahmoodi Chalbatani et al. 2019) (**Figure 29E-H**). In humans, four Argonaute proteins (AGO-1 to AGO-4) are expressed, but only AGO-2 possesses endonuclease "slicer" activity, enabling it to directly cleave target mRNA (Liu et al. 2004). This mechanism

effectively silences the expression of the corresponding protein, thereby modulating cellular processes or disease pathways (Ranasinghe et al. 2023).

The high specificity of siRNA-mediated silencing has firmly established this mechanism as a powerful tool for both functional genomics and therapeutic applications (Friedrich and Aigner 2022; Ozcan et al. 2015).

4.3. Challenges of siRNA-based therapy

Despite the promising potential of siRNA for targeted gene silencing, their therapeutic application faces several biological and technical challenges (**Figure 30**).

4.3.1. Intracellular barriers limiting the conception of siRNA therapeutics

4.3.1.1. Off-target effects and efficacy

The first limitation of siRNA therapy lies in its potential for off-target gene silencing. Although siRNA are designed to hybridize with a perfect complementary sequence to their target mRNA, partial sequence homology can allow miRNA-like interactions, leading to unintended downregulation of non-target transcripts (Hu et al. 2020; Mahmoodi Chalbatani et al. 2019; Ozcan et al. 2015). These off-target effects may result in cellular toxicity, phenotypic alterations, or compromised therapeutic outcomes (Ozcan et al. 2015).

Moreover, RNAi efficacy varies widely depending on siRNA design and target accessibility. Only a subset of siRNA demonstrate high silencing potency, with studies showing that just ~15% of randomly selected siRNA induce >90% knockdown efficiency (Ozcan et al. 2015). This necessitates careful selection and optimization of siRNA sequences through computational screening approaches (Ranasinghe et al. 2023).

4.3.1.2. Immune response and toxicity

In addition, siRNA can stimulate innate immune responses via recognition of Toll-like receptors (TLR3, TLR7, TLR8) and cytosolic receptors like RIG-I, leading to the induction of type I interferon responses and pro-inflammatory cytokines (Ranasinghe et al. 2023; Robbins et al. 2009). Sequence motifs such as 5’-UGUGU-3’ and 5’-GUCCUUCAA-3’ have been implicated in TLR-mediated immune activation, particularly through dendritic cells and monocytes (Ozcan et al. 2015).

siRNA may also exert sequence-dependent cytotoxicity, even in the absence of target knockdown. Toxic motifs such as UGGC tetramers or AU-rich pentamers have been associated with increased cellular stress and apoptosis (Ozcan et al. 2015).

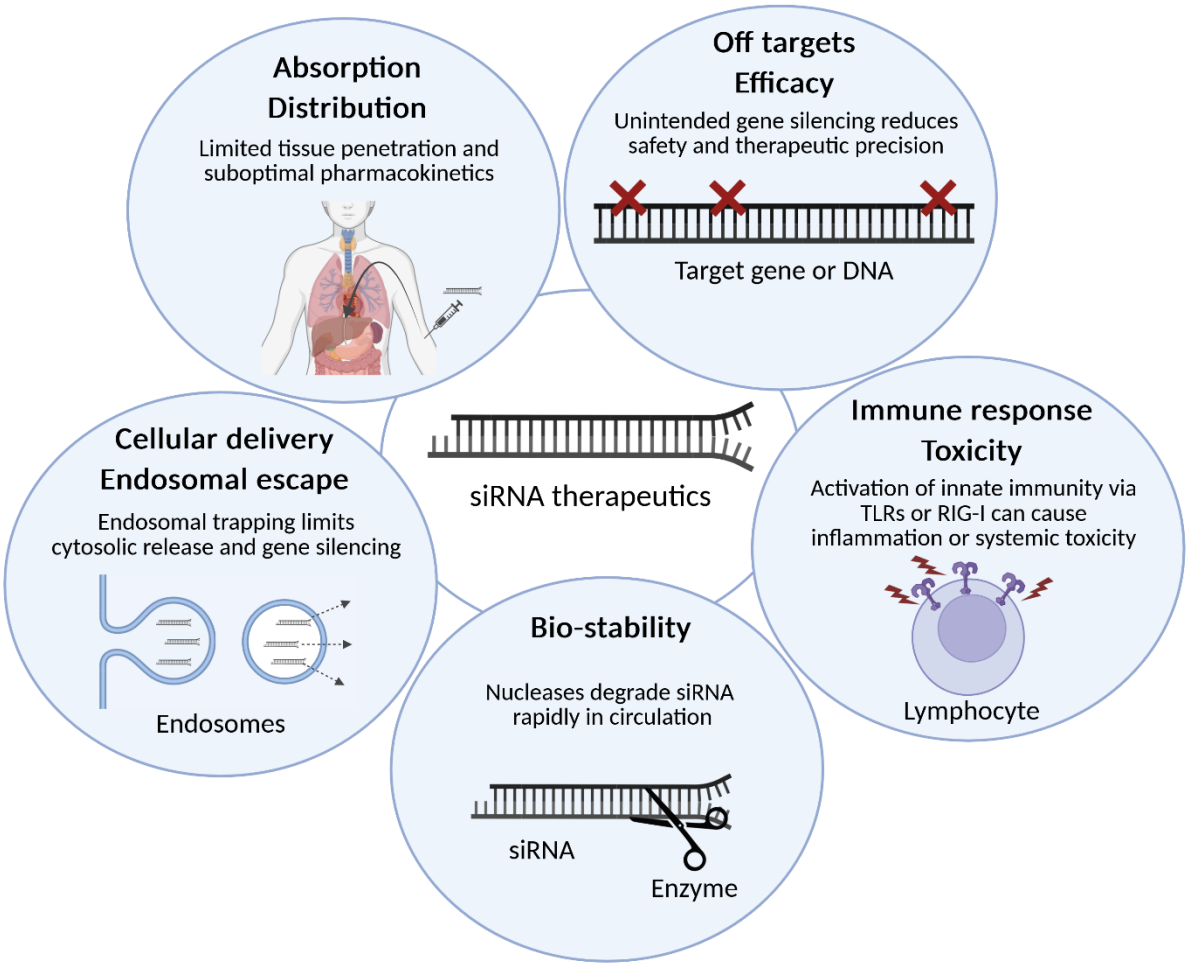

Figure 30: Challenges in siRNA therapeutics.
Even though siRNA technology has numerous benefits over conventional small molecule therapies, there are still certain issues that must be resolved, including biodistribution, stability, immunological stimulation, transport efficiency, and possible off-target consequences.
Adapted from Ebenezer et al., 2025.

4.3.1.3. Bio-stability

siRNA are quickly degraded by serum nucleases, leading to short half-lives in circulation (Ebenezer et al. 2025). Indeed, the plasma half-life for a free siRNA molecule in the blood stream has been calculated to be about only 6 min (Dassie et al. 2009). Ensuring siRNA bio-stability remains pivotal for achieving effective gene silencing (Ebenezer et al. 2025). To improve siRNA stability effectively, a combination of chemical modifications targeting the ribose sugar (2'-O-methyl, 2'-fluoro, 4'-thio), backbone (phosphorothioate), and overhangs (amide-linked) is often employed. These modifications enhance resistance to nucleases and

prolong half-life in biological fluids while maintaining or even enhancing RNAi potency (Alagia and Eritja 2016; Ku et al. 2016).

4.3.1.4. Cellular delivery and endosomal escape

Once administered, siRNA rely on cellular uptake mechanisms to reach their site of action in the cytoplasm. Due to their relatively large molecular weight (~13-15 kDa) and pronounced negative charge, naked siRNA are poorly internalized by cells. Mainly unable to cross the plasma membrane by themselves, they are highly susceptible to rapid degradation by extracellular nucleases (Ebenezer et al. 2025; Kanasty et al. 2013). Formulation strategies, such as nanoparticle encapsulation, cyclodextrin conjugation, and polymer crosslinking, further protect siRNA from degradation and improve their delivery to target cells (Dastgerdi et al. 2024; Ho et al. 2016). siRNA are generally internalized via endocytic pathways rather than passive diffusion across cell membranes (Juliano et al. 2012). Most siRNA are sequestered in endosomal compartments, from which efficient escape is essential for RISC loading and gene silencing (Juliano et al. 2012). Only 1-2% of siRNA are probably able to escape from endosomes (Ranasinghe et al. 2023). Without effective endosomal release, internalized siRNA are often trafficked to lysosomes and degraded, resulting in decreased silencing activity.

4.3.2. Pharmacological challenges: absorption and distribution

Orally administered siRNA are particularly problematic because their polyanionic charge and hydrophilic nature make them vulnerable to degradation in the GI tract environment and prevents them from efficiently crossing biological membranes (Ranasinghe et al. 2023). As a result, currently approved siRNA therapies targeting systemic diseases require parenteral administration via intravenous or subcutaneous injection (Yasuda et al. 2023). In some cases, local administration offers an alternative by delivering siRNA directly to target tissues such as the eyes, mucous membranes, or skin, thereby avoiding systemic barriers and achieving higher local bioavailability (Ranasinghe et al. 2023). However, only a limited number of diseases are suitable for this approach, which restricts its broader therapeutic use.

Once in the bloodstream, siRNA are rapidly distributed but face difficulties to reach certain tissues, because of the passage in the vascular endothelium. The ability of siRNA to penetrate tissues largely depends on the nature of the capillaries involved: organs with tight capillary junctions pose significant barriers, whereas discontinuous capillaries, such as those found in

the liver or within tumor vasculature, permit easier passage (Ranasinghe et al. 2023). This explains why siRNA often accumulate preferentially in the liver or tumor sites, where vascular permeability is higher. Consequently, the liver has emerged as the most common target organ for successful siRNA-based therapies (Ebenezer et al. 2025; Ranasinghe et al. 2023; Yasuda et al. 2023).

4.3.3. How to develop an optimal siRNA for efficient silencing without side effects

Developing an optimal siRNA requires balancing efficiency, specificity, and safety. An ideal siRNA must effectively silence its target without activating the innate immune system, causing off-target effects or exhibiting toxicity (Friedrich and Aigner 2022; Ozcan et al. 2015).

Firstly, the GC content should be between 30% and 60%, as low GC content risks weak binding, while excessive GC hinders dsRNA fragment unwinding and RISC incorporation (Khvorova and Watts 2017).

Position-specific nucleotide preferences also improve siRNA efficacy. Efficient siRNA tend to have more A/U bases at the 5’-end of the antisense strand and more G/C bases at the 5’-end of the sense strand, favoring correct antisense loading into RISC and reducing off-target-effects (Ozcan et al. 2015).

To avoid off-target effects and immune activation, siRNA sequences must exclude secondary structures, repeats, palindromes and long siRNA (>24 pb) (Friedrich and Aigner 2022).

Target site selection is equally crucial. Regulatory elements or highly structured regions, such as 5’- and 3’-untranslated region or sequences near the start codon, can interfere with RISC binding (Friedrich and Aigner 2022).

Chemical modifications have emerged as key strategies to enhance siRNA performance. Modifications such as phosphorothioate linkages at the 3’ end, 2’-O-methylation, 2’-fluoro, and 2’-deoxy homologs, or incorporation of locked nucleic acids can stabilize siRNA duplexes (Ebenezer et al. 2025; Fakhr et al. 2016). These techniques can significantly improve siRNA stability against nucleases, reduce immunogenicity, and diminish off-target interactions without compromising the silencing efficacy of the guide strand. Moreover, maintaining a free 5’-phosphate or hydroxyl group on the antisense strand is crucial for RISC recognition (Fakhr et al. 2016; Hu et al. 2020).

Finally, free bioinformatics tools can help to find good siRNA candidates (e.g., RNAxs web tool, http://rna.tbi.univie.ac.at/cgi-bin/RNAxs/RNAxs.cgi) (Fakhr et al. 2016).

4.4. siRNA therapeutics and their challenges

4.4.1. Food and Drug Administration-approved siRNA drugs

The clinical landscape of siRNA therapeutics has advanced over the past few years, with six siRNA-based drugs now approved by the U.S. FDA (**Table 5**). The following therapies exemplify the advancements in the design and delivery of siRNA, which are intended to address distinct genetic or metabolic disorders (Ebenezer et al. 2025). These drugs use chemical modifications such as 2'-O-methylation and phosphorothioate linkages to enhance stability, reduce immunogenicity, and improve the pharmacokinetics of siRNA (Friedrich and Aigner 2022; Hu et al. 2020).

Moreover, a common feature among these approved drugs is their hepatic tropism. Although the first therapeutic siRNA involved siRNA encapsulation in lipid nanoparticles (LNP), most of the FDA-approved siRNA employ a GalNAc (N-acetylgalactosamine) conjugation strategy, where the siRNA is covalently linked to a triantennary $GalNAc_3$ moiety at the 3' end of the sense strand. These conjugates enable targeted delivery of siRNA specifically to hepatocytes since GalNAc is a sugar ligand that binds with high affinity to the asialoglycoprotein receptor, a receptor highly expressed on hepatocytes. This receptor-mediated endocytosis pathway allows efficient and selective uptake of siRNA into the liver following subcutaneous injection, without the need for more complex delivery vehicles (Friedrich and Aigner 2022).

Despite these achievements, current siRNA drugs are largely restricted to liver and circulatory system diseases due to the lack of broadly applicable delivery systems for tissues beyond the liver. As a result, many potential therapeutic applications of siRNA remain untapped. Nevertheless, the pipeline continues to grow, with more than 60 siRNA drugs currently in clinical trials for diverse indications including oncology, fibrosis, infectious diseases, and neurological disorders (Ebenezer et al. 2025; Friedrich and Aigner 2022; Mahmoodi Chalbatani et al. 2019; Ranasinghe et al. 2023).

Table 5: FDA-approved siRNA therapeutics.

Drug name	Target molecule	Disease	Year of FDA approval	Delivery system (vectorization)	Route of administration	Reference
Patisiran	Transthyretin (TTR)	Hereditary ATTR amyloidosis	2018	Lipid nanoparticles (LNP)	Intravenous infusion (IV)	(Adams et al. 2018)
Givosiran	ALAS1	Acute hepatic porphyria	2019	GalNAc conjugate	Subcutaneous injection (SC)	(Scott 2020)
Lumasiran	Glycolate oxidase (GO)	Primary hyperoxaluria type 1	2020			(Scott and Keam 2021)
Inclisiran	PCSK9	Hypercholesterolemia	2021			(Lamb 2021)
Vutrisiran	Transthyretin (TTR)	Hereditary ATTR amyloidosis	2022			(Keam 2022)
Nedosiran	LDHA	Primary hyperoxaluria type 1	2023			(Syed 2023)

Footnote: This table summarizes the six siRNA drugs approved by the FDA, specifying their molecular targets, clinical indications, year of approval, delivery platforms, and routes of administration.

GalNAc refers to N-acetylgalactosamine conjugation, which enables targeted delivery to hepatocytes via the asialoglycoprotein receptor. Patisiran is unique among these drugs for using lipid nanoparticles as its delivery system; all others employ GalNAc conjugation for vectorization.

4.4.2. siRNA as cancer therapy

The therapeutic application of siRNA in cancer treatment has been explored over the past two decades, supported by its ability to specifically inhibit oncogenic drivers and that support tumor growth, cell survival, angiogenesis, and metastasis in tumors (Singh et al. 2025). For example, in preclinical mouse studies, the silencing of VEGF and VEGFR has been used to block angiogenesis, the targeting of KRAS or PLK1 (polo-like kinase 1) has been used to impact tumor cell survival directly, and BCL-2 has been targeted to enhance apoptosis (Liu et al. 2025). These

preclinical studies have provided a solid basis for the clinical translation of siRNA as an anti-cancer therapy.

Several siRNA-based therapeutics have since entered early-phase clinical trials, providing proof-of-concept for RNAi in cancer patients. Concerning pancreatic adenocarcinoma, ATU027 has reached Phase II (Liu et al. 2025; Singh et al. 2025). It is a siRNA-loaded lipid nanoparticle targeting protein kinase N3 (PKN3), a PI3K-Rho-family GTPases axis effector linked to tumor invasion and metastatic spread. After a favorable first-in-human safety experience in advanced solid tumors (NCT00938574), phase II combined ATU027 with gemcitabine (NCT01808638) and reported significantly prolonged progression-free survival in metastatic disease, supporting continued evaluation of vascular-targeted RNAi in pancreatic cancer (Aleku et al. 2008; Schultheis et al. 2020). Another siRNA therapeutic developed for pancreatic cancer is siG12D-LODER (Local Drug EluteR), a local prolonged siRNA delivery system targeting mutated *KRAS* (Liu et al. 2025; Singh et al. 2025). This drug showed a favorable safety profile without dose-limiting toxicities and disease control in combination with chemotherapy in phase I (NCT01188785). The phase II study (NCT01676259) was initiated in 2017 and tested repeated siG12D-LODER dosing with chemotherapy *versus* chemotherapy alone, but results have not published yet (Golan et al. 2015). In prostate cancer, siRNA EphA2-DOPC (EPHARNA), a neutral liposomal formulation targeting the EphA2 receptor frequently overexpressed in epithelial tumors, has advanced to a first-in-human phase I trial (NCT01591356) following robust preclinical tumor growth inhibition and anti-angiogenic activity (Landen et al. 2005; Wagner et al. 2017). A selection of representative siRNA candidates evaluated in oncology is summarized in **Table 6**.

These trials highlight both the therapeutic promise of RNAi and the persistent challenges to its clinical translation. They encompass a diverse set of targets, such as endothelial PKN3, cell cycle kinase PLK1, receptor EphA2, and enzymes such as RRM2, as well as different delivery strategies, ranging from intravenous administration of LNP formulations to intratumoral injection. Although no siRNA anticancer therapy has yet received regulatory approval, the numerous clinical trials reinforce the view of RNAi as a versatile and precision-oriented therapeutic approach in oncology (Ebenezer et al. 2025; Liu et al. 2025; Redhwan et al. 2023; Singh et al. 2025).

Table 6: siRNA-based therapeutics investigated in oncology clinical trials (non-exhaustive list).

Drug name / Candidate	Target molecule	Cancer type	Delivery system (vectorization)	Trial phase / status	Reference
ATU027	PKN3	Advanced solid tumors, pancreatic adenocarcinoma	Cationinc liposomal formulation (Atuplex® LNP)	Phase I/II; favorable safety, preliminary efficacy	(Aleku et al. 2008; Schultheis et al. 2020)
siG12D-LODER	KRAS G12D	Pancreas cancer	Polymeric nanoparticles (LODER)	Phase I/II	(Golan et al. 2015)
siRNA-EphA2-DOPC	EphA2	prostate cancer	Neutral liposomal DOPC nanoparticles	Phase I – good tolerability, biomarker knockdown	(Wagner et al. 2017)
CALAA-01	RRM2	Solid tumors (e.g., melanoma)	Cyclodextrin-based polymer nanoparticles	Phase I; first targeted siRNA in humans, discontinued due to PK/safety	(Zuckerman et al. 2014)
TKM-080301 (TKM-PLK1)	PLK1	Hepatocellular carcinoma, neuroendocrine tumors, refractory solid tumors	Lipid nanoparticles (LNP)	Phase I/II; target engagement, limited efficacy	(El Dika et al. 2019)
DCR-MYC	MYC	Solid tumors, multiple myeloma, or lymphoma	LNP	Phase I; well tolerated and showed promising initial promising responses	(Tolcher et al. 2015)

According to Singh et al., 2025.

4.4.3. Delivery challenges

As we saw before, one of the most significant challenges limiting the broader application of siRNA therapeutics remains efficient and tissue-specific delivery other than the liver. To overcome these challenges, numerous delivery systems are under investigation (Dowdy 2017). However, given that, among all smRNA molecules, only shRNA can be vectorized by viruses, the subsequent section will center on non-viral delivery systems (**Figure 31**).

Lipid nanoparticles (LNP) were already used in the FDA-approved siRNA drug *Patisiran* (Onpattro®, 2018), and in mRNA vaccines (notably mRNA-based COVID-19 vaccines such as

BNT162b2 (Comirnaty®, Pfizer-BioNTech) and *mRNA-1273* (Spikevax®, Moderna) (Baden et al. 2021; Polack et al. 2020). This delivery system allows the encapsulation of unmodified siRNA, thereby allowing higher protection from nuclease degradation. Other synthetic nanoparticles can also be used (Dowdy 2017).

Polymeric systems, including polyethyleneimine and dendrimers, provide strong siRNA binding but require optimization to minimize cytotoxicity.

More recently, CPP have emerged as promising carriers, also because they can form peptide-based nanoparticles (PBN) (Hammond et al. 2021). However, achieving precise tissue specificity while minimizing off-target effects and immunogenicity remains a central challenge in siRNA drug development whatever the delivery system (Dowdy 2017; Hu et al. 2020; Ranasinghe et al. 2023).

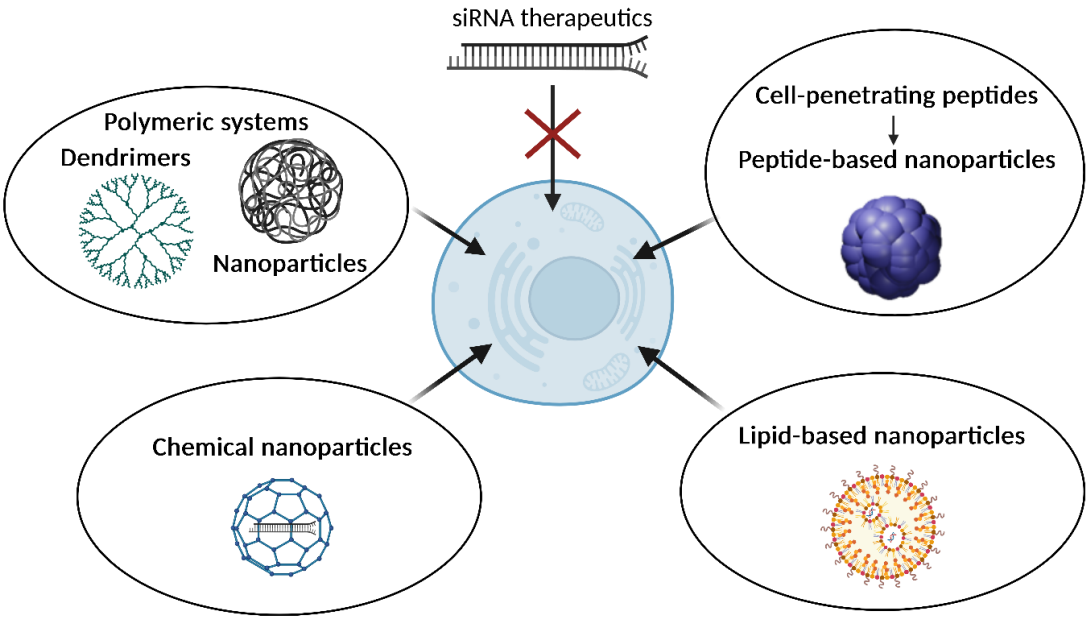

Figure 31: Examples of siRNA delivery systems
Beside others, the most common siRNA delivery systems used polymeric, chemical, peptide-based or lipid-based nanoparticles.
Homemade figure.

4.5. Cell-Penetrating Peptides for cellular siRNA delivery

4.5.1. A brief presentation of cell-penetrating peptides

Among the various strategies explored to facilitate cytoplasmic delivery of nucleic acids, CPP have attracted increasing attention due to their versatility, biocompatibility, and capacity to promote cellular uptake through non-invasive mechanisms (Bottens and Yamada 2022).

INTRODUCTION

CPP are short peptides, typically comprising 5 to 30 amino acids, amphipathic or cationic, often derived from viral proteins or designed synthetically to enhance membrane interaction (Habault and Poyet 2019). They are capable of translocating across biological membranes and facilitate intracellular transport of a broad range of cargoes, including antibodies, peptides, or nucleic acids such as plasmids and smRNA (Bottens and Yamada 2022; Habault and Poyet 2019; Shoari et al. 2021). One of the earliest and most studied CPP is the TAT peptide, derived from the HIV-1 transactivator of transcription protein, which demonstrated the feasibility of peptide-mediated intracellular delivery (Vivès et al. 1997). Around the same time, another CPP, Penetratin, derived from the Antennapedia homeodomain of *Drosophila*, was shown to facilitate cellular uptake of various cargoes (Derossi D et al. 1998; Peck and Isacke 1998). Since then, a wide variety of CPP have been developed or engineered to improve delivery efficiency, reduce toxicity, and enhance selectivity (Bottens and Yamada 2022).

CPP have been extensively studied as transfection agents, with hundreds of studies attempting to elucidate their mechanisms of cellular uptake (Okafor et al. 2025; Ruseska and Zimmer 2020). It is now widely accepted that endocytosis-dependent pathways represent the principal mode of CPP internalization. These include macropinocytosis, clathrin-mediated, and caveolin-mediated endocytosis, which often result in the entrapment of CPP-cargo complexes in endosomal compartments and limit their bioavailability in the cytoplasm (Deshayes et al. 2020; Klipp et al. 2023; Xu et al. 2019). Interestingly, direct membrane translocation has also been reported under certain conditions, particularly at high CPP concentrations, although this mechanism is considered less prevalent (Brock 2014; Tünnemann et al. 2008).

To improve the efficiency of intracellular delivery, modern CPP designs increasingly incorporate features that enhance endosomal escape, a key point for functional siRNA activity. Modifications such as histidine-rich motifs, pH-sensitive domains, or membrane-disruptive sequences have been used to promote cytosolic release (Klipp et al. 2023). Moreover, structural refinement, especially the promotion of α-helical secondary structures, has been shown to significantly improve membrane interaction and delivery efficiency (McCarthy et al. 2014; Wickline et al. 2023).

4.5.2. Covalent CPP to deliver cargoes

These peptides can be broadly classified into cationic, amphipathic, and hydrophobic groups based on their amino acid composition and structure (Lindgren and Langel 2011). The positive charge density, mainly due to arginine and lysine residues, enables CPP to electrostatically interact with negatively charged molecules such as siRNA and cell membranes, facilitating cellular uptake (Ellert-Miklaszewska et al. 2017). In covalent CPP-siRNA conjugates (**Figure 32**), the direct linkage may neutralize the positive charges of CPP (theoretically one CPP for one siRNA), thereby reducing its ability to interact with the cell membrane and to promote uptake (Meade and Dowdy 2007). To address this limitation, cleavable linkers sensitive to intracellular conditions, such as disulfide bonds or enzyme-cleavable sequences, are often employed to release the siRNA once inside the cell, restoring CPP functionality (Juliano 2016; Sohrabi et al. 2016). Covalent conjugation strategies have been especially explored with charge-neutral oligonucleotides such as peptide nucleic acids (PNA) and phosphorodiamidate morpholino oligomers (PMO), which do not mask the cationic properties of CPP (Betts et al. 1995; Lebleu et al. 2008).

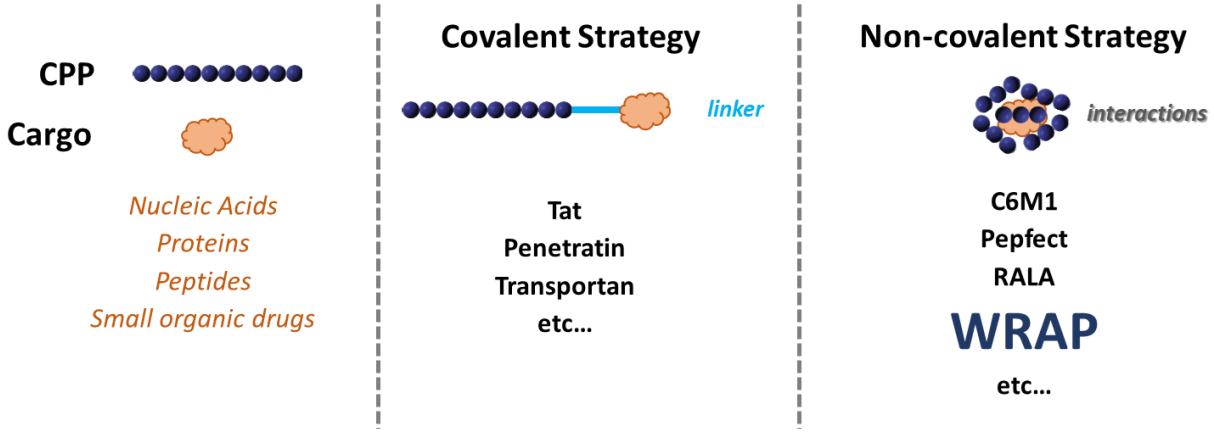

Figure 32: Overview of different Cell-Penetrating Peptides (CPP) (non-exhaustive examples).

Covalent-CPP have been widely studied in preclinical models, particularly in the context of oncology, neurodegeneration, and genetic disorders. For instance, TAT- or Penetratin-fused proteins and nucleic acids have been shown to cross cellular membranes and even the blood-brain barrier, facilitating targeted delivery of therapeutic enzymes, siRNAs, or gene-editing components (Guidotti et al. 2017). Despite their potential, issues such as off-target effects, endosomal entrapment, and immunogenicity remain significant hurdles to clinical translation. Nevertheless, covalent CPP systems continue to be refined and represent a versatile field for addressing intracellular delivery challenges.

4.5.3. From non-covalent CPP to peptide-based nanoparticles

The first reports on the use of non-covalent CPP for the delivery of nucleic acids were published in the late 1990s, with the short amphipathic peptides MPG (Morris et al. 1997) and KALA (Wyman et al. 1997). Later, CPP have been developed to form PBN capable of protecting siRNA by non-covalent interactions, improving serum stability, and enhancing biodistribution (Wickline et al. 2023). In non-covalent complexes (**Figure 32**), CPP (in larger quantity) condense siRNA through interactions such as electrostatic binding, hydrophobic assembly, or π-π stacking, forming nanoparticles where the overall positive surface charge remains available for membrane interaction and internalization (Bechara and Sagan 2013). Moreover, when siRNA are incorporated into PBN, the ratio of CPP to siRNA can be adjusted to maintain an overall positive surface charge, enhancing delivery efficiency without relying on 1:1 stoichiometry (Bechara and Sagan 2013) (**Figure 32**). In this way, amphipathic peptides can organize into particles that condense siRNA into core-shell-like architectures, shielding them from nucleases and phagocytic clearance (McCarthy et al. 2014; Tarvirdipour et al. 2020). In this way, PBN function analogously to LNP but with added biological flexibility and reduced toxicity (McCarthy et al. 2014; Shoari et al. 2021).

In parallel, the therapeutic landscape has expanded beyond simple delivery. Several CPP have been engineered to include tumor-targeting motifs or therapeutic activity themselves, such as inhibition of oncogenic signaling pathways, thus acting as dual-function agents (Bottens and Yamada 2022; Shoari et al. 2021). Notably, amphipathic CPP, such as RALA (McCarthy et al. 2014) or PepFect (Ezzat et al. 2011) variants, have shown promise for nucleic acid delivery, thanks to their ability to self-assemble into complexes with siRNA and to induce endosomal escape (Lehto et al. 2016). In 2023, the first clinically non-covalent CPP-containing product was even approved by the FDA: DAXXIFY™ (Revance Therapeutics, Inc.). It is a botulinum toxin type A formulation containing the peptide excipient RTP004. This synthetic, positively charged, lysine- and arginine-rich CPP binds noncovalently to the neurotoxin and enhances cellular uptake, prevents protein aggregation, stabilizes the formulation, improves presynaptic binding, and increases the intracellular activity of the neurotoxin (Dowdy et al. 2023).

Still, the broader clinical translation of these CPP was not achieved, a lack of tissue specificity, variable *in vivo* stability, and the risk of off-target effects through nonspecific membrane

interactions. To address these concerns, researchers are increasingly designing hybrid systems, where CPP are functionalized with targeting ligands (tumor-homing peptides, antibodies) or integrated into multicomponent nanoparticles with lipids, polymers, or inorganic scaffolds (Tarvirdipour et al. 2020; Wickline et al. 2023).

Among the newest and most promising CPP delivery systems are those that employ highly structured amphipathic peptides capable of forming stable PBN with siRNA. These delivery systems are designed to imitate how natural proteins interact with cell membranes (in terms of charges). As a result, they show improved delivery efficiency and better ability to escape from endosomes after cellular uptake. One such innovative class is the "WRAP" family, which will be explored in detail in the next section. These peptides represent a significant advance in the field of peptide-mediated delivery and open new possibilities for extrahepatic gene silencing therapies (Boisguérin et al. 2021).

4.6. WRAP5 as a delivery tool for siRNA-based gene silencing

In this context, a novel family of amphipathic peptides termed **WRAP**, for tryptophan (**W**) and arginine (**R**) rich **A**mphipathic **P**eptides, has emerged as a powerful tool for siRNA delivery (Patent PCT/EP2019/069149).

4.6.1. Characteristics of the WRAP family

WRAP are short (15/16 mer) amphipathic peptides only composed of three residues: tryptophan (aromatic), arginine (hydrophilic), and leucine (hydrophobic). Developed by our group in 2019, more than 15 different WRAP sequences were screened, resulting in two lead compounds: WRAP1 and WRAP5 (**Table 7**).

Table 7: Two main WRAP sequences (Konate et al., 2019).

ID	Sequences	AA	Charges	W
WRAP1	LLWRLWRLLWRLWRLL	16	5	4
WRAP5	LLRLLRWWWRLLRLL	16	5	3

The acronym "WRAP" reflects both their physicochemical properties (W/R-rich content, amphipathicity) and their ability to wrap around siRNA through electrostatic and hydrophobic interactions (Konate et al. 2019). Notably, tryptophan residues contribute not only to the hydrophobic interactions but also display a strong propensity to intercalate into the minor

grooves of double-stranded DNA or RNA, further stabilizing the PBN. These characteristics allows WRAP to bind negatively charged siRNA, resulting in the spontaneous formation of compact and stable PBN (non-covalent complexes) that facilitate their cellular uptake (**Figure 33A**).

WRAP spontaneously condense siRNA into nanoparticles with a mean size of around 100 nm in diameter (**Figure 33B**) (Konate et al. 2021). Moreover, transmission electron microscopy images show the nanoparticles to be globular in shape, like a blackberry (**Figure 33C**) (Konate et al. 2019).

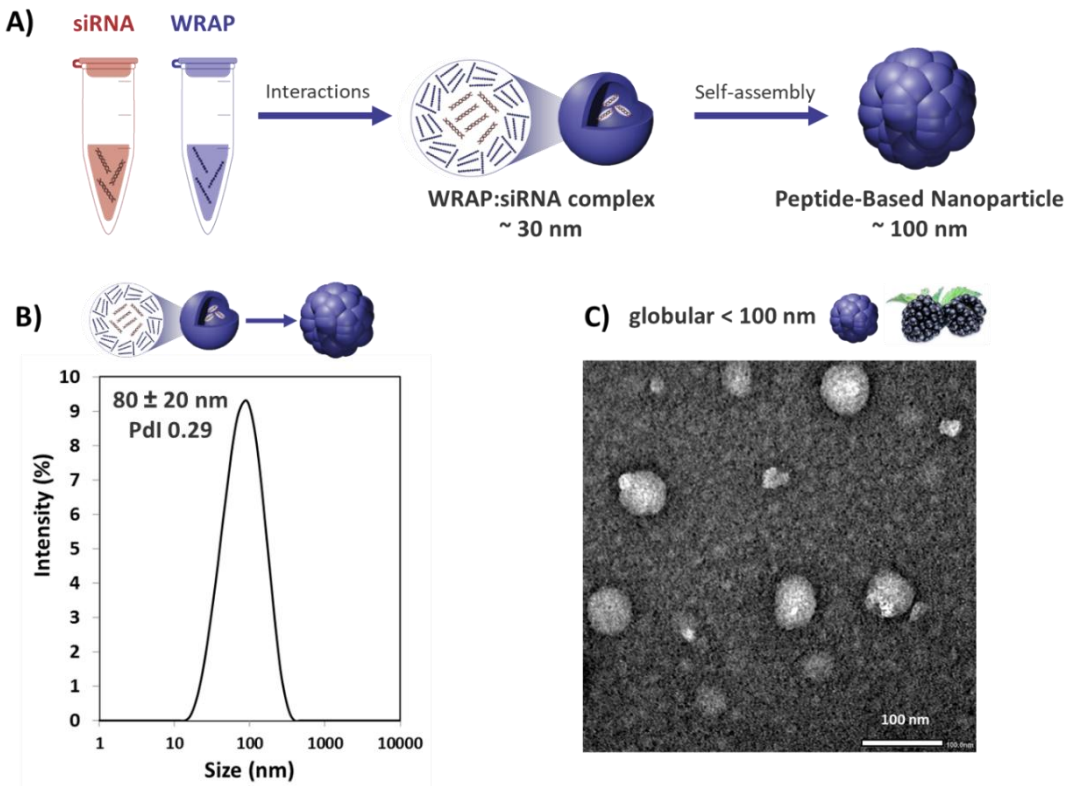

Figure 33: WRAP-based nanoparticles characteristics.

A) Schematic nanoparticles formation. **B**) WRAP mean size measured by dynamic lightning scattering. **C**) Transmission electron microscopy image showing a mainly globular form, like a blackberry, of the WRAP5:siRNA nanoparticles.

Adapted from Konate et al., 2019; Boisguérin et al., 2021.

To obtain more specific PBN, WRAP can also be chemically modified to enhance resistance to proteases (PEGylation with PEG as polyethylene glycol), to respond to specific microenvironmental triggers, or to obtain a more precise tissue-targeting (see also section 4.6.4 for more details) (Di Gregorio et al. 2025; Faria et al. 2024; Neves et al. 2022; Teko-Agbo et al. 2025).

4.6.2. The internalization mechanism of WRAP-based nanoparticles

WRAP:siRNA nanoparticles have favorable colloidal stability and surface properties, such as a slightly positive zeta potential, which supports close interaction with the negatively charged cell surface and then the entrance into cells (Deshayes et al. 2020; Konate et al. 2019). Internalization mechanisms of WRAP-based nanoparticles involve two types of mechanisms with evidence indicating that both routes can operate in parallel depending on factors such as peptide concentration, charge, and cargo size (Deshayes et al. 2020). The first is endocytosis-based uptake (**Figure 34A**), and the second corresponds to the direct translocation through the plasma membrane.

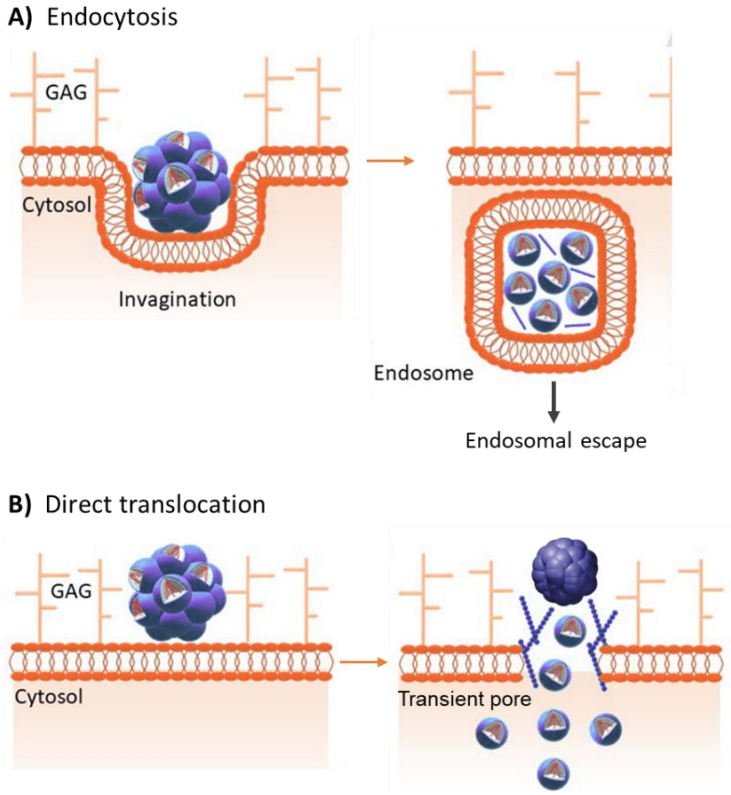

Figure 34: Mechanism of WRAP:siRNA nanoparticles cellular internalization.
Schematic representation of the two ways of WRAP:siRNA internalization by endocytosis (**A**) and direct translocation (**B**).
Abbreviation: GAG: Glycosaminoglycans. Adapted from Boisguerin et al., 2021.

Importantly, WRAP-based nanoparticles remain active at 4 °C or under ATP depletion, strongly supporting the occurrence of direct membrane translocation. This mechanism was further confirmed using cells in which all three isoforms of dynamin, key GTPases required for the endocytosis pathway, were chemically knocked out. In this dynamin triple KO model, where all classical endocytic pathways are blocked, siRNA delivery by WRAP still occurred efficiently, providing strong evidence that it is direct membrane translocation, an endocytosis-

independent route of cellular entry (Deshayes et al. 2020). Direct membrane translocation could occur through transient pore-like structure formation upon contact of the nanoparticle with the membrane as evidence by biophysical experiments previously (Deshayes et al. 2004) (**Figure 34B**).

Nevertheless, it remains challenging to define a single predominant uptake pathway, as endocytosis is a constitutive process at the cell surface and may also contribute to nanoparticle internalization (Deshayes et al. 2020; 2022). Crucially, the ability of WRAP peptides to directly translocate across cell membranes represents a significant advantage for therapeutic applications, as it bypasses the reliance on endosomal escape, a well-known limitation of LNP, which predominantly enter cells via endocytosis (Konate et al. 2021). Biophysical assays, including fluorescent leakage studies, have shown that WRAP transiently destabilize lipid bilayers, facilitating cytosolic delivery of the siRNA payload either via direct penetration or rapid endosomal escape following endocytic uptake (Deshayes et al. 2020; 2022; Konate et al. 2021).

4.6.3. WRAP5-based nanoparticles siRNA delivery

Among this family of non-covalent CPP, WRAP5 has emerged as an effective system for siRNA delivery. Specifically optimized for this purpose, WRAP5 exhibits a high degree of efficiency and reproducibility in gene silencing applications (Boisguérin et al. 2021). The formulation is based on an optimal peptide-to-siRNA molar ratio of 20:1, which has been shown to ensure maximal condensation, cellular uptake, and biological activity *in vitro*. Moreover, comparatively to conventional transfection agents (non-peptides), WRAP5-based siRNA delivery systems not only achieve equivalent levels of gene silencing efficiency but also exhibit significantly lower cytotoxicity, as demonstrated by clonogenic assays (Konate et al. 2021), making them a safer alternative for therapeutic applications. Although WRAP5 has shown potential for the delivery of other nucleic acids, such as plasmid DNA and mRNA, its highest performance and optimization remain in siRNA delivery (Faria et al. 2024; Neves et al. 2022; Teko-Agbo et al. 2025). This specialization, combined with demonstrated *in vitro* and *in vivo* efficacy, positions WRAP5 as a leading PBN delivery system for siRNA-based therapeutic strategies. Several *in vitro* studies have demonstrated the broad applicability of WRAP5:siRNA nanoparticles across different human and murine cell lines, including U87 (glioblastoma), MCF7 (breast cancer), HT29 (colorectal cancer), Neuro2a (neuroblastoma), EA.hy296 (human

vascular endothelial cells), hiPSC-derived cardiomyocytes, and GIST-T1, among others (Boisguérin et al. 2021; Di Gregorio et al. 2025; Konate et al. 2021; Konate, Pezzati, et al. 2025). For each cell line, optimization concerning siRNA concentration, evaluation of cytotoxicity and biological application were carried out. These results confirm the versatility and robustness of the WRAP5 system across various cellular contexts and disease models (Boisguérin et al. 2021).

The therapeutic relevance of WRAP5-mediated siRNA delivery has also been validated in zebrafish embryos (Konate, Teko-Agbo, et al. 2025) and *in vivo* (Ferreiro et al. 2021). A key study demonstrated successful gene silencing in a glioblastoma mouse model following systemic administration of WRAP5:siRNA nanoparticles, highlighting their ability to achieve functional delivery and gene knockdown in a complex tumor microenvironment (Ferreiro et al. 2021).

4.6.4. Optimizing to "smart" WRAP5 PBN for siRNA delivery

Ongoing optimization aims to further improve WRAP5-based nanoparticle efficiency, specificity, and suitability for therapeutic applications.

In one hand, the accessible surface area of the nanoparticles can be improved through chemical peptide grafting strategies (**Figure 35A**). The first optimization strategy involved the grafting of a PEG onto the nanoparticles (independently of their composition) to increase their stability and circulation time *in vivo* (Suk et al. 2016). However, the design of the PEG layer (its length, density, and conformation) is critical as 100% PEGylation severely impaired siRNA internalization and gene silencing, likely due to steric hindrance inhibiting cell entry (Aldrian et al. 2017). In response to acidic microenvironments such as those found in ischemic tissues or tumors, pH-sensitive PEG linkers were designed and added between the PEG moiety and the nanoparticle. These pH-cleavable PEGylated WRAP5 displayed dual behavior: under neutral pH, full PEGylation blocked transfection efficiency, as expected. But in acidic conditions, such as those mimicking myocardial infarction, PEG detachment restored the transfection capability. Our team has exemplified this using the WRAP nanoparticle. This pH-sensitive modification resulted in enhanced siRNA delivery and gene knockdown, whereas naked WRAP5 lost efficacy entirely (Di Gregorio et al. 2025). To target tumor cells, the strategy was also to graft an RGD (Arg-Gly-Asp) motif onto the WRAP5 sequence to target integrin

receptors commonly overexpressed (*unpublished data*). Finally, multi-grafted nanoparticles (containing a mixture of naked, RGD-, and PEG-modified WRAP5 peptides) successfully retained silencing efficacy comparable to 100% native WRAP5, while offering improved biocompatibility and targeting potential (*unpublished data*).

On the other hand, the core of the nanoparticles can be optimized by adapting and diversifying the siRNA cargo (**Figure 35B**). A proof-of-concept study was recently conducted to evaluate the capacity of a single nanoparticle to deliver multiple siRNA simultaneously (Konate, Pezzati, et al. 2025). Using fluorescence microscopy, we confirmed the co-internalization of three distinct siRNA in the same cells, each labeled with a different fluorophore, compared to the control conditions without signal detection. Furthermore, functional assays showed effective gene silencing of the 3 targeted protein (CD1, CDK4, and MCL-1) in at least two different cell lines, validating the feasibility of multiple gene knockdown using WRAP5 (Konate, Pezzati, et al. 2025). This strategy opens the door to combinatorial therapies targeting multiple disease pathways.

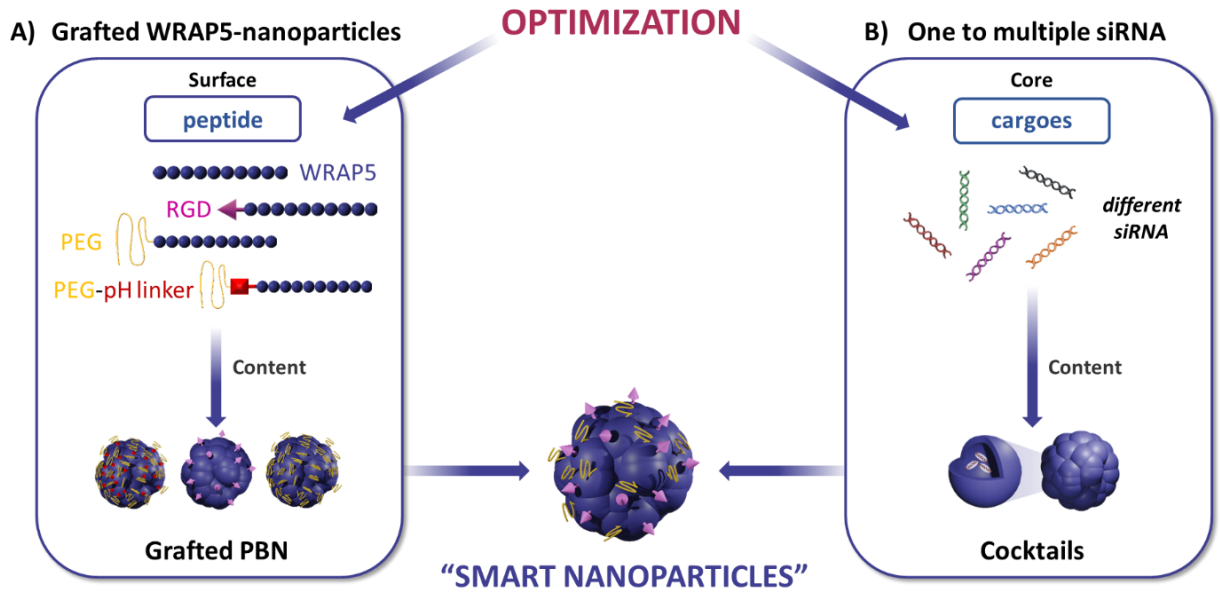

Figure 35: Overview of WRAP5 optimization to develop "smart" WRAP5 nanoparticles.
Engineering can be performed on the surface of the nanoparticle by grafting WRAP5 (**A**) or in the core to encapsulate multiple siRNA (**B**).
Abbreviations: WRAP5: W- and R- Amphipathic Peptide 5, RGD: Arg-Gly-Asp, PEG: polyethylene glycol, siRNA: small interfering RNA. Homemade figure.

In conclusion, optimizing WRAP5 nanoparticles, from the surface or the core, leads to "smart" PBN. These findings support the potential of WRAP5 functionalization for condition-specific therapeutic strategies.

THESIS OBJECTIVES

THESIS OBJECTIVES

Building on this substantial introduction and in light of current knowledge on GIST pathogenesis and resistance, the next step is to outline and contextualize the objectives of this thesis.

Previous work from our group identified LIX1 as a regulator of GIST cellular plasticity and a contributor to adaptation under KIT inhibition, notably through upstream modulation of the Hippo signaling pathway. In this context, the transcriptional co-activators YAP1 and TAZ, downstream effectors of Hippo signaling, emerged as potential mediators of LIX1-driven effects. Their growing roles in tumorigenesis in general, or in GIST, make them promising targets to bypass drug resistance and limit disease progression. Yet, their respective and distinct contributions to GIST biology remain poorly defined. This is partly due to their high structural similarities, overlapping transcriptional programs, which often lead to their consideration as a single functional unit.

Accordingly, the central aim of this thesis is to decipher the individual and combined contributions of YAP1 and TAZ in GIST biology and therapeutic resistance.

To this end, a targeted RNAi strategy will be employed, combining siRNA molecules that specifically bind to the mRNA of interest (i.e., YAP1 or TAZ) with a novel delivery system. This system, known as WRAP5, has been optimized for efficient and non-toxic nucleic acid delivery *in vitro* with promising *in vivo* applications.

This research will be structured around three main objectives, each corresponding to a dedicated results chapter:

1) **To validate WRAP5-based nanoparticles as a siRNA delivery system in GIST for multi-protein silencing**

In a first step, we will validate the use of WRAP5 nanoparticles in the GIST-T1 cell line by assessing siRNA delivery efficiency, intracellular trafficking, and cytotoxicity. This work will confirm their suitability for functional gene silencing in this sarcoma model. Importantly, this system will give us the opportunity to simultaneously silence multiple genes, exemplified by CDK4, CD1, and MCL-1, highlighting its potential for combinatorial therapeutic strategies.

2) To dissect the individual roles of YAP1 and TAZ in GIST tumor biology

Building on the established WRAP5 nanoparticles loaded with multiple siRNA as an efficient tool in GIST cells, we will selectively silence YAP1, TAZ, or both in three different IM-sensitive GIST cell lines. We will evaluate phenotypic changes in proliferation and migration, and will determine canonical downstream targets. Finally, we will correlate the association of YAP1 and TAZ overexpression (and for the identified downstream targets) with progression-free survival and metastatic status in GIST patient datasets. These analyses will provide insights into the relative contributions of each protein during early GIST development.

3) To investigate the role of YAP1 and TAZ in IM-resistant GIST cells

The final objective of our study will be to explore the influence of silencing YAP1 and/or TAZ in relation to cellular adaptation to IM exposure. Thanks to our collaborator Dr. César Serrano (VHIO, Barcelona), we will have access to three IM-resistant GIST cell lines and will be able to assess their respective levels of YAP1 and TAZ protein expression. Then, we will evaluate the silencing of these two proteins in the different IM-resistant GIST cells. We will perform time-course analyses and IC_{50} determinations using the GIST-T1 cell line to assess the potential role of these targets in TKI resistance.

Achieving these objectives will advance our understanding of GIST development and allow us to propose novel perspectives for combinatorial strategies to overcome TKI resistance.

RESULTS

Chapter 1: Multi-siRNA delivery using WRAP5-based nanoparticles in GIST cells

Chapter 2: Studying individual roles of YAP1 and TAZ in GIST tumor biology

Chapter 3: YAP1 and TAZ: playing around with IM resistance?

CHAPTER 1: Multi-siRNA delivery using WRAP5-based nanoparticles in GIST cells

This work has been published as:

Konate K*, **Pezzati I***, et al. Multiprotein Silencing Using WRAP-Based Nanoparticles: A Proof of Concept. Bioconjug Chem. 2025;36(6):1218–1233. doi:10.1021/acs.bioconjchem.5c00069 .

* equal contributions

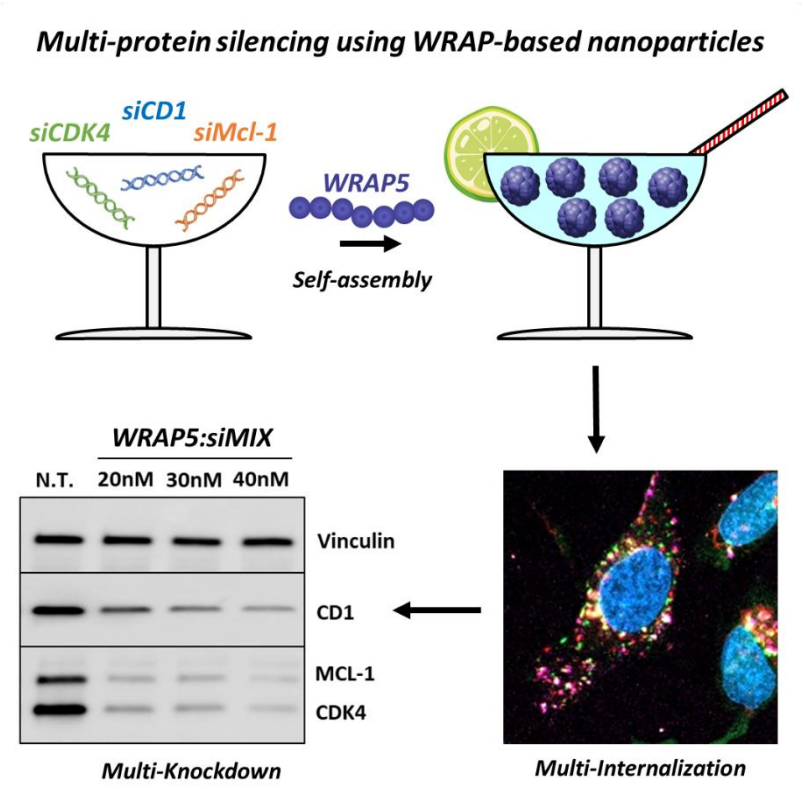

CHAPTER 1

1. Structured summary

1.1. Introduction

The WRAP5-based nanoparticle was developed by our team as siRNA delivery system in various cell types, with the most extensive validation carried out in human U87 glioblastoma cells *in vitro* and *in vivo* (Ferreiro et al. 2021; Konate et al. 2019). Previous work demonstrated the ability of WRAP5:siRNA nanoparticles to downregulate one protein, exogenous (overexpressed luciferase) or endogenous (Cyclin-dependent kinase 4, CDK4) (Konate et al. 2019; 2021). Despite the success of the silencing process, the targeting of a single protein within glioblastoma cells did not result in significant alterations in phenotype. This is likely due to the functional redundancy of oncogenic pathways, particularly within the cell cycle, where several proteins can compensate for the loss of a single player (e.g., CDK6 for CDK4).

Based on these findings, we hypothesized that optimizing the core of the WRAP5-based nanoparticle by encapsulating one to multiple siRNA could be particularly relevant for achieving multi-silencing and phenotypic impact. For this proof-of-concept, we chose proteins involved in cell cycle regulation and apoptosis resistance. We initially evaluated this approach in the U87 glioblastoma cell line. To further strengthen the study, explore the potential translational relevance, and test this approach in a different tumor type, we included the GIST-T1 cell line as a complementary model. The present section focuses on this last aspect, evaluating the ability of WRAP5-based nanoparticles to co-deliver multiple siRNA for the simultaneous inhibition of several proteins in GIST cells.

1.2. Methods

Three siRNA sequences targeting different proteins were selected. Two of them targeted proteins involved in cell cycle progression: CDK4, a regulator of the G1 to S phase transition, and CD1, the principal activator of CDK4. The third targeted MCL-1, an anti-apoptotic protein member of the BCL-2 family. These three proteins are all frequently upregulated in tumors.

Each siRNA was individually delivered thanks to WRAP5-based nanoparticles, following established protocols described for U87 cells.

For the multi-silencing experiments, we first assessed whether the three siRNA could be internalized into the same cell by confocal microscopy. We used three fluorescence-labeled siRNA: siCDK4-Alexa488, siCD1-Atto550, and MCL-1-Atto654.

Next, to evaluate protein knockdown efficiency by Western blot, the three siRNA were mixed before nanoparticle formation at different molar ratios of 3/14/3 and 4/12/4, then 5/10/5 and 6/8/6 for siCD1, siCDK4, and siMcl-1, respectively. These ratios were adapted from experiments conducted on the U87 cell line, based on comparison of the basal protein expression between the two cell lines and individual silencing results. The resulting formulations, referred to as siMIX, were used to transfect GIST-T1 cells under the same culture conditions as U87 cells. Cytotoxicity was assessed using a lactate dehydrogenase (LDH) assay.

Finally, to see the long-term impact on cell growth, a clonogenic assay was performed.

1.3. Results

When delivered individually, siCDK4, siCD1, or siMCl-1 induced a substantial reduction in their respective protein levels of more than 60% at a concentration of 40 nM compared to the siRNA control (**Figure S3** of the publication). This result confirmed the capacity of WRAP5-based nanoparticles to address efficient delivery of a single siRNA into GIST-T1 cells.

Confocal images revealed that WRAP5 nanoparticles loaded with the siMIX formulation successfully delivered the three fluorescence-labeled siRNA into the same cells, with distinct signals observed in the cytoplasm of nearly all cells. Internalization patterns were similar whether the siRNA were delivered individually or in combination (**Figure 4** of the publication).

Among the four siRNA ratios tested, the 6/8/6 ratio best matched the basal protein expression profile of GIST-T1 compared to U87. Indeed, only the WRAP5 nanoparticles encapsulating the 6/8/6 siRNA ratio led to homogeneous silencing of the three proteins (around 70% for the three proteins at 60 nM total siRNA concentration). This demonstrated that WRAP5:siMIX enabled suitable simultaneous protein silencing in GIST-T1 cells (**Figure 5** of the publication).

Functionally, only the WRAP5:siMIX condition exhibited a significant decrease in colony-forming (30% at 40 nM total siRNA concentration) capacity compared to cells treated with single siRNA or siRNA control WRAP5-based nanoparticles. This reduction suggests that multi-target silencing more effectively impairs cell proliferation than the inhibition of individual

proteins. However, given that the observed effect did not result in a 50% reduction, it is plausible that alternative compensatory mechanisms within the cell cycle and survival pathways were engaged.

1.4. Discussion

These findings confirm that WRAP5-based nanoparticles can serve as an efficient tool for both single and multiple siRNA silencing, enabling the simultaneous knockdown of several oncogenic targets in GIST-T1 cells. The ability to co-silence targets involved in both cell cycle progression and apoptosis resistance appears to enhance the anti-proliferative response compared to single-target inhibition. The confocal images validate the capacity for co-delivery within the same cell, while the clonogenic assay indicates a functional impact of this multi-target approach.

Additionally, this supports the flexibility and adaptability of our WRAP5-based nanoparticles tool, allowing us to modulate the ratio between siRNA, depending on the protein expression profiles in different cancers. These characteristics are crucial for optimizing therapeutic strategies aimed at heterogeneous cancers.

1.5. Conclusion and perspectives

This proof-of-concept study thus lays the methodological foundations for the subsequent investigations presented in this thesis. This study not only demonstrated the feasibility of WRAP5-based nanoparticles siRNA delivery in GIST-T1 cells but also opens the possibility to functionally interrogate complex signaling pathways involving multiple effectors, such as the Hippo pathway, through combinatorial gene knockdown.

The successful validation of WRAP5-based nanoparticles in this sarcoma model establishes a key tool for the following work, as this strategy can easily be transposed to investigate the functional roles of the transcriptional co-activators YAP1 and TAZ in GIST, which is the central goal of the following chapter.

2. Published Work “Multiprotein Silencing Using WRAP-Based Nanoparticles: A Proof of Concept”

Bioconjugate Chemistry

Editors' Choice

pubs.acs.org/bc

Article

Multiprotein Silencing Using WRAP-Based Nanoparticles: A Proof of Concept

Karidia Konate,[§] Irène Pezzati,[§] Karima Redjatti, Estelle Agnel, Eric Vivès, Sandrine Faure, Pascal de Santa Barbara, Prisca Boisguérin,* and Sébastien Deshayes*

Cite This: *Bioconjugate Chem.* 2025, 36, 1218−1233

Read Online

ACCESS | Metrics & More | Article Recommendations | Supporting Information

ABSTRACT: Cancer remains the leading cause of death, with chemotherapy, radiotherapy, and surgical resection being the primary treatment methods. However, chemotherapy's side effects, surgical limitations, and drug resistance present significant challenges. Small interfering RNA (siRNA) has emerged as a promising tool in cancer therapy due to its ability to silence disease-related genes selectively. Recent advancements in nonviral delivery systems, particularly cell-penetrating peptides (CPPs), have enhanced the efficacy of siRNA delivery. The use of siRNA as a therapeutic tool in cancer treatment has been reported in the literature. However, silencing only one target protein has only a minor effect on tumor cell proliferation, as previously shown for WRAP-based nanoparticles targeting cyclin-dependent kinase 4 (CDK4) in human U87 glioblastoma cells. Here, we designed a more sophisticated approach to enhance therapeutic efficacy, encapsulating multiple siRNAs targeting CDK4, cyclin D1 (CD1), and MCL-1 proteins. The siRNA cocktail, delivered via WRAP5 nanoparticles, effectively silenced these targets and reduced cell proliferation in human U87 glioblastoma cells. Furthermore, the nanoparticles also demonstrated potential therapeutic impact in gastrointestinal stromal tumors (GIST), a rare cancer characterized by its tendency to resist standard treatments. This study highlights the versatility of WRAP5 nanoparticles as a platform for personalized cancer therapy, suggesting that siRNA delivery systems may be tailored to specific cancer types for more effective treatment strategies.

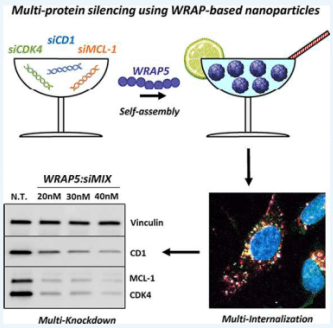

Downloaded via UNIV MONTPELLIER on July 14, 2025 at 16:20:01 (UTC).
See https://pubs.acs.org/sharingguidelines for options on how to legitimately share published articles.

INTRODUCTION

Based on the global cancer statistics database provided by the Global Cancer Observatory (GLOBOCAN) estimation for 2022, cancer is the first leading cause of death worldwide, accounting for almost 10 million deaths per year (nearly one in six deaths).[1] Despite the considerable progress made in the field of anticancer therapy, particularly in the development of chemotherapy, radio-chemotherapy, and hormonal therapy, surgical resection in combination with chemo-radiotherapy remains the established method for treating malignant cancers.[2] However, chemotherapy is not without its drawbacks, as evidenced by the occurrence of adverse side effects and the potential for inadvertent damage to healthy cells.[3] Moreover, the inadequacy of surgical resection can result in cancer recurrence in a variety of cases, including glioblastoma multiform.[4] In addition, the primary challenge to the effective treatment of cancer patients concerns the appearance of drug resistance as observed for gastrointestinal stromal tumors (GIST) mainly through secondary mutations.[5]

Consequently, novel therapeutic approaches are now being developed to target the fundamental mechanisms and acquired capacities that transform healthy cells and tissues into cancerous tumors. In this context, a particularly fruitful area of research in the domain of precision medicine employs small interfering RNA (siRNA).[2,6,7] In detail, the potential efficacy of siRNA in treating diseases is attributable to the binding to specific mRNA sequences, resulting in an efficient silencing of disease-related genes. This was further demonstrated by the fact that six siRNAs have been approved by the FDA (US Food and Drug Administration) and the EMA (European Medicines Agency).[8] As siRNA did not enter the cells by themselves, they were all delivered using carriers: five of them used GalNAc conjugates, and one siRNA, named Patisiran,[9] was formulated as lipid-based nanoparticles.[10,11] However, all these FDA-approved siRNAs were designed to target the liver. To target other tissues, various delivery systems have been designed, including nonviral carriers composed of polymers, lipids, or inorganic materials, tested in preclinical and clinical studies.[12] However, for some of them, several side effects were observed, such as the activation of Fas Ligand-mediated cell death by polyethylenimine (PEI), or toxicity due to platelets and CD11-*b*-positive cells aggregation in the lung by poly(L-lysine) (PLL).[13]

Received: February 14, 2025
Revised: April 11, 2025
Accepted: May 5, 2025
Published: May 29, 2025

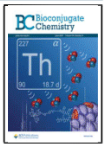

ACS Publications

© 2025 The Authors. Published by American Chemical Society

https://doi.org/10.1021/acs.bioconjchem.5c00069
Bioconjugate Chem. 2025, 36, 1218−1233

In the field of safer delivery systems, cell-penetrating peptides (CPPs, comprising up to 30 amino acids) have been proposed as an up-and-coming alternative. Notably, those CPPs capable of forming nanoparticles in the presence of siRNAs are particularly interesting.[14−16] This noncovalent strategy is based on electrostatic and hydrophobic interactions between both the peptide and the siRNA, thus opening peptides to the field of nanomedicine.[17]

In this context, we designed a family of amphipathic peptides called WRAP (W- and R-rich Amphipathic Peptides) able to form peptide-based nanoparticles (PBNs) once incubated with siRNA at a specific CPP/siRNA molar ratio (MR).[18] The proof-of-concept study showing the transfection potency of the WRAP peptides was first established in human U87 glioblastoma cells on overexpressed and endogenous proteins. Afterward, we evaluated the siRNA transfection activity in 9 other cell lines,[18] and later on also in vascular endothelial cells or hiPSC-derived cardiomyocytes.[19] The high efficacy of the WRAP-based PBNs in delivering siRNAs across different cancer cell lines can be attributed to their rapid cellular internalization (∼15 min) mainly through direct membrane translocation, with only a minor fraction entering via endocytosis-dependent pathways.[18,20] This determination was made using various approaches, including a leakage assay on liposomes to validate membrane interaction, as well as endocytosis inhibitors or cell markers for endosomes/lysosomes. Most notably, we observed an accumulation of fluorescently labeled siRNAs delivered by WRAP-based nanoparticles in Dynamin triple-KO cells, where the primary endocytic pathways are compromised.[20]

Based on a structure−activity relationship (SAR) study, we identified two lead peptides WRAP1 (LLWRLWRLL-WRLWRLL) and WRAP5 (LLRLLRWWWRLLRLL), showing nearly the same delivery properties.[21] Compared to lipid-based reagents for siRNA transfection (e.g., RNAiMAX), we demonstrated that WRAP:siRNA nanoparticles are as efficient for protein silencing without cytotoxicity as shown through a clonogenic assay.[21] Finally, the first in vivo investigation performed with WRAP:siRNA nanoparticles demonstrated effective luciferase silencing in a mouse xenograft model using glioblastoma cancer cells that overexpress luciferase,[22] or green fluorescence protein (GFP) silencing in Zebrafish that overexpress GFP in vascular endothelial cells.[23]

In our previous works, we focused mainly on glioblastoma, which represents the most prevalent form of malignant brain and other central nervous system (CNS) tumors.[24] The incidence of glioblastoma is 3.21 per 100,000 population.[25] Characteristics of this cancer were dysregulation of signal pathways and an aberrant cell cycle due to cyclin-dependent kinase 4 (CDK4) amplification or overexpression, as reported for most of the cyclin-dependent kinases (CDKs) in human cancers.[26,27] Therefore, we aimed to target glioblastoma cell proliferation by WRAP:siRNA nanoparticles downregulating CDK4 to develop a pharmacological treatment. However, despite observing significant CDK4 protein silencing, no phenotypical changes, such as a reduction in proliferation, were induced.[18,21] One potential explanation for this phenomenon is that the inhibition of one single protein is not sufficient to arrest the whole cell cycle. Therefore, our next objective was to develop a more sophisticated approach to simultaneously downregulate multiple proteins using WRAP5-based nanoparticles encapsulating several siRNAs. Specifically, we aimed to target both the cell cycle and cell survival, to inhibit cell proliferation and direct cancer cells to death. To target the cell cycle, we selected CDK4 as previously described[18,21] and its activator, the cyclin D1 (CD1), whose overexpression resulted in dysregulated CDK activity, rapid cell growth, bypass of key cellular checkpoints, and ultimately cancer progression.[28] To target cell survival, we selected the myeloid leukemia cell differentiation protein MCL-1, a key antiapoptotic protein within the BCL-2 family.[29] Indeed, it has been established that many cancers evade pro-apoptotic stress signals by upregulating antiapoptotic proteins, such as MCL-1, to maintain their survival.[30] Furthermore, MCL-1 overexpression is often linked to therapeutic resistance.[31−33]

In the present study, we reported on the encapsulation of three siRNAs targeting CDK4, CD1, and MCL-1 proteins as a potential cancer treatment. First, we confirmed that the three proteins could be silenced individually through transfection by the WRAP5:siRNA nanoparticles in human U87 glioblastoma cells. Subsequently, we performed knockdown using different ratios of 2 or 3 encapsulated siRNAs. Following this screening, we demonstrated that WRAP5 nanoparticles encapsulating the three siRNAs with a defined ratio of 14/3/3 for siCD1/siCDK4/siMCL-1 (=siMIX) silenced the three proteins by more than 80% in U87 cells. Furthermore, this particular siRNA cocktail was found to have a physiological impact on cell proliferation, in comparison to the nanoparticles encapsulating a single siRNA.

Encouraged by these results, we analyzed WRAP5:siMIX nanoparticles in gastrointestinal stromal tumors (GIST), which are rare cancers but represent the most common form of sarcoma of the digestive tract, with an incidence of 0.82 per 100,000 population.[34] GISTs develop predominantly in the stomach and are caused in approximately 75% of cases by gain-of-function mutations in the receptor tyrosine kinase c-KIT gene. Imatinib (IM), a tyrosine kinase inhibitor (TKI), is the standard first-line treatment for GIST. However, it is important to note that complete remission is rare, and resistance is frequent, highlighting the need for the development of novel therapeutics.

As performed in the human U87 glioblastoma cells, we first analyzed the silencing of the three proteins individually and then all together using WRAP nanoparticles encapsulating single siRNA or the siMIX. Interestingly, we found a similar effect on cell proliferation when the WRAP5:siMIX was applied on GIST cells, however, with another siRNA ratio. These results suggest that the efficacy of cancer treatment using siRNAs should be adapted according to the specific type of cancer being treated. This approach could represent a significant advancement in the field of personalized cancer therapy.

■ MATERIALS AND METHODS

Materials. WRAP5 peptide was synthesized at the SynBio3 platform (IBMM Montpellier) and the crude product was purified in house following a qualitative analysis by HPLC/MS (∼95% purity). The different siRNA sequences were purchased from Eurogentec (see Table S1). The siRNA stock solutions were prepared in RNase-free water.

WRAP5:siRNA Nanoparticle Formulation. WRAP5 solutions were prepared in pure water (Sigma-Aldrich). Nanoparticles were formulated in pure water supplemented by 5% glucose (Sigma-Aldrich) by mixing equal volumes of siRNA and WRAP5 at the corresponding molar ratio (R = 20) at room temperature.[18] The molar ratio R = 20 corresponded

https://doi.org/10.1021/acs.bioconjchem.5c00069
Bioconjugate Chem. 2025, 36, 1218−1233

to a 20-fold higher molar concentration of WRAP5 compared to the siRNA, as already described.[18] For WRAP5:siMIX nanoparticles, siRNA cocktails were premixed according to siRNA stoichiometry: 80% siCD1 and 20% siCDK4 for 4/1 "binary cocktail" and 70% siCD1, 15% siCDK4 and 15% siMCL-1 for 14/3/3 "tertiary cocktail" in human U87 glioblastoma cells as well as 30% siCD1, 40% siCDK4 and 30% siMCL-1 for 6/8/6 "tertiary cocktail" in human GIST-T1 cells.

Dynamic Light Scattering. The mean particle size (*Z*-average diameter) and the polydispersity index (PdI) of the WRAP5:siRNA nanoparticles (WRAP5 = 10 μM, siRNA = 500 nM, R = 20) were evaluated with a Zetasizer NanoZS (Malvern). *Z*-average diameter corresponded to the intensity weighted mean hydrodynamic size, and the PdI indicated the homogeneity of nanoparticle suspension. A perfectly uniform sample would have a single defined size (e.g., 100 nm) with a PdI close to zero. For peptide-based nanoparticle, a mean size between 80 and 150 nm and PdI < 0.3 generally indicated a homogeneous population. All results were obtained from three independent measurements (three runs for each measurement at 25 °C).

Culture Conditions. Human U87 glioblastoma cells were grown in a complete medium: DMEM with GlutaMAX (Thermo Fisher Scientific), penicillin/streptomycin (Thermo Fisher Scientific), 10% fetal bovine serum (FBS, Thermo Fisher Scientific), nonessential amino acids NEAA 1× (Thermo Fisher Scientific) and 0.1% hygromycin (Invitrogen). Human gastrointestinal stromal tumor (GIST-T1) cells (Cosmo Bio, Japan) were grown in a complete medium: DMEM (4.5 g/L glucose, L-glutamine and sodium pyruvate) (Corning), 1% penicillin/streptomycin (Sigma), and 10% fetal bovine serum (FBS, Sigma). All the cells were maintained in a humidified incubator with 5% CO_2 at 37 °C.

Western Blotting. For Western blot assays, 75,000 U87 and 150,000 GIST-T1 cells were seeded 24 h before the experiment into 24-well plates. For siRNA transfection with WRAP5-based nanoparticles, the cells were incubated with 175 μL of fresh prewarmed serum-free DMEM + 75 μL of the nanoparticle solutions at the indicated concentrations or 75 μL 5% glucose for the nontreated cells. After 1.5 h of incubation, 250 μL DMEM supplemented with 20% FBS (final FBS concentration = 10%) were added to each well without withdrawing the WRAP5:siRNA nanoparticles. Cells were then incubated for another 24 h (or 72 h) and finally lysed for Western blot evaluation.

Transfected cells were washed in PBS and lysed in RIPA buffer [50 mM tris pH 8.0, 150 mM sodium chloride, 1% Triton X-100, 0.1% SDS (sodium dodecyl sulfate, Sigma-Aldrich), including protease inhibitors (SigmaFAST, Sigma-Aldrich)]. Cells were incubated for 5 min on ice with 130 μL/24-well lysis buffer. Thereafter, cells were scraped and transferred to a 1.5 mL tube. After 5 min on ice, the cell lysates were centrifuged (10 min, 16,100*g*, 4 °C), supernatants were collected, and protein concentrations were determined using the Pierce BCA Protein Assay (Thermo Fisher Scientific). Cell extracts were separated by 4−20% Mini-PROTEAN TGXTM Precast Gel (Bio-Rad). After electrophoresis, samples were transferred onto Trans-Blot Turbo Mini PVDF Transfer membrane (Bio-Rad). As antibodies, we used anti-CDK4 rabbit mAb D9G3E, anti-MCL-1 rabbit, anti-Vinculin rabbit mAb E1E9 V, antimouse IgG HRP and antirabbit IgG HRP(all from Cell Signaling) as well as anti-CD1 (SP4) (Thermo Fisher Scientific). Blots were revealed with the Pierce ECL plus Western blotting substrate (Thermo Fisher Scientific) on an Amersham imager 600 (GE Healthcare Life Science) or a Sapphire RGB & NIR Biomolecular Scanner (Azure biosystems). The signal intensities of the blots were quantified using Fidji ImageJ software. Each band intensity corresponding to a distinguished condition was then normalized to the band intensity of nontreated cells (=100%) as previously described[18]

$$\text{Signal Intensity (\% of N.T.)} = \text{intensity (condition} \times\text{)/intensity (N.T.)} \times 100$$

Cell Cytotoxicity Measurement. The cytotoxicity induced by the nanoparticles was evaluated using the Cytotoxicity Detection Kit (Lactate DeHydrogenase, Sigma-Aldrich) following the manufacturer's instructions using the supernatant of the Western blot incubations. At least one well of the 24-well plate was used as LDH positive control (100% toxicity) by adding Triton X-100 (Sigma-Aldrich) to a final concentration of 0.1% (~15 min incubation at 37 °C). Afterward, 50 μL supernatant of each well were transferred to a new clear 96-well plate. 50 μL of the "dye solution/catalyst" mixture was added to the supernatant and incubated in the darkness for 30 min at room temperature. The reaction was stopped by adding 25 μL of HCl (1 N) to each well before measuring the absorption at 490 nm. Relative cytotoxicity was calculated according to the manufacturer.[35]

$$\text{Relative toxicity (\%)} = [(\text{exp. value} - \text{value N.T. cells})/(\text{value Triton} - \text{value N.T. cells})] \times 100$$

Clonogenic Assay. For clonogenic assays, 350 U87 or GIST-T1 cells were seeded 24 h before the experiment into 6-well plates. For nanoparticle incubation, the cells were incubated with 1.7 mL of fresh prewarmed serum-free DMEM + 300 μL of the nanoparticle solutions at the indicated concentrations or 300 μL 5% glucose for the nontreated cells (N.T.). After 1.5 h of incubation, the medium was removed and replaced by 2 mL DMEM supplemented with 10% FBS. Cells were then incubated for 14 days.

The medium of the transfected U87 cells was removed, and 1.5 mL/well of methanol/acetic acid solution (3/1, vol/vol) was added to fix the cell colonies. After 20 min incubation, the solution was replaced by 1.5 mL/well of Giemsa (Sigma-Aldrich)/H_2O (3.5/10, vol/vol) for 20 min.

The medium of the transfected GIST-T1 cells was removed, and the cells were washed two times with PBS1X. Then, cells were fixed using 0.5 mL/well of 4% paraformaldehyde (PFA) solution. After 10 min incubation, cells were rinsed two times with PBS1X, and 0.5 mL/well of crystal violet solution (in 10% ethanol) was added to color cell colonies for 10 min. Finally, the dye solution was removed and the wells were rinsed many times with H_2O or PBS1X until the background of the wells was clear. After air-drying the wells, an image of the whole 6-well plate was acquired on an Amersham imager 600 (GE Healthcare Life Science) or a Sapphire RGB & NIR Biomolecular Scanner (Azure biosystems).

The colonies of each 6-well plate were counted manually and normalized to the nontreated (N.T.) control condition of the same plate, as shown in the equation[21]

https://doi.org/10.1021/acs.bioconjchem.5c00069
Bioconjugate Chem. 2025, 36, 1218−1233

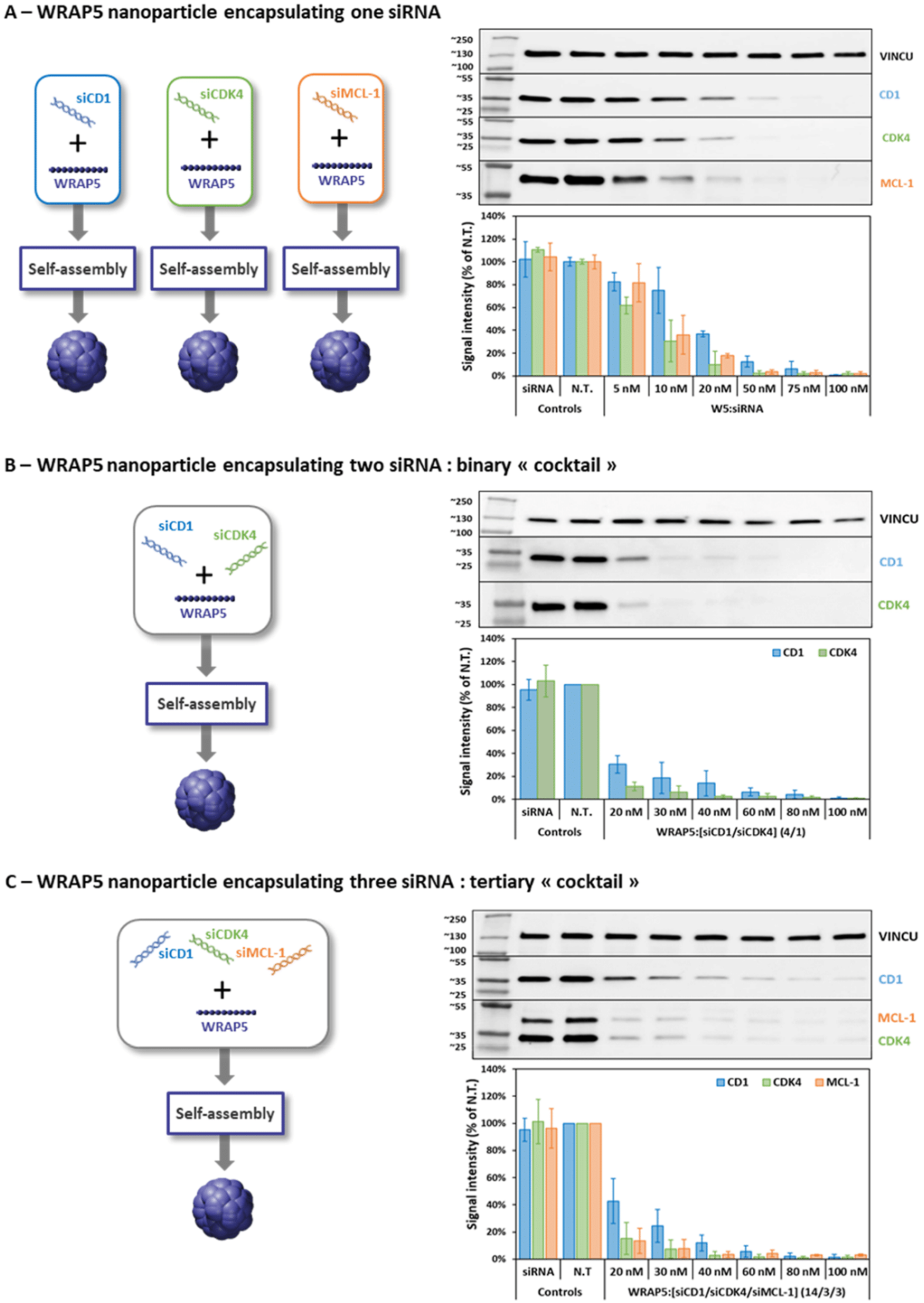

Figure 1. Evaluation of the dose-dependent silencing of WRAP5:siRNA nanoparticles in U87 cells (A) WRAP5 nanoparticles encapsulating one siRNA (schematic representation on the left side) induced the dose-dependent silencing of CD1, CDK4, and MCL-1 proteins in human U87 glioblastoma cells at the indicated siRNA concentrations revealed by Western Blot after a 24 h incubation. (B) WRAP5 nanoparticles encapsulating

https://doi.org/10.1021/acs.bioconjchem.5c00069
Bioconjugate Chem. 2025, 36, 1218−1233

Figure 1. continued

two siRNAs (schematic representation on the left side) in a siRNA ratio 4/1 induced the dose-dependent simultaneous silencing of two proteins (CD1/CDK4) in human U87 glioblastoma cells at the indicated siRNA concentrations revealed by Western Blot after a 24 h incubation. (C) WRAP5 nanoparticles encapsulating three siRNAs (schematic representation on the left side) in a siRNA ratio 14/3/3 induced the dose-dependent simultaneous silencing of three proteins (CD1/CDK4/MCL-1) in human U87 glioblastoma cells at the indicated siRNA concentrations revealed by Western Blot after a 24 h incubation. Data represent mean ± SD, with $n = 2$ independent experiments in duplicates. Vinculin (VINCU) was used as an internal loading control. Controls: nontreated cells (N.T.) and siRNA alone.

colonies counted [% of N.T.]

= number of colonies (condition ×)/number of colonies (N.T.) × 100

Confocal Microscopy. For confocal microscopy, 300,000 GIST cells were seeded 24 h before the experiment into a glass-bottom dish (FluoroDish, 35 mm). For nanoparticle incubation, the cells were incubated with 1800 μL of prewarmed serum-free DMEM FluoroBrite + 200 μL of the nanoparticle solutions at the indicated concentrations or 200 μL 5% glucose for the nontreated cells.

Transfected cells were incubated for 10 min Hoechst 33342 dye (Sigma-Aldrich) for nucleus labeling. Afterward, cells were washed twice with D-PBS and covered with FluoroBrite DMEM medium (Thermo Fisher Scientific). Live cell images were acquired on an inverted Zeiss LSM800 microscope using a lens Apo 63x/1.2 W DICIII. All confocal acquisitions were performed using the following diode lasers: 405 nm with a Hoechst filter (400 nm−456 nm), 488 nm with an Alexa488 filter (500 nm−542 nm), 561 nm with an Atto550 filter (560 nm−617 nm) and 640 nm with an Atto655 filter (656 nm−700 nm). Image acquisition was done sequentially to minimize crosstalk between the fluorophores. Each confocal image was merged and adjusted with the same brightness and contrast parameters using the Fidji ImageJ software.

■ RESULTS

WRAP5:siRNA Targeting Three Different Proteins in U87 Cells. As previously revealed by confocal microscopy, WRAP5-based nanoparticles are a suitable delivery system to transfect siRNAs in human U87 glioblastoma cells.[18,20] However, our studies using WRAP5-loaded with siRNA targeting CDK4 did not reveal the expected phenotypic activity in terms of cancer cell proliferation reduction.[18,21] We assumed that reducing the expression of only one targeted protein involved in the cell cycle regulation was not sufficient to disturb cell growth because other cyclin-dependent kinases (e.g., CDK2, CDK6) could compensate the CDK4 activity.[36,37] To overcome this fact, we decided to silence simultaneously different proteins of the cell cycle such as CDK4 and Cyclin D1 (CD1) as well as the antiapoptotic protein MCL-1 to stop the cell cycle progression and reduce cell survival.

First, we evaluated the dose-dependent silencing capacity of three different siRNAs, especially designed to target proteins CD1, CDK4, and MCL-1 (siCD1, siCDK4, and siMCL-1) separately. For that, one of the three siRNAs was encapsulated by the WRAP5-based nanoparticle and applied to human U87 glioblastoma cells (Figure 1A). We used the same WRAP5:siRNA molar ratio between the peptide and the siRNA (molar ratio 20:1) for all tested conditions, which was described as optimal for siRNA delivery.[18,20,22]

WRAP5 nanoparticles encapsulating the siCDK4 revealed an important knock-down of the CDK4 protein expression (>80% using 20 nM siCDK4) as observed previously,[18] as well as for the MCL-1 protein (~80% using 20 nM siMCL-1) (Figure 1A). Curiously, a higher siCD1 concentration (50 nM) was required to obtain the same knock-down efficiency (~80%). This was not explained by different sizes of the nanoparticles (all between 50 and 150 nm, see Table 1) but probably by an increased stability, a longer turnover, or a higher expression of the CD1 protein compared to CDK4 and MCL-1 proteins in U87 cells. CD1 was described as a key protein involved in different cancers,[38,39] suggesting that its expression fluctuated according to cell types. This latter observation could explain why the CD1 silencing needed more than twice the siRNA concentration of the other targets (CDK4, MCL-1).

Table 1. WRAP5 Nanoparticles Characterization by DLS Measurements[a]

	dye	mean size (nm)	PdI
WRAP5:siCD1	no	72.2 ± 4.1	0.270 ± 0.058
	yes	121.2 ± 4.3	0.373 ± 0.040
WRAP5:siCDK4	no	98.4 ± 15.2	0.242 ± 0.052
	yes	77.1 ± 14.2	0.204 ± 0.047
WRAP5:siMCL-1	no	106.2 ± 0.1	0.216 ± 0.014
	yes	75.9 ± 2.4	0.238 ± 0.008
WRAP5:siMIX(14/3/3)	no	79.3 ± 7.9	0.275 ± 0.028
	yes	n.d.	n.d.
WRAP5:siMIX(6/8/6)	no	62.8 ± 6.6	0.252 ± 0.006
	yes	n.d.	n.d.
WRAP5:siMIX(3/3/3)	no	140.8 ± 54.2	0.255 ± 0.028
	yes	75.3 ± 0.7	0.263 ± 0.080

[a]All WRAP5:siRNA complexes were formed at $R = 20$ using a final siRNA concentration of 500 nM in an aqueous solution of 5% glucose for mean size and PdI acquisition. $n \geq 2$ independent formulations (3 measures per run). siMIX: a cocktail of [siCD1/siCD4/siMCL-1] at the indicated ratio, n.d.: not determined, PdI: Polydispersity Index. Dye indicated the presence of fluorescence-labeled siRNA.

WRAP5 Nanoparticles Encapsulating up to 3 siRNA for Protein Silencing in U87 Cells. To avoid using high concentrations of CD1 siRNA, we decided to perform a "binary cocktail" approach by encapsulating together siCD1 and siCDK4 into one nanoparticle (=WRAP5:siMIX). With this condition, we expected the silencing of both proteins. First, we encapsulated into the WRAP5 nanoparticle the same amount of siCD1 and siCDK4 (1/1 or 50%/50%), but with this ratio, we observed a significantly higher CDK4 knock-down compared to CD1 (Data not shown). To obtain a more equivalent silencing of both proteins, we combined 80% of siCD1 with 20% of siCDK4, corresponding to a final ratio of 4/1 [siCD1/siCDK4] into WRAP5 nanoparticles (Figure 1B). As described below, the molar ratio between WRAP5 and siRNA was 20/1, and this will be kept constant for all following experiments, regardless of whether one, two, or three siRNAs were encapsulated.

https://doi.org/10.1021/acs.bioconjchem.5c00069
Bioconjugate Chem. 2025, 36, 1218−1233

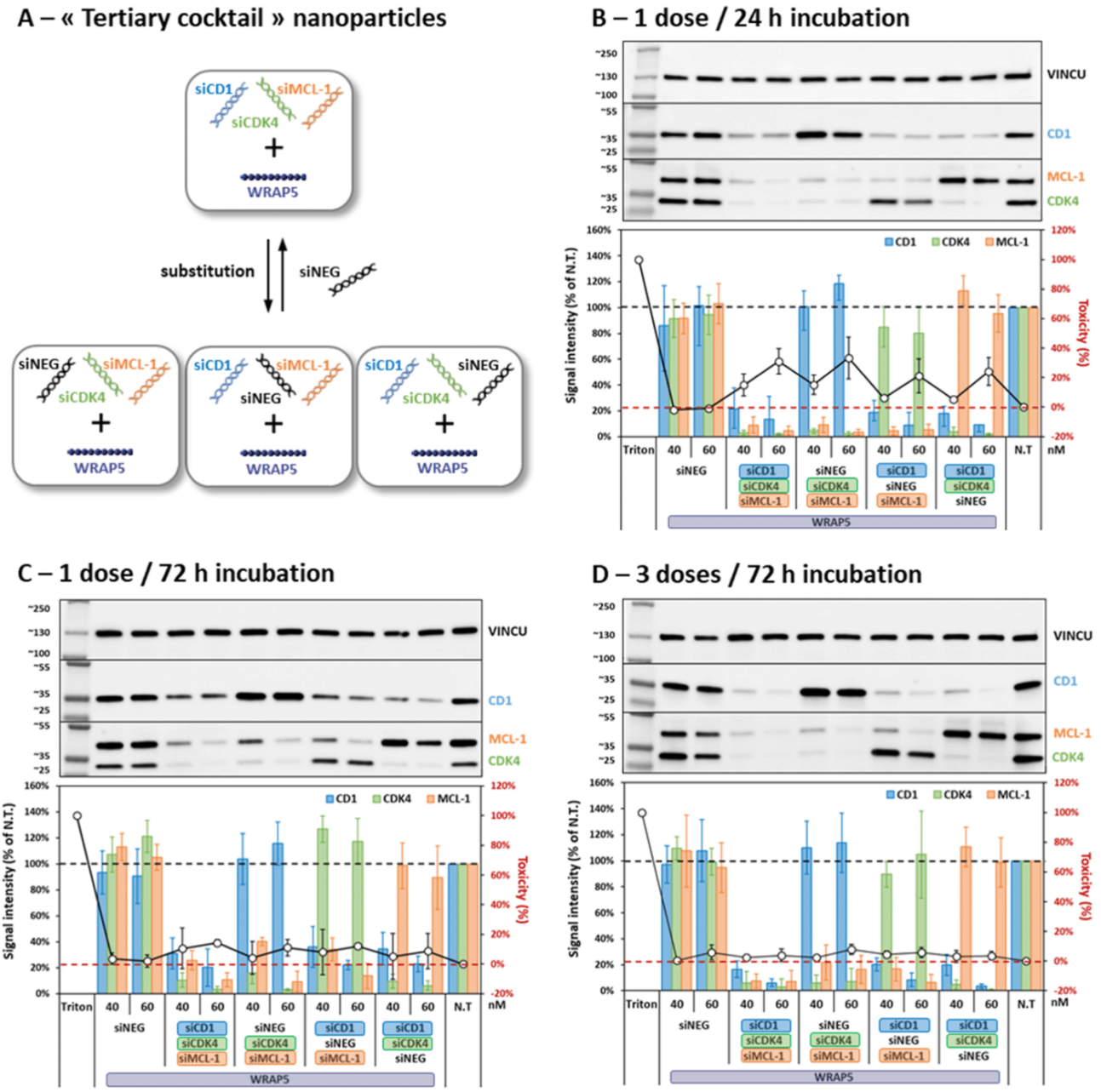

Figure 2. Evaluation of the dose-dependent silencing of WRAP5:[siCD1/siCDK4/siMCL-1] (14/3/3) nanoparticles. (A) Schematic representation of WRAP5 nanoparticles encapsulating three siRNAs with or without siNEG substitution. (B) Single dose application of WRAP5:[siCD1/siCDK4/siMCL-1] nanoparticles at a ratio 14/3/3 induced a simultaneous silencing of three proteins (CD1, CDK4, and MCL-1) in human U87 glioblastoma cells at the indicated siRNA concentrations revealed by Western Blot after a 24 h incubation. (C) Single dose application of WRAP5:[siCD1/siCDK4/siMCL-1] nanoparticles at a ratio 14/3/3 induced a simultaneous silencing of three proteins (CD1, CDK4, and MCL-1) in human U87 glioblastoma cells at the indicated siRNA concentrations revealed by Western Blot after a 72 h incubation. (D) Three-dose application of WRAP5:[siCD1/siCDK4/siMCL-1] nanoparticles at a ratio 14/3/3 induced a simultaneous silencing of three proteins (CD1, CDK4, and MCL-1) in human U87 glioblastoma cells at the indicated siRNA concentrations revealed by Western Blot after a 72 h incubation. Data represent mean ± SD, with n = 3 independent experiments in duplicates. Vinculin (VINCU) was used as an internal loading control. Nontreated cells (N.T.)/Triton were used to determine 100% toxicity using the LDH assay. The dashed black line represented 100% protein expression, and the dashed red line represented 0% cytotoxicity.

By looking in detail at the "40 nM" condition corresponding to a nanoparticle encapsulating 32 nM siCD1 and 8 nM siCDK4 (4/1 ratio), three important points could be revealed in human U87 glioblastoma cells. First, we showed an important dose-dependent simultaneous silencing of CD1 and CDK4 using this 4/1 siRNA ratio. Second, we observed a synergic effect as the knock-down as CDK4 silencing was higher (>90%) compared to the single siRNA-loaded nanoparticles at a similar concentration (~70% for WRAP5:siCDK4 at 10 nM) (Figure 1A). Interestingly, we also illustrated a slight synergic effect for the CD1 protein with a knock-down of ~80% in the binary condition (siRNAs at 30 nM with siCD1 at

https://doi.org/10.1021/acs.bioconjchem.5c00069
Bioconjugate Chem. 2025, 36, 1218−1233

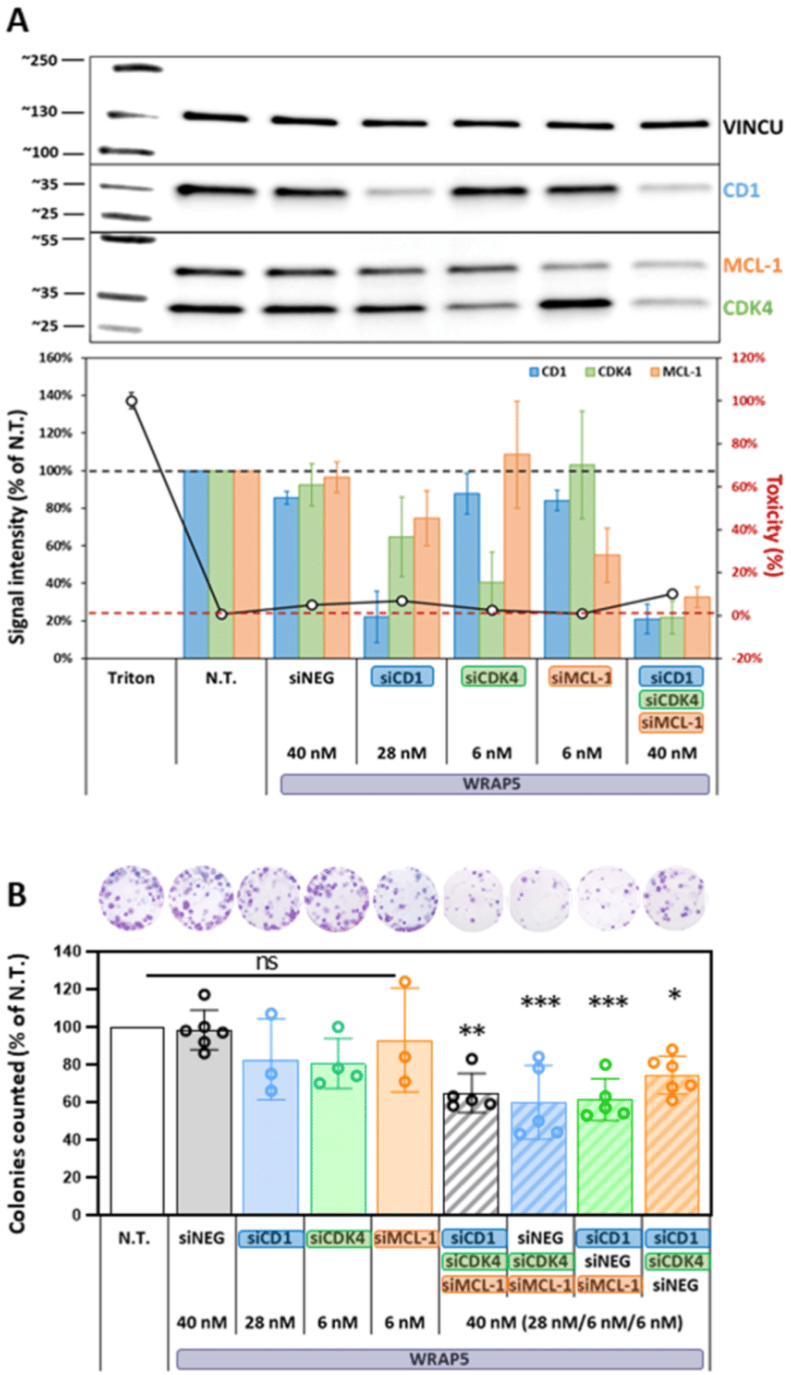

Figure 3. WRAP5:siMIX (14/3/3) nanoparticles affect cell proliferation on U87 cells depending on the incubation time. (A) WRAP5:[siCD1/siCDK4/siMCL-1] nanoparticles at a ratio 14/3/3 induced a simultaneous silencing of three proteins (CD1, CDK4, and MCL-1) in human U87 glioblastoma cells at the indicated siRNA concentrations revealed by Western Blot after a 24 h incubation. Data represent mean ± SD, with $n = 2$ independent experiments in duplicates. Vinculin (VINCU) was used as an internal loading control. Nontreated cells (N.T.)/Triton were used to determine 100% toxicity using the LDH assay. The dashed black line represented 100% protein expression, and the dashed red line represented 0% cytotoxicity. (B) WRAP5:[siCD1/siCDK4/siMCL-1] nanoparticles at a ratio 14/3/3 induced a reduction in cell proliferation in human U87 glioblastoma cells at the indicated siRNA concentrations, revealed by clonogenic assay after a 14 day incubation.Data represent mean ± SD using ≥3 independent experiments. Statistics using Kruskal–Wallis test: WRAP5:siNEG ns > 0.9999, WRAP5:siCD1 ns > 0.9999, WRAP5:siCDK4 ns = 0.2773, WRAP5:siMCL-1 ns > 0.9999, WRAP:[siCD1/siCDK4/siMCL-1] $p^{**} = 0.0010$, WRAP5:[siNEG/siCDK4/siMCL-1] $p^{***} = 0.0004$, WRAP5:[siCD1/siNEG/siMCL-1] $p^{***} = 0.0003$ and WRAP5:[siCD1/siCDK4/siNEG] $p^{*} = 0.0110$ vs N.T.

24 nM and siCDK4 at 6 nM, Figure 1B) compared to the single-loaded nanoparticle (siCD1 at 50 nM, Figure 1A).

We observed similar behavior for the encapsulation of a "binary cocktail" targeting both CD1 and MCL-1 at a final siRNA ratio of 4/1 [siCD1/MCL-1] (Figure S1). This led us

https://doi.org/10.1021/acs.bioconjchem.5c00069
Bioconjugate Chem. 2025, 36, 1218−1233

to extend the idea of siRNA combination, considering a "tertiary cocktail" formulation.

Knowing that a higher siCD1 concentration was needed to obtain the same silencing efficiency as CDK4 and MCL-1, we encapsulated the three different siRNAs in a "tertiary cocktail" using 70% siCD1, 15% siCDK4 and 15% siMCL-1, corresponding to a siRNA ratio of 14/3/3 [siCD1/siCDK4/siMCL-1] (Figure 1C) and we evaluated their effect in a dose-dependent manner in human U87 glioblastoma cells.

Then, the "20 nM" condition was selected to assess the synergistic effects between the three knock-downs, which corresponded to 14 nM siCD1, 3 nM siCDK4, and 3 nM siMCL-1. Interestingly, we observed a positive effect of the transfection of the three siRNAs because the impact of the "tertiary cocktail" was higher on the three proteins (70% for CD1, 90% for CDK4 and 80% for MCL-1) compared to the corresponding single siRNA-loaded nanoparticles at the same concentrations (~25% for WRAP5:siCD1 at 10 nM, 40% for WRAP5:CDK4 at 5 nM and 20% for WRAP5:MCL-1 at 5 nM—Figure 1A).

Finally, we evaluated the WRAP5 nanoparticle loaded with the siRNAs cocktail [siCD1/siCDK4/siMCL-1] (=WRAP5:-siMIX) compared to single siRNA-loaded nanoparticles by DLS (Table 1). The measurements revealed that WRAP5 encapsulating one or three siRNAs all formed nanoparticles with a mean size between 70 and 100 nm with a PdI < 0.3. Graphical representations of the measured mean sizes are visualized in Figure S2. Moreover, these nanoparticles were stable over 7 days when stored at 4 °C (data not shown).

WRAP5-Based siRNA Cocktail: Optimal Dosing for Silencing in U87 Cells. The next step was the evaluation of the WRAP5:siMIX nanoparticles for their silencing efficiency compared to a negative control condition (WRAP5 encapsulating an inactive siRNA = siNEG). This negative control was selected as the WRAP5 peptide alone did not form nanoparticles (data not shown). In the same experiment, we also compared the WRAP5:siMIX with nanoparticles with one siRNA substituted by the siNEG to estimate if a synergic effect could be shown (Figure 2A). Two final siRNA concentrations (40 nM, 60 nM) were selected for this screening within the middle range of our previous dose response (Figure 1C) to ensure sufficient concentration for inhibiting target proteins. As reported before for PBNs, these concentrations were known to have no cytotoxic effects.[18,21,40,41]

When applying one single dose of the WRAP5:siMIX nanoparticles, we observed after 24 h incubation of the U87 cells a clear silencing (≥80%) for the three proteins, which was not observed with the WRAP5:siNEG (Figure 2B). Moreover, if one siRNA of the cocktail was replaced by the siNEG, the corresponding protein was expressed in the same manner as in the nontreated cells, confirming the specificity of the WRAP5:siMIX. For the 60 nM siMIX concentration, we could observe a slight cell cytotoxicity (20%−40%), which was not shown for the WRAP5:siNEG at the same concentration. The results demonstrated that WRAP5:siMIX nanoparticles appeared to alter cell survival mechanisms, regardless of whether two or three siRNAs were encapsulated.

Next, we assessed the duration of the silencing effect of a single dose of WRAP5:siMIX by analyzing the protein expression of CD1, CDK4, and MCL-1 at 72 h post-transfection. Indeed, the silencing observed at 24 h was maintained over time, revealing a still important knock-down of more than 70% of all three proteins (Figure 2C). However, the previously observed cytotoxicity (>20%) was lost. This could have several explanations. First, the lactate dehydrogenase (LDH) enzyme used to detect LDH release into the medium after plasma membrane alteration has a low stability over the 72 h of incubation. Second, U87 cells were sensitive to WRAP5:siRNA incubation during the first 24 h, but resistant cells persisted over time, resulting in no cytotoxicity after 72 h.

We then investigated whether using WRAP5:siMIX nanoparticles at a reduced concentration, in conjunction with repetitive doses, would have any further impact on protein silencing. To this end, we applied lower concentrations of siMIX (20 and 40 nM) daily for three consecutive days and observed the effects after 72 h post-transfection. As shown in Figure 2D, the results indicated that three repeated doses of WRAP5:siMIX induced the same silencing effect on the three targeted proteins (CD1/CDK4/MCL-1) as observed for the single dose while using 2-fold lower concentrations (20 nM and 40 nM) (Figure 2C). However, no specific cytotoxic effects were observed due to the siMIX incubation, even with the three doses applied. At the time of the third treatment (48 h), cells were still proliferating, resulting in a higher cell density compared to the conditions at 24 h. It is known that the possible cytotoxicity of nanoparticles depends on the cell density in the well: cells with a lower density are more affected than cells with a higher density.[42]

WRAP5:siMIX Nanoparticles: Impact on U87 Cell Proliferation. As we observed a slight increase in cytotoxicity with the WRAP5:siMIX nanoparticles (Figure 2A), we aimed to compare them with the WRAP5 nanoparticles encapsulating the single siRNA. For that, the siRNA concentrations within the "single"-loaded nanoparticles corresponded to those used in the "tertiary siMIX" using a short (24 h) and a longer (14 days) incubation period.

First, we evaluated the 24 h condition and revealed efficient silencing (~80%) of the three proteins using the WRAP5:siMIX nanoparticles (Figure 3A), comparable to the knockdown observed above in Figure 1C. This important silencing (80%) was only observed with WRAP5 nanoparticles loaded with the single siCD1 with the highest siRNA concentration (28 nM). For the two other single siRNA-loaded WRAP5 nanoparticles (siCDK4 and siMCL-1) the knock-downs reached lower values (60% and 45% for CDK4 and MCL-1, respectively) compared to siMIX, supporting synergistic effects. In addition, all observed protein silencing phenomena were specific because WRAP5:siNEG gave nearly no knock-down activity (100% ± 20%) for the three targeted proteins. Moreover, no significant levels of cellular toxicity were detected by LDH after 24 h.

Then, we compared the effect of WRAP5:siMIX nanoparticles on a long (14 days) incubation period using a clonogenic assay (Figure 3B). The clonogenic assay is a well-established experimental approach that quantifies the ability of a single cell to form a colony. It is a widely utilized technique for assessing the effects of pharmaceutical agents on the growth and proliferative characteristics of cells in vitro.

First, we showed that the single siRNA-loaded WRAP5 nanoparticles (same concentration as in the siMIX) had no significant effect on cell proliferation compared to the nontreated or the WRAP5:siNEG-treated cells. More interestingly, WRAP5:siMIX (40 nM) nanoparticles demonstrated a significant proliferation reduction of ~40% (**$p < 0.01$). Afterward, we evaluated the potent synergic effect of the three siRNAs within the siMIX by replacing each of them with the siNEG as shown previously (Figure 2B). When siCD1 or

https://doi.org/10.1021/acs.bioconjchem.5c00069
Bioconjugate Chem. 2025, 36, 1218−1233

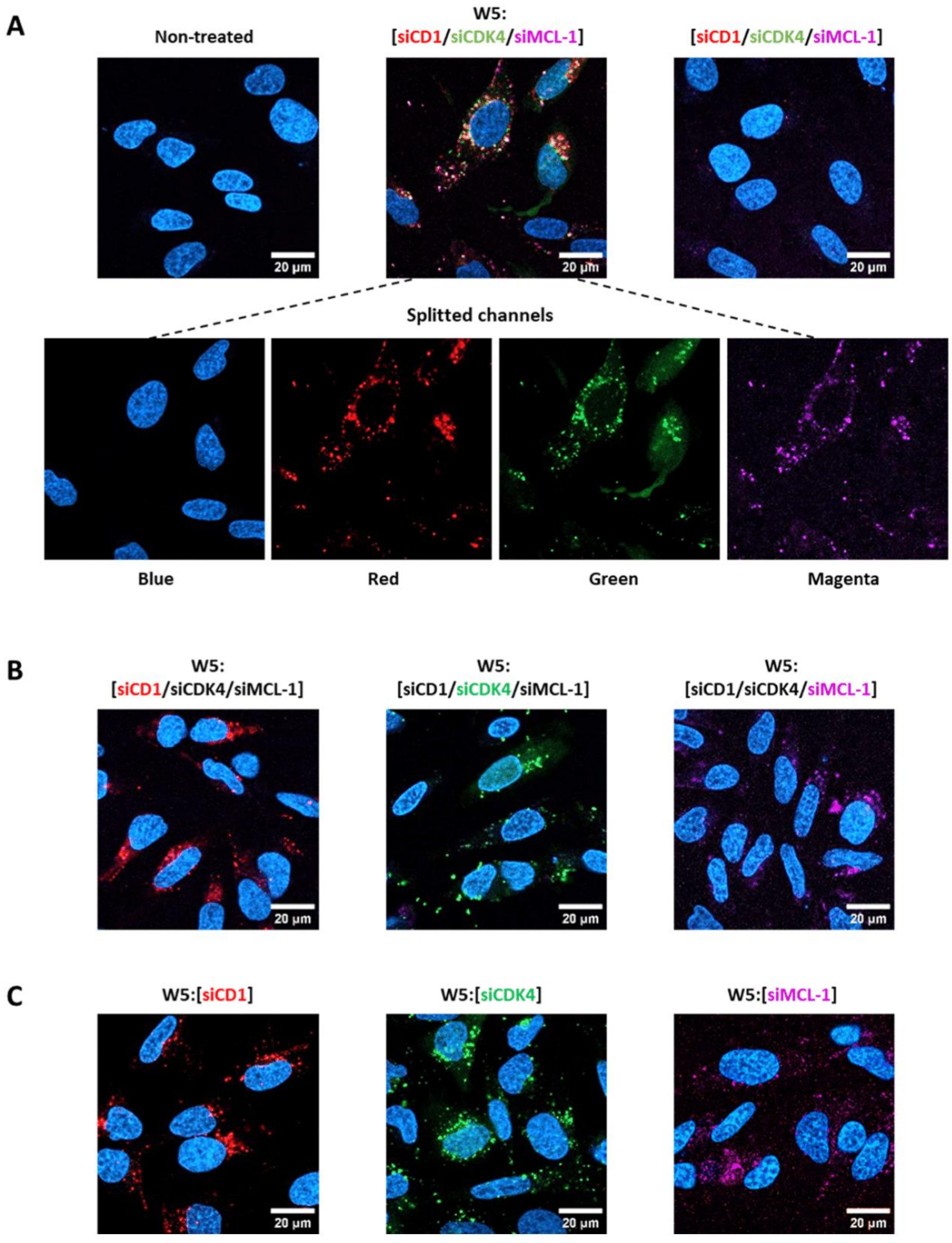

Figure 4. Evaluation of WRAP5:[siCD1/siCDK4/siMCL-1] nanoparticles transfection in GIST-T1 cells. (A) Representative live images of confocal microscopy acquisitions of fully fluorescence-labeled WRAP5:[siCD1/siCDK4/siMCL-1] nanoparticles (ratio 1/1/1, with 40 nM total siRNA concentration) compared to nontreated GIST cells or those treated with the siRNA alone [siCD1/siCDK4/siMCL-1] (without WRAP5). As a control for the uniform cellular internalization, representative live images of confocal microscopy acquisitions WRAP5:[siCD1/siCDK4/siMCL-1] nanoparticles (ratio 1/1/1, with 40 nM total siRNA concentration) with only one fluorescence-labeled siRNA (B) compared to those incubated the single siRNA-loaded WRAP5 nanoparticles (40 nM) (C).Conditions: GIST-T1 cells were incubated for 6 h at the indicated siRNA compositions. Red = siCD1-Atto550, green = siCDK4-Alexa488, magenta = siMCL-1-Atto654 and blue = Hoechst dye. White bar = 20 μm.

https://doi.org/10.1021/acs.bioconjchem.5c00069
Bioconjugate Chem. 2025, 36, 1218−1233

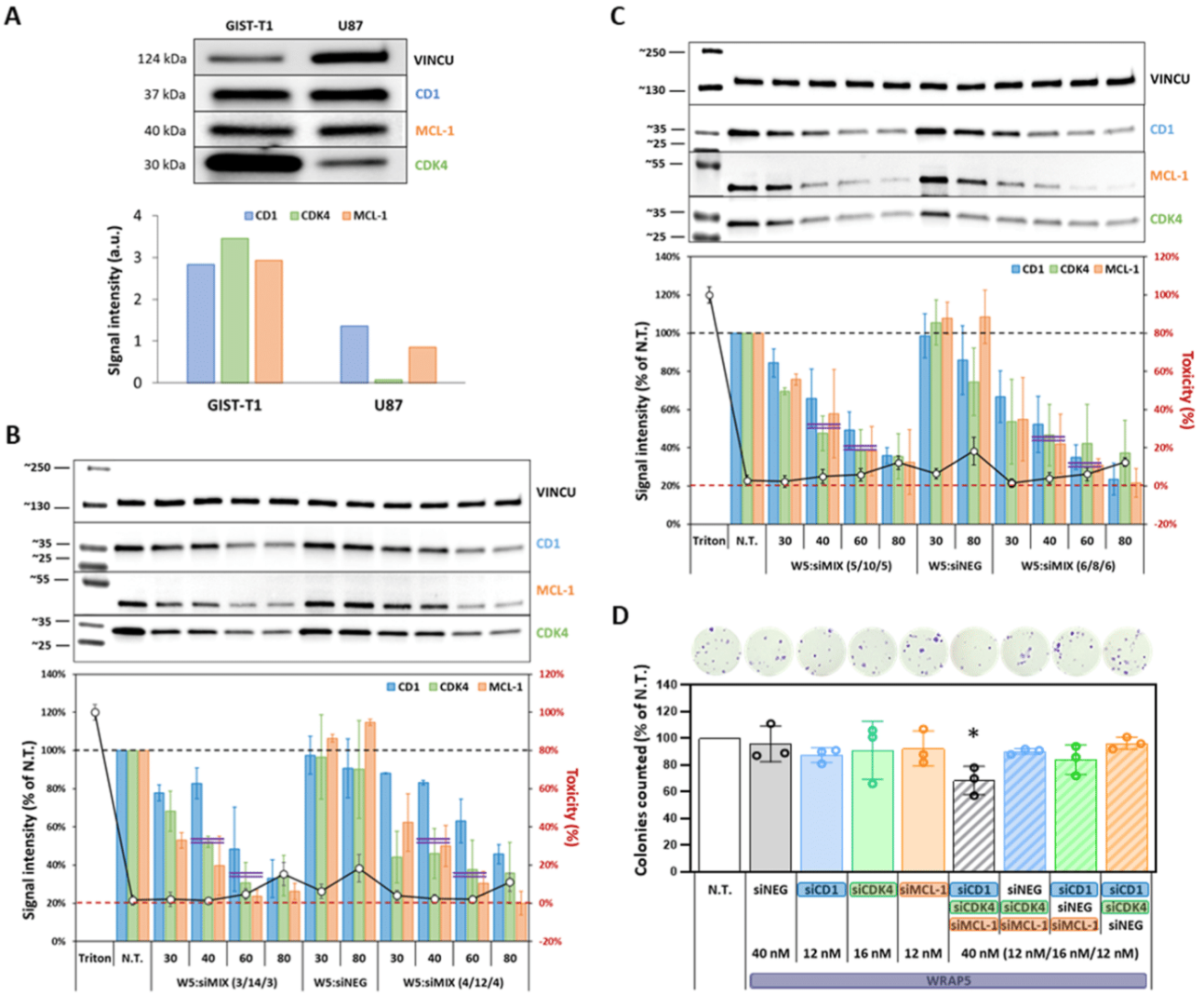

Figure 5. Evaluation of WRAP5:[siCD1/siCDK4/siMCL-1] nanoparticles transfection in GIST-T1 cells. (A) Basal expression levels of CD1, CDK4, and MCL-1 proteins in human GIST-T1 compared to U87 cells. We determined an equal expression level for CD1 and MCL-1 proteins but a higher expression pattern for CDK4 in GIST-T1 cells, contrary to U87 cells, where CDK4 was less expressed than CD1 and MCL-1. (B) Comparison of single-dose application of WRAP5:[siCD1/siCDK4/siMCL-1] nanoparticles at a ratio 3/14/3 or 4/12/4 at the indicated siRNA concentrations revealed by Western Blot after a 24 h incubation. Both conditions induced a simultaneous silencing of CD1 and MCL-1 proteins in GIST cells with less efficiency for the CD1 protein (see magenta double bars). Data represent mean ± SD using 3 independent experiments. (C) Comparison of single-dose application of WRAP5:[siCD1/siCDK4/siMCL-1] nanoparticles at a ratio 5/10/5 or 6/8/6 at the indicated siRNA concentrations revealed by Western Blot after a 24 h incubation. Only the condition with a siRNA ratio of 6/8/6 induced a simultaneous silencing of all three proteins in GIST cells (see magenta double bars). Data represent mean ± SD using 3 independent experiments. (D) WRAP5:[siCD1/siCDK4/siMCL-1] nanoparticles at a ratio 6/8/6 induced a reduction in cell proliferation in U87 cells at the indicated siRNA concentrations, revealed by clonogenic assay after a 14 day incubation. Data represent mean ± SD using 3 independent experiments. Statistics using Kruskal–Wallis test: WRAP5:siNEG ns > 0.9999, WRAP5:siCD1 ns = 0.9999, WRAP5:siCDK4 ns > 0.9999, WRAP5:siMCL-1 ns > 0.9999, WRAP:[siCD1/siCDK4/siMCL-1] p^* = 0.0434, WRAP5:[siNEG/siCDK4/siMCL-1] ns > 0.9999 WRAP5:[siCD1/siNEG/siMCL-1] ns = 0.7139 and WRAP5:[siCD1/siCDK4/siNEG] ns > 0.9999 vs nontreated cells (N.T.).

siCDK4 was replaced by the siNEG, we observed a comparable reduction in cell proliferation as the WRAP5:siMIX condition. However, in the case of replacing the siMCL-1 by the siNEG, cell proliferation was less reduced (20%, $*p < 0.05$), suggesting that, compared to siCDK4 and siCD1, the "tertiary cocktail" required siMCL-1 to ensure a greater impact. We hypothesized that the resulting inhibition of MCL-1 could be correlated to apoptosis induction, as the knockdown of *Mcl-1* was already associated with an increased level of apoptotic markers.[43]

In conclusion, applying a long-term incubation of WRAP5:siMIX nanoparticles to the U87 cells we could observe for the first time a physiological effect of the WRAP5-mediated silencing of three proteins resulting in the significant reduction of proliferation.

WRAP5:siMIX Nanoparticles: Suitable for GIST Cell Transfection. In order to evaluate the potential of the "tertiary cocktail" approach in another cancer type, we considered the multiple protein targeting using WRAP-based nanoparticles in the gastrointestinal stromal tumor (GIST). To this aim, we first examined the ability of WRAP5 nanoparticles to deliver each siRNA targeting CDK4, CD1, and MCL-1 (siCD1, siCDK4, and siMCL-1) individually in human GIST-

https://doi.org/10.1021/acs.bioconjchem.5c00069
Bioconjugate Chem. 2025, 36, 1218−1233

T1 cells.[44,45] Although significant knock-downs were detected for siCD1 and siMCL-1 (>90% for 60 nM), the targeting of CDK4 seemed to reach a plateau of 60% silencing, whatever the applied siCDK4 concentration (40, 60, 80 nM), suggesting a different silencing behavior of CDK4 (Figure S3). The siCDK4 has been previously validated in human U87 glioblastoma cells[18,40,41] but this is the first instance of its use in GIST-T1. Consequently, we tried additional CDK4-targeting siRNAs to identify the most effective siCDK4 for GIST-T1 cells. Three new siRNAs targeting CDK4 were compared to the first, which finally appeared to be the most suitable (Figure S4).

Having the optimal siRNA to silence CD1, CDK4, and MCL-1 in human GIST-T1 cells, our next objective was to examine the capacity of WRAP5 nanoparticles to deliver the siMIX in human GIST-T1 cells using an equivalent ratio (1/1/1) to determine if the three siRNAs were internalized in the same way. For this purpose, WRAP5:siMIX was formulated using fluorescence-labeled siRNA (siCDK4-Alexa488, siCD1-Atto550, and siMCL-1-Atto-655). Nanoparticle formulations in the presence of fluorescence-labeled siRNA were checked by DLS measurements in terms of size and stability and compared to unlabeled siRNA (Table 1). All nanoparticles formulated with fluorescence-labeled siRNA revealed a size between 75 and 100 nm with a PdI < 0.3, which was more or less equivalent to the unlabeled nanoparticles. We observed a slight discrepancy for the nanoparticle WRAP5:siCD1-Atto550, probably due to the fluorescent properties of the Atto550 compared to green laser features of the Zetasizer NanoZS (Malvern). Indeed, the green laser of the DLS produced a 532 nm excitation (50 mW), which could slightly excite Atto550, whose absorbance spectrum starts at 520 nm with a maximum/optimal excitation at 550 nm. This slight excitation could result in a signal noise increase and a higher polydispersity index (***Malvern FAQ Web site***).[46]

The internalization of WRAP5:siMIX nanoparticles encapsulating the three fluorescence-labeled siRNAs was visualized by confocal microscopy, thereby revealing a visible cytoplasmic signal in nearly all transfected cells compared to the nontreated cells or those treated with the siMIX without WRAP5 as the delivery system (Figure 4A). Live-cell imaging revealed the typical dotter pattern of internalized siRNA (siCD1-Atto550, siCDK4-Alexa488, and siMCL-1-Atto654) visible in the cytoplasm of GIST-T1 cells as previously reported for human U87 glioblastoma cells.[18,20]

Afterward, the internalization of WRAP5:siMIX nanoparticles containing solely one fluorescence-labeled siRNA out of the three available siRNA (Figure 4B) was compared to the internalization of WRAP5:siRNA encapsulating a single labeled siRNA, siCD1 or siCDK4 or siMCL-1 (Figure 4C). This comparison revealed that the internalization of the labeled siRNAs occurred similarly, irrespective of whether they were encapsulated alone or in combination with the others.

In conclusion, these microscopy results indicated that the presence of the three siRNAs within a single nanoparticle induced simultaneous cell transfection. In all cases, the observed fluorescence signals were specific for WRAP5-based transfection as no fluorescence signal was observed when siMIX was applied to the cells alone.

WRAP5:siMIX Nanoparticles: Suitable Simultaneous Protein in GIST Cells. Before evaluating the silencing abilities of the WRAP/siMIX to silence the expression of CDK4, CD1, and MCL-1 in human GIST-T1 cells, we first investigated their basal expression levels in GIST-T1 cells compared to human U87 glioblastoma cells. At equal total protein quantity, we determined by Western blot an equal expression level for CD1 and MCL-1 proteins in both cell lines, but a different expression profile for CDK4 depending on the cell type. Compared to the other two targets (CD1 and MCL-1), CDK4 showed lower and higher expression in U87 and GIST-T1 cells, respectively (Figure 5A). Due to this fact, we considered that the siRNA ratio in the cocktail should be modified to fit with protein expression profiles in human GIST-T1 cells. We used a higher amount of siCDK4 compared to CD1 and MCL-1 to reach an equal silencing of all three proteins. First, we evaluated the two siRNA ratios of 3/14/3 and 4/12/4 for siCD1, siCDK4, and siMCL-1, respectively (Figure 5B), revealing a dose-dependent silencing of the three targets. However, the knockdown of CD1 seemed to be less pronounced than for the other two proteins (CDK4 and MCL-1), suggesting that higher siCD1 concentrations were needed. To consider a higher amount of siCD1 in the cocktail, two other 5/10/5 and 6/8/6 siRNA ratios were evaluated in a dose-dependent manner in GIST-T1 cells (Figure 5C). In this context, compared to nontreated or GIST-T1 cells treated with the nanoparticles loaded with siNEG, only the WRAP5 nanoparticles encapsulating the 6/8/6 siRNA ratio revealed a homogeneous silencing of the three proteins of around 50% and 70% at a concentration of 40 nM and 60 nM, respectively. Under these conditions, slight cytotoxicity (LDH assay) was shown at high siRNA concentration, independent of the used siRNA (also siNEG), suggesting that this phenomenon was due to the transfection conditions rather than silencing effects.

WRAP5:siMIX Nanoparticles: Suitable to Reduce Cell Proliferation in GIST-T1 Cells. Finally, as described for U87 cells, the long-term impact of the WRAP5:siMIX nanoparticles on cell proliferation was investigated in human GIST-T1 cells through a similar clonogenic assay with a 14 days incubation period (Figure 5D). First, we analyzed the WRAP nanoparticles encapsulating the single siRNA, showing no effect on GIST-T1 cell proliferation. Then, we selected WRAP5:siMIX nanoparticles at the 6/8/6 siRNA ratio for siCD1, siCDK4, and siMCL-1, respectively, as the optimal transfection condition showing the highest knock-down efficiency. Using this condition, we demonstrated a significant reduction of cell proliferation of ∼30% ($*p < 0.05$). Interestingly, this WRAP/siMIX appeared as the only condition showing a physiological impact on GIST-T1 cells. Indeed, nanoparticles encapsulating siNEG substitution did not induce any effect on GIST-T1 colony formations (Figure 5D).

In conclusion, these results revealed that a physiological effect could be only detected for the simultaneous silencing of three proteins in GIST-T1 cells through a long-term incubation (14 days without medium change) of WRAP5:siMIX nanoparticles. Furthermore, the difference in silencing of the three targets was found to be associated with the discrepancy of physiological impact (cell proliferation) between human U87 and GIST-1-T1 cells. This emphasized the importance of adapting the siRNA ratio in siMIX according to the cell types and the expression profile of the corresponding targets.

■ DISCUSSION

WRAP5-Based siRNA Delivery in Human U87 Glioblastoma Cells: From One to Multiple Silencing. First, we investigated the use of WRAP5-based nanoparticles to transfer

https://doi.org/10.1021/acs.bioconjchem.5c00069
Bioconjugate Chem. 2025, 36, 1218−1233

siRNA such as siCDK4, siCD1, and siMCL-1 individually in human U87 glioblastoma cells to estimate the efficiency of gene silencing for each target and their potential physiological impact (Figure 1A). As already published, we observed that the targeting of CDK4 was significant (95% inhibition with 20 nM siCDK4) and in agreement with our previous work,[18] supporting here the robustness of the WRAP5 technology in siRNA delivery. The siRNA-mediated inhibition of CD1 expression was significant but required a higher siRNA concentration (50 nM) to reach a similar CDK4 extinction, suggesting a difference in the level of expression or half-life of CD1 compared to CDK4. However, as for CDK4, the CD1 inhibition did not induce any significant phenotype. Concerning MCL-1, a strong knockdown (85% inhibition) was detected at 20 nM. Belonging to the anti-apoptotic BCL-2 family proteins, MCL-1 was known to have a very short biological half-life of only 20−30 min, which could explain the siRNA-mediated knock-down efficiency.[47] However, we did not detect any impact on the cell proliferation for the three single siRNAs used in this study. We correlated this observation with the fact that CDK4, as well as CD1, could be replaced by other CDK or Cyclin proteins.[36,48]

In the context of glioblastoma cells, it is known that Bcl-2 inhibition triggers MCL-1 upregulation. This compensatory mechanism is a cellular response to the role typically played by Bcl-2 in preventing cell death.[49] Thus, it is possible that MCL-1 antiapoptotic activity could be replaced by other antiapoptotic proteins such as Bcl-2.

As for other drug delivery systems, we tried to improve the cellular impact of gene silencing by using siRNA combinations through WRAP5 nanoparticles encapsulating siRNA cocktails. We first investigated a "binary cocktail" approach by encapsulating two siRNAs within the nanoparticle. We tested the association of siCD1 with siCDK4 to knock-down the CDK4/CD1 complex involved in the cell cycle checkpoint of human U87 glioblastoma cells, expecting a cell cycle arrest.

Indeed, CDK4 played a pivotal role in regulating the G1 to S phase transition, a critical checkpoint in the cell cycle.[50] In the early G1 phase, CD1 bound to CDK4, forming a cyclin D-CDK4 complex, which translocated into the nucleus. The binding of CD1 to CDK4 resulted in a conformational change that activated the kinase activity of CDK4, enabling it to phosphorylate the retinoblastoma (RB) protein. Once phosphorylated, Rb underwent conformational changes, releasing the E2F transcription factors, previously bound to and inhibited by Rb. The free E2F transcription factor activated the expression of genes required for DNA synthesis and replication, important for the transition into S phase.

As the CD1 inhibition alone required a higher amount of siRNA, we mixed 80% of siCD1 with 20% of siCDK4, corresponding to a 4/1 stoichiometry between siCD1/siCDK4 (Figure 1B). Results revealed the ability to silence both proteins at a similar level for this siRNA molar ratio, confirming the rationale of the "binary cocktail" strategy. However, as with previous single-target extinction, no physiological impact was observed, suggesting that potential cell cycle arrest may not be sufficient to generate a net biological effect.[48]

Then, we decided to incorporate a siRNA targeting the antiapoptotic MCL-1, to orient the approach toward a "tertiary cocktail" strategy with two siRNAs targeting the cell cycle and one targeting antiapoptotic characteristics (Figure 1C). The idea was to affect the cell cycle progression and simultaneously activate apoptosis. Based on a single siRNA and "binary cocktail" formulation, we used a siRNA cocktail with a higher siCD1 concentration (70%) compared to equivalent amounts of both siCDK4 (15%) and siMCL-1 (15%), resulting in a 14/3/3 stoichiometry (70%/15%/15%). The WRAP5-mediated delivery of such a "tertiary cocktail" enabled an equivalent knock-down of the three targets CD1, CDK4, and MCL-1, revealing the force of the WRAP5 nanoparticles as a delivery system.

Using the WRAP5:siMIX, we observed an 80% extinction of the three respective protein targets at the low siRNA concentration (40 nM siMIX = 28 nM siCD1, 6 nM siCDK4, 6 nM siMCL-1), compared to the 40% to 60% extinction detected for the siRNA individually. These data indicated a synergic effect between the three siRNAs of the siMIX, supporting the potency of the "tertiary cocktail" combination for multiple silencing by WRAP5 nanoparticles. Our results were in agreement with previously reported nanoparticles loaded with different siRNAs. One example is given through a cholesterol-modified antimicrobial peptide (AMP) DP7, which encapsulated multiple siRNA elements and exhibited a synergic antitumor effect compared to single-target therapy.[51] Also, dendrimers were shown to be able to encapsulate three distinct siRNAs targeting the *Bcl-xl*, *Bcl-2*, and *MCL-1* genes for simultaneous protein silencing as a new treatment for breast cancer.[52] Similarly, lipid nanoparticles were associated with siRNA cocktails enabling inhibition of *MCL-1*, *Bcl-2*, and *CD1* genes in the Mantle cell lymphoma.[48]

Finally, we evaluated the impact of WRAP5:siMIX on the proliferation of human U87 glioblastoma cells using the commonly used clonogenic assay. We first demonstrated that single siRNA-loaded nanoparticles were ineffective in altering cell proliferation. Remarkably, we highlighted that WRAP5:-siMIX nanoparticles significantly reduced cell proliferation (−40% with 40 nM), underscoring the importance of multitargeting genes for effective cancer inhibition.

siRNA Cocktail Optimization Based on Targeted Cancer Cell Types. After validation in human U87 glioblastoma cells, we applied our multiple targeting strategies to other cancers by considering gastrointestinal stromal tumors (GIST), a common form of sarcoma of the digestive tract. A rapid comparison of the basal expression levels of targeted proteins revealed a difference in the CDK4 expression profile with a higher level in GIST-T1 than in U87 cells. To translate the WRAP5:siMIX to human GIST-T1 cells, modification of the siRNA molar ratio within the siMIX should be changed in order to reach a similar silencing efficiency.

This first observation was not surprising as cancer cell types have different properties and protein expression, suggesting that the siRNA ratio should be adapted. An example is given by Knapp et al., mentioning the treatment of human mantle cell lymphoma (JeKo-1 cells) using a "tertiary siMIX" at a dose of 210 nM, which contained 10 nM siMCL-1, 100 nM siBcl-2, and 100 nM siCD1 (1/10/10 siRNA molar ratio).[48] In our study, a low siMCL-1 concentration was sufficient in comparison to the siCD1/siBcl-2 concentrations.

For GIST-T1 cells, we used the same three siRNAs (siCD1, siCDK4, and siMCL-1) as all were represented in this cell line associated with the development of the pathology. CD1 was described as a potential therapeutic target in KIT-independent GISTs, with bortezomib-mediated inhibition proposed as a novel therapeutic strategy.[53] Furthermore, CD1 played a crucial role in GIST-KIT independence, as its suppression

https://doi.org/10.1021/acs.bioconjchem.5c00069
Bioconjugate Chem. 2025, 36, 1218−1233

exhibited antiproliferative and pro-apoptotic effects.[39] Besides that, recurrent genomic aberrations by in-cell cycle regulators were determined which caused coactivation of the CDK2 and CDK4/6 pathways in clinical GIST samples.[36] Finally, MCL-1 overexpression in GIST patients was associated with OSTEOPONTIN, a secreted phosphoprotein involved in the malignant potential and aggressive phenotypes.[54]

After having screened several siRNA ratios, we identified the ratio of 6/8/6 [siCD1/siCDK4/siMCL-1] as the optimal one for human GIST-T1 cells (Figure 5C). In detail, we observed with this optimized siMIX the silencing of around 50% (40 nM) of the three proteins CD1, CDK4, and MCL-1. Curiously, using the same siMIX concentration of 40 nM, the knockdown efficiency in GIST-T1 cells was lower than in human U87 glioblastoma cells. Clonogenic assay on GIST-T1 cells using WRAP5:siMIX nanoparticles revealed a significant reduction (−30% with 40 nM) compared to single siRNA or siNEG-substituted siMIX, highlighting their impact on GIST-T1 cell proliferation (Figure 5D).

These results supported the fact that a stoichiometric siRNA adjustment should be performed according to the cellular type, i.e., targeted cancer. This also indicated that for similar targeted proteins, the innate nature of cells determined the siRNA cocktail stoichiometry.

■ CONCLUSION

In the present work, we demonstrated the ability of WRAP5-based nanoparticles to deliver a siRNA cocktail (siMIX) in order to silence three distinct proteins in neuroblastoma and sarcoma-derived cells. The siRNA molar ratio within the siMIX had to be adapted to the level of expression of each targeted protein with regard to the cancer cell type used. However, working on siRNA cocktails encapsulated in delivery systems raised several questions as highlighted by Guo et al.[55] Before the selection of the targeted proteins that should be silenced, researchers should ask themselves if multigene silencing will be more efficient than single gene knockdown, if targeting different signaling pathways should be more suitable than focusing on a single pathway. Furthermore, it is important to identify the main target/siRNA couple to define the optimal combination (ratio) that should be applied to obtain the best synergic therapeutic gene silencing.

For the future, to potentiate WRAP5-based siRNA cocktails, other parameters could be further optimized as reported previously to increase their in vivo stability by PEGylation,[41] their localization in specific intracellular compartments by targeting motif grafting,[56] or more recently, their dependence on the nature of the microenvironment by integration of a pH-sensitive linker.[19] WRAP5-based nanoparticles have already been successfully applied for the siRNA delivery in vivo in different animal models. Through intratumoral injection in mice or recently by simple bath immersion for the Zebra fish,[23] peptide-based nanoparticles constituted a promising alternative to existing lipid-based siRNA delivery methods. Therefore, their use for a multiprotein silencing in vivo should be of a real interest.

Taken together, these innovative results with respect to peptide-based nanoparticle technology will pave the way for developments that could lead to an improvement in the approach to personalized medicine.

■ ASSOCIATED CONTENT

Supporting Information

The Supporting Information is available free of charge at https://pubs.acs.org/doi/10.1021/acs.bioconjchem.5c00069.

Whole Experimental Section. Table S1 referred to the used siRNA sequences; Figure S1 to the evaluation of the dose-dependent silencing of WRAP5:siRNA nanoparticles in U87 cells; Figure S2 to graphical representations of the measured mean sizes of WRAP5-based nanoparticles; Figure S3 to the evaluation of the dose-dependent silencing of WRAP5:siRNA nanoparticles in GIST cells; Figure S4 to the evaluation of the silencing of WRAP5:siRNA nanoparticles encapsulating different siCDK4 in GIST-T1 cells (PDF)

■ AUTHOR INFORMATION

Corresponding Authors

Prisca Boisguérin − *PhyMedExp, University of Montpellier, INSERM U1046, CNRS UMR 9214371, 34295 Montpellier, Cedesx 5, France;* orcid.org/0000-0002-6955-1340; Email: prisca.boisguerin@inserm.fr

Sébastien Deshayes − *PhyMedExp, University of Montpellier, INSERM U1046, CNRS UMR 9214371, 34295 Montpellier, Cedesx 5, France;* orcid.org/0000-0002-4684-9152; Email: sebastien.deshayes@inserm.fr

Authors

Karidia Konate − *PhyMedExp, University of Montpellier, INSERM U1046, CNRS UMR 9214371, 34295 Montpellier, Cedesx 5, France*

Irène Pezzati − *PhyMedExp, University of Montpellier, INSERM U1046, CNRS UMR 9214371, 34295 Montpellier, Cedesx 5, France*

Karima Redjatti − *University of Montpellier, 34090 Montpellier, France*

Estelle Agnel − *University of Montpellier, 34090 Montpellier, France*

Eric Vivès − *PhyMedExp, University of Montpellier, INSERM U1046, CNRS UMR 9214371, 34295 Montpellier, Cedesx 5, France*

Sandrine Faure − *PhyMedExp, University of Montpellier, INSERM U1046, CNRS UMR 9214371, 34295 Montpellier, Cedesx 5, France*

Pascal de Santa Barbara − *PhyMedExp, University of Montpellier, INSERM U1046, CNRS UMR 9214371, 34295 Montpellier, Cedesx 5, France*

Complete contact information is available at: https://pubs.acs.org/10.1021/acs.bioconjchem.5c00069

Author Contributions

[§]K.K. and I.P. contributed equally to the work.

Notes

Patent entitled "Non-naturally occurring peptides for use as cell-penetrating peptides" WO2020/016242.

The authors declare no competing financial interest.

■ ACKNOWLEDGMENTS

This research was funded by the "Fondation ARC pour la Recherche sur le Cancer" (PJA20171206171 to P.B.), the "Agence Nationale de la Recherche" (ANR-21-CE18-0022-01 to P.B.), AFM-Téléthon (n°23800 to S.F.), and by institutional

funds from INSERM, CNRS and University of Montpellier. The authors are grateful to Pascal Verdié from the SynBio3 platform for providing peptide synthesis facilities, and to Pierre Sanchez for performing LCMS analysis, both from the Institut des Biomolécules Max Mousseron (IBMM), Montpellier (France).

REFERENCES

(1) Bray, F.; Laversanne, M.; Sung, H.; Ferlay, J.; Siegel, R. L.; Soerjomataram, I.; Jemal, A. Global Cancer Statistics 2022: GLOBOCAN Estimates of Incidence and Mortality Worldwide for 36 Cancers in 185 Countries. *Ca-Cancer J. Clin.* **2024**, *74* (3), 229−263.

(2) Tripathi, P. P.; Arami, H.; Banga, I.; Gupta, J.; Gandhi, S. Cell Penetrating Peptides in Preclinical and Clinical Cancer Diagnosis and Therapy. *Oncotarget* **2018**, *9* (98), 37252−37267.

(3) van den Boogaard, W. M. C.; Komninos, D. S. J.; Vermeij, W. P. Chemotherapy Side-Effects: Not All DNA Damage Is Equal. *Cancers* **2022**, *14* (3), 627.

(4) Vaz-Salgado, M. A.; Villamayor, M.; Albarrán, V.; Alía, V.; Sotoca, P.; Chamorro, J.; Rosero, D.; Barrill, A. M.; Martín, M.; Fernandez, E.; Gutierrez, J. A.; Rojas-Medina, L. M.; Ley, L. Recurrent Glioblastoma: A Review of the Treatment Options. *Cancers* **2023**, *15* (17), 4279.

(5) Cicala, C. M.; Olivares-Rivas, I.; Aguirre-Carrillo, J. A.; Serrano, C. KIT/PDGFRA Inhibitors for the Treatment of Gastrointestinal Stromal Tumors: Getting to the Gist of the Problem. *Expert Opin. Invest. Drugs* **2024**, *33* (3), 159−170.

(6) Shoari, A.; Tooyserkani, R.; Tahmasebi, M.; Löwik, D. W. P. M. Delivery of Various Cargos into Cancer Cells and Tissues via Cell-Penetrating Peptides: A Review of the Last Decade. *Pharmaceutics* **2021**, *13* (9), 1391.

(7) Mikutis, S.; Bernardes, G. J. L. Technologies for Targeted RNA Degradation and Induced RNA Decay. *Chem. Rev.* **2024**, *124* (23), 13301−13330.

(8) Tang, Q.; Khvorova, A. RNAi-Based Drug Design: Considerations and Future Directions. *Nat. Rev. Drug Discovery* **2024**, *23* (5), 341−364.

(9) Hoy, S. M. Patisiran: First Global Approval. *Drugs* **2018**, *78* (15), 1625−1631.

(10) Brown, C. R.; Gupta, S.; Qin, J.; Racie, T.; He, G.; Lentini, S.; Malone, R.; Yu, M.; Matsuda, S.; Shulga-Morskaya, S.; Nair, A. V.; Theile, C. S.; Schmidt, K.; Shahraz, A.; Goel, V.; Parmar, R. G.; Zlatev, I.; Schlegel, M. K.; Nair, J. K.; Jayaraman, M.; Manoharan, M.; Brown, D.; Maier, M. A.; Jadhav, V. Investigating the Pharmacodynamic Durability of GalNAc−siRNA Conjugates. *Nucleic Acids Res.* **2020**, *48* (21), 11827−11844.

(11) Yonezawa, S.; Koide, H.; Asai, T. Recent Advances in siRNA Delivery Mediated by Lipid-Based Nanoparticles. *Adv. Drug Delivery Rev.* **2020**, *154*−*155*, 64−78.

(12) Ahn, I.; Kang, C. S.; Han, J. Where Should siRNAs Go: Applicable Organs for siRNA Drugs. *Exp. Mol. Med.* **2023**, *55* (7), 1283−1292.

(13) Guo, F.; Ke, J.; Fu, Z.; Han, W.; Wang, L. Cell Penetrating Peptide-Based Self-Assembly for PD-L1 Targeted Tumor Regression. *Int. J. Mol. Sci.* **2021**, *22* (24), 13314.

(14) Falato, L.; Gestin, M.; Langel, U. Cell-Penetrating Peptides Delivering siRNAs: An Overview. In *Design and Delivery of SiRNA Therapeutics*; Humana: New York, NY, 2021; pp 329−352.

(15) Boisguérin, P.; Konate, K.; Josse, E.; Vivès, E.; Deshayes, S. Peptide-Based Nanoparticles for Therapeutic Nucleic Acid Delivery. *Biomedicines* **2021**, *9* (5), 583.

(16) Wickline, S. A.; Hou, K. K.; Pan, H. Peptide-Based Nanoparticles for Systemic Extrahepatic Delivery of Therapeutic Nucleotides. *Int. J. Mol. Sci.* **2023**, *24* (11), 9455.

(17) Mendes, B. B.; Conniot, J.; Avital, A.; Yao, D.; Jiang, X.; Zhou, X.; Sharf-Pauker, N.; Xiao, Y.; Adir, O.; Liang, H.; Shi, J.; Schroeder, A.; Conde, J. Nanodelivery of Nucleic Acids. *Nat. Rev. Methods Primers* **2022**, *2* (1), 1−21.

(18) Konate, K.; Dussot, M.; Aldrian, G.; Vaissière, A.; Viguier, V.; Neira, I. F.; Couillaud, F.; Vivès, E.; Boisguerin, P.; Deshayes, S. Peptide-Based Nanoparticles to Rapidly and Efficiently "Wrap 'n Roll" siRNA into Cells. *Bioconjugate Chem.* **2019**, *30* (3), 592−603.

(19) Di Gregorio, G.; Vallée, C.; Konate, K.; Teko-Agbo, C.; Hammoum, T.; Faure-Gautron, H.; Bessin, Y.; Deshayes, S.; Vivès, E.; Meli, A. C.; de Santa Barbara, P.; Faure, S.; Barrère-Lemaire, S.; Ulrich, S.; Boisguérin, P. Enhancing WRAP-Based Nanoparticles for siRNA Delivery in pH-Sensitive Environments. *ChemMedChem* **2025**, No. e202400885.

(20) Deshayes, S.; Konate, K.; Dussot, M.; Chavey, B.; Vaissière, A.; Van, T. N. N.; Aldrian, G.; Padari, K.; Pooga, M.; Vivès, E.; Boisguérin, P. Deciphering the Internalization Mechanism of WRAP:siRNA Nanoparticles. *Biochim. Biophys. Acta, Biomembr.* **2020**, *1862* (6), 183252.

(21) Konate, K.; Josse, E.; Tasic, M.; Redjatti, K.; Aldrian, G.; Deshayes, S.; Boisguérin, P.; Vivès, E. WRAP-Based Nanoparticles for siRNA Delivery: A SAR Study and a Comparison with Lipid-Based Transfection Reagents. *J. Nanobiotechnol.* **2021**, *19* (1), 236.

(22) Ferreiro, I.; Genevois, C.; Konate, K.; Vivès, E.; Boisguérin, P.; Deshayes, S.; Couillaud, F. Vivo Follow-Up of Gene Inhibition in Solid Tumors Using Peptide-Based Nanoparticles for siRNA Delivery. *Pharmaceutics* **2021**, *13* (5), 749.

(23) Konate, K.; Agbo, C. T.; Pezzati, I.; Hammoum, T.; Deshayes, S.; Descamps, S.; Vivès, E.; Faure, S.; de Santa Barbara, P.; Boisguérin, P. WRAP-Based Nanoparticles for siRNA Delivery in Zebrafish Embryos by Simple Bath Immersion. *Mol. Ther.—Methods Clin. Dev.* **2025**, *33*, 101458.

(24) Hanif, F.; Muzaffar, K.; Perveen, K.; Malhi, S.; Simjee, S. Glioblastoma Multiforme: A Review of Its Epidemiology and Pathogenesis through Clinical Presentation and Treatment. *Asian Pac. J. Cancer Prev.* **2017**, *18* (1), 3.

(25) Farooq, M.; Scalia, G.; Umana, G. E.; Parekh, U. A.; Naeem, F.; Abid, S. F.; Khan, M. H.; Zahra, S. G.; Sarkar, H. P.; Chaurasia, B. A Systematic Review of Nanomedicine in Glioblastoma Treatment: Clinical Efficacy, Safety, and Future Directions. *Brain Sci.* **2023**, *13* (12), 1727.

(26) Friedman, A.; Bigner, D.; Van Meir, E. G.; Brat, D. J.; M Mastrogianakis, G.; Olson, J. J.; Mikkelsen, T.; Lehman, N.; Aldape, K.; Alfred Yung, W. K.; Bogler, O.; VandenBerg, S.; Berger, M.; Prados, M.; Muzny, D.; Morgan, M.; Scherer, S.; Sabo, A.; Nazareth, L.; Lewis, L.; Hall, O.; Zhu, Y.; Ren, Y.; Alvi, O.; Yao, J.; Hawes, A.; Jhangiani, S.; Fowler, G.; San Lucas, A.; Kovar, C.; Cree, A.; Dinh, H.; Santibanez, J.; Joshi, V.; Gonzalez-Garay, M. L.; Miller, C. A.; Milosavljevic, A.; Donehower, L.; Wheeler, D. A.; Gibbs, R. A.; Cibulskis, K.; Sougnez, C.; Fennell, T.; Mahan, S.; Wilkinson, J.; Ziaugra, L.; Onofrio, R.; Bloom, T.; Nicol, R.; Ardlie, K.; Baldwin, J.; Gabriel, S.; Lander, E. S.; Ding, L.; Fulton, R. S.; McLellan, M. D.; Wallis, J.; Larson, D. E.; Shi, X.; Abbott, R.; Fulton, L.; Chen, K.; Koboldt, D. C.; Wendl, M. C.; Meyer, R.; Tang, Y.; Lin, L.; Osborne, J. R.; Dunford-Shore, B. H.; Miner, T. L.; Delehaunty, K.; Markovic, C.; Swift, G.; Courtney, W.; Pohl, C.; Abbott, S.; Hawkins, A.; Leong, S.; Haipek, C.; Schmidt, H.; Wiechert, M.; Vickery, T.; Scott, S.; Dooling, D. J.; Chinwalla, A.; Weinstock, G. M.; Mardis, E. R.; Wilson, R. K.; Getz, G.; Winckler, W.; Verhaak, R. G. W.; Lawrence, M. S.; O'Kelly, M.; Robinson, J.; Alexe, G.; Beroukhim, R.; Carter, S.; Chiang, D.; Gould, J.; Gupta, S.; Korn, J.; Mermel, C.; Mesirov, J.; Monti, S.; Nguyen, H.; Parkin, M.; Reich, M.; Stransky, N.; Weir, B. A.; Garraway, L.; Golub, T.; Meyerson, M.; Chin, L.; Protopopov, A.; Zhang, J.; Perna, I.; Aronson, S.; Sathiamoorthy, N.; Ren, G.; Yao, J.; Wiedemeyer, W. R.; Kim, H.; Won Kong, S.; Xiao, Y.; Kohane, I. S.; Seidman, J.; Park, P. J.; Kucherlapati, R.; Laird, P. W.; Cope, L.; Herman, J. G.; Weisenberger, D. J.; Pan, F.; Van Den Berg, D.; Van Neste, L.; Mi Yi, J.; Schuebel, K. E.; Baylin, S. B.; Absher, D. M.; Li, J. Z.; Southwick, A.; Brady, S.; Aggarwal, A.; Chung, T.; Sherlock, G.; Brooks, J. D.; Myers, R. M.; Spellman, P. T.; Purdom, E.; Jakkula, L. R.; Lapuk, A. V.; Marr, H.; Dorton, S.; Gi Choi, Y.; Han, J.; Ray, A.;

Wang, V.; Durinck, S.; Robinson, M.; Wang, N. J.; Vranizan, K.; Peng, V.; Van Name, E.; Fontenay, G. V.; Ngai, J.; Conboy, J. G.; Parvin, B.; Feiler, H. S.; Speed, T. P.; Gray, J. W.; Brennan, C.; Socci, N. D.; Olshen, A.; Taylor, B. S.; Lash, A.; Schultz, N.; Reva, B.; Antipin, Y.; Stukalov, A.; Gross, B.; Cerami, E.; Qing Wang, W.; Qin, L.-X.; Seshan, V. E.; Villafania, L.; Cavatore, M.; Borsu, L.; Viale, A.; Gerald, W.; Sander, C.; Ladanyi, M.; Perou, C. M.; Neil Hayes, D.; Topal, M. D.; Hoadley, K. A.; Qi, Y.; Balu, S.; Shi, Y.; Wu, J.; Penny, R.; Bittner, M.; Shelton, T.; Lenkiewicz, E.; Morris, S.; Beasley, D.; Sanders, S.; Kahn, A.; Sfeir, R.; Chen, J.; Nassau, D.; Feng, L.; Hickey, E.; Zhang, J.; Weinstein, J. N.; Barker, A.; Gerhard, D. S.; Vockley, J.; Compton, C.; Vaught, J.; Fielding, P.; Ferguson, M. L.; Schaefer, C.; Madhavan, S.; Buetow, K. H.; Collins, F.; Good, P.; Guyer, M.; Ozenberger, B.; Peterson, J.; Thomson, E.; The Cancer Genome Atlas Research Network. Comprehensive Genomic Characterization Defines Human Glioblastoma Genes and Core Pathways. *Nature* **2008**, *455* (7216), 1061−1068.

(27) Malumbres, M.; Barbacid, M. To Cycle or Not to Cycle: A Critical Decision in Cancer. *Nat. Rev. Cancer* **2001**, *1* (3), 222−231.

(28) Qie, S.; Diehl, J. A. Cyclin D1, Cancer Progression, and Opportunities in Cancer Treatment. *J. Mol. Med.* **2016**, *94* (12), 1313−1326.

(29) Yamaguchi, R.; Lartigue, L.; Perkins, G. Targeting Mcl-1 and Other Bcl-2 Family Member Proteins in Cancer Therapy. *Pharmacol. Ther.* **2019**, *195*, 13−20.

(30) Wang, L.; Chen, Y.; Zhang, M.; Liu, J.; Li, H.; Liu, M.; Wu, S.; Zhang, Y.; Li, W.; Wang, B. Chemical Dissection of Selective Myeloid Leukemia-1 Inhibitors: How They Were Found and Evolved. *Eur. J. Med. Chem.* **2025**, *283*, 117168.

(31) Fofaria, N. M.; Frederick, D. T.; Sullivan, R. J.; Flaherty, K. T.; Srivastava, S. K. Overexpression of Mcl-1 Confers Resistance to BRAFV600E Inhibitors Alone and in Combination with MEK1/2 Inhibitors in Melanoma. *Oncotarget* **2015**, *6* (38), 40535−40556.

(32) Reiner, T.; de las Pozas, A.; Parrondo, R.; Palenzuela, D.; Cayuso, W.; Rai, P.; Perez-Stable, C. Mcl-1 Protects Prostate Cancer Cells from Cell Death Mediated by Chemotherapy-Induced DNA Damage. *Oncoscience* **2015**, *2* (8), 703−715.

(33) Zervantonakis, I. K.; Iavarone, C.; Chen, H.-Y.; Selfors, L. M.; Palakurthi, S.; Liu, J. F.; Drapkin, R.; Matulonis, U.; Leverson, J. D.; Sampath, D.; Mills, G. B.; Brugge, J. S. Systems Analysis of Apoptotic Priming in Ovarian Cancer Identifies Vulnerabilities and Predictors of Drug Response. *Nat. Commun.* **2017**, *8*, 365.

(34) Vaamonde-Martín, R. J.; Ballesta-Ruiz, M.; Sánchez-Gil, A.; Fernández, J. A.; Martínez-Barba, E.; Martínez-García, J.; Gatta, G.; Chirlaque-López, M. D. Incidence Trends and Main Features of Gastro-Intestinal Stromal Tumours in a Mediterranean Region: A Population-Based Study. *Cancers* **2023**, *15* (11), 2994.

(35) ROCHE. Cytotoxicity Detection Kit, 2020 https://www.sigmaaldrich.com/deepweb/assets/sigmaaldrich/product/documents/167/504/11644793001.pdf?srsltid=AfmBOorrPGoZj3Hyg_ZkI5isSAWUkBJmcRMQamrM_36566KKjAPZgcgs.

(36) Schaefer, I.-M.; Hemming, M. L.; Lundberg, M. Z.; Serrata, M. P.; Goldaracena, I.; Liu, N.; Yin, P.; Paulo, J. A.; Gygi, S. P.; George, S.; Morgan, J. A.; Bertagnolli, M. M.; Sicinska, E. T.; Chu, C.; Zheng, S.; Mariño-Enríquez, A.; Hornick, J. L.; Raut, C. P.; Ou, W.-B.; Demetri, G. D.; Saka, S. K.; Fletcher, J. A. Concurrent Inhibition of CDK2 Adds to the Anti-Tumour Activity of CDK4/6 Inhibition in GIST. *Br. J. Cancer* **2022**, *127* (11), 2072−2085.

(37) Malumbres, M.; Barbacid, M. Cell Cycle, CDKs and Cancer: A Changing Paradigm. *Nat. Rev. Cancer* **2009**, *9* (3), 153−166.

(38) Champagne, J.; Linares, L. K.; Maurel, B.; Zampieri, A.; Moreno, M.; Fuentes, I.; Dubois, E.; Severac, D.; Decorsière, A.; Bienvenu, F. TAG-RNAi Overcomes off-Target Effects in Cancer Models. *Oncogene* **2020**, *39* (4), 935−945.

(39) Ou, W.-B.; Ni, N.; Zuo, R.; Zhuang, W.; Zhu, M.; Kyriazoglou, A.; Wu, D.; Eilers, G.; Demetri, G. D.; Qiu, H.; Li, B.; Marino-Enriquez, A.; Fletcher, J. A. Cyclin D1 Is a Mediator of Gastrointestinal Stromal Tumor KIT-Independence. *Oncogene* **2019**, *38* (39), 6615−6629.

(40) Vaissière, A.; Aldrian, G.; Konate, K.; Lindberg, M. F.; Jourdan, C.; Telmar, A.; Seisel, Q.; Fernandez, F.; Viguier, V.; Genevois, C.; Couillaud, F.; Boisguerin, P.; Deshayes, S. A Retro-Inverso Cell-Penetrating Peptide for siRNA Delivery. *J. Nanobiotechnol.* **2017**, *15* (1), 34.

(41) Aldrian, G.; Vaissière, A.; Konate, K.; Seisel, Q.; Vivès, E.; Fernandez, F.; Viguier, V.; Genevois, C.; Couillaud, F.; Démènè, H.; Aggad, D.; Covinhes, A.; Barrère-Lemaire, S.; Deshayes, S.; Boisguerin, P. PEGylation Rate Influences Peptide-Based Nanoparticles Mediated siRNA Delivery in Vitro and in Vivo. *J. Controlled Release* **2017**, *256*, 79−91.

(42) Heng, B. C.; Zhao, X.; Xiong, S.; Ng, K. W.; Boey, F. Y.-C.; Loo, J. S.-C. Cytotoxicity of Zinc Oxide (ZnO) Nanoparticles Is Influenced by Cell Density and Culture Format. *Arch. Toxicol.* **2011**, *85* (6), 695−704.

(43) Takagi, S.; Nakajima, M.; Koike, S.; Takami, M.; Sugiura, Y.; Sakata, S.; Baba, S.; Takemoto, A.; Huang, T.; Seto, Y.; Saito, M.; Funauchi, Y.; Ae, K.; Takeuchi, K.; Fujita, N.; Katayama, R. Frequent Copy Number Gain of MCL1 Is a Therapeutic Target for Osteosarcoma. *Oncogene* **2024**, *44*, 794−804.

(44) Taguchi, T.; Sonobe, H.; Toyonaga, S.; Yamasaki, I.; Shuin, T.; Takano, A.; Araki, K.; Akimaru, K.; Yuri, K. Conventional and Molecular Cytogenetic Characterization of a New Human Cell Line, GIST-T1, Established from Gastrointestinal Stromal Tumor. *Lab. Invest.* **2002**, *82* (5), 663−665.

(45) Ruiz-Demoulin, S.; Trenquier, E.; Dekkar, S.; Deshayes, S.; Boisguérin, P.; Serrano, C.; de Santa Barbara, P.; Faure, S. LIX1 Controls MAPK Signaling Reactivation and Contributes to GIST-T1 Cell Resistance to Imatinib. *Int. J. Mol. Sci.* **2023**, *24* (8), 7138.

(46) Can_fluorescent_samples_be_measured_with_DLS_. https://macro.lsu.edu/HowTo/MALVERN/FAQ_HTML/can_fluorescent_samples_be_measured_with_dls/can_fluorescent_samples_be_measured_with_dls_.htm (accessed 2025−02−03).

(47) Kelly, G. L.; Strasser, A. Toward Targeting Antiapoptotic MCL-1 for Cancer Therapy. *Annu. Rev. Cancer Biol.* **2020**, *4* (4), 299−313.

(48) Knapp, C. M.; He, J.; Lister, J.; Whitehead, K. A. Lipid Nanoparticle siRNA Cocktails for the Treatment of Mantle Cell Lymphoma. *Bioeng. Transl. Med.* **2018**, *3* (2), 138−147.

(49) Tagscherer, K. E.; Fassl, A.; Campos, B.; Farhadi, M.; Kraemer, A.; Böck, B. C.; Macher-Goeppinger, S.; Radlwimmer, B.; Wiestler, O. D.; Herold-Mende, C.; Roth, W. Apoptosis-Based Treatment of Glioblastomas with ABT-737, a Novel Small Molecule Inhibitor of Bcl-2 Family Proteins. *Oncogene* **2008**, *27* (52), 6646−6656.

(50) Pellarin, I.; Dall'Acqua, A.; Favero, A.; Segatto, I.; Rossi, V.; Crestan, N.; Karimbayli, J.; Belletti, B.; Baldassarre, G. Cyclin-Dependent Protein Kinases and Cell Cycle Regulation in Biology and Disease. *Signal Transduction Targeted Ther.* **2025**, *10* (1), 1−62.

(51) Liu, M.; Xie, D.; Hu, D.; Zhang, R.; Wang, Y.; Tang, L.; Zhou, B.; Zhao, B.; Yang, L. In Situ Cocktail Nanovaccine for Cancer Immunotherapy. *Adv. Sci.* **2023**, *10* (31), 2207697.

(52) Jain, A.; Mahira, S.; Majoral, J.-P.; Bryszewska, M.; Khan, W.; Ionov, M. Dendrimer Mediated Targeting of siRNA against Polo-like Kinase for the Treatment of Triple Negative Breast Cancer. *J. Biomed. Mater. Res., Part A* **2019**, *107* (9), 1933−1944.

(53) Chen, T.; Ni, N.; Yuan, L.; Xu, L.; Bahri, N.; Sun, B.; Wu, Y.; Ou, W.-B. Proteasome Inhibition Suppresses KIT-Independent Gastrointestinal Stromal Tumors Via Targeting Hippo/YAP/Cyclin D1 Signaling. *Front. Pharmacol* **2021**, *12*, 686874.

(54) Hsu, K.-H.; Tsai, H.-W.; Lin, P.-W.; Hsu, Y.-S.; Lu, P.-J.; Shan, Y.-S. Anti-Apoptotic Effects of Osteopontin through the up-Regulation of Mcl-1 in Gastrointestinal Stromal Tumors. *World J. Surg. Oncol.* **2014**, *12*, 189.

(55) Guo, F.; Ji, X.; Xiong, C.; Sun, H.; Liang, Z.; Yan-Do, R.; Gai, B.; Gao, F.; Huang, L.; Li, Z.; Kuang, B. Y.; Shi, P. Single-Cell Encoded Gene Silencing for High-Throughput Combinatorial siRNA Screening. *Nat. Commun.* **2024**, *15* (1), 9985.

(56) Faria, R.; Vivés, E.; Boisguerin, P.; Sousa, A.; Costa, D. Development of Peptide-Based Nanoparticles for Mitochondrial Plasmid DNA Delivery. *Polymers* **2021**, *13* (11), 1836.

https://doi.org/10.1021/acs.bioconjchem.5c00069
Bioconjugate Chem. 2025, 36, 1218−1233

CHAPTER 1

SUPPORTING INFORMATION

Table S1: Used siRNA sequences

ID	Anti-sense sequences	References
siCDK4*	5'-CAG-AUC-UCG-GUG-AAC-GAU-GdTdT-3'	Mao 2014 [1]
siCDK4 (2)	5'-UGU-GGG-UUA-AAA-GUC-AGC-AdTdT-3'	Ikai 2016 [2]
siCDK4 (3)	5'-CUC-CAU-CUU-UCU-ACA-GAU-UAC-dTdT-3'	Kathryn 2013 [3]
siCDK4 (4)	5'-CUC-UUA-UCU-ACA-UAA-GGA-UGA-AGG-dTdT-3'	Kathryn 2013 [3]
siCD1	5'-AAA-UGA-ACU-UCA-CAU-CUG-UdTdT-3'	Champagne 2020 [4]
siMCL-1	5'-GGA-CUU-UUA-UAC-CUG-UUA-UdTdT-3'	Dzmitruk 2015 [5]
siSCR	5'-CAU-CAU-CCCUGC-CUC-UAC-UdTdT-3'	Konate 2019 [6]

Footnotes: * corresponds to siCDK4 (1) in Figure S4 and was used in all cocktails formulations

Table S2: Used antibodies

Name	Clone / Catalog Number	Supplier	RRID*
CDK4	D9G3E / #12790	Cell Signaling	AB_2631166
MCL-1	D5V5L / #39224	Cell Signaling	AB_2799149
CD1	SP4 / #MA5-16356	Thermo Fisher Scientific	AB_2537875
Vinculin	E1E9V / #13901	Cell Signaling	AB_2728768
Anti-Rabbit-HRP	#7074	Cell Signaling	AB_2099233

Footnotes: * corresponds to "Research Resource Identification Portal" references

REFERENCES

(1) Mao, C.-Q.; Xiong, M.-H.; Liu, Y.; Shen, S.; Du, X.-J.; Yang, X.-Z.; Dou, S.; Zhang, P.-Z.; Wang, J. Synthetic Lethal Therapy for KRAS Mutant Non-Small-Cell Lung Carcinoma with Nanoparticle-Mediated CDK4 siRNA Delivery. *Mol. Ther. J. Am. Soc. Gene Ther.* **2014**, *22* (5), 964–973. https://doi.org/10.1038/mt.2014.18.

(2) Ikai, A.; Watanabe, M.; Sowa, Y.; Kishimoto, M.; Yanagisawa, A.; Fujiwara, H.; Otsuji, E.; Sakai, T. Phosphorylated Retinoblastoma Protein Is a Potential Predictive Marker of Irinotecan Efficacy for Colorectal Cancer. *Int. J. Oncol.* **2016**, *48* (3), 1297–1304. https://doi.org/10.3892/ijo.2016.3332.

(3) Harrison Pitner, M. K.; Saavedra, H. I. Cdk4 and Nek2 Signal Binucleation and Centrosome Amplification in a Her2+ Breast Cancer Model. *PloS One* **2013**, *8* (6), e65971. https://doi.org/10.1371/journal.pone.0065971.

(4) Champagne, J.; Linares, L. K.; Maurel, B.; Zampieri, A.; Moreno, M.; Fuentes, I.; Dubois, E.; Severac, D.; Decorsière, A.; Bienvenu, F. TAG-RNAi Overcomes off-Target Effects in Cancer Models. *Oncogene* **2020**, *39* (4), 935–945. https://doi.org/10.1038/s41388-019-1020-2.

(5) Dzmitruk, V.; Szulc, A.; Shcharbin, D.; Janaszewska, A.; Shcharbina, N.; Lazniewska, J.; Novopashina, D.; Buyanova, M.; Ionov, M.; Klajnert-Maculewicz, B.; Gómez-Ramirez, R.; Mignani, S.; Majoral, J.-P.; Muñoz-Fernández, M. A.; Bryszewska, M. Anticancer siRNA Cocktails as a Novel Tool to Treat Cancer Cells. Part (B). Efficiency of Pharmacological Action. *Int. J. Pharm.* **2015**, *485* (1–2), 288–294. https://doi.org/10.1016/j.ijpharm.2015.03.034.

(6) Konate, K.; Dussot, M.; Aldrian, G.; Vaissière, A.; Viguier, V.; Neira, I. F.; Couillaud, F.; Vivès, E.; Boisguerin, P.; Deshayes, S. Peptide-Based Nanoparticles to Rapidly and Efficiently "Wrap 'n Roll" siRNA into Cells. *Bioconjug. Chem.* **2019**, *30* (3), 592–603. https://doi.org/10.1021/acs.bioconjchem.8b00776.

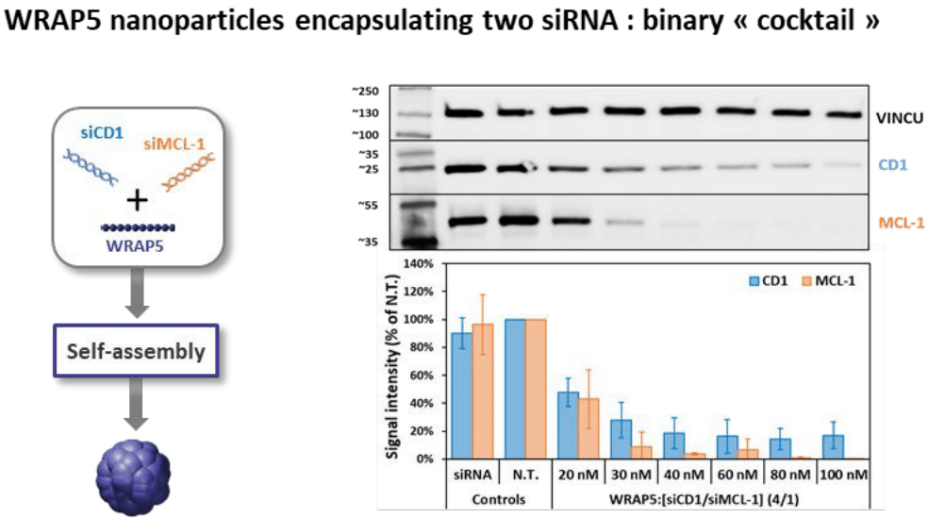

Figure S1: Evaluation of the dose-dependent silencing of WRAP5:siRNA nanoparticles in U87 cells

WRAP5 nanoparticles encapsulating two siRNA (schematic representation on the left side) in a final siRNA ratio 4/1 induced the dose-dependent simultaneous silencing of two proteins (CD1/MCL-1) in U87 cells at the indicated siRNA concentrations revealed by Western Blot after a 24 h incubation. Graphical representation of mean ± SD using 3 independent experiments. Vinculin (VINCU) was used as an internal loading control.

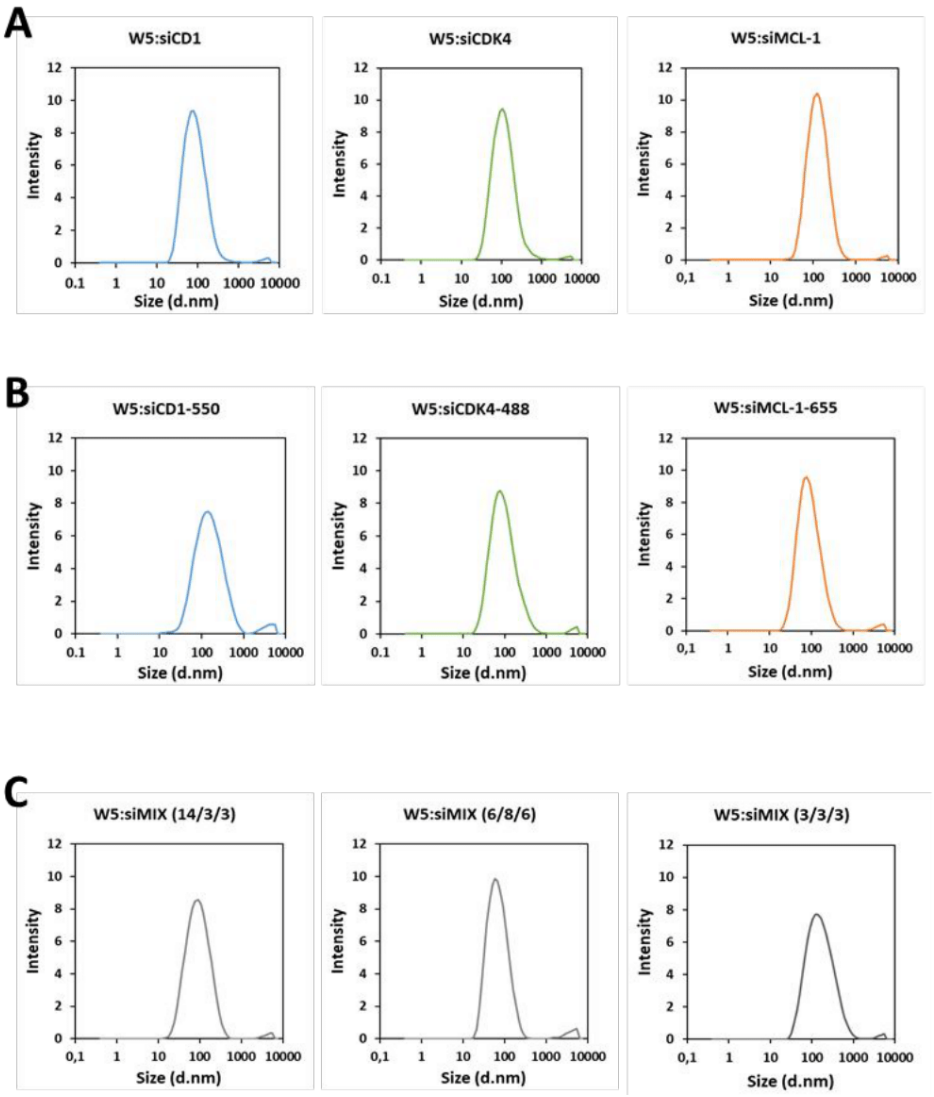

Figure S2: Graphical representations of the measured mean sizes of WRAP5:siRNA nanoparticles

Mean size distribution of WRAP5:siRNA nanoparticles (W5:siRNA) for **(A)** single siRNA (siCD1, CDK4, MCL-1) **(B)** single fluorescence-labeled siRNA (siCD1-550, siCDK4-488, siMCL-1-655) and **(C)** siMIX with siRNA ratio at 14/3/3, 6/8/6, and 3/3/3 molar ratio.

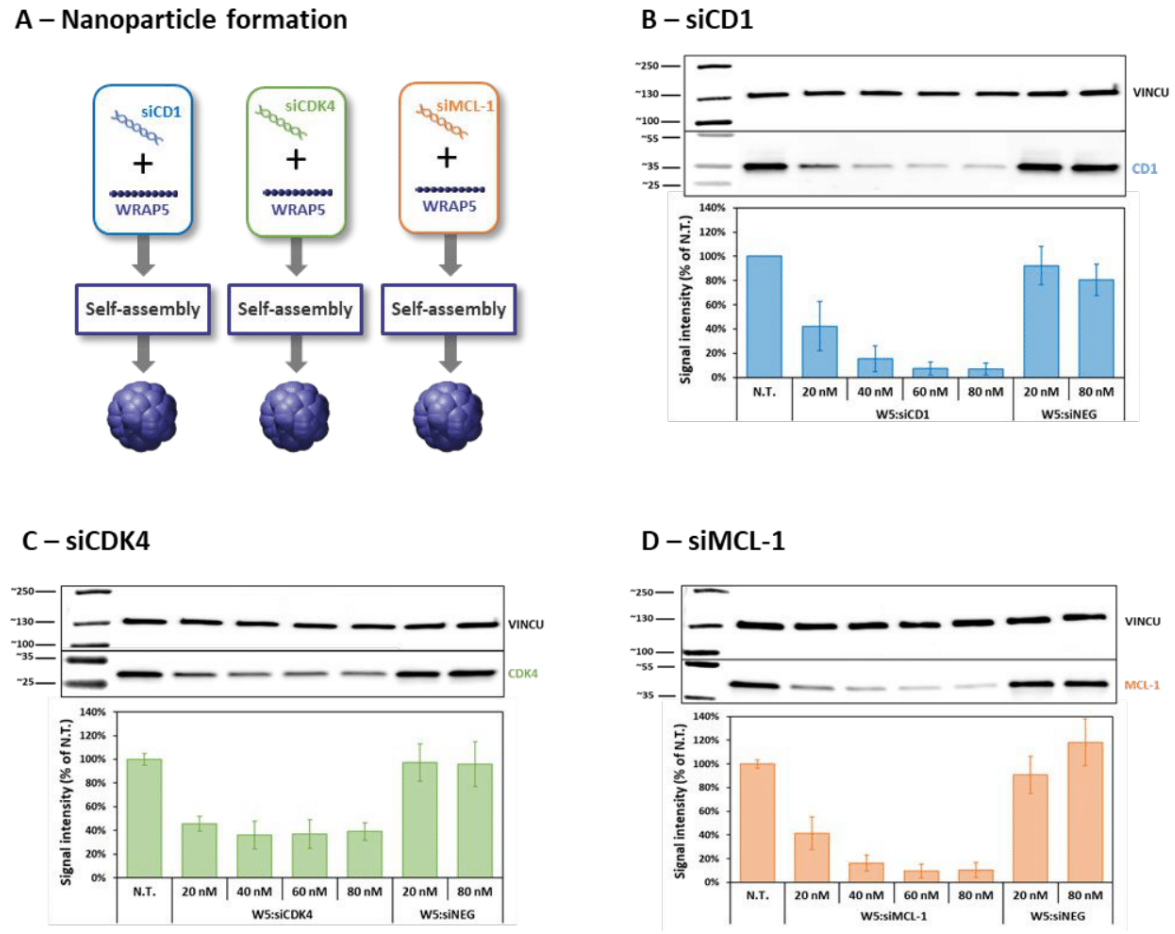

Figure S3: Evaluation of the dose-dependent silencing of WRAP5:siRNA nanoparticles in GIST-T1 cells
(**A**) Schematic representation of the nanoparticle formulation using WRAP encapsulating one siRNA. siCD1 (**B**), siCDK4 (**C**) and siMCL-1 (**D**).
Graphical representation of mean ± SD using 3 independent experiments. Vinculin (VINCU) was used as an internal loading control.

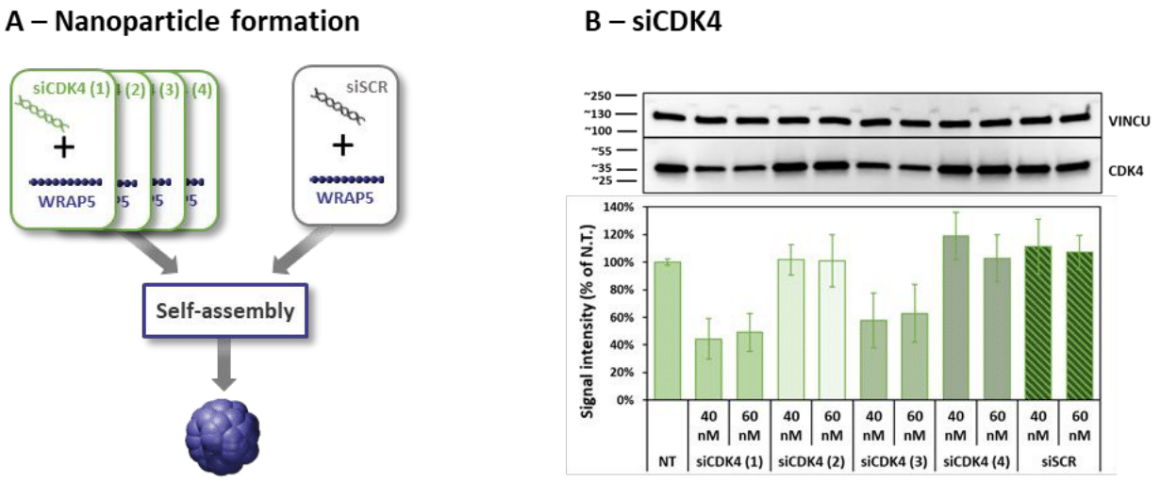

Figure S4: Evaluation of the silencing of WRAP5:siRNA nanoparticles encapsulating different siCDK4 in GIST-T1 cells

(**A**) Schematic representation of the nanoparticle formulation using WRAP encapsulating one siRNA.
(**B**) Four different siRNA targeting CDK4 (siCDK4(1), siCDK4(2), siCDK4(3) and siCDK4(4)) were encapsulated in WRAP5-based nanoparticles at both 40 nM / 60nM siRNA concentration in order to check their targeting efficiency in GIST-T1.
Graphical representation of mean ± SD using 2 independent experiments. Vinculin (VINCU) was used as an internal loading control.

RESULTS

Chapter 1: Multi-siRNA delivery using WRAP5-based nanoparticles in GIST cells

Chapter 2: Studying individual roles of YAP1 and TAZ in GIST tumor biology

Chapter 3: YAP1 and TAZ: playing around with IM resistance?

CHAPTER 2: Studying individual roles of YAP1 and TAZ in GIST tumor biology

This work has been submitted to Cell Communication and Signaling as:

Pezzati I et al., Breaking the redundancy: TAZ outperforms YAP1 in GIST progression. Preprint: doi:https://doi.org/10.1101/2025.09.02.673653

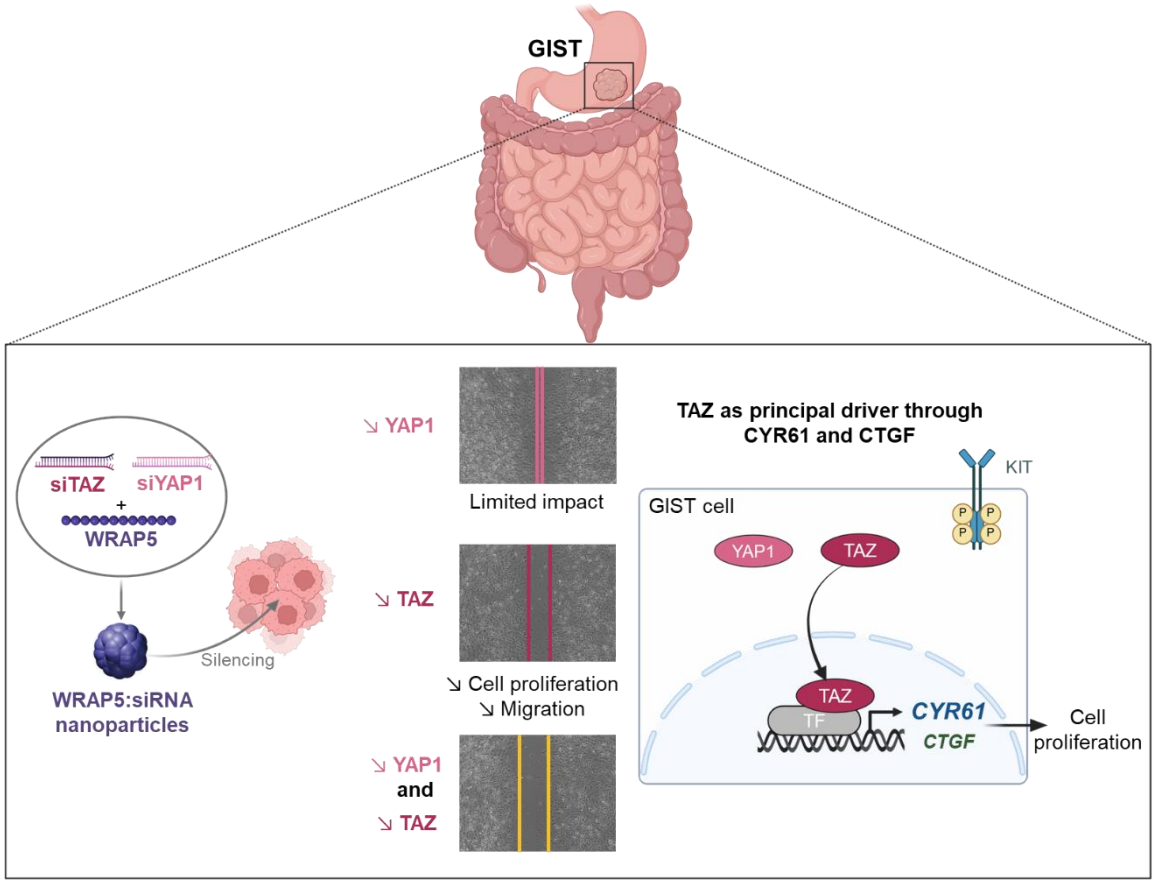

CHAPTER 2

1. Structured summary

1.1. Introduction

GIST are mainly driven by oncogenic *KIT* or *PDGFRA* mutations, which primarily activate MAPK/ERK and PI3K/AKT signaling cascades to promote cell proliferation and survival. Over the past decade, additional factors indirectly modulating these pathways have been analyzed, such as SH3BP2, SPRY4, SOCS2, ACK1, and LIX1, which have been shown to strongly contribute to tumor progression and therapeutic IM resistance. Among these, the Hippo pathway effectors YAP1 and TAZ have been linked to aggressive tumor behavior and drug resistance in various cancers, including GIST. However, their precise role in *KIT*-dependent IM-sensitive GIST remains poorly defined. Although YAP1 and TAZ are frequently co-activated and often studied as a single functional unit, emerging evidence indicates distinct regulatory mechanisms, expression profiles, and biological functions that may vary across tumor types.

Building on our demonstration in Chapter 1 that siRNA-loaded WRAP5 nanoparticles enable efficient and specific multiprotein silencing in GIST-T1 cells, we applied this approach to investigate the individual roles of YAP1 and TAZ in several *KIT*-dependent IM-sensitive GIST cell lines. We then compared the impact of single *versus* combined silencing on cell proliferation, migration, and expression of canonical Hippo target genes.

Through this work, we sought to determine whether YAP1 and TAZ exert distinct functional contributions to GIST development, and whether their selective inhibition could represent a therapeutic strategy to overcome tumor heterogeneity and progression.

1.2. Methods

We first analyzed a clinically annotated gene expression data set (ATGsarc) of localized, untreated GIST, sorting cases into low- and high-expression groups for each gene of interest and comparing overall survival using Kaplan-Meier curves or metastasis progression by box blot representation (collaboration with Dr. F. Chibon, Toulouse).

At least two siRNA sequences per protein of interest were designed in-house and their specificity and absence of cytotoxicity were validated in the GIST-T1 cell line through Western blot analysis and lactate dehydrogenase (LDH) release assay, respectively. Silencing

experiments were then performed by delivering siRNA individually, or in combination using the WRAP5 delivery system formulated according to established protocols. Knockdown was quantified at protein and transcript levels by Western blot and quantitative PCR (qPCR), respectively. For YAP1 and TAZ, protein silencing was also evaluated by confocal microscopy.

Functional consequences of protein inhibition were evaluated through MTT and cell counting assays for proliferation, and wound-healing assays for migration. In parallel, we examined the activation status of downstream KIT effectors in the MAPK/ERK and PI3K/AKT pathways, as well as the expression of canonical Hippo pathway targets CYR61, CTGF, and CD1. To confirm the generalizability of our findings, these experiments were extended to two additional *KIT*-dependent IM-sensitive GIST cell lines, GIST-430 and GIST-882 (Collaboration with Pr. C. Serrano, Barcelona).

1.3. Results

At the beginning of the study, YAP1 and TAZ expression levels were evaluated using a GIST patient data set (ATGsarc). Here, *TAZ* expression was significantly associated with shorter progression-free survival and higher metastasis formation, whereas the prognostic impact of *YAP1* expression was less pronounced (**Figure 1** of the publication). These clinical observations supported the hypothesis that *TAZ*, and to a lesser extent *YAP1*, contributes to GIST progression.

Selective silencing of YAP1 or TAZ using WRAP5:siRNA nanoparticles resulted in efficient and specific knockdown (60% to 80% at an siRNA concentration of 60 nM) without cross-effects (**Figures 2 and S2** of the publication). Only slight cytotoxicity was observed at the highest concentration (~20% at 80 nM).

Simultaneous delivery of siYAP1 and siTAZ achieved robust dual protein inhibition in GIST-T1 cells (~50% at a siRNA concentration of 20 nM + 20 nM), a level comparable to that obtained with single-protein inhibition (**Figure 3** of the publication). Immunofluorescence analysis confirmed efficient and specific silencing of YAP1 and TAZ in GIST-T1 cells treated with WRAP5 nanoparticles, showing significant reductions upon individual knockdowns (-35% YAP1, -40% TAZ) and even stronger inhibition when both were targeted simultaneously (-55% YAP1, -61% TAZ), without evidence of compensatory nuclear relocalization (**Figure 4** of the publication).

Functionally, TAZ silencing led to an important reduction in proliferation (-30% in MTT or -21% in cell counting assay) and migration (-24%) after 72 hours post-transfection (**Figure 5** of the publication). In contrast, YAP1 silencing had a more non-significant inhibitory effect. Combined silencing induced only a slight additional effect compared to TAZ silencing alone on migration as revealed in the wound healing assay. KIT activation and its canonical MAPK/ERK and PI3K/AKT pathways remained unchanged (**Figure 6** of the publication), indicating that the anti-proliferative effects of TAZ inhibition were independent of direct KIT modulation. To investigate the downstream effects of TAZ on Hippo pathway effectors, we analyzed CYR61 and CTGF expression and observed that TAZ knockdown, alone or combined with YAP1, strongly downregulated CYR61 (-65%) and CTGF (-55%) at the protein level and their mRNA expression (>80%), whereas YAP1 silencing alone had no inhibitory effect. In contrast, CD1 expression remained unchanged upon YAP1 or TAZ silencing, indicating its regulation in GIST-T1 cells is independent of these factors under the tested conditions (**Figure 6** of the publication).

In GIST-430 and GIST-882 cells, TAZ retained a major role, but YAP1 contributed more substantially in certain contexts, likely reflecting differences in basal protein levels. At the protein level, TAZ silencing strongly reduced CYR61 and CTGF expression (50% for both proteins). As expected, YAP1 silencing induced minimal non-significant changes. Combined silencing (YAP1 and TAZ) seems to repress more effectively *CYR61* and *CFTGF* genes in cell lines with distinct basal YAP1 and TAZ protein expression profiles in the different cell lines (**Figure 7** of the publication).

Functional validation showed that CYR61 knockdown reproduced the anti-proliferative effect observed with TAZ inhibition, whereas CTGF or both proteins knockdown had less impact (**Figure 8** in the publication). High *CYR61* expression correlated with poor prognosis in patient datasets, mirroring the role of TAZ-CYR61 axis in the GIST development.

1.4. Discussion

This work demonstrates, for the first time, that YAP1 and TAZ can be selectively targeted and studied for their respective roles in *KIT*-dependent IM-sensitive GIST cells. Using WRAP5-based nanoparticles, we achieved efficient and specific silencing of YAP1 or TAZ individually, or in combination. Across three evaluated GIST cell lines, TAZ emerged as the dominant

functional effector in GIST cells. Its inhibition significantly impaired proliferation and migration, and downregulated key Hippo pathway targets, particularly CYR61.

In contrast, YAP1 knockdown had more modest effects, and combined silencing produced only limited additive benefit than TAZ silencing alone. Nevertheless, variability between cell lines suggests that YAP1 may assume greater importance in specific molecular contexts, likely influenced by basal expression levels.

CYR61 downregulation exhibited a stronger correlation with impaired proliferation than CTGF, in line with its established association with a poor prognosis in GIST datasets. These results further support the hypothesis that CYR61 is a clinically relevant downstream effector of TAZ in GIST.

Our findings are in accordance with reports in other cancers where there is divergence of Hippo pathway activity between YAP1 and TAZ in terms of transcriptional output and biological function, thus reinforcing the concept of tissue- and lineage-specific Hippo pathway activity. Although the molecular mechanisms underlying this divergence remain unclear, they may involve differences in TEAD isoform affinity, the recruitment of distinct nuclear cofactors, or chromatin accessibility.

1.5. Conclusions and perspectives

This central work of this thesis identified TAZ as a key driver of GIST cell proliferation and migration, highlighting its promising therapeutic potential in *KIT*-dependent IM-sensitive GIST. TAZ acted here through the major regulation of the Hippo pathway effector CYR61, and with a smaller contribution from CTGF. YAP1 could have a potential complementary role in some specific GIST subtypes. Given the heterogeneity of YAP1 and TAZ expression in GIST, combined targeting strategies may offer broader clinical benefit, particularly in advanced and metastatic disease.

The developed WRAP5-based nanoparticles proved to be a robust tool for selective and sustained YAP1/TAZ silencing. Knowing that six siRNA-based drugs are now FDA- and EMA-approved, this strategy could complement existing TKI therapies, especially in the context of resistance.

Future studies should elucidate the mechanisms underlying YAP1 and TAZ functional divergence, evaluate WRAP5:siTAZ and WRAP5:siYAP1+siTAZ formulations *in vivo*, and assess their efficacy in IM-resistant models (see Chapter 3 for preliminary results). Finally, the optimization of nanoparticles, in terms of stability and tumor targeting, will probably be essential to improve their specificity for clinical application.

2. Submitted work "Breaking the redundancy: TAZ outperforms YAP1 in GIST progression"

CHAPTER 2

Breaking the redundancy: TAZ outperforms YAP1 in GIST progression

Irène Pezzati[1], Eric Vivès[1], Frédéric Chibon[3, 4], Sandrine Faure[1], Pascal de Santa Barbara[1], César Serrano[2], Sébastien Deshayes[1#], Prisca Boisguérin[1#]

[1]PhyMedExp, University of Montpellier, INSERM, CNRS UMR, 641 Avenue du Doyen G. Giraud, CHU Arnaud de Villeneuve, Bâtiment IURC, 34093 Montpellier, Cedex 5, France.

[2] Sarcoma Translational Research Laboratory, Vall d'Hebron Institute of Oncology, Barcelona, Spain

[3] Oncosarc, INSERM UMR1037, Univ Toulouse, CNRS, Inserm, CRCT, Toulouse, France ;

[4] Oncopole Claudius Régaud, IUCT-Oncopole, Department of Pathology, Toulouse, France.

[#]Corresponding authors: sebastien.deshayes@inserm.fr; prisca.boisguerin@inserm.fr

ABSTRACT

Background Gastrointestinal stromal tumors (GIST) are mainly caused by gain-of-function mutations in *KIT* or *PDGFRA* genes and constitute the most common malignant neoplasm of mesenchymal origin. Imatinib (IM), a tyrosine kinase inhibitor (TKI) targeting these oncogenic drivers, has considerably improved patient outcomes, although resistance remains a major challenge. The transcriptional co-activators YAP1 and TAZ, downstream effectors of the Hippo pathway, have emerged as potential oncogenic drivers in various cancers, including GIST. However, their specific roles in *KIT*-dependent tumor development remain unclear.

Methods We used WRAP5-based nanoparticles loaded with specifically designed siRNA to selectively silence YAP1 and/or TAZ proteins in *KIT*-dependent IM-sensitive GIST cell lines. This nucleic acid delivery system enabled efficient and specific knockdown without cytotoxicity. We assessed the impact on cell proliferation, migration, and gene expression, focusing on YAP1/TAZ targets *CYR61* and *CTGF*.

Results TAZ silencing resulted in a substantial reduction in cell proliferation and migration, whereas YAP1 knockdown was comparatively limited. This finding was consistent with an increased *TAZ* expression in GIST patients, which was associated with shorter progression-free survival and an increased tendency for metastasis development. A slight additive effect was observed upon a combined YAP1/TAZ silencing, suggesting a more complex regulation between these two proteins. Expression of CYR61 and CTGF was predominantly regulated by TAZ, although a stronger downregulation was observed upon YAP1/TAZ knockdown in a subset of GIST cell lines, which may depend on differences in YAP1 and TAZ basal expression. Finally, CYR61 seemed to be more implicated in cell proliferation inhibition, which is further supported by the correlation between high *CYR61* expression and poor prognosis in the GIST patients.

Conclusion Our results highlight the central regulatory function of TAZ-CYR61 axis in oncogenic processes in *KIT*-dependent GIST, with a modest contribution from YAP1. Targeting TAZ, alone or in combination with YAP1, may represent a promising therapeutic approach, particularly in the context of tumor heterogeneity.

Keywords GIST, YAP1, TAZ, siRNA, WRAP5, nanoparticle, CYR61

CHAPTER 2

BACKGROUND

Gastrointestinal stromal tumors (GIST) are the most prevalent mesenchymal cancers of the digestive tract, with an estimated annual incidence of 10-15 per million individuals worldwide [1,2]. The histogenesis of these rare sarcomas is attributed to interstitial cells of Cajal (ICC), which act as pacemakers regulating gastrointestinal motility, or related mesenchymal progenitors [3]. GIST are primarily driven by oncogenic gain-of-function mutations in receptor tyrosine kinase genes, most notably *KIT* (75-80% of cases) and, to a lesser extent, *PDGFRA* (5-10%) [4,5]. These mutations lead to the constitutive activation of downstream signaling pathways, resulting in uncontrolled cellular proliferation and survival [6,7]. The process of oncogenic signaling cascades downstream of KIT involves the PI3K/AKT/mTOR and RAS/MAPK/ERK pathways. These pathways play critical roles in GIST development and progression, contributing to tumor initiation, growth, and metastatic dissemination [1,8,9].

The introduction of tyrosine kinase inhibitors (TKI) in the early 21st century, such as imatinib mesylate (IM), has significantly improved patient outcomes by effectively inhibiting KIT-downstream PI3K and MAPK pathways [10]. Nevertheless, resistance remains a major clinical challenge in advanced and metastatic GIST, as most patients experience disease progression within 18 to 24 months of treatment, due to secondary resistance mechanisms [7]. Second- and third-line TKI therapies, including sunitinib and regorafenib, have been demonstrated to induce temporary disease control [11,12]. However, their clinical efficacy is constrained by their capacity to target only a subset of secondary *KIT* mutations and by the molecular heterogeneity of resistance [5,6,13]. Another limitation shared by these therapies is their common mechanism of action: they do not address the emergence of additional mutations or the broader cellular adaptations that occur during prolonged TKI exposure [1]. In certain instances, resistance to TKI treatment can result from mechanisms that entirely bypass KIT, such as the loss of KIT expression. This results in a *KIT*-independent GIST phenotype, which is unresponsive to TKI treatments [14–16]. Together, these limitations underscore the urgent need for alternative therapeutic strategies and a deeper understanding of the molecular pathways that drive GIST progression and resistance.

Recent studies have identified LImb eXpression 1 (LIX1) as a novel contributor of GIST progression and therapeutic resistance. LIX1 is overexpressed in aggressive and relapsed tumors, and its levels increase upon TKI resistance [17,18]. Functionally, LIX1 promotes MAPK pathway reactivation following KIT inhibition, thereby limiting TKI efficacy. LIX1 also regulates mitochondrial function, proliferation, and tumoral lineage identity in GIST cells in *KIT*-dependent contexts through the Hippo pathway and its two paralogous downstream effectors, the Yes-associated protein (YAP1) and the WW domain-containing transcription regulator protein 1 (WWTR1), also known as TAZ [17–19].

The Hippo signaling pathway is a highly conserved regulator of organ size, cell proliferation, and apoptosis, playing a crucial role in tissue homeostasis [20]. In its active form, the Hippo core function is to restrict YAP1 and TAZ to the cytoplasm by LAST1/2-depending phosphorylation of both proteins [21]. Upon Hippo inactivation, YAP1 and TAZ are dephosphorylated and translocate to the nucleus, where they mainly bind TEAD transcription factors [21]. Together, YAP1/TAZ/TEAD complex drives the expression of genes involved in cell growth, migration, survival, and tissue identity in numerous organs, including the digestive tract, such as *CTGF*, *CYR61*, *AREG, MYC, MCL-1, BIRC5, AXL, etc.* [22–25]. Furthermore, in the nucleus, YAP1 and TAZ also participate in the expression of Cyclin D1 (CD1), a key cell cycle regulator of the G1/S transition implicated in tumor invasion and resistance to therapy in solid tumors [26,27].

Focusing on GIST, recent proof-of-concept studies have shown that dysregulation of the Hippo pathway, with YAP1 and TAZ as positive regulators of CD1, can drive tumor growth and progression. These findings establish Hippo/YAP1/CD1 signaling as a key oncogenic mechanism in *KIT*-independent IM-resistant GIST [14,15]. In *KIT*-dependent GIST cells, both sensitive and resistant to IM through KIT secondary mutations, pharmacological inhibition by the Bcl-2 inhibitor, AT101, of the YAP1/TAZ-CD1 axis has been recently shown to reduce tumor growth and induce apoptosis in preclinical GIST models [28]. Moreover, pharmacological inhibition of YAP1/TAZ with verteporfin promotes ferroptosis in KIT-

dependent IM-sensitive and -resistant human GIST cells. This result correlates with aggressive tumor behavior, underscoring its therapeutic potential in cases resistant to TKI [29,30].

It has been reported that the Hippo pathway is often dysregulated in combination with hyperactivation of YAP1/TAZ in various human cancers, including solid tumors and sarcomas [31]. In these cases, dysregulation contributes to aggressive phenotypes, therapy resistance, and metastatic dissemination [32,33]. Despite their frequent co-activation in cancers, the term "YAP1/TAZ" is often described as interchangeable transcriptional co-activators within the Hippo signaling pathway and studied as a single unit without any distinction in functional assays [34,35]. Yet accumulating evidence reveals fundamental differences between them, not only in their protein domain composition and transcriptional partners, but also in their patterns of expression and regulatory behavior, which vary depending on tissue context and physiological conditions [36,37]. These distinctions call for a careful evaluation of their respective roles in cancer, especially in sarcomas [38–41].

Based on these facts, we hypothesized that YAP1 and TAZ could be promising therapeutic targets for GIST. Therefore, we aimed to individually and jointly evaluate the contribution of YAP1 and TAZ in *KIT*-dependent IM-sensitive GIST cells using specifically designed small interfering RNA (siRNA). For cellular internalization, we opted for the tryptophan and arginine-rich amphipathic peptide, WRAP5, which self-assembled into peptide-based nanoparticles (PBN) in the presence of siRNA as payload [42]. Formulated at a specific molar ratio (WRAP5:siRNA = 20:1), WRAP5-based nanoparticles were selected from a performed structure-activity study as one of the lead peptides [43], which was mainly evaluated in the U87 glioblastoma cell line [42]. More recently, we have demonstrated that WRAP5 could encapsulate up to three distinct siRNA, enabling the simultaneous silencing of three different proteins within GIST cells [44]. Compared to conventional lipid-based transfection reagents, the PBN demonstrated superior safety profiles with minimal cytotoxicity in long-term assays, while maintaining high intracellular delivery efficiency [43,45]. Its versatility has been validated across multiple cell types, both cancerous and non-cancerous, as well as in animal models (mouse and zebrafish), making it particularly suitable for studying dose-dependent gene silencing effects in therapeutic contexts as exemplified through different protein silencing [44,46–48].

In the present study, the efficacy of YAP1 and/or TAZ silencing was first confirmed in human *KIT*-dependent IM-sensitive GIST-T1 cells. For the first time, we could demonstrate that TAZ is a regulator of proliferation and migration in GIST-T1 cells, with a limited contribution of YAP1. This predominant role was in accordance with a bad prognosis in GIST patients with a high level of *TAZ* that we revealed from the ATGsarc database. Consequently, we demonstrated that this phenomenon is attributable to the transcriptional activity of TAZ on *CTGF* and *CYR61* genes. Finally, the role of TAZ, and a slight additive effect of combined YAP1 and TAZ, was also validated in other GIST cell lines (GIST-430 and GIST-882). In summary, the present findings newly underscore the significance of TAZ as a key player in GIST development.

METHODS

Peptide. WRAP5 peptide (LLRLLRWWWRLLRLL) was synthesized at the SynBio3 platform (IBMM Montpellier), and the crude product was purified in-house following a qualitative analysis by HPLC/MS (~95% purity). WRAP5 stock solutions were prepared at 400 µM or 40 µM and stored at 4°C.

siRNA design. To design siRNA targeting the gene of interest, a systematic bioinformatics approach was performed. First, the nucleotide sequence of the target gene was retrieved from the National Center for Biotechnology Information (NCBI) database. The coding sequence (CDS) was extracted in FASTA format. Next, potential siRNA candidates were designed using the RNAxs web tool (http://rna.tbi.univie.ac.at/cgi-bin/RNAxs/RNAxs.cgi). The extracted FASTA sequence was input into RNAxs with default design options, and the maximum number of siRNA was set to five. To ensure specificity, each proposed siRNA sequence (generally 19 to 21 nucleotides long) was subjected to a BLAST (Basic Local Alignment Search Tool) search (https://blast.ncbi.nlm.nih.gov/Blast.cgi) using the nucleotide BLAST (blastn) tool. Each siRNA was analyzed for sequence specificity by evaluating identity

percentages, gaps, and alignment length. Only siRNA with high specificity to the target gene, minimal off-target interactions, and no significant matches with essential receptors or proteins were considered. Finally, selected siRNAs were synthesized and purchased through Eurogentec (see **Table S1**). The siRNA stock solutions were prepared in RNase-free water at 200 µM or 20 µM and stored at -20°C, as recommended by the provider. Each siRNA was tested for specificity and efficacy in targeting the gene of interest before selecting the most effective one for subsequent experiments.

WRAP5:siRNA nanoparticle formulation. Nanoparticles were formulated in pure water supplemented by 5% glucose (Sigma-Aldrich) by mixing equal volumes of WRAP5 and siRNA at the corresponding molar ratio (WRAP5:siRNA = 20:1) at room temperature [42]. For PBN combining two siRNA (siYAP1+siNEG or siTAZ+siNEG or siYAP1+siTAZ), the two siRNA were pre-mixed according to siRNA stoichiometry 1:1 as described [44].

Dynamic light scattering (DLS). WRAP5:siRNA nanoparticles (WRAP5 = 10 µM, siRNA = 500 nM, R = 20) were evaluated with a Zetasizer NanoZS (Malvern) in terms of mean particle size (Z-average diameter) of the particle distribution and the polydispersity index (PdI). All results were obtained from three independent measurements (three runs for each measurement at 25°C) as described [42].

Cell culture conditions. The experiments were conducted on human *KIT*-dependent IM-sensitive GIST cells. The GIST-T1 cell line (primary mutation in KIT exon 11 Δ560–578 in-frame deletion), from Cosmo Bio (Japan, Catalog No: PMC-GIST01C), was established from a metastatic Asian female human untreated GIST sample [49,50]. GIST-882 (KIT exon 13 K642E mutation) [51] and GIST-430 (KIT exon 11 Δ560-576 in-frame deletion) [52] were a gift from our collaborator, Dr. C. Serrano (Sarcoma Translational Research Laboratory, Vall d'Hebron Institute of Oncology [VHIO], Barcelona, Spain).

GIST-T1 cells were grown in Dulbecco's Modified Eagle's Medium (DMEM) (Corning, #10-013-CV) supplemented with 10% fetal bovine serum (FBS) (Sigma-Aldrich, #F7524) and 1% penicillin-streptomycin (Sigma-Aldrich, #P4333). GIST-430 and GIST-882 cells were cultured in Iscove's Modified Dulbecco's Medium (IMDM) (Sigma-Aldrich, #I3390) supplemented with 15% FBS, 1% penicillin-streptomycin, and 1% L-Glutamine (Thermo Fisher Scientific, #11524456). All the cells were passaged using Gibco™ Trypsin-EDTA (0.05%), phenol red (Thermo Fisher Scientific, #25300062). All the cells were maintained in a humidified incubator with 5% CO_2 at 37°C. All cultures were tested monthly to be mycoplasma-free using the **MycoAlert™ PLUS Mycoplasma Detection Kit (Lonza,** #LT07-710**).** GIST-T1 cell lines were incubated with IM (STI571, Euromedex, France) at the concentrations indicated in the figure legends.

GIST data set. Kaplan–Meier curves of progression-free survival stratified by *YAP1*, *TAZ*, *CYR61* or *CTGF* were obtained based on a clinically annotated gene expression data set (ATGsarc) of localized, untreated GIST (n = 60), quantified by microarray (ArrayExpress: E-MTAB-373) [53]. For each gene, patients were divided into high and low expression groups. The cut-off for stratifications was first set at the mean expression value, a standard approach in survival analysis to minimize bias from outliers (log-rank test). In parallel, box plot analyses were performed to compare the expression levels of these four genes between GIST patients with and without metastasis, providing additional insight into their potential association with disease aggressiveness.

Cell cytotoxicity measurement. The cytotoxicity induced by the nanoparticles was evaluated using Cytotoxicity Detection Kit^{Plus} (LDH, Sigma-Aldrich) following the manufacturer's instructions and as described before [42].

Transfection experiments. For Western blot assays and RNA extraction, 300,000 GIST-T1 and 700,000 GIST-430 cells were seeded into 6-well plates (Sarstedt, #83.3920) 24 hours before the experiment. For GIST-882 cells, 500,000 cells were seeded 48 hours before the experiment into 6-well plates. For nanoparticle incubation, cells were treated with 800 µL of fresh, pre-warmed serum-free culture medium and 200 µL of nanoparticle solutions at the specified concentrations, or 200 µL of 5% glucose when required. After 1.5 h, 1,000 µL of the appropriate culture medium supplemented with 20% FBS for GIST-T1 (final FBS concentration = 10%) or 30% FBS for GIST-430 and GIST-882 (final FBS concentration = 15%) was added to each well, without removing the transfection reagents. The cells were incubated for an additional 24 hours or 48 hours before being lysed for RNA extraction or Western blot analysis, respectively.

Western blotting. Transfected cells were treated as described before, with some differences [44]. To standardize protein loading, all samples were diluted in RIPA buffer to match the lowest protein concentration. A 1:1 volume of 2X Laemmli Sample Buffer (Bio-Rad, #1610737) containing 5% β-mercaptoethanol was then added to each sample. Samples were heated at 95°C for 10 minutes, immediately placed on ice, and stored at -20°C until electrophoresis. Cell extracts were loaded with 5 to 10 µg of proteins. Electrophoresis and membrane transfer were achieved following [44]. Membranes were then blocked with TBS-0.5% or 0.2% Tween (Euromedex, #EU0660-B) containing 5% BSA (Sigma-Aldrich, #A2135). The 10X Tris-Buffered Saline (TBS) solution was prepared by dissolving 80 g NaCl, 2 g KCl, and 61 g Tris base (all from Sigma-Aldrich) in 800 mL of Milli-Q water, adjusting the pH to 8.0 with HCl, and completing the volume to 1 L with Milli-Q water. Membranes were subsequently incubated with the appropriate primary antibody in the same blocking buffer overnight at 4°C. After three washes with TBS-0.05% or 0.02% Tween, membranes were incubated for 1.5 h with the corresponding HRP-conjugated secondary antibody. Three additional washes were performed before chemiluminescent detection using luminol. The revelation was done following [44] and imaged using a Sapphire RGB & NIR Biomolecular Scanner (Azure Biosystems). VINCULIN, α-ACTININ, or β-ACTIN proteins were used as loading controls depending on the experiment. Primary and secondary antibodies were used according to the manufacturer's recommendations. The details of the antibodies, including their source, catalog number, dilution, and application, are summarized in Supplemental Materials (see **Table S2**).

The signal intensities of the blots were quantified using Fiji ImageJ software as described in [44].

Confocal microscopy. For confocal microscopy, 150,000 GIST-T1 cells were seeded onto 18 mm cover slips in 12-well plates (Sarstedt, #83.3921). 24 hours post-seeding, cells were incubated with 400 µL of fresh, pre-warmed serum-free DMEM and 100 µL of nanoparticle solutions at the specified concentrations. After 1.5 hours, 500 µL of DMEM supplemented with 20% FBS was added. After transfection, cells were fixed with 2% paraformaldehyde (PFA), and simultaneously, permeabilized and blocked using a solution of PBS containing 0.1% Tween-20/4% donkey serum (SIGMA, #D9663). Afterward, cells were incubated overnight with primary antibodies, followed by a 1-hour incubation with secondary antibodies. Nuclear staining was performed using Hoechst (1 mg/mL, Sigma, #14533), and membrane actin was labeled with Phalloidin Alexa Fluor™ Plus 647 (1:800, Thermo Fisher Scientific, #A22287). To visualize YAP1 and TAZ simultaneously, a mixed antibody staining approach was used. Finally, the cells were washed with D-PBS three times and mounted on glass slides with poly-(vinyl alcohol) Mowiol™ 4–88 glycerol Tris buffer (Biovalley). Confocal images were acquired using an inverted Zeiss LSM800 microscope with an Apo 63x/1.2 W DICIII objective. To minimize fluorophore crosstalk, sequential image acquisition was applied. For each biological replicate, 2 different arbitrary positions were selected for a z-stack mode acquisition (15 images with a z-stack interval of 0.22 µm). Acquired images were analyzed using Fiji (ImageJ) software. The sum of the fluorescence intensity for each z-stack projection was performed to obtain one image. The threshold of each sample was adjusted to quantify the mean fluorescence of the image. Mean fluorescence of YAP1 and TAZ was normalized by the mean fluorescence of the nucleus (Hoechst signal) and then adjusted to the WRAP5:siNEG condition.

Cell Proliferation Assay by MTT. For the MTT assay, 10,000 GIST-T1 cells were seeded into 96-well plates (Corning Falcon, #353072) 24 hours before the experiment. Cell proliferation was assessed using the CellTiter 96® Non-Radioactive Cell Proliferation Assay (Promega, #G4000), in which the luciferase-catalyzed luciferin/ATP reaction provides an indicator of cell number, based on the enzymatic conversion of MTT into a colored formazan product. The manufacturer's protocol was followed with slight modifications. The transfection with WRAP5:siRNA (1,200 nM:60 nM) and IM treatment (200 nM, Euromedex, #TO-I031) was performed in a total volume of 100 µL per well. Cells were incubated with 80 µL of serum-free DMEM and 10 µL of nanoparticle solutions. After 1.5 h, 10 µL of pure FBS was added, without removing the transfection reagents. All experiments were conducted in quintuplicate. At 24 h or 48 h post-transfection, 15 µL of the Dye Solution was added to each well, and the plate was incubated for 2 h. Subsequently, 100 µl of the Solubilization Solution/Stop Mix was added to each well, and the plate was incubated at room temperature for 1 h on a rocker to ensure a uniformly colored

solution. Cell proliferation was measured using an Infinity M200 Pro microplate reader (Tecan Group Ltd) at 570 nm to quantify formazan formation and at 630 nm to minimize background interference from cell debris and nonspecific absorbance.
Cell proliferation was obtained using the following formulas:

Corrected Absorbance = [(Abs_{570}(Sample) - Abs_{570}(Background)) - (Abs_{630}(Sample) - Abs_{630}(Background))]

$$\text{Cell Proliferation Index} = \frac{\text{Corrected Absorbance (Sample)}}{\text{Mean Corrected Absorbance (WRAP5:siNEG)}}$$

This approach normalizes the absorbance readings by removing background interference and comparing sample proliferation to the WRAP5:siNEG control. The background group was defined as the absorbance of wells containing medium without cells.
Cell proliferation assay by cell counting. For cell proliferation analysis by cell counting, 100,000 GIST-T1 cells were seeded into 12-well plates 24 hours before the experiment. The transfection of WRAP5:siRNA (800 nM:40 nM) and IM treatment (50 nM) were performed in duplicate 24 hours after seeding. Transfection was performed using 400 µL of serum-free DMEM and 100 µL of nanoparticle solution. After 1.5 h, 500 µL of DMEM supplemented with 20% FBS was added. Measurements were taken at 0 h, 24 h, 48 h, and 72 h post-treatment following an established protocol. Before counting, viable cells were washed twice with DPBS 1X and incubated for 5 min with Trypsin-EDTA (0.05%) containing phenol red to detach the adherent cells. The resulting suspension was brought to a final volume of 1,000 µL by adding 800 µL of DPBS 1X. Proliferation was assessed using the CellDrop BFx automated counter (DeNovix, Wilmington, DE, USA) with the Brightfield program. A custom program optimized for GIST-T1 was used to ensure precise quantification. For each well, four independent counts were performed on 10 µL aliquots, and the average was used to determine the final cell concentration (cells/mL). To assess cell growth, counts at each time point were normalized to the mean count at t = 0 h.
Wound healing assay. A wound healing assay was performed to assess the migratory capacity of GIST-T1 cells. To standardize the procedure, a Culture-Insert 4 Well (ibidi GmbH, #80469) was used in a 12-well plate. To minimize evaporation, 700 µL of medium was added to the area surrounding the insert. Next, 110 µL of a cell suspension containing 100,000 cells in complete DMEM was carefully added to each well of the insert. Transfection with WRAP5:siRNA (1,600 nM:80nM) was performed 24 h after seeding. The medium was gently removed, and 90 µL of serum-free medium was added, followed by 10 µL of WRAP5:siRNA nanoparticle solution. The cells were incubated for 1.5 hours at 37°C, after which 10 µL of pure serum was added to each well. After 24 hours, the insert was carefully removed from each well and filled with 1 mL of complete DMEM. If necessary, 1-2 washes with serum-free medium were performed to remove detached cells and debris.
Images of the wound area were captured immediately after scratching (time 0) and at 48 hours (72 hours post-transfection) using the EVOS® LX Core microscope system (#AMEX1000, Thermo Fisher Scientific), equipped with a 3.1 megapixel color camera (2048 x 1536 pixels, 1/2-inch sensor) and a resolution of 1024 x 768 pixels. The wound area was quantified using the Wound_healing_size_tool.ijm plugin in ImageJ, with adjusted parameters: Variance 10, Threshold 25, and Saturation 0.200. The percentage of wound closure was calculated by subtracting the area at t0 from the area at t48, and the results were normalized to the siNEG condition to assess cell migration.
Reverse transcription and quantitative polymerase chain reaction (RT-qPCR). Total RNA was extracted from cell cultures using the RNeasy® Mini Kit (Qiagen, # 74104), following the manufacturer's protocol with some modifications. Specifically, cells were lysed in 230 µL of RLT buffer per well in a 6-well plate. The lysates were then processed according to the manufacturer's instructions to obtain RNA samples. RNA quality and concentration were assessed using a NanoDrop™ One spectrophotometer (Thermo Scientific). The extracted RNA was then reverse transcribed into complementary DNA (cDNA) using 500 ng of RNA as the input material. The reverse transcription was carried out using the Verso

cDNA Synthesis Kit (Thermo Scientific, #AB-1453/B), according to the manufacturer's instructions. Following the synthesis, the cDNA was diluted in ultra pure RNase-free water to a final concentration of 2.5 ng/µL for use in subsequent qPCR analysis. Quantitative PCR (qPCR) was performed using the LightCycler® technology (Roche Diagnostics). PCR primers were designed using the LightCycler Probe Design 2.0 software for some targets, while others were sourced from the literature. Detailed primer sequences are provided in **Table S3**. To ensure primer specificity, each primer was verified through a BLAST search to confirm that there were no mismatches and that only the target of interest was amplified. Additionally, the efficiency of each primer was validated by performing a dilution series of cDNA ranging from 10 ng to 0.001 ng of cDNA per reaction. For each qPCR reaction, 5 ng of cDNA was added per well in a 96-well qPCR plate, in a final reaction volume of 10 µL. Reactions were carried out using the SYBR Green detection method (Roche Diagnostics, #04887352001), qPCR was conducted in technical triplicate, and standard curves were generated for each primer pair to assess amplification efficiency. Data were normalized to the reference gene *HPRT1*, and relative gene expression was calculated using the 2^−ΔΔCt method, which compares the Ct values (threshold cycle) of the target genes relative to the reference genes and the calibrator sample. All qPCR reactions were performed in a LightCycler® 480 System (Roche Diagnostics, #05015243001), and the results were analyzed and presented as mean gene expression levels relative to the reference genes.

Statistical analysis. All statistical analyses were performed using GraphPad Prism (version 8.0.1). Data are presented as mean ± standard deviation (SD) or standard error of the mean (SEM) when appropriate, based on at least three independent experiments. Normality of data distribution was assessed using the Shapiro-Wilk test. When data did not follow a normal distribution, the Kruskal-Wallis test was used for multiple comparisons, as it is a non-parametric alternative to one-way ANOVA that does not assume normality, with Dunn's correction applied for pairwise comparisons to either siNEG-treated cells or untreated cells. When residuals followed a Gaussian distribution and equal standard deviations were confirmed, a one-way ANOVA was performed for multiple comparisons, followed by Dunnett's post-hoc test to compare each condition to either untreated cells or the siNEG-treated cells. In a case of two-group comparison, an unpaired two-tailed Student's t-test was applied. A 95% confidence interval was applied to all tests, and statistical significance (p-value) was defined as follows: ns (not significant) >0.05, * <0.05, ** <0.01, *** <0.001, and **** <0.0001. In the figures, the number of biological replicates (N) and the number of measurements made within each biological replicate (n) are shown.

RESULTS

Role of YAP1 and TAZ in GIST prognosis

In our previous work, we identified LIX1 expression in GIST tissue microarrays in 79% of all GIST specimens (61/77) as well as in 79% of high-grade GIST (34/43) [17]. Moreover, *LIX1* was assessed as a negative prognostic factor in GIST, with high expression levels associated with shorter disease-free survival and increased metastatic risk. Importantly, LIX1 was suspected to regulate GIST cell plasticity through the modulation of YAP1 activity, suggesting a mechanistic link between these factors [17,54].

In the present study, we first evaluated whether the expression of *YAP1* and *TAZ* (*WWTR1*) was also associated with clinical outcome in GIST patients, as we previously did for *LIX1*. We analyzed a cohort of 60 patients from the ATGsarc microarray database [53]. The first analyzed data set comprised 28 GIST patients with high and 32 with low *TAZ* expression, and the second one contained 35 GIST patients with high and 25 with low *YAP1* expression (**Figure 1A**). Both blotted Kaplan-Meier curves revealed that a tendentially high expression of *YAP1* (p = 0.054) or a significantly high expression of *TAZ* (p = 0.0021) could be associated with shorter disease-free survival, indicating a potential role in tumor progression.

Similarly, high transcript levels of both *YAP1* and *TAZ* correlated with the presence of metastases. Both analyzed datasets comprised 15 GIST patients with and 45 without metastases

(**Figure 1B**). Both boxplots indicated a significant correlation of *YAP1* expression (p = 0.027) or *TAZ* expression (p = 0.0217) and metastasis formation, linking both genes to an aggressive tumor behavior.

Collectively, these results support that *TAZ* and, to a lesser extent, *YAP1* contribute to GIST progression. To further prove their role in GIST, we functionally assessed experimentally their individual contributions *in vitro*.

Specific silencing of YAP1 or TAZ using WRAP5:siRNA nanoparticles in GIST-T1 cells

To selectively investigate the individual and combined roles of YAP1 and TAZ in *KIT*-dependent IM-sensitive GIST-T1 cells, we designed for each gene different siRNA using the RNAxs web tool. Each siRNA was blasted to ensure the specificity of the sequence for its target. Two siRNA with the highest score, each targeting two different complementary regions of the targeted mRNA, were selected for evaluation (**Table S1**).

For the cellular internalization of the siRNA, we used the WRAP5-based nanoparticle delivery system previously validated for efficient and low-toxicity gene silencing across diverse cancerous and non-cancerous cellular models [42,43,46]. First, we used dynamic light scattering (DLS) to validate WRAP5:siRNA nanoparticle integrity, showing an average diameter ranging from 90 to 120 nm, with a polydispersity index (PdI) of around 0.3 (**Figure S1**). These relatively homogeneous populations of nanoparticles were consistent with previous reports [42,44] and were, therefore, suitable for gene silencing experiments.

YAP1 and TAZ silencing were evaluated in GIST-T1 cells using WRAP5:siYAP1 and WRAP5:siTAZ in a dose-dependent manner (20 nM to 80 nM) by Western blot (**Figures 2A** and **2B**). This analysis was performed compared to non-treated GIST-T1 cells as well as to those incubated with WRAP5 nanoparticles encapsulating a siRNA without any cellular target (siNEG) to ensure that the nanoparticles do not influence cell physiology.

Concerning the YAP1 and TAZ silencing, we observed, in both cases, a specific knockdown of YAP1 with the WRAP5:siYAP1 nanoparticles without any effect on the TAZ protein expression (**Figure 2A)**. The same specificity has been shown for WRAP5:siTAZ nanoparticles on the TAZ and YAP1 expression (**Figure 2B)**. This knockdown specificity was further confirmed with additional controls: (1) alternative siRNA sequences targeting another region of the *YAP1* and *TAZ* mRNA showed no cross-silencing between YAP1 and TAZ, depending on the siRNA used (**Figures S2A, S2B**), and (2) WRAP5:siNEG nanoparticles did not induce any YAP1 or TAZ silencing compared to the untreated GIST-T1 cells **Figures 2A, 2B, S2A, S2B**).

For both proteins, YAP1 and TAZ, the maximal silencing efficacy reached a plateau of approximately 70% at a siRNA concentration of 60 nM, depending on the used siRNA (**Figures 2A, 2B, S2A, S2B**). To confirm that this range of silencing was correct for both proteins, we encapsulated a siRNA (siYAP1TAZ) [55] that silenced both proteins (**Figure S3**). Using this siRNA, a silencing of around 70% for both proteins was revealed, confirming the specificity and efficacy of our designed siRNA.

To ensure that the nanoparticles did not interfere with the cell viability, we performed for all analyzed conditions (**Figures 2A, 2B, S2A, S2B**) cytotoxicity assays (LDH) before cell lysis for Western blot. Indeed, we revealed minimal cytotoxicity below 20% for siRNA concentrations up to 60 nM and only some slight effects (20%-30%) using the highest siRNA concentration of 80 nM (**Figures 2C, 2D, S2C, S2D**). These thresholds for cytotoxicity were in the acceptable range as described in the standard ISO 10993-5 used to evaluate the *in vitro* cytotoxicity of medical devices [56].

Finally, we compared YAP1 and TAZ expression levels depending on different percentages of GIST-T1 cell confluence (30%, 50%, 80%, and 100%) to ensure that, for both, protein quantity will be the same under different transfection protocols used in the next experiments. Western blot analyses confirmed that, at working cell confluence ranges between 50% and 100%, no significant difference between YAP1 or TAZ expressions was observed (**Figure S4**). This finding confirmed that GIST-T1 cell confluence and potent resulting contact inhibition did not affect the protein quantity of YAP1 and TAZ [57,58].

Simultaneous silencing of YAP1 and TAZ in GIST-T1 cells

Knowing that the WRAP5:siYAP1 and the WRAP5:siTAZ nanoparticles could perform specific YAP1 or TAZ silencing (at 40 nM siRNA), we wanted to combine both siRNA to further evaluate if a phenotypic synergistic effect could be observed. The delivery of two or three siRNA simultaneously by the WRAP5 nanoparticles was previously described in glioblastoma U87 cells, but also in GIST-T1 cells [44]. Furthermore, as the WRAP5:siNEG nanoparticles did not affect cell physiology and cytotoxicity, we decided to use this condition for the result normalization for all further assays.

The siRNA cocktail with an equimolar ratio (1:1) of siYAP1 and siTAZ (WRAP5:siYAP1+siTAZ) was formulated with a constant siRNA concentration (40 nM) across conditions, meaning that [20 nM siYAP1+20 nM siTAZ] were used for the (WRAP5:siYAP1+siTAZ) condition (**Figures 3A, 3B**). Western blot analyses showed a significant YAP1 (p <0.01) and TAZ (p <0.05) silencing, respectively, of around 50%, compared to WRAP5:siNEG, which was in coherence with the results shown in **Figures 2A** and **2B**. The 50% silencing was also observed when one of the two loaded siRNA was replaced by the siNEG, showing that there was probably no cross-talk between both silenced proteins.

Analyses by qPCR confirmed the robust silencing (up to 70%) of *YAP1* (p <0.05) and *TAZ* (p <0.05) mRNA when the WRAP5 nanoparticle encapsulated both siRNA (siYAP1+siTAZ) compared to WRAP5:siNEG (**Figures 3C, 3D**). Here again, comparable mRNA silencing efficiency was observed for siRNA delivered alone or in combination, allowing us to rule out any cross-talk due to simultaneous knockdown of YAP1 and TAZ.

To further confirm the specificity and efficiency of YAP1 and TAZ silencing at the cellular level, we performed immunofluorescence staining of both proteins in GIST-T1 cells treated with WRAP5 nanoparticles loaded with siNEG, siYAP1, siTAZ, or siYAP1+siTAZ (**Figure 4A**). Cells were co-stained for YAP1 and TAZ, and fluorescence intensity was quantified across individual cells. A significant decrease in TAZ signal (-45%, p <0.01) was observed in cells treated with siTAZ (**Figure 4B**), while YAP1 signal was significantly reduced (-40%, p <0.01) in cells treated with siYAP1 (**Figure 4C**) compared to the siNEG condition. Notably, no nuclear relocalization or compensatory accumulation of one protein was observed when the other was silenced. This absence of compensatory nuclear recruitment suggests that YAP1 and TAZ do not substitute for each other in GIST-T1 cells under these conditions. However, it seems that the fluorescence signal of TAZ is significantly lower (-64%, p <0.0001) when both siRNA (siYAP1+siTAZ) were used, in contrast to the YAP1 fluorescence signal, which was constant (-40%, p <0.01; equal to siYAP1 alone) (**Figures 4B, 4C**).

These results established WRAP5:siRNA nanoparticles as a reliable and non-toxic tool for selective and combinatorial gene silencing of YAP1 and TAZ in GIST cells, enabling us to dissect the role of both proteins individually or together in GIST biology.

Selective effect of TAZ silencing on GIST-T1 cell migration and proliferation

After proving the effectiveness of our WRAP5:siRNA nanoparticles in silencing YAP1 and TAZ individually or together in GIST-T1 cells, we next investigated the functional consequences of their knockdown on the cellular mechanisms, such as cell migration and proliferation.

To assess cell migration, we performed a wound healing assay on confluent GIST-T1 cells seeded on a culture insert to reproduce a homogeneous scratch (wound). 72 hours after transfection with siRNA-loaded WRAP5 nanoparticles, we observed that TAZ silencing resulted in a substantial decrease (-24%) in wound closure compared to the siNEG control condition (p <0.01), suggesting an impaired migratory capacity (**Figure 5A**). With regard to YAP1 silencing, it is interesting to note that no significant effects (p = ns) has been observed, despite previous reports of its involvement in migration phenomena in other cancers [59,60]. Co-silencing of YAP1 and TAZ using WRAP5:(siYAP1+siTAZ) resulted in cell migration reduction compared to the siNEG control (-31%, p <0.001) (**Figure 5**). This slightly higher migration revealed that the co-silencing may have an additive effect compared to TAZ silencing alone, as observed previously in confocal microscopy (**Figure 4**). However, most of this effect is driven by targeted TAZ silencing.

We next evaluated cell proliferation firstly using the MTT assay, an approach that measured metabolic cell activity with the same incubation conditions as used for the wound healing assay (**Figure 5B**). Evaluation of the assay 48 hours post-transfection showed no statistical differences between the

WRAP5-based conditions (**Figure S5**). Only GIST-T1 cells incubated with IM (200 nM used as control) revealed a significant reduction in cell proliferation (-85%, p <0.0001). In contrast, when the assay was evaluated 72 hours post-transfection, a marked decline in proliferation rate was observed for TAZ silencing (-30%, p <0.05) in comparison to the control condition siNEG or siYAP1. Interestingly, we observed an equivalent effet on proliferation when GIST-T1 cells were co-treated with (siYAP1+siTAZ), also supporting the predominant role of TAZ (-20%, p <0.05).

Similar results were observed when performing a direct cell counting over time (**Figure 5C**). Following transfection with WRAP5-based nanoparticles, YAP1 silencing alone did not result in a statistically significant reduction in cell proliferation. However, a reduction in the number of cells was observed 48 hours or 72 hours post-transfection when TAZ was silenced alone or in combination with YAP1 (around -21% at 72 h, p <0.01). No potential additive effect of the applied siYAP1+siTAZ combination could be detected in both cell proliferation assays.

Together, these findings revealed that TAZ, more than YAP1, could drive GIST-T1 cell proliferation and migration, and that its silencing had a stronger inhibitory effect on these tumorigenic properties.

Impact of TAZ silencing on Hippo pathway effectors in GIST-T1 cells

Following the observed phenotypic effects of TAZ silencing on *KIT*-dependent IM-sensitive GIST-T1 cell migration and proliferation, we aimed to explore the molecular mechanisms underlying its function. Following activation by phosphorylation, YAP1 and TAZ translocate into the nucleus, where they bind to the TEAD1-4 proteins, thereby facilitating the expression of downstream target genes (*CTGF, CYR61, AREG, MYC, MCL-1, BIRC5, AXL*, etc.) implicated in cell migration, proliferation, invasion, and resistance to apoptosis [23–25].

As we observed an effect of TAZ on cell migration and proliferation, we first examined the expression of CYR61 and CTGF. Western blot analyses on GIST-T1 cells incubated with the WRAP5 nanoparticles encapsulating the siYAP1 alone induced no downstream effect on CYR61 and CTGF expression (p = ns). Conversely, WRAP5:siTAZ nanoparticles revealed a significant downregulation of CYR61 protein (-65%, p <0.001) and of CTGF (-55%, p <0.01) compared to the control condition (WRAP5:siNEG) (**Figures 6A, 6B**). This effect on CYR61 and CTGF protein expression was also observed when siTAZ was used in combination with siYAP1. All these results were confirmed by qPCR analyses that revealed a significant downregulation of *CYR61* and *CTGF* genes on mRNA levels upon TAZ knockdown, either alone or in combination with YAP1 (>80%, p <0.0001 for both, respectively) compared to WRAP5:siNEG. In contrast, YAP1 silencing alone had no measurable effect on *CYR61* mRNA level, but, curiously, we observed an increase of *CTGF* mRNA upon siYAP1 silencing (**Figure 6D**). These indicated that TAZ, rather than YAP1, was the main driver of Hippo pathway output in GIST-T1 cells.

We also analyzed Cyclin D1 (CD1) expression to determine whether this key cell cycle regulator was modulated by YAP1 or TAZ in our model. Surprisingly, CD1 expression remained unchanged following TAZ or YAP1 silencing (p = ns for all conditions *versus* siNEG), suggesting that its regulation in GIST-T1 cells was independent of these factors under the tested conditions (**Figure 6C**).

Finally, to investigate the potential connection between the Hippo and KIT signaling pathways, we assessed ratios of total and phosphorylated levels of KIT, AKT, and ERK, mimicking the activation of MAPK and PI3K/mTOR pathways. They represent the key effectors of KIT oncogenic signaling [24,33]. No significant changes were observed following YAP1 or TAZ knockdown in GIST-T1 cells (**Figure 6E**), indicating that the anti-tumorigenic effects of TAZ silencing were independent of direct modulation of KIT or its canonical downstream cascades.

In conclusion, these results showed that TAZ promoted GIST-T1 proliferation and migration primarily through activation of specific Hippo pathway targets, rather than by influencing CD1 and the KIT signaling axis. We thus hypothesized that CYR61 and CTGF were specific downstream effectors of TAZ in GIST-T1 cells.

WRAP5:siRNA as an effective tool for YAP1/TAZ silencing other GIST cells

As the GIST pathology was characterized by different mutations resulting in *KIT*-dependent IM-sensitive GIST, we decided to quantify YAP1 and TAZ expression in GIST-430 and GIST-882 cells [51,52]. These two cell lines harbors different *KIT* mutations than the primary mutation in GIST-T1 cell (*KIT* exon 11 Δ560–578 in frame-deletion versus respectively KIT exon 11 Δ560-576 in-frame deletion and KIT exon 13 K642E mutation). These cells displayed distinct basal expression profiles of YAP1, and TAZ compared to GIST-T1 cells, as confirmed by Western blot analyses (**Figure S6**). Notably, TAZ expression was markedly lower in GIST-882 cells, while both YAP1 and TAZ were expressed at higher levels in GIST-430, underscoring the molecular heterogeneity that characterized GIST tumors [61]. Importantly, total and phosphorylated KIT levels appeared comparable across the three cell lines, suggesting that differences in YAP1 and TAZ expression and downstream target regulation were not attributable to variations in KIT signaling (**Figure S6**). However, given the differing morphologies (**Figure S7**) and proliferation rates of the three GIST cell lines, the protocol was adapted to each cell line in terms of cell density and siRNA concentrations (see Materials & Methods section for details).

Using WRAP5:siRNA nanoparticles previously used, we evaluated YAP1 and TAZ silencing depending on the applied siRNA (siYAP1, siTAZ, siYAP1+siTAZ, siNEG) in GIST-430 and GIST-882 cells. In both cell lines, YAP1 and TAZ knockdown were efficient when the corresponding siRNA was used compared to the siNEG (between 40% and 70%, depending on the condition used) (**Figures 7A, 7B**). Surprisingly, for the WRAP5 nanoparticles delivering the equimolar siRNA cocktail of siYAP1 and siTAZ, we observed a slightly higher protein knockdown than with the single siRNA, which was not observed previously on GIST-T1 cells. However, when applying the one-way ANOVA statistical test followed by Dunnett's post-hoc test with multiple comparisons versus siTAZ or (siYAP1+siTAZ), no significant difference was observed between these groups (data not shown).

Then, we also analyzed YAP1/TAZ silencing on downstream protein expression of CYR61 and CTGF in GIST-430 and GIST-882 cells, as previously done for GIST-T1 cells. In details, in GIST-430 cells, YAP1 or TAZ silencing alone led to a non-significant reduction in CYR61 and CTGF even if there was a trend for both proteins (p = ns *versus* WRAP5:siNEG), while their combination (siYAP1+siTAZ) significantly decreased both targets (50%, p <0.01 for CYR61 and 50%, p <0.01 for CTGF) (**Figure 7A**). In contrast, YAP1 knockdown did not affect either of these both downstream proteins. In GIST-882 cells, TAZ silencing alone did not significantly reduce CYR61 (p = ns), but a significant reduction in protein expression was observed for CTGF (45%, p <0.05), while YAP1 knockdown had no effect (p = ns versus WRAP5:siNEG). Again, dual silencing significantly reduced both gene expressions (50%, p <0.01 for CYR61 and 65%, p <0.01 for CTGF) (**Figure 7B**).

These results suggested that although TAZ appeared to play a predominant role, YAP1 could potently contribute in a complementary way in GIST-430 and GIST-882 cells. As we observed a higher basal YAP1 expression (**Figure S6**), it is probably possible that YAP1 has a more predominant role in these two GIST cell lines. Given the variability between three cell lines, both factors should be considered when targeting the YAP1/TAZ axis in GIST.

CYR61 and CTGF as key downstream effectors mediating TAZ-induced proliferation in GIST-T1 cells

We decided to silence CYR61 and CTGF to ensure that they were effectors of the impact on cell proliferation observed for TAZ. For each gene, we designed two siRNA. Their specific knockdown efficiency and their potent cytotoxic effect were assessed by Western blot and by LDH assay, respectively (**Figures S8A-H**). Selected siCYR61 and siCTGF led to 90% and 60% of protein inhibition at 40 nM, respectively (**Figures S8A, S8E**) without any toxic effect for the cells (**Figures S8C, S8G**. The efficacy of these selected siRNA was also validated in qPCR analyses. This experiment led to significant downregulation of *CYR61* and *CTGF* mRNA levels 24 hours after treatment with WRAP5:siCYR61 and WRAP5:siCTGF nanoparticles, respectively (-60%, p <0.001 for both, **Figure 8A**).

To assess the functional impact of CYR61 and CTGF silencing on cell proliferation, we performed cell counting assays over a 72-hour time-course following WRAP5:siRNA delivery. Following GIST-T1 cellular transfection with WRAP5-based nanoparticles, we observed a downward trend in the number of cells at 48 hours or 72 hours post-transfection when CTGF was silenced alone or in combination with CYR61, respectively (around -22% at 72h, p = ns)(**Figure 8B**). Interestingly, CYR61

silencing alone resulted in a statistically significant reduction in cell proliferation (-34% at 72h, $p<0.01$) compared to the siNEG control.

Finally, to explore the clinical relevance of these findings, we analyzed the same cohort of 60 patients from the ATGsarc microarray database [53] as previously performed for YAP1 and TAZ (**Figure 1**). Kaplan-Meier survival analyses stratified patients by high versus low gene expression levels of *CYR61* or *CTGF*. High *CYR61* expression was significantly associated with reduced disease-free survival ($p = 0.011$; **Figure 8C**) and with the presence of metastasis during GIST evolution ($p = 0.0203$; **Figure 8D**). In contrast, *CTGF* expression showed no significant correlation with either disease-free survival ($p = 0.43$) or metastatic status ($p = 0.583$). *CYR61* is identified as a clinically relevant effector of TAZ, linking its overexpression to both increased tumor cell proliferation and poor clinical outcomes in GIST.

These results support the role of CYR61 as a downstream effector of TAZ in GIST-T1 cells, to promote tumor cell proliferation. This correlates with a high *CYR61* expression associated with critical clinical features, including shorter progression-free survival and metastatic status.

DISCUSSION

In this study, we provided the first investigation of the individual roles of YAP1 and TAZ, the two Hippo pathway effectors, in *KIT*-dependent IM-sensitive GIST cells. Indeed, it is well known that YAP1 and TAZ are implicated in cancer development and progression, even if most publications presented YAP1/TAZ as functionally redundant due to their structural similarity and shared transcriptional partners [24,34,35]. However, some reports suggest that both proteins have distinct roles as reviewed by Reggiani, *et al*. [37].

We aimed to evaluate whether it was possible to target YAP1 or TAZ separately using interfering RNA to elucidate which of these oncogenic proteins participated in GIST development and proliferation. Using our WRAP5-based nanoparticles as a delivery tool previously validated for therapeutic delivery [43–46], we vectorized specifically developed siRNA targeting the mRNA of *YAP1* and *TAZ*, individually, but also together using a siRNA cocktail containing an equimolar combination of both (siYAP1+siTAZ).

With this tool in our hand, we observed a specific and significant silencing of YAP1 or TAZ individually or in combination in *KIT*-dependent IM-sensitive GIST-T1 (**Figure 3**). However, only the silencing of TAZ resulted in a reduction in cell migration and cell proliferation (**Figure 5**). More interestingly, transcriptional activation of downstream targets such as *CYR61* and *CTGF* genes was shown after TAZ silencing, while YAP1 exerted limited or nearly no effects on these genes implicated in cell proliferation. Notably, inhibition of TAZ alone prevented the induction of oncogenic characteristics, and dual silencing showed only a slight additive effect on phenotypic outcomes. These results thus reinforce the idea of non-redundant roles in GIST cells and a more complex regulatory mechanism.

The functional divergence between YAP1 and TAZ protein function observed here was consistent with reports in other malignancies especially cancers. In hepatocellular carcinoma and cholandiocarcinoma, only YAP1 played crucial roles in the development and progression [62,63]. In non-small cell lung cancer, TAZ preferentially regulated genes involved in extracellular matrix remodeling and metastasis, whereas YAP1 controlled proliferation-related genes [64]. Moreover, the activation of TAZ nuclear translocation was associated with the highly aggressive in triple-negative subtype of breast cancer [65]. Importantly, such divergence has also been described in sarcomas, a relevant context for GIST. For example, two research articles revealed an upregulated YAP1 expression level in osteosarcoma and participated to cell differentiation [41,66], even if the role of TAZ was not evaluated. In contrast, TAZ activity was modulated for the myogenic differentiation in rhabdomyosarcoma without the participation of YAP1 [67]. Our study extended this paradigm to GIST, establishing TAZ as a main oncogenic driver and supporting the notion of tissue- and lineage-specific YAP1/TAZ activity. However, our results supported the idea that TAZ could represent a more relevant therapeutic target in the context of GIST, in line with the clinical data identifying TAZ as a superior prognostic marker (**Figure 1**).

Despite these findings, the mechanistic basis of this functional separation remained unclear as both proteins, YAP1 and TAZ, mainly bound to TEAD transcription factors to regulate gene expression involved in cancer development. This raised the possibility that differential nuclear co-factor recruitment (co-activators or co-repressors) or divergent affinity for specific TEAD isoforms could underlie the selective transcriptional activity of TAZ [37,60]. Further research should help to define these regulatory mechanisms, including chromatin context, transcriptional partner preferences, or post-translational modifications, which could fine-tune TEAD-dependent transcriptional output.

By comparing in detail the three analyzed GIST cell lines, we observed heterogeneous YAP1 and TAZ protein expression, while TAZ emerged as the dominant effector for downstream *CYR61* and *CTGF* gene downregulation (**Figures 6A, 6B, 6D, 7**). However, depending on the cellular YAP1/TAZ expression profile, a combined silencing of both proteins further repressed downstream gene expression. This suggested a possible context-dependent or co-operative role of YAP1/TAZ. This heterogeneity in YAP1/TAZ protein expression could reflect the diversity found within tumors in GIST patients and highlighted the possible advantage of targeting both pathways in more aggressive or advanced cases. Indeed, similar strategies have been effective in other cancers. In KRAS G12C mutant cells, dual knockdown of YAP1 and TAZ maximized reduction in **CYR61** expression and sensitized tumors to targeted therapies [68]. Likewise, in BRAF inhibitor-resistant melanoma, dual YAP1/TAZ silencing restored drug sensitivity and suppressed proliferation [69,70]. These findings supported our conclusion that dual inhibition, while not always synergistic, could provide broader efficacy in complex tumor environments.

In the present study, it was demonstrated that upon Hippo inactivation, the TAZ-CYR61 axis is activated as evidenced by the proliferation assay (**Figure 8B**). This activation exerts a negative impact on clinical progression as shown by correlating TAZ/CYR61 expression in the GIST database for progression-free survival and metastasis formation (**Figures 8C, 8D**). Indeed, the two genes are well established downstream targets of the YAP1/TAZ-TEAD complex and are implicated in cell proliferation, angiogenesis, extracellular matrix deposition, and metastasis across multiple tumor types [24,35].

In the three used GIST cell models, their expression was consistently regulated by TAZ and less by YAP1, reinforcing the specificity of TAZ-mediated transcription in GIST. Similar finding was revealed in gastric cancer, another digestive cancer, showing that TAZ upregulation was an important inducer of epithelial-mesenchymal transition and gastric cancer stem cell [55].

Although CD1 expression remained unaffected when YAP1 and TAZ were inhibited, this does not exclude the involvement of other cell-cycle regulators such as cyclin D2, cyclin D3, CDK2, or CDK4 notably in TAZ-driven proliferation [71]. Moreover, a modulation of apoptosis-related markers such as MCL-1 or BCL-2 could not be disregarded, leading to an indirect impact through other survival pathways [72]. Our results suggest that YAP1 and TAZ silencing does not significantly alter the major downstream signaling pathways of KIT activation, ERK/MAPK, and PI3K/AKT/mTOR, indicating that TAZ-driven transcriptional programs may promote tumor progression through pathways at least partly independent of canonical KIT signaling.

In conclusion, the use of WRAP5:siRNA nanoparticles could be an innovative therapeutic strategy for GIST treatment, as these nanoparticles exhibited low cytotoxicity and enabled sustained delivery of siRNA *in vitro* and *in vivo,* as previously reported in other pathologies or in GIST [42,44,46–48,73]. This approach opened new avenues for RNA-based therapeutics in GIST, where current treatment options remained limited for GIST patients to kinase inhibition using TKI [74]. Notably, siRNA-based drugs are now commonly accepted as six vectorized siRNA have been approved by the FDA (US Food and Drug Administration) and the EMA (European Medicines Agency) [75]. In the context of the presented siTAZ or (siYAP1+siTAZ)-loaded WRAP5-based nanoparticles as a therapeutic entity, further *in vivo* investigations will be needed to further promote their development. Especially, further work should be performed in order to determine if both siRNA should be used to overcome GIST patient heterogenicity (variation in the mutation profile).

Finally, to potentiate siRNA-loaded WRAP5 nanoparticles, other parameters should also be taken into account, such as the optimization of the nanoparticle itself through PEGylation (increasing

the stability) or targeting motif insertion as reported previously in other physio-pathological contexts [46,48,73]. Given emerging links between Hippo pathway reactivation and TKI resistance [18], future work should also explore how YAP1/TAZ modulation impacts IM response and resistance mechanisms.

FIGURES

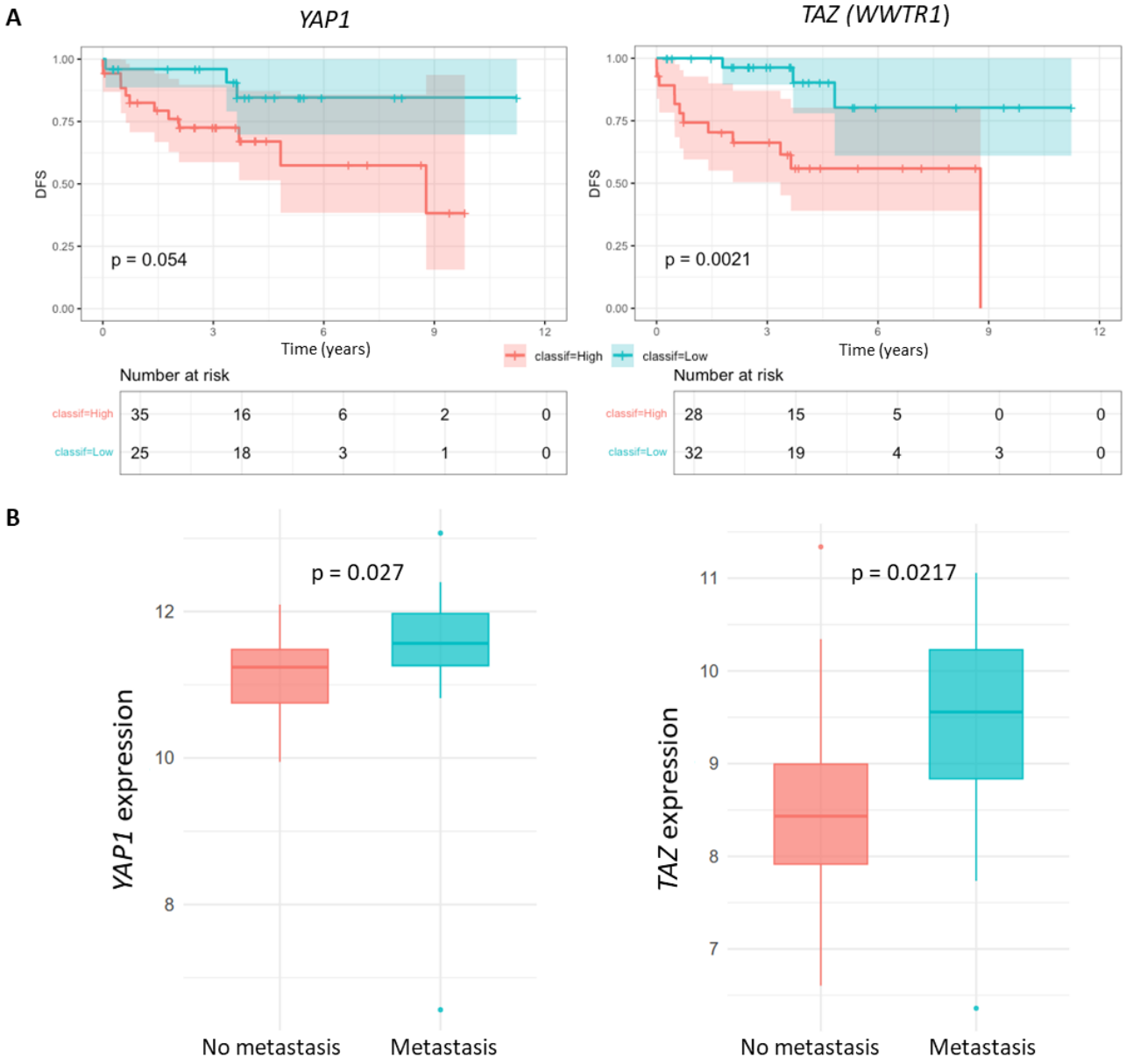

Figure 1: Correlation of *YAP1* and *TAZ* expression with the prognosis of GIST patients.
(**A**) Kaplan-Meier curves of disease-free survival (DFS) from 60 total GIST patients in the ATGsarc microarray database, stratified by *YAP1* or *TAZ* (*WWTR1*) expression levels. Group 1 (red): patients with high gene expression (initial number of patients = 35); Group 2 (blue): patients with low gene expression (initial number of patients = 25). Number at risk = number of patients at risk over time. They are summarized in the table below the curves.
(**B**) Comparison between *YAP1* or *TAZ* transcript levels and the presence of metastasis. n = 45 (red) and n = 15 (blue) in the no metastatic and metastatic groups, respectively. p-values from the log-rank test are indicated.

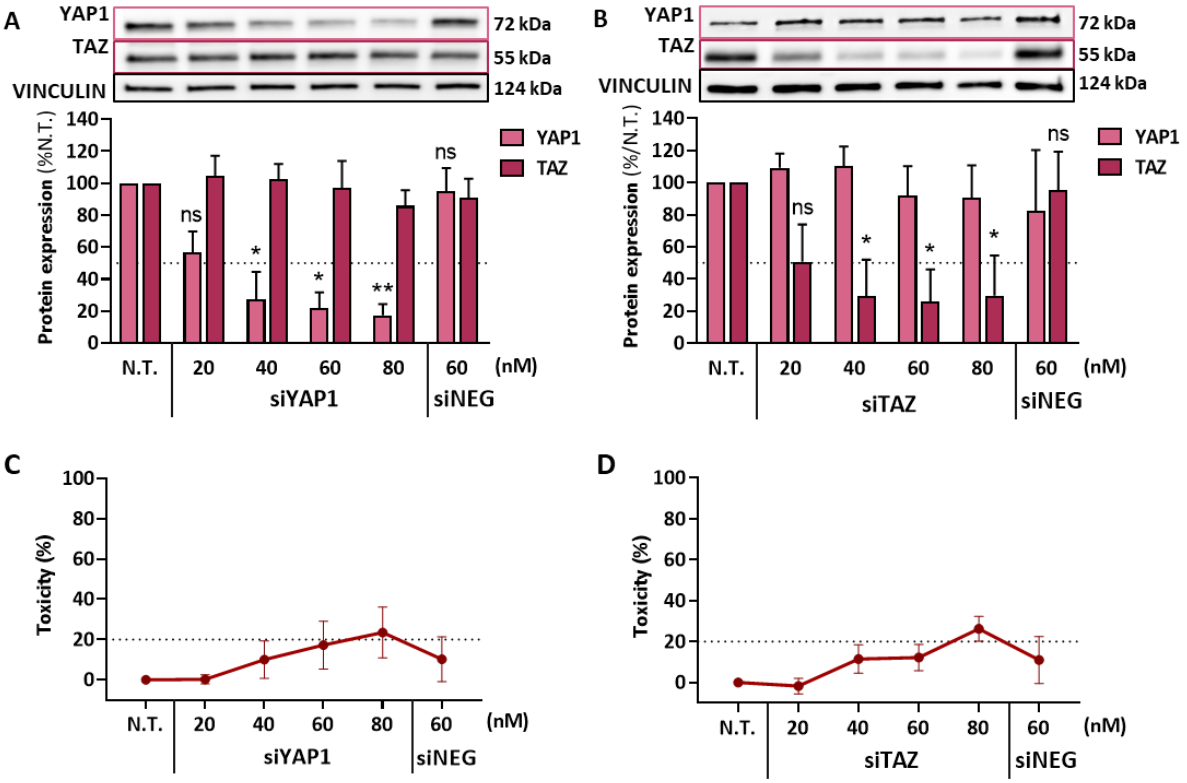

Figure 2: Evaluation of YAP1 or TAZ silencing in GIST-T1 cells with WRAP5:siRNA nanoparticles.
WRAP5:siRNA nanoparticles delivering siYAP1 (**A**) or siTAZ (**B**) induced a dose-dependent inhibition of YAP1 or TAZ protein expression in GIST-T1 cells after 48 h of incubation, as shown by Western blot quantification. No significant toxicity was observed for siYAP1 (**C**) or siTAZ (**D**) within the tested concentration range (20 – 60 nM), as assessed by LDH assay. A slight toxicity was observed for 80 nM.
Controls included untreated (N.T.) and siNEG-treated cells. Data are presented as mean ± SD from N=4 experiments. Statistical analysis was performed using Kruskal-Wallis followed by Dunn's multiple comparisons test *versus* N.T. (**A**, **B**); ns >0.05, * <0.05, ** <0.01. Analysis of TAZ expression following siYAP1 treatment and YAP1 expression following siTAZ treatment showed no significant differences compared to N.T. (data not annotated on the graph for clarity).

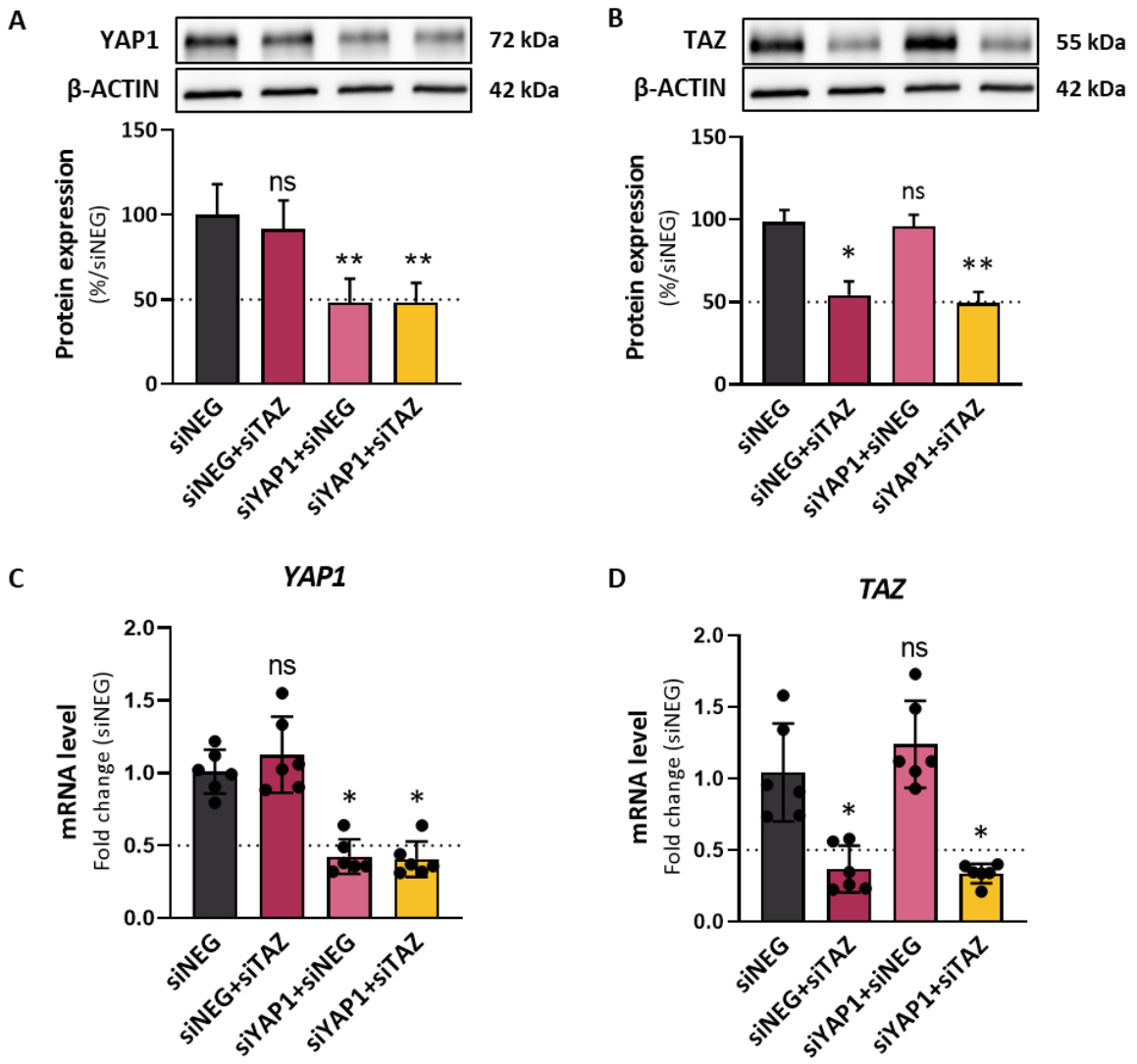

Figure 3: Specific targeting of YAP1 and TAZ, individually or simultaneously, using WRAP5:siRNA cocktails. WRAP5:siRNA nanoparticles delivering an equimolar cocktail of siRNAs targeting YAP1 and/or TAZ specifically inhibited YAP1 and TAZ protein expression (**A, B**) and mRNA levels (**C, D**) in GIST-T1 cells, as assessed by Western blot quantification and qPCR analysis, respectively.
Conditions: WRAP5:siRNA (MR 20 with [siRNA] = 40 nM), siNEG-treated cells were used as a control condition. Data were presented as mean ± SD for N=6 individual experiments. Statistical analyses were performed using Kruskal-Wallis followed by Dunn's multiple comparisons test *versus* siNEG; ns >0.05, * <0.05, ** <0.01.

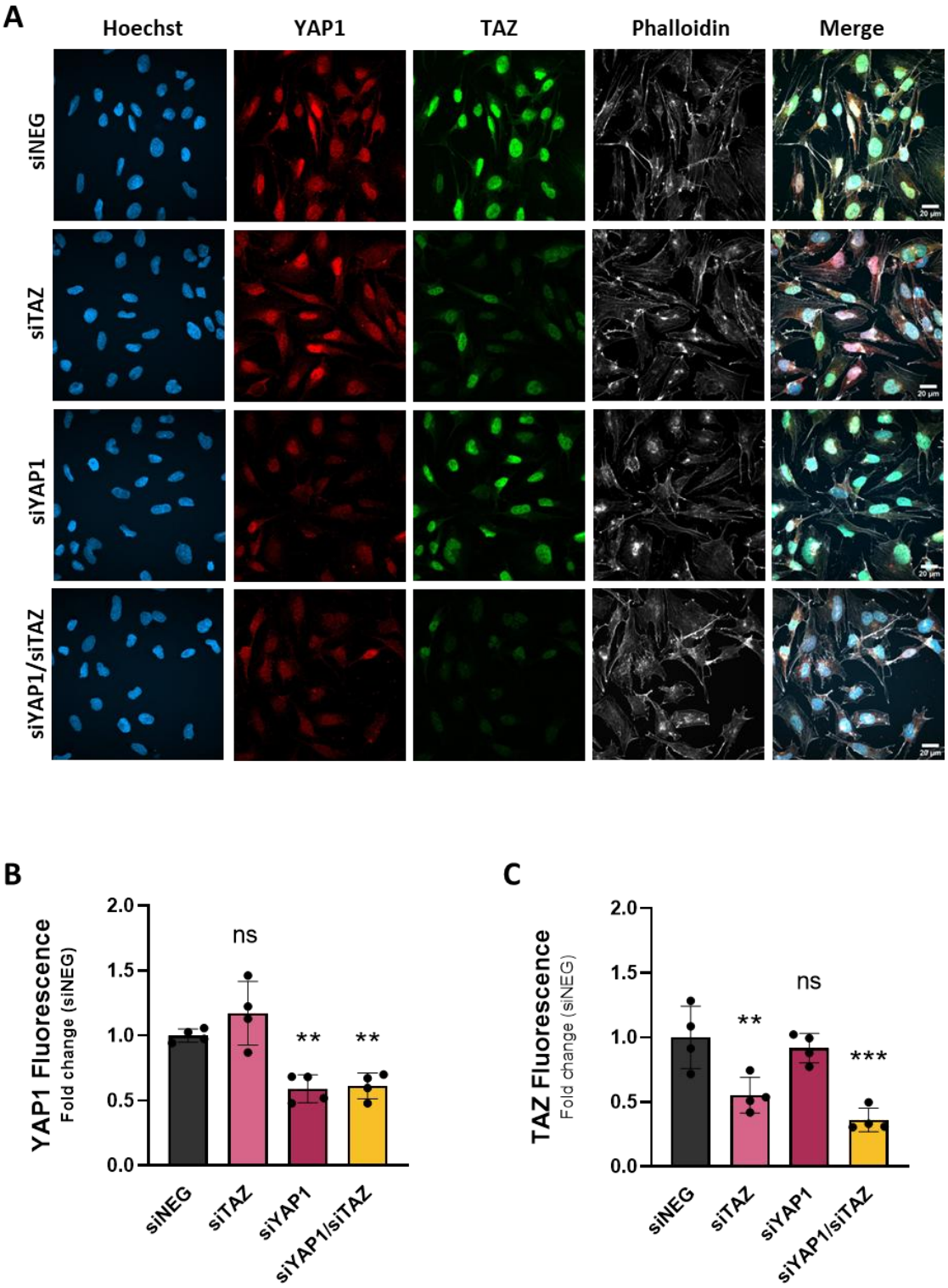

Figure 4: Immunofluorescence analysis of YAP1 and TAZ expression following siRNA-mediated silencing in GIST-T1 cells.

GIST-T1 cells were treated with WRAP5 nanoparticles loaded with 40 nM of siNEG (control), 20 nM of siYAP1 or siTAZ, or a combination of siYAP1+siTAZ (20 nM each). Immunofluorescence staining was performed to detect endogenous YAP1 (red) and TAZ (green), with nuclei counterstained using Hoechst (blue) and Phalloidin (gray). Representative images are shown for each condition (**A**). Scale bars = 20 µm.

Quantification of fluorescence intensity by Image J was performed for YAP1 (**B**) and for TAZ (**C**) in the four conditions. Data were represented as mean ± SD for N = 2 with n=2. Statistical analyses were performed using Kruskal-Wallis followed by Dunn's multiple comparisons test *versus* siNEG.

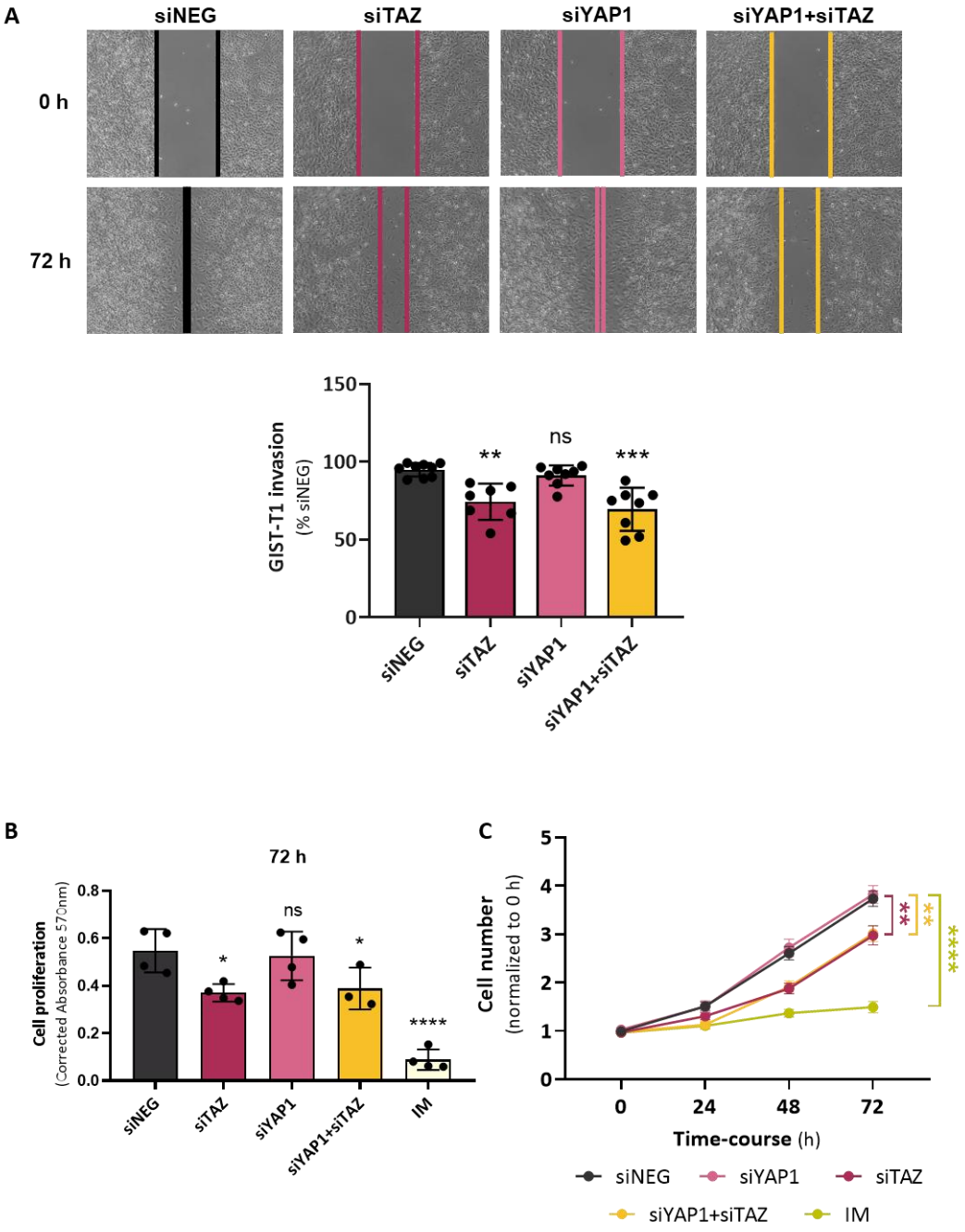

Figure 5: TAZ silencing reduced GIST-T1 cell migration and proliferation.

(**A**) WRAP5:siRNA nanoparticles targeting TAZ, YAP1, or both (siYAP1+siTAZ) were analyzed in a wound healing assay 72 h post-transfection in GIST-T1 cells. The graph shows the percentage of wound closure relative to the initial scratch and normalized to the siNEG condition (N=8 independent experiments).

(**B**) WRAP5:siRNA nanoparticles targeting TAZ, YAP1, or both (siYAP1+siTAZ) were analyzed using the CellTiter 96® Non-Radioactive Cell Proliferation Assay 72 h post-transfection in GIST-T1 cells (N=4 independent experiments with n=5 replicates).

(**C**) WRAP5:siRNA nanoparticles targeting TAZ, YAP1, or both (siYAP1+siTAZ) were analyzed by cell counting over a 72 h time course post-transfection (N=5 independent experiments with n=2 replicates).

Abbreviation: IM = Imatinib. Conditions: WRAP5:siRNA (MR 20) with siRNA concentrations as indicated in the Materials & Methods section, siNEG was used as the control condition, IM = 200 nM. Data are presented as mean ± SD (**A**, **B**) or mean ± SEM (**C**). Statistical analyses were performed using Kruskal-Wallis followed by Dunn's post-hoc test *versus* siNEG (**A**); one-way ANOVA followed by Holm-Sidak's post-hoc test *versus* siNEG (**B**,**C**). ns >0.05, * <0.05, ** <0.01, *** <0.001, and **** <0.0001.

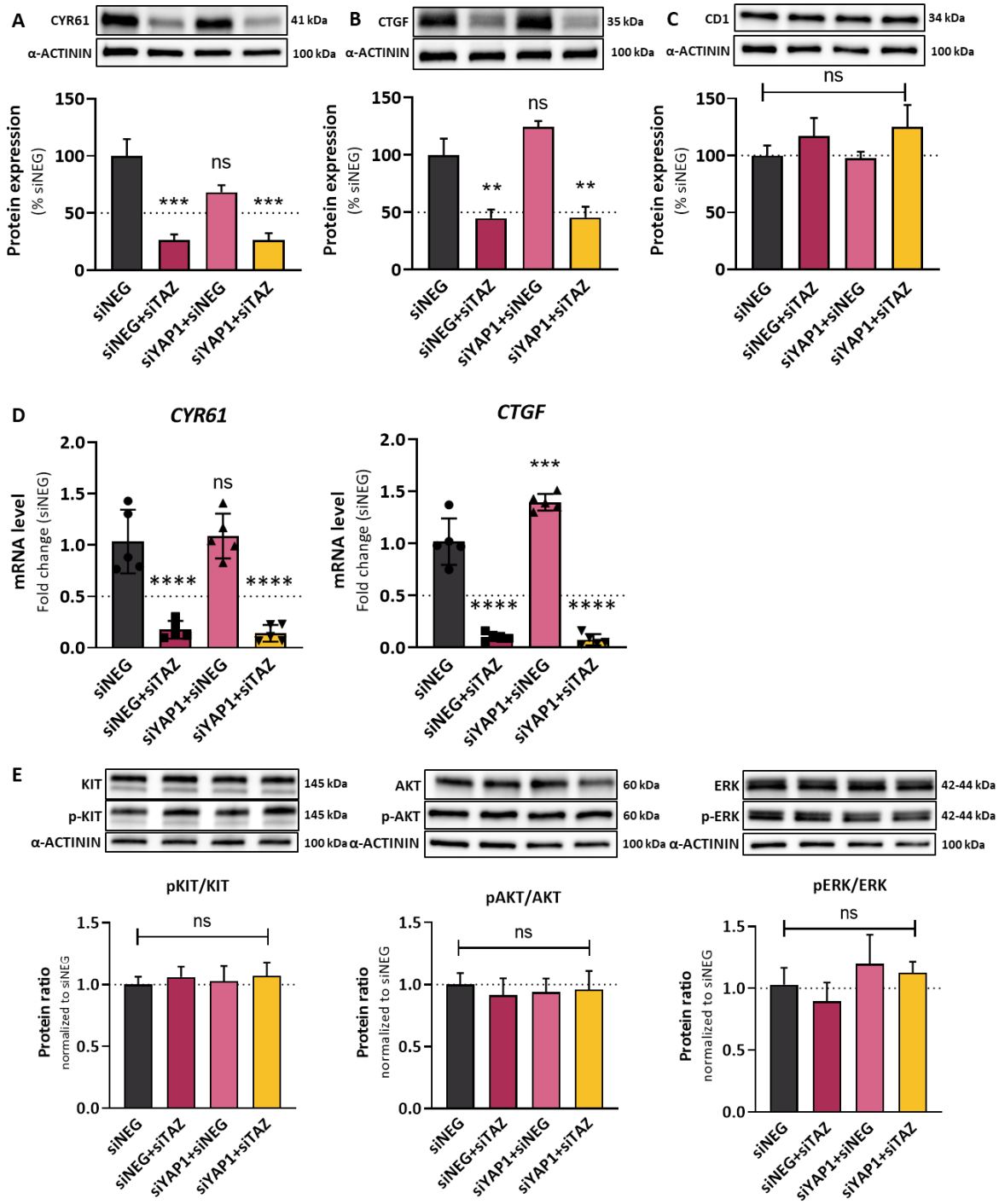

Figure 6: Evaluating TAZ silencing on different signaling pathways in GIST-T1 cells.

Effect of WRAP5:siRNA nanoparticles targeting TAZ, YAP1, or both (siYAP1+siTAZ) on CYR61 (**A**), CTGF (**B**), and CD1 (**C**) protein expression in GIST-T1 cells was analyzed by Western blot analysis 48 h post-transfection. (**D**) Effect of WRAP5:siRNA nanoparticles targeting TAZ, YAP1, or both (siYAP1+siTAZ) on CYR61 and CTGF mRNA levels in GIST-T1 cells was analyzed by qPCR analysis 24 h post-transfection.

(**E**) Effect of WRAP5:siRNA nanoparticles targeting TAZ, YAP1, or both (siYAP1+siTAZ) on of KIT signaling components (KIT, pKIT, AKT, pAKT, ERK, pERK) in GIST-T1 cells was analyzed by Western blot analysis 48 h post-transfection.

Conditions: WRAP5:siRNA (MR 20 with [siRNA] = 40 nM), siNEG was used as the control condition. Data are presented as mean ± SD with N = 4 - 6 individual experiments. Statistical analyses were performed using one-way ANOVA followed by Dunnett's post-hoc test *versus* siNEG (**A**,**B,C,D**); Kruskal-Wallis followed by Dunn's multiple comparisons test *versus* siNEG (**E**) ns >0.05, ** <0.01, *** <0.001, ****<0.0001.

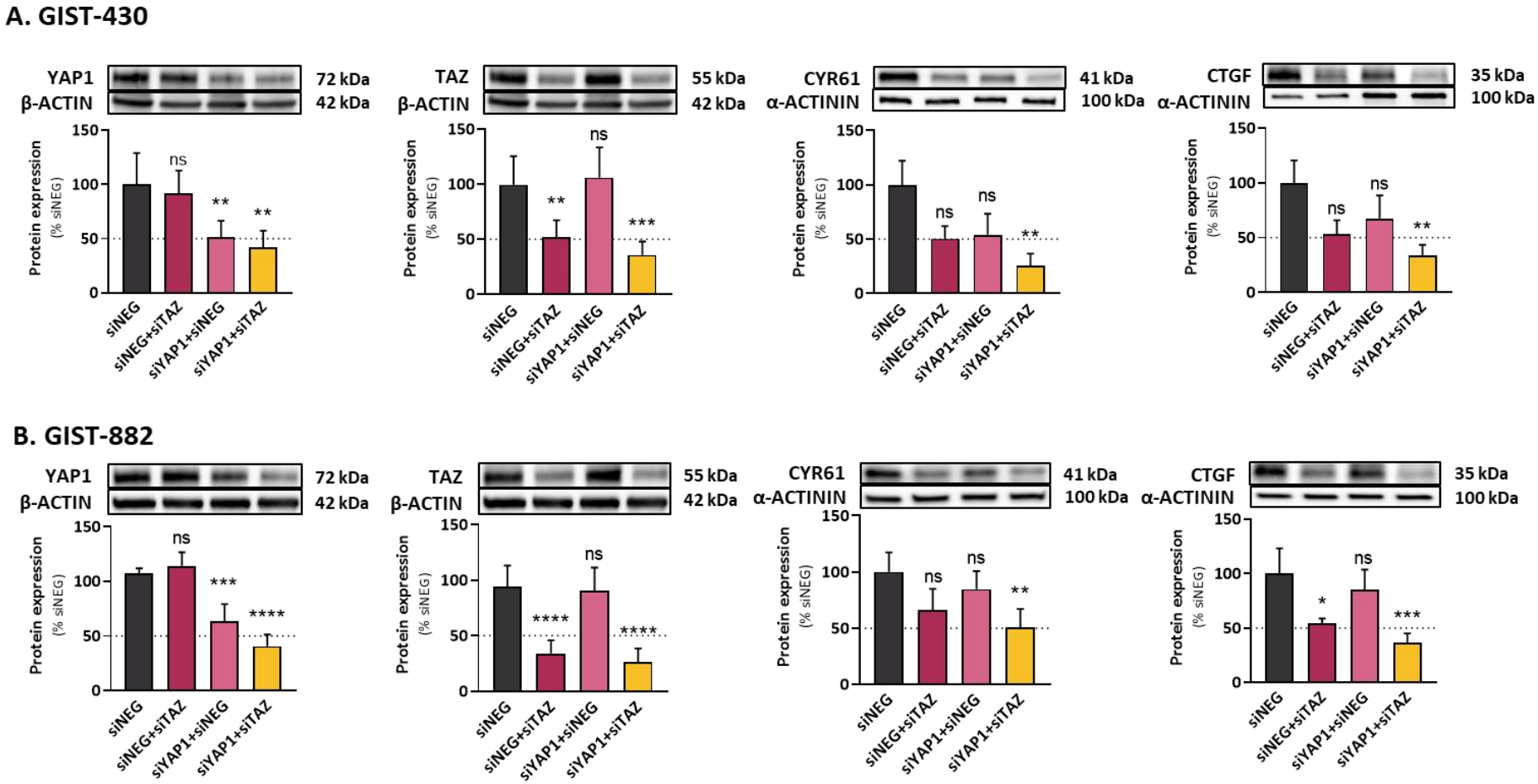

Figure 7: WRAP5:siRNA nanoparticles enabled selective silencing of YAP1 and TAZ across GIST cell lines, with conserved downstream regulation of CYR61 and CTGF.

Effect of WRAP5:siRNA nanoparticles targeting TAZ, YAP1, or both (siYAP1+siTAZ) on YAP1 and TAZ or CYR61 and CTGF protein expression in GIST-430 (**A**) and GIST-882 (**B**) cells was analyzed by Western blot 48 h post-transfection

Conditions: WRAP5:siRNA (MR 20 with [siRNA] = 80 nM), siNEG was used as a control. Data are presented as mean ± SD for N=5 individual experiments. Statistical analyses were performed using one-way ANOVA followed by Dunnett's post-hoc test *versus* siNEG (**B,C**); Kruskal-Wallis followed by Dunn's multiple comparisons *versus* siNEG (**D,E**); ns >0.05, * <0.05, ** <0.01, *** <0.001, **** <0.0001.

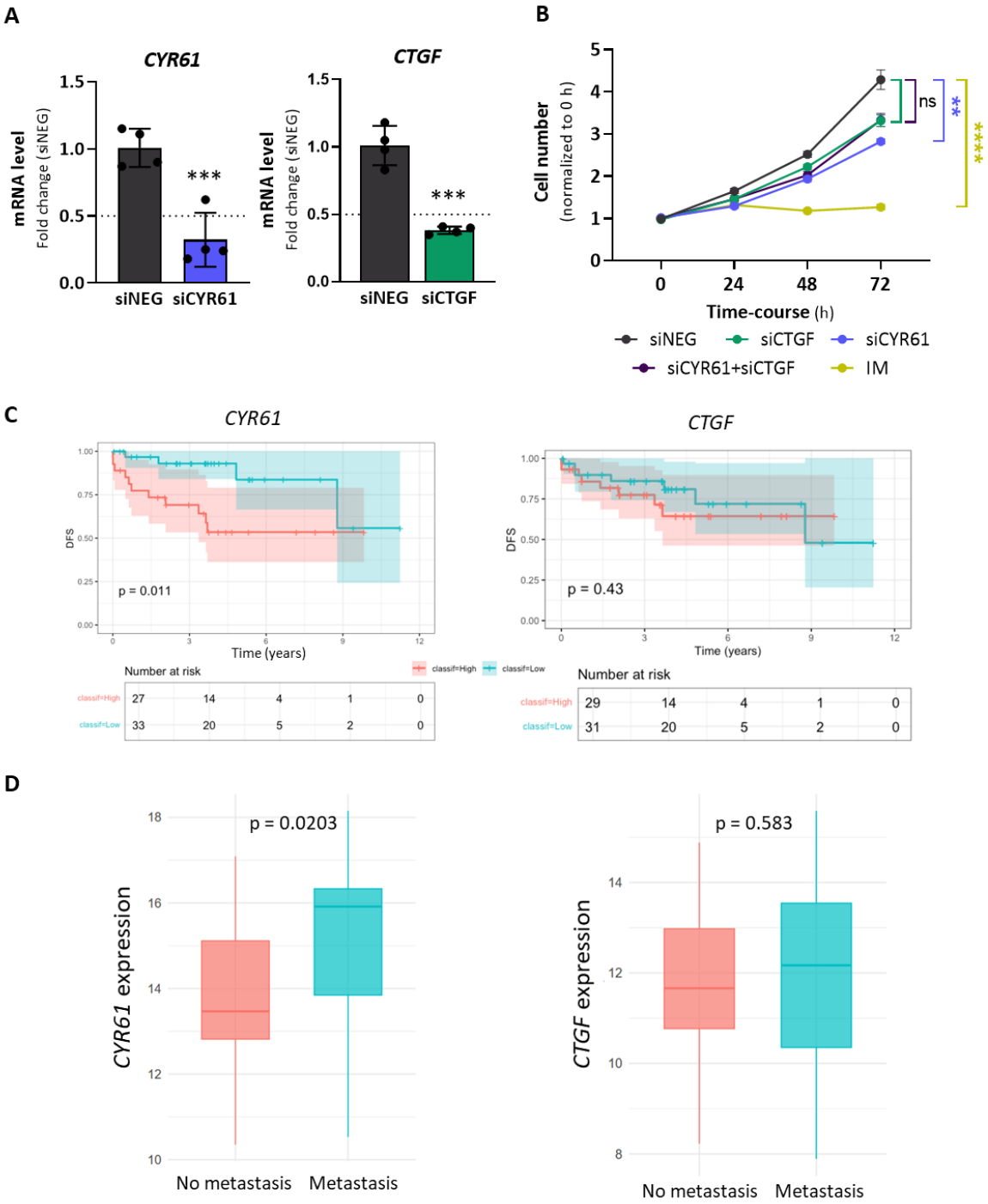

Figure 8: CYR61 and CTGF are effectors of TAZ for cell proliferation control

(**A**) Effect of WRAP5:siRNA nanoparticles targeting CYR61 and CTGF mRNA levels in GIST-T1 cells was analyzed by qPCR analysis 24 h post-transfection.

(**B**) WRAP5:siRNA nanoparticles targeting CYR61, CTGF, or both (siCYR61+siCTGF) were analyzed by cell counting over a 72 h time course post-transfection (N=4 independent experiments with n=2 replicates).

Abbreviation: IM = Imatinib. Conditions: WRAP5:siRNA (MR 20) with [siCYR61], [siCTGF] = 20 nM and [siNEG], [siCYR61/siCTGF] = 40 nM, siNEG was used as the control condition, IM = 50 nM. Data are presented as mean ± SD (**A**) or mean ± SEM (**B**). Statistical analyses were performed using unpaired two-tailed Student's t-test *versus* siNEG (**A**) or using Kruskal-Wallis followed by Dunn's multiple comparisons *versus* siNEG (**B**), ns >0.05, ** <0.01, *** <0.001, **** <0.0001.

(**C**) Kaplan-Meier curves of disease-free survival (DFS) from 60 total GIST patients in the ATGsarc microarray database, stratified by *CYR61* or *CTGF* expression levels. Group 1 (red): patients with high gene expression (initial number of patients = 27); Group 2 (blue): patients with low gene expression (initial number of patients = 33). Number at risk = number of patients at risk over time. They are summarized in the table below the curves.
(**D**) Correlation between *CYR61* or *CTGF* transcript levels and the presence of metastasis. n = 45 (red) and n = 15 (blue) in the non-metastatic and metastatic groups, respectively. p-values from the log-rank test are indicated.

SUPPLEMENTAL INFORMATION
Supplementary Material and Figures

ETHICS APPROVAL AND CONSENT TO PARTICIPATE
Not applicable.

CONSENT FOR PUBLICATION
Not applicable

AVAILABILITY OF DATA AND MATERIALS
GIST database (ATGsarc) is available at https://atg-sarc.sarcomabcb.org/

COMPETING INTERESTS
C.S. has received research funding (institution) from IDRX, Blueprint, Karyopharm, Pfizer, Deciphera, and Bayer; consulting fees (advisory role) from IDRX, CogentBio, Immunicum AB, Deciphera, and Blueprint; payment for lectures from Deciphera, PharmaMar, Pfizer, Bayer, and Blueprint; and travel grants from PharmaMar, Gilead, Pfizer, and Bayer. The remaining authors declare no competing interests.

FUNDING
This research was funded by the “Agence Nationale de la Recherche” (ANR-21-CE18-0022-01 to P.B.; ANR-21-CE17-0017 to S.F.; ANR-23-CE14-0071 to P.d.S.B.), and by institutional funds from INSERM, CNRS, and the University of Montpellier.

AUTHORS’ CONTRIBUTIONS
Conceptualization, I.P., P.B., S.D., P.D.S.B., S.F., C.S.; Methodology, I.P., P.B., S.D., E.V., F.C.; Experiments, I.P., P.B., S.D.; Figures, I.P., P.B., S.D., F.C.; Statistical analysis, I.P., P.B., F.C.; Writing-original draft preparation, I.P., P.B., S.D., S.F., P.D.S.B., C.S., E.V., F.C.; Funding acquisition, P.B., S.F., P.D.S.B. All authors have read and agreed to the published version of the manuscript.

ACKNOWLEDGMENTS
The authors are grateful to Pascal Verdié from the SynBio3 platform for providing peptide synthesis facilities, and to Pierre Sanchez for performing LC-MS analysis, both from the Institut des Biomolécules Max Mousseron (IBMM), Montpellier (France). The authors thank Dr. Karidia Konate and Thanian Hammoum for their critical reading of the manuscript.

REFERENCES
1. Blay J-Y, Kang Y-K, Nishida T, von Mehren M. Gastrointestinal stromal tumours. Nat Rev Dis Primer. 2021;7:22.

2. Casali PG, Blay JY, Abecassis N, Bajpai J, Bauer S, Biagini R, et al. Gastrointestinal stromal tumours: ESMO-EURACAN-GENTURIS Clinical Practice Guidelines for diagnosis, treatment and follow-up. Ann Oncol Off J Eur Soc Med Oncol. 2022;33:20–33.
3. Min KW, Leabu M. Interstitial cells of Cajal (ICC) and gastrointestinal stromal tumor (GIST): facts, speculations, and myths. J Cell Mol Med. 2006;10:995–1013.
4. Hirota S, Isozaki K, Moriyama Y, Hashimoto K, Nishida T, Ishiguro S, et al. Gain-of-function mutations of c-kit in human gastrointestinal stromal tumors. Science. 1998;279:577–80.
5. Schaefer I-M, DeMatteo RP, Serrano C. The GIST of Advances in Treatment of Advanced Gastrointestinal Stromal Tumor. Am Soc Clin Oncol Educ Book. 2022;42:1–15.
6. Bauer S, George S, von Mehren M, Heinrich MC. Early and Next-Generation KIT/PDGFRA Kinase Inhibitors and the Future of Treatment for Advanced Gastrointestinal Stromal Tumor. Front Oncol. 2021;11.
7. Serrano C, George S. Gastrointestinal Stromal Tumor: Challenges and Opportunities for a New Decade. Clin Cancer Res Off J Am Assoc Cancer Res. 2020;26:5078–85.
8. Duan Y, Haybaeck J, Yang Z. Therapeutic Potential of PI3K/AKT/mTOR Pathway in Gastrointestinal Stromal Tumors: Rationale and Progress. Cancers. 2020;12:2972.
9. Zhou S, Abdihamid O, Tan F, Zhou H, Liu H, Li Z, et al. KIT mutations and expression: current knowledge and new insights for overcoming IM resistance in GIST. Cell Commun Signal. 2024;22:153.
10. Demetri GD, von Mehren M, Blanke CD, Van den Abbeele AD, Eisenberg B, Roberts PJ, et al. Efficacy and safety of imatinib mesylate in advanced gastrointestinal stromal tumors. N Engl J Med. 2002;347:472–80.
11. Demetri GD, Oosterom AT van, Garrett CR, Blackstein ME, Shah MH, Verweij J, et al. Efficacy and safety of sunitinib in patients with advanced gastrointestinal stromal tumour after failure of imatinib: a randomised controlled trial. The Lancet. 2006;368:1329–38.
12. Demetri GD, Reichardt P, Kang Y-K, Blay J-Y, Rutkowski P, Gelderblom H, et al. Efficacy and safety of regorafenib for advanced gastrointestinal stromal tumours after failure of imatinib and sunitinib (GRID): an international, multicentre, randomised, placebo-controlled, phase 3 trial. The Lancet. 2013;381:295–302.
13. Serrano C, Fletcher JA. Overcoming heterogenity in imatinib-resistant gastrointestinal stromal tumor. Oncotarget. 2019;10:6286–7.
14. Chen T, Ni N, Yuan L, Xu L, Bahri N, Sun B, et al. Proteasome Inhibition Suppresses KIT-Independent Gastrointestinal Stromal Tumors Via Targeting Hippo/YAP/Cyclin D1 Signaling. Front Pharmacol. 2021;12:686874.
15. Ou W-B, Ni N, Zuo R, Zhuang W, Zhu M, Kyriazoglou A, et al. Cyclin D1 is a mediator of gastrointestinal stromal tumor KIT-independence. Oncogene. 2019;38:6615–29.
16. Tu Y, Zuo R, Ni N, Eilers G, Wu D, Pei Y, et al. Activated tyrosine kinases in gastrointestinal stromal tumor with loss of KIT oncoprotein expression. Cell Cycle Georget Tex. 2018;17:2577–92.
17. Guérin A, Martire D, Trenquier E, Lesluyes T, Sagnol S, Pratlong M, et al. LIX1 regulates YAP activity and controls gastrointestinal cancer cell plasticity. J Cell Mol Med. 2020;24:9244–54.
18. Ruiz-Demoulin S, Trenquier E, Dekkar S, Deshayes S, Boisguérin P, Serrano C, et al. LIX1 Controls MAPK Signaling Reactivation and Contributes to GIST-T1 Cell Resistance to Imatinib. Int J Mol Sci. 2023;24:7138.
19. Guérin A, Angebault C, Kinet S, Cazevieille C, Rojo M, Fauconnier J, et al. LIX1-mediated changes in mitochondrial metabolism control the fate of digestive mesenchyme-derived cells. Redox Biol. 2022;56:102431.
20. Fu M, Hu Y, Lan T, Guan K-L, Luo T, Luo M. The Hippo signalling pathway and its implications in human health and diseases. Signal Transduct Target Ther. 2022;7:376.
21. Ma S, Meng Z, Chen R, Guan K-L. The Hippo Pathway: Biology and Pathophysiology. Annu Rev Biochem. 2019;88:577–604.
22. Boopathy GTK, Hong W. Role of Hippo Pathway-YAP/TAZ Signaling in Angiogenesis. Front Cell Dev Biol. 2019;7.

23. LeBlanc L, Ramirez N, Kim J. Context-dependent roles of YAP/TAZ in stem cell fates and cancer. Cell Mol Life Sci CMLS. 2021;78:4201–19.
24. Messina B, Lo Sardo F, Scalera S, Memeo L, Colarossi C, Mare M, et al. Hippo pathway dysregulation in gastric cancer: from Helicobacter pylori infection to tumor promotion and progression. Cell Death Dis. 2023;14:1–12.
25. Mouillet-Richard S, Laurent-Puig P. YAP/TAZ Signalling in Colorectal Cancer: Lessons from Consensus Molecular Subtypes. Cancers. 2020;12:3160.
26. Montalto FI, De Amicis F. Cyclin D1 in Cancer: A Molecular Connection for Cell Cycle Control, Adhesion and Invasion in Tumor and Stroma. Cells. 2020;9:2648.
27. Qie S, Diehl JA. Cyclin D1, Cancer Progression and Opportunities in Cancer Treatment. J Mol Med Berl Ger. 2016;94:1313–26.
28. Wu X, Yamashita K, Lou M, Matsumoto C, Zhang W, Baba H, et al. AT101 Suppresses Gastrointestinal Stromal Tumor Growth and Promotes Apoptosis via YAP/TAZ-CCND1 and FBXW7-MCL1 Axes. Ann Surg Oncol. 2025;32:5991–6004.
29. Delvaux M, Hagué P, Craciun L, Wozniak A, Demetter P, Schöffski P, et al. Ferroptosis Induction and YAP Inhibition as New Therapeutic Targets in Gastrointestinal Stromal Tumors (GISTs). Cancers. 2022;14:5050.
30. Vandenberghe P, Delvaux M, Hagué P, Erneux C, Vanderwinden J-M. Potentiation of imatinib by cilostazol in sensitive and resistant gastrointestinal stromal tumor cell lines involves YAP inhibition. Oncotarget. 2019;10:1798–811.
31. Moroishi T, Hansen CG, Guan K-L. The emerging roles of YAP and TAZ in cancer. Nat Rev Cancer. 2015;15:73–9.
32. Driskill JH, Dermawan JK, Antonescu CR, Pan D. YAP, TAZ, and Hippo-Dysregulating Fusion Proteins in Cancer. Annu Rev Cancer Biol. 2024;8:331–50.
33. Wei Y, Hui VLZ, Chen Y, Han R, Han X, Guo Y. YAP/TAZ: Molecular pathway and disease therapy. MedComm. 2023;4:e340.
34. Cunningham R, Hansen CG. The Hippo pathway in cancer: YAP/TAZ and TEAD as therapeutic targets in cancer. Clin Sci Lond Engl 1979. 2022;136:197–222.
35. Luo J, Deng L, Zou H, Guo Y, Tong T, Huang M, et al. New insights into the ambivalent role of YAP/TAZ in human cancers. J Exp Clin Cancer Res CR. 2023;42:130.
36. Piccolo S, Panciera T, Contessotto P, Cordenonsi M. YAP/TAZ as master regulators in cancer: modulation, function and therapeutic approaches. Nat Cancer. 2023;4:9–26.
37. Reggiani F, Gobbi G, Ciarrocchi A, Sancisi V. YAP and TAZ Are Not Identical Twins. Trends Biochem Sci. 2021;46:154–68.
38. Bae JS, Kim SM, Lee H. The Hippo signaling pathway provides novel anti-cancer drug targets. Oncotarget. 2016;8:16084–98.
39. Chen C, Zhou H, Zhang X, Liu Z, Ma X. PRMT1 potentiates chondrosarcoma development through activation of YAP activity. Mol Carcinog. 2019;58:2193–206.
40. Patterson MR, Cogan JA, Cassidy R, Theobald DA, Wang M, Scarth JA, et al. The Hippo pathway transcription factors YAP and TAZ play HPV-type dependent roles in cervical cancer. Nat Commun. 2024;15:5809.
41. Zhang Y-H, Li B, Shen L, Shen Y, Chen X-D. The role and clinical significance of YES-associated protein 1 in human osteosarcoma. Int J Immunopathol Pharmacol. 2013;26:157–67.
42. Konate K, Dussot M, Aldrian G, Vaissière A, Viguier V, Neira IF, et al. Peptide-Based Nanoparticles to Rapidly and Efficiently “Wrap 'n Roll” siRNA into Cells. Bioconjug Chem. 2019;30:592–603.
43. Konate K, Josse E, Tasic M, Redjatti K, Aldrian G, Deshayes S, et al. WRAP-based nanoparticles for siRNA delivery: a SAR study and a comparison with lipid-based transfection reagents. J Nanobiotechnology. 2021;19:236.
44. Konate K, Pezzati I, Redjatti K, Agnel E, Vivès E, Faure S, et al. Multiprotein Silencing Using WRAP-Based Nanoparticles: A Proof of Concept. Bioconjug Chem. 2025;36:1218–33.
45. Boisguérin P, Konate K, Josse E, Vivès E, Deshayes S. Peptide-Based Nanoparticles for Therapeutic Nucleic Acid Delivery. Biomedicines. 2021;9:583.

46. Di Gregorio G, Vallée C, Konate K, Teko-Agbo CA, Hammoum T, Faure-Gautron H, et al. Enhancing WRAP-Based Nanoparticles for Small Interfering Ribonucleic Acid Delivery in pH-Sensitive Environments. ChemMedChem. 2025;e2400885.
47. Ferreiro I, Genevois C, Konate K, Vivès E, Boisguérin P, Deshayes S, et al. In Vivo Follow-Up of Gene Inhibition in Solid Tumors Using Peptide-Based Nanoparticles for siRNA Delivery. Pharmaceutics. 2021;13:749.
48. Konate K, Teko-Agbo CA, Pezzati I, Hammoum T, Deshayes S, Descamps S, et al. WRAP-based nanoparticles for siRNA delivery in zebrafish embryos by simple bath immersion. Mol Ther Methods Clin Dev. 2025;33:101458.
49. García-Valverde A, Rosell J, Serna G, Valverde C, Carles J, Nuciforo P, et al. Preclinical Activity of PI3K Inhibitor Copanlisib in Gastrointestinal Stromal Tumor. Mol Cancer Ther. 2020;19:1289–97.
50. Taguchi T, Sonobe H, Toyonaga S, Yamasaki I, Shuin T, Takano A, et al. Conventional and molecular cytogenetic characterization of a new human cell line, GIST-T1, established from gastrointestinal stromal tumor. Lab Investig J Tech Methods Pathol. 2002;82:663–5.
51. Lux ML, Rubin BP, Biase TL, Chen C-J, Maclure T, Demetri G, et al. KIT Extracellular and Kinase Domain Mutations in Gastrointestinal Stromal Tumors. Am J Pathol. 2000;156:791–5.
52. Garner AP, Gozgit JM, Anjum R, Vodala S, Schrock A, Zhou T, et al. Ponatinib inhibits polyclonal drug-resistant KIT oncoproteins and shows therapeutic potential in heavily pretreated gastrointestinal stromal tumor (GIST) patients. Clin Cancer Res Off J Am Assoc Cancer Res. 2014;20:5745–55.
53. Lagarde P, Pérot G, Kauffmann A, Brulard C, Dapremont V, Hostein I, et al. Mitotic checkpoints and chromosome instability are strong predictors of clinical outcome in gastrointestinal stromal tumors. Clin Cancer Res Off J Am Assoc Cancer Res. 2012;18:826–38.
54. McKey J, Martire D, de Santa Barbara P, Faure S. LIX1 regulates YAP1 activity and controls the proliferation and differentiation of stomach mesenchymal progenitors. BMC Biol. 2016;14:34.
55. Tiffon C, Giraud J, Molina-Castro SE, Peru S, Seeneevassen L, Sifré E, et al. TAZ Controls Helicobacter pylori-Induced Epithelial-Mesenchymal Transition and Cancer Stem Cell-Like Invasive and Tumorigenic Properties. Cells. 2020;9:1462.
56. Burkhardt F, Spies BC, Wesemann C, Schirmeister CG, Licht EH, Beuer F, et al. Cytotoxicity of polymers intended for the extrusion-based additive manufacturing of surgical guides. Sci Rep. 2022;12:7391.
57. Pavel M, Renna M, Park SJ, Menzies FM, Ricketts T, Füllgrabe J, et al. Contact inhibition controls cell survival and proliferation via YAP/TAZ-autophagy axis. Nat Commun. 2018;9:2961.
58. Zhang Q, Han X, Chen J, Xie X, Xu J, Zhao Y, et al. Yes-associated protein (YAP) and transcriptional coactivator with PDZ-binding motif (TAZ) mediate cell density–dependent proinflammatory responses. J Biol Chem. 2018;293:18071–85.
59. Ghaboura N. Unraveling the Hippo pathway: YAP/TAZ as central players in cancer metastasis and drug resistance. EXCLI J. 2025;24:612–37.
60. Zanconato F, Cordenonsi M, Piccolo S. YAP/TAZ at the Roots of Cancer. Cancer Cell. 2016;29:783–803.
61. Mao X, Yang X, Chen X, Yu S, Yu S, Zhang B, et al. Single-cell transcriptome analysis revealed the heterogeneity and microenvironment of gastrointestinal stromal tumors. Cancer Sci. 2021;112:1262–74.
62. Li S, Hao L, Li N, Hu X, Yan H, Dai E, et al. Targeting the Hippo/YAP1 signaling pathway in hepatocellular carcinoma: From mechanisms to therapeutic drugs (Review). Int J Oncol. 2024;65:1–17.
63. Pei T, Li Y, Wang J, Wang H, Liang Y, Shi H, et al. YAP is a critical oncogene in human cholangiocarcinoma. Oncotarget. 2015;6:17206–20.
64. Shreberk-Shaked M, Dassa B, Sinha S, Di Agostino S, Azuri I, Mukherjee S, et al. A Division of Labor between YAP and TAZ in Non-Small Cell Lung Cancer. Cancer Res. 2020;80:4145–57.

65. Díaz-Martín J, López-García MÁ, Romero-Pérez L, Atienza-Amores MR, Pecero ML, Castilla MÁ, et al. Nuclear TAZ expression associates with the triple-negative phenotype in breast cancer. Endocr Relat Cancer. 2015;22:443–54.
66. Basu-Roy U, Han E, Rattanakorn K, Gadi A, Verma N, Maurizi G, et al. PPARγ agonists promote differentiation of cancer stem cells by restraining YAP transcriptional activity. Oncotarget. 2016;7:60954–70.
67. Hebron KE, Perkins OL, Kim A, Jian X, Girald-Berlingeri SA, Lei H, et al. ASAP1 and ARF1 Regulate Myogenic Differentiation in Rhabdomyosarcoma by Modulating TAZ Activity. Mol Cancer Res. 2025;23:95–106.
68. Edwards AC, Stalnecker CA, Jean Morales A, Taylor KE, Klomp JE, Klomp JA, et al. TEAD Inhibition Overcomes YAP1/TAZ-Driven Primary and Acquired Resistance to KRASG12C Inhibitors. Cancer Res. 2023;83:4112–29.
69. Kim H, Son S, Ko Y, Lee JE, Kim S, Shin I. YAP, CTGF and Cyr61 are overexpressed in tamoxifen-resistant breast cancer and induce transcriptional repression of ERα. J Cell Sci. 2021;134:jcs256503.
70. Kim MH, Kim J, Hong H, Lee S, Lee J, Jung E, et al. Actin remodeling confers BRAF inhibitor resistance to melanoma cells through YAP/TAZ activation. EMBO J. 2016;35:462–78.
71. Knapp CM, He J, Lister J, Whitehead KA. Lipid nanoparticle siRNA cocktails for the treatment of mantle cell lymphoma. Bioeng Transl Med. 2018;3:138–47.
72. Wang L, Chen Y, Zhang M, Liu J, Li H, Liu M, et al. Chemical dissection of selective myeloid leukemia-1 inhibitors: How they were found and evolved. Eur J Med Chem. 2025;283:117168.
73. Faria R, Vivès E, Boisguérin P, Descamps S, Sousa Â, Costa D. Upgrading Mitochondria-Targeting Peptide-Based Nanocomplexes for Zebrafish In Vivo Compatibility Assays. Pharmaceutics. 2024;16:961.
74. Joensuu H, Miyashita H, George S, Sicklick J. Navigating Ongoing Challenges in GI Stromal Tumors. Am Soc Clin Oncol Educ Book Am Soc Clin Oncol Annu Meet. 2025;45:e473224.
75. Tang Q, Khvorova A. RNAi-based drug design: considerations and future directions. Nat Rev Drug Discov. 2024;23:341–64.

CHAPTER 2

SUPPORTING INFORMATION

Supporting Tables

Table S1: Used siRNA sequences

ID	Sense sequence	Anti-sense sequence	Reference
siYAP1	5’-CUA-UGU-UCA-UUC-CAU-CUC-CdTdT-3’	5’-GGA-GAU-GGA-AUG-AAC-AUA-GdTdT-3’	This work
siYAP1’	5’-AUA-GUA-AAU-UUC-UCC-AUC-CdTdT-3’	5’-GGA-UGG-AGA-AAU-UUA-CUA-UdTdT-3’	This work
siTAZ	5’-AAA-UCA-GGG-AAA-CGG-GUC-UdTdT-3’	5’-AGA-CCC-GUU-UCC-CUG-AUU-UdTdT-3’	This work
siTAZ’	5’-AUU-AUU-AGU-GAU-GGA-UCU-CdTdT-3’	5’-GAG-AUC-CAU-CAC-UAA-UAA-UdTdT-3’	This work
si(YAPTAZ)	5’-UGU-GGA-UGA-GAU-GGA-UAC-AdTdT-3’	5’-UGU-AUC-CAU-CUC-AUC-CAC-AdTdT-3’	(Tiffon et al., 2020)
siCYR61	5’-AUC-AUC-AUG-ACG-UUC-UUG-GdTdT-3’	5’-CCA-AGA-ACG-UCA-UGA-UGA-UdTdT-3’	This work
siCYR61’	5’-UGG-AGU-UGA-CGA-GAA-ACA-AdTdT-3’	5’-UUG-UUU-CUC-GUC-AAC-UCC-AdTdT-3’	This work
siCTGF	5'-AAU-UUA-GCU-CGG-UAU-GUC-UdTdT-3'	5'-AGA-CAU-ACC-GAG-CUA-AAU-UdTdT-3'	This work
siCTGF’	5’-AUU-UUG-GGA-GUA-CGG-AUG-CpTpT-3’	5’-GCA-UCC-GUA-CUC-CCA-AAA-UpTpT-3’	This work
siNEG	Confidential	Confidential	Negative Control siRNA, Eurogentec, Réf. SR-CL000-005

Table S2: List of antibodies

Target (Protein)	MW (kDa)	Host Species	Clone / Catalog Number	Dilution	Company / Supplier	Application	RRID
YAP1	65 - 78	Rabbit	D8H1X / #14074	1:1,000 (GIST-T1) 1:5,000 (GIST-882) 1:10,000 (GIST-430)	Cell Signaling	WB	AB_2650491
YAP1	65-70	Mouse	66900-1	1:800	Proteintech	If	AB_2882229
TAZ	55	Rabbit	E9J5A / #72804	1:1,000 (GIST-T1 and GIST-882) 1:5,000 (GIST-430) 1:500 (If)	Cell Signaling	WB, If	AB_2904134
KIT (CD117)	145	Rabbit	#DB062	1:1,000	DB Biotech	WB	AB_2315699
Phospho-KIT (pKIT)	145	Rabbit	Tyr703 D12E12 / #3073	1:1,000	Cell Signaling	WB	AB_1147635
AKT	60	Rabbit	#9272	1:1,000	Cell Signaling	WB	AB_329827
Phospho-AKT (pAKT)	60	Rabbit	Ser473 D9E / #4060	1:1,000	Cell Signaling	WB	AB_2315049
p44/42 MAPK (Erk1/2)	42, 44	Mouse	L34F12 / #4696	1:1,000	Cell Signaling	WB	AB_390780
Phospho-p44/42 MAPK (Erk1/2)	42, 44	Rabbit	Thr202/Tyr204 20G11 / #4376	1:1,000	Cell Signaling	WB	AB_331772
CYR61	41	Rabbit	D4H5D / #14479	1:1,000	Cell Signaling	WB	AB_2798492
CTGF	35	Rabbit	D8Z8U / #86641	1:1,000	Cell Signaling	WB	AB_2800085
CD1	34	Rabbit	SP4 / #MA5-16356	1:1,000	ThermoFisher Scientific	WB	AB_2537875
VINCULIN	124	Rabbit	E1E9V / #13901	1:1,000	Cell Signaling	WB	AB_2728768
α-ACTININ	100	Rabbit	D6F6 / #6487	1:1,000	Cell Signaling	WB	AB_11179206

β-ACTIN	42	Mouse	#A5441	1:10,000	Sigma-Aldrich	WB	AB_476744
Anti-Rabbit	/	IgG, HRP	#7074	1:1,000	Cell Signaling	WB	AB_2099233
Anti-Mouse	/	IgG, HRP	#7076	1:10,000 (β-Actin) 1:1,000 (others)	Cell Signaling	WB	AB_330924
Anti-Rabbit Alexa Fluor™ 488	/	Donkey	#A31570	1:1,000	Invitrogen	If	/
Anti-Mouse Alexa Fluor™ 555	/	Donkey	#A21206	1:1,000	Invitrogen	If	/

Footnotes: WB: Western Blot / If: Immunofluorescence.

Table S3: Human gene-specific primers used for RT-qPCR.

Target	Forward primer (5'-3')	Reverse primer (5'-3')	Amplicon (bp)	Reference
YAP1	CACAGCATGTTCGAGCTCAT	GATGCTGAGCTGTGGGTGTA	120	(Molina-Castro et al., 2020)
TAZ	TGCCGTCAGTTCCACAC	GTTCTGCTGGCTCAGGGT	115	This work
CYR61	GGAGCCTCGCATCCTAT	ATTGGTAACTCGTGTGGAGA	115	(Guérin et al., 2020)
CTGF	TTCAAGTGCCCTGACGG	GCGATTCAAAGATGTCATTGTCTC	117	This work
HPRT1	TGGTCAGGCAGTATAATCCA	GGTCCTTTTCACCAGCAAGCT	59	(Molina-Castro et al., 2020)

REFERENCES

1. Guérin, A., Martire, D., Trenquier, E., Lesluyes, T., Sagnol, S., Pratlong, M., Lefebvre, E., Chibon, F., de Santa Barbara, P., & Faure, S. (2020). LIX1 regulates YAP activity and controls gastrointestinal cancer cell plasticity. Journal of Cellular and Molecular Medicine, 24(16), 9244-9254. https://doi.org/10.1111/jcmm.15569
2. Molina-Castro, S. E., Tiffon, C., Giraud, J., Boeuf, H., Sifre, E., Giese, A., Belleannée, G., Lehours, P., Bessède, E., Mégraud, F., Dubus, P., Staedel, C., & Varon, C. (2020). The Hippo Kinase LATS2 Controls Helicobacter pylori-Induced Epithelial-Mesenchymal Transition and Intestinal Metaplasia in Gastric Mucosa. Cellular and Molecular Gastroenterology and Hepatology, 9(2), 257-276. https://doi.org/10.1016/j.jcmgh.2019.10.007
3. Tiffon, C., Giraud, J., Molina-Castro, S. E., Peru, S., Seeneevassen, L., Sifré, E., Staedel, C., Bessède, E., Dubus, P., Mégraud, F., Lehours, P., Martin, O. C. B., & Varon, C. (2020). TAZ Controls Helicobacter pylori-Induced Epithelial-Mesenchymal Transition and Cancer Stem Cell Like Invasive and Tumorigenic Properties. Cells, 9(6), 1462. https://doi.org/10.3390/cells9061462

Supporting Figures

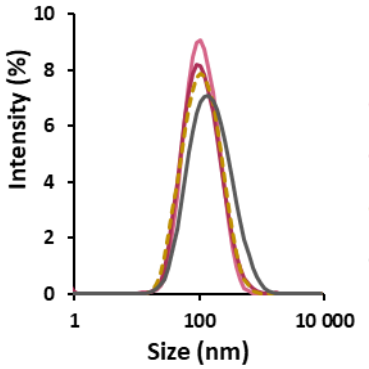

Size (nm)	PdI
92.7 ± 2.1	0.29 ± 0.06
92.8 ± 11.9	0.30 ± 0.04
89.3 ± 8.9	0.29 ± 0.02
121.9 ± 7.3	0.36 ± 0.01

Figure S1: Characterization of WRAP5:siRNA nanoparticles by dynamic light scattering (DLS).
Mean size distribution of WRAP5:siRNA nanoparticles (W5 = 10 µM, MR = 20)
DLS measurements were performed on all nanoparticles, with three individual experiments (N = 3) and three runs per condition.

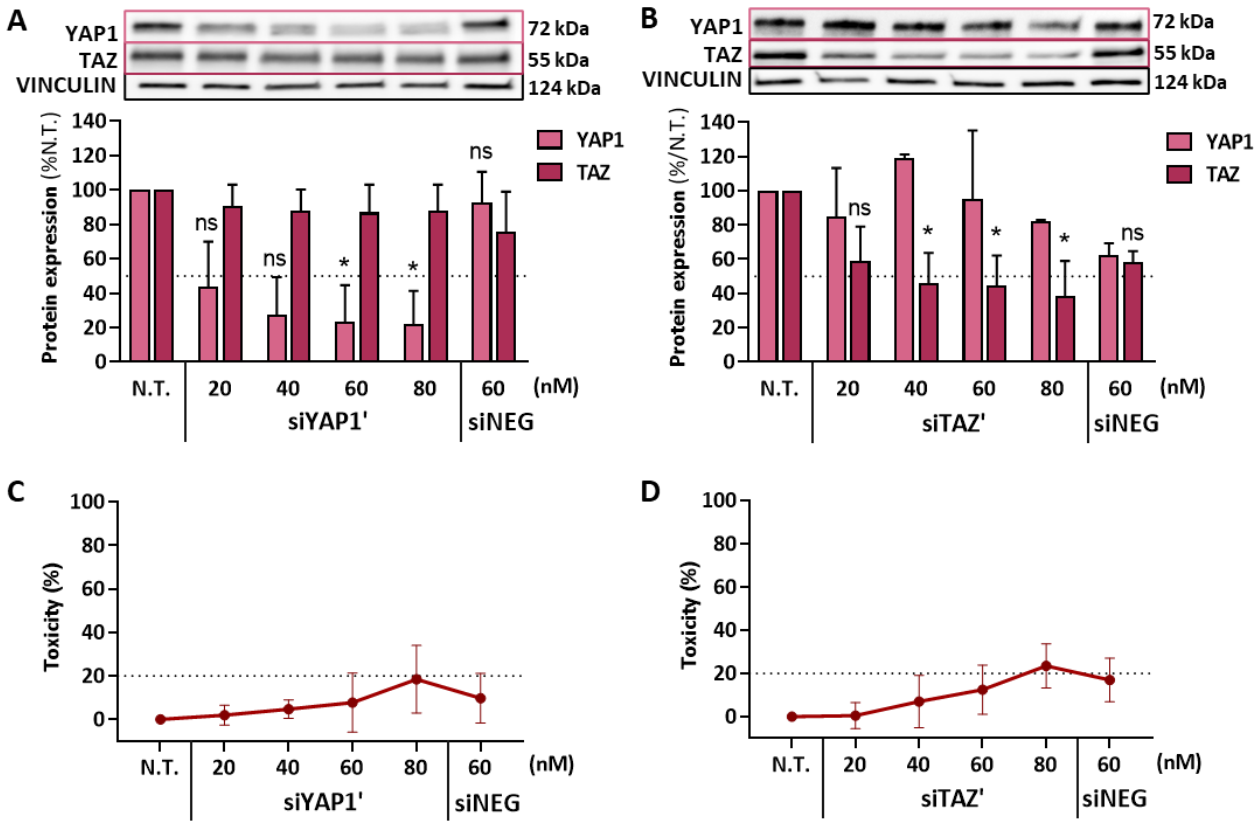

Figure S2: Evaluation of YAP1 or TAZ silencing in GIST-T1 cells with WRAP5:siRNA' nanoparticles
WRAP5:siRNA nanoparticles delivering siYAP1' (**A**) or siTAZ' (**B**) induced a dose-dependent inhibition of YAP1 or TAZ in GIST-T1 cells after 48 h of incubation, as shown by Western blot quantification. A slight toxicity was observed respectively for siYAP1' (**C**) and siTAZ' (**D**) at 80 nM and above, as assessed by LDH assay.
Controls include untreated (N.T.) and siNEG-treated cells. Data are presented as mean ± SD from N=4 independent experiments. Statistical analysis was performed using Kruskal-Wallis followed by Dunn's multiple comparisons test *versus* N.T. (**A**, **B**); ns >0.05, * <0.05. Analysis of TAZ expression following siYAP1 treatment and YAP1 expression following siTAZ treatment showed no significant differences compared to N.T. (data not annotated on the graph for clarity).

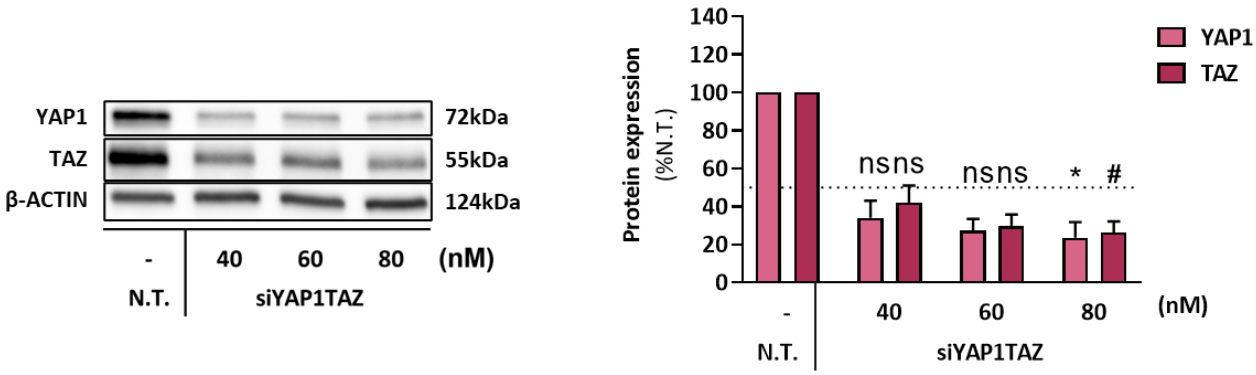

Figure S3: Silencing YAP1 and TAZ protein expression using a single siRNA in GIST-T1 cells
WRAP5-based nanoparticles encapsulating a single siRNA (siYAP1TAZ) published by Tiffon et al., 2020 induced a dose-dependent inhibition of YAP1 and TAZ simultaneously in GIST-T1 cells after 48 h of incubation, as shown by Western blot quantification.
Values are the mean ± SD for N=3 independent experiments. Statistical test: Kruskal-Wallis followed by Dunn with ns >0.05 and * or # <0.05 comparisons test *versus* siNEG.

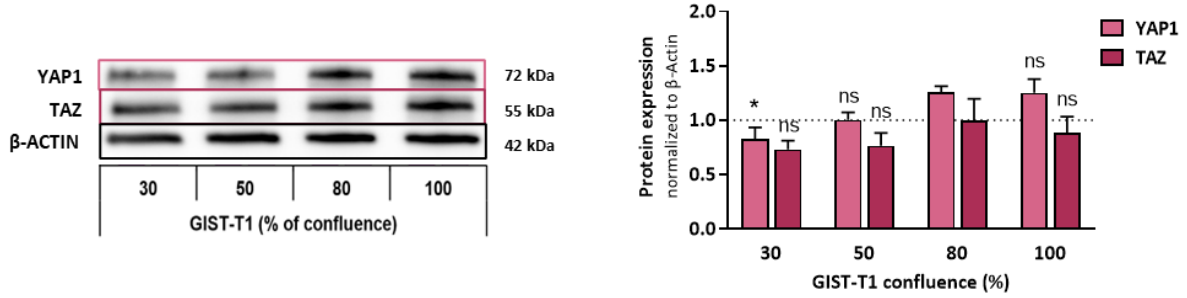

Figure S4 : YAP1 and TAZ protein expression in GIST-T1 cells
Western blot analysis and quantification of YAP1 and TAZ protein expression in GIST-T1 cells according to cell confluence. Values are the mean ± SEM for N=4 independent experiments. Statistical test: Kruskal-Wallis followed by Dunn with ns >0.05 and * <0.05 for YAP1 or TAZ expression at different confluences *versus* 80% confluence.

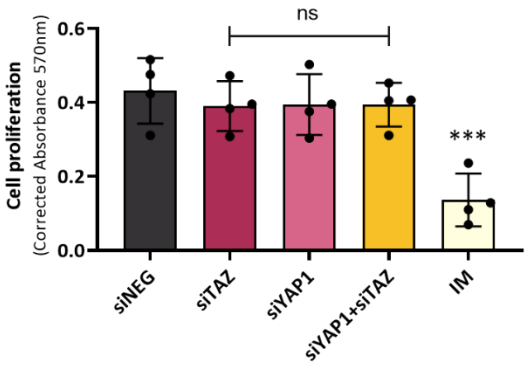

Figure S5: Cell proliferation remains unaffected at 48 h post siRNA transfection
Proliferation of GIST-T1 cells was assessed 48 h after transfection using the CellTiter 96® Non-Radioactive Cell Proliferation Assay for N=4 independent experiments with n=5 replicates each.
siNEG was used as a control. Abbreviation: IM = Imatinib. Data are presented as mean ± SD. Statistical analysis was performed using one-way ANOVA followed by Dunnett's multiple comparisons test *versus* siNEG; ns > 0.05, *** < 0.001.

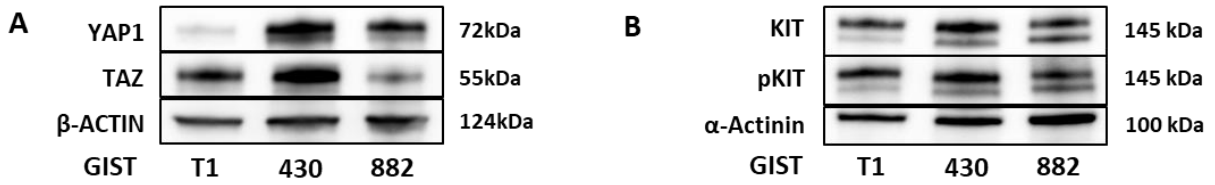

Figure S6: Basal expression of YAP1, TAZ, KIT, pKIT in GIST cell lines.
Comparison of the basal protein expression levels of YAP1 and TAZ (**A**) as well as KIT and phosphorylated KIT (pKIT) (**B**) in GIST-T1, GIST-430, and GIST-882 cell lines, as assessed by Western blot.

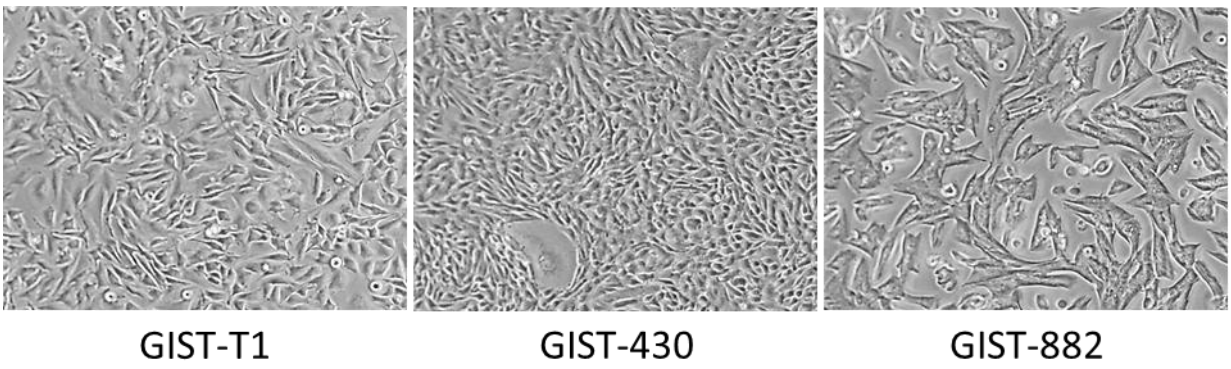

Figure S7: Morphology of three different GIST cell lines
GIST-T1, GIST-430, GIST-882 images taken using the EVOS® LX Core microscope system with an 10x objective (#AMEX1000, Thermo Fisher Scientific).

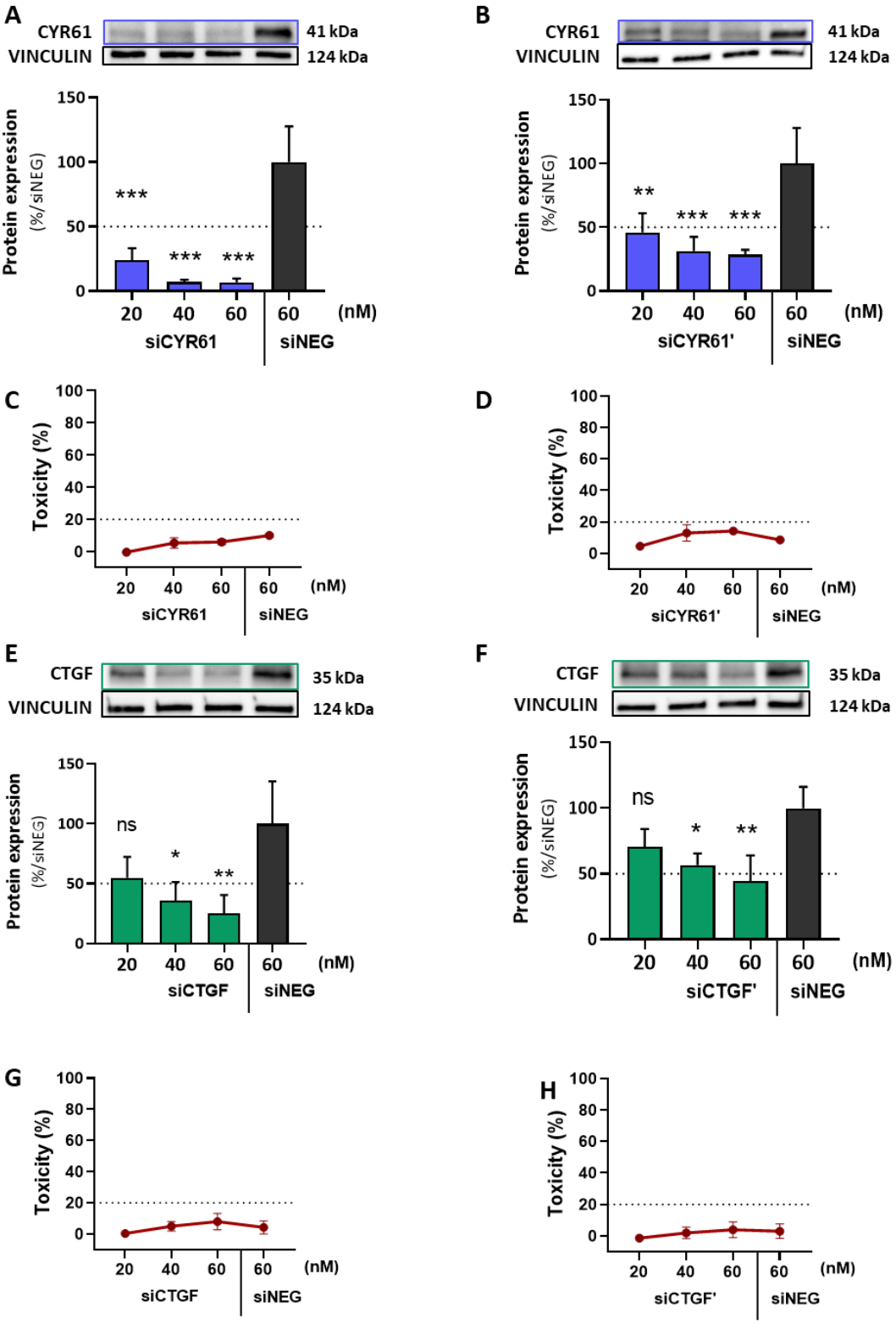

Figure S8: Evaluation of CYR61 or CTGF silencing in GIST-T1 cells with WRAP5:siRNA nanoparticles

WRAP5:siRNA nanoparticles delivering siCYR61 and siCYR61' (**A,B**) or siCTGF and siCTGF' (**E,F**) induced a dose-dependent inhibition of CYR61 or CTGF in GIST-T1 cells after 48 h of incubation, as shown by Western blot quantification. No toxicity was observed respectively for siCYR61 and siCYR61' (**C,D**) and siCTGF and siCTGF' (**G,H**), as assessed by LDH assay.

Controls include untreated (N.T.) and siNEG-treated cells. Data are presented as mean ± SD from N=4 independent experiments. Statistical analysis was performed using Kruskal-Wallis followed by Dunn's multiple comparisons test *versus* siNEG. (**A**, **B**); ns >0.05, * <0.05, ** <0.01, *** <0.001.

RESULTS

Chapter 1: Multi-siRNA delivery using WRAP5-based nanoparticles in GIST cells

Chapter 2: Studying individual roles of YAP1 and TAZ in GIST tumor biology

Chapter 3: YAP1 and TAZ: playing around with IM resistance?

CHAPTER 3: YAP1 and TAZ: playing around with IM resistance?

1. Aim of the study

The standard first-line therapy for GIST patients remains IM, a selective inhibitor of KIT and PDGFRA tyrosine kinases (César Serrano et al. 2023). The introduction of this treatment has significantly changed the natural progression of the disease, especially in cases of advanced and metastatic GIST (Demetri et al. 2002). Nevertheless, complete remission in these cases is rarely achieved, and long-term disease control is limited. Most patients eventually experience GIST progression after 20 to 24 months of continuous IM treatment (Kelly et al. 2021). This relapse is primarily driven by the emergence of resistant subclones harboring heterogeneous secondary mutations in the *KIT* gene (Serrano 2021; Serrano et al. 2019). Subsequent lines of treatment, including SU, RE, and more recently, RI, offer only modest clinical benefit, with progression-free survival levels below 6 months and objective response rates of less than 10% (Schaefer et al. 2022). A significant constraint imposed by these therapeutic small molecules lies in their shared mechanism of action (refer to Section 2.1 of the Introduction). It has been demonstrated that these agents inhibit RTK activity; however, they are ineffective in addressing the emergence of additional mutations or the broader cellular adaptations that occur during long-term TKI exposure (Blay et al. 2021). As a result, these treatments frequently fail to address the inherent complexity and adaptability of GIST resistance mechanisms to IM (Schaefer et al. 2022).

Deciphering the molecular processes driving GIST progression and therapy failure remains a key priority for the development of more effective and durable next-generation treatment strategies. Mechanisms of resistance extend beyond KIT reactivation and involve complex cellular adaptations and compensatory signaling networks (Serrano and George 2020). In this context, growing attention has been paid to non-canonical pathways that may promote tumor cell survival under therapeutic pressure (Zhou et al. 2024). Among these, the Hippo pathway effectors YAP1 and TAZ have been the subject of notable research (Franklin et al. 2023). These paralogous proteins have been identified as key regulators of mechanotransduction and cellular plasticity. They function as transcription co-activators, playing an important role in various biological processes (refer to Section 3 in the Introduction). Their implication in the progression and metastasis of a wide range of solid tumors underscores their potential as

therapeutic targets (Fu et al. 2022; Piccolo et al. 2014). Moreover, both proteins have emerged as possible modulators of resistance mechanisms in various cancers, including those driven by oncogenic kinases (Guo et al. 2022; Piccolo et al. 2023; Zanconato et al. 2016).

Within GIST, however, their functional roles remain incompletely characterized. As stated in Chapter 2, novel insights were provided into TAZ activity in *KIT*-dependent IM-sensitive cell lines. In particular, we identified a significant role for TAZ, whose activity appeared to support cell proliferation and migration, while the impact of YAP1 seemed to have less pronounced, or even undetectable effects. TAZ was shown to regulate the expression of pro-oncogenic transcriptional targets, including *CYR61* and *CTGF*. Among them, *CYR61* was identified as the main regulator of GIST cell proliferation.

However, the precise behavior of YAP1 and TAZ in the context of acquired resistance remains to be fully elucidated. Some evidence already suggests their involvement: Ruiz-Demoulin and colleagues reported an early increase in YAP1 and TAZ expression upon IM exposure in GIST-T1 cells (at 48h) (Ruiz-Demoulin et al. 2023), while Wu and colleagues showed that both proteins are overexpressed in a long-term IM-treated derived GIST-T1 cell line that has developed resistance (Wu, Yamashita, Lou, et al. 2025). Nevertheless, it is still unclear whether YAP1 and TAZ retain distinct biological functions in this context, or whether a functional shift occurs that may allow YAP1 to assume a more dominant role. Given the potent interplay between the two proteins, it is imperative to analyze their behavior in an IM-resistant GIST context.

Considering these unresolved questions, we initiated some preliminary experiments, which were conducted during the final period of my thesis. This work was designed to address two main objectives.

First, we sought to characterize the expression and cellular distribution of YAP1 and TAZ across a panel of IM-resistant GIST cell lines, in order to better understand their involvement in resistance mechanisms. In parallel, their phosphorylation state and the expression of KIT and phospho-KIT were also analyzed. After comparing the expression profile of these different proteins between sensitive and resistant cell lines, we then evaluated YAP1 and/or TAZ silencing in IM-resistant cells using the WRAP:siRNA nanoparticles.

Second, based on our previous observations of TAZ activity in IM-sensitive cells, we hypothesized that inhibiting its expression could improve the therapeutic efficacy of IM. We therefore evaluated the levels of YAP1 and TAZ in GIST-T1 cells through IM treatment. Then, we assessed whether TAZ silencing could decrease the IC_{50} value of IM in GIST-T1 cells, allowing us to reduce the IM dose without compromising efficacy. Such an approach, if validated, could not only allow lower drug concentrations without compromising therapeutic efficacy but also delay the emergence of resistance by decreasing the selective pressure exerted on tumor cells.

In conclusion, these experiments will provide new insights into the contribution of Hippo pathway dysregulation to GIST resistance and explore the potential of YAP1 and TAZ as therapeutic targets in both IM-sensitive and IM-resistant GIST.

2. Preliminary results

2.1. YAP1 and TAZ heterogeneity in IM-sensitive and IM-resistant GIST cell lines

To assess whether IM resistance is associated with alterations in the Hippo signaling pathway, we first evaluated the expression levels of YAP1 and TAZ in a panel of six GIST cell lines available in the laboratory. These include three IM-sensitive and *KIT*-dependent lines: GIST-T1, GIST-430, and GIST-882. These cell lines harbor a primary activating mutation in the *KIT* gene, thereby mimicking the molecular profile of untreated GIST tumors. GIST-T1/670 and GIST-430/654 are IM-resistant and *KIT*-dependent cell lines obtained after long-term IM exposure of cultured GIST-T1 and GIST-430, respectively. These lines carry both primary and secondary *KIT* mutations, which mimic acquired resistance mechanisms observed clinically. Finally, GIST-48B is an IM-resistant, *KIT*-independent line, which lacks *KIT* expression and thus represents a model of alternative oncogenic escape. The mutational status and origin of each cell line are detailed in the Materials and Methods section ("Used cell lines and culture conditions") and in the Introduction, with a summary provided in **Table 1**.

Table 1: GIST cell lines used in this study.

.Cell lines	*KIT* mutations
IM-sensitive *KIT*-mutant	
GIST-T1	Exon 11: V560-Y578del
GIST-882	Exon 13: K642E
GIST-430	Exon 11: V560-L576del
IM-resistant *KIT*-mutant	
GIST-T1/670	Exon 11 + Exon 14: T670I
GIST-430/654	Exon 11 + Exon 13: V564A
***KIT*-independent GIST**	
GIST48B	None

Footnote: Adapted from Zhou et al., 2024; Serrano et al., 2019

Western blot analysis of total YAP1 and TAZ protein levels revealed clear differences across the cell lines. YAP1 (**Figure 1A**) and TAZ (**Figure 1C**), respectively, appeared to be more strongly expressed in the two *KIT*-dependent IM-resistant lines (GIST-T1/670 and GIST-430/654) compared to their respective IM-sensitive cell lines (GIST-T1 and GIST-430). The variations were most noticeable in high-contrast images for the GIST-T1 and GIST-T1/670 lines and less pronounced between GIST-430 and GIST-430/654 (**Figures 1A', 1C'**). These results suggest a potential upregulation of YAP1 and TAZ in the context of acquired resistance to KIT inhibition, which depends on the type of secondary mutation.

Surprisingly, both YAP1 (**Figures 1A, 1A'**) and TAZ (**Figures 1C, 1C'**) were also expressed in the *KIT*-independent line GIST-48B. In this experimental condition, the YAP1 level was found to be noticeably higher than that of TAZ, suggesting no immediate evidence for a functional divergence between the two proteins in this context. However, this finding suggests the persistence of Hippo pathway effectors in the absence of KIT signaling.

As we had the IM-sensitive GIST-882 cell lines also in culture, we evaluated YAP1 and TAZ expression levels. YAP1 was clearly more expressed than TAZ in GIST 882 compared to the others (**Figures 1A, 1C**).

To gain insight into the activation status of YAP1 (**Figures 1A, 1A'**) and TAZ (**Figures 1C, 1C'**), we examined the respective phosphorylated forms of these proteins. Since phosphorylation typically leads to cytoplasmic sequestration and inactivation (Meng et al. 2016), the presence or absence of pYAP1 and pTAZ is indicative of Hippo pathway activity.

Remarkably, GIST-T1 and GIST-T1/670 exhibited very low levels of pYAP1 (**Figures 1A, 1A'**) and pTAZ (**Figures 1C, 1C'**), confirmed by calculating pYAP1/YAP1 and pTAZ/TAZ ratios, which were well below 1 (**Figures 1B, 1D**). For quantification, the intensity of the blots has no influence. These results suggest that most of the YAP1 and TAZ pools are in an active, dephosphorylated state, likely localized to the nucleus.

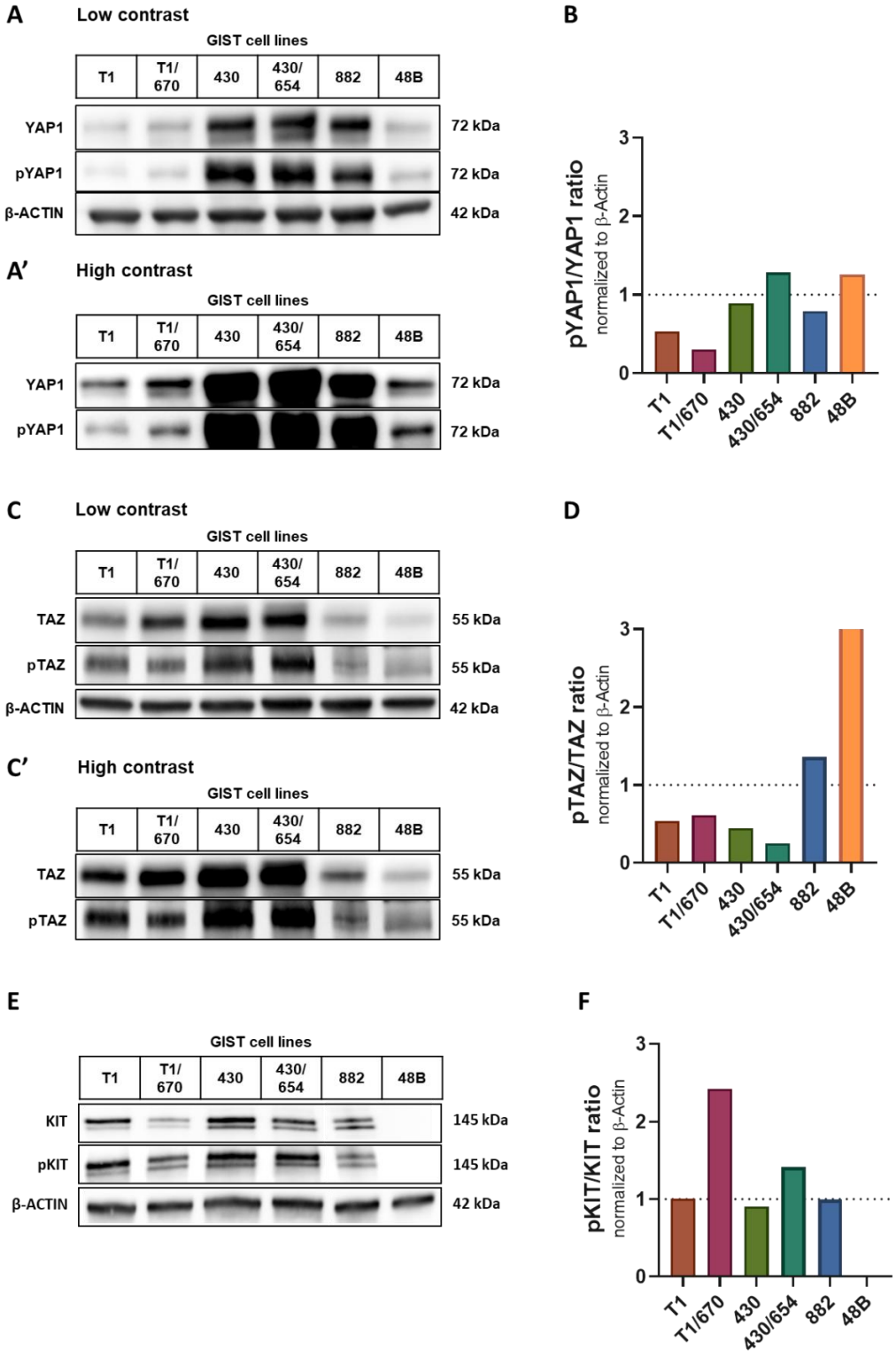

Figure 1: Analysis of protein expression in different GIST cell lines.

Western blot analysis of YAP1 and pYAP1, TAZ and pTAZ expressions with low (**A** or **C**) and high (**A'** or **C'**) contrast in six different GIST cell lines, and the respective phosphorylated form/non-phosphorylated form ratio (**B** or **D**). Western blot analysis of KIT and pKIT expression (**E**) and its relative pKIT/KIT ratio (**F**). Three cell lines are IM-sensitive: GIST-T1, -430, and -882. Three others are IM-resistant: GIST-T1/670, -430/654 and -48B (also *KIT*-independent). β-Actin was used as a loading control. Variations in band intensity reflect differential protein expression among the GIST cell lines, possibly related to mutational background or drug response profiles.

GIST-430 and GIST-430/654 showed both higher and comparable levels of pYAP1 than those observed in GIST-T1 and GIST-T1/670 cell lines (**Figures 1A, 1A'**). However, the pYAP1/YAP1 ratio indicated a more balanced distribution between active and inactive pools (ratio ~ 1) (**Figure 1B**). Concerning the pTAZ/TAZ ratio in GIST-430 and GIST-430/654, the non-phosphorylated form predominated (ratio < 1), suggesting an important TAZ activity (**Figure 1D**).

GIST-882 also displayed phosphorylated YAP1 and TAZ (**Figures 1A, 1C**). The ratios pYAP1/YAP1 and pTAZ/TAZ seemed to be fairly balanced between the two forms (ratio ~1) (**Figures 1B, 1D**).

Finally, for GIST-48B, the ratio pYAP1/YAP1 indicated a good balance between the two forms (ratio ~ 1) (**Figures 1A, 1B**). Surprisingly, pTAZ seemed to predominate (pTAZ/TAZ>1), suggesting a reduced activity for TAZ (**Figure 1D**).

All these data indicate that, depending on the lineage, and notably on the secondary *KIT* mutations for IM-resistant GIST cell lines, the pools of phosphorylated and non-phosphorylated forms of YAP1 and TAZ proteins may vary, thus leaning toward greater activation or non-activation of the Hippo pathway. IM resistance, particularly in the GIST-T1/670 background, is associated not only with increased expression but also with decreased phosphorylation of YAP1 and TAZ, reinforcing the idea of persistent activation of both co-regulators in resistant status.

Additionally, we evaluated total KIT and phospho-KIT expression (**Figure 1E**). These experiments were performed using the same whole cell lysates without any prior treatment as used before for YAP1/TAZ and pYAP1/pTAZ quantifications, thus reflecting the baseline oncogenic state of KIT signaling in each cell line. As expected, KIT was absent in GIST-48B, confirming its *KIT*-independent status. KIT and pKIT levels were generally well-balanced within each line and did not exhibit marked differences between IM-sensitive and -resistant contexts,

except for GIST-T1/670. Indeed, calculated pKIT/KIT ratio indicated a predominance for pKIT (ratio>1) (**Figure 1F**). This result could indicate that for the secondary *KIT* mutation in Exon 14, there is an overexpression of KIT activation. Excluding that, each cell line displayed its expected KIT protein activation profile, confirming the validity of the model system.

These data confirm the interest of understanding the role of YAP1 and TAZ in IM-resistant GIST lines, also due to their high expression heterogeneity.

2.2. YAP1 and TAZ silencing in GIST-T1/670 and GIST-430/654 using WRAP5:siRNA nanoparticles

To validate YAP1 and/or TAZ silencing in IM-resistant GIST models using the WRAP5:siRNA nanoparticle-based delivery system, we applied the same experimental setup as described as used for the IM-sensitive GIST cells (see Chapter 2).

First, cell density and culture conditions for GIST-T1/670 and GIST-430/654 cell lines were optimized, as these cells have a different morphology (**Figure 2**) and proliferation rates.

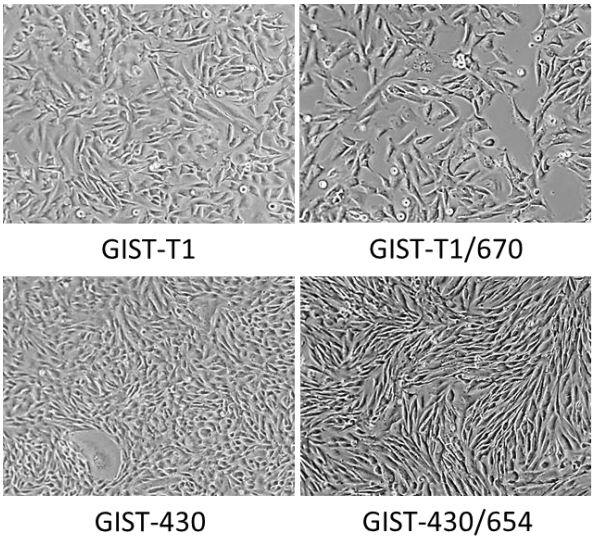

Figure 2: Representative images of GIST cell lines
GIST-T1, GIST-T1/670, GIST-430, and GIST-430/654, images taken using the EVOS™ LX Core microscope system, 10x (Thermo Fisher Scientific).

Given the stronger functional implication of TAZ in GIST-T1 migration and proliferation (see Chapter 2), we focused subsequent experiments on its selective inhibition. A dose-response assay was performed using WRAP5:siTAZ nanoparticles at final siRNA concentrations ranging from 40 to 80 nM, with the classic fixed WRAP5-to-siRNA charge ratio (R = 20). Western blot

analyses revealed a clear reduction of TAZ protein levels at 40 nM, with no consistent additional knockdown observed from 60 to 80 nM. Indeed, at the lowest siTAZ concentration used, TAZ inhibition reached approximately 70% in GIST-T1/670 and 50% in GIST-430/654, relative to siNEG control. Importantly, in line with the results presented in Chapter 2, no effect on YAP1 protein expression was observed (**Figures 3A, 3B**). These results, although based on only two independent replicates, support the functional delivery of siTAZ in IM-resistant cells and justify further phenotypic assessments in the context of GIST IM resistance.

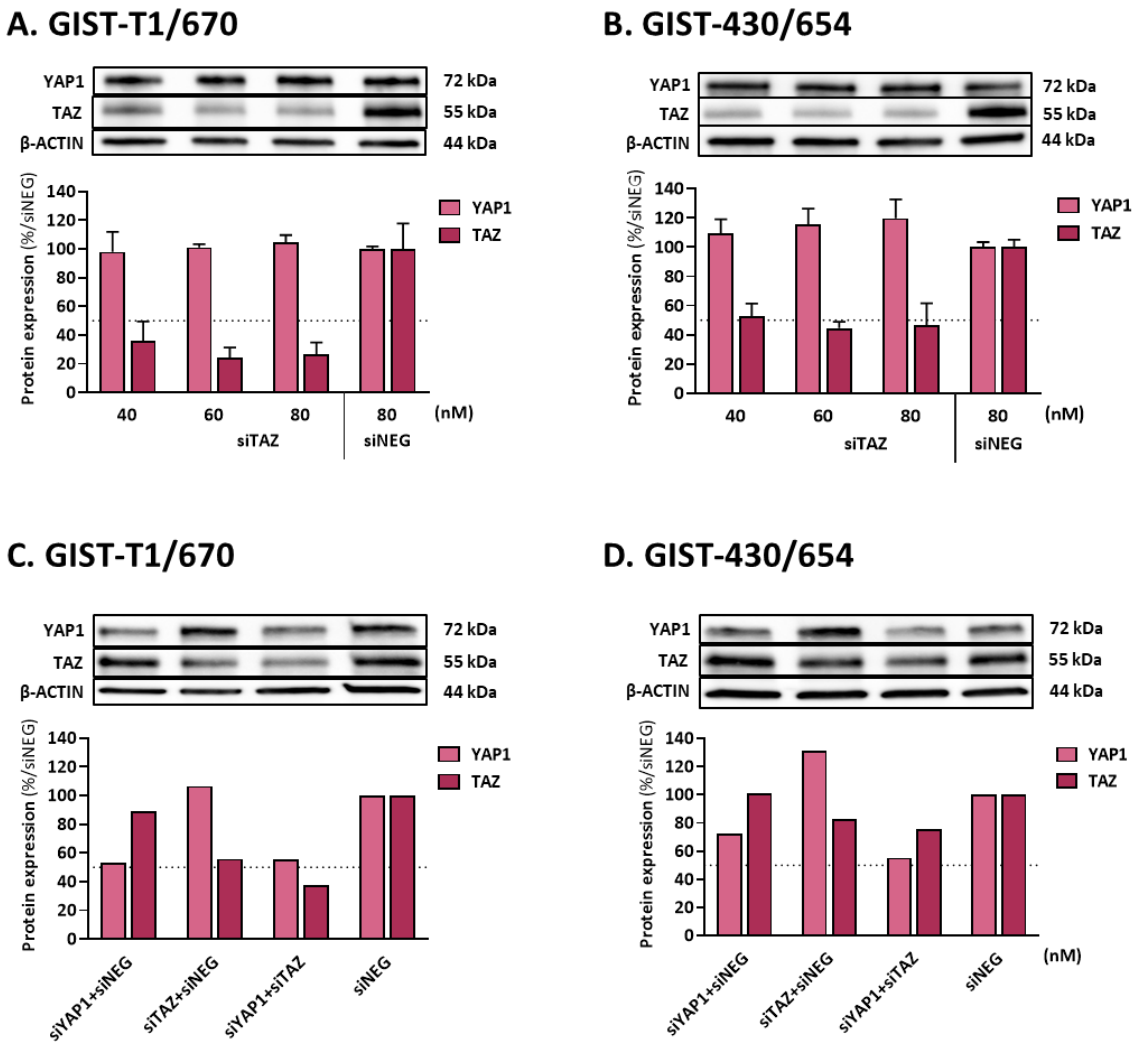

Figure 3: Specific YAP1/TAZ silencing, individually or simultaneously, using WRAP:siRNA nanoparticles in GIST-T1/670 and GIST-430/654.

WRAP5:siRNA nanoparticles delivering siTAZ induced a dose-dependent inhibition of TAZ protein expression in both GIST-T1/670 (**A**) and GIST-430/654 (**B**) within the tested concentration range (40 - 80 nM). WRAP5:siRNA nanoparticles delivering an equimolar cocktail of siRNA targeting YAP1 and/or TAZ specifically inhibited TAZ protein expression but not YAP1 in both GIST-T1/670 (**C**) and GIST-430/654 (D).

Conditions: WRAP5:siRNA (MR 20 with [siRNA] = 40 - 80 nM), siNEG-treated cells were used as a control condition (80 nM or 40 nM). Data were presented as mean ± SD for N=2 (**A, B**) or N=1 (**C, D**).

Afterwards, a siRNA cocktail targeting YAP1 and TAZ in an equimolar ratio (WRAP5:siYAP1+siTAZ) was transfected, maintaining a total siRNA concentration of 40 nM (20 nM siYAP1 + 20 nM siTAZ). A negative control (WRAP5:siNEG) was included in parallel, having the same siRNA concentration of 40 nM. Under these preliminary conditions, performed only once (N = 1), we observed a satisfying profile in GIST-T1/670 cells, with approximately 50% reduction of protein expression for siYAP1, siTAZ, and their combination (**Figure 3C**). In contrast, in GIST-430/654 cells, this concentration was insufficient, especially for TAZ, which was only inhibited of approximately 20%. A higher siRNA dose will be required to achieve a stronger knockdown, since it is known that expressing more protein increases the concentration of siRNA. (**Figure 3D**). Indeed, keeping each siRNA (siYAP1 or siTAZ) at 20 nM was not enough. This was also the case previously in GIST-430 cells, where we later increased the total siRNA dose to 80 nM to obtain more robust silencing. Importantly, in both resistant lines, YAP1 and TAZ could be silenced independently: inhibition of one did not appear to affect the protein levels of the other. Thus, regardless of IM sensitivity, YAP1 and TAZ do not seem to exhibit reciprocal regulation.

These preliminary findings confirm the feasibility of WRAP5-mediated siRNA delivery in IM-resistant GIST lines, changing the dose of siRNA depending on the cell line.

2.3. IM treatment impact on YAP1 and TAZ protein expression

Following the previously established role of TAZ in IM-sensitive GIST-T1 cells, we investigated whether KIT inhibition could influence the expression of YAP1 and TAZ. To this end, we used the GIST-T1 cell line, which harbors a KIT exon 11 mutation and remains fully sensitive to IM, allowing us to capture direct molecular effects of KIT inhibition over time. Cells were treated with a high dose of IM (0,5 µM) and analyzed at 0, 4-, 24-, 48-, and 72-hours post-treatment for phenotypic observation and protein quantification by Western blots.

GIST-T1 cells, in the absence of IM treatment, displayed a continuous proliferation rate, reaching full confluence by 72 hours, based on visual observation (**Figure 4A**). In contrast, IM-treated GIST-T1 cells exhibited a lack of proliferation by adopting a quiescent phenotype, as evidenced by the acquired microscope pictures showing no confluency over time. Moreover, a progressive accumulation of floating cells was observed at later time points, particularly

after 72 hours, which could correspond to reduced adhesion and potential cell death or dormancy (to be confirmed).

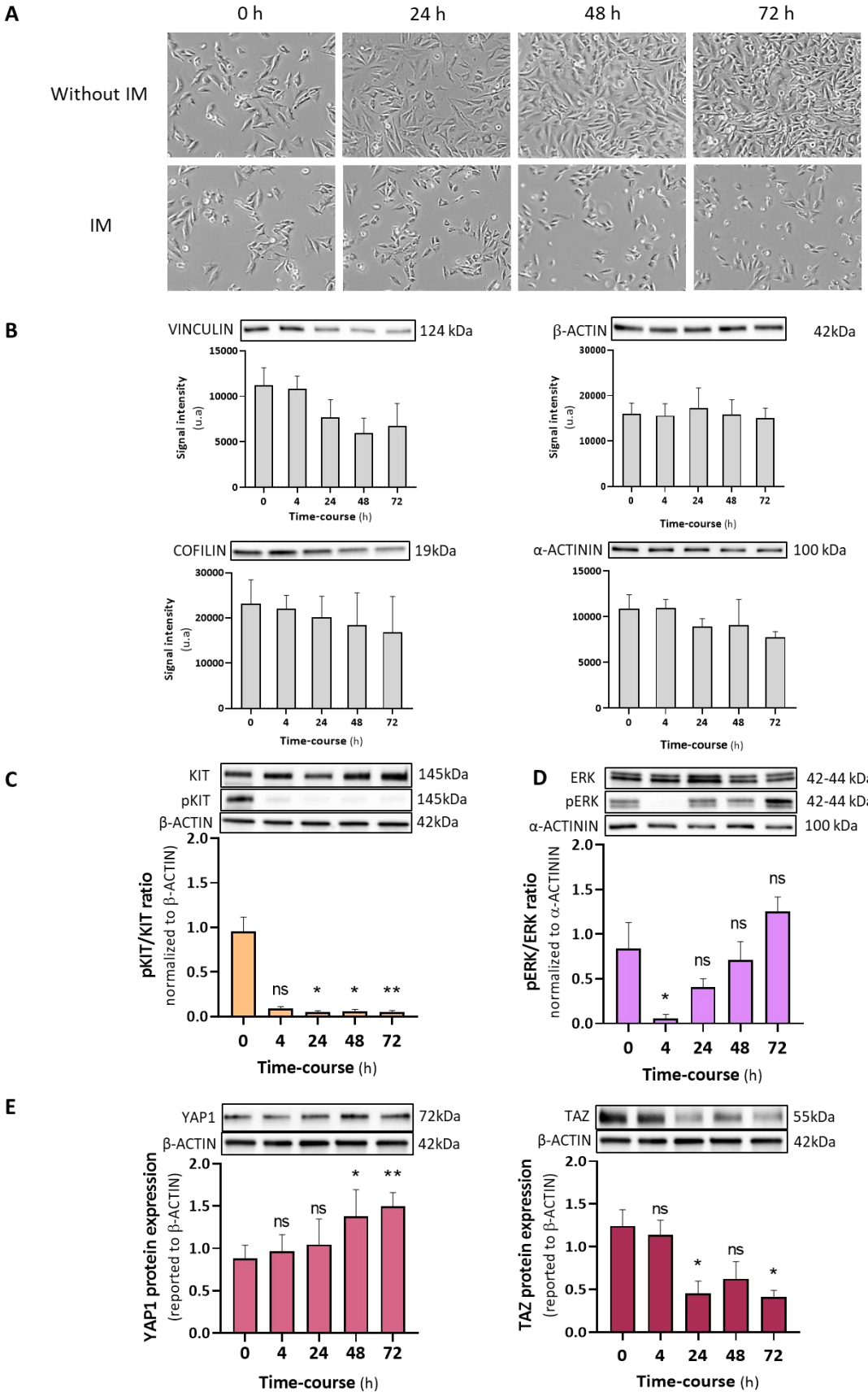

Figure 4: Time-dependent IM impact on GIST-T1 cells.

(**A**) GIST-T1 images during IM treatment taken at each time point using the EVOS^{TM} LX Core microscope system with a 10× objective lens (Thermo Fisher Scientific). (**B**) Variation of loading control protein (VINCULIN, COFILIN, β-ACTIN, α-ACTININ) during time-dependent IM incubation on GSIT-T1 cells.

Analysis of protein expression by Western blot with the corresponding quantification for KIT and pKIT (**C**), ERK and pERK (**D**), and YAP1 and TAZ (**E**), after a time-dependent IM treatment on GIST-T1 cells. β-ACTIN was used as a final loading control. Data were presented as mean ± SD for N=4 (**B, C, D, E**). Statistical analysis was performed using Kruskal-Wallis followed by Dunn's multiple comparisons test versus 0 hours. (**C, D, E**); ns >0.05, * <0.05, ** <0.01.

Before assessing the protein levels of the protein of interest by Western blot, we evaluated several loading controls commonly used in this assay, given the known impact of IM on cellular signaling and cytoskeletal dynamics (Kuželová et al. 2010; Procaccia et al. 2014). Among the tested candidates, such as VINCULIN, COFILIN, β-ACTIN, and α-ACTININE, the most stable across all measured timepoints following IM exposure was the β-ACTIN (**Figure 4B**). Both VINCULIN and COFILIN exhibited decreased protein levels from 24 hours, probably reflecting IM-induced cytoskeletal remodeling. β-ACTIN was therefore selected as the reference for all subsequent immunoblots, as well as α-ACTININE, staying the second most stably expressed during IM treatment.

To confirm the efficacy of IM, we monitored total and phosphorylated KIT protein levels in treated and untreated cells (**Figure 4C**). As expected, the ratio of pKIT to total KIT fell sharply as early as 4 hours after treatment and remained suppressed throughout the 72 hours, very significantly from 24 hours (p-value <0.05). This confirms effective KIT inhibition in our experimental setup and strengthens the association between altered YAP1 and TAZ levels and the pharmacological blockade of KIT signaling.

Then, the activation status of the MAPK signaling pathway under IM treatment was evaluated. It has previously been shown that there is a rebound of this pathway during early IM resistance onset (Ruiz-Demoulin et al., 2023). This can be calculated using the pERK/ERK ratio. Under these experimental conditions, there is indeed inhibition of the MAPK pathway at 4 hours and a gradual reactivation of the pathway, observed with a significant ratio <1 after 48 hours of treatment, as described (Ruiz-Demoulin et al., 2023).

Finally, Western blot analysis of YAP1 and TAZ expression in response to IM treatment is presented (**Figure 4D**). YAP1 protein levels increased progressively from 4 hours after IM treatment and remained significantly elevated throughout 48 and 72 hours (1.5-fold increase).

In contrast, TAZ levels showed a marked significant decrease as early as 24 hours, with sustained suppression up to 72 hours (0.5-fold change relative to the control).

These findings reveal that IM treatment induces a selective downregulation of TAZ while concomitantly increasing YAP1 expression in IM-sensitive GIST cells. Further experiments will be needed to better understand YAP1/TAZ roles in IM-resistance. It appears that GIST-T1 behave differently between YAP1 and TAZ during IM treatment, reinforcing the idea of two distinct roles (as observed in Chapter 2).

2.4. Combined effect of TAZ silencing and IM treatment on GIST cell proliferation

To evaluate whether a more pronounced targeted inhibition of TAZ could enhance the antiproliferative effect of IM, we performed a combinatorial assay in GIST-T1 cells. Cells were first transfected with WRAP5:siTAZ nanoparticles (60 nM) or control nanoparticles (WRAP5:siNEG), then treated with increasing concentrations of IM for 48 hours (from 0.1 to 1,000 nM). A preliminary experiment was conducted to assess cell proliferation using a metabolic-based assay (CellTiter 96® Non-Radioactive Cell Proliferation Assay (MTT), Promega), and dose-response curves were generated from three biological replicates (N=3, n=9).

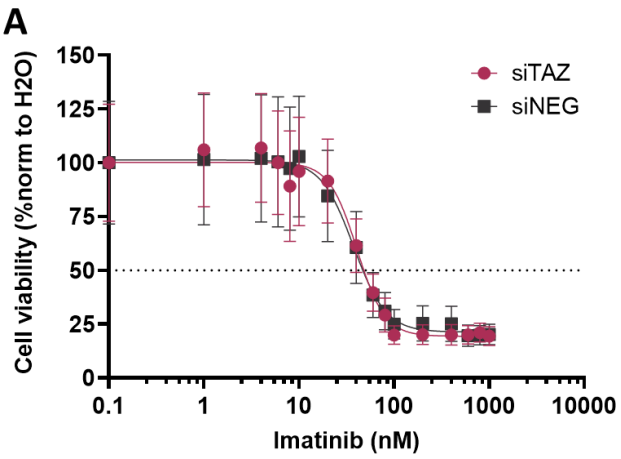

B

siRNA condition	IC50 (nM)
siTAZ	40.66
siNEG	37.31

Figure 5: Effect of TAZ silencing on imatinib sensitivity in GIST-T1 cells.

(**A**) Dose-response curves were generated after 48 h of imatinib treatment in cells transfected with either a negative control siRNA (siNEG) or a TAZ-targeting siRNA (siTAZ). Cell viability was measured using CellTiter 96® Non-Radioactive Cell Proliferation Assay (Promega) (N=3 with n=9 replicates) and normalized to H_2O. Curves were fitted with a four-parameter logistic regression model (log[inhibitor] vs. normalized response, variable slope) in GraphPad Prism. (**B**) IC50 values were compared by an extra sum-of-squares F test, revealing no significant difference between siNEG and siTAZ conditions ($p>0.5$).

IM treatment induced a dose-dependent inhibition of cell proliferation in both control and TAZ-silenced conditions (**Figure 5**). The calculated IC_{50} for IM was 37.31 nM in WRAP5:siNEG-transfected cells and 40.66 nM in cells treated with WRAP5:siTAZ, based on nonlinear regression analysis. No significant shift in IM sensitivity was observed upon TAZ knockdown under these conditions.

Although preliminary, these results suggest that TAZ silencing alone does not sensitize GIST-T1 cells to IM over 48 hours post-treatment. Further experiments will be required to confirm these findings in independent replicates and to explore longer-term or phenotypic consequences of TAZ inhibition in combination with IM.

3. Discussion

The investigation of IM resistance in GIST has facilitated the comprehension of the biological mechanisms behind therapeutic adaptation to targeted KIT inhibition, thereby paving the way for the development of new treatment strategies. In this study, we established the preliminary foundations for understanding the role of YAP1 and TAZ in GIST resistance to IM.

We first explored the expression of YAP1 and TAZ in GIST cell lines with distinct sensitivity profiles to TKI, especially IM. Our findings show that YAP1 and TAZ protein levels are higher in IM-resistant cell lines, including GIST-T1/670 and GIST-430/654, compared to their IM-sensitive counterparts. This observation aligns with previous reports suggesting that components of the Hippo pathway may be upregulated as part of adaptive resistance mechanisms to targeted therapies in various cancer types, including GIST (Mouillet-Richard and Laurent-Puig 2020; Yu et al. 2015; Zanconato et al. 2016). However, few studies have directly assessed YAP1 and TAZ levels in the context of GIST IM-resistance, warranting further investigation (Wu, Yamashita, Lou, et al. 2025).

In addition, when considering the phosphorylation status of YAP1 and TAZ, we observed that their activation profiles do not appear to strictly correlate with IM resistance. Indeed, both GIST-T1 and its IM-resistant derivative GIST-T1/670 predominantly display non-phosphorylated forms of YAP1 and TAZ, whereas GIST-430 and GIST-430/654 exhibit a more balanced distribution between phosphorylated and non-phosphorylated YAP1, while phosphorylated TAZ tends to predominate over its non-phosphorylated counterpart. These

observations suggest that YAP1 and TAZ regulation may be influenced more by the mutational background. However, as Western blot analysis cannot provide spatial information on nuclear *versus* cytoplasmic localization, these results remain descriptive. Further immunohistochemical studies would be required to determine the precise subcellular distribution of YAP1 and TAZ, which is critical to understand how the Hippo signaling regulation differs across GIST cell lines.

Interestingly, YAP1 and TAZ were also expressed in the *KIT*-independent cell line GIST-48B, reinforcing the hypothesis that their role may extend beyond the canonical KIT-driven signaling. This independence could reflect a compensatory or alternative pathway that sustains cell survival and plasticity when KIT is no longer a primary driver. The role of the Hippo pathway in *KIT*-independent GIST has been initially reported as the first proof (Chen et al. 2021). In this context, they demonstrated that proteasome inhibition suppresses *KIT*-independent GIST growth by targeting the Hippo/YAP1/CD1 axis, thereby providing the first evidence that Hippo pathway dysregulation may be a key for tumor maintenance in the absence of KIT signaling. This observation suggests that YAP1 activation could have an oncogenic role, integrating upstream signals from diverse origins to maintain proliferation and survival, particularly in resistant or KIT-negative disease states, and highlights the therapeutic potential of targeting the Hippo pathway in this subset of GIST.

To evaluate whether YAP1 and TAZ could be functionally targeted in IM-resistant GIST cells, we transfected WRAP5:siRNA nanoparticles designed to silence both proteins. The WRAP5 delivery system was previously validated in three IM-sensitive lines (referred to in Chapters 1 and 2), and we then wanted to test its silencing efficiency in IM-resistant models. Preliminary experiments confirmed that the WRAP5:siRNA delivery system is effective, initially tested in a dose-dependent manner against TAZ, and subsequently using a combination of siRNA targeting both YAP1 and TAZ. However, we assume that higher doses would be used in the GIST-430/654 cell line to achieve efficient knockdown compared to the GIST-T1/670 cell line. This observation may reflect the intrinsically higher expression levels of YAP1 and TAZ in this model. Nevertheless, these findings indicate that our WRAP5:siRNA nanoparticles constitute a valuable tool to further explore the phenotypic consequences of YAP1 and TAZ inhibition in IM-resistant GIST cells.

Inactivation of the KIT molecular cascade with TKI such as IM reduces cell proliferation and induces a quiescent state, primarily through inhibition of signaling pathways such as ERK/MAPK and PI3K/AKT/mTOR (Zhou et al. 2024). To investigate the early adaptive response to IM, we performed a 72-hour time-course treatment in GIST-T1 cells. Our data indicate that KIT inhibition actively modulates YAP1 and TAZ protein dynamics. Surprisingly, YAP1 levels progressively increased following IM exposure, whereas TAZ levels decreased. These two opposite trajectories suggest divergent regulation and potentially distinct functions downstream of KIT inhibition. This pattern implies that YAP1 and TAZ are not functionally redundant in this context but rather respond differently to signaling rewiring under pharmacological pressure, a hypothesis also seen in other cancers (Chorzalska et al. 2017; Shreberk-Shaked et al. 2020). The increase in YAP1 may reflect an alternative, possibly compensatory function linked to survival or stress adaptation (Shibata et al. 2018). Part of this trend aligns with previous observations showing that IM treatment upregulates LIX1 as well as YAP1 and TAZ expression (Ruiz-Demoulin et al. 2023). However, our results diverge from those findings in one key aspect: whereas the earlier study reported a simultaneous increase in both YAP1 and TAZ, we observed a marked decrease in TAZ as early as 4 hours post IM-treatment. Given the known role of TAZ in promoting cell growth and motility (Zhou and Lei 2016), and our own data from Chapter 2 showing that TAZ silencing reduces proliferation in IM-sensitive GIST-T1 cells, this early drop in TAZ may correlate with the observed proliferation arrest. Moreover, the rebound of the ratio of phosphorylated ERK to total ERK levels in our experiments confirms the occurrence of an early adaptive response to IM. These opposing YAP1 and TAZ dynamics point to differential regulation in response to KIT inhibition and raise the possibility that they engage in distinct downstream programs, or in parallel to KIT signaling (**Table 2**). To confirm these protein-level observations, it will be essential to assess their transcript levels by qPCR. MAPK pathway reactivation during early IM exposure has been linked to survival signaling in GIST (Ruiz-Demoulin et al. 2023). The rise in YAP1 despite proliferation arrest suggests that it might contribute to survival or early resistance mechanisms, potentially in cooperation with other signaling pathways or with the involvement of other transcriptional networks. However, our data in IM-sensitive GIST cells showed no direct relation between the YAP1/TAZ axis and MAPK signaling, suggesting instead that MAPK reactivation may occur in parallel to the observed YAP1 and TAZ protein levels variations. Moreover, these results could reflect more complex upstream regulatory events,

with YAP1 upregulation and TAZ downregulation being secondary to differential modulation of Hippo pathway kinases such as MST1/2 and LATS1/2. Therefore, evaluating the activity of these kinases will be essential to clarify whether the observed changes result from direct signaling rewiring or from upstream control mechanisms. Further exploration of canonical YAP1 and TAZ target genes associated with proliferation, such as *CYR61* and *CTGF* (Koo et al. 2020; Li et al. 2024), and survival, such as *AXL* or *BIRC5* (Goyette et al. 2018; Hansen et al. 2015), could also help understand YAP1/TAZ roles respectively in IM-treated GIST cells.

Table 2: Summary of YAP1 and TAZ profiles in relation to IM response in GIST cells based on obtained results.

	IM sensitivity	Early adaptive response to IM	IM acquired resistance
KIT	One primary mutation	Primary mutation	Primary and secondary mutations
YAP1	Limited role in proliferation/migration. Possible contribution to survival or stress adaptation.	Progressive increase in protein levels upon IM exposure.	High protein expression. Potential role in adaptation and survival.
TAZ	Key role in proliferation and migration.	Early decrease in protein levels following IM exposure.	High protein expression. Likely contributes to proliferation and resistance.

In our combinatorial assays, we tested whether TAZ silencing could sensitize GIST-T1 cells to IM. While no shift in IC_{50} was observed in a preliminary experiment, we cannot exclude that a more potent or sustained silencing of TAZ, particularly in the presence of high IM concentrations, might improve the antiproliferative effect. Our assay was not designed to detect subtle survival phenotypes or compensatory signaling over time. Further experiments, including long-term assays, combination with optimized TAZ inhibition, or silencing TAZ after IM treatment, will be necessary to address this question. Moreover, performing MTT assay upon TAZ silencing in IM-resistant GIST cells could clarify whether partial resensitization to IM occurs in the context of acquired resistance with *KIT* secondary mutations. Although we performed three preliminary experiments with siTAZ, pushing this approach further might also help refine the role of YAP1 in resistance. Based on our observations in sensitive cells, YAP1 silencing is unlikely to alter the IC_{50} in the MTT assay, given its limited role in proliferation. Instead, YAP1 upregulation upon IM treatment may reflect a compensatory or stress-related

response, supporting the idea that YAP1 is more a biomarker of cellular adaptation than a direct effector.

In conclusion, these results support the complexity of YAP1 and TAZ regulation in GIST and their potential roles in response to IM (early adaptation and long-term effect). While TAZ appears directly involved in proliferation, YAP1 may contribute to adaptation and survival under therapeutic pressure. A deeper understanding of their respective transcriptional outputs, binding partners, and regulation under KIT inhibition is essential. From a translational perspective, deciphering the temporal activation of YAP1 during IM exposure could facilitate the identification of a therapeutic window to suppress resistance emergence. This, in turn, could allow for IM dose reduction or improving the efficacy of combined approaches. Importantly, our data indicate that YAP1 and TAZ are not functionally redundant in this context, but rather respond to KIT inhibition through divergent functional dynamics.

DISCUSSION

DISCUSSION

This thesis was conducted to decipher different signaling pathways in GIST cell lines, with the objective of gaining a deeper understanding of tumor development and therapeutic resistance. Although considered as a rare cancer type, GIST represent the most common mesenchymal neoplasms of the GI tract (Blay et al. 2021), resulting in 800 to 900 new diagnoses annually in France (Landi et al. 2010). The introduction of IM has transformed the management of GIST patients, a selective KIT and PDGFRA TKI, which remains the gold standard first-line therapy (Demetri et al. 2002). However, despite initial efficacy, a proportion of locally advanced and metastatic GIST patients eventually develop resistance after 20-24 months, and disease relapse is frequent (Schaefer et al. 2022). This therapeutic limitation highlights the importance of identifying further molecular drivers that could complement or improve the current treatment model.

Previous work from our group identified LIX1 as an upstream regulator of Hippo signaling, suggesting that YAP1 and TAZ could act as key mediators of adaptive responses in GIST (Guérin et al. 2020; McKey et al. 2016). While Hippo dysregulation is known to drive tumorigenesis in multiple cancers (Piccolo et al. 2023; Plouffe et al. 2018), the respective roles of YAP1 and TAZ in GIST remain poorly defined. Our study was based on the hypothesis that YAP1 and TAZ may not always function as a single unit, but instead exert distinct contributions to tumor biology and therapeutic resistance (Reggiani et al. 2021).

To achieve this aim, three objectives were defined. The first was to validate WRAP5-based nanoparticles as an efficient tool for siRNA delivery in GIST, with the additional advantage of enabling multi-protein silencing. The second was to investigate the individual roles of YAP1 and TAZ in GIST biology, focusing on their impact on cell proliferation, migration, and canonical downstream targets in IM-sensitive cell lines. The third was to assess the significance of YAP1 and TAZ in IM-resistant conditions to establish if their activity plays a role in therapeutic evasion and adaptation.

To contextualize our results, the discussion will address (1) the promise of WRAP5 nanoparticles for siRNA delivery in GIST, (2) the distinct contributions of YAP1 and TAZ in GIST biology, (3) their implications in IM sensitivity and resistance, (4) limitations of the study, and future perspectives.

DISCUSSION

1. WRAP5-based nanoparticles as promising therapeutic tools?

Small molecules remain indispensable in cancer therapeutics due to their favorable pharmacological properties and ease of administration. However, their development is hampered by challenges in achieving high target specificity and the risk of resistance and toxicity. Especially, complex targets like protein-protein interaction (PPI), implicated in cellular signaling pathways, do not present obvious “hot spots” or cavities suitable to small-molecule binding, complicating rational drug design (Demirel et al. 2018). Indeed, PPI interfaces often span large surface areas (typically 1,500–3,000 Å²) with shallow and featureless topographies, lacking well-defined pockets for small molecules to bind tightly and specifically (Sheng et al. 2015). These considerations underscore the need for alternative therapeutic modalities capable of targeting YAP1 and TAZ more specifically and safely. Among these, RNAi emerges as a promising strategy, supported by both preclinical and clinical validation (Esteller 2011). By allowing precise knockdown of specific mRNA, RNAi enables selective inhibition of YAP1 or TAZ individually, addressing their partially distinct roles in GIST. This concept is not purely theoretical: RNA-based therapies are already clinically validated, with six FDA-approved drugs demonstrating the feasibility of systemic nucleic acid therapeutics (Friedrich and Aigner 2022). Moreover, recent FDA approval of DAXXIFY™, a botulinum toxin formulation containing the CPP RTP004, illustrates that non-covalent CPP-based delivery systems can achieve clinical efficacy and safety (Dowdy et al. 2023).

Our choice of WRAP5-based nanoparticles as a siRNA delivery system builds on this translational rationale. Developed in our laboratory, WRAP5 is a non-covalent CPP optimized for siRNA transport (Konate et al. 2019) (**Figure 1**). *In vitro*, we demonstrated in this thesis that it efficiently silences single or multiple protein targets in GIST-T1 cell lines, while maintaining low cytotoxicity compared to conventional lipid-based transfection reagents (Konate et al. 2021). In detail, we have explored the combined inhibition of CDK4, CD1, and MCL-1 in the GIST-T1 model using WRAP5-based multi-protein silencing (Konate, Pezzati, et al. 2025) (see also Chapter 1). While individual knockdowns yielded limited phenotypic changes, simultaneous silencing of the three targets markedly reduced long-term proliferative capacity, as evidenced by clonogenic assays, reinforcing the notion that combinatorial targeting of oncogenic drivers is required for sustained growth inhibition.

Importantly, WRAP5 nanoparticles can be engineered to enhance stability, targeting, and payload versatility by modifying their core composition or their surface. For example, core modifications allow multi-siRNA delivery, as demonstrated in proof-of-concept studies, the 3 proteins listed above, which significantly reduced proliferation in GIST-T1 cells (Konate, Pezzati, et al. 2025). Concerning the surface modification, PEGylation has been shown to improve nanoparticle stability *in vitro* (Di Gregorio et al. 2025) and *in vivo* for immunization strategies (Teko-Agbo et al. 2025).

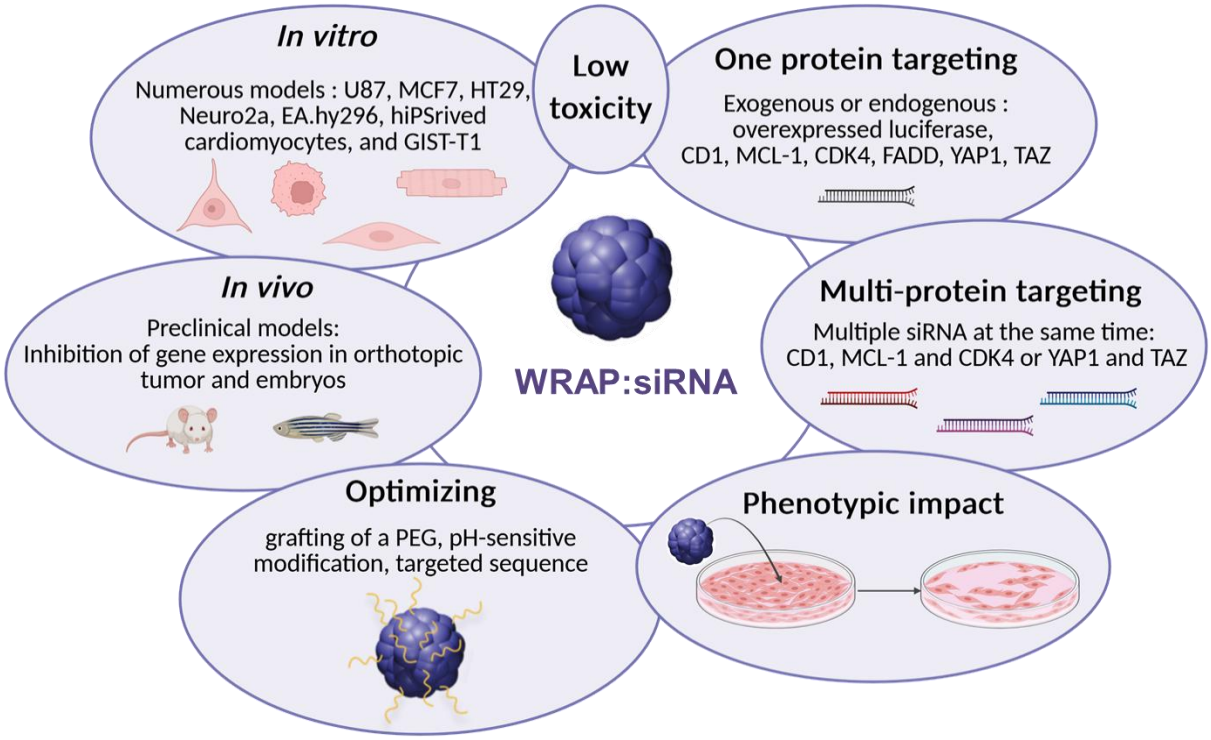

Figure 1: WRAP5-based nanoparticles for siRNA therapeutic delivery system

Beyond *in vitro* applications, WRAP5 has been successfully applied *in vivo* in preclinical models including mice, rabbits, and zebrafish, highlighting its translational potential (Ferreiro et al. 2021; Konate, Teko-Agbo, et al. 2025; Teko-Agbo et al. 2025). Additional strategies, such as pH-sensitive linkers that release siRNA in acidic tumor microenvironments, further exemplify how these nanoparticles could be tailored to improve both efficacy and safety (Di Gregorio et al. 2025). We could think of apply this approach to incorporate sequences recognizing GIST-specific nuclear factors (e.g., ETV1) (Chi et al. 2010).

2. Distinct roles of YAP1 and TAZ in GIST biology

This thesis constitutes the first dedicated analysis of the individual contributions of YAP1 and TAZ, the two paralogous downstream effectors of the Hippo pathway, in *KIT*-dependent IM-sensitive GIST cells. While both proteins share a high degree of structural homology and mainly bind with TEAD1-4 family of TF to regulate overlapping transcriptional programs (Cunningham and Hansen 2022; Luo et al. 2023; Piccolo et al. 2023), increasing evidence suggests that YAP1 and TAZ may exert distinct and non-redundant functions depending on the cellular and tissue context (Reggiani et al. 2021). Our results support this hypothesis by demonstrating that TAZ plays a predominant role in promoting the proliferation and migration of GIST-T1 cells, whereas YAP1 silencing alone produced only limited effects.

In detail, using WRAP5-based nanoparticles as a delivery system for siRNA, we achieved efficient and specific downregulation of YAP1 or TAZ, either individually or in combination (refer to Chapter 2). Only TAZ inhibition resulted in a significant reduction of proliferation and migration. In contrast, YAP1 knockdown alone did not significantly impact the phenotype, and combined YAP1/TAZ silencing produced only a modest synergic effect in this model. This observation marked a functional divergence between YAP1 and TAZ in GIST, suggesting that TAZ may act as the main driver of Hippo-mediated oncogenic transcriptional programs in this sarcoma. It was also confirmed by an increased *TAZ* expression in GIST patients, which was associated with shorter disease-free survival and an increased tendency for metastasis development.

This finding is in line with evidence from other types of cancers, in which it has been demonstrated that YAP1 and TAZ diverge in their oncogenic effects. For example, in hepatocellular carcinoma and cholangiocarcinoma, YAP1 has been identified as the dominant effector , whereas in non-small cell lung cancer, TAZ preferentially regulated extracellular matrix remodeling and metastasis, while YAP1 primarily drove proliferation-related genes (Shreberk-Shaked et al. 2020). Similarly, in triple-negative breast cancer, TAZ nuclear translocation has been associated with aggressive tumor behavior (Díaz-Martín et al. 2015). In sarcomas, lineage-specific roles of YAP1 and TAZ have also been documented: YAP1 upregulation promotes proliferation and differentiation in osteosarcoma (Zhang et al. 2013),

while TAZ regulates myogenic differentiation programs in rhabdomyosarcoma (Hebron et al. 2025).

This finding highlights that the predominant role of TAZ is particularly relevant in GIST, as previous studies have mainly focused on YAP1 as the principal effector. In *KIT*-independent GIST, activation of the YAP1-CD1 axis has been described as a major oncogenic driver, with CD1 overexpression sustaining proliferation and survival (Chen et al. 2021; Ou et al. 2019) (**Figure 2**). In *KIT*-dependent GIST, FBXW7-YAP1 axis has been recently associated with tumor progression, either through its prognostic value as an independent marker of recurrence (Wu, Yamashita, Matsumoto, et al. 2025). Beyond this, accumulating evidence underscores the importance of YAP1 activity, as its pharmacological inhibition, either indirectly through a PDE3 (Phosphodiesterase 3) inhibitor cilostazol or directly with verteporfin, has been shown to

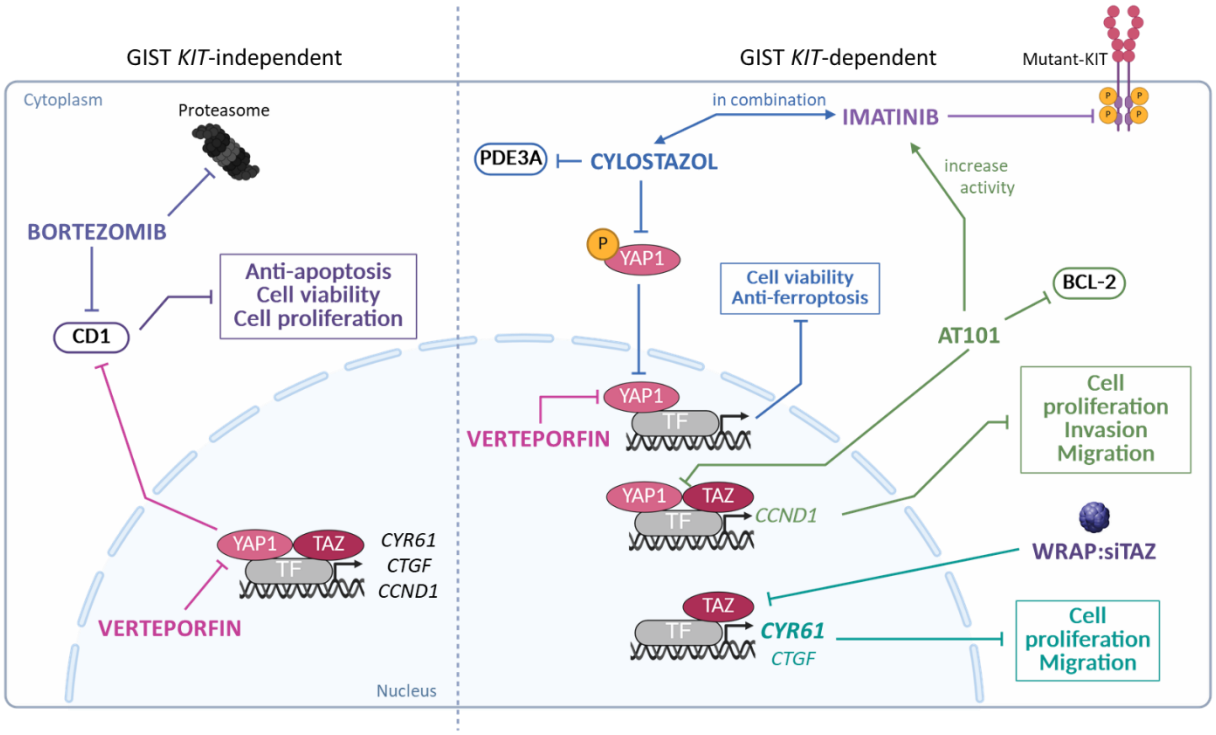

Figure 2: Pharmacologic and genetic strategies targeting YAP1/TAZ in *KIT*-independent and *KIT*-dependent GIST.

***KIT*-independent (left):** Bortezomib (proteasome inhibitor) reduces pro-survival/proliferative signaling by inhibiting Cyclin D1 (CD1) and limits cell viability. Verteporfin directly disrupts the YAP1-TEAD transcriptional complex, lowering expression of canonical targets (*CYR61, CTGF, CCND1*) and limiting proliferation.

***KIT*-dependent (right):** Inhibition of phosphodiesterase 3A (PDE3A) by cilostazol increases YAP1 cytoplasmic retention, attenuating nuclear YAP1 activity; functionally, this associates with improved cell viability control and anti-ferroptotic effects. AT101 (pan-BCL-2 family inhibitor) suppresses YAP1/TAZ-driven programs linked to proliferation, invasion, and migration. Imatinib (KIT/PDGFRA tyrosine-kinase inhibitor) is shown as a combination partner that can increase these YAP1/TAZ modulations. Targeted gene silencing with WRAP:siTAZ selectively knocks down TAZ, decreasing expression of mostly *CYR61* and minority *CTGF* target genes and inhibiting cell proliferation and migration.

restore sensitivity to IM and limit resistance by inducing ferroptosis (Delvaux et al. 2022; Vandenberghe et al. 2019).

More recently, activation of the YAP1/TAZ-CD1 axis has been identified as a hallmark of IM resistance, and its pharmacological inhibition with AT101, a BCL-2 inhibitor, has been shown to suppress GIST growth and metastasis, while enhancing the efficacy of IM (Wu, Yamashita, Lou, et al. 2025). In 2024, the company BAYER performed a high-throughput screening to identify small molecules. After a multi-parameter optimization, they obtained BAY-593, an *in vivo* probe with favorable PK properties, which demonstrated anti-tumor activity and blockade of YAP1 signaling *in vivo* (Graham et al. 2024). Despite these findings, the clinical data on YAP1 remain limited and, importantly, to our best knowledge, no study to date has demonstrated a functional role for TAZ in GIST. Our results therefore provide the first evidence that TAZ can act as a main effector in this tumor type. This underlines the need for future work to assess its potential as a prognostic marker and therapeutic target.

Following the observed phenotypic effects of TAZ silencing on *KIT*-dependent IM-sensitive GIST-T1 cell migration and proliferation, we delineated the downstream effectors mediating this response. Mechanistically, co-transcriptional factors YAP1 and TAZ activate numerous target genes implicated in proliferation, survival, and invasion (including *CTGF, CYR61, CCND1, AREG, MYC*, and *MCL-1*) (Boopathy and Hong 2019; Glinkina et al. 2023; Hansen et al. 2015; LeBlanc et al. 2021). In our model, TAZ knockdown, but not YAP1 inhibition, led to a significant downregulation of CYR61 and CTGF. Both CYR61 and CTGF are well-characterized YAP1/TAZ-TEAD targets implicated in extracellular matrix remodeling, angiogenesis, and tumor proliferation (Boopathy and Hong 2019; Zhou et al. 2016). In contrast, CD1 expression remained unchanged after YAP1/TAZ silencing. The absence of CD1 modulation in our models does not exclude the possible involvement of other cell cycle regulators, such as CYCLIN D2/D3, CDK2, or CDK4 (Knapp et al. 2018), or survival pathways mediated by anti-apoptotic proteins such as MCL-1 or BCL-2 (Wang et al. 2025). Moreover, the discrepancy between our results and those reporting a YAP1/TAZ-CCND1 axis may be explained by differences in experimental conditions, including the use of distinct CD1 and YAP1 antibodies, siRNA targeting different regions of the mRNA, variations in cell culture conditions such as confluency, and differences in the transfection reagent employed.

Finally, no alterations were detected in the activation of KIT, AKT, or ERK, indicating that TAZ exerts its pro-tumorigenic effects through selective transcriptional targets rather than modulation of KIT signaling. While both the Hippo pathway and KIT signaling are well-characterized in cellular regulation, there is currently no evidence in the literature indicating a functional link between them.

Physiological experiments further established CYR61 as a key effector of TAZ, since its silencing significantly impaired GIST-T1 proliferation, whereas CTGF inhibition produced only a modest and non-significant effect. Importantly, high CYR61 expression correlated with reduced desease-free survival and metastatic status in a GIST patient dataset, underscoring its clinical relevance as a mediator of TAZ-driven oncogenicity. Nevertheless, the lack of a significant effect of CTGF silencing on proliferation does not exclude a potential role in other oncogenic programs, such as promoting cell migration and invasion, supporting angiogenesis, or modulating the tumor microenvironment. Indeed, as TAZ inhibition reduces both CYR61 and CTGF expressions, it is plausible that CTGF exerts complementary functions to CYR61 in driving tumor progression. These results suggest that the oncogenic activity of TAZ in GIST is largely mediated by CYR61-dependent transcriptional outputs, with CYR61 emerging as a key effector that bridges Hippo pathway dysregulation to clinically aggressive behavior. Our identification of TAZ-CYR61 axis as a pivotal effector in GIST is supported by findings in other cancers. In breast cancer cells, TAZ-induced taxol resistance is mediated via CYR61 and CTGF. Knockdown of these factors reverses resistance, emphasising their functional relevance downstream of TAZ (Lai et al. 2011). Similarly, in alveolar rhabdomyosarcoma, TAZ suppression reduces CYR61 and CTGF expression, leading to growth inhibition and apoptosis (Deel et al. 2018). Moreover, CYR61 and CTGF are well-described YAP1/TAZ targets across many epithelial cancers, including pancreatic, glioma, prostate, and breast cancers (Boopathy and Hong 2019; Juan and Hong 2016; Zhou et al. 2016). Thus, we highlight the TAZ-CYR61 axis in our study for the first time in GIST.

Interestingly, the divergence between YAP1 and TAZ functions in GIST can not be explained solely by their shared ability to interact with TEAD transcription factors (**Figure 3**). Both proteins largely rely on TEAD for transcriptional activation (Reggiani et al. 2021; Zanconato et al. 2016), yet the selective regulation of *CYR61* and *CTGF* by TAZ suggests that additional mechanisms, such as preferential cofactor recruitment, post-translational modifications, or

differential affinity for TEAD isoforms, may underlie their distinct outputs. This hypothesis is supported by previous studies showing that TAZ can function as a coactivator for lineage-determining transcription factors such as RUNX2 and MyoD (Hong et al. 2005; Jeong et al. 2010), or act as a repressor by antagonizing PPARγ-driven transcription (Hong and Guan 2012). YAP1, conversely, is known to engage in unique interactions with partners such as p73 (Strano et al. 2001) or ERBB4 (Hong and Guan 2012), further illustrating that the divergence observed in GIST likely arises from differential transcriptional partnerships and chromatin contexts.

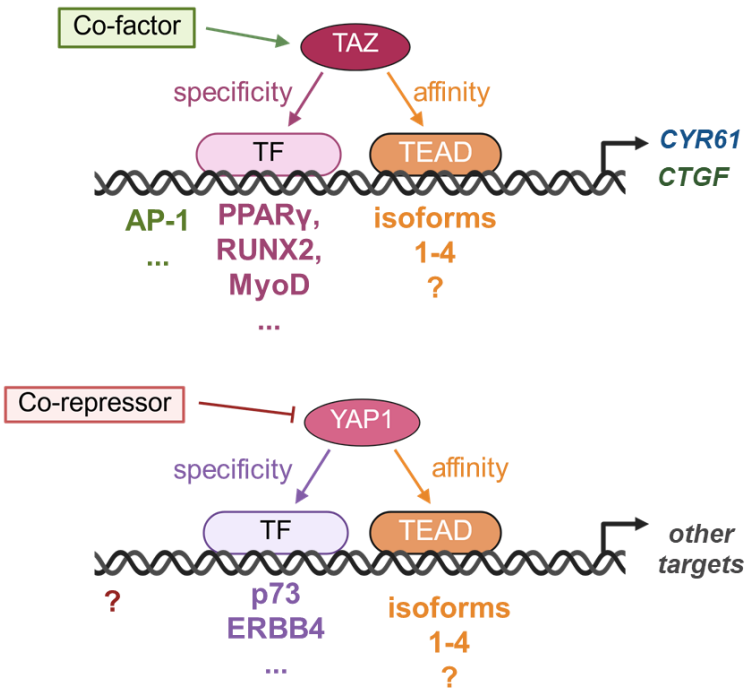

Figure 3: Proposed model of differential interactions of YAP1 and TAZ in GIST biology.

TAZ may preferentially interact with specific transcription factors (TF) such as PPARγ, RUNX2, or MyoD, possibly in addition with co-factors, leading to regulation of targets like *CYR61* and *CTGF*.

YAP1, in contrast, may associate with a distinct set of TF (p73, ERBB4) and co-repressors, influencing different downstream targets.

Both YAP1 and TAZ can bind TEAD isoforms 1-4, with potential differences in affinity. This schematic illustrates the hypothesized specificity and partner-dependent modulation of transcriptional programs by YAP1 *versus* TAZ in GIST cells.

Another important dimension of our work lies in the YAP1/TAZ expression heterogeneity across the GIST cell lines analyzed. While TAZ emerged as the dominant regulator of CYR61 and had a minor effect on CTGF expression, dual YAP1/TAZ silencing occasionally enhanced repression of the two downstream targets, suggesting a cellular type context-dependent cooperative effect. This heterogeneity may reflect the molecular diversity observed in GIST tumors. Indeed, the mutations in a tumour depend on the cells that compose it and are

therefore heterogeneous. This notion implies that, although TAZ is likely the more relevant target, combined inhibition of both paralogs could be advantageous in aggressive or advanced disease. Similar strategies have proven effective in other cancers: in KRAS G12C mutant cells, dual knockdown of YAP1 and TAZ amplified suppression of CYR61 and sensitized tumors to targeted therapies (Edwards et al. 2023), while in BRAF inhibitor-resistant melanoma, concomitant silencing of both proteins restored drug sensitivity (Kim et al. 2021; 2016).

3. YAP1 and TAZ implications in IM sensitivity and resistance

Another relevant observation of our study was the differential YAP1/TAZ expression in IM-sensitive *versus* resistant GIST cell lines, with higher basal protein levels in resistant lines compared to sensitive counterparts. While TAZ silencing reduced proliferation across IM-sensitive models, resistant lines exhibited distinct patterns of YAP1/TAZ expression, suggesting that YAP1 and TAZ activity might contribute to therapeutic evasion and adaptation. It should be noted that these observations in resistant models remain preliminary and require further validation.

Our first results indicate that KIT inhibition induced by time-course experiments with IM produced contrasting results, with YAP1 levels increasing and TAZ levels decreasing. This suggests that they could play distinct roles in early adaptive responses to TKI. Importantly, TAZ remains susceptible to siRNA-loaded WRAP5 nanoparticle silencing in resistant cells, providing a functional avenue to explore combinatorial strategies aimed at overcoming TKI resistance. Investigating IM resistance is particularly pertinent in light of recent work of our team, which identified a potential involvement of the LIX1/YAP1/TAZ axis in early adaptive responses to KIT inhibition (Ruiz-Demoulin et al. 2023). Indeed, YAP1 and TAZ have been linked to drug resistance in several cancers, including lung, breast, and melanoma, where they confer tolerance to targeted therapies and chemotherapy. Further work should investigate whether YAP1/TAZ inhibition restores sensitivity to imatinib in resistant models, or whether their activity is enhanced by resistance-associated mutations.

Insights from other malignancies further strengthen this perspective. In CML, YAP1 and TAZ have emerged as important mediators of resistance to TKI targeting the BCR-ABL fusion protein, which drives the uncontrolled proliferation, enhanced survival, and disrupted differentiation of hematopoietic cells. YAP1 is upregulated at the protein level in BCR-ABL$^+$

cells and phosphorylated on Tyr-357 by Src family kinases, thereby promoting the expression of SURVIVIN, MYC, and CD1 (Li et al. 2016; Moriyama and Hori 2019). Silencing YAP1 reduces proliferation and induces G1 arrest, restoring sensitivity to IM even in resistant lines. In the blast phase of CML, TAZ, not YAP1, becomes epigenetically activated through FLT3/JAK/STAT3 signaling, where it drives TKI resistance via TEAD-dependent transcriptional programs (Shin et al. 2023). Importantly, pharmacological inhibition of the TAZ/TEAD axis restored drug sensitivity in these models.

These findings illustrate how YAP1/TAZ can act as transcriptional "back-up" systems that sustain tumor cell survival despite blockade of primary oncogenic drivers. In our GIST models, the observation that YAP1 protein levels increase while TAZ levels decrease following KIT inhibition suggests that they may play complementary but distinct roles in early adaptive responses.

4. Limitations of this study and future perspectives

While our study provides novel insights into the roles of YAP1 and TAZ in GIST, we acknowledge several limitations that highlight promising directions for future research.

First, our work was conducted *in vitro* using a limited number of GIST cell lines. Although these models capture certain biological features, they can not fully reproduce tumor heterogeneity or the influence of the microenvironment. Extending the investigation to spheroids, organoids, PDX, or genetically engineered mouse models would provide more physiological relevance. This could also help determine whether TAZ inhibition can reduce tumor growth and impact survival *in vivo*. Access to patient tumor samples would also be a helpful tool to validate the predominant role of the TAZ-CYR61 axis as a poor prognostic factor and to evaluate TAZ or YAP1/TAZ as biomarkers. IHC studies correlating expression and localization (nuclear/cytoplasmic) with clinical outcomes may ultimately support their use in patient stratification.

A further challenge in our study concerns the difficulty of achieving a complete knockdown of both proteins, YAP1 and TAZ. Even at high siRNA concentrations, inhibition rarely exceeded 70%, suggesting that a residual active pool of proteins may persist. This is likely related to their intrinsic stability, as YAP1 and TAZ display distinct half-lives: YAP1 is relatively stable (≈6 h),

whereas TAZ is rapidly degraded (≈2 h) in mouse embryonic fibroblasts (Miranda et al. 2017). These kinetics may vary across cell lines, further complicating interpretation. We attempted to experimentally determine the half-life of both proteins in GIST cells using cycloheximide assays, but these experiments proved technically challenging and ultimately inconclusive. As the knockdown of YAP1 and TAZ is not complete, the therapeutic significance of residual YAP1/TAZ activity after silencing remains uncertain.

Another limitation of our study is the restricted scope of downstream targets explored. Beyond CYR61, CTGF, and CD1, the transcriptional networks specifically regulated by TAZ remain largely unexplored. Transcriptomic and epigenomic profiling (RNA-seq and ChIP-seq) would be crucial to delineate the transcriptional networks governed by YAP1/TAZ and uncover additional oncogenic mechanisms or therapeutic adaptations. Moreover, future work dissecting their protein-protein interactions, post-translational modifications, and nuclear partners through approaches such as co-immunoprecipitation could provide mechanistic explanations for the preferential oncogenic impact of TAZ.

Finally, our findings raise therapeutic perspectives. Combination strategies integrating TEAD inhibitors or other Hippo modulators with IM or newer TKI warrant evaluation in preclinical settings. Understanding how YAP1/TAZ influence stromal remodeling, immune infiltration, or angiogenesis may reveal indirect mechanisms of resistance and broaden the therapeutic landscape. In parallel, optimizing silencing technologies such as WRAP5:siRNA delivery or indirectly modulating upstream Hippo regulators (e.g., LATS1/2, MST1/2) and metabolic pathways dependent on YAP1/TAZ could broaden treatment options.

CONCLUSION

CONCLUSION

The collected results of this three-year doctoral thesis have given us insights into the cellular biological signaling pathways of GIST cells using WRAP5 nanoparticles loaded with siRNA (**Figure 1**).

First, we validated the strategy by which we aimed to silence multiple proteins at the same time to obtain a more specific response on cell proliferation in GIST cells using WRAP5:siRNA nanoparticles. Secondly, we provided the first comprehensive study of the individual roles of the two Hippo pathway effectors YAP1 and TAZ in *KIT*-dependent GIST cells. Our findings demonstrate a functional divergence between these paralogs, with the TAZ-CYR61 axis emerging as the principal driver of proliferation and migration in IM-sensitive GIST cells. Thirdly, preliminary results demonstrated a higher expression of YAP1 and TAZ in IM-resistant GIST cells and a functional divergence upon IM treatment.

Beyond providing mechanistic insights, our study highlights the therapeutic potential of targeting TAZ, alone or in combination with YAP1, as a strategy to limit tumor growth and potentially overcome TKI resistance. Transient knockdown strategy, and partial exploration of downstream transcriptional programs, need comprehensive molecular analyses and further validation *in vivo*.

However, this approach not only confirms the translational relevance of RNAi-based therapeutics but also opens avenues for future preclinical optimization, including tumor-targeted delivery, combinatorial strategies with IM or TEAD inhibitors, and exploration of TAZ as a predictive biomarker.

In conclusion, the results of this thesis work advance the field of sarcomas by demonstrating that TAZ is a key oncogenic effector in GIST, capable of sustaining proliferation and that YAP1 and TAZ potentially contributing to therapeutic adaptation. These insights pave the way for future studies aiming to translate Hippo pathway modulation into clinically relevant strategies, ultimately improving outcomes for patients with resistant or aggressive GIST.

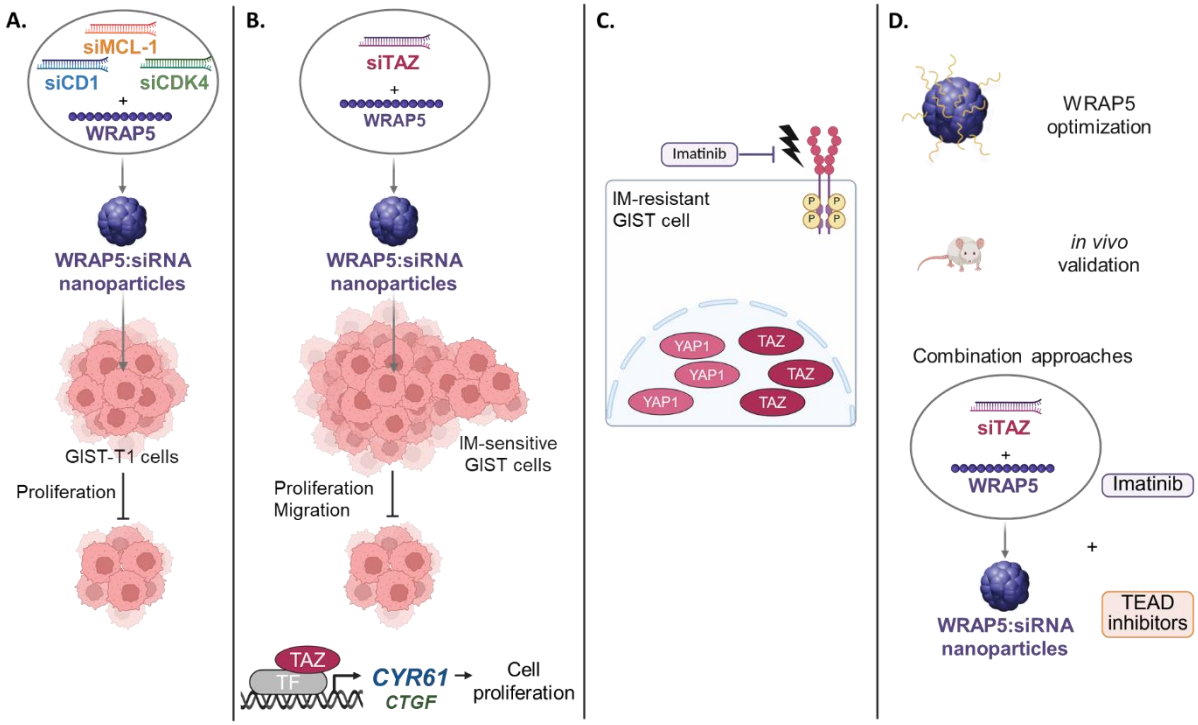

Figure 1: Summary of the main findings and perspectives of this thesis.

WRAP5:siRNA nanoparticles were validated as a versatile tool for simultaneous silencing of multiple targets, effectively reducing GIST cell proliferation (**A**). Functional characterization revealed that TAZ, rather than YAP1, acts as the principal Hippo pathway effector in *KIT*-dependent GIST-T1 cells, driving proliferation and migration through the TAZ-CYR61 axis (**B**). In the context of imatinib resistance, both YAP1 and TAZ remain high expressed, suggesting potential involvement in adaptive mechanisms (**C**). Beyond these mechanistic insights, our results highlight the translational potential of targeting TAZ using WRAP5:siRNA nanoparticles, either alone or in combination with imatinib or TEAD inhibitors. Future directions include optimization of nanoparticle delivery, *in vivo* validation, and exploration of TAZ as a predictive biomarker (**D**).

MATERIALS AND METHODS

1. Used cell lines and culture conditions

Human GIST cells were classified according to *KIT* gene status and their TKI sensitivity (**Table1**). IM-sensitive *KIT*-dependent GIST cell lines had heterozygous primary activating mutations in *KIT*. They included **GIST-T1** (*KIT* exon 11 Δ560-578 in-frame deletion) (García-Valverde et al. 2020; Taguchi et al. 2002), **GIST-882** (*KIT* exon 13 K642E mutation) (Lux et al. 2000), and **GIST-430** cells (*KIT* exon 11 Δ560-576 in-frame deletion) (Garner et al. 2014). IM-resistant *KIT*-dependent GIST cell lines included **GIST-T1/670** (subcell line of GIST-T1 with a secondary exon 14 missense T670I mutation) and **GIST-430/654** cells (subcell line of GIST-430 with a secondary exon 13 missense V654A mutation) (García-Valverde et al. 2020; Garner et al. 2014; Ou et al. 2008). These two human cell lines were established under KIT-selective pressure with IM and have secondary mutations in the ATP-binding pocket. KIT-independent GIST cell line included **GIST-48B** (Garner et al. 2014).

Table 1: List of GIST cell lines available in the laboratory with their KIT mutations, sensitivity to TKI, and corresponding references.

Cell line	KIT status	TKI sensitivity				Reference
		IM	SU	RE	RI	
GIST-T1	Ex. 11 Δ560-578					Cosmo Bio (Japan, Catalog No: PMC-GIST01C)
GIST-T1/670	Ex. 11 Δ560–578 + Ex. 14 T670I					Gift from C. Serrano (Sarcoma Translational Research Laboratory, Vall d'Hebron Institute of Oncology (VHIO), Barcelona, Spain)
GIST-430	Ex. 11 Δ560-576					
GIST-430/654	Ex. 11 Δ560-576 + Ex. 13 V654A					
GIST-882	Ex. 13 K642E					
GIST-48B	KIT-independent					

IM: imatinib; SU: sunitinib; RE : regorafenib ; RI : ripretinib

Sensitive cell line: green / Resistant cell line: red / Uncertain: gray

Sensitivity to TKIs was based on published data and experimental findings (Garner et al., 2014; Schaefer et al., 2022; Serrano et al., 2019).

The GIST-T1 cell line was purchased from Cosmo Bio (Japan, Catalog No: PMC-GIST01C). Initially, it was established from a metastatic sample of an untreated Asian female GIST patient. GIST-882, GIST-430, GIST-T1/670, GIST-430/654, and GIST-48B cell lines were a gift from Dr. C. Serrano (Sarcoma Translational Research Laboratory, Vall d'Hebron Institute of

Oncology (VHIO), Barcelona, Spain). Besides the different genetic mutations, every cell line had a particular morphology (**Figure 1**). All cell lines display an adherent, spindle-shaped morphology characteristic of mesenchymal origin, with cells forming interlacing bundles. Some cell lines, such as GIST-48B, exhibit a more heterogeneous appearance with areas of increased refractility and less uniform cell shapes ("globular-like"), while others like GIST-882 present a more homogeneous, elongated morphology ("lace-like"). These morphological differences may reflect intrinsic genetic variations or responses to specific treatments within each cell line. The growth rate also differs between cell lines and which therefore implies different seeding conditions.

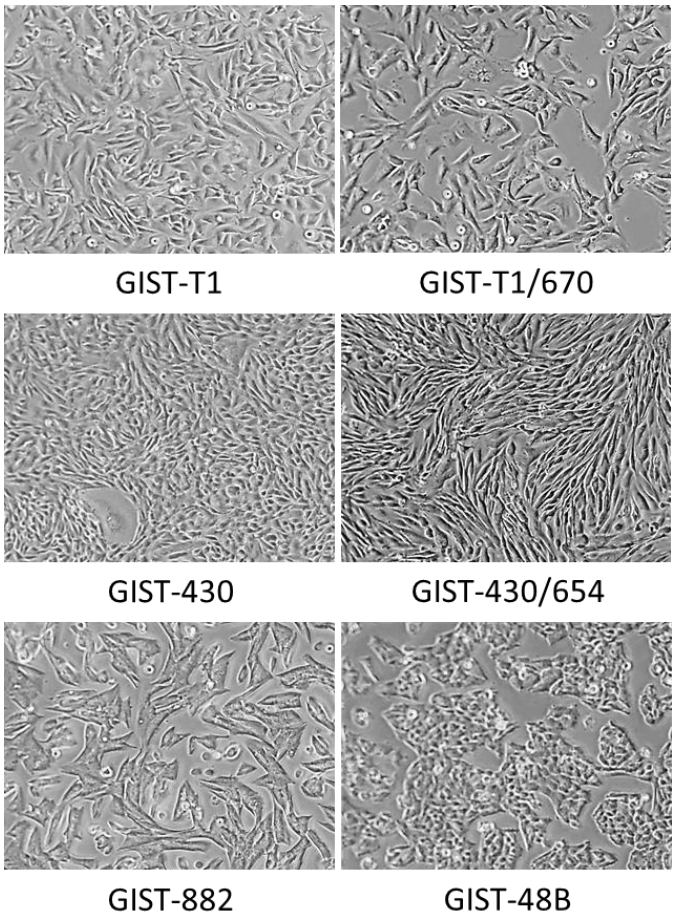

Figure1 : Representative images of GIST cell lines

GIST-T1, GIST-T1/670, GIST-430, GIST-430/654, GIST-882, and GIST-48B images taken using the EVOSTM LX Core microscope system, 100x (AMEX1000, Thermo Fisher Scientific).

GIST-T1 and GIST-T1/670 cells were grown in Dulbecco's Modified Eagle's Medium (DMEM) (Corning, #10-013-CV) supplemented with 10% fetal bovine serum (FBS) (Sigma-Aldrich, #F7524-500ML) and 1% penicillin-streptomycin (Sigma-Aldrich, #P4333-100ML). GIST-430, GIST 430/654, GIST-882, GIST-48B cells were cultured in Iscove's Modified Dulbecco's Medium

(IMDM) (Sigma-Aldrich, #I3390-500ML) supplemented with 15% FBS (Sigma-Aldrich, #F7524-500ML), 1% penicillin-streptomycin (Sigma-Aldrich, #P4333-100ML), and 1% L-Glutamine (Thermo Fisher Scientific, #25030024). GIST430/654 and GIST-T1/670 were maintained with IM (100 nM, Euromedex, STI571, #EU0660-B). All the cells were passaged using Gibco™ Trypsin-EDTA (0.05%), phenol red (Thermo Fisher Scientific, #25300062) and were maintained in a humidified incubator with 5% CO_2 at 37°C. All cultures were tested monthly for mycoplasma contamination using the MycoAlert™ PLUS Mycoplasma Detection Kit (Lonza, #LT07-710**).**

For IM treatment, a stock solution of 1 mM in H_2O was prepared, aliquoted, and stored at -20°C. When mentioned in the Figure legend, GIST-T1 cell lines were incubated with IM at the indicated concentrations.

2. Screening protein expression using a GIST clinical data set

Kaplan–Meier curves of progression-free survival stratified by *YAP1*, *WWTR1* (*TAZ*), *CYR61* and *CTGF* were obtained based on a clinically annotated gene expression data set (ATGsarc) of localized, untreated GIST (n = 60), quantified by microarray (Lagarde et al. 2012). For each gene, patients were divided into high and low expression groups. The cut-off for stratifications was first set at the median expression value, a standard approach in survival analysis to minimize bias from outliers. In addition, the use of the mean expression value as a cut-off was explored to identify the threshold yielding the most significant separation between survival curves (log-rank test). In parallel, box plot analyses were performed to compare the expression levels of these four genes between GIST patients with and without metastasis, providing additional insight into their potential association with disease aggressiveness.

3. Characteristics of the used cell-penetrating peptide

WRAP5 peptide (W5, Patent n°EP18183966) was synthesized at the SynBio3 platform (IBMM Montpellier), and the crude product was purified in-house following a qualitative analysis by HPLC/MS (~95% purity). Its biochemical characteristics are shown in **Table 2**.

Table 2: Biochemical characteristics of WRAP5

ID	Sequence	Number AA	Charges	Reference
WRAP5 (W5)	LLRLLRWWWRLLRLL	15	+5	(Konate et al. 2019)

Stock solution of the WRAP5 peptide were made by dissolving the peptide in pure water (Sigma-Aldrich, #D8537) at a concentration of 400 µM or 40 µM. Absorbance of the peptide solution measured at 280 nm (NanoDrop) was used to calculate the peptide concentration using the Lambert-Beer's Law (ε = 5,550 $L \cdot mol^{-1} \cdot cm^{-1}$ for each tryptophan). W5 stock solution was stored at 4°C.

4. Design of the used siRNA sequences and their characteristics

To design siRNA targeting the gene of interest, we followed a systematic bioinformatics approach for *YAP1*, *TAZ*, *CYR61* and *CTGF* genes. First, the nucleotide sequences of the target gene were retrieved from the National Center for Biotechnology Information (NCBI) database (https://www.ncbi.nlm.nih.gov/nucleotide/) by selecting the appropriate species (*Homo sapiens*) and by choosing the most reliable transcript variant, avoiding predicted versions. The coding sequence (CDS) was extracted in FASTA format. Next, potential siRNA candidates were designed using the RNAxs web tool (http://rna.tbi.univie.ac.at/cgi-bin/RNAxs/RNAxs.cgi). The extracted FASTA sequence was input into RNAxs with default design options, and the maximum number of siRNAs was set to five. The output files containing candidate siRNA sequences were downloaded.

The sequences of the siRNA targeting *CDK4*, *MCL-1*, and *CD1* are taken from the literature.

To ensure specificity, each proposed siRNA sequence (generally 19 to 21 nucleotides long) was subjected to a BLAST search (https://blast.ncbi.nlm.nih.gov/Blast.cgi) using the nucleotide BLAST (blastn) tool. The human genome (taxid:9606) was selected as the reference organism. Each siRNA was analyzed for sequence specificity by evaluating identity percentages, gaps, and alignment length. Only siRNA with high specificity to the target gene, minimal off-target interactions, and no significant matches with essential receptors or proteins were considered. Predicted genes and chromosome sequences were excluded from selection.

siNEG is a control siRNA specifically designed by Eurogentec and guaranteed to have no cellular targets *in vitro* or *in vivo*.

Finally, selected siRNA were synthesized and purchased through Eurogentec (https://www.eurogentec.com/en/) (See **Table 3**). The siRNA stock solutions were prepared in RNase-free water at 200 µM or 20 µM as recommended by the provider and were stored at -20°C. Each siRNA was tested for specificity and efficacy in targeting the gene of interest before selecting the most effective one for subsequent experiments.

Table 3: Used siRNA sequences.

ID	Sense sequence	Anti-sense sequence	Reference
siCDK4	5'-CAU-CGU-UCA-CGA-UCU-GdTdT-3'	5'-CAG-AUC-UCG-GUG-AAC-GAU-GdTdT-3'	(Mao et al. 2014)
siMCL-1	5'-AUA-ACA-GGU-AUA-AAA-GUC-CdTdT-3'	5'-GGA-CUU-UUA-UAC-CUG-UUA-UdTdT-3'	(Dzmitruk et al. 2015)
siCD1	5'-ACA-GAU-GUG-AUC-AUU-UdTdT-3'	5'-AAA-UGA-ACU-UCA-CAU-CUG-UdTdT-3'	(Champagne et al. 2020)
siYAP1	5'-CUA-UGU-UCA-UUC-CAU-CUC-CdTdT-3'	5'-GGA-GAU-GGA-AUG-AAC-AUA-GdTdT-3'	This work
siYAP1'	5'-AUA-GUA-AAU-UUC-UCC-AUC-CdTdT-3'	5'-GGA-UGG-AGA-AAU-UUA-CUA-UdTdT-3'	This work
siTAZ'	5'-AUU-AUU-AGU-GAU-GGA-UCU-CdTdT-3'	5'-GAG-AUC-CAU-CAC-UAA-UAA-UdTdT-3'	This work
siTAZ	5'-AAA-UCA-GGG-AAA-CGG-GUC-UdTdT-3'	5'-AGA-CCC-GUU-UCC-CUG-AUU-UdTdT-3'	This work
si(YAPTAZ)	5'-UGU-GGA-UGA-GAU-GGA-UAC-AdTdT-3'	5'-UGU-AUC-CAU-CUC-AUC-CAC-AdTdT-3'	(Tiffon et al. 2020)
siCYR61	5'-AUC-AUC-AUG-ACG-UUC-UUG-GdTdT-3'	5'-CCA-AGA-ACG-UCA-UGA-UGA-UdTdT-3'	This work
siCYR61'	5'-UUG UUU CUC GUC AAC UCC AdTdT-3'	5'-U GGA GUU GAC GAG AAA CAA-dTdT-3'	This work
siCTGF	5'-AAU-UUA-GCU-CGG-UAU-GUC-UdTdT-3'	5'-AGA-CAU-ACC-GAG-CUA-AAU-UdTdT-3'	This work
siCTGF'	5'- AUU UUG GGA GUA CGG AUG CdTdT-3'	5'- GCA UCC GUA CUC CCA AAA U-dTdT-3'	This work
siNEG	Confidential	Confidential	Negative Control siRNA, Eurogentec, Réf. SR-CL000-005

In order to evaluate the cellular internalization of siRNA in confocal microscopy, fluorescence-labeled siRNA were used : red = siCD1-Alexa550, green = siCDK4-Alexa488, magenta = siMCL-1-Atto654.

5. How to formulate and characterize WRAP-based nanoparticles

5.1. Formulation of the WRAP5:siRNA nanoparticles

Nanoparticles were formulated in pure water supplemented by 5% glucose (Sigma-Aldrich, #50-99-7) by mixing equal volumes of siRNA and WRAP5 at the corresponding molar ratio (R = 20) at room temperature (**Figure 2**). The molar ratio R = 20 corresponded to a 20-fold higher molar concentration of WRAP5 compared to the siRNA, as already described (Konate et al. 2019). As an example, R=20 corresponds to 20-fold higher molar concentration of peptides compared to the siRNA (800 nM WRAP5 for 40 nM siRNA).

For WRAP5 nanoparticles encapsulating three siRNA, a cocktail was pre-mixed according to siRNA stoichiometry 30% siCD1, 40% siCDK4, and 30% siMCL-1 (ratio 6/8/6) before mixing with the WRAP5 peptide. For WRAP5 nanoparticles encapsulating two siRNA (siYAP1+siNEG or siTAZ+siNEG or siYAP1+siTAZ), the two siRNAs were pre-mixed according to siRNA stoichiometry 1:1 and then mixed to the WRAP5 peptide.

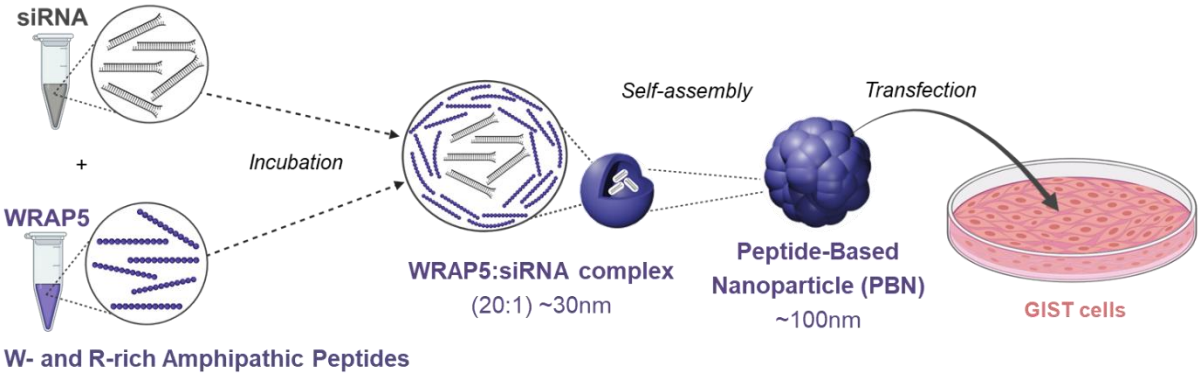

Figure 2: Schematic representation of WRAP:siRNA nanoparticle formulation for the subsequent cell transfection.

5.2. Characterization of the WRAP5:siRNA nanoparticles by dynamic light scattering

WRAP5:siRNA nanoparticles (WRAP5 = 10 µM, siRNA = 500 nM, R = 20) were evaluated with a Zetasizer NanoZS (Malvern) in terms of mean particle size (Z-average diameter) of the particle distribution and the polydispersity index (PdI). Z-average diameter corresponded to the intensity-weighted mean hydrodynamic size of the ensemble collection of nanoparticles measured, and the PdI indicated the homogeneity of nanoparticle suspension (a perfectly

uniform sample would have a PDI close to 0.0). All results were obtained from three independent measurements (three runs for each measurement at 25°C) as described (Konate et al. 2019).

6. WRAP5:siRNA evaluation in cells

6.1. Cell transfection of WRAP5:siRNA nanoparticles

In most of the transfection reactions, WRAP5:siRNA transfection was performed by first adding 4/10 of the total well volume with serum-free medium, followed by 1/10 of the total volume with the nanoparticle solution. After 1.5 hours, 5/10 of the total volume with serum-containing medium was added to achieve a final 10% or 15% FBS concentration, depending on the cell line, without removing the transfection reagents as described before (Konate et al. 2019; 2021; Konate, Pezzati, et al. 2025).

For Western blot assays, RNA extraction, qPCR analysis, protein localization by microscopy, cell counting, and wound healing, GIST cell lines were seeded and transfected as described in **Table 4**. After 1.5 hours, the appropriate culture medium supplemented with 20% FBS for GIST-T1 and GIST-T1/670 (final FBS concentration = 10%) or 30% FBS for GIST-430, GIST-882 and GIST-430/654 (final FBS concentration = 15%) was added to each well, without removing the transfection reagents. The cells were incubated for an additional period of 24 to 48 hours, depending on the assay.

For cellular internalization in leaving cells, GIST-T1 cells were seeded and transfected in serum free medium (1,800 µL = 9/10) by adding the WRAP5:siRNA-fluo nanoparticles (200 µL = 1/10) (**Table 4**), for 4 hours and then directly imaged.

For MTT assay, GIST-T1 cells were seeded and transfected in serum free medium (80 µL = 8/10) by adding the WRAP5:siRNA nanoparticles (10 µL = 1/10). After 1.5 hours, pure FBS (10 µL = 1/10) was added to reach a final FBS concentration of 10%, without removing the transfection reagents (**Table 4**). The cells were incubated for an additional period of 24 hours.

Table 4: Experimental conditions for GIST cell transfection.

Cell line	Seeding	Time *	well	Transfection			Experiment
				Medium 0% FBS	WRAP5: siRNA	Medium	
GIST-T1	300,000 150,000	24 h	P6 P12	800 µl 200 µl	200 µl 50 µl	1,000 µl # 250 µl #	WB, RNA extraction, qPCR
GIST-430	700,000	24 h	P6	800 µl	200 µl	1,000 µl ##	
GIST-882	500,000	48 h	P6	800 µl	200 µl	1,000 µl ##	
GIST-T1	300,000	24 h	P6	1,800 µl	200 µl	/	Cellular internalization
	150,000	24 h	P12	400 µl	100 µl	500 µl #	Protein localization
	10,000	24 h	P96	80 µl	10 µl	10 µl ###	MTT assay
	100,000	24 h	P12	400 µl	100 µl	500 µl #	Cell counting
	100,000	24 h	P12	90 µL	10 µL	10 µL ###	Wound healing
	350	24 h	P6	1,700 µL	300 µL	2,000 µL ####	Clonogenic assay

Footnote: * = time before transfection; #Medium with 20% FBS, ##Medium with 30% FBS, ###Pure FBS, ####replacement of the media by fresh DMEM media containing 10% FBS.

6.2. Cell toxicity measurement by LDH assay

To confirm that the WRAP5-based nanoparticles do not affect cell viability, an evaluation of the toxicity was performed in parallel to the Western blot analyses using the Cytotoxicity Detection Kit^{Plus} (ref. 4744926001, Sigma-Aldrich) following the manufacturer's instructions.

The LDH cytotoxicity assay is a simple and rapid method for measuring cell death by detecting lactate dehydrogenase (LDH) released from damaged cells. LDH is a stable enzyme present in all cells and is quickly released into the culture medium when the plasma membrane is compromised. The assay quantifies LDH activity through a coupled enzymatic reaction that produces a colored formazan product, with the intensity of the color directly reflecting the number of lysed cells and thus the level of cytotoxicity (**Figure 3**).

At least one well of the 6-well plate was used as an LDH positive control (100% toxicity) by adding Triton X-100 (Sigma-Aldrich, #3402420090) to a final concentration of 0.1% (~15 min incubation at 25°C). Afterward, 50 µL supernatant of each well was transferred to a new clear Greiner Bio-One 96-well plate (Dutscher, #655101). 50 µL of the “dye solution/catalyst” mixture was added to the supernatant and incubated in the darkness for 30 min at room

temperature. The reaction was stopped by adding 25 µL of HCl (1 N) to each well before measuring the absorption at 490 nm.

Cell toxicity was obtained using the following formula:

$$\text{Relative toxicity (\%)} = \frac{\text{value(sample)} - \text{value(non treated cells or WRAP5:siNEG)}}{\text{value(triton)} - \text{value(non treated cells or WRAP5:siNEG)}} * 100$$

This approach normalizes the absorbance readings by comparing sample cell toxicity to the non-treated group or WRAP5:siNEG control.

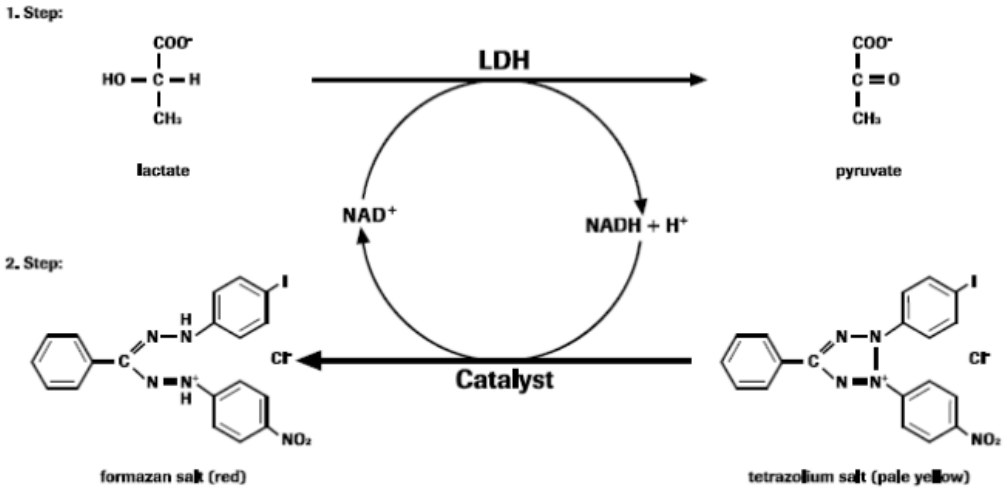

Figure 3: Schematic representation of the LDH cytotoxicity assay.
In the first step, lactate dehydrogenase (LDH) catalyzes the conversion of lactate to pyruvate, accompanied by the reduction of NAD^+ to NADH + H^+. In the second step, a catalyst mediates the transfer of electrons from NADH to a tetrazolium salt (pale yellow), reducing it to a colored formazan product (red). The amount of formazan formed is proportional to the LDH activity and thus to the extent of cell membrane damage.

6.3. Protein expression evaluation by Western blot

Transfected cells were washed with Dulbecco's Phosphate-Buffered Saline (DPBS) 1X (Corning, #21-031-CV) and lysed in RIPA buffer [50 mM Tris pH 8.0, 150 mM sodium chloride, 1% Triton X-100, 0.1% SDS (sodium dodecyl sulfate, Sigma-Aldrich, #436143)], supplemented with SigmaFAST protease inhibitors (S8820, Sigma-Aldrich) and PhosSTOP phosphatase inhibitors (Roche, #04906845001). Cells were incubated for 5 min on ice with 130 µL RIPA lysis buffer, then scraped and transferred to a 1.5 mL tube. After an additional 5-minute incubation on ice, lysates were centrifuged (10 min, 16,100 g, 4°C), and the supernatants were collected. Protein concentrations were determined using the Pierce BCA Protein Assay (Thermo Fisher Scientific, #10741395) according to the manufacturer's instructions. To standardize protein loading, all samples were diluted in lysis buffer to match the lowest protein concentration. A 1:1 volume

of 2X Laemmli Sample Buffer (Bio-Rad, #1610737) containing 5% β-mercaptoethanol was then added to each sample. Samples were heated at 95°C for 10 minutes, immediately placed on ice, and stored at -20°C until performing SDS-PAGE (sodium dodecyl sulfate–polyacrylamide gel electrophoresis).

Cell extracts (5 to 10 µg of proteins) were separated on a 4-20% Mini-PROTEAN® TGX™ Precast Gel (Bio-Rad, #4561094) using 1X Tris-Glycerine-SDS running buffer (TG-SDS 10X, Euromedex, #EU0510) and then transferred onto a Trans-Blot® Turbo™ Mini PVDF Transfer Membrane (Bio-Rad, #1704156).

For membrane incubation, 10X Tris-Buffered Saline (TBS) solution was prepared by dissolving 80 g NaCl, 2 g KCl, and 61 g Tris base (all from Sigma) in 800 mL of Milli-Q water, adjusting the pH to 8.0 with HCl, and completing the volume to 1 L with Milli-Q water. Membranes were then blocked with 1X TBS solution containing 0.2% or 0.5% Tween (Euromedex, #EU0660-B) and 5% BSA (Sigma-Aldrich, #A2135-100G). The membranes were subsequently incubated with the appropriate primary antibody (**Table 5**) in the same blocking buffer overnight at 4°C. After three washes with 1X TBS-Tween, membranes were incubated for 1.5 hours with the corresponding HRP-conjugated secondary antibody in blocking buffer. Three additional washes were performed before chemiluminescent detection.

Table 5: List of antibodies for Western blot.

Target (Protein)	MW (kDa)	Host Species	Clone / Catalog Number	Dilution	Company / Supplier
CDK4	30	Rabbit	D9G3E / #12790	1:1,000	Cell Signaling
CD1	37	Rabbit	SP4 / #MA5-16356	1:1,000	Thermo Fisher Scientific
Mcl-1	40	Rabbit	D5V5L / #39224	1:1,000	Cell Signaling
YAP1	65 - 78	Rabbit	D8H1X / #14074	1:1,000 (GIST-T1) 1:5,000 (GIST-882) 1:10,000 (GIST-430)	Cell Signaling
TAZ	55	Rabbit	E9J5A / #72804	1:1,000 (GIST-T1 and GIST-882) 1:5,000 (GIST-430)	Cell Signaling
Phospho-YAP (Ser127) (pYAP1)	65-78	Rabbit	#4911	1:1000	Cell Signaling
Phospho-WWTR1 (Ser89) (pTAZ)	50-55	Rabbit	#PA5-105066	1:1000	ThermoFisher Scientific

KIT (CD117)	145	Rabbit	#DB062	1:1,000	DB Biotech
Phospho-c-KIT (pKIT)	145	Rabbit	Tyr703 D12E12 / #3073	1:1,000	Cell Signaling
AKT	60	Rabbit	#9272	1:1,000	Cell Signaling
Phospho-AKT (pAKT)	60	Rabbit	Ser473 D9E / #4060	1:1,000	Cell Signaling
p44/42 MAPK (Erk1/2)	42, 44	Mouse	L34F12 / #4696	1:1,000	Cell Signaling
Phospho-p44/42 MAPK (Erk1/2)	42, 44	Rabbit	Thr202/Tyr204 20G11 / #4376	1:1,000	Cell Signaling
CYR61	41	Rabbit	D4H5D / #14479	1:1,000	Cell Signaling
CTGF	35	Rabbit	D8Z8U / #86641	1:1,000	Cell Signaling
CD1	34	Rabbit	SP4 / #MA5-16356	1:1,000	ThermoFisher Scientific
Vinculin	124	Rabbit	E1E9V / #13901	1:1,000	Cell Signaling
α-Actinin	100	Rabbit	D6F6 / #6487	1:1,000	Cell Signaling
β-Actin	42	Mouse	#A5441	1:10,000	Sigma-Aldrich
Cofilin	19	Rabbit	D59/#3318S	1:1,000	Cell Signaling
Anti-Rabbit	/	IgG, HRP	#7074	1:1,000	Cell Signaling
Anti-Mouse	/	IgG, HRP	#7076	1:10,000 (β-Actin) 1:1,000 (others)	Cell Signaling

Proteins on the PVDF membrane were revealed by chemiluminescence using either the SuperSignal™ West Pico^{PLUS} Chemiluminescent Substrate (Thermo Fisher Scientific, #34578) or the SuperSignal™ West Femto Maximum Sensitivity Substrate (Thermo Fisher Scientific, #34095), depending on the used antibody, and imaged using a Sapphire RGB & NIR Biomolecular Scanner (Azure Biosystems). Vinculin, α-actinin, or β-actin proteins were used as loading controls depending on the experiment.

The signal intensities of the blots were quantified using Fidji ImageJ software. Each band intensity corresponding to a distinguished condition was then normalized to the band intensity of non-treated cells or WRAP5:siNEG control (= 100%):

$$\text{Relative Signal Intensity (\%)} = \frac{\text{Intensity(sample)}}{\text{Intensity(non treated cells or WRAP5:siNEG)}} * 100$$

6.4. RNA extraction and qPCR

Total RNA was extracted from cell cultures using the RNeasy® Mini Kit (Qiagen, #74104), following the manufacturer's protocol with some modifications. Specifically, cells were lysed in 230 µL of RLT buffer per well for a 6-well plate. RLT buffer contains primarily guanidine isothiocyanate, a potent chaotropic agent that denatures proteins and inactivates RNases, thereby protecting RNA during extraction.

The lysates were then processed according to the manufacturer's instructions to obtain RNA samples. RNA quality and concentration were assessed using a NanoDrop™ One spectrophotometer (Thermo Scientific).

The extracted RNA was then reverse transcribed into complementary DNA (cDNA) using 500 ng of RNA as the input material. The reverse transcription was carried out using the Verso cDNA Synthesis Kit (AB-1453/B, Thermo Scientific), according to the manufacturer's instructions. Following the synthesis, the cDNA was diluted to a final concentration of 2.5 ng/µL for use in subsequent qPCR analysis.

qPCR was performed using LightCycler® technology (Roche Diagnostics). PCR primers were designed using the LightCycler Probe Design 2.0 software for some targets, while others were sourced from the literature. Detailed primer sequences were provided in **Table 6**. Primers were ordered at Eurofins, solubilized in RNAse-free water, and stored at -20°C. To ensure primer specificity, each primer was verified through a BLAST (Basic Local Alignment Search Tool) search to confirm that there were no mismatches and that only the target of interest was amplified. Additionally, the efficiency of each primer was validated by performing a dilution series of cDNA ranging from 10 ng to 0.001 ng of cDNA per reaction. This validation step ensured that the primers worked efficiently across a wide range of template concentrations and that amplification was specific to the target sequence. For each qPCR reaction, 5 ng of cDNA was added per well in a 96-well qPCR plate, in a final reaction volume of 10 µL. Reactions were carried out using the SYBR Green detection method (Roche Diagnostics, #04887352001), qPCR was conducted in technical triplicate, and standard curves were generated for each primer pair to assess amplification efficiency. Data were normalized to the reference genes HPRT1, and relative gene expression was calculated using the 2^−ΔΔCt method, which compared the Ct values (threshold cycle) of the target genes relative to the

reference genes and the calibrator sample. All qPCR reactions were performed in a LightCycler® 480 System (Roche Diagnostics, #05015243001), and the results were analyzed and presented as mean gene expression levels relative to the reference genes.

Table 6: Human gene-specific primers used for RT-qPCR

Target	Forward primer (5'-3')	Reverse primer (5'-3')	Amplicon (bp)	Reference
YAP1	CACAGCATGTTCGAGCTCAT	GATGCTGAGCTGTGGGTGTA	120	(Molina-Castro et al. 2020)
TAZ	TGCCGTCAGTTCCACAC	GTTCTGCTGGCTCAGGGT	115	This work
CYR61	GGAGCCTCGCATCCTAT	ATTGGTAACTCGTGTGGAGA	115	(Guérin et al. 2020)
CTGF	TTCAAGTGCCCTGACGG	GCGATTCAAAGATGTCATTGTCTC	117	This work
HPRT1	TGGTCAGGCAGTATAATCCA	GGTCCTTTTCACCAGCAAGCT	59	(Molina-Castro et al. 2020)

7. Confocal microscopy

7.1. WRAP5-based nanoparticles cellular internalization

To assess the cellular internalization of WRAP5-based nanoparticles, confocal microscopy was performed using fluorescence-labeled siRNA (Alexa550, Alexa488, Alexa655). GIST-T1 cells (300,000 per well) were seeded in glass-bottom dishes (FluoroDish, 35 mm, Dutscher, #WFD35-100) 24 hours before imaging. Cells were incubated with the nanoparticles as described in section 6.1. After 4 hours incubation, nuclei were stained with Hoechst 33342 dye (Sigma-Aldrich) for 10 minutes. Cells were then washed twice with DPBS 1X and maintained in FluoroBrite DMEM (Thermo Fisher Scientific, #A1896701) for live imaging.

Confocal images were acquired using an inverted Zeiss LSM800 microscope with an Apo 63x/1.2 W DICIII objective. Fluorescence detection was performed with the following diode lasers: 405 nm (Hoechst, 400–456 nm), 488 nm with an Alexa488 filter (500 nm - 542 nm), 561 nm with an Alexa550 filter (560 nm - 617 nm) and 640 nm with an Alexa655 filter (656 nm - 700 nm). To minimize crosstalk between fluorophores, sequential image acquisition was used. All images were processed with Fiji ImageJ software, applying uniform brightness and contrast adjustments across all samples.

7.2. YAP1 and TAZ localization by immunofluorescence

To visualize the cytoplasmic and nuclear localization of YAP1 and TAZ in GIST-T1 cells following WRAP5:siRNA-mediated knockdown (siYAP1 and/or siTAZ for 24 hours), we performed immunofluorescence analysis using confocal microscopy. After transfection, cells were fixed with 2% paraformaldehyde (PFA, EUROMEDEX, #EM-15714), permeabilized with DPBS1X containing 0.1% TritonX100, blocked with DPBS1X containing 0.1% Tween-20 and 4% donkey serum. Afterward, cells were incubated overnight with primary antibodies (see

Table 7), followed by a 1-hour incubation with secondary antibodies. Nuclear staining was performed using Hoechst (1 mg/mL, Sigma-Aldrich, #14533), and membrane actin was labeled with Phalloidin Alexa Fluor™ Plus 647 (1:800, Thermo Fisher Scientific, #A22287). To visualize YAP1 and TAZ simultaneously, a mixed antibody staining approach was used. Finally, the cells were washed with DPBS three times and mounted with poly-(vinyl alcohol) Mowiol™ 4–88 glycerol Tris buffer (Biovalley) on glass slides. Confocal images were acquired using an inverted Zeiss LSM800 microscope with an Apo 63x/1.2 W DICIII objective. To minimize fluorophore crosstalk, sequential image acquisition was applied. For each sample, 4 different position were selected for a z-stack mode acquisition (15 images with a z-stack interval of 0.22 µm. Acquired images were analyzed using Fiji (ImageJ) software. Z-projection for each sample was performed by summing fluorescence intensities to one image. The threshold of each sample was adjusted to quantify the mean fluorescence of the image.

Table 7: List of antibodies for Immunofluorescence.

Target (Protein)	MW (kDa)	Host Species	Clone / Catalog Number	Dilution	Company / Supplier
YAP1	65-70	Mouse	66900-1	1:800	Proteintech
TAZ	55	Rabbit	E9J5A / #72804	1:500	Cell Signaling
Anti-Rabbit Alexa Fluor™ 488	/	Donkey	#A31570	1:1,000	Invitrogen
Anti-Mouse Alexa Fluor™ 555	/	Donkey	#A21206	1:1,000	Invitrogen

8. Assays for cellular biological activities

8.1. Clonogenic assay

We chose to perform a clonogenic assay to assess cell survival. The clonogenic assay measures the ability of a single cell to grow into a colony, reflecting its capacity for unlimited proliferation. Cells were first plated at low density and allowed to grow for several weeks; colonies formed were then fixed, stained, and counted. The number of colonies indicates the fraction of cells that retained their reproductive viability after treatment, making this assay a gold standard for assessing the long-term effects of therapeutics, specifically anti-cancer, on cell survival and proliferation.

A total of 350 GIST-T1 cells were plated in 6-well plates 24 hours before the start of the experiment. For nanoparticle exposure, cells were treated with 1.7 mL of fresh, pre-warmed serum-free DMEM supplemented with 300 µL of nanoparticle solution at the desired concentrations, or with 300 µL of 5% glucose solution for the untreated control condition (N.T.). Following a 1.5-hour incubation period, the medium was aspirated and replaced with 2 mL of DMEM containing 10% FBS. The cells were then maintained in culture for 14 days. After this incubation period, the medium was discarded, and the transfected GIST-T1 cells were washed twice with PBS1X. Cells were subsequently fixed using 0.5 mL per well of 4% PFA solution. After a 10-minute fixation, cells were rinsed twice with PBS1X, and 0.5 mL per well of crystal violet staining solution (prepared in 10% ethanol) was applied for 10 minutes to visualize cell colonies. The staining solution was then removed, and the wells were thoroughly rinsed with water or PBS1X until the background was clear. Once air-dried, images of the entire 6-well plate were captured using the Sapphire RGB & NIR Biomolecular Scanner (Azure Biosystems).

Colony counts for each condition were performed manually and expressed relative to the non-treated control on the same plate, using the following formula:

$$\text{Colonies counted } [\%\text{ of N.T.}] = \frac{\text{number of colonies (condition x)}}{\text{number of colonies (N.T.)}} * 100$$

8.2. Cell proliferation

Cell proliferation, defined as the increase in cell number over time due to cell growth and division, was assessed in this study using two complementary methods: the MTT (CellTiter96®) assay to measure metabolic activity and by counting cells to determine cell density.

8.2.1. MTT assay using the CellTiter96® kit

Cell proliferation was assessed using the CellTiter 96® Non-Radioactive Cell Proliferation Assay (Promega, #G4000), in which the luciferase-catalyzed luciferin/ATP reaction provided an indicator of cell number, based on the enzymatic conversion of MTT (3-[4,5-dimethylthiazol-2-yl]-2,5 diphenyl tetrazolium bromide) into a colored formazan product (**Figure 4**). The manufacturer's protocol was followed with slight modifications. GIST-T1 cells were plated in complete DMEM using 96-well plates at a density of 10,000 cells per well and incubated for 24 h. Following this, transfection with WRAP5:siRNA (1,200 nM:60 nM) or IM treatment when needed (200 nM) were performed in a total volume of 100 µL per well, as described in section 6.1. All experiments were conducted in quintuplicate. To obtain the IC50 value of imatinib (IM) in GIST-T1 cells, IM treatment was conducted 24 hours after transfection. At 48 hours post-transfection, depending on the experiment, 15 µl of the Dye Solution was added to each well, and the plate was incubated for 2 hours. Subsequently, 100 µl of the Solubilization Solution/Stop Mix was added to each well, and the plate was incubated at room temperature for 1 hour on a shaker to ensure a uniformly colored solution. Cell proliferation was measured using a microplate reader (Tecan M200) at 570 nm to quantify formazan formation and at 630 nm to minimize background interference from cell debris and nonspecific absorbance.

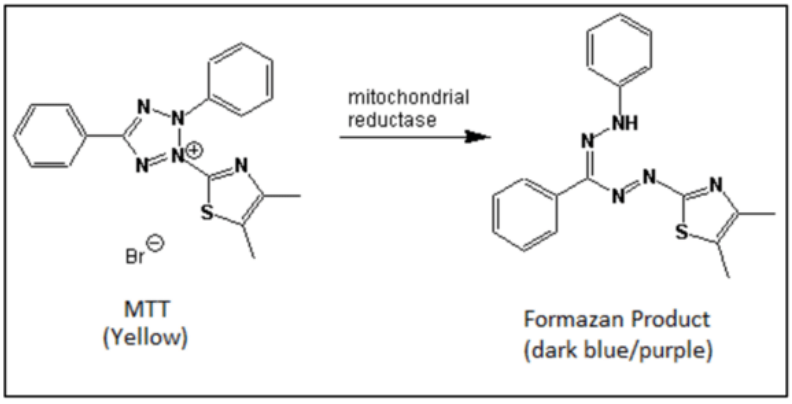

Figure 4: Schematic representation of the MTT assay.

The yellow MTT compound (3-(4,5-dimethylthiazol-2-yl)-2,5-diphenyltetrazolium bromide) is reduced by mitochondrial reductase enzymes in metabolically active cells to form an insoluble dark blue/purple formazan product. This colorimetric change is commonly used to assess cell viability and metabolic activity.

Cell proliferation was obtained using the following formulas:

Corrected Absorbance = [(Abs_{570}(Sample) - Abs_{570}(Background)) - (Abs_{630}(Sample) - Abs_{630}(Background))]

$$\text{Cell Proliferation Index} = \frac{\text{Corrected Absorbance (Sample)}}{\text{Mean Corrected Absorbance (WRAP5:siNEG)}}$$

This approach normalized the absorbance readings by removing background interference and by comparing sample proliferation to the WRAP5:siNEG control. The background group was defined as the absorbance of wells containing medium without cells and could be attributed to the chemical interference of certain compounds with the tetrazolium reduction reactions.

8.2.2. Counting cells

GIST-T1 cells were seeded at a density of 100,000 per well in complete DMEM using 12-well plates. Transfection of WRAP5:siRNA (800 nM: 40 nM) and IM treatment (50 nM) were performed in duplicate 24 hours after seeding as previously described in section 6.1. Measurements were taken at 0, 24, 48, and 72 hours post-treatment following an established protocol. Before counting, viable cells were washed twice with DPBS 1X and incubated for 5 minutes with 100 µL of Trypsin-EDTA (0.05%) containing phenol red to detach the adherent cells. The resulting suspension was brought to a final volume of 1,000 µL by adding 900 µL of DPBS 1X. Proliferation was assessed using the CellDrop BFx automated counter (DeNovix) with the Brightfield program. A custom program optimized for GIST-T1 was used to ensure precise quantification. For each well, three or four independent counts were performed on 10 µL aliquots, and the average was used to determine the final cell concentration (cells/mL). To assess cell growth, counts at each time point were normalized to the mean count at 0 hour. After the measurements, the plates were discarded.

8.3. Wound healing assay

A wound healing assay was performed to assess the migratory capacity of GIST-T1 cells. To standardize the procedure, a 4-well culture insert (Ibidi GmbH, #80469) was used in a 12-well plate. To minimize evaporation, 700 µL of medium was added to the area surrounding the insert. Next, 110 µL of a cell suspension at a density of 110,000 cells per well in complete DMEM was carefully added to each well of the insert. Transfection with WRAP5:siRNA

(1,600 nM:80nM) was performed 24 hours after seeding. The medium was gently removed, and 90 µL of serum-free medium was added, followed by 10 µL of WRAP5:siRNA nanoparticle solution. The cells were incubated for 1.5 hours at 37°C, after which 10 µL of pure serum was added to each well. After 24 hours, the insert was carefully removed from each well. If necessary, 1-2 washes with serum-free DMEM medium were performed to remove detached cells and debris. Each well was then filled with 1 mL of complete DMEM and further incubated at 37°C in an humid incubator.

Images of the wound area were captured immediately after insert removal (t=0 hour) and at 48 hours (72 hours post-transfection) using the EVOS® LX Core microscope system (AMEX1000, Thermo Fisher Scientific), equipped with a 3.1 megapixel color camera (2048 x 1536 pixels, 1/2-inch sensor) and a resolution of 1024 x 768 pixels. The wound area on the acquired images was quantified using the Wound_healing_size_tool.ijm plugin in ImageJ, with adjusted parameters: Variance 10, Threshold 25, and Saturation 0.200. The percentage of wound closure was calculated by subtracting the area at t=0 hour from the area at t=48 hour, and the results were normalized to the WRAP5:siNEG condition to assess cell migration.

9. Impact of an IM treatment on GIST-T1 cells

9.1. Time-dependent effect of IM on protein expression in GIST-T1 cells

GIST-T1 cells were seeded in 35-mm diameter dishes at a density of 300,000 cells per dish. After 24 hours, cells were treated with 0.5 µM IM or left untreated as a control. Cells were collected at 4, 24, 48, and 72 hours post-treatment. For collection, the culture medium was removed, and cells were washed once with DPBS 1X. Cells were then scraped, pooled from three dishes per condition, and transferred into 1.5 mL tubes. Samples were centrifuged at 300 × g for 10 minutes at 4°C. The supernatant was discarded, and the cell pellets were flash-frozen in liquid nitrogen before storage at -80°C until further experimentation. Finally, cell pellets were lysed, protein amounts were quantified, and Western blot analyses were performed, as described in Section 6.3. KIT, phospho-KIT, YAP1, and TAZ protein expression levels were calculated, normalized to β-ACTIN or α-ACTININ.

9.2. Determination of the IM IC_{50} value after GIST-T1 cell incubation

The IC_{50} of IM was determined using the CellTiter96® assay at 48 hours post-treatment. The IC_{50}, or half-maximal inhibitory concentration, represented the concentration of IM required to reduce cell viability by 50% compared to untreated controls. GIST-T1 cells were seeded following the same procedure described in Section 5.1.1, with modifications. 24 hours after seeding, cells were treated with increasing concentrations of IM (0.1, 1, 4, 6, 8, 10, 20, 40, 60, 80, 100, 200, 400, 600, 800, and 1,000 nM) prepared from a 1 µM stock solution. After 48 hours of treatment, cell proliferation was assessed by measuring the corrected absorbance using the CellTiter96® kit following the formula:

$$\text{Corrected Absorbance} = [(Abs_{570}(\text{Sample}) - Abs_{570}(\text{Background})) - (Abs_{630}(\text{Sample}) - Abs_{630}(\text{Background}))]$$

To determine the IC_{50} value, IM concentrations were transformed to a logarithmic scale in GraphPad Prism 8.0.1 software (GraphPad Software, Inc.) and plotted against the corrected absorbance. A nonlinear regression analysis using the log(inhibitor) *versus* normalized response-variable slope (four parameters: top, bottom, logIC_{50} and hill slope) model was applied to derive from the resulting dose-response curve the IC_{50} value. IC_{50} values were compared between conditions by an extra sum-of-squares F test and reported IC_{50} were mean estimated with 95% confidence intervals.

10. Statistical analyses

All statistical analyses were performed using GraphPad Prism (version 8.0.1). Data are presented as mean ± standard deviation (SD) or standard error of the mean (SEM) when appropriate, based on at least three independent experiments. Normality of data distribution was assessed using the Shapiro-Wilk test. When data did not follow a normal distribution, the Kruskal-Wallis test was used for multiple comparisons, as it is a non-parametric alternative to one-way ANOVA that does not assume normality, with Dunn's correction applied for pairwise comparisons to either siNEG-treated cells or untreated cells. When residuals followed a Gaussian distribution and equal standard deviations were confirmed, a one-way ANOVA was performed for multiple comparisons, followed by Dunnett's post-hoc test to compare each condition to either untreated cells or the siNEG-treated cells. In a case of two-group

comparison, an unpaired two-tailed Student's t-test was applied. A 95% confidence interval was applied to all tests, and statistical significance (p-value) was defined as follows: ns (not significant) >0.05, * <0.05, ** <0.01, *** <0.001, and **** <0.0001. In the figures, the number of biological replicates (N) and the number of measurements made within each biological replicate (n) are shown.

11. Editorial assistance

To improve the clarity and fluency of the English writing, digital writing assistance tools were used (Grammarly, DeepL Write, ChatGPT and PerplexityPRO). These tools were employed solely for language refinement. The accuracy and scientific content of the thesis were carefully verified through manual reviewing.

12. Illustration tools

Most of the figures and graphical representations included in this thesis were created with BioRender (www.biorender.com).

REFERENCES

REFERENCES

Adams, David, Alejandra Gonzalez-Duarte, William D. O'Riordan, et al. 2018. "Patisiran, an RNAi Therapeutic, for Hereditary Transthyretin Amyloidosis." *The New England Journal of Medicine* 379 (1): 11–21. https://doi.org/10.1056/NEJMoa1716153.

Ainsua-Enrich, Erola, Eva Serrano-Candelas, Damiana Álvarez-Errico, et al. 2015. "The Adaptor 3BP2 Is Required for KIT Receptor Expression and Human Mast Cell Survival." *Journal of Immunology* 194 (9): 4309–18. https://doi.org/10.4049/jimmunol.1402887.

Akao, Ken, Tatsuhiro Sato, Emi Mishiro-Sato, et al. 2025. "TEAD-Independent Cell Growth of Hippo-Inactive Mesothelioma Cells: Unveiling Resistance to TEAD Inhibitor K-975 through MYC Signaling Activation." *Molecular Cancer Therapeutics* 24 (5): 709–19. https://doi.org/10.1158/1535-7163.MCT-24-0308.

Alagia, Adele, and Ramon Eritja. 2016. "siRNA and RNAi Optimization." *WIREs RNA* 7 (3): 316–29. https://doi.org/10.1002/wrna.1337.

Aldrian, Gudrun, Anaïs Vaissière, Karidia Konate, et al. 2017. "PEGylation Rate Influences Peptide-Based Nanoparticles Mediated siRNA Delivery in Vitro and in Vivo." *Journal of Controlled Release* 256: 79–91. https://doi.org/10.1016/j.jconrel.2017.04.012.

Aleku, Manuela, Petra Schulz, Oliver Keil, et al. 2008. "Atu027, a Liposomal Small Interfering RNA Formulation Targeting Protein Kinase N3, Inhibits Cancer Progression." *Cancer Research* 68 (23): 9788–98. https://doi.org/10.1158/0008-5472.CAN-08-2428.

American Cancer Society. 2019. "How Gastrointestinal Stromal Tumors Are Diagnosed." American Cancer Society. https://www.cancer.org/cancer/types/gastrointestinal-stromal-tumor/detection-diagnosis-staging/how-diagnosed.html.

Antonescu, Cristina R., Peter Besmer, Tianhua Guo, et al. 2005. "Acquired Resistance to Imatinib in Gastrointestinal Stromal Tumor Occurs through Secondary Gene Mutation." *Clinical Cancer Research* 11 (11): 4182–90. https://doi.org/10.1158/1078-0432.CCR-04-2245.

Aragón, Eric, Nina Goerner, Qiaoran Xi, et al. 2012. "Structural Basis for the Versatile Interactions of Smad7 with Regulator WW Domains in TGF-β Pathways." *Structure* 20 (10): 1726–36. https://doi.org/10.1016/j.str.2012.07.014.

Baden, Lindsey R., Hana M. El Sahly, Brandon Essink, et al. 2021. "Efficacy and Safety of the mRNA-1273 SARS-CoV-2 Vaccine." *The New England Journal of Medicine* 384 (5): 403–16. https://doi.org/10.1056/NEJMoa2035389.

Bae, Jun Sang, Jeong Yeol Park, See-Hyoung Park, et al. 2017. "Expression of ANO1/DOG1 Is Associated with Shorter Survival and Progression of Breast Carcinomas." *Oncotarget* 9 (1): 607–21. https://doi.org/10.18632/oncotarget.23078.

Bae, June Sung, Sun Mi Kim, and Ho Lee. 2016. "The Hippo Signaling Pathway Provides Novel Anti-Cancer Drug Targets." *Oncotarget* 8 (9): 16084–98. https://doi.org/10.18632/oncotarget.14306.

Baroja, Isabel, Nikolaos C. Kyriakidis, Georg Halder, and Iván M. Moya. 2024. "Expected and Unexpected Effects after Systemic Inhibition of Hippo Transcriptional Output in Cancer." *Nature Communications* 15 (1): 2700. https://doi.org/10.1038/s41467-024-46531-1.

REFERENCES

Barry, Evan R., Vladimir Simov, Iris Valtingojer, and Olivier Venier. 2021. "Recent Therapeutic Approaches to Modulate the Hippo Pathway in Oncology and Regenerative Medicine." *Cells* 10 (10): 2715. https://doi.org/10.3390/cells10102715.

Bartel, David P. 2004. "MicroRNAs: Genomics, Biogenesis, Mechanism, and Function." *Cell* 116 (2): 281–97. https://doi.org/10.1016/s0092-8674(04)00045-5.

Bauer, Sebastian, Suzanne George, Margaret von Mehren, and Michael C. Heinrich. 2021. "Early and Next-Generation KIT/PDGFRA Kinase Inhibitors and the Future of Treatment for Advanced Gastrointestinal Stromal Tumor." *Frontiers in Oncology* 11. https://doi.org/10.3389/fonc.2021.672500.

Bechara, Chérine, and Sandrine Sagan. 2013. "Cell-Penetrating Peptides: 20 Years Later, Where Do We Stand?" *FEBS Letters* 587 (12): 1693–702. https://doi.org/10.1016/j.febslet.2013.04.031.

Betts, L., J. A. Josey, J. M. Veal, and S. R. Jordan. 1995. "A Nucleic Acid Triple Helix Formed by a Peptide Nucleic Acid-DNA Complex." *Science* 270 (5243): 1838–41. https://doi.org/10.1126/science.270.5243.1838.

Bierbaumer, Lisa, Anna M. Katschnig, Branka Radic-Sarikas, et al. 2021. "YAP/TAZ Inhibition Reduces Metastatic Potential of Ewing Sarcoma Cells." *Oncogenesis* 10 (1): 2. https://doi.org/10.1038/s41389-020-00294-8.

Blair, Peter J., Yulia Bayguinov, Kenton M. Sanders, and Sean M. Ward. 2012. "Interstitial Cells in the Primate Gastrointestinal Tract." *Cell and Tissue Research* 350 (2): 199–213. https://doi.org/10.1007/s00441-012-1468-7.

Blanke, Charles D., George D. Demetri, Margaret von Mehren, et al. 2008. "Long-Term Results from a Randomized Phase II Trial of Standard- versus Higher-Dose Imatinib Mesylate for Patients with Unresectable or Metastatic Gastrointestinal Stromal Tumors Expressing KIT." *Journal of Clinical Oncology* 26 (4): 620–25. https://doi.org/10.1200/JCO.2007.13.4403.

Blay, Jean-Yves, Yoon-Koo Kang, Toshiroo Nishida, and Margaret von Mehren. 2021. "Gastrointestinal Stromal Tumours." *Nature Reviews* 7 (1): 22. https://doi.org/10.1038/s41572-021-00254-5.

Blay, Jean-Yves, César Serrano, Michael C. Heinrich, et al. 2020. "Ripretinib in Patients with Advanced Gastrointestinal Stromal Tumours (INVICTUS): A Double-Blind, Randomised, Placebo-Controlled, Phase 3 Trial." *The Lancet. Oncology* 21 (7): 923–34. https://doi.org/10.1016/S1470-2045(20)30168-6.

Boisguérin, Prisca, Karidia Konate, Emilie Josse, Eric Vivès, and Sébastien Deshayes. 2021. "Peptide-Based Nanoparticles for Therapeutic Nucleic Acid Delivery." *Biomedicines* 9 (5): 583. https://doi.org/10.3390/biomedicines9050583.

Boopathy, Gandhi T. K., and Wanjin Hong. 2019. "Role of Hippo Pathway-YAP/TAZ Signaling in Angiogenesis." *Frontiers in Cell and Developmental Biology* 7. https://doi.org/10.3389/fcell.2019.00049.

Bosbach, Benedikt, Shayu Deshpande, Ferdinand Rossi, et al. 2012. "Imatinib Resistance and Microcytic Erythrocytosis in a KitV558Δ;T669I/+ Gatekeeper-Mutant Mouse Model of Gastrointestinal Stromal Tumor." *Proceedings of the National Academy of Sciences of the United States of America* 109 (34): E2276-2283. https://doi.org/10.1073/pnas.1115240109.

REFERENCES

Bosbach, Benedikt, Ferdinand Rossi, Yasemin Yozgat, et al. 2017. "Direct Engagement of the PI3K Pathway by Mutant KIT Dominates Oncogenic Signaling in Gastrointestinal Stromal Tumor." *Proceedings of the National Academy of Sciences* 114 (40): E8448–57. https://doi.org/10.1073/pnas.1711449114.

Bottens, Ryan A., and Tohru Yamada. 2022. "Cell-Penetrating Peptides (CPPs) as Therapeutic and Diagnostic Agents for Cancer." *Cancers* 14 (22): 5546. https://doi.org/10.3390/cancers14225546.

Bourret, Annick, Norbert Chauvet, Pascal de Santa Barbara, and Sandrine Faure. 2017. "Colonic Mesenchyme Differentiates into Smooth Muscle before Its Colonization by Vagal Enteric Neural Crest-Derived Cells in the Chick Embryo." *Cell and Tissue Research* 368 (3): 503–11. https://doi.org/10.1007/s00441-017-2577-0.

Brock, Roland. 2014. "The Uptake of Arginine-Rich Cell-Penetrating Peptides: Putting the Puzzle Together." *Bioconjugate Chemistry* 25 (5): 863–68. https://doi.org/10.1021/bc500017t.

Bucher, Pascal, Peter Villiger, Jean-François Egger, Leo H. Buhler, and Philippe Morel. 2004. "Management of Gastrointestinal Stromal Tumors: From Diagnosis to Treatment." *Swiss Medical Weekly* 134 (11–12): 145–53. https://doi.org/10.4414/smw.2004.10530.

Bure, Irina, Alexander Braun, Claudia Kayser, et al. 2017. "The Expression of Hematopoietic Progenitor Cell Antigen CD34 Is Regulated by DNA Methylation in a Site-Dependent Manner in Gastrointestinal Stromal Tumours." *International Journal of Cancer* 141 (11): 2296–304. https://doi.org/10.1002/ijc.30905.

Cai, Jing, Anirban Maitra, Robert A. Anders, Makoto M. Taketo, and Duojia Pan. 2015. "β-Catenin Destruction Complex-Independent Regulation of Hippo-YAP Signaling by APC in Intestinal Tumorigenesis." *Genes & Development* 29 (14): 1493–506. https://doi.org/10.1101/gad.264515.115.

Cao, Lei, Wencong Tian, Yongjie Zhao, et al. 2024. "Gene Mutations in Gastrointestinal Stromal Tumors: Advances in Treatment and Mechanism Research." *Global Medical Genetics* 11 (4): 251–62. https://doi.org/10.1055/s-0044-1789204.

Casali, P. G., J. Y. Blay, N. Abecassis, et al. 2022. "Gastrointestinal Stromal Tumours: ESMO-EURACAN-GENTURIS Clinical Practice Guidelines for Diagnosis, Treatment and Follow-Up." *Annals of Oncology: Official Journal of the European Society for Medical Oncology* 33 (1): 20–33. https://doi.org/10.1016/j.annonc.2021.09.005.

Champagne, Julien, Laetitia K. Linares, Benjamin Maurel, et al. 2020. "TAG-RNAi Overcomes off-Target Effects in Cancer Models." *Oncogene* 39 (4): 935–45. https://doi.org/10.1038/s41388-019-1020-2.

Chapeau, Emilie A., Laurent Sansregret, Giorgio G. Galli, et al. 2024. "Direct and Selective Pharmacological Disruption of the YAP–TEAD Interface by IAG933 Inhibits Hippo-Dependent and RAS–MAPK-Altered Cancers." *Nature Cancer* 5 (7): 1102–20. https://doi.org/10.1038/s43018-024-00754-9.

Chen, Changbao, Hua Zhou, Xiaolin Zhang, Zhongjun Liu, and Xinlong Ma. 2019. "PRMT1 Potentiates Chondrosarcoma Development through Activation of YAP Activity." *Molecular Carcinogenesis* 58 (12): 2193–206. https://doi.org/10.1002/mc.23108.

REFERENCES

Chen, Qian, Nailing Zhang, Ryan S. Gray, et al. 2014. "A Temporal Requirement for Hippo Signaling in Mammary Gland Differentiation, Growth, and Tumorigenesis." *Genes & Development* 28 (5): 432–37. https://doi.org/10.1101/gad.233676.113.

Chen, Ting, Nan Ni, Li Yuan, et al. 2021. "Proteasome Inhibition Suppresses KIT-Independent Gastrointestinal Stromal Tumors Via Targeting Hippo/YAP/Cyclin D1 Signaling." *Frontiers in Pharmacology* 12: 6874. https://doi.org/10.3389/fphar.2021.686874.

Chen, Yingzhun, Xiaoguang Zhao, Jian Sun, et al. 2019. "YAP1/Twist Promotes Fibroblast Activation and Lung Fibrosis That Conferred by miR-15a Loss in IPF." *Cell Death and Differentiation* 26 (9): 1832–44. https://doi.org/10.1038/s41418-018-0250-0.

Chen, Yu-An, Chen-Yu Lu, Tian-You Cheng, Szu-Hua Pan, Hsin-Fu Chen, and Nan-Shan Chang. 2019. "WW Domain-Containing Proteins YAP and TAZ in the Hippo Pathway as Key Regulators in Stemness Maintenance, Tissue Homeostasis, and Tumorigenesis." *Frontiers in Oncology* 9: 60. https://doi.org/10.3389/fonc.2019.00060.

Chi, Ping, Yu Chen, Lei Zhang, et al. 2010. "ETV1 Is a Lineage Survival Factor That Cooperates with KIT in Gastrointestinal Stromal Tumours." *Nature* 467 (7317): 849–53. https://doi.org/10.1038/nature09409.

Chi, Ping, Li-Xuan Qin, Bastien Nguyen, et al. 2022. "Phase II Trial of Imatinib Plus Binimetinib in Patients With Treatment-Naive Advanced Gastrointestinal Stromal Tumor." *Journal of Clinical Oncology: Official Journal of the American Society of Clinical Oncology* 40 (9): 997–1008. https://doi.org/10.1200/JCO.21.02029.

Chorzalska, Anna, Javier Flores Kim, Karim Roder, et al. 2017. "Long-Term Exposure to Imatinib Mesylate Downregulates Hippo Pathway and Activates YAP in a Model of Chronic Myelogenous Leukemia." *Stem Cells and Development* 26 (9): 656–77. https://doi.org/10.1089/scd.2016.0262.

Cilloni, Daniela, Beatrice Maffeo, Arianna Savi, Alice Costanza Danzero, Valentina Bonuomo, and Carmen Fava. 2024. "Detection of KIT Mutations in Systemic Mastocytosis: How, When, and Why." *International Journal of Molecular Sciences* 25 (20): 10885. https://doi.org/10.3390/ijms252010885.

Corless, Christopher L., Christine M. Barnett, and Michael C. Heinrich. 2011. "Gastrointestinal Stromal Tumours: Origin and Molecular Oncology." *Nature Reviews. Cancer* 11 (12): 865–78. https://doi.org/10.1038/nrc3143.

Corless, Christopher L., Jonathan A. Fletcher, and Michael C. Heinrich. 2004. "Biology of Gastrointestinal Stromal Tumors." *Journal of Clinical Oncology* 22 (18): 3813–25. https://doi.org/10.1200/JCO.2004.05.140.

Cunningham, Richard, and Carsten Gram Hansen. 2022. "The Hippo Pathway in Cancer: YAP/TAZ and TEAD as Therapeutic Targets in Cancer." *Clinical Science* 136 (3): 197–222. https://doi.org/10.1042/CS20201474.

Dassie, Justin P., Xiu-Ying Liu, Gregory S. Thomas, et al. 2009. "Systemic Administration of Optimized Aptamer-siRNA Chimeras Promotes Regression of PSMA-Expressing Tumors." *Nature Biotechnology* 27 (9): 839–49. https://doi.org/10.1038/nbt.1560.

REFERENCES

Dastgerdi, Nazgol Karimi, Nazanin Karimi Dastgerdi, Hulya Bayraktutan, et al. 2024. "Enhancing siRNA Cancer Therapy: Multifaceted Strategies with Lipid and Polymer-Based Carrier Systems." *International Journal of Pharmaceutics* 663: 124545. https://doi.org/10.1016/j.ijpharm.2024.124545.

Debiec-Rychter, Maria, Raf Sciot, Axel Le Cesne, et al. 2006. "KIT Mutations and Dose Selection for Imatinib in Patients with Advanced Gastrointestinal Stromal Tumours." *European Journal of Cancer* 42 (8): 1093–103. https://doi.org/10.1016/j.ejca.2006.01.030.

Deel, Michael D., Katherine K. Slemmons, Ashley R. Hinson, et al. 2018. "The Transcriptional Coactivator TAZ Is a Potent Mediator of Alveolar Rhabdomyosarcoma Tumorigenesis." *Clinical Cancer Research* 24 (11): 2616–30. https://doi.org/10.1158/1078-0432.CCR-17-1207.

Delvaux, Marine, Perrine Hagué, Ligia Craciun, et al. 2022. "Ferroptosis Induction and YAP Inhibition as New Therapeutic Targets in Gastrointestinal Stromal Tumors (GISTs)." *Cancers* 14 (20): 5050. https://doi.org/10.3390/cancers14205050.

Demetri, George D., Robert S. Benjamin, Charles D. Blanke, et al. 2007. "NCCN Task Force Report: Management of Patients with Gastrointestinal Stromal Tumor (GIST)--Update of the NCCN Clinical Practice Guidelines." *Journal of the National Comprehensive Cancer Network.* 5 Suppl 2: S1-29.

Demetri, George D., Christopher R. Garrett, Patrick Schöffski, et al. 2012. "Complete Longitudinal Analyses of the Randomized, Placebo-Controlled, Phase III Trial of Sunitinib in Patients with Gastrointestinal Stromal Tumor Following Imatinib Failure." *Clinical Cancer Research: An Official Journal of the American Association for Cancer Research* 18 (11): 3170–79. https://doi.org/10.1158/1078-0432.CCR-11-3005.

Demetri, George D., Margaret von Mehren, Charles D. Blanke, et al. 2002. "Efficacy and Safety of Imatinib Mesylate in Advanced Gastrointestinal Stromal Tumors." *The New England Journal of Medicine* 347 (7): 472–80. https://doi.org/10.1056/NEJMoa020461.

Demetri, George D., Allan T. van Oosterom, Christopher R. Garrett, et al. 2006. "Efficacy and Safety of Sunitinib in Patients with Advanced Gastrointestinal Stromal Tumour after Failure of Imatinib: A Randomised Controlled Trial." *The Lancet* 368 (9544): 1329–38. https://doi.org/10.1016/S0140-6736(06)69446-4.

Demetri, George D., Peter Reichardt, Yoon-Koo Kang, et al. 2013. "Efficacy and Safety of Regorafenib for Advanced Gastrointestinal Stromal Tumours after Failure of Imatinib and Sunitinib (GRID): An International, Multicentre, Randomised, Placebo-Controlled, Phase 3 Trial." *The Lancet* 381 (9863): 295–302. https://doi.org/10.1016/S0140-6736(12)61857-1.

Demirel, Habibe Cansu, Tunca Dogan, and Nurcan Tuncbag. 2018. "A Structural Perspective on the Modulation of Protein-Protein Interactions with Small Molecules." *Current Topics in Medicinal Chemistry* 18 (8): 700–713. https://doi.org/10.2174/1568026618666180601080824.

Derossi D, Chassaing G, and Prochiantz A. 1998. "Trojan Peptides: The Penetratin System for Intracellular Delivery." *Trends in Cell Biology* 8 (2). https://pubmed.ncbi.nlm.nih.gov/9695814/.

Deshayes, Sébastien, Sabine Gerbal-Chaloin, May C. Morris, et al. 2004. "On the Mechanism of Non-Endosomial Peptide-Mediated Cellular Delivery of Nucleic Acids." *Biochimica Et Biophysica Acta* 1667 (2): 141–47. https://doi.org/10.1016/j.bbamem.2004.09.010.

REFERENCES

Deshayes, Sébastien, Karidia Konate, Marion Dussot, et al. 2020. “Deciphering the Internalization Mechanism of WRAP:siRNA Nanoparticles.” *Biochimica Et Biophysica Acta (BBA). Biomembranes* 1862 (6): 183252. https://doi.org/10.1016/j.bbamem.2020.183252.

Deshayes, Sébastien, Karidia Konate, Eric Vivès, and Prisca Boisguérin. 2022. “Tips and Tools to Understand Direct Membrane Translocation of siRNA-Loaded WRAP-Based Nanoparticles.” *Methods in Molecular Biology* 2383: 475–90. https://doi.org/10.1007/978-1-0716-1752-6_30.

Deshpande, Shayu, Benedikt Bosbach, Yasemin Yozgat, Christopher Y. Park, Malcolm A. S. Moore, and Peter Besmer. 2013. “KIT Receptor Gain-of-Function in Hematopoiesis Enhances Stem Cell Self-Renewal and Promotes Progenitor Cell Expansion.” *Stem Cells* 31 (8): 1683–95. https://doi.org/10.1002/stem.1419.

Di Gregorio, Giulia, Coélio Vallée, Karidia Konate, et al. 2025. “Enhancing WRAP-Based Nanoparticles for Small Interfering Ribonucleic Acid Delivery in pH-Sensitive Environments.” *ChemMedChem*, e2400885. https://doi.org/10.1002/cmdc.202400885.

Di Palma, Tina, Barbara D’Andrea, Giovanna Lucia Liguori, et al. 2009. “TAZ Is a Coactivator for Pax8 and TTF-1, Two Transcription Factors Involved in Thyroid Differentiation.” *Experimental Cell Research* 315 (2): 162–75. https://doi.org/10.1016/j.yexcr.2008.10.016.

Díaz-Martín, Juan, María Ángeles López-García, Laura Romero-Pérez, et al. 2015. “Nuclear TAZ Expression Associates with the Triple-Negative Phenotype in Breast Cancer.” *Endocrine-Related Cancer* 22 (3): 443–54. https://doi.org/10.1530/ERC-14-0456.

Dowdy, Steven F. 2017. “Overcoming Cellular Barriers for RNA Therapeutics.” *Nature Biotechnology* 35 (3): 222–29. https://doi.org/10.1038/nbt.3802.

Dowdy, Steven F., Conor J. Gallagher, Domenico Vitarella, and Jessica Brown. 2023. “A Technology Evaluation of the Atypical Use of a CPP-Containing Peptide in the Formulation and Performance of a Clinical Botulinum Toxin Product.” *Expert Opinion on Drug Delivery* 20 (9): 1157–66. https://doi.org/10.1080/17425247.2023.2251399.

Druker, Brian J., Shu Tamura, Elisabeth Buchdunger, et al. 1996. “Effects of a Selective Inhibitor of the Abl Tyrosine Kinase on the Growth of Bcr–Abl Positive Cells.” *Nature Medicine* 2 (5): 561–66. https://doi.org/10.1038/nm0596-561.

Duan, Yi, Johannes Haybaeck, and Zhihui Yang. 2020. “Therapeutic Potential of PI3K/AKT/mTOR Pathway in Gastrointestinal Stromal Tumors: Rationale and Progress.” *Cancers* 12 (10): 2972. https://doi.org/10.3390/cancers12102972.

Dzmitruk, Volha, Aleksandra Szulc, Dzmitry Shcharbin, et al. 2015. “Anticancer siRNA Cocktails as a Novel Tool to Treat Cancer Cells. Part (B). Efficiency of Pharmacological Action.” *International Journal of Pharmaceutics* 485 (1–2): 288–94. https://doi.org/10.1016/j.ijpharm.2015.03.034.

Ebenezer, Oluwakemi, Abel Kolawole Oyebamiji, John Oludele Olanlokun, Jack A. Tuszynski, and Gane Ka-Shu Wong. 2025. “Recent Update on siRNA Therapeutics.” *International Journal of Molecular Sciences* 26 (8): 3456. https://doi.org/10.3390/ijms26083456.

Edwards, A. Cole, Clint A. Stalnecker, Alexis Jean Morales, et al. 2023. “TEAD Inhibition Overcomes YAP1/TAZ-Driven Primary and Acquired Resistance to KRASG12C Inhibitors.” *Cancer Research* 83 (24): 4112–29. https://doi.org/10.1158/0008-5472.CAN-23-2994.

REFERENCES

El Dika, Imane, Ho Yeong Lim, Wei Peng Yong, et al. 2019. "An Open-Label, Multicenter, Phase I, Dose Escalation Study with Phase II Expansion Cohort to Determine the Safety, Pharmacokinetics, and Preliminary Antitumor Activity of Intravenous TKM-080301 in Subjects with Advanced Hepatocellular Carcinoma." *The Oncologist* 24 (6): 747-e218. https://doi.org/10.1634/theoncologist.2018-0838.

Elbashir, S. M., J. Harborth, W. Lendeckel, A. Yalcin, K. Weber, and T. Tuschl. 2001. "Duplexes of 21-Nucleotide RNAs Mediate RNA Interference in Cultured Mammalian Cells." *Nature* 411 (6836): 494–98. https://doi.org/10.1038/35078107.

Ellert-Miklaszewska, Aleksandra, Katarzyna Poleszak, and Bozena Kaminska. 2017. "Short Peptides Interfering with Signaling Pathways as New Therapeutic Tools for Cancer Treatment." *Future Medicinal Chemistry* 9 (2): 199–221. https://doi.org/10.4155/fmc-2016-0189.

Esteban-Amo, María J., Patricia Jiménez-Cuadrado, Pablo Serrano-Lorenzo, Miguel Á de la Fuente, and María Simarro. 2024. "Succinate Dehydrogenase and Human Disease: Novel Insights into a Well-Known Enzyme." *Biomedicines* 12 (9): 2050. https://doi.org/10.3390/biomedicines12092050.

Esteller, Manel. 2011. "Non-Coding RNAs in Human Disease." *Nature Reviews. Genetics* 12 (12): 861–74. https://doi.org/10.1038/nrg3074.

Ezzat, Kariem, Samir E. L. Andaloussi, Eman M. Zaghloul, et al. 2011. "PepFect 14, a Novel Cell-Penetrating Peptide for Oligonucleotide Delivery in Solution and as Solid Formulation." *Nucleic Acids Research* 39 (12): 5284–98. https://doi.org/10.1093/nar/gkr072.

Fakhr, E., F. Zare, and L. Teimoori-Toolabi. 2016. "Precise and Efficient siRNA Design: A Key Point in Competent Gene Silencing." *Cancer Gene Therapy* 23 (4): 73–82. https://doi.org/10.1038/cgt.2016.4.

Faria, Rúben, Eric Vivès, Prisca Boisguérin, Simon Descamps, Ângela Sousa, and Diana Costa. 2024. "Upgrading Mitochondria-Targeting Peptide-Based Nanocomplexes for Zebrafish In Vivo Compatibility Assays." *Pharmaceutics* 16 (7): 961. https://doi.org/10.3390/pharmaceutics16070961.

Ferreiro, Isabel, Coralie Genevois, Karidia Konate, et al. 2021. "In Vivo Follow-Up of Gene Inhibition in Solid Tumors Using Peptide-Based Nanoparticles for siRNA Delivery." *Pharmaceutics* 13 (5): 749. https://doi.org/10.3390/pharmaceutics13050749.

Ferrigno, Olivier, François Lallemand, Franck Verrecchia, et al. 2002. "Yes-Associated Protein (YAP65) Interacts with Smad7 and Potentiates Its Inhibitory Activity against TGF-Beta/Smad Signaling." *Oncogene* 21 (32): 4879–84. https://doi.org/10.1038/sj.onc.1205623.

Fire, A., S. Xu, M. K. Montgomery, S. A. Kostas, S. E. Driver, and C. C. Mello. 1998. "Potent and Specific Genetic Interference by Double-Stranded RNA in Caenorhabditis Elegans." *Nature* 391 (6669): 806–11. https://doi.org/10.1038/35888.

Fitamant, Julien, Filippos Kottakis, Samira Benhamouche, et al. 2015. "YAP Inhibition Restores Hepatocyte Differentiation in Advanced HCC, Leading to Tumor Regression." *Cell Reports* 10 (10): 1692–707. https://doi.org/10.1016/j.celrep.2015.02.027.

REFERENCES

Fletcher, Christopher D. M., Jules J. Berman, Christopher Corless, et al. 2002. "Diagnosis of Gastrointestinal Stromal Tumors: A Consensus Approach." *Human Pathology* 33 (5): 459–65. https://doi.org/10.1053/hupa.2002.123545.

Floris, Giuseppe, Agnieszka Wozniak, Raf Sciot, et al. 2013. "A Potent Combination of the Novel PI3K Inhibitor, GDC-0941, with Imatinib in Gastrointestinal Stromal Tumor Xenografts: Long-Lasting Responses after Treatment Withdrawal." *Clinical Cancer Research* 19 (3): 620–30. https://doi.org/10.1158/1078-0432.CCR-12-2853.

Franklin, J. Matthew, Zhengming Wu, and Kun-Liang Guan. 2023. "Insights into Recent Findings and Clinical Application of YAP and TAZ in Cancer." *Nature Reviews. Cancer* 23 (8): 512–25. https://doi.org/10.1038/s41568-023-00579-1.

Friedrich, Maik, and Achim Aigner. 2022. "Therapeutic siRNA: State-of-the-Art and Future Perspectives." *BioDrugs: Clinical Immunotherapeutics, Biopharmaceuticals and Gene Therapy* 36 (5): 549–71. https://doi.org/10.1007/s40259-022-00549-3.

Fu, Minyang, Yuan Hu, Tianxia Lan, Kun-Liang Guan, Ting Luo, and Min Luo. 2022. "The Hippo Signalling Pathway and Its Implications in Human Health and Diseases." *Signal Transduction and Targeted Therapy* 7 (1): 376. https://doi.org/10.1038/s41392-022-01191-9.

Fukuda, Kazumasa, Yoshiro Saikawa, Hiroyuki Sako, et al. 2013. "Establishment and Characterization of Novel Cell Lines and Xenografts from Patients with Gastrointestinal Stromal Tumors." *Oncology Reports* 30 (1): 71–78. https://doi.org/10.3892/or.2013.2425.

Fullenkamp, Colleen A., Sarah L. Hall, Omar I. Jaber, et al. 2016. "TAZ and YAP Are Frequently Activated Oncoproteins in Sarcomas." *Oncotarget* 7 (21): 30094–108. https://doi.org/10.18632/oncotarget.8979.

Gabella, Giorgio. 2002. "Development of Visceral Smooth Muscle." *Results and Problems in Cell Differentiation* 38: 1–37. https://doi.org/10.1007/978-3-540-45686-5_1.

Gao, Jiaxin, Zide Liu, Xingxing Liu, et al. 2024. "Follow-up Analysis and Research of Very Low-Risk and Low-Risk Gastrointestinal Stromal Tumors after Endoscopic Resection." *Scientific Reports* 14 (1): 17872. https://doi.org/10.1038/s41598-024-68460-1.

García-Valverde, Alfonso, Jordi Rosell, Sergi Sayols, et al. 2021. "E3 Ubiquitin Ligase Atrogin-1 Mediates Adaptive Resistance to KIT-Targeted Inhibition in Gastrointestinal Stromal Tumor." *Oncogene* 40 (48): 6614–26. https://doi.org/10.1038/s41388-021-02049-0.

García-Valverde, Alfonso, Jordi Rosell, Garazi Serna, et al. 2020. "Preclinical Activity of PI3K Inhibitor Copanlisib in Gastrointestinal Stromal Tumor." *Molecular Cancer Therapeutics* 19 (6): 1289–97. https://doi.org/10.1158/1535-7163.MCT-19-1069.

Garner, Andrew P., Joseph M. Gozgit, Rana Anjum, et al. 2014. "Ponatinib Inhibits Polyclonal Drug-Resistant KIT Oncoproteins and Shows Therapeutic Potential in Heavily Pretreated Gastrointestinal Stromal Tumor (GIST) Patients." *Clinical Cancer Research* 20 (22): 5745–55. https://doi.org/10.1158/1078-0432.CCR-14-1397.

Gelderblom, Hans, Robin L. Jones, Suzanne George, et al. 2020. "Imatinib in Combination with Phosphoinositol Kinase Inhibitor Buparlisib in Patients with Gastrointestinal Stromal Tumour Who Failed Prior Therapy with Imatinib and Sunitinib: A Phase 1b, Multicentre Study." *British Journal of Cancer* 122 (8): 1158–65. https://doi.org/10.1038/s41416-020-0769-y.

REFERENCES

George, Suzanne, William D. Tap, Margaret von Mehren, et al. 2023. "Initial Results from the Phase (Ph) 1 Portion of a Ph 1/2 Study of THE-630 in Patients (Pts) with Advanced Gastrointestinal Stromal Tumor (GIST)." *Journal of Clinical Oncology* 41 (16): e23508–e23508. https://doi.org/10.1200/JCO.2023.41.16_suppl.e23508.

Giraud, Julie, Silvia Molina-Castro, Lornella Seeneevassen, et al. 2020. "Verteporfin Targeting YAP1/TAZ-TEAD Transcriptional Activity Inhibits the Tumorigenic Properties of Gastric Cancer Stem Cells." *International Journal of Cancer* 146 (8): 2255–67. https://doi.org/10.1002/ijc.32667.

Glinkina, Kseniya A., Amina F. A. S. Teunisse, Maria Chiara Gelmi, Jelle de Vries, Martine J. Jager, and Aart G. Jochemsen. 2023. "Combined Mcl-1 and YAP1/TAZ Inhibition for Treatment of Metastatic Uveal Melanoma." *Melanoma Research* 33 (5): 345–56. https://doi.org/10.1097/CMR.0000000000000911.

Golan, Talia, Elina Zorde Khvalevsky, Ayala Hubert, et al. 2015. "RNAi Therapy Targeting KRAS in Combination with Chemotherapy for Locally Advanced Pancreatic Cancer Patients." *Oncotarget* 6 (27): 24560–70. https://doi.org/10.18632/oncotarget.4183.

Goulev, Youlian, Jean Daniel Fauny, Beatriz Gonzalez-Marti, Domenico Flagiello, Joël Silber, and Alain Zider. 2008. "SCALLOPED Interacts with YORKIE, the Nuclear Effector of the Hippo Tumor-Suppressor Pathway in Drosophila." *Current Biology* 18 (6): 435–41. https://doi.org/10.1016/j.cub.2008.02.034.

Goyette, Marie-Anne, Stéphanie Duhamel, Léo Aubert, et al. 2018. "The Receptor Tyrosine Kinase AXL Is Required at Multiple Steps of the Metastatic Cascade during HER2-Positive Breast Cancer Progression." *Cell Reports* 23 (5): 1476–90. https://doi.org/10.1016/j.celrep.2018.04.019.

Graham, Keith, Philip Lienau, Benjamin Bader, et al. 2024. "Discovery of YAP1/TAZ Pathway Inhibitors through Phenotypic Screening with Potent Anti-Tumor Activity via Blockade of Rho-GTPase Signaling." *Cell Chemical Biology* 31 (7): 1247-1263.e16. https://doi.org/10.1016/j.chembiol.2024.02.013.

Grannas, Karin, Linda Arngården, Peter Lönn, et al. 2015. "Crosstalk between Hippo and TGFβ: Subcellular Localization of YAP/TAZ/Smad Complexes." *Journal of Molecular Biology* 427 (21): 3407–15. https://doi.org/10.1016/j.jmb.2015.04.015.

Gregorieff, Alex, Yu Liu, Mohammad R. Inanlou, Yuliya Khomchuk, and Jeffrey L. Wrana. 2015. "Yap-Dependent Reprogramming of Lgr5(+) Stem Cells Drives Intestinal Regeneration and Cancer." *Nature* 526 (7575): 715–18. https://doi.org/10.1038/nature15382.

Guérin, Amandine, Claire Angebault, Sandrina Kinet, et al. 2022. "LIX1-Mediated Changes in Mitochondrial Metabolism Control the Fate of Digestive Mesenchyme-Derived Cells." *Redox Biology* 56: 102431. https://doi.org/10.1016/j.redox.2022.102431.

Guérin, Amandine, Delphine Martire, Eva Trenquier, et al. 2020. "LIX1 Regulates YAP Activity and Controls Gastrointestinal Cancer Cell Plasticity." *Journal of Cellular and Molecular Medicine* 24 (16): 9244–54. https://doi.org/10.1111/jcmm.15569.

Guidotti, Giulia, Liliana Brambilla, and Daniela Rossi. 2017. "Cell-Penetrating Peptides: From Basic Research to Clinics." *Trends in Pharmacological Sciences* 38 (4): 406–24. https://doi.org/10.1016/j.tips.2017.01.003.

REFERENCES

Guo, Yibo, Juan Luo, Hailin Zou, Chenxin Liu, Liang Deng, and Peng Li. 2022. "Context-Dependent Transcriptional Regulations of YAP/TAZ in Cancer." *Cancer Letters* 527: 164–73. https://doi.org/10.1016/j.canlet.2021.12.019.

Ha, Minju, and V. Narry Kim. 2014. "Regulation of microRNA Biogenesis." *Nature Reviews. Molecular Cell Biology* 15 (8): 509–24. https://doi.org/10.1038/nrm3838.

Ha, Taekyu, Hidetaka Ohnuki, and Giovanna Tosato. 2018. "Novel Insights into Endothelial Cell Malignancies." *Oncotarget* 9 (101): 37468–70. https://doi.org/10.18632/oncotarget.26516.

Habault, Justine, and Jean-Luc Poyet. 2019. "Recent Advances in Cell Penetrating Peptide-Based Anticancer Therapies." *Molecules* 24 (5): 927. https://doi.org/10.3390/molecules24050927.

Hagenbeek, Thijs J., Jason R. Zbieg, Marc Hafner, et al. 2023. "An Allosteric Pan-TEAD Inhibitor Blocks Oncogenic YAP/TAZ Signaling and Overcomes KRAS G12C Inhibitor Resistance." *Nature Cancer* 4 (6): 812–28. https://doi.org/10.1038/s43018-023-00577-0.

Hammond, Suzan M., Annemieke Aartsma-Rus, Sandra Alves, et al. 2021. "Delivery of Oligonucleotide-Based Therapeutics: Challenges and Opportunities." *EMBO Molecular Medicine* 13 (4): e13243. https://doi.org/10.15252/emmm.202013243.

Hansen, Carsten Gram, Toshiro Moroishi, and Kun-Liang Guan. 2015. "YAP and TAZ: A Nexus for Hippo Signaling and Beyond." *Trends in Cell Biology* 25 (9): 499–513. https://doi.org/10.1016/j.tcb.2015.05.002.

Harvey, Kieran F., Cathie M. Pfleger, and Iswar K. Hariharan. 2003. "The Drosophila Mst Ortholog, Hippo, Restricts Growth and Cell Proliferation and Promotes Apoptosis." *Cell* 114 (4): 457–67. https://doi.org/10.1016/s0092-8674(03)00557-9.

He, Chunxiao, Zilong Wang, Jiaying Yu, Shuang Mao, and Xi Xiang. 2024. "Current Drug Resistance Mechanisms and Treatment Options in Gastrointestinal Stromal Tumors: Summary and Update." *Current Treatment Options in Oncology* 25 (11): 1390–405. https://doi.org/10.1007/s11864-024-01272-7.

He, Wangzhen, Liangliang Xu, Jiongyan Ding, et al. 2023. "Co-Targeting of ACK1 and KIT Triggers Additive Anti-Proliferative and -Migration Effects in Imatinib-Resistant Gastrointestinal Stromal Tumors." *Biochimica Et Biophysica Acta (BBA). Molecular Basis of Disease* 1869 (5): 166690. https://doi.org/10.1016/j.bbadis.2023.166690.

Hebron, Katie E., Olivia L. Perkins, Angela Kim, et al. 2025. "ASAP1 and ARF1 Regulate Myogenic Differentiation in Rhabdomyosarcoma by Modulating TAZ Activity." *Molecular Cancer Research* 23 (2): 95–106. https://doi.org/10.1158/1541-7786.MCR-24-0490.

Heinrich, Michael C., Christopher L. Corless, George D. Demetri, et al. 2003. "Kinase Mutations and Imatinib Response in Patients with Metastatic Gastrointestinal Stromal Tumor." *Journal of Clinical Oncology* 21 (23): 4342–49. https://doi.org/10.1200/JCO.2003.04.190.

Heinrich, Michael C., Christopher L. Corless, Anette Duensing, et al. 2003. "PDGFRA Activating Mutations in Gastrointestinal Stromal Tumors." *Science* 299 (5607): 708–10. https://doi.org/10.1126/science.1079666.

REFERENCES

Heng, Boon Chin, Xuehui Zhang, Dominique Aubel, et al. 2021. "An Overview of Signaling Pathways Regulating YAP/TAZ Activity." *Cellular and Molecular Life Sciences* 78 (2): 497–512. https://doi.org/10.1007/s00018-020-03579-8.

Hiemer, Samantha E., Aleksander D. Szymaniak, and Xaralabos Varelas. 2014. "The Transcriptional Regulators TAZ and YAP Direct Transforming Growth Factor β-Induced Tumorigenic Phenotypes in Breast Cancer Cells." *The Journal of Biological Chemistry* 289 (19): 13461–74. https://doi.org/10.1074/jbc.M113.529115.

Hillmer, Ryan E., and Brian A. Link. 2019. "The Roles of Hippo Signaling Transducers Yap and Taz in Chromatin Remodeling." *Cells* 8 (5): 502. https://doi.org/10.3390/cells8050502.

Hilman, Dror, and Uri Gat. 2011. "The Evolutionary History of YAP and the Hippo/YAP Pathway." *Molecular Biology and Evolution* 28 (8): 2403–17. https://doi.org/10.1093/molbev/msr065.

Hirota, S., K. Isozaki, Y. Moriyama, et al. 1998. "Gain-of-Function Mutations of c-Kit in Human Gastrointestinal Stromal Tumors." *Science* 279 (5350): 577–80. https://doi.org/10.1126/science.279.5350.577.

Ho, William, Xue-Qing Zhang, and Xiaoyang Xu. 2016. "Biomaterials in siRNA Delivery: A Comprehensive Review." *Advanced Healthcare Materials* 5 (21): 2715–31. https://doi.org/10.1002/adhm.201600418.

Holden, Jeffrey K., and Christian N. Cunningham. 2018. "Targeting the Hippo Pathway and Cancer through the TEAD Family of Transcription Factors." *Cancers* 10 (3): 81. https://doi.org/10.3390/cancers10030081.

Hong, Jeong-Ho, Eun Sook Hwang, Michael T. McManus, et al. 2005. "TAZ, a Transcriptional Modulator of Mesenchymal Stem Cell Differentiation." *Science* 309 (5737): 1074–78. https://doi.org/10.1126/science.1110955.

Hong, Wanjin, and Kun-Liang Guan. 2012. "The YAP and TAZ Transcription Coactivators: Key Downstream Effectors of the Mammalian Hippo Pathway." *Seminars in Cell & Developmental Biology* 23 (7): 785–93. https://doi.org/10.1016/j.semcdb.2012.05.004.

Hornick, Jason L., and Christopher D. M. Fletcher. 2007. "The Role of KIT in the Management of Patients with Gastrointestinal Stromal Tumors." *Human Pathology* 38 (5): 679–87. https://doi.org/10.1016/j.humpath.2007.03.001.

Hou, Ying-Yong, Yun-Shan Tan, Meng-Hong Sun, et al. 2004. "C-Kit Gene Mutation in Human Gastrointestinal Stromal Tumors." *World Journal of Gastroenterology* 10 (9): 1310–14. https://doi.org/10.3748/wjg.v10.i9.1310.

Hu, Bo, Liping Zhong, Yuhua Weng, et al. 2020. "Therapeutic siRNA: State of the Art." *Signal Transduction and Targeted Therapy* 5 (1): 101. https://doi.org/10.1038/s41392-020-0207-x.

Hu, Xiangchen, Zhe Wang, Peng Su, Qiqi Zhang, and Youwei Kou. 2022. "Advances in the Research of the Mechanism of Secondary Resistance to Imatinib in Gastrointestinal Stromal Tumors." *Frontiers in Oncology* 12. https://doi.org/10.3389/fonc.2022.933248.

Huang, Jianbin, Shian Wu, Jose Barrera, Krista Matthews, and Duojia Pan. 2005. "The Hippo Signaling Pathway Coordinately Regulates Cell Proliferation and Apoptosis by Inactivating Yorkie, the Drosophila Homolog of YAP." *Cell* 122 (3): 421–34. https://doi.org/10.1016/j.cell.2005.06.007.

REFERENCES

Huang, Zhihui, Jinxia Hu, Jinxiu Pan, et al. 2016. "YAP Stabilizes SMAD1 and Promotes BMP2-Induced Neocortical Astrocytic Differentiation." *Development* 143 (13): 2398–409. https://doi.org/10.1242/dev.130658.

Huizinga, Jan D., Natalia Zarate, and Gianrico Farrugia. 2009. "Physiology, Injury, and Recovery of Interstitial Cells of Cajal: Basic and Clinical Science." *Gastroenterology* 137 (5): 1548–56. https://doi.org/10.1053/j.gastro.2009.09.023.

Ibrahim, Ahmad, and Shefali Chopra. 2020. "Succinate Dehydrogenase-Deficient Gastrointestinal Stromal Tumors." *Archives of Pathology & Laboratory Medicine* 144 (5): 655–60. https://doi.org/10.5858/arpa.2018-0370-RS.

Isfort, Ilka, Sandra Elges, Magdalene Cyra, et al. 2019. "Prevalence of the Hippo Effectors YAP1/TAZ in Tumors of Soft Tissue and Bone." *Scientific Reports* 9 (1): 19704. https://doi.org/10.1038/s41598-019-56247-8.

Jeong, Hana, Sujung Bae, Su Yeon An, et al. 2010. "TAZ as a Novel Enhancer of MyoD-Mediated Myogenic Differentiation." *FASEB Journal: Official Publication of the Federation of American Societies for Experimental Biology* 24 (9): 3310–20. https://doi.org/10.1096/fj.09-151324.

Jia, Jianhang, Wensheng Zhang, Bing Wang, Richard Trinko, and Jin Jiang. 2003. "The Drosophila Ste20 Family Kinase dMST Functions as a Tumor Suppressor by Restricting Cell Proliferation and Promoting Apoptosis." *Genes & Development* 17 (20): 2514–19. https://doi.org/10.1101/gad.1134003.

Jiang, Cheng-Gang, Ling Lv, Fu-Rong Liu, et al. 2011. "Downregulation of Connective Tissue Growth Factor Inhibits the Growth and Invasion of Gastric Cancer Cells and Attenuates Peritoneal Dissemination." *Molecular Cancer* 10: 122. https://doi.org/10.1186/1476-4598-10-122.

Jiao, Shi, Huizhen Wang, Zhubing Shi, et al. 2014. "A Peptide Mimicking VGLL4 Function Acts as a YAP Antagonist Therapy against Gastric Cancer." *Cancer Cell* 25 (2): 166–80. https://doi.org/10.1016/j.ccr.2014.01.010.

Jones, Robin L., César Serrano, Margaret von Mehren, et al. 2021. "Avapritinib in Unresectable or Metastatic PDGFRA D842V-Mutant Gastrointestinal Stromal Tumours: Long-Term Efficacy and Safety Data from the NAVIGATOR Phase I Trial." *European Journal of Cancer* 145: 132–42. https://doi.org/10.1016/j.ejca.2020.12.008.

Juan, Wen Chun, and Wanjin Hong. 2016. "Targeting the Hippo Signaling Pathway for Tissue Regeneration and Cancer Therapy." *Genes* 7 (9): 55. https://doi.org/10.3390/genes7090055.

Juliano, Rudolph L. 2016. "The Delivery of Therapeutic Oligonucleotides." *Nucleic Acids Research* 44 (14): 6518–48. https://doi.org/10.1093/nar/gkw236.

Juliano, Rudolph L., Xin Ming, and Osamu Nakagawa. 2012. "Cellular Uptake and Intracellular Trafficking of Antisense and siRNA Oligonucleotides." *Bioconjugate Chemistry* 23 (2): 147–57. https://doi.org/10.1021/bc200377d.

Justice, R. W., O. Zilian, D. F. Woods, M. Noll, and P. J. Bryant. 1995. "The Drosophila Tumor Suppressor Gene Warts Encodes a Homolog of Human Myotonic Dystrophy Kinase and Is Required for the Control of Cell Shape and Proliferation." *Genes & Development* 9 (5): 534–46. https://doi.org/10.1101/gad.9.5.534.

REFERENCES

Kaan, Hung Yi Kristal, Siew Wee Chan, Siew Kim Joyce Tan, et al. 2017. "Crystal Structure of TAZ-TEAD Complex Reveals a Distinct Interaction Mode from That of YAP-TEAD Complex." *Scientific Reports* 7 (1): 2035. https://doi.org/10.1038/s41598-017-02219-9.

Kamide, Daisuke, Taku Yamashita, Koji Araki, et al. 2016. "Selective Activator Protein-1 Inhibitor T-5224 Prevents Lymph Node Metastasis in an Oral Cancer Model." *Cancer Science* 107 (5): 666–73. https://doi.org/10.1111/cas.12914.

Kanai, F., P. A. Marignani, D. Sarbassova, et al. 2000. "TAZ: A Novel Transcriptional Co-Activator Regulated by Interactions with 14-3-3 and PDZ Domain Proteins." *The EMBO Journal* 19 (24): 6778–91. https://doi.org/10.1093/emboj/19.24.6778.

Kanasty, Rosemary, Joseph Robert Dorkin, Arturo Vegas, and Daniel Anderson. 2013. "Delivery Materials for siRNA Therapeutics." *Nature Materials* 12 (11): 967–77. https://doi.org/10.1038/nmat3765.

Kaneda, Ayumi, Toshihiro Seike, Tomohiro Danjo, et al. 2020. "The Novel Potent TEAD Inhibitor, K-975, Inhibits YAP1/TAZ-TEAD Protein-Protein Interactions and Exerts an Anti-Tumor Effect on Malignant Pleural Mesothelioma." *American Journal of Cancer Research* 10 (12): 4399–415.

Kang, Yoon-Koo, Suzanne George, Robin L. Jones, et al. 2021. "Avapritinib Versus Regorafenib in Locally Advanced Unresectable or Metastatic GI Stromal Tumor: A Randomized, Open-Label Phase III Study." *Journal of Clinical Oncology* 39 (28): 3128–39. https://doi.org/10.1200/JCO.21.00217.

Kango-Singh, Madhuri, Riitta Nolo, Chunyao Tao, et al. 2002. "Shar-Pei Mediates Cell Proliferation Arrest during Imaginal Disc Growth in Drosophila." *Development* 129 (24): 5719–30. https://doi.org/10.1242/dev.00168.

Kays, Joshua K., Jeffrey D. Sohn, Bradford J. Kim, Katherine Goze, and Leonidas G. Koniaris. 2018. "Approach to Wild-Type Gastrointestinal Stromal Tumors." *Translational Gastroenterology and Hepatology* 3 (0): 0. https://doi.org/10.21037/tgh.2018.10.13.

Keam, Susan J. 2022. "Vutrisiran: First Approval." *Drugs* 82 (13): 1419–25. https://doi.org/10.1007/s40265-022-01765-5.

Kelly, Ciara M., Laura Gutierrez Sainz, and Ping Chi. 2021. "The Management of Metastatic GIST: Current Standard and Investigational Therapeutics." *Journal of Hematology & Oncology* 14 (1): 2. https://doi.org/10.1186/s13045-020-01026-6.

Khan, Jaffar, Asad Ullah, Abdul Waheed, et al. 2022. "Gastrointestinal Stromal Tumors (GIST): A Population-Based Study Using the SEER Database, Including Management and Recent Advances in Targeted Therapy." *Cancers* 14 (15): 3689. https://doi.org/10.3390/cancers14153689.

Khvorova, Anastasia, and Jonathan K. Watts. 2017. "The Chemical Evolution of Oligonucleotide Therapies of Clinical Utility." *Nature Biotechnology* 35 (3): 238–48. https://doi.org/10.1038/nbt.3765.

Kim, Hyungjoo, Seogho Son, Yunhyo Ko, Jeong Eon Lee, Sangmin Kim, and Incheol Shin. 2021. "YAP, CTGF and Cyr61 Are Overexpressed in Tamoxifen-Resistant Breast Cancer and Induce Transcriptional Repression of ERα." *Journal of Cell Science* 134 (11): jcs256503. https://doi.org/10.1242/jcs.256503.

REFERENCES

Kim, Min Hwan, Jongshin Kim, Hyowon Hong, et al. 2016. "Actin Remodeling Confers BRAF Inhibitor Resistance to Melanoma Cells through YAP/TAZ Activation." *The EMBO Journal* 35 (5): 462–78. https://doi.org/10.15252/embj.201592081.

Kindblom, L. G., H. E. Remotti, F. Aldenborg, and J. M. Meis-Kindblom. 1998. "Gastrointestinal Pacemaker Cell Tumor (GIPACT): Gastrointestinal Stromal Tumors Show Phenotypic Characteristics of the Interstitial Cells of Cajal." *The American Journal of Pathology* 152 (5): 1259–69.

Klipp, Alexander, Michael Burger, and Jean-Christophe Leroux. 2023. "Get out or Die Trying: Peptide- and Protein-Based Endosomal Escape of RNA Therapeutics." *Advanced Drug Delivery Reviews* 200: 115047. https://doi.org/10.1016/j.addr.2023.115047.

Knapp, Christopher M., Jia He, John Lister, and Kathryn A. Whitehead. 2018. "Lipid Nanoparticle siRNA Cocktails for the Treatment of Mantle Cell Lymphoma." *Bioengineering & Translational Medicine* 3 (2): 138–47. https://doi.org/10.1002/btm2.10088.

Koga, Yuki, Masaaki Iwatsuki, Kohei Yamashita, et al. 2019. "The Role of FBXW7, a Cell-Cycle Regulator, as a Predictive Marker of Recurrence of Gastrointestinal Stromal Tumors." *Gastric Cancer* 22 (6): 1100–1108. https://doi.org/10.1007/s10120-019-00950-y.

Konate, Karidia, Marion Dussot, Gudrun Aldrian, et al. 2019. "Peptide-Based Nanoparticles to Rapidly and Efficiently 'Wrap 'n Roll' siRNA into Cells." *Bioconjugate Chemistry* 30 (3): 592–603. https://doi.org/10.1021/acs.bioconjchem.8b00776.

Konate, Karidia, Emilie Josse, Milana Tasic, et al. 2021. "WRAP-Based Nanoparticles for siRNA Delivery: A SAR Study and a Comparison with Lipid-Based Transfection Reagents." *Journal of Nanobiotechnology* 19 (1): 236. https://doi.org/10.1186/s12951-021-00972-8.

Konate, Karidia, Irène Pezzati, Karima Redjatti, et al. 2025. "Multiprotein Silencing Using WRAP-Based Nanoparticles: A Proof of Concept." *Bioconjugate Chemistry* 36 (6): 1218–33. https://doi.org/10.1021/acs.bioconjchem.5c00069.

Konate, Karidia, Clémentine A. Teko-Agbo, Irène Pezzati, et al. 2025. "WRAP-Based Nanoparticles for siRNA Delivery in Zebrafish Embryos by Simple Bath Immersion." *Molecular Therapy. Methods & Clinical Development* 33 (2): 101458. https://doi.org/10.1016/j.omtm.2025.101458.

Kondo, Jumpei, Won Jae Huh, Jeffrey L. Franklin, Michael C. Heinrich, Brian P. Rubin, and Robert J. Coffey. 2020. "A Smooth Muscle-Derived, Braf-Driven Mouse Model of Gastrointestinal Stromal Tumor (GIST): Evidence for an Alternative GIST Cell-of-Origin." *The Journal of Pathology* 252 (4): 441–50. https://doi.org/10.1002/path.5552.

Koo, Ja Hyun, Steven W. Plouffe, Zhipeng Meng, et al. 2020. "Induction of AP-1 by YAP/TAZ Contributes to Cell Proliferation and Organ Growth." *Genes & Development* 34 (1–2): 72–86. https://doi.org/10.1101/gad.331546.119.

Koontz, Laura M., Yi Liu-Chittenden, Feng Yin, et al. 2013. "The Hippo Effector Yorkie Controls Normal Tissue Growth by Antagonizing Scalloped-Mediated Default Repression." *Developmental Cell* 25 (4): 388–401. https://doi.org/10.1016/j.devcel.2013.04.021.

Kovar, Heinrich, Lisa Bierbaumer, and Branka Radic-Sarikas. 2020. "The YAP/TAZ Pathway in Osteogenesis and Bone Sarcoma Pathogenesis." *Cells* 9 (4): 972. https://doi.org/10.3390/cells9040972.

REFERENCES

Ku, Sook Hee, Sung Duk Jo, Yeon Kyung Lee, Kwangmeyung Kim, and Sun Hwa Kim. 2016. "Chemical and Structural Modifications of RNAi Therapeutics." *Advanced Drug Delivery Reviews* 104: 16–28. https://doi.org/10.1016/j.addr.2015.10.015.

Kurahashi, Masaaki, Haifeng Zheng, Laura Dwyer, Sean M. Ward, Sang Don Koh, and Kenton M. Sanders. 2011. "A Functional Role for the 'fibroblast-like Cells' in Gastrointestinal Smooth Muscles." *The Journal of Physiology* 589: 697–710. https://doi.org/10.1113/jphysiol.2010.201129.

Kurokawa, Y., Y. Honma, A. Sawaki, et al. 2022. "Pimitespib in Patients with Advanced Gastrointestinal Stromal Tumor (CHAPTER-GIST-301): A Randomized, Double-Blind, Placebo-Controlled Phase III Trial." *Annals of Oncology* 33 (9): 959–67. https://doi.org/10.1016/j.annonc.2022.05.518.

Kurppa, Kari J., Yao Liu, Ciric To, et al. 2020. "Treatment-Induced Tumor Dormancy through YAP-Mediated Transcriptional Reprogramming of the Apoptotic Pathway." *Cancer Cell* 37 (1): 104-122.e12. https://doi.org/10.1016/j.ccell.2019.12.006.

Kuželová, K., M. Pluskalová, D. Grebeňová, K. Pavlásková, P. Halada, and Z. Hrkal. 2010. "Changes in Cell Adhesivity and Cytoskeleton-Related Proteins during Imatinib-Induced Apoptosis of Leukemic JURL-MK1 Cells." *Journal of Cellular Biochemistry* 111 (6): 1413–25. https://doi.org/10.1002/jcb.22868.

Kwon, Ji Eun, Hyun Ju Kang, Se Hoon Kim, et al. 2009. "Pathological Characteristics of Gastrointestinal Stromal Tumours with PDGFRA Mutations." *Pathology* 41 (6): 544–54. https://doi.org/10.1080/00313020903071421.

Lagarde, Pauline, Gaëlle Pérot, Audrey Kauffmann, et al. 2012. "Mitotic Checkpoints and Chromosome Instability Are Strong Predictors of Clinical Outcome in Gastrointestinal Stromal Tumors." *Clinical Cancer Research* 18 (3): 826–38. https://doi.org/10.1158/1078-0432.CCR-11-1610.

Lai, Dulcie, King Ching Ho, Yawei Hao, and Xiaolong Yang. 2011. "Taxol Resistance in Breast Cancer Cells Is Mediated by the Hippo Pathway Component TAZ and Its Downstream Transcriptional Targets Cyr61 and CTGF." *Cancer Research* 71 (7): 2728–38. https://doi.org/10.1158/0008-5472.CAN-10-2711.

Lai, Zhi-Chun, Xiaomu Wei, Takeshi Shimizu, et al. 2005. "Control of Cell Proliferation and Apoptosis by Mob as Tumor Suppressor, Mats." *Cell* 120 (5): 675–85. https://doi.org/10.1016/j.cell.2004.12.036.

Lamb, Yvette N. 2021. "Inclisiran: First Approval." *Drugs* 81 (3): 389–95. https://doi.org/10.1007/s40265-021-01473-6.

Landen, Charles N., Arturo Chavez-Reyes, Corazon Bucana, et al. 2005. "Therapeutic EphA2 Gene Targeting in Vivo Using Neutral Liposomal Small Interfering RNA Delivery." *Cancer Research* 65 (15): 6910–18. https://doi.org/10.1158/0008-5472.CAN-05-0530.

Landi, B., O. Bouché, R. Guimbaud, and J.-A. Chayvialle. 2010. "[Gastrointestinal stromal tumors (GIST)<5 cm in size: review of the literature and expert propositions for clinical management]." *Gastroenterologie Clinique Et Biologique* 34 (2): 120–33. https://doi.org/10.1016/j.gcb.2009.06.019.

REFERENCES

Le Guen, Ludovic, Stéphane Marchal, Sandrine Faure, and Pascal de Santa Barbara. 2015. "Mesenchymal-Epithelial Interactions during Digestive Tract Development and Epithelial Stem Cell Regeneration." *Cellular and Molecular Life Sciences: CMLS* 72 (20): 3883–96. https://doi.org/10.1007/s00018-015-1975-2.

LeBlanc, Lucy, Nereida Ramirez, and Jonghwan Kim. 2021. "Context-Dependent Roles of YAP/TAZ in Stem Cell Fates and Cancer." *Cellular and Molecular Life Sciences: CMLS* 78 (9): 4201–19. https://doi.org/10.1007/s00018-021-03781-2.

Lebleu, Bernard, Hong M. Moulton, Rachida Abes, et al. 2008. "Cell Penetrating Peptide Conjugates of Steric Block Oligonucleotides." *Advanced Drug Delivery Reviews* 60 (4–5): 517–29. https://doi.org/10.1016/j.addr.2007.09.002.

Lee, Cheng-Han, Cher-wei Liang, and Inigo Espinosa. 2010. "The Utility of Discovered on Gastrointestinal Stromal Tumor 1 (DOG1) Antibody in Surgical Pathology-the GIST of It." *Advances in Anatomic Pathology* 17 (3): 222–32. https://doi.org/10.1097/PAP.0b013e3181d973c2.

Lehto, Taavi, Kariem Ezzat, Matthew J. A. Wood, and Samir El Andaloussi. 2016. "Peptides for Nucleic Acid Delivery." *Advanced Drug Delivery Reviews* 106 (Pt A): 172–82. https://doi.org/10.1016/j.addr.2016.06.008.

Lei, Qun-Ying, Heng Zhang, Bin Zhao, et al. 2008. "TAZ Promotes Cell Proliferation and Epithelial-Mesenchymal Transition and Is Inhibited by the Hippo Pathway." *Molecular and Cellular Biology* 28 (7): 2426–36. https://doi.org/10.1128/MCB.01874-07.

Lewin, Jeremy, Jean-Charles Soria, Anastasios Stathis, et al. 2018. "Phase Ib Trial With Birabresib, a Small-Molecule Inhibitor of Bromodomain and Extraterminal Proteins, in Patients With Selected Advanced Solid Tumors." *Journal of Clinical Oncology* 36 (30): 3007–14. https://doi.org/10.1200/JCO.2018.78.2292.

Li, George Z., and Chandrajit P. Raut. 2019. "Targeted Therapy and Personalized Medicine in Gastrointestinal Stromal Tumors: Drug Resistance, Mechanisms, and Treatment Strategies." *OncoTargets and Therapy* 12: 5123–33. https://doi.org/10.2147/OTT.S180763.

Li, Hui, Zhenglan Huang, Miao Gao, et al. 2016. "Inhibition of YAP Suppresses CML Cell Proliferation and Enhances Efficacy of Imatinib in Vitro and in Vivo." *Journal of Experimental & Clinical Cancer Research : CR* 35 (1): 134. https://doi.org/10.1186/s13046-016-0414-z.

Li, Qi, Yang Sun, Gopala K. Jarugumilli, et al. 2020. "Lats1/2 Sustain Intestinal Stem Cells and Wnt Activation through TEAD-Dependent and Independent Transcription." *Cell Stem Cell* 26 (5): 675-692.e8. https://doi.org/10.1016/j.stem.2020.03.002.

Li, Shenghao, Liyuan Hao, Na Li, et al. 2024. "Targeting the Hippo/YAP1 Signaling Pathway in Hepatocellular Carcinoma: From Mechanisms to Therapeutic Drugs (Review)." *International Journal of Oncology* 65 (3): 1–17. https://doi.org/10.3892/ijo.2024.5676.

Li, Shujing, Sien Zhao, Nianhai Liang, et al. 2023. "SPRY4 Inhibits and Sensitizes the Primary KIT Mutants in Gastrointestinal Stromal Tumors (GISTs) to Imatinib." *Gastric Cancer: Official Journal of the International Gastric Cancer Association and the Japanese Gastric Cancer Association* 26 (5): 677–90. https://doi.org/10.1007/s10120-023-01402-4.

REFERENCES

Lihuang, Li, Guo Qiuyan, Liu Yanxiu, et al. 2021. "Targeted Combination Therapy for Glioblastoma by Co-Delivery of Doxorubicin, YAP-siRNA and Gold Nanorods." *Journal of Materials Science & Technology* 63 (February): 81–90. https://doi.org/10.1016/j.jmst.2020.03.009.

Lim, Taekyu, Inkyoung Lee, Jungmin Kim, and Won Ki Kang. 2015. "Synergistic Effect of Simvastatin Plus Radiation in Gastric Cancer and Colorectal Cancer: Implications of BIRC5 and Connective Tissue Growth Factor." *International Journal of Radiation Oncology, Biology, Physics* 93 (2): 316–25. https://doi.org/10.1016/j.ijrobp.2015.05.023.

Lin, Chunli, and Xiaofeng Xu. 2017. "YAP1-TEAD1-Glut1 Axis Dictates the Oncogenic Phenotypes of Breast Cancer Cells by Modulating Glycolysis." *Biomedicine & Pharmacotherapy = Biomedecine & Pharmacotherapie* 95 (November): 789–94. https://doi.org/10.1016/j.biopha.2017.08.091.

Lin, Ming-Tsai, Chung-Yaou Zuon, Cheng-Chi Chang, et al. 2005. "Cyr61 Induces Gastric Cancer Cell Motility/Invasion via Activation of the Integrin/Nuclear Factor-kappaB/Cyclooxygenase-2 Signaling Pathway." *Clinical Cancer Research: An Official Journal of the American Association for Cancer Research* 11 (16): 5809–20. https://doi.org/10.1158/1078-0432.CCR-04-2639.

Lindblad, Oscar, Julhash U. Kazi, Lars Rönnstrand, and Jianmin Sun. 2015. "PI3 Kinase Is Indispensable for Oncogenic Transformation by the V560D Mutant of C-Kit in a Kinase-Independent Manner." *Cellular and Molecular Life Sciences: CMLS* 72 (22): 4399–407. https://doi.org/10.1007/s00018-015-1944-9.

Lindgren, Maria, and Ulo Langel. 2011. "Classes and Prediction of Cell-Penetrating Peptides." *Methods in Molecular Biology (Clifton, N.J.)* 683: 3–19. https://doi.org/10.1007/978-1-60761-919-2_1.

Liu, Jidong, Michelle A. Carmell, Fabiola V. Rivas, et al. 2004. "Argonaute2 Is the Catalytic Engine of Mammalian RNAi." *Science (New York, N.Y.)* 305 (5689): 1437–41. https://doi.org/10.1126/science.1102513.

Liu, Mohan, Yusi Wang, Yibing Zhang, et al. 2025. "Landscape of Small Nucleic Acid Therapeutics: Moving from the Bench to the Clinic as next-Generation Medicines." *Signal Transduction and Targeted Therapy* 10 (1): 73. https://doi.org/10.1038/s41392-024-02112-8.

Liu, Renjing, Kristen L. Leslie, and Kathleen A. Martin. 2015. "Epigenetic Regulation of Smooth Muscle Cell Plasticity." *Biochimica Et Biophysica Acta* 1849 (4): 448–53. https://doi.org/10.1016/j.bbagrm.2014.06.004.

Liu, Weizhen, Xiangyu Zeng, Yuping Yin, et al. 2020. "Targeting the WEE1 Kinase Strengthens the Antitumor Activity of Imatinib via Promoting KIT Autophagic Degradation in Gastrointestinal Stromal Tumors." *Gastric Cancer: Official Journal of the International Gastric Cancer Association and the Japanese Gastric Cancer Association* 23 (1): 39–51. https://doi.org/10.1007/s10120-019-00977-1.

Liu, Ying, Wenjie Liu, Ziqiang Yu, et al. 2021. "A Novel BRD4 Inhibitor Suppresses Osteoclastogenesis and Ovariectomized Osteoporosis by Blocking RANKL-Mediated MAPK and NF-κB Pathways." *Cell Death & Disease* 12 (7): 654. https://doi.org/10.1038/s41419-021-03939-7.

Liu-Chittenden, Yi, Bo Huang, Joong Sup Shim, et al. 2012. "Genetic and Pharmacological Disruption of the TEAD-YAP Complex Suppresses the Oncogenic Activity of YAP." *Genes & Development* 26 (12): 1300–1305. https://doi.org/10.1101/gad.192856.112.

REFERENCES

Lopez-Hernandez, Alejandro, Silvia Sberna, and Stefano Campaner. 2021. “Emerging Principles in the Transcriptional Control by YAP and TAZ.” *Cancers* 13 (16): 4242. https://doi.org/10.3390/cancers13164242.

Lu, Yi, Lu Chen, Jiachuan Wu, et al. 2023. “Artificial Intelligence in Endoscopic Ultrasonography: Risk Stratification of Gastric Gastrointestinal Stromal Tumors.” *Therapeutic Advances in Gastroenterology* 16: 17562848231177156. https://doi.org/10.1177/17562848231177156.

Luo, Juan, Liang Deng, Hailin Zou, et al. 2023. “New Insights into the Ambivalent Role of YAP/TAZ in Human Cancers.” *Journal of Experimental & Clinical Cancer Research* 42: 130. https://doi.org/10.1186/s13046-023-02704-2.

Lux, Marcia L., Brian P. Rubin, Tara L. Biase, et al. 2000. “KIT Extracellular and Kinase Domain Mutations in Gastrointestinal Stromal Tumors.” *The American Journal of Pathology* 156 (3): 791–95. https://doi.org/10.1016/S0002-9440(10)64946-2.

Lv, Liemei, and Xiangxiang Zhou. 2023. “Targeting Hippo Signaling in Cancer: Novel Perspectives and Therapeutic Potential.” *MedComm* 4 (5): e375. https://doi.org/10.1002/mco2.375.

Ma, Shenghong, Zhipeng Meng, Rui Chen, and Kun-Liang Guan. 2019. “The Hippo Pathway: Biology and Pathophysiology.” *Annual Review of Biochemistry* 88 (June): 577–604. https://doi.org/10.1146/annurev-biochem-013118-111829.

Macleod, A. Robert. 2021. “Abstract ND11: The Discovery and Characterization of ION-537: A next Generation Antisense Oligonucleotide Inhibitor of YAP1 in Preclinical Cancer Models.” *Cancer Research* 81 (13_Supplement). https://doi.org/10.1158/1538-7445.AM2021-ND11.

Maeda, H., A. Yamagata, S. Nishikawa, et al. 1992. “Requirement of C-Kit for Development of Intestinal Pacemaker System.” *Development (Cambridge, England)* 116 (2): 369–75. https://doi.org/10.1242/dev.116.2.369.

Mahmoodi Chalbatani, Ghanbar, Hassan Dana, Elahe Gharagouzloo, et al. 2019. “Small Interfering RNAs (siRNAs) in Cancer Therapy: A Nano-Based Approach.” *International Journal of Nanomedicine* 14: 3111–28. https://doi.org/10.2147/IJN.S200253.

Mao, Cheng-Qiong, Meng-Hua Xiong, Yang Liu, et al. 2014. “Synthetic Lethal Therapy for KRAS Mutant Non-Small-Cell Lung Carcinoma with Nanoparticle-Mediated CDK4 siRNA Delivery.” *Molecular Therapy* 22 (5): 964–73. https://doi.org/10.1038/mt.2014.18.

Mavroeidis, Leonidas, Foteini Kalofonou, Ruth Casey, Andrea Napolitano, Ramesh Bulusu, and Robin L. Jones. 2025. “Identifying and Managing Rare Subtypes of Gastrointestinal Stromal Tumors.” *Expert Review of Gastroenterology & Hepatology* 19 (5): 549–61. https://doi.org/10.1080/17474124.2025.2486304.

Mayo Foundation for Medical Education and Research. 2025. “Gastrointestinal Stromal Tumors: Diagnosis and Treatment.” Mayo Clinic, February. https://www.mayoclinic.org/diseases-conditions/gastrointestinal-stromal-tumors/diagnosis-treatment/drc-20579539.

Mazur, M. T., and H. B. Clark. 1983. “Gastric Stromal Tumors. Reappraisal of Histogenesis.” *The American Journal of Surgical Pathology* 7 (6): 507–19. https://doi.org/10.1097/00000478-198309000-00001.

REFERENCES

McCarthy, Helen O., Joanne McCaffrey, Cian M. McCrudden, et al. 2014. "Development and Characterization of Self-Assembling Nanoparticles Using a Bio-Inspired Amphipathic Peptide for Gene Delivery." *Journal of Controlled Release* 189: 141–49. https://doi.org/10.1016/j.jconrel.2014.06.048.

McIntyre, Glen J., Allison J. Arndt, Kirsten M. Gillespie, Wendy M. Mak, and Gregory C. Fanning. 2011. "A Comparison of Multiple shRNA Expression Methods for Combinatorial RNAi." *Genetic Vaccines and Therapy* 9 (1): 9. https://doi.org/10.1186/1479-0556-9-9.

McKey, Jennifer, Delphine Martire, Pascal de Santa Barbara, and Sandrine Faure. 2016. "LIX1 Regulates YAP1 Activity and Controls the Proliferation and Differentiation of Stomach Mesenchymal Progenitors." *BMC Biology* 14 (April): 34. https://doi.org/10.1186/s12915-016-0257-2.

Meade, BR, and SF Dowdy. 2007. "Exogenous siRNA Delivery Using Peptide Transduction Domains/Cell Penetrating Peptides." *Advanced Drug Delivery Reviews* 59 (2–3). https://doi.org/10.1016/j.addr.2007.03.004.

Meng, Zhipeng, Toshiro Moroishi, and Kun-Liang Guan. 2016. "Mechanisms of Hippo Pathway Regulation." *Genes & Development* 30 (1): 1–17. https://doi.org/10.1101/gad.274027.115.

Menge, Franka, Jens Jakob, Bernd Kasper, Armand Smakic, Timo Gaiser, and Peter Hohenberger. 2018. "Clinical Presentation of Gastrointestinal Stromal Tumors." *Visceral Medicine* 34 (5): 335–40. https://doi.org/10.1159/000494303.

Merker, Weitz J, and Stange De. 2016. "Gastrointestinal Organoids: How They Gut It Out." *Developmental Biology* 420 (2). https://doi.org/10.1016/j.ydbio.2016.08.010.

Merritt, Nicole M., Colleen A. Fullenkamp, Sarah L. Hall, et al. 2018. "A Comprehensive Evaluation of Hippo Pathway Silencing in Sarcomas." *Oncotarget* 9 (60): 31620–36. https://doi.org/10.18632/oncotarget.25824.

Messina, Beatrice, Federica Lo Sardo, Stefano Scalera, et al. 2023. "Hippo Pathway Dysregulation in Gastric Cancer: From Helicobacter Pylori Infection to Tumor Promotion and Progression." *Cell Death & Disease* 14 (1): 1–12. https://doi.org/10.1038/s41419-023-05568-8.

Miettinen, M., L. H. Sobin, and M. Sarlomo-Rikala. 2000. "Immunohistochemical Spectrum of GISTs at Different Sites and Their Differential Diagnosis with a Reference to CD117 (KIT)." *Modern Pathology: An Official Journal of the United States and Canadian Academy of Pathology, Inc* 13 (10): 1134–42. https://doi.org/10.1038/modpathol.3880210.

Miettinen, M., M. Virolainen, and null Maarit-Sarlomo-Rikala. 1995. "Gastrointestinal Stromal Tumors--Value of CD34 Antigen in Their Identification and Separation from True Leiomyomas and Schwannomas." *The American Journal of Surgical Pathology* 19 (2): 207–16. https://doi.org/10.1097/00000478-199502000-00009.

Miettinen, Markku, and Jerzy Lasota. 2006. "Gastrointestinal Stromal Tumors: Review on Morphology, Molecular Pathology, Prognosis, and Differential Diagnosis." *Archives of Pathology & Laboratory Medicine* 130 (10): 1466–78. https://doi.org/10.5858/2006-130-1466-GSTROM.

Min, K. W., and M. Leabu. 2006. "Interstitial Cells of Cajal (ICC) and Gastrointestinal Stromal Tumor (GIST): Facts, Speculations, and Myths." *Journal of Cellular and Molecular Medicine* 10 (4): 995–1013. https://doi.org/10.1111/j.1582-4934.2006.tb00541.x.

REFERENCES

Miranda, Maria Zena, Janne Folke Bialik, Pam Speight, et al. 2017. "TGF-B1 Regulates the Expression and Transcriptional Activity of TAZ Protein via a Smad3-Independent, Myocardin-Related Transcription Factor-Mediated Mechanism." *Journal of Biological Chemistry* 292 (36): 14902–20. https://doi.org/10.1074/jbc.M117.780502.

Mizuno, T., H. Murakami, M. Fujii, et al. 2012. "YAP Induces Malignant Mesothelioma Cell Proliferation by Upregulating Transcription of Cell Cycle-Promoting Genes." *Oncogene* 31 (49): 5117–22. https://doi.org/10.1038/onc.2012.5.

Mo, Fan-E., Andrew G. Muntean, Chih-Chiun Chen, Donna B. Stolz, Simon C. Watkins, and Lester F. Lau. 2002. "CYR61 (CCN1) Is Essential for Placental Development and Vascular Integrity." *Molecular and Cellular Biology* 22 (24): 8709–20. https://doi.org/10.1128/MCB.22.24.8709-8720.2002.

Mol, Clifford D., Douglas R. Dougan, Thomas R. Schneider, et al. 2004. "Structural Basis for the Autoinhibition and STI-571 Inhibition of c-Kit Tyrosine Kinase." *The Journal of Biological Chemistry* 279 (30): 31655–63. https://doi.org/10.1074/jbc.M403319200.

Molina-Castro, Silvia Elena, Camille Tiffon, Julie Giraud, et al. 2020. "The Hippo Kinase LATS2 Controls Helicobacter Pylori-Induced Epithelial-Mesenchymal Transition and Intestinal Metaplasia in Gastric Mucosa." *Cellular and Molecular Gastroenterology and Hepatology* 9 (2): 257–76. https://doi.org/10.1016/j.jcmgh.2019.10.007.

Monges, Geneviève, Ségolène Bisot-Locard, Jean-Yves Blay, et al. 2010. "The Estimated Incidence of Gastrointestinal Stromal Tumors in France. Results of PROGIST Study Conducted among Pathologists." *Bulletin Du Cancer* 97 (3): E16–22. https://doi.org/10.1684/bdc.2010.1041.

Montalto, Francesca Ida, and Francesca De Amicis. 2020. "Cyclin D1 in Cancer: A Molecular Connection for Cell Cycle Control, Adhesion and Invasion in Tumor and Stroma." *Cells* 9 (12): 2648. https://doi.org/10.3390/cells9122648.

Morice, Sarah, Mathilde Mullard, Regis Brion, et al. 2020. "The YAP/TEAD Axis as a New Therapeutic Target in Osteosarcoma: Effect of Verteporfin and CA3 on Primary Tumor Growth." *Cancers* 12 (12): 3847. https://doi.org/10.3390/cancers12123847.

Moriyama, Kenta, and Toshiyuki Hori. 2019. "BCR-ABL Induces Tyrosine Phosphorylation of YAP Leading to Expression of Survivin and Cyclin D1 in Chronic Myeloid Leukemia Cells." *International Journal of Hematology* 110 (5): 591–98. https://doi.org/10.1007/s12185-019-02726-7.

Morris, M. C., P. Vidal, L. Chaloin, F. Heitz, and G. Divita. 1997. "A New Peptide Vector for Efficient Delivery of Oligonucleotides into Mammalian Cells." *Nucleic Acids Research* 25 (14): 2730–36. https://doi.org/10.1093/nar/25.14.2730.

Mouillet-Richard, Sophie, and Pierre Laurent-Puig. 2020. "YAP/TAZ Signalling in Colorectal Cancer: Lessons from Consensus Molecular Subtypes." *Cancers* 12 (11): 3160. https://doi.org/10.3390/cancers12113160.

Mucciarini, Claudia, Giulio Rossi, Federica Bertolini, et al. 2007. "Incidence and Clinicopathologic Features of Gastrointestinal Stromal Tumors. A Population-Based Study." *Cancer* 7: 230. https://doi.org/10.1186/1471-2407-7-230.

Mullen, Dorinda, Rajkumar Vajpeyi, Jose-Mario Capo-Chichi, Klaudia Nowak, Newton Wong, and Runjan Chetty. 2023. "Gastrointestinal Stromal Tumours (GISTs) with KRAS Mutation: A Rare

but Important Subset of GISTs." *Case Reports in Gastrointestinal Medicine* 2023: 4248128. https://doi.org/10.1155/2023/4248128.

Murakami, Masao, Junji Tominaga, Ryosuke Makita, et al. 2006. "Transcriptional Activity of Pax3 Is Co-Activated by TAZ." *Biochemical and Biophysical Research Communications* 339 (2): 533–39. https://doi.org/10.1016/j.bbrc.2005.10.214.

Na, Young-Soon, Min-Hee Ryu, Changhoon Yoo, et al. 2017. "Establishment and Characterization of Patient-Derived Xenograft Models of Gastrointestinal Stromal Tumor Resistant to Standard Tyrosine Kinase Inhibitors." *Oncotarget* 8 (44): 76712–21. https://doi.org/10.18632/oncotarget.20816.

Nakamura, K., and T. Yamamoto. 1988. "Morphology of Smooth Muscle Cells in the Rat Thoracic Duct. A Scanning and Transmission Electron-Microscope Study." *Cell and Tissue Research* 251 (2): 243–48. https://doi.org/10.1007/BF00215831.

Nannini, Margherita, Alessandro Rizzo, Valentina Indio, Angela Schipani, Annalisa Astolfi, and Maria Abbondanza Pantaleo. 2021. "Targeted Therapy in SDH-Deficient GIST." *Therapeutic Advances in Medical Oncology* 13: 17588359211023278. https://doi.org/10.1177/17588359211023278.

Neppala, Pushpa, Sudeep Banerjee, Paul T. Fanta, et al. 2019. "Current Management of Succinate Dehydrogenase-Deficient Gastrointestinal Stromal Tumors." *Cancer Metastasis Reviews* 38 (3): 525–35. https://doi.org/10.1007/s10555-019-09818-0.

Neunlist, Michel, Laurianne Van Landeghem, Maxime M. Mahé, Pascal Derkinderen, Stanislas Bruley des Varannes, and Malvyne Rolli-Derkinderen. 2013. "The Digestive Neuronal-Glial-Epithelial Unit: A New Actor in Gut Health and Disease." *Nature Reviews. Gastroenterology & Hepatology* 10 (2): 90–100. https://doi.org/10.1038/nrgastro.2012.221.

Neves, Ana Raquel, Tânia Albuquerque, Rúben Faria, et al. 2022. "Development of WRAP5 Peptide Complexes for Targeted Drug/Gene Co-Delivery toward Glioblastoma Therapy." *Pharmaceutics* 14 (10): 2213. https://doi.org/10.3390/pharmaceutics14102213.

Nimmakayala, Rama Krishna, Ayoola O. Ogunleye, Seema Parte, et al. 2022. "PAF1 Cooperates with YAP1 in Metaplastic Ducts to Promote Pancreatic Cancer." *Cell Death & Disease* 13 (10): 839. https://doi.org/10.1038/s41419-022-05258-x.

Nishida, Toshirou, Yoichi Naito, Tsuyoshi Takahashi, et al. 2024. "Molecular and Clinicopathological Features of KIT/PDGFRA Wild-Type Gastrointestinal Stromal Tumors." *Cancer Science* 115 (3): 894–904. https://doi.org/10.1111/cas.16058.

Noland, Cameron L., Sarah Gierke, Paul D. Schnier, et al. 2016. "Palmitoylation of TEAD Transcription Factors Is Required for Their Stability and Function in Hippo Pathway Signaling." *Structure* 24 (1): 179–86. https://doi.org/10.1016/j.str.2015.11.005.

Okafor, Michael, David Schmitt, Stéphane Ory, et al. 2025. "The Different Cellular Entry Routes for Drug Delivery Using Cell Penetrating Peptides." *Biology of the Cell* 117 (6): e70012. https://doi.org/10.1111/boc.70012.

Oosterom, A. T. van, I. Judson, J. Verweij, et al. 2001. "Safety and Efficacy of Imatinib (STI571) in Metastatic Gastrointestinal Stromal Tumours: A Phase I Study." *Lancet* 358 (9291): 1421–23. https://doi.org/10.1016/s0140-6736(01)06535-7.

REFERENCES

Ou, W.-b, M.-j Zhu, G. D. Demetri, C. D. M. Fletcher, and J. A. Fletcher. 2008. "Protein Kinase C-θ Regulates KIT Expression and Proliferation in Gastrointestinal Stromal Tumors." *Oncogene* 27 (42): 5624–34. https://doi.org/10.1038/onc.2008.177.

Ou, Wen-Bin, Nan Ni, Rui Zuo, et al. 2019. "Cyclin D1 Is a Mediator of Gastrointestinal Stromal Tumor KIT-Independence." *Oncogene* 38 (39): 6615–29. https://doi.org/10.1038/s41388-019-0894-3.

Ozcan, Gulnihal, Bulent Ozpolat, Robert L. Coleman, Anil K. Sood, and Gabriel Lopez-Berestein. 2015. "Preclinical and Clinical Development of siRNA-Based Therapeutics." *Advanced Drug Delivery Reviews* 87: 108–19. https://doi.org/10.1016/j.addr.2015.01.007.

Paddison, Patrick J., and Gregory J. Hannon. 2002. "RNA Interference: The New Somatic Cell Genetics?" *Cancer Cell* 2 (1): 17–23. https://doi.org/10.1016/s1535-6108(02)00092-2.

Pantalacci, Sophie, Nicolas Tapon, and Pierre Léopold. 2003. "The Salvador Partner Hippo Promotes Apoptosis and Cell-Cycle Exit in Drosophila." *Nature Cell Biology* 5 (10): 921–27. https://doi.org/10.1038/ncb1051.

Pantaleo, Maria A., Michael C. Heinrich, Antoine Italiano, et al. 2022. "A Multicenter, Dose-Finding, Phase 1b Study of Imatinib in Combination with Alpelisib as Third-Line Treatment in Patients with Advanced Gastrointestinal Stromal Tumor." *Cancer* 22 (1): 511. https://doi.org/10.1186/s12885-022-09610-4.

Parab, Trisha M., Michael J. DeRogatis, Alexander M. Boaz, et al. 2019. "Gastrointestinal Stromal Tumors: A Comprehensive Review." *Journal of Gastrointestinal Oncology* 10 (1): 144–54. https://doi.org/10.21037/jgo.2018.08.20.

Paramasivam, Murugan, Ali Sarkeshik, John R. Yates, Maria J. G. Fernandes, and Dannel McCollum. 2011. "Angiomotin Family Proteins Are Novel Activators of the LATS2 Kinase Tumor Suppressor." *Molecular Biology of the Cell* 22 (19): 3725–33. https://doi.org/10.1091/mbc.E11-04-0300.

Park, Kwon-Sik, Jeffrey A. Whitsett, Tina Di Palma, Jeong-Ho Hong, Michael B. Yaffe, and Mariastella Zannini. 2004. "TAZ Interacts with TTF-1 and Regulates Expression of Surfactant Protein-C." *The Journal of Biological Chemistry* 279 (17): 17384–90. https://doi.org/10.1074/jbc.M312569200.

Patel, Shreyaskumar. 2013. "Exploring Novel Therapeutic Targets in GIST: Focus on the PI3K/Akt/mTOR Pathway." *Current Oncology Reports* 15 (4): 386–95. https://doi.org/10.1007/s11912-013-0316-6.

Patterson, Molly R., Joseph A. Cogan, Rosa Cassidy, et al. 2024. "The Hippo Pathway Transcription Factors YAP and TAZ Play HPV-Type Dependent Roles in Cervical Cancer." *Nature Communications* 15 (1): 5809. https://doi.org/10.1038/s41467-024-49965-9.

Peck, D., and C. M. Isacke. 1998. "Hyaluronan-Dependent Cell Migration Can Be Blocked by a CD44 Cytoplasmic Domain Peptide Containing a Phosphoserine at Position 325." *Journal of Cell Science* 111: 1595–601. https://doi.org/10.1242/jcs.111.11.1595.

Perciavalle, Rhonda M., Daniel P. Stewart, Brian Koss, et al. 2012. "Anti-Apoptotic MCL-1 Localizes to the Mitochondrial Matrix and Couples Mitochondrial Fusion to Respiration." *Nature Cell Biology* 14 (6): 575–83. https://doi.org/10.1038/ncb2488.

REFERENCES

Piccolo, Stefano, Sirio Dupont, and Michelangelo Cordenonsi. 2014. "The Biology of YAP/TAZ: Hippo Signaling and Beyond." *Physiological Reviews* 94 (4): 1287–312. https://doi.org/10.1152/physrev.00005.2014.

Piccolo, Stefano, Tito Panciera, Paolo Contessotto, and Michelangelo Cordenonsi. 2023. "YAP/TAZ as Master Regulators in Cancer: Modulation, Function and Therapeutic Approaches." *Nature Cancer* 4 (1): 9–26. https://doi.org/10.1038/s43018-022-00473-z.

Plouffe, Steven W., Kimberly C. Lin, Jerrell L. Moore, et al. 2018. "The Hippo Pathway Effector Proteins YAP and TAZ Have Both Distinct and Overlapping Functions in the Cell." *The Journal of Biological Chemistry* 293 (28): 11230–40. https://doi.org/10.1074/jbc.RA118.002715.

Polack, Fernando P., Stephen J. Thomas, Nicholas Kitchin, et al. 2020. "Safety and Efficacy of the BNT162b2 mRNA Covid-19 Vaccine." *The New England Journal of Medicine* 383 (27): 2603–15. https://doi.org/10.1056/NEJMoa2034577.

Proaño-Pérez, Elizabeth, Eva Serrano-Candelas, Alfonso García-Valverde, et al. 2023. "The Microphthalmia-Associated Transcription Factor Is Involved in Gastrointestinal Stromal Tumor Growth." *Cancer Gene Therapy* 30 (2): 245–55. https://doi.org/10.1038/s41417-022-00539-1.

Proaño-Pérez, Elizabeth, Eva Serrano-Candelas, Cindy Mancia, Arnau Navinés-Ferrer, Mario Guerrero, and Margarita Martin. 2022. "SH3BP2 Silencing Increases miRNAs Targeting ETV1 and Microphthalmia-Associated Transcription Factor, Decreasing the Proliferation of Gastrointestinal Stromal Tumors." *Cancers* 14 (24): 6198. https://doi.org/10.3390/cancers14246198.

Procaccia, Vera, Hironao Nakayama, Akio Shimizu, and Michael Klagsbrun. 2014. "Gleevec/Imatinib, an ABL2 Kinase Inhibitor, Protects Tumor and Endothelial Cells from Semaphorin-Induced Cytoskeleton Collapse and Loss of Cell Motility." *Biochemical and Biophysical Research Communications* 448 (2): 134–38. https://doi.org/10.1016/j.bbrc.2014.04.063.

Qie, Shuo, and J. Alan Diehl. 2016. "Cyclin D1, Cancer Progression and Opportunities in Cancer Treatment." *Journal of Molecular Medicine* 94 (12): 1313–26. https://doi.org/10.1007/s00109-016-1475-3.

Qiu, Dandan, Lingling Gao, and Xingwei Yu. 2024. "Knockdown of YAP1 Reduces YTHDF3 to Stabilize SMAD7 and Thus Inhibit Bladder Cancer Stem Cell Stemness." *Discovery Medicine.* 36 (186): 1486–98. https://doi.org/10.24976/Discov.Med.202436186.138.

Ramazani, Yasaman, Noël Knops, Mohamed A. Elmonem, et al. 2018. "Connective Tissue Growth Factor (CTGF) from Basics to Clinics." *Matrix Biology* 68–69: 44–66. https://doi.org/10.1016/j.matbio.2018.03.007.

Ran, Leili, Inna Sirota, Zhen Cao, et al. 2015. "Combined Inhibition of MAP Kinase and KIT Signaling Synergistically Destabilizes ETV1 and Suppresses GIST Tumor Growth." *Cancer Discovery* 5 (3): 304–15. https://doi.org/10.1158/2159-8290.CD-14-0985.

Ranasinghe, Priyanga, Melisande L. Addison, James W. Dear, and David J. Webb. 2023. "Small Interfering RNA: Discovery, Pharmacology and Clinical Development-An Introductory Review." *British Journal of Pharmacology* 180 (21): 2697–720. https://doi.org/10.1111/bph.15972.

REFERENCES

Redhwan, Moqbel Ali Moqbel, Hariprasad M G, Suman Samaddar, et al. 2023. "Small Interference (RNAi) Technique: Exploring Its Clinical Applications, Benefits and Limitations." *European Journal of Clinical Investigation* 53 (10): e14039. https://doi.org/10.1111/eci.14039.

Reggiani, Francesca, Giulia Gobbi, Alessia Ciarrocchi, and Valentina Sancisi. 2021. "YAP and TAZ Are Not Identical Twins." *Trends in Biochemical Sciences* 46 (2): 154–68. https://doi.org/10.1016/j.tibs.2020.08.012.

Robbins, Marjorie, Adam Judge, and Ian MacLachlan. 2009. "siRNA and Innate Immunity." *Oligonucleotides* 19 (2): 89–102. https://doi.org/10.1089/oli.2009.0180.

Robinson, Tim L., Kanishka Sircar, Bryan R. Hewlett, Katherine Chorneyko, Robert H. Riddell, and Jan D. Huizinga. 2000. "Gastrointestinal Stromal Tumors May Originate from a Subset of CD34-Positive Interstitial Cells of Cajal." *The American Journal of Pathology* 156 (4): 1157–63. https://doi.org/10.1016/S0002-9440(10)64984-X.

Rosenbluh, Joseph, Deepak Nijhawan, Andrew G. Cox, et al. 2012. "β-Catenin-Driven Cancers Require a YAP1 Transcriptional Complex for Survival and Tumorigenesis." *Cell* 151 (7): 1457–73. https://doi.org/10.1016/j.cell.2012.11.026.

Rothzerg, Emel, Evan Ingley, Benjamin Mullin, Wei Xue, David Wood, and Jiake Xu. 2021. "The Hippo in the Room: Targeting the Hippo Signalling Pathway for Osteosarcoma Therapies." *Journal of Cellular Physiology* 236 (3): 1606–15. https://doi.org/10.1002/jcp.29967.

Rubin, Brian P., Cristina R. Antonescu, James P. Scott-Browne, et al. 2005. "A Knock-in Mouse Model of Gastrointestinal Stromal Tumor Harboring Kit K641E." *Cancer Research* 65 (15): 6631–39. https://doi.org/10.1158/0008-5472.CAN-05-0891.

Ruiz-Demoulin, Salomé, Eva Trenquier, Sanaa Dekkar, et al. 2023. "LIX1 Controls MAPK Signaling Reactivation and Contributes to GIST-T1 Cell Resistance to Imatinib." *International Journal of Molecular Sciences* 24 (8): 7138. https://doi.org/10.3390/ijms24087138.

Ruseska, Ivana, and Andreas Zimmer. 2020. "Internalization Mechanisms of Cell-Penetrating Peptides." *Beilstein Journal of Nanotechnology* 11: 101–23. https://doi.org/10.3762/bjnano.11.10.

Rutkowski, Piotr, Katarzyna Seliga, and Maria Dębiec-Rychter. 2022. "SDH-Deficient Gastrointestinal Stromal Tumours." *Nowotwory. Journal of Oncology* 72 (5): 5. https://doi.org/10.5603/NJO.2022.0052.

Salguero-Aranda, Carmen, Joaquín Olmedo-Pelayo, Enrique de Álava, Ana Teresa Amaral, and Juan Díaz-Martín. 2022. "Genetic Alterations and Deregulation of Hippo Pathway as a Pathogenetic Mechanism in Bone and Soft Tissue Sarcoma." *Cancers* 14 (24): 6211. https://doi.org/10.3390/cancers14246211.

Sanchez-Vega, Francisco, Marco Mina, Joshua Armenia, et al. 2018. "Oncogenic Signaling Pathways in The Cancer Genome Atlas." *Cell* 173 (2): 321-337.e10. https://doi.org/10.1016/j.cell.2018.03.035.

Sandvik, Oddvar M., Kjetil Søreide, Jan Terje Kvaløy, Einar Gudlaugsson, and Jon Arne Søreide. 2011. "Epidemiology of Gastrointestinal Stromal Tumours: Single-Institution Experience and Clinical Presentation over Three Decades." *Cancer Epidemiology* 35 (6): 515–20. https://doi.org/10.1016/j.canep.2011.03.002.

REFERENCES

Sano, Daisuke, Takako Kihara, Jiayin Yuan, et al. 2023. "Characterization of Cell Line with Dedifferentiated GIST-like Features Established from Cecal GIST of Familial GIST Model Mice." *Pathology International* 73 (5): 181–87. https://doi.org/10.1111/pin.13315.

Santoro, Massimo, and Francesca Carlomagno. 2013. "Central Role of RET in Thyroid Cancer." *Cold Spring Harbor Perspectives in Biology* 5 (12): a009233. https://doi.org/10.1101/cshperspect.a009233.

Sbaraglia, Marta, Elena Bellan, and Angelo P. Dei Tos. 2021. "The 2020 WHO Classification of Soft Tissue Tumours: News and Perspectives." *Pathologica* 113 (2): 70–84. https://doi.org/10.32074/1591-951X-213.

Schaefer, Inga-Marie, Ronald P. DeMatteo, and César Serrano. 2022. "The GIST of Advances in Treatment of Advanced Gastrointestinal Stromal Tumor." *American Society of Clinical Oncology Educational Book* 42: 1–15. https://doi.org/10.1200/EDBK_351231.

Schipani, Angela, Margherita Nannini, Annalisa Astolfi, and Maria A. Pantaleo. 2023. "SDHA Germline Mutations in SDH-Deficient GISTs: A Current Update." *Genes* 14 (3): 646. https://doi.org/10.3390/genes14030646.

Schöffski, P., P. Reichardt, J.-Y. Blay, et al. 2010. "A Phase I-II Study of Everolimus (RAD001) in Combination with Imatinib in Patients with Imatinib-Resistant Gastrointestinal Stromal Tumors." *Annals of Oncology* 21 (10): 1990–98. https://doi.org/10.1093/annonc/mdq076.

Schroeder, Molly C., and Georg Halder. 2012. "Regulation of the Hippo Pathway by Cell Architecture and Mechanical Signals." *Seminars in Cell & Developmental Biology* 23 (7): 803–11. https://doi.org/10.1016/j.semcdb.2012.06.001.

Schultheis, Beate, Dirk Strumberg, Jan Kuhlmann, et al. 2020. "Safety, Efficacy and Pharcacokinetics of Targeted Therapy with The Liposomal RNA Interference Therapeutic Atu027 Combined with Gemcitabine in Patients with Pancreatic Adenocarcinoma. A Randomized Phase Ib/IIa Study." *Cancers* 12 (11): 3130. https://doi.org/10.3390/cancers12113130.

Scirocco, Annunziata, Paola Matarrese, Marilia Carabotti, Barbara Ascione, Walter Malorni, and Carola Severi. 2016. "Cellular and Molecular Mechanisms of Phenotypic Switch in Gastrointestinal Smooth Muscle." *Journal of Cellular Physiology* 231 (2): 295–302. https://doi.org/10.1002/jcp.25105.

Scott, Lesley J. 2020. "Givosiran: First Approval." *Drugs* 80 (3): 335–39. https://doi.org/10.1007/s40265-020-01269-0.

Scott, Lesley J., and Susan J. Keam. 2021. "Lumasiran: First Approval." *Drugs* 81 (2): 277–82. https://doi.org/10.1007/s40265-020-01463-0.

Seeneevassen, Lornella, Pierre Dubus, Caroline Gronnier, and Christine Varon. 2022. "Hippo in Gastric Cancer: From Signalling to Therapy." *Cancers* 14 (9): 2282. https://doi.org/10.3390/cancers14092282.

Serrano, C., S. Bauer, D. Gómez-Peregrina, et al. 2023. "Circulating Tumor DNA Analysis of the Phase III VOYAGER Trial: KIT Mutational Landscape and Outcomes in Patients with Advanced Gastrointestinal Stromal Tumor Treated with Avapritinib or Regorafenib." *Annals of Oncology* 34 (7): 615–25. https://doi.org/10.1016/j.annonc.2023.04.006.

REFERENCES

Serrano, César. 2021. "New Treatments in Advanced Gastrointestinal Stromal Tumor." *Current Opinion in Oncology* 33 (4): 323–28. https://doi.org/10.1097/CCO.0000000000000745.

Serrano, César, and Sebastian Bauer. 2022. "New Tyrosine Kinase Inhibitors for the Treatment of Gastrointestinal Stromal Tumors." *Current Oncology Reports* 24 (2): 151–59. https://doi.org/10.1007/s11912-021-01165-0.

Serrano, César, and Jonathan A. Fletcher. 2019. "Overcoming Heterogenity in Imatinib-Resistant Gastrointestinal Stromal Tumor." *Oncotarget* 10 (59): 6286–87. https://doi.org/10.18632/oncotarget.27277.

Serrano, César, and Suzanne George. 2020. "Gastrointestinal Stromal Tumor: Challenges and Opportunities for a New Decade." *Clinical Cancer Research* 26 (19): 5078–85. https://doi.org/10.1158/1078-0432.CCR-20-1706.

Serrano, César, Adrián Mariño-Enríquez, Derrick L. Tao, et al. 2019. "Complementary Activity of Tyrosine Kinase Inhibitors against Secondary Kit Mutations in Imatinib-Resistant Gastrointestinal Stromal Tumours." *British Journal of Cancer* 120 (6): 612–20. https://doi.org/10.1038/s41416-019-0389-6.

Serrano, César, Javier Martín-Broto, José Manuel Asencio-Pascual, et al. 2023. "2023 GEIS Guidelines for Gastrointestinal Stromal Tumors." *Therapeutic Advances in Medical Oncology* 15: 17588359231192388. https://doi.org/10.1177/17588359231192388.

Serrano-Candelas, Eva, Erola Ainsua-Enrich, Arnau Navinés-Ferrer, et al. 2018. "Silencing of Adaptor Protein SH3BP2 Reduces KIT/PDGFRA Receptors Expression and Impairs Gastrointestinal Stromal Tumors Growth." *Molecular Oncology* 12 (8): 1383–97. https://doi.org/10.1002/1878-0261.12332.

Shen, He, Yanmin Chen, Yin Wan, et al. 2021. "Identification of TAZ-Dependent Breast Cancer Vulnerabilities Using a Chemical Genomics Screening Approach." *Frontiers in Cell and Developmental Biology* 9: 673374. https://doi.org/10.3389/fcell.2021.673374.

Shen, Le. 2009. "Functional Morphology of the Gastrointestinal Tract." *Current Topics in Microbiology and Immunology* 337: 1–35. https://doi.org/10.1007/978-3-642-01846-6_1.

Sheng, Chunquan, Guoqiang Dong, Zhenyuan Miao, Wannian Zhang, and Wei Wang. 2015. "State-of-the-Art Strategies for Targeting Protein-Protein Interactions by Small-Molecule Inhibitors." *Chemical Society Reviews* 44 (22): 8238–59. https://doi.org/10.1039/c5cs00252d.

Shibata, Masahiro, Kendall Ham, and Mohammad Obaidul Hoque. 2018. "A Time for YAP1: Tumorigenesis, Immunosuppression and Targeted Therapy." *International Journal of Cancer* 143 (9): 2133–44. https://doi.org/10.1002/ijc.31561.

Shin, Ji Eun, Soo-Hyun Kim, Mingyu Kong, et al. 2023. "Targeting FLT3-TAZ Signaling to Suppress Drug Resistance in Blast Phase Chronic Myeloid Leukemia." *Molecular Cancer* 22 (1): 177. https://doi.org/10.1186/s12943-023-01837-4.

Shoari, Alireza, Raheleh Tooyserkani, Mehdi Tahmasebi, and Dennis W. P. M. Löwik. 2021. "Delivery of Various Cargos into Cancer Cells and Tissues via Cell-Penetrating Peptides: A Review of the Last Decade." *Pharmaceutics* 13 (9): 1391. https://doi.org/10.3390/pharmaceutics13091391.

REFERENCES

Shorstova, Tatiana, William D. Foulkes, and Michael Witcher. 2021. "Achieving Clinical Success with BET Inhibitors as Anti-Cancer Agents." *British Journal of Cancer* 124 (9): 1478–90. https://doi.org/10.1038/s41416-021-01321-0.

Shreberk-Shaked, Michal, Bareket Dassa, Sanju Sinha, et al. 2020. "A Division of Labor between YAP and TAZ in Non-Small Cell Lung Cancer." *Cancer Research* 80 (19): 4145–57. https://doi.org/10.1158/0008-5472.CAN-20-0125.

Shrestha, Madhu, Toshinori Ando, Chanbora Chea, et al. 2019. "The Transition of Tissue Inhibitor of Metalloproteinases from -4 to -1 Induces Aggressive Behavior and Poor Patient Survival in Dedifferentiated Liposarcoma via YAP/TAZ Activation." *Carcinogenesis* 40 (10): 1288–97. https://doi.org/10.1093/carcin/bgz023.

Simon, Susanne, Florian Grabellus, Loretta Ferrera, et al. 2013. "DOG1 Regulates Growth and IGFBP-5 in Gastrointestinal Stromal Tumors." *Cancer Research* 73 (12): 3661–70. https://doi.org/10.1158/0008-5472.CAN-12-3839.

Singh, Jyoti, Abdulaziz S. Saeedan, Gaurav Kaithwas, and Mohd Nazam Ansari. 2025. "Small Interfering RNA: From Designing to Therapeutic in Cancer." *Journal, Genetic Engineering & Biotechnology* 23 (2): 100484. https://doi.org/10.1016/j.jgeb.2025.100484.

Sohrabi, Nasrin, Alireza Valizadeh, Samad Mussa Farkhani, and Abolfazl Akbarzadeh. 2016. "Basics of DNA Biosensors and Cancer Diagnosis." *Artificial Cells, Nanomedicine, and Biotechnology* 44 (2): 654–63. https://doi.org/10.3109/21691401.2014.976707.

Sommer, Gunhild, Valter Agosti, Imke Ehlers, et al. 2003. "Gastrointestinal Stromal Tumors in a Mouse Model by Targeted Mutation of the Kit Receptor Tyrosine Kinase." *Proceedings of the National Academy of Sciences of the United States of America* 100 (11): 6706–11. https://doi.org/10.1073/pnas.1037763100.

Song, Shumei, Min Xie, Ailing W. Scott, et al. 2018. "A Novel YAP1 Inhibitor Targets CSC-Enriched Radiation-Resistant Cells and Exerts Strong Antitumor Activity in Esophageal Adenocarcinoma." *Molecular Cancer Therapeutics* 17 (2): 443–54. https://doi.org/10.1158/1535-7163.MCT-17-0560.

Søreide, Kjetil, Oddvar M. Sandvik, Jon Arne Søreide, Vanja Giljaca, Andrea Jureckova, and V. Ramesh Bulusu. 2016. "Global Epidemiology of Gastrointestinal Stromal Tumours (GIST): A Systematic Review of Population-Based Cohort Studies." *Cancer Epidemiology* 40: 39–46. https://doi.org/10.1016/j.canep.2015.10.031.

Strano, S., E. Munarriz, M. Rossi, et al. 2001. "Physical Interaction with Yes-Associated Protein Enhances P73 Transcriptional Activity." *The Journal of Biological Chemistry* 276 (18): 15164–73. https://doi.org/10.1074/jbc.M010484200.

Sudol, M. 1994. "Yes-Associated Protein (YAP65) Is a Proline-Rich Phosphoprotein That Binds to the SH3 Domain of the Yes Proto-Oncogene Product." *Oncogene* 9 (8): 2145–52.

Suk, Jung Soo, Qingguo Xu, Namho Kim, Justin Hanes, and Laura M. Ensign. 2016. "PEGylation as a Strategy for Improving Nanoparticle-Based Drug and Gene Delivery." *Advanced Drug Delivery Reviews* 99 (Pt A): 28–51. https://doi.org/10.1016/j.addr.2015.09.012.

REFERENCES

Sun, Yang, Lu Hu, Zhipeng Tao, et al. 2022. "Pharmacological Blockade of TEAD-YAP Reveals Its Therapeutic Limitation in Cancer Cells." *Nature Communications* 13 (1): 6744. https://doi.org/10.1038/s41467-022-34559-0.

Swalchick, William, Rania Shamekh, and Marily M. Bui. 2015. "Is DOG1 Immunoreactivity Specific to Gastrointestinal Stromal Tumor?" *Cancer Control: Journal of the Moffitt Cancer Center* 22 (4): 498–504. https://doi.org/10.1177/107327481502200416.

Syed, Yahiya Y. 2023. "Nedosiran: First Approval." *Drugs* 83 (18): 1729–33. https://doi.org/10.1007/s40265-023-01976-4.

Taguchi, Takahiro, Hiroshi Sonobe, Shin-ichi Toyonaga, et al. 2002. "Conventional and Molecular Cytogenetic Characterization of a New Human Cell Line, GIST-T1, Established from Gastrointestinal Stromal Tumor." *Laboratory Investigation* 82 (5): 663–65. https://doi.org/10.1038/labinvest.3780461.

Tang, Tracy T., Andrei W. Konradi, Ying Feng, et al. 2021. "Small Molecule Inhibitors of TEAD Auto-Palmitoylation Selectively Inhibit Proliferation and Tumor Growth of NF2-Deficient Mesothelioma." *Molecular Cancer Therapeutics* 20 (6): 986–98. https://doi.org/10.1158/1535-7163.MCT-20-0717.

Tapon, Nicolas, Kieran F. Harvey, Daphne W. Bell, et al. 2002. "Salvador Promotes Both Cell Cycle Exit and Apoptosis in Drosophila and Is Mutated in Human Cancer Cell Lines." *Cell* 110 (4): 467–78. https://doi.org/10.1016/s0092-8674(02)00824-3.

Tarvirdipour, Shabnam, Xinan Huang, Voichita Mihali, Cora-Ann Schoenenberger, and Cornelia G. Palivan. 2020. "Peptide-Based Nanoassemblies in Gene Therapy and Diagnosis: Paving the Way for Clinical Application." *Molecules* 25 (15): 3482. https://doi.org/10.3390/molecules25153482.

Teko-Agbo, Clémentine Ayélé, Emilie Josse, Karidia Konate, et al. 2025. "A Short Peptide for Efficient Cellular mRNA Delivery: A Potential Application for Inducing an Immune Response." *Molecular Therapy. Nucleic Acids* 36 (3): 102650. https://doi.org/10.1016/j.omtn.2025.102650.

Thrash, Hannah L., and Ann Marie Pendergast. 2023. "Multi-Functional Regulation by YAP/TAZ Signaling Networks in Tumor Progression and Metastasis." *Cancers* 15 (19): 19. https://doi.org/10.3390/cancers15194701.

Tiffon, Camille, Julie Giraud, Silvia Elena Molina-Castro, et al. 2020. "TAZ Controls Helicobacter Pylori-Induced Epithelial-Mesenchymal Transition and Cancer Stem Cell-Like Invasive and Tumorigenic Properties." *Cells* 9 (6): 1462. https://doi.org/10.3390/cells9061462.

Tolcher, Anthony W., Kyriakos P. Papadopoulos, Amita Patnaik, et al. 2015. "Safety and Activity of DCR-MYC, a First-in-Class Dicer-Substrate Small Interfering RNA (DsiRNA) Targeting MYC, in a Phase I Study in Patients with Advanced Solid Tumors." *Journal of Clinical Oncology* 33 (15_suppl): 11006–11006. https://doi.org/10.1200/jco.2015.33.15_suppl.11006.

Torihashi, S., K. Nishi, Y. Tokutomi, T. Nishi, S. Ward, and K. M. Sanders. 1999. "Blockade of Kit Signaling Induces Transdifferentiation of Interstitial Cells of Cajal to a Smooth Muscle Phenotype." *Gastroenterology* 117 (1): 140–48. https://doi.org/10.1016/s0016-5085(99)70560-3.

REFERENCES

Tünnemann, Gisela, Gohar Ter-Avetisyan, Robert M. Martin, Martin Stöckl, Andreas Herrmann, and M. Cristina Cardoso. 2008. "Live-Cell Analysis of Cell Penetration Ability and Toxicity of Oligo-Arginines." *Journal of Peptide Science* 14 (4): 469–76. https://doi.org/10.1002/psc.968.

Tuveson, D. A., N. A. Willis, T. Jacks, et al. 2001. "STI571 Inactivation of the Gastrointestinal Stromal Tumor C-KIT Oncoprotein: Biological and Clinical Implications." *Oncogene* 20 (36): 5054–58. https://doi.org/10.1038/sj.onc.1204704.

Tzen, Chin-Yuan, and Bey-Liing Mau. 2005. "Analysis of CD117-Negative Gastrointestinal Stromal Tumors." *World Journal of Gastroenterology* 11 (7): 1052–55. https://doi.org/10.3748/wjg.v11.i7.1052.

Udan, Ryan S., Madhuri Kango-Singh, Riitta Nolo, Chunyao Tao, and Georg Halder. 2003. "Hippo Promotes Proliferation Arrest and Apoptosis in the Salvador/Warts Pathway." *Nature Cell Biology* 5 (10): 914–20. https://doi.org/10.1038/ncb1050.

Van Looy, Thomas, Agnieszka Wozniak, Giuseppe Floris, et al. 2014. "Phosphoinositide 3-Kinase Inhibitors Combined with Imatinib in Patient-Derived Xenograft Models of Gastrointestinal Stromal Tumors: Rationale and Efficacy." *Clinical Cancer Research* 20 (23): 6071–82. https://doi.org/10.1158/1078-0432.CCR-14-1823.

Vandenberghe, Pierre, Marine Delvaux, Perrine Hagué, Christophe Erneux, and Jean-Marie Vanderwinden. 2019. "Potentiation of Imatinib by Cilostazol in Sensitive and Resistant Gastrointestinal Stromal Tumor Cell Lines Involves YAP Inhibition." *Oncotarget* 10 (19): 1798–811. https://doi.org/10.18632/oncotarget.26734.

Varelas, Xaralabos, Rui Sakuma, Payman Samavarchi-Tehrani, et al. 2008. "TAZ Controls Smad Nucleocytoplasmic Shuttling and Regulates Human Embryonic Stem-Cell Self-Renewal." *Nature Cell Biology* 10 (7): 837–48. https://doi.org/10.1038/ncb1748.

Varelas, Xaralabos, Payman Samavarchi-Tehrani, Masahiro Narimatsu, et al. 2010. "The Crumbs Complex Couples Cell Density Sensing to Hippo-Dependent Control of the TGF-β-SMAD Pathway." *Developmental Cell* 19 (6): 831–44. https://doi.org/10.1016/j.devcel.2010.11.012.

Verschoor, Arie J., J. V. M. G. Bovée, L. I. H. Overbeek, PALGA group, P. C. W. Hogendoorn, and H. Gelderblom. 2018. "The Incidence, Mutational Status, Risk Classification and Referral Pattern of Gastro-Intestinal Stromal Tumours in the Netherlands: A Nationwide Pathology Registry (PALGA) Study." *An International Journal of Pathology* 472 (2): 221–29. https://doi.org/10.1007/s00428-017-2285-x.

Vivès, E., P. Brodin, and B. Lebleu. 1997. "A Truncated HIV-1 Tat Protein Basic Domain Rapidly Translocates through the Plasma Membrane and Accumulates in the Cell Nucleus." *The Journal of Biological Chemistry* 272 (25): 16010–17. https://doi.org/10.1074/jbc.272.25.16010.

Wagner, Michael J., Rahul Mitra, Mark J. McArthur, et al. 2017. "Preclinical Mammalian Safety Studies of EPHARNA (DOPC Nanoliposomal EphA2-Targeted siRNA)." *Molecular Cancer Therapeutics* 16 (6): 1114–23. https://doi.org/10.1158/1535-7163.MCT-16-0541.

Wallace, Adam S., and Alan J. Burns. 2005. "Development of the Enteric Nervous System, Smooth Muscle and Interstitial Cells of Cajal in the Human Gastrointestinal Tract." *Cell and Tissue Research* 319 (3): 367–82. https://doi.org/10.1007/s00441-004-1023-2.

REFERENCES

Wang, Luyao, Yuxiang Chen, Maoqian Zhang, et al. 2025. "Chemical Dissection of Selective Myeloid Leukemia-1 Inhibitors: How They Were Found and Evolved." *European Journal of Medicinal Chemistry* 283: 117168. https://doi.org/10.1016/j.ejmech.2024.117168.

Ward, S. M., and K. M. Sanders. 2001. "Physiology and Pathophysiology of the Interstitial Cell of Cajal: From Bench to Bedside. I. Functional Development and Plasticity of Interstitial Cells of Cajal Networks." *American Journal of Physiology. Gastrointestinal and Liver Physiology* 281 (3): G602-611. https://doi.org/10.1152/ajpgi.2001.281.3.G602.

Wei, Yuzi, Victoria Lee Zhi Hui, Yilin Chen, Ruiying Han, Xianglong Han, and Yongwen Guo. 2023. "YAP/TAZ: Molecular Pathway and Disease Therapy." *MedComm* 4 (4): e340. https://doi.org/10.1002/mco2.340.

West, Robert B., Christopher L. Corless, Xin Chen, et al. 2004. "The Novel Marker, DOG1, Is Expressed Ubiquitously in Gastrointestinal Stromal Tumors Irrespective of KIT or PDGFRA Mutation Status." *The American Journal of Pathology* 165 (1): 107–13. https://doi.org/10.1016/S0002-9440(10)63279-8.

Wheatley, Sally P., and Dario C. Altieri. 2019. "Survivin at a Glance." *Journal of Cell Science* 132 (7): jcs223826. https://doi.org/10.1242/jcs.223826.

Wickline, Samuel A., Kirk K. Hou, and Hua Pan. 2023. "Peptide-Based Nanoparticles for Systemic Extrahepatic Delivery of Therapeutic Nucleotides." *International Journal of Molecular Sciences* 24 (11): 9455. https://doi.org/10.3390/ijms24119455.

Wu, Chiao-En, Chin-Yuan Tzen, Shang-Yu Wang, and Chun-Nan Yeh. 2019. "Clinical Diagnosis of Gastrointestinal Stromal Tumor (GIST): From the Molecular Genetic Point of View." *Cancers* 11 (5): 679. https://doi.org/10.3390/cancers11050679.

Wu, Shian, Jianbin Huang, Jixin Dong, and Duojia Pan. 2003. "Hippo Encodes a Ste-20 Family Protein Kinase That Restricts Cell Proliferation and Promotes Apoptosis in Conjunction with Salvador and Warts." *Cell* 114 (4): 445–56. https://doi.org/10.1016/s0092-8674(03)00549-x.

Wu, Xiyu, Masaaki Iwatsuki, Masakazu Takaki, et al. 2024. "FBXW7 Regulates the Sensitivity of Imatinib in Gastrointestinal Stromal Tumors by Targeting MCL1." *Gastric Cancer* 27 (2): 235–47. https://doi.org/10.1007/s10120-023-01454-6.

Wu, Xiyu, Kohei Yamashita, Meiyue Lou, et al. 2025. "AT101 Suppresses Gastrointestinal Stromal Tumor Growth and Promotes Apoptosis via YAP/TAZ-CCND1 and FBXW7-MCL1 Axes." *Annals of Surgical Oncology* 32 (8): 5991–6004. https://doi.org/10.1245/s10434-025-17247-3.

Wu, Xiyu, Kohei Yamashita, Chihiro Matsumoto, et al. 2025. "YAP Acts as an Independent Prognostic Marker and Regulates Growth and Metastasis of Gastrointestinal Stromal Tumors via FBXW7-YAP Pathway." *Journal of Gastroenterology* 60 (3): 275–84. https://doi.org/10.1007/s00535-024-02180-1.

Wyman, T. B., F. Nicol, O. Zelphati, P. V. Scaria, C. Plank, and F. C. Szoka. 1997. "Design, Synthesis, and Characterization of a Cationic Peptide That Binds to Nucleic Acids and Permeabilizes Bilayers." *Biochemistry* 36 (10): 3008–17. https://doi.org/10.1021/bi9618474.

Xu, Jiangkang, Abdur Rauf Khan, Manfei Fu, Rujuan Wang, Jianbo Ji, and Guangxi Zhai. 2019. "Cell-Penetrating Peptide: A Means of Breaking through the Physiological Barriers of Different

Tissues and Organs." *Journal of Controlled Release* 309: 106–24. https://doi.org/10.1016/j.jconrel.2019.07.020.

Xu, Jin, Xia-Fei Wang, Peng Chen, et al. 2016. "RNA Interference in Moths: Mechanisms, Applications, and Progress." *Genes* 7 (10): 88. https://doi.org/10.3390/genes7100088.

Xu, M. Z., S. W. Chan, A. M. Liu, et al. 2011. "AXL Receptor Kinase Is a Mediator of YAP-Dependent Oncogenic Functions in Hepatocellular Carcinoma." *Oncogene* 30 (10): 1229–40. https://doi.org/10.1038/onc.2010.504.

Xu, Song-Hui, Jin-Zhou Huang, Min Chen, et al. 2017. "Amplification of ACK1 Promotes Gastric Tumorigenesis via ECD-Dependent P53 Ubiquitination Degradation." *Oncotarget* 8 (8): 12705–16. https://doi.org/10.18632/oncotarget.6194.

Xu, T., W. Wang, S. Zhang, R. A. Stewart, and W. Yu. 1995. "Identifying Tumor Suppressors in Genetic Mosaics: The Drosophila Lats Gene Encodes a Putative Protein Kinase." *Development* 121 (4): 1053–63. https://doi.org/10.1242/dev.121.4.1053.

Yagi, R., L. F. Chen, K. Shigesada, Y. Murakami, and Y. Ito. 1999. "A WW Domain-Containing Yes-Associated Protein (YAP) Is a Novel Transcriptional Co-Activator." *The EMBO Journal* 18 (9): 2551–62. https://doi.org/10.1093/emboj/18.9.2551.

Yasuda, Makiko, Siobán Keel, and Manisha Balwani. 2023. "RNA Interference Therapy in Acute Hepatic Porphyrias." *Blood* 142 (19): 1589–99. https://doi.org/10.1182/blood.2022018662.

Ye, Shuai, Dinara Sharipova, Marya Kozinova, et al. 2021. "Identification of Wee1 as a Target in Combination with Avapritinib for Gastrointestinal Stromal Tumor Treatment." *JCI Insight* 6 (2): e143474, 143474. https://doi.org/10.1172/jci.insight.143474.

Yu, Fa-Xing, Bin Zhao, and Kun-Liang Guan. 2015. "Hippo Pathway in Organ Size Control, Tissue Homeostasis, and Cancer." *Cell* 163 (4): 811–28. https://doi.org/10.1016/j.cell.2015.10.044.

Zanconato, Francesca, Giusy Battilana, Mattia Forcato, et al. 2018. "Transcriptional Addiction in Cancer Cells Is Mediated by YAP/TAZ through BRD4." *Nature Medicine* 24 (10): 1599–610. https://doi.org/10.1038/s41591-018-0158-8.

Zanconato, Francesca, Michelangelo Cordenonsi, and Stefano Piccolo. 2016. "YAP/TAZ at the Roots of Cancer." *Cancer Cell* 29 (6): 783–803. https://doi.org/10.1016/j.ccell.2016.05.005.

Zanconato, Francesca, Mattia Forcato, Giusy Battilana, et al. 2015. "Genome-Wide Association between YAP/TAZ/TEAD and AP-1 at Enhancers Drives Oncogenic Growth." *Nature Cell Biology* 17 (9): 1218–27. https://doi.org/10.1038/ncb3216.

Zhang, Heng, Chen-Ying Liu, Zheng-Yu Zha, et al. 2009. "TEAD Transcription Factors Mediate the Function of TAZ in Cell Growth and Epithelial-Mesenchymal Transition." *The Journal of Biological Chemistry* 284 (20): 13355–62. https://doi.org/10.1074/jbc.M900843200.

Zhang, Jianmin, Jun-Yuan Ji, Min Yu, et al. 2009. "YAP-Dependent Induction of Amphiregulin Identifies a Non-Cell-Autonomous Component of the Hippo Pathway." *Nature Cell Biology* 11 (12): 1444–50. https://doi.org/10.1038/ncb1993.

REFERENCES

Zhang, Liangying, Kun Xiao, Shaoting Zhang, et al. 2025. "SOCS2 Inhibits the Tumorigenesis of GISTs and Increases the Sensitivity of GISTs to Imatinib by Suppression of KIT Activation." *Scientific Reports* 15 (1): 4779. https://doi.org/10.1038/s41598-025-89477-0.

Zhang, Wenjing, Yijun Gao, Peixue Li, et al. 2014. "VGLL4 Functions as a New Tumor Suppressor in Lung Cancer by Negatively Regulating the YAP-TEAD Transcriptional Complex." *Cell Research* 24 (3): 331–43. https://doi.org/10.1038/cr.2014.10.

Zhang, Y.-H., B. Li, L. Shen, Y. Shen, and X.-D. Chen. 2013. "The Role and Clinical Significance of YES-Associated Protein 1 in Human Osteosarcoma." *International Journal of Immunopathology and Pharmacology* 26 (1): 157–67. https://doi.org/10.1177/039463201302600115.

Zhao, Bin, Li Li, Qing Lu, et al. 2011. "Angiomotin Is a Novel Hippo Pathway Component That Inhibits YAP Oncoprotein." *Genes & Development* 25 (1): 51–63. https://doi.org/10.1101/gad.2000111.

Zhao, Bin, Li Li, Karen Tumaneng, Cun-Yu Wang, and Kun-Liang Guan. 2010. "A Coordinated Phosphorylation by Lats and CK1 Regulates YAP Stability through SCF(Beta-TRCP)." *Genes & Development* 24 (1): 72–85. https://doi.org/10.1101/gad.1843810.

Zhao, Bin, Karen Tumaneng, and Kun-Liang Guan. 2011. "The Hippo Pathway in Organ Size Control, Tissue Regeneration and Stem Cell Self-Renewal." *Nature Cell Biology* 13 (8): 877–83. https://doi.org/10.1038/ncb2303.

Zhao, Zhan, Shenghui Qiu, Xiangwei Zhang, et al. 2025. "Characterization of a Novel Cell Line Established from Mice Gastrointestinal Stromal Model by Chemical Induction." *Translational Oncology* 56: 102388. https://doi.org/10.1016/j.tranon.2025.102388.

Zhou, Shishan, Omar Abdihamid, Fengbo Tan, et al. 2024. "KIT Mutations and Expression: Current Knowledge and New Insights for Overcoming IM Resistance in GIST." *Cell Communication and Signaling* 22 (1): 153. https://doi.org/10.1186/s12964-023-01411-x.

Zhou, Xin, and Qun-Ying Lei. 2016. "Regulation of TAZ in Cancer." *Protein & Cell* 7 (8): 548–61. https://doi.org/10.1007/s13238-016-0288-z.

Zhou, Yuhang, Tingting Huang, Alfred S. L. Cheng, Jun Yu, Wei Kang, and Ka Fai To. 2016. "The TEAD Family and Its Oncogenic Role in Promoting Tumorigenesis." *International Journal of Molecular Sciences* 17 (1): 138. https://doi.org/10.3390/ijms17010138.

Zhou, Zheng, Taishan Hu, Zhiheng Xu, et al. 2015. "Targeting Hippo Pathway by Specific Interruption of YAP-TEAD Interaction Using Cyclic YAP-like Peptides." *FASEB Journal: Official Publication of the Federation of American Societies for Experimental Biology* 29 (2): 724–32. https://doi.org/10.1096/fj.14-262980.

Zhu, Guangrong, Jun Shi, Shaoting Zhang, et al. 2020. "Loss of PI3 Kinase Association Improves the Sensitivity of Secondary Mutation of KIT to Imatinib." *Cell & Bioscience* 10: 16. https://doi.org/10.1186/s13578-020-0377-9.

Zuckerman, Jonathan E., Ismael Gritli, Anthony Tolcher, et al. 2014. "Correlating Animal and Human Phase Ia/Ib Clinical Data with CALAA-01, a Targeted, Polymer-Based Nanoparticle Containing siRNA." *Proceedings of the National Academy of Sciences of the United States of America* 111 (31): 11449–54. https://doi.org/10.1073/pnas.1411393111.

APPENDICES

APPENDICES

1. Appendix 1: Other publication during thesis

Molecular Therapy
Methods & Clinical Development
Original Article

WRAP-based nanoparticles for siRNA delivery in zebrafish embryos by simple bath immersion

Karidia Konate,[1] Clémentine A. Teko-Agbo,[1] Irène Pezzati,[1] Thania Hammoum,[1] Sébastien Deshayes,[1] Simon Descamps,[2] Eric Vivès,[1] Sandrine Faure,[1] Pascal de Santa Barbara,[1] and Prisca Boisguérin[1]

[1]PHYMEDEXP, University of Montpellier, INSERM U1046, CNRS UMR 9214, Montpellier, France; [2]Cell Biology Research of Montpellier (CRBM), University of Montpellier, UMR5237, Montpellier, France

The use of RNA interference (RNAi) is becoming more widespread in several areas of biomedical research. However, the success of RNAi depends on the effective delivery of siRNA *in vitro* or *in vivo*. Efforts are under way to identify universally effective delivery systems. Promising candidates include cell-penetrating peptides, such as the WRAP (tryptophan and arginine-rich amphipathic peptide) family, which forms nanoparticles in the presence of short interfering RNA (siRNA). Here, we optimized the WRAP-based nanoparticles for zebrafish embryo transfection by first determining the ideal formulation compatible with the saline solution required for zebrafish embryo care. We found that adding 20% polyethylene glycol (PEG) to the WRAP1 nanoparticles provided the best nanoparticles in terms of size (around 100 nm) and uniformity (PdI ≤0.3), compared with other nanoparticles tested. We then performed a simple soaking procedure in which we exposed dechorionated zebrafish embryos expressing GFP in their vascular cells to siRNA-loaded 20% PEG-WRAP1 nanoparticles. Under these conditions, we showed dose-dependent siRNA internalization and efficient GFP silencing. Although still in its early stages, this proof-of-concept study provides promising prospects for further *in vivo* research in zebrafish embryos to evaluate the efficacy of gene silencing using PEGylated WRAP1 nanoparticles by skin transfection in a pathophysiological context.

INTRODUCTION

Besides small molecules, proteins, or antibodies, therapeutic nucleic acids (NAs) are increasingly considered as a new generation of pharmacological drugs in biomedical research.[1] Therapeutic NAs can be RNA or DNA molecules with different functions, specifically acting on gene regulation. Recent optimization of NA synthesis, chemical modifications, and delivery has rapidly accelerated the development of therapeutic NA. To date, 17 NA-based therapeutics have been approved by the Food and Drug Administration (FDA) or the European Medicines Agency (EMA).[1] In particular, double-stranded short interfering RNAs (siRNAs) have been developed as a major therapeutic tool to silence gene expression by degrading the target mRNA.[2,3] Today, six siRNA-based therapeutics have been approved by the FDA[4] with ONPATTRO (Partisiran) being the first in 2018.[5]

The majority of gene therapies are based on viral gene carriers, and recent years have shown both successes and challenges for this approach.[6] This highlights the need for a broader range of gene carriers that reduce the risk of insertional mutagenesis and potential carcinogenicity, but also allow for complex manufacturing processes and associated large-scale production. In recent decades, non-viral entities such as various naturally derived, synthetic, or hybrid (natural and synthetic) lipids, polymers, or peptides have become promising alternatives to viral carriers due to their greater genetic payload capacity, biocompatibility, and scalability.[6]

Cell-penetrating peptides (CPPs), usually defined as short (up to 30 amino acids) peptides, have been developed as a promising non-viral NA internalization strategy as they constitute a great alternative to the existing viral (adenovirus, retrovirus, etc.), lipid-based, or polymer-based methods.[7] More specifically, amphipathic or chemically modified CPPs have been increasingly used in non-covalent strategies based on electrostatic and hydrophobic interactions between both the peptide and the siRNA (Figure 1), thus opening peptides to the field of nanomedicine.[8–11] CPPs could be used for nanoparticle formulation in the naked version or as grafted conjugates to improve the stability and/or targeting of the nanoparticles. The most common entity used for the grafting is polyethylene glycol (PEG), which reduces the interactions between the nanoparticle and the environment.[12]

In this context, we designed a family of amphipathic peptides called WRAP (W- and R-rich Amphipathic Peptides), which can self-assemble into peptide-based nanoparticles (PBNs) after incubation with siRNA at a specific CPP:siRNA molar ratio (MR).[13] The high siRNA delivery efficacy of WRAP-PBNs in various cell lines was mainly due to their direct cellular membrane translocation, although a small fraction entered via endocytosis-dependent pathways.[14] Intracellular delivery of Cy3b-labeled siRNAs by WRAP-based nanoparticles was demonstrated to reach the half-maximal value (=50% of

Received 6 September 2024; accepted 27 March 2025;
https://doi.org/10.1016/j.omtm.2025.101458.

Correspondence: Prisca Boisguérin, PHYMEDEXP, University of Montpellier, INSERM U1046, CNRS UMR 9214, Montpellier, France.
E-mail: prisca.boisguerin@inserm.fr

Published by Elsevier Inc. on behalf of The American Society of Gene and Cell Therapy.
This is an open access article under the CC BY-NC-ND license (http://creativecommons.org/licenses/by-nc-nd/4.0/).

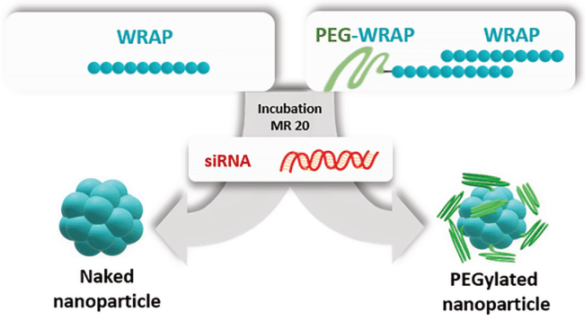

Figure 1. Principle of the WRAP1 nanoparticle formulation as naked or PEGylated versions in the presence of siRNA

WRAP or a mixture of PEGylated WRAP/WRAP are added to a siRNA solution at a molar ratio (MR) of 20 (e.g., 800 nM WRAP + 40 nM siRNA) to obtain nanoparticles ready for siRNA transfection.

fluorescent cells) after ~210 s of incubation and the maximal level of fluorescence (~95%) after ~15 min of incubation.[13] A structure-activity relationship (SAR) study revealed the major role of the N- and C-terminal leucine doublets within the WRAP peptide sequence, which are important to the nanoparticle formation in the presence of siRNA and gene silencing activity.[15] Based on this SAR study, two lead peptides were identified, WRAP1 (LLWRLWRLL WRLWRLL) and WRAP5 (LLRLLRWWWRLLRLL), which have nearly identical delivery properties.

In the same study,[15] we compared the WRAP-based delivery systems with lipid-based reagents for siRNA transfection (RNAiMAX [Life Technologies], INTERFERin [PolyPlus], DharmaFect [Dharmacon], and HiPerFect [Qiagen]). Our findings demonstrated that all transfection reagents (peptide- or lipid-based) exhibited equivalent efficiency, achieving specific luciferase silencing (>80%) without any observed cytotoxic effects (lactate dehydrogenase [LDH] assay, 36 h post-transfection). However, in a long-term incubation (clonogenic assay, 14 days post-transfection), we observed some cytotoxic effects (up to 80%) for all lipid-based delivery systems, except for HiPerFect, thereby demonstrating the safety of the WRAP-based system. Finally, the first *in vivo* study performed with WRAP:siRNA nanoparticles demonstrated effective luciferase silencing in a mouse xenograft model.[16]

In general, the development of therapeutic molecules requires proof-of-concept studies in animal models (e.g., mice or rats). In this context, zebrafish (*Danio rerio*), initially used for decades as a classical developmental and embryological model, has received growing attention as a model for human disease and drug discovery (more than 1,700 reviews in PubMed with the keywords "zebrafish for human disease" @January 2025). The zebrafish is an excellent *in vivo* model due to (1) rapid reproduction and development, (2) high gene conservation compared with humans, and (3) a transparent body for any phenotypic visualization.

Gene regulation could be performed in zebrafish by injecting nanoparticles at different stages of development (one-cell or two-cell stage, 24 h postfertilization [hpf] or even later). However, micro-needle injections require specific materials (micro-needles, injectors, etc.) and the experimenter's skills. Furthermore, zebrafish embryo mortality is known to be very high during the first 1–6 hpf following micro-needle injections, and the expression of specific cellular tracers (e.g., GFP, mCHERRY) required for some experiments may be too low to detect, as the expressing cell types are not developed at these early stages. Therefore, we propose a simple bath immersion protocol to perform the siRNA transfection using WRAP-based nanoparticles on dechorionated zebrafish embryos. In this context, we wanted to compare our two lead CPPs, WRAP1 and WRAP5, to determine which one is more appropriate for *in vivo* applications.

First, we evaluated the GFP silencing in HEK293 cells overexpressing GFP using different siRNA targeting different regions of the *GFP* mRNA. Afterward, we compared the size and stability of WRAP5- and WRAP1-based nanoparticles formulated in several conditions (media containing 5% glucose, 5 mM NaCl, or zebrafish culture medium) by dynamic light scattering (DLS) measurements. We selected WRAP1:siRNA nanoparticles with 20% PEGylation as the stable ones under all conditions evaluated. Finally, using a simple bathing protocol, we demonstrated the dose-dependent siRNA (Cy3-labeled) internalization and the efficient GFP silencing in dechorionated *Tg* [*fli1*:EGFP]^{y1} transgenic zebrafish embryos.

This novel application of peptide-based nanoparticles through the skin paves the way for the possible use of zebrafish embryos as an *in vivo* model for protein knockdown using vectorized siRNA in a pathophysiological context to advance the development of new therapeutic applications.

RESULTS

Determination of efficient siGFP-loaded WRAP nanoparticles for GFP silencing in HEK293 cells

Cells with stable expression of GFP are often used as cellular models to quantify the uptake and knockdown efficiency of developed transfection reagents. Therefore, many different siRNA sequences have been published in the literature or even proposed by various manufacturers. For this study, we selected three different siRNAs (siGFP-M,[17] siGFP-G,[18] and siGFP-W[19], with the letter corresponding to the name of the first author) to evaluate their silencing properties using cellular delivery systems of the WRAP peptides we developed.[13] Indeed, the use of different siRNAs may lead to the induction of different silencing activities, depending on the model employed (i.e., cellular or animal). In addition, the silencing activity may be influenced by various off-target effects, which should be considered, as indicated in Figure S1. In the supplemental information, details of the selection procedure for the three siRNAs (siGFP-M, siGFP-G, and siGFP-W) are highlighted.

In detail, stably GFP-transfected HEK293 cells were seeded in a microtiter plate. Twenty-four hours post-seeding, the cells were

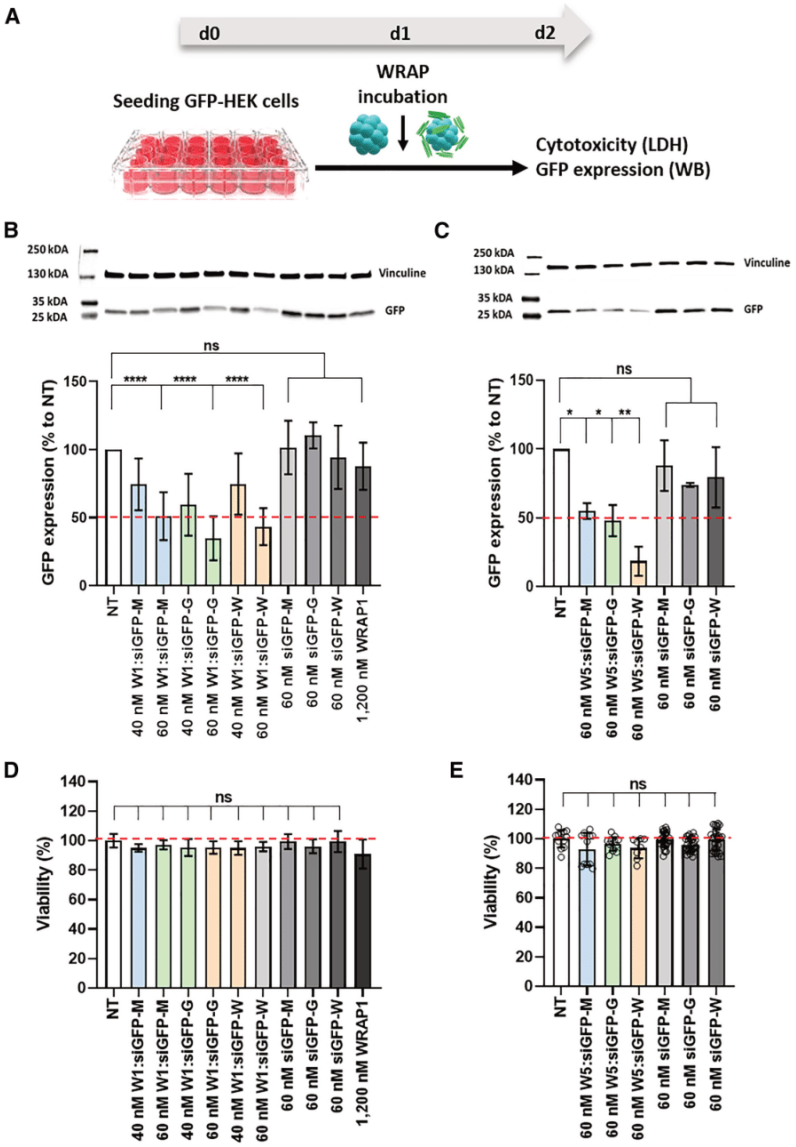

Figure 2. Comparison of GFP silencing and cytotoxicity using different siRNA vectorized by WRAP nanoparticles

(A) Schematic representation of WRAP:siGFP incubation protocol on GFP-overexpressing HEK293 cells. At day zero (d0), cells were seeded in a 24-well plate. Twenty-four hours post-seeding (d1), cells were incubated with the WRAP:siRNA PBNs. Twenty-four hours post-incubation (d2), supernatants were collected for cytotoxicity measurements (LDH) and afterward, cells were lysed for GFP knockdown evaluation by western blots (WB). (B and C) Western blot evaluation and quantification for WRAP1:siGFP compared with siGFP or WRAP1 alone (B) and for WRAP5:siGFP (C) compared with siGFP alone in GFP-overexpressing HEK293 cells. Data represent mean ± SD, with $n \geq 2$ independent experiments in duplicate. Transfection condition: Nanoparticles with MR = 20 and an siRNA concentration of 40 nM or 60 nM/Non-treated cells (NT)/Dashed line indicated 50% of GFP expression. Statistical analysis: One-way ANOVA with a Dunnett post-test, ns > 0.05, $^{*}p < 0.05$, $^{**}p = 0.001$, and $^{****}p < 0.0001$ vs. NT cells. (D and E) Viability (%) of WRAP1:siGFP compared with siGFP or WRAP1 alone (D) and for WRAP5:siGFP (E) compared with siGFP alone in GFP-overexpressing HEK293 cells. LDH release was measured from the supernatant of conditions highlighted in (B) and (C). Triton was used to determine 0% viability in the LDH assay (not shown)/Non-treated cells (NT = 100% viability)/Dashed line indicated 100% viability. Statistical analysis: One-way ANOVA with a Dunnett post-test, ns > 0.05 vs. NT cells.

transfected with the WRAP:siRNA complexes to evaluate the GFP silencing by western blot (Figure 2A). First, we observed knockdown efficiency for all siRNA-GFP compared with the untreated cells in our incubation condition (Figure 2B). We observed GFP silencing efficiencies of ∼25% and 40% for WRAP1:siGFP-M, 40% and 65% for WRAP1:siGFP-G, and 25% and 56% for WRAP1:siGFP-W at the two siRNA concentrations used, 40 nM and 60 nM, respectively. At the highest concentration of 60 nM, the GFP knockdown was statistically significant for all used siRNA ($^{****}p < 0.0001$ vs. non-treated [NT] cells). Furthermore, no GFP silencing effect was observed when HEK293 cells were transfected with the siRNA or the WRAP1 peptide separately, showing the importance of WRAP1-based siRNA transfection.

Subsequently, we evaluated the GFP silencing using the WRAP5 peptide as another transfection reagent. This evaluation was conducted employing the same transfection protocol and an siRNA concentration of 60 nM, which resulted in 50% silencing, as previously observed for WRAP1 (Figure 2C). Similarly, we revealed a reduction in GFP expression of around 50% for WRAP5:siGFP-M and WRAP5:siGFP-G ($^{*}p < 0.05$ vs. NT cells), and even higher for WRAP5:siGFP-W (∼80%, $^{**}p = 0.001$ vs. NT cells). Again, as shown for WRAP1, no GFP silencing is observed with either the siGFP or the WRAP5 peptide alone.

Finally, for all conditions analyzed by western blot, we also evaluated the potential cytotoxicity that the transfection reagent could have on the HEK293 cells by measuring the release of lactate dehydrogenase (LDH). In this context, the cytotoxicity evaluation was important to avoid false-positive results, as the toxic effect would impact the GFP expression. To normalize the assay, NT cells were used as a positive

Table 1. WRAP:siRNA and 20% PEG-WRAP:siRNA characterization by DLS measurements in different solutions

Nanoparticle	Medium	Mean size (nm)	PdI
WRAP1:siRNA	5% Gluc	81.9 ± 10.5	0.387 ± 0.080
	5% Gluc +5 mM NaCl	117.2 ± 29.7	0.341 ± 0.072
	E3 medium	81.6 ± 2.1	0.323 ± 0.086
	E3 medium (d+1)	>1,000	>0.8
WRAP5:siRNA	5% Glucose	77.7 ± 8.6	0.255 ± 0.041
	5% Glucose +5 mM NaCl	>900	>0.5
	E3 medium	>500	>0.5
	E3 medium (d+1)	>1,000	>0.8
20PWRAP1:siRNA	5% Glucose	98.1 ± 19.3	0.299 ± 0.041
	5% Glucose +5 mM NaCl	128.2 ± 53.9	0.264 ± 0.049
	5% Glucose +5 mM NaCl (d+1)	122.5 ± 39.8	0.342 ± 0.088
	E3 medium	85.6 ± 9.5	0.259 ± 0.006
	E3 medium (d+1)	163.6 ± 29.1	0.327 ± 0.076
20PWRAP5:siRNA	5% Glucose	77.9 ± 4.9	0.296 ± 0.066
	5% Glucose +5 mM NaCl	128.8 ± 20.1	0.269 ± 0.057
	5% Glucose +5 mM NaCl (d+1)	ND	ND
	E3 medium	121.9 ± 71.7	0.347 ± 0.067
	E3 medium (d+1)	>1,000	>0.5

All WRAP:siGFP-M complexes were formed at molar ratio (MR) = 20 in an aqueous solution of 5% glucose and thereafter diluted (1:10) in the indicated medium (final peptide concentration of 10 μM). E3 medium contains 5 mM NaCl, 0.17 mM KCl, 0.33 mM $CaCl_2$, 0.33 mM $MgSO_4$. Mean sizes were measured using the intensity distribution (for mean sizes by number distribution see Table S3); $n \geq 2$ independent formulations (3 measures per run). PdI, Polydispersity Index, (d+1) = complexes were stored at 4°C and measured one day post-dilution. ND, not determined.

control (100% viability), and Triton X-100 treated cells were considered as a negative control (0% viability). Regarding the different WRAP1:siRNA conditions, all values were close to those measured for untreated cells and not lower than 95% (ns > 0.05 vs. NT) (Figure 2D). The same was observed for all WRAP5:siRNA conditions (ns > 0.05 vs. NT) (Figure 2E).

As previously reported, amphipathic WRAP1 and WRAP5 peptides can spontaneously form peptide-based nanoparticles (PBNs) in the presence of siRNA.[13,15] DLS measurements were performed to confirm similar nanoparticle sizes and polydispersity (PdI) values for all WRAP1/WRAP5 formulations performed with the three different siRNAs (Table S2; Figure S2). When formulated in an aqueous solution of 5% glucose, we observed the formation of small particles with a size of ∼20–30 nm, as revealed by the size distribution based on the number (%) (Tables S2 and S3). Afterward, these small particles self-associate to the final PBN of ∼80–100 nm as shown by the size distribution based on intensity (%), as previously reported.[13]

Considering that there are no differences among the three nanoparticles formulated with WRAP1, this suggests that their observed silencing properties in GFP-overexpression HEK293 cells are also equivalent (Figure 2B). However, at this stage, we have no explanation for the higher GFP knockdown observed for WRAP5:siGFP-W (Figure 2C) compared with the other two formulations (WRAP5:siGFP-M and WRAP5:siGFP-G), which exhibit GFP expression reduction in the same range as shown for the three WRAP1:siGFP nanoparticles.

PEGylation of WRAP-based nanoparticles to provide compatibility with zebrafish medium incubation

The stability of the nanoparticles in saline solutions of different ionic forces was analyzed to evaluate the potential of WRAP-based nanoparticles as a delivery system for zebrafish embryo transfection (Table 1). For this purpose, both WRAP:siRNA nanoparticles were formulated in water and thereafter diluted (1:10) in saline solutions such as 5% glucose supplemented with 5 mM NaCl (low ionic strength) or in the zebrafish medium (E3 medium containing 5 mM NaCl, 0.17 mM KCl, 0.33 mM $CaCl_2$, 0.33 mM $MgSO_4$) (high ionic strength) (Table 1).

WRAP1:siRNA nanoparticles appeared to be stable after dilution in both saline solutions, i.e., we observed no change in nanoparticle size, nor aggregation or flocculation in the solution. However, the complexes were destabilized with time as reflected by the measurement 1-day post-dilution in E3 medium. In contrast, for WRAP5:siRNA, we observed the formation of large complexes or aggregates (>500 nm) with a correspondingly increased polydispersity index (PdI >0.5) in the presence of salt. The increasing PdI values correspond to a loss of particle homogeneity, which means that the variability of the detected particles can range from 100 nm small objects

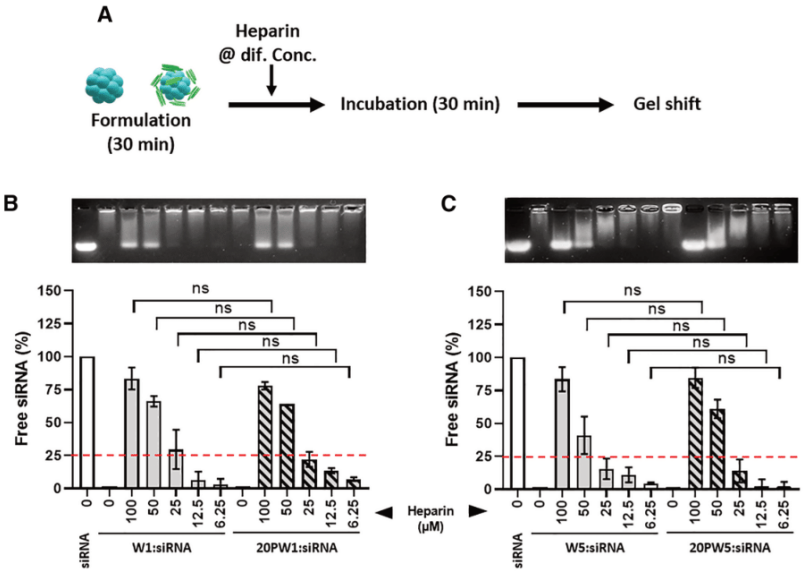

Figure 3. Evaluation of WRAP-based nanoparticle stability in the presence of heparin

(A) Schematic representation of incubation protocol of WRAP:siGFP-M with increasing heparin concentrations. Representative images of gel shift assays of WRAP1- (B) or WRAP5-based nanoparticles (C) incubated with heparin (100 μM–6.25 μM). Below the images, the graphical representations show the percentage of free siRNA normalized to siRNA alone (100%) and the nanoparticles without heparin (0%). Conditions: Nanoparticles with MR = 20 and an siGFP-M concentration of 40 nM; Dashed line indicated 25% of free siRNA; Data represent mean ± SD, with $n \geq 2$ independent experiments. Statistical analysis: One-way ANOVA with a Tukey multiple comparisons test, ns > 0.05.

to microparticles, making them unsuitable for cellular transfection. The differences between the two sequences are given by the number and the distribution of the tryptophan residues: WRAP1 has four tryptophan residues that are scattered all along the sequence, whereas WRAP5 has only three tryptophan residues that are clustered in the middle of the sequence. At this time, it is not clear whether the number and/or position of the tryptophan residues could impact the destabilization of the nanoparticle in the presence of ionic forces.

To confer stability to the colloidal properties of nanoparticles in the E3 medium, we sought to optimize nanoparticles by grafting protective entities. A common method to stabilize or protect the nanoparticle from interaction with serum proteins when administered via an intravenous injection[20] is to graft polyethylene (PEG) moieties onto nanoparticles. Based on previous results obtained with PEGylated RICK:siRNA[21] or PEGylated MTS-WRAP:pDNA,[22] we combined 20% PEG-WRAP peptide with 80% of naked WRAP peptide prior to siRNA addition and the resulting nanoparticle formation. The two nanoparticles WRAP1:siRNA or WRAP5:siRNA, formulated in an aqueous solution containing 5% glucose, have the same size as the versions containing 20% of PEG-WRAP1 or PEG-WRAP5 (Table 1). It appears that the addition of 20% PEG-peptide does not affect the nanoparticle size, as previously reported for PEG-RICK:siRNA[21] or for PEG-HyOMe-WRAP5:siRNA (with a pH-sensitive hydrazine linker).[23]

As previously done for the naked WRAP:siRNA nanoparticles, 20% PEG-WRAP:siRNA complexes were formulated in water and then diluted in both saline media (1:10 dilution) to evaluate the effect of PEGylation on nanoparticle stability. As expected, nanoparticles formulated with 20% PEG-WRAP seemed to support a higher tolerance to salt-containing solutions, as exemplified by both nanoparticles measured immediately after the dilution (Table 1). Twenty percent PEG-WRAP1:siRNA nanoparticles were stable in the presence of 5 mM NaCl with a size of 128.2 ± 53.9 nm and a PdI of 0.264 ± 0.049 as well as in E3 medium with a size of 85.6 ± 9.5 nm and a PdI of 0.259 ± 0.006. Also, 20% PEG-WRAP5:siRNA nanoparticles were stable in both media with sizes of 128.8 ± 20.1 nm and 121.9 ± 71.7 with PdI values of 0.269 ± 0.057 and 0.347 ± 0.067, respectively. However, only the WRAP1-based nanoparticles were stable even 1-day post-dilution in the E3 solution with an acceptable mean size of ∼160 nm compared with the WRAP5-based nanoparticles (>1,000 nm, Table 1).

Another method of assessing the stability of nanoparticles is to evaluate them in the presence of heparin. Heparin is a linear, acidic polysaccharide belonging to the glycosaminoglycan family. It is frequently used in the field of siRNA-loaded nanoparticles to perform a competition assay with the siRNA for binding with the delivery vector (positively charged peptides or polymers). This assay also could be used to indirectly evaluate the stability of nanoparticles using gel shift assays.[15,24] For this purpose, nanoparticles were formulated in an aqueous solution containing 5% glucose and then supplemented with increasing concentrations of heparin (6.25 μM–100 μM, Figure 3A). Curiously, we observed no significant differences between naked WRAP1/5:siRNA nanoparticles and those formed with 20% PEG-WRAP1/5:siRNA with increasing heparin concentrations. Setting an arbitrary threshold of 25% free siRNA for a positive heparin impact (= siRNA release), we could show that naked or PEGylated WRAP1:siRNA nanoparticles tolerated heparin concentrations of up to 12.5 μM (Figure 3B), whereas naked or PEGylated WRAP5-based nanoparticles tolerated higher heparin concentrations (50 μM) (Figure 3C). The same experiments were repeated with 100% PEG-WRAP1/5 nanoparticles incubated with the same increasing heparin concentrations to confirm the nanoparticle stabilizing property of the PEG moiety (Figure S3). Indeed, fully

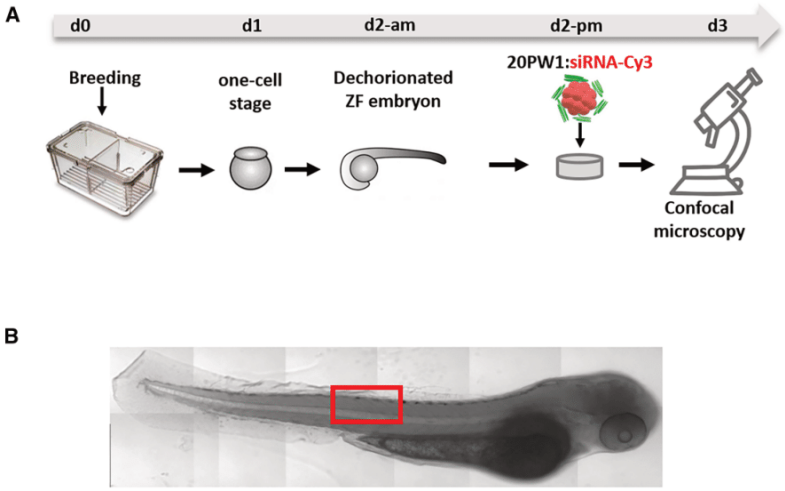

Figure 4. Evaluation of the internalization potential of 20% PEG-WRAP1:siRNA nanoparticles in the zebrafish embryo

(A) Schematic representation of the zebrafish embryo incubation protocol. At day zero (d0), zebrafish breeding was performed to collect one-cell stage embryos at d1. In the morning of d2 (~24 hpf), the zebrafish embryos were dechorionated and left for 6 h in E3 medium before adding in the afternoon the fluorescence-labeled 20% PEG-WRAP1:siRNA (20PW1:siRNA-Cy3) nanoparticles. After ~20 h, the embryos were washed, fixed (PFA), and imaged by confocal microscopy. (B) Visualization of the area that was used for confocal image acquisition (red square). (C) Representative images of the z stack confocal microscopy acquisition of non-treated zebrafish embryo compared with the one incubated with 20% PEG-WRAP1:siRNA-Cy3 nanoparticles at the indicated final siRNA concentrations (MR = 20). Green = GFP-expressing vascular endothelial cells, red = siRNA-Cy3. White bar = 100 μm.

PEGylated WRAP1/5 nanoparticles released less siRNA at the same heparin concentration compared with the naked or 20% PEGylated version.

Next, the stability of the nanoparticles (WRAP1/5, 20% PEG-WRAP1/5, and 100% PEG-WRAP1/5) was evaluated by gel shift assay in saline E3 medium (data not shown). Here, we observed no siRNA release for all conditions, meaning that in the presence of salt, the nanoparticles tend to aggregate (as observed by DLS through larger sizes) without destabilizing the nanoparticle itself (aggregates are not able to migrate through the gel).

In conclusion, based on the results obtained from DLS measurements and gel shift assays, we selected the 20% PEG-WRAP1:siRNA formulation to evaluate the activity of the siRNA in a GFP-expressing zebrafish model.

A simple bathing incubation of zebrafish embryos with PEGylated WRAP1 nanoparticles for siRNA internalization

Gene silencing in zebrafish embryos is commonly performed by injecting oligonucleotides such as a phosphorodiamidate morpholino oligomer (PMO) at the one-cell stage. However, there is a high mortality rate at this stage (depending on the zebrafish line used) because zebrafish embryos are generally very fragile during the first 24 hpf. To avoid this delicate injection procedure, we decided to simply bathe the dechorionated zebrafish embryos for 24 h with the PEGylated WRAP1 nanoparticles for the siRNA transfection.

For this purpose, we used zebrafish embryos derived from the breeding of a *Tg*[*fli1*:EGFP]^{y1} transgenic line having GFP-labeled vascular endothelial cells. Two days post-breeding, the embryos were dechorionated in the early morning, washed, and left in an E3 medium (6 h) before the addition of nanoparticles with different concentrations of Cy3-labeled siRNA. To improve GFP signal detection by confocal microscopy, embryos were treated with 1-phenyl 2-thiourea (PTU) to remove zebrafish pigmentation as reported previously.[25] After 20 h, zebrafish embryos were washed and fixed with PFA for confocal microscopy imaging to evaluate the potential internalization of the fluorescence-labeled siRNA (Figure 4A). Approximately the same dorsal region of the zebrafish embryo was used for z stack image acquisition by confocal microscopy (see red square in Figure 4B). For an accurate comparison of the different conditions, all images were acquired and processed using the same parameters each time.

Zebrafish embryos incubated only in an E3 medium alone showed almost no red auto-fluorescence (Figure 4C, first panel). By adding 20%-PEG-WRAP1 nanoparticles encapsulating different amounts of Cy3-labeled siRNA (35 nM, 70 nM, or 140 nM), we observed a dose-dependent accumulation of red fluorescence at the surface and within the inner regions of the zebrafish embryos (Figure 4C). To the best of our knowledge, these very encouraging results confirm for the first time, that a simple bathing procedure with the PEGylated WRAP1 nanoparticles allows the transfection of siRNA in a zebrafish embryo as a potent gene silencing strategy.

Moreover, by incubating a dechorionated zebrafish embryo with the 20% PEG-WRAP1 nanoparticles for 72 h, we confirmed that the incubation condition had no impact on zebrafish development (Figure S4). No morphological changes or differences in the embryo size were observed between untreated zebrafish embryos (704 ± 12 μm, $n = 18$) and those incubated with the nanoparticles (702 ± 24 μm, $n = 20$). More importantly, no zebrafish embryo died during the incubation (siRNA = 140 nM). The result showed that the nanoparticle incubation has no cytotoxic impact on the zebrafish embryos even if the nanoparticles are internalized.

Quantification of GFP silencing in zebrafish embryos after nanoparticle bathing

Having confirmed that siRNA internalization using 20% PEG-WRAP1 nanoparticles was possible by simply bathing the zebrafish embryos, we wanted to know if a specific GFP knockdown could be observed. In a protocol similar to that used for the siRNA-Cy3 internalization/visualization, dechorionated zebrafish embryos were incubated with 20% PEG-WRAP1:siGFP nanoparticles. Using siGFP-G as an example, the same three siRNA doses (35 nM, 70 nM, and 140 nM) were used to quantify by western blot GFP silencing after 24 h of incubation (Figure S5). However, the overwhelming presence of vitellogenin yolk proteins could potentially interfere with the identification of cellular proteins by SDS-PAGE to an unknown extent. Therefore, we performed a de-yolking procedure before the lysis of zebrafish embryos to reduce the yolk proteins in the lysate, as has been performed in several studies on zebrafish embryos and larvae at different stages postfertilization.[26,27]

Under these conditions, we observed a significant dose-dependent GFP silencing: ∼40% for 35 nM (**$p = 0.0014$), ∼50% for 70 nM (****$p > 0.0001$), and ∼80% for 140 nM siGFP-G (****$p > 0.0001$), vs. NT, respectively (Figure S5B). In addition, we repeated the experiment and extended the nanoparticle incubation to 48 h to ensure that the correct bathing procedure was used for optimal GFP knockdown. As shown in Figure S5C, the overall GFP/α-Actinin levels of the untreated and control conditions were less pronounced after 48 h of incubation compared with 24 h, probably due to the growth of the embryos (changes in the GFP/α-Actinin ratios). Also, the dose-dependent GFP silencing seems to be lower: ∼10% for 35 nM (ns = 0.9630), ∼30% for 70 nM (ns = 0.1451), and ∼50% for 140 nM siGFP-G (*$p > 0.0125$), respectively, vs. NT, respectively (Figure S5C).

Since the siGFP concentration of 140 nM induced the highest GFP silencing for both incubation periods, the specificity of GFP knockdown with 20% PEG-WRAP1 nanoparticles loaded with the three siGFP (siGFP-M, -G, and -W) was evaluated by western blot analyses (Figure 5A). Western blot analyses of the GFP protein expression showed a clear and specific silencing effect induced by the three PEGylated nanoparticles in the zebrafish embryos. In detail, we observed a 68% reduction in GFP expression (***$p < 0.001$ vs. NT) for 20% PEG-WRAP1:siGFP-M, of 80% reduction (****$p < 0.0001$ vs. NT) for 20% PEG-WRAP1:siGFP-G, and of 63% reduction (**$p < 0.01$ vs. NT) for 20% PEG-WRAP1:siGFP-W (Figure 5B). In contrast, the applied control conditions (the three siRNAs alone or 20% PEG-WRAP1:siCtrl) had no GFP silencing properties (ns > 0.5 vs. NT) demonstrating the specificity of the siRNA-loaded PEGylated nanoparticles.

Visualization of GFP silencing in zebrafish embryos after nanoparticle bathing

Having confirmed that a siRNA transfection using 20% PEG-WRAP1 nanoparticles was possible by simply bathing the zebrafish embryos, we wanted to know if a specific GFP knockdown could be observed. Using a protocol similar to that used for the siRNA-Cy3 internalization/visualization, dechorionated zebrafish embryos were incubated with 20% PEG-WRAP1 encapsulating the three siGFP previously tested on HEK293 cells (Figure 6A). All z stack images of the zebrafish embryos were acquired by confocal microscopy in the same dorsal region as previously described (see Figure 4B) and images were processed consistently, using the same parameters each time.

Confocal images acquired after tissue fixation showed a well-defined pattern of blood vessels due to GFP-expressing endothelial cells in untreated zebrafish embryos (Figure 5C). In contrast, the 20% PEG-WRAP1 nanoparticles encapsulating the three GFP-targeting siRNA (siGFP-M, siGFP-G, and siGFP-W) showed a remarkable reduction in green fluorescence. More importantly, this silencing appeared to be sequence-specific, as embryos incubated with the nanoparticles encapsulating a control siRNA (20% PEG-WRAP1:siCtrl) showed no reduction in the GFP signal. The importance of the drug delivery system was highlighted in embryos treated with the three GFP-targeting siRNA alone as another negative control condition showing no GFP silencing.

To obtain a more global view of the results, the green fluorescence signal intensity of each acquired image was quantified by ImageJ software. As shown in the graph (Figure 5D), we were able to quantify approximatively 50% GFP silencing for the three 20% PEG-WRAP1:siGFP nanoparticles (**$p < 0.01$ for 20% PEG-WRAP1:siGFP-G, and ***$p < 0.001$ for 20% PEG-WRAP1:siGFP-M/W vs. non-treated embryos), which was not observed with the four control conditions (3x siRNA alone or 20% PEG-WRAP1:siCtrl).

DISCUSSION

In this study, we established a protocol for efficient and specific gene silencing by immersing zebrafish embryos in an E3 medium containing PEGylated WRAP1-based nanoparticles encapsulating siRNA. First, we confirmed the silencing efficiency of three different published siRNAs targeting the GFP protein[17–19] in GFP-overexpressing HEK293 cells. Transfections were performed with the WRAP-based nanoparticles as previously described,[13–15] and the GFP silencing of three different siGFP-loaded nanoparticles in GFP-overexpressing HEK293 cells was evaluated by western blot in comparison to the siRNA transfection without delivery system (Figure 2). We obtained a GFP silencing of ∼50% for all WRAP:siGFP transfected HEK293

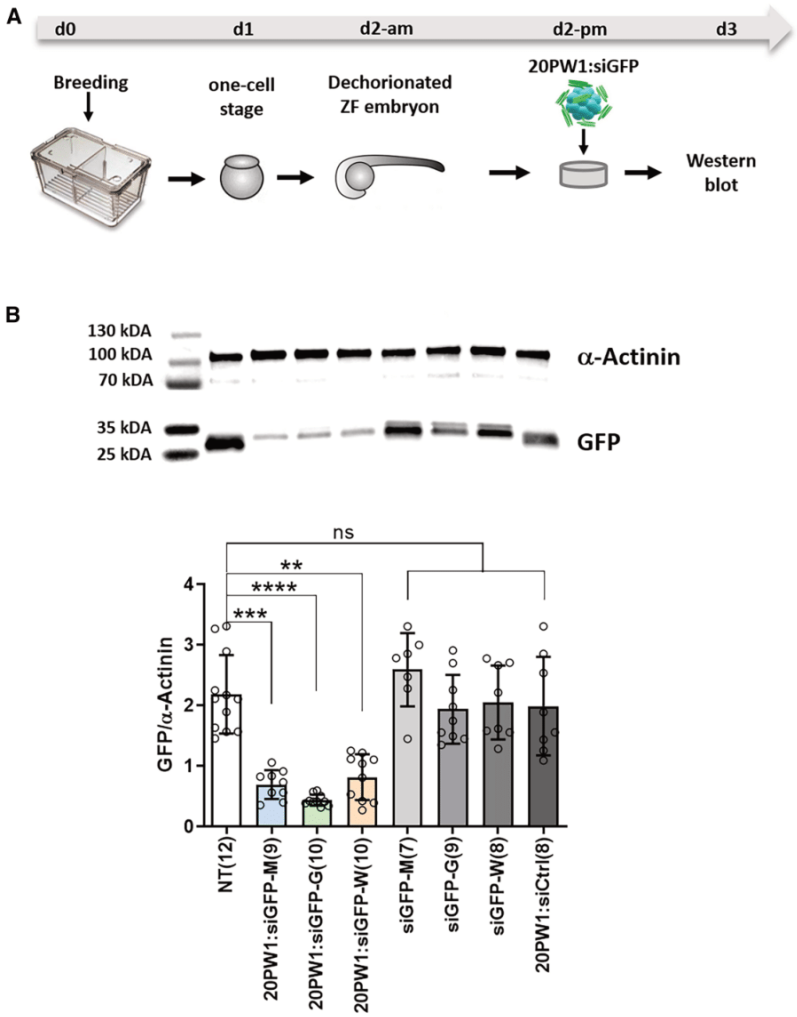

Figure 5. Quantification of the GFP silencing in zebrafish embryos by 20% PEG-WRAP1:siRNA nanoparticle bathing

(A) Schematic representation of the zebrafish embryo incubation protocol. At day zero (d0), zebrafish breeding was performed to collect one-cell stage embryos at d1. In the morning of d2 (~24 hpf), zebrafish embryos were dechorionated and left for 6 h in E3 medium before adding the fluorescence-labeled 20% PEG-WRAP1:siRNA (20PW1:siGFP) nanoparticles. After ~20 h, the embryos were washed, de-yolked, and lysed. Finally, proteins were quantified by western blot. (B) Representative images of western blots comparing non-treated zebrafish embryos with those incubated with 20% PEG-WRAP1:siGFP and 20% PEG-WRAP1:siCtrl nanoparticles or with the siRNA alone. The final siRNA concentration was 140 nM for all conditions (MR = 20). α-Actinin was used as a loading control. The graphical representation shows the GFP signal intensities normalized to the α-Actinin signal intensities. Brackets indicate the number of zebrafish embryos analyzed. Statistical evaluation: ns > 0.5, $^{**}p < 0.01$, $^{***}p < 0.001$, and $^{****}p < 0.0001$ vs. NT.

cells. This was consistent with the fact that wild-type GFP protein has a half-life of around 26 h,[28] meaning that during a 24-h incubation period for GFP knockdown, only newly synthesized GFP proteins are inhibited.

We then performed a proof of concept of *in vivo* WRAP-based siRNA transfection in *Tg*[*fli1*:EGFP]^{y1} zebrafish embryos using a simple immersion method. *Tg*(*fli1*:EGFP) (y1) fish express enhanced GFP throughout the vasculature under the control of the fli1 promoter.[29] To ensure the stability of the WRAP nanoparticles in the saline solution in which the zebrafish embryos were maintained, we evaluated the PEGylation of the WRAP nanoparticles. As previously reported by our team and others,[21,22,30,31] peptide-based nanoparticles could be improved by introducing PEG moieties on their surface to obtain a higher stabilization and/or lower interaction with molecules of the media or *in vivo* (e.g., blood or cytosol). In our case, we showed that the addition of PEG entities (20%) increased the stability of the colloidal properties (size and PdI) of WRAP1:siRNA nanoparticles in the presence of different saline solutions in contrast to the WRAP5:siRNA nanoparticles (Table 1). This result was further confirmed by a higher resistance to heparin of the 20% PEG-WRAP1:siRNA nanoparticles (Figure 3). Moreover, these results also emphasized the versatility of formulating such nanoparticles, which could be adapted to the ionic strength of the incubation conditions and transfection protocol.

Indeed, the ionic strength, which influences the intermolecular forces of the nanoparticles, affects the colloidal stability of the nanoparticles, leading to flocculation or precipitation phenomena based on changes in the van der Waals forces.[32] The negative effect of environmental salt on colloidal systems has been demonstrated for several nanoparticles, such as latex particles,[33] ethyl cellulose nanoparticles,[34] and gold nanoparticles.[35] Likewise, many examples have been published showing the positive effect of PEG coating on the colloidal stability of different nanoparticles such as iron oxide, gold, and SiO_2 but also on polymers or liposomes (see reviews in Lee[36], Li et al.,[37] Hristov et al.,[38] and Shi et al.[39]).

Subsequently, dechorionated zebrafish embryos (24 hpf) were incubated (bathed) in an E3 medium containing the siRNA-loaded PEGylated WRAP1 nanoparticles to evaluate the feasibility of a skin transfection. First, we showed a dose-dependent internalization of the Cy3-labeled siRNA by confocal microscopy (Figure 4). Then,

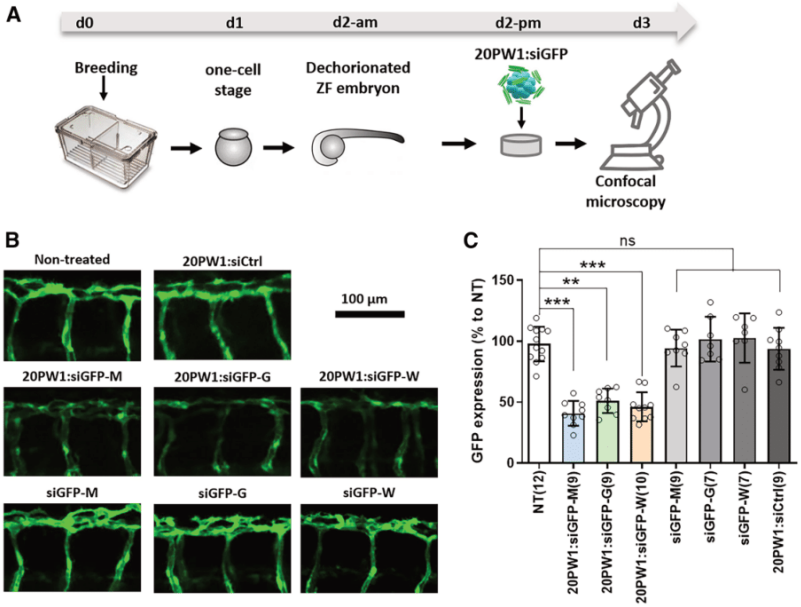

Figure 6. Visualization of the GFP silencing in zebrafish embryos by 20% PEG-WRAP1:siRNA nanoparticle bathing

(A) Schematic representation of the zebrafish embryo incubation protocol. At day zero (d0), zebrafish breeding was performed to collect one-cell stage embryos at d1. In the morning of d2 (~24 hpf), the zebrafish embryos were dechorionated and left for 6 h in E3 medium before adding in the afternoon the fluorescence-labeled 20% PEG-WRAP1:siRNA (20PW1:siGFP) nanoparticles. After ~20 h, the embryos were washed, fixed (PFA), and imaged by confocal microscopy. (B) Representative images of the z stack confocal microscopy acquisition of non-treated zebrafish embryo compared with those incubated with 20% PEG-WRAP1:siGFP and 20% PEG-WRAP1:siCtrl nanoparticles or with the siRNA alone. The final siRNA concentration was 140 nM for all conditions. Green = GFP-expressing endothelial cells. White bar = 100 µm. (C) Quantification of the GFP fluorescence signal intensity of the conditions shown in (C). Brackets indicate the number of zebrafish embryos analyzed. Statistical evaluation: ns > 0.5, $^{**}p < 0.01$, and $^{***}p < 0.001$ vs. non-treated embryos (NT).

we determined the optimal siRNA dose and incubation time (24 h vs. 48 h) (Figure S4). Finally, significant GFP silencing was quantified for all three WRAP:siGFP nanoparticles by western blot (more than 60%) (Figure 5) and by confocal microscopy (about 50%) (Figure 6) compared with the control conditions (WRAP:siCtrl or the siGFP alone). We selected specifically the western blot assay to evaluate knockdown at the protein level given the fact that only a fraction of RNA-induced silencing complexes (RISCs) are capable of carrying out small RNA-directed RNA cleavage, while the remainder suppresses expression by interfering with protein synthesis. Consequently, evaluating knockdown exclusively through the measurement of RNA levels (e.g., by quantitative PCR or northern blotting) can potentially lead to an overestimation of knockdown for long-lived proteins or an underestimation of knockdown caused by contributions from non-catalytic RISCs.[40]

Zebrafish embryos between 0 hpf and 72 hpf (=3 days) have a closed mouth (feeding through the yolk). Oral absorption and excretion are fully functional only between 72 hpf and 126 hpf, when zebrafish morphogenesis is complete.[41] Since the PEGylated WRAP nanoparticles in our case were incubated by immersion with the zebrafish embryo between 48 hpf and 72 hpf, it is most likely that internalization is mainly by dermal translocation and not by oral adsorption.

The specificity of the GFP silencing by the siRNAs was controlled by a blast search of zebrafish nucleotides, which revealed some potential off-targets for siGFP-G and siGFP-W (see supplemental results). Slightly higher GFP knockdown observed in zebrafish embryos (~60%) compared with GFP-overexpressing HEK293 cells (~50%) could be explained by different promoters (CMV for the HEK293 cells vs. fli1 for the zebrafish embryos) resulting in a higher GFP expression level in the HEK293 cells. Finally, the knockdown efficiencies for the three 20% PEG-WRAP1:siGFP nanoparticles measured by western blot analysis seemed to be more important than those quantified by confocal microscopy. However, GFP quantification by the two methods could not be directly compared because the GFP detection (fluorescence vs. antibody) is completely different, and more probably, the antibody detection may be more sensitive.

One potential strategy to improve the efficacy of RNAi-based silencing involves using chemically modified siRNAs. This approach involves the development of three modifications designed to diminish the siRNA degradation by ribonucleases. These modifications encompass alterations to the ribose (e.g., locked nucleic acid [LNA]), the phosphate (e.g., phosphorothioate [PS]), and base modifications (e.g., pseudouridine).[42] It is imperative to consider these modifications when conducting further *in vivo* studies.

There are many advantages in zebrafish handling, such as conserved vertebrate biology, ease of husbandry, high fecundity, small size, rapid development, and transparent juveniles. The zebrafish genome has been sequenced, and it has been shown that 70% of human genes have a zebrafish homolog, and more remarkably, 82% of human genes associated with the disease are mapped to a homologous gene in zebrafish.[43] For these reasons, zebrafish have long been studied for embryology, cell biology, genetics, and toxicology. Most toxicology studies on zebrafish have been focused on environmental pollutants, but there are also an increasing number of studies in the field of pharmaceutical toxicology.[44]

For all these studies, the incubation of zebrafish embryos by immersion in media containing various compounds or nanoparticles has

already been reported, with inconclusive results in most cases. For instance, Guarin et al. evaluated the spatiotemporal distribution of seven fluorescent alkyne compounds following immersion or microinjection (pericardial cavity, intraperitoneally, and yolk sac) of 72 hpf zebrafish embryos. The results of this study indicated that after 48 h, less signal was observed with immersion compared with microinjection.[45] Another example is given with different functionalized mesoporous silica nanoparticles (MSNs), which were incubated with zebrafish embryos by immersion. Confocal microscopy revealed that only polyethyleneimine-MSNs penetrated the embryos, whereas amino-, succinic acid-, or polyethyleneglycol-MSNs remained aggregated on the skin surface.[46]

In a study by van Pomeren et al.,[47] the authors evaluated the uptake of polystyrene particles of different sizes (25, 50, 250, and 700 nm) by immersion of zebrafish embryo. Irrespective of the size, internalization of the particles occurs only through oral uptake (between 72 and 120 hpf), which leads to dispersion in the body and ultimately to accumulation in certain organs such as the eyes or the digestive tract. Similar results were observed in adult zebrafish having a bath administration of surfactant-free poly(lactic acid) nanoparticles (PLA-NPs, 200 nm). Penetration and translocation through epithelial barriers were observed only from all exposed mucosae (gills, thymus, intestines, and the olfactory mucosa) and not from the fish skin.[48]

We recognize that the transfection of zebrafish embryos is not trivial and depends on the appropriate delivery systems, especially for skin transfection in the first-hour postfertilization. Here, we present the efficient skin transfection of siRNA via PEGylated WRAP1 using a simple immersion protocol showing a remarkable silencing effect exemplified by the GFP knockdown. Since the WRAP-based delivery system can encapsulate any siRNA, this technique could be useful in studying molecular interactions in early zebrafish embryo development and associated pathologies. It also opens up possibilities for novel RNAi-based pharmacological developments.

MATERIALS AND METHODS

Materials

WRAP1 (W1) and WRAP5 (W5) peptides were synthesized on the SynBio3 platform (Institut des Biomolécules Max Mousseron Montpellier) and crude products were purified in-house following a qualitative analysis by high-performance liquid chromatography/mass spectrometry as reported elsewhere.[13] PEG-WRAP1 (PW1) and PEG-WRAP5 (PW5) peptides were synthesized by coupling a PEG moiety to the N-terminal end of the WRAP peptide on resin, as described in more detail in the supplemental information. Peptide stock solutions were prepared in pure water (Sigma-Aldrich) and stored at 4°C. The different siRNA sequences (unlabeled and Cy3-labeled) were purchased from Eurogentec (see Table S1), resuspended in RNase-free water, and stored at −20°C. The siRNA stock solutions were prepared in RNase-free water. Stably transfected GFP HEK293 cell lines were used. As antibodies, we used anti-GFP rabbit (#600-401-215, Rockland), anti-Vinculin rabbit mAb E1E9V (#13901, Cell Signaling), anti-α-actinin (#3134, Cell Signaling), and anti-rabbit immunoglobulin (Ig)G horseradish peroxidase (HRP) (#7074S, Cell Signaling).

Nanoparticle formation

Nanoparticle formation was performed in pure water supplemented by 5% glucose (G7021, Sigma-Aldrich) by adding first the peptide and then the corresponding amount of siRNA at a molar ratio (MR) of 20:1 (peptide:siRNA) at room temperature.

DLS and Zeta potential

Peptide:siRNA nanoparticles (peptide = 10 μM, siRNA = 500 nM, MR = 20) were evaluated with a Zetasizer NanoZS (Malvern) in terms of mean size (Z-average) of the particle distribution and of homogeneity (PdI). Zeta potential was determined in 5% glucose complemented with 1 mM or 5 mM NaCl (S5886, Sigma-Aldrich). All results were obtained from three independent measurements (three runs for each measurement at 25°C) using the Zetasizer software 7.11.

Agarose gel shift retardation assay

WRAP:siRNA complexes (siRNA = 3.5 μM in 20 μL of an aqueous solution containing 5% glucose) were formed at a peptide:siRNA ratio of 20:1 and pre-incubated for 30 min at room temperature. Then, 5 μL of heparin (H3149, Sigma-Aldrich) solutions were added to obtain a final concentration of 100 μM, 50 μM, 25 μM, 12.5 μM, and 6.25 μM and again incubated for 30 min at room temperature. Finally, 20 μL of each solution was loaded on an agarose gel (1% w/v, A9539, Sigma-Aldrich) and electrophoresis was performed at 50 V for 25 min. To visualize the siRNA, the agarose gel was stained with GelRed (BY1740, Interchim) for UV detection, and images were acquired using a FAS-Digi PRO Gel Imaging System imager (Nippon Genetics) equipped with a DMC-GF7 camera (Panasonic). The signal intensities were quantified using ImageJ software (gel analysis tool) (version 1.54m). Each band intensity corresponding to a distinguished condition was then normalized to the band intensity of the siRNA alone (=100%): Relative fluorescence (%) = fluorescence intensity (condition x)/fluorescence intensity (siRNA alone) × 100.

Cell culture and transfection conditions

HEK293 (human embryonic kidney) cells stably transfected with an integrative GFP encoding plasmid were grown in a complete medium: DMEM with L-glutamine/pyruvate (COR10-013-CV, Ozyme), 1% penicillin/streptomycin (P4333, Sigma-Aldrich), and 10% heat-inactivated fetal bovine serum (FBS, P40-37500A, Dutscher). For western blot assay, 100,000 HEK293-GFP cells were seeded 24 h before the experiment into 24-well plates. The cells were incubated with 175 μL of fresh pre-warmed serum-free DMEM +75 μL of the nanoparticle solutions for standard incubation. After 1.5 h of incubation, 250 μL DMEM supplemented with 20% FBS (final FBS concentration = 10%) was added to each well without withdrawing the transfection reagents. Cells were then incubated for another 24 h and finally lysed for western blotting (see below).

Zebrafish experiments

Zebrafishes (*Danio rerio*) were raised and used according to standard laboratory protocols. Zebrafish use was performed in agreement with European Union guidelines for the handling of laboratory animals. All experiments were approved by the Comité d'Ethique pour l'Expérimentation Animale and the Direction Sanitaire et Vétérinaire de l'Hérault (Aquatic model facility, ZEFIX from CRBM C-34-172-39). *Tg*[*fli1*:EGFP]^{y1} transgenic line was used with enhanced GFP-labeling of all endothelial cells.[29]

Zebrafish embryos were kept for 24 h in a dish (100 mm) in E3 medium (5 mM NaCl, 0.17 mM KCl, 0.33 mM $CaCl_2$, 0.33 mM $MgSO_4$, 0.01 mg/L methylene blue) in an incubator at 28°C. Thereafter, the zebrafish embryo chorions were removed with sharp forceps and the embryos were kept in an E3 medium containing 75 μM N-Phenylthiourea (PTU, P7629, Sigma-Aldrich) to avoid pigment formation. Six hours after chorion removal, zebrafish embryos were washed twice with E3+PTU medium and then incubated with the nanoparticles for 24 h at 28°C. The nanoparticles were formulated at a peptide:siRNA molar ratio of 20:1 (see the preceding section "nanoparticle formation") with an siRNA concentration of 3 mM and then directly diluted in the E3+PTU medium at the desired siRNA concentration. For western blot analysis or confocal microscopy imaging, zebrafish embryos were previously washed twice with E3+PTU medium before proceeding (see the following sections). Three independent experiments were performed with 3–5 zebrafish embryos per condition.

Relative viability measurement

The Cytotoxicity Detection Kit^{Plus} (LDH, #04744934001, Sigma-Aldrich) was used to evaluate the cytotoxicity induced by the PBNs. After the PBN incubation (36 h), at least one well was used as LDH negative control (0% viability) by adding Triton X-100 (T9797, Sigma-Aldrich) to a final concentration of 0.1% (∼15 min incubation at 37°C). Non-treated cells were considered as 100% viability (= positive control). Afterward, 50 μL supernatant of each well was transferred in a new clear 96-well plate (Greiner) and completed with 50 μL/well of the "dye solution/catalyst" mixture as recommended by the manufacturer. The plate was then incubated in the dark for 30 min at room temperature. The reaction was stopped by adding 25 μL/well of HCl (1 N) before measuring the absorption at 490 nm using the Infinite M200 pro plate reader (Tecan). Relative viability (%) was calculated with the following formula: [100 – ((value treated cells – value non-treated cells)/(value Triton – value non-treated cells) × 100)].

Western blot

HEK293-GFP cells

Transfected cells were lysed in 130 μL/24-well RIPA buffer (50 mM Tris pH 8.0, 150 mM NaCl, 1% Triton X-100, 0.1% SDS [sodium dodecyl sulfate, L4509, Sigma-Aldrich], including SigmaFAST protease inhibitor cocktail [diluted 1/10, S8820, Sigma-Aldrich]) on ice for 5 min. Thereafter, cells were scraped and transferred in a 1.5-mL tube and kept a further 5 min on ice.

Zebrafish embryos

At 48 hpf (= 24 h post PBN incubation), one embryo was placed in one 1.5-mL tube. Embryos were de-yolked using an ice-cold Ringer solution (11.6 mM NaCl, 0.29 mM KCl, 0.18 mM CaCl,[2] 0.5 mM HEPES, pH 7.2) by triturating with a P200 pipette. The de-yolked embryo was rinsed twice with the same Ringer solution before adding 70 μL RIPA buffer (see above). The embryos were incubated on a rotating wheel at 4°C for complete lysis, followed by a sonication step of 20 min.

Afterward, for both sample types (from cells or zebrafish embryos), lysates were centrifuged (10 min, 13,500 × *g*, 4°C), supernatants were collected in novel tubes and protein concentrations were determined using the Pierce BCA Protein Assay (#23225, Thermo Fisher). Proteins (15 μg and 8 μg from cell and zebrafish embryo lyses, respectively) were separated by 4%–20% Mini-PROTEAN TGXTM Precast Gels (#4561094 or #4561095, Bio-Rad) and transferred onto Trans-Blot Turbo PVDF Transfer Membranes (#1704157, Bio-Rad). Primary and secondary antibodies were incubated in 5% BSA TBS-T buffer overnight at 4°C or for 1 h at room temperature, respectively. Western blots were revealed with the Pierce ECL plus western blotting substrate (Thermo Fisher) on an Amersham imager 600 (GE Healthcare Life Science). The signal intensities of the blots were quantified using ImageJ software (version 1.54m). Each band intensity corresponding to a distinguished condition is then normalized to the band intensity of non-treated cells (NT) (= 100%): Relative Signal Intensity (%) = intensity (condition x)/intensity (NT) × 100.

Confocal microscopy

Zebrafish embryos were fixed in 4% PFA in phosphate-buffered saline (PBS) for 30 min at room temperature. Afterward, embryos were washed five times with PBS buffer and kept in PBS buffer at 4°C until imaging. Image acquisition was performed by confocal microscopy on an inverted Zeiss LSM800 microscope using a lens Apo 63x/1.2 W DICIII. All confocal acquisitions were performed using a diode laser 488 nm with the specific GFP filter (486 nm–561 nm) and a diode laser 561 nm with the specific Alexa 594 filter (592 nm–614 nm). Fifteen images per sample were acquired using z stack mode with a z stack interval of 3 μm. Acquired images were analyzed using the ImageJ software (version 1.54m). Z projection for each sample was performed by summing fluorescence intensities to one image. The threshold of each sample was adjusted to quantify the mean fluorescence of the image.

Statistical evaluation

Statistical analysis was performed only for independent experiments. Data (mean ± SD) were analyzed with an ordinary one-way ANOVA and the Dunnett's post-test. Data were analyzed with GraphPad Prism version 8.0.2.

ACKNOWLEDGMENTS

This research was funded by the "Fondation ARC pour la Recherche sur le Cancer" (PJA20171206171 to P.B.), the "Agence Nationale de la Recherche" (ANR-21-CE18-0022-01 to P.B.), AFM-Téléthon (n 23800 to S.F.), and by institutional funds from

Inserm, CNRS, and University of Montpellier. The authors are grateful to Pascal Verdié from the SynBio3 platform for providing peptide synthesis facilities, and to Pierre Sanchez for performing LCMS analysis, both from the Institut des Biomolécules Max Mousseron (IBMM), Montpellier (France). The authors thank Marc Plays and Bénédicte Delaval from the Aquatic model platform ZEFIX situated at the Cell Biology Research of Montpellier (CRBM) for technical support.

AUTHOR CONTRIBUTIONS

Conceptualization, S.Deshayes and P.B.; methodology and formal analysis, C.T.A., K.K., S. Descamps, E.V., S. Deshayes, I.P., T.H., and P.B.; writing – original draft preparation, P.B.; writing – review and editing, E.V., K.K., S. Deshayes, S.F., and P.d.S.B.; funding acquisition, P.B., S.F., and P.d.S.B. All authors have read and agreed to the published version of the manuscript.

DECLARATION OF INTERESTS

Patent entitled "Non-naturally occurring peptides for use as cell-penetrating peptides" WO2020/016242.

SUPPLEMENTAL INFORMATION

Supplemental information can be found online at https://doi.org/10.1016/j.omtm.2025.101458.

REFERENCES

1. Talap, J., Zhao, J., Shen, M., Song, Z., Zhou, H., Kang, Y., Sun, L., Yu, L., Zeng, S., and Cai, S. (2021). Recent advances in therapeutic nucleic acids and their analytical methods. J. Pharm. Biomed. Anal. *206*, 114368. https://doi.org/10.1016/j.jpba.2021.114368.

2. Tolia, N.H., and Joshua-Tor, L. (2007). Slicer and the argonautes. Nat. Chem. Biol. *3*, 36–43. https://doi.org/10.1038/nchembio848.

3. Whitehead, K.A., Langer, R., and Anderson, D.G. (2009). Knocking down barriers: advances in siRNA delivery. Nat. Rev. Drug Discov. *8*, 129–138. https://doi.org/10.1038/nrd2742.

4. Tang, Q., and Khvorova, A. (2024). RNAi-based drug design: considerations and future directions. Nat. Rev. Drug Discov. *23*, 341–364. https://doi.org/10.1038/s41573-024-00912-9.

5. Hoy, S.M. (2018). Patisiran: First Global Approval. Drugs *78*, 1625–1631. https://doi.org/10.1007/s40265-018-0983-6.

6. Paunovska, K., Loughrey, D., and Dahlman, J.E. (2022). Drug delivery systems for RNA therapeutics. Nat. Rev. Genet. *23*, 265–280. https://doi.org/10.1038/s41576-021-00439-4.

7. Roberts, T.C., Langer, R., and Wood, M.J.A. (2020). Advances in oligonucleotide drug delivery. Nat. Rev. Drug Discov. *19*, 673–694. https://doi.org/10.1038/s41573-020-0075-7.

8. Boisguérin, P., Deshayes, S., Gait, M.J., O'Donovan, L., Godfrey, C., Betts, C.A., Wood, M.J.A., and Lebleu, B. (2015). Delivery of therapeutic oligonucleotides with cell penetrating peptides. Adv. Drug Deliv. Rev. *87*, 52–67. https://doi.org/10.1016/j.addr.2015.02.008.

9. Lehto, T., Ezzat, K., Wood, M.J.A., and El Andaloussi, S. (2016). Peptides for nucleic acid delivery. Adv. Drug Deliv. Rev. *106*, 172–182. https://doi.org/10.1016/j.addr.2016.06.008.

10. Kurrikoff, K., and Langel, Ü. (2019). Recent CPP-based applications in medicine. Expert Opin. Drug Deliv. *16*, 1183–1191. https://doi.org/10.1080/17425247.2019.1665021.

11. Boisguérin, P., Konate, K., Josse, E., Vivès, E., and Deshayes, S. (2021). Peptide-Based Nanoparticles for Therapeutic Nucleic Acid Delivery. Biomedicines *9*, 583. https://doi.org/10.3390/biomedicines9050583.

12. Pasut, G., and Veronese, F.M. (2012). State of the art in PEGylation: the great versatility achieved after forty years of research. J. Control. Release *161*, 461–472. https://doi.org/10.1016/j.jconrel.2011.10.037.

13. Konate, K., Dussot, M., Aldrian, G., Vaissière, A., Viguier, V., Neira, I.F., Couillaud, F., Vivès, E., Boisguerin, P., and Deshayes, S. (2019). Peptide-Based Nanoparticles to Rapidly and Efficiently "Wrap 'n Roll" siRNA into Cells. Bioconjug. Chem. *30*, 592–603. https://doi.org/10.1021/acs.bioconjchem.8b00776.

14. Deshayes, S., Konate, K., Dussot, M., Chavey, B., Vaissière, A., Van, T.N.N., Aldrian, G., Padari, K., Pooga, M., Vivès, E., and Boisguérin, P. (2020). Deciphering the internalization mechanism of WRAP:siRNA nanoparticles. Biochim. Biophys. Acta. Biomembr. *1862*, 183252. https://doi.org/10.1016/j.bbamem.2020.183252.

15. Konate, K., Josse, E., Tasic, M., Redjatti, K., Aldrian, G., Deshayes, S., Boisguérin, P., and Vivès, E. (2021). WRAP-based nanoparticles for siRNA delivery: a SAR study and a comparison with lipid-based transfection reagents. J. Nanobiotechnology *19*, 236. https://doi.org/10.1186/s12951-021-00972-8.

16. Ferreiro, I., Genevois, C., Konate, K., Vivès, E., Boisguérin, P., Deshayes, S., and Couillaud, F. (2021). In Vivo Follow-Up of Gene Inhibition in Solid Tumors Using Peptide-Based Nanoparticles for siRNA Delivery. Pharmaceutics *13*, 749. https://doi.org/10.3390/pharmaceutics13050749.

17. Molla, M.R., Chakraborty, S., Munoz−Sagredo, L., Drechsler, M., Orian−Rousseau, V., and Levkin, P.A. (2020). Combinatorial Synthesis of a Lipidoid Library by Thiolactone Chemistry: In Vitro Screening and In Vivo Validation for siRNA Delivery. Bioconjug. Chem. *31*, 852–860. https://doi.org/10.1021/acs.bioconjchem.0c00013.

18. Gruber, J., Manninga, H., Tuschl, T., Osborn, M., and Weber, K. (2005). Specific RNAi Mediated Gene Knockdown in Zebrafish Cell Lines. RNA Biol. *2*, 101–105. https://doi.org/10.4161/rna.2.3.2060.

19. Wen, Y., Bai, H., Zhu, J., Song, X., Tang, G., and Li, J. (2020). A supramolecular platform for controlling and optimizing molecular architectures of siRNA targeted delivery vehicles. Sci. Adv. *6*, eabc2148. https://doi.org/10.1126/sciadv.abc2148.

20. Allen, C., Dos Santos, N., Gallagher, R., Chiu, G.N.C., Shu, Y., Li, W.M., Johnstone, S.A., Janoff, A.S., Mayer, L.D., Webb, M.S., and Bally, M.B. (2002). Controlling the physical behavior and biological performance of liposome formulations through use of surface grafted poly(ethylene glycol). Biosci. Rep. *22*, 225–250. https://doi.org/10.1023/a:1020186505848.

21. Aldrian, G., Vaissière, A., Konate, K., Seisel, Q., Vivès, E., Fernandez, F., Viguier, V., Genevois, C., Couillaud, F., Démèné, H., et al. (2017). PEGylation rate influences peptide-based nanoparticles mediated siRNA delivery in vitro and in vivo. J. Control. Release *256*, 79–91. https://doi.org/10.1016/j.jconrel.2017.04.012.

22. Faria, R., Vivès, E., Boisguérin, P., Descamps, S., Sousa, Â., and Costa, D. (2024). Upgrading Mitochondria-Targeting Peptide-Based Nanocomplexes for Zebrafish In Vivo Compatibility Assays. Pharmaceutics *16*, 961. https://doi.org/10.3390/pharmaceutics16070961.

23. Di Gregorio, G., Coléo, V., Karidia, K., Clémentine, T.-A., Hammoum, T.F., Gautron, H., Bessin, Y., Deshayes, S., Vivès, E., Meli, A.C., et al. (2025). Enhancing WRAP-based nanoparticles for siRNA delivery in pH-sensitive environments. ChemMedChem, e202400885. https://doi.org/10.1002/cmdc.202400885.

24. Porosk, L., Härk, H.H., Arukuusk, P., Haljasorg, U., Peterson, P., and Kurrikoff, K. (2023). The Development of Cell-Penetrating Peptides for Efficient and Selective In Vivo Expression of mRNA in Spleen Tissue. Pharmaceutics *15*, 952. https://doi.org/10.3390/pharmaceutics15030952.

25. Karlsson, J., von Hofsten, J., and Olsson, P.E. (2001). Generating transparent zebrafish: a refined method to improve detection of gene expression during embryonic development. Mar. Biotechnol. *3*, 522–527. https://doi.org/10.1007/s1012601-0053-4.

26. Schnabel, D., Castillo-Robles, J., and Lomeli, H. (2019). Protein Purification and Western Blot Detection from Single Zebrafish Embryo. Zebrafish *16*, 505–507. https://doi.org/10.1089/zeb.2019.1761.

27. Purushothaman, K., Das, P.P., Presslauer, C., Lim, T.K., Johansen, S.D., Lin, Q., and Babiak, I. (2019). Proteomics Analysis of Early Developmental Stages of Zebrafish Embryos. Int. J. Mol. Sci. *20*, 6359. https://doi.org/10.3390/ijms20246359.

28. Corish, P., and Tyler-Smith, C. (1999). Attenuation of green fluorescent protein half-life in mammalian cells. Protein Eng. *12*, 1035–1040. https://doi.org/10.1093/protein/12.12.1035.

29. Lawson, N.D., and Weinstein, B.M. (2002). In Vivo Imaging of Embryonic Vascular Development Using Transgenic Zebrafish. Dev. Biol. *248*, 307–318. https://doi.org/10.1006/dbio.2002.0711.

30. Veiman, K.-L., Künnapuu, K., Lehto, T., Kiisholts, K., Pärn, K., Langel, Ü., and Kurrikoff, K. (2015). PEG shielded MMP sensitive CPPs for efficient and tumor specific gene delivery in vivo. J. Control. Release *209*, 238–247. https://doi.org/10.1016/j.jconrel.2015.04.038.

31. Kurrikoff, K., Veiman, K.-L., Künnapuu, K., Peets, E.M., Lehto, T., Pärnaste, L., Arukuusk, P., and Langel, Ü. (2017). Effective in vivo gene delivery with reduced toxicity, achieved by charge and fatty acid -modified cell penetrating peptide. Sci. Rep. *7*, 17056. https://doi.org/10.1038/s41598-017-17316-y.

32. Intermolecular and Surface Forces - 3rd Edition https://www.elsevier.com/books/intermolecular-and-surface-forces/israelachvili/978-0-12-391927-4.

33. Takács, D., Tomšič, M., and Szilagyi, I. (2022). Effect of Water and Salt on the Colloidal Stability of Latex Particles in Ionic Liquid Solutions. Colloids Interfaces *6*, 2. https://doi.org/10.3390/colloids6010002.

34. Bizmark, N., and Ioannidis, M.A. (2015). Effects of Ionic Strength on the Colloidal Stability and Interfacial Assembly of Hydrophobic Ethyl Cellulose Nanoparticles. Langmuir *31*, 9282–9289. https://doi.org/10.1021/acs.langmuir.5b01857.

35. Pamies, R., Cifre, J.G.H., Espín, V.F., Collado-González, M., Baños, F.G.D., and de la Torre, J.G. (2014). Aggregation behaviour of gold nanoparticles in saline aqueous media. J. Nanoparticle Res. *16*, 2376. https://doi.org/10.1007/s11051-014-2376-4.

36. Lee, H. (2020). Molecular Simulations of PEGylated Biomolecules, Liposomes, and Nanoparticles for Drug Delivery Applications. Pharmaceutics *12*, E533. https://doi.org/10.3390/pharmaceutics12060533.

37. Li, D., Wang, F., Di, H., Liu, X., Zhang, P., Zhou, W., and Liu, D. (2019). Cross-Linked Poly(ethylene glycol) Shells for Nanoparticles: Enhanced Stealth Effect and Colloidal Stability. Langmuir *35*, 8799–8805. https://doi.org/10.1021/acs.langmuir.9b01325.

38. Hristov, D.R., Lopez, H., Ortin, Y., O'Sullivan, K., Dawson, K.A., and Brougham, D. F. (2021). Impact of dynamic sub-populations within grafted chains on the protein binding and colloidal stability of PEGylated nanoparticles. Nanoscale *13*, 5344–5355. https://doi.org/10.1039/d0nr08294e.

39. Shi, L., Zhang, J., Zhao, M., Tang, S., Cheng, X., Zhang, W., Li, W., Liu, X., Peng, H., and Wang, Q. (2021). Effects of polyethylene glycol on the surface of nanoparticles for targeted drug delivery. Nanoscale *13*, 10748–10764. https://doi.org/10.1039/d1nr02065j.

40. Chang, K., Marran, K., Valentine, A., and Hannon, G.J. (2012). RNAi in Cultured Mammalian Cells Using Synthetic siRNAs. Cold Spring Harb. Protoc. *2012*, 957–961. https://doi.org/10.1101/pdb.prot071076.

41. Ng, A.N.Y., de Jong-Curtain, T.A., Mawdsley, D.J., White, S.J., Shin, J., Appel, B., Dong, P.D.S., Stainier, D.Y.R., and Heath, J.K. (2005). Formation of the digestive system in zebrafish: III. Intestinal epithelium morphogenesis. Dev. Biol. *286*, 114–135. https://doi.org/10.1016/j.ydbio.2005.07.013.

42. Chernikov, I.V., Ponomareva, U.A., and Chernolovskaya, E.L. (2023). Structural Modifications of siRNA Improve Its Performance In Vivo. Int. J. Mol. Sci. *24*, 956. https://doi.org/10.3390/ijms24020956.

43. Howe, K., Clark, M.D., Torroja, C.F., Torrance, J., Berthelot, C., Muffato, M., Collins, J.E., Humphray, S., McLaren, K., Matthews, L., et al. (2013). The zebrafish reference genome sequence and its relationship to the human genome. Nature *496*, 498–503. https://doi.org/10.1038/nature12111.

44. Cassar, S., Adatto, I., Freeman, J.L., Gamse, J.T., Iturria, I., Lawrence, C., Muriana, A., Peterson, R.T., Van Cruchten, S., and Zon, L.I. (2020). Use of Zebrafish in Drug Discovery Toxicology. Chem. Res. Toxicol. *33*, 95–118. https://doi.org/10.1021/acs.chemrestox.9b00335.

45. Guarin, M., Faelens, R., Giusti, A., De Croze, N., Léonard, M., Cabooter, D., Annaert, P., de Witte, P., and Ny, A. (2021). Spatiotemporal imaging and pharmacokinetics of fluorescent compounds in zebrafish eleuthero-embryos after different routes of administration. Sci. Rep. *11*, 12229. https://doi.org/10.1038/s41598-021-91612-6.

46. Paatero, I., Casals, E., Niemi, R., Özliseli, E., Rosenholm, J.M., and Sahlgren, C. (2017). Analyses in zebrafish embryos reveal that nanotoxicity profiles are dependent on surface-functionalization controlled penetrance of biological membranes. Sci. Rep. *7*, 8423. https://doi.org/10.1038/s41598-017-09312-z.

47. van Pomeren, M., Brun, N.R., Peijnenburg, W.J.G.M., and Vijver, M.G. (2017). Exploring uptake and biodistribution of polystyrene (nano)particles in zebrafish embryos at different developmental stages. Aquat. Toxicol. *190*, 40–45. https://doi.org/10.1016/j.aquatox.2017.06.017.

48. Rességuier, J., Delaune, E., Coolen, A.-L., Levraud, J.-P., Boudinot, P., Le Guellec, D., and Verrier, B. (2017). Specific and Efficient Uptake of Surfactant-Free Poly(Lactic Acid) Nanovaccine Vehicles by Mucosal Dendritic Cells in Adult Zebrafish after Bath Immersion. Front. Immunol. *8*, 190. https://doi.org/10.3389/fimmu.2017.00190.

2. Appendix 2: Scientific contributions related to this thesis

2.1. Publications

Pezzati, I., Serrano, C., Vivès, E., Chibon, F., Faure, S., de Santa Barbara, P., Deshayes, S., Boisguérin, P. (2025) Breaking the redundancy: TAZ outperforms YAP1 in GIST progression. bioRxiv 2025.09.02.673653; doi: https://doi.org/10.1101/2025.09.02.673653

Konate, K., Pezzati, I., Redjatti, K., Agnel, E., Vivès, E., Faure, S., de Santa Barbara, P., Boisguérin, P., & Deshayes, S. (2025). Multiprotein Silencing Using WRAP-Based Nanoparticles: A Proof of Concept. Bioconjugate chemistry, 36(6), 1218–1233. https://doi.org/10.1021/acs.bioconjchem.5c00069

Konate, K., Teko-Agbo, C. A., Pezzati, I., Hammoum, T., Deshayes, S., Descamps, S., Vivès, E., Faure, S., de Santa Barbara, P., & Boisguérin, P. (2025). WRAP-based nanoparticles for siRNA delivery in zebrafish embryos by simple bath immersion. Molecular therapy. Methods & clinical development, 33(2), 101458. https://doi.org/10.1016/j.omtm.2025.101458

2.2. Oral presentations

EuSARC The Biology of Sarcoma: from Basic Mechanisms to Innovative Therapies. *Venezia, VE, ITALY*. June 5th-7th, 2025

Irene Pezzati, Sandrine Faure, Pascal de Santa Barbara, Cesar Serrano, Sébastien Deshayes, Prisca Boisguérin. Deciphering YAP1/TAZ roles using WRAP-Based Nanoparticles in Gastrointestinal Stromal Tumors (GIST).

Cell-penetrating peptides: next generation delivery systems. *Montpellier, FRANCE.* 10th-12nd, June 2024

Irene Pezzati, Giulia Di Gregorio, Karidia Konate, Sandrine Faure, Pascal de Santa Barbara, Eric Vivès, Sébastien Deshayes, Prisca Boisguérin. Optimizing the WRAP family: "Smart peptide-based nanoparticles" for siRNA-cocktail delivery.

20th Meeting of Doctoral Students in Chemical and Biological Health Sciences. *Montpellier, FRANCE*. September 29th, 2023

Irene Pezzati, Sébastien Deshayes, Prisca Boisguérin. Dissecting the YAP/TAZ pathway in chemotherapy-resistant gastrointestinal stromal tumors (GIST) to develop new pharmacological molecules.

2.3. Posters

ESMO Sarcoma and Rare Cancers. *Lugano, TI, SWITZERLAND.* March 20th-22nd, 2025

Irene Pezzati, Sandrine Faure, Pascal de Santa Barbara, Cesar Serrano, Sébastien Deshayes, Prisca Boisguérin. Deciphering YAP1/TAZ roles using WRAP-Based Nanoparticles in Gastrointestinal Stromal Tumors (GIST).

21th Meeting of Doctoral Students in Chemical and Biological Health Sciences. *Montpellier, FRANCE.* September 26th, 2024

Irene Pezzati, Sandrine Faure, Pascal de Santa Barbara, Eric Vivès, Karidia Konate, Sébastien Deshayes, Prisca Boisguérin. Tools for YAP1/TAZ silencing in gastrointestinal stromal tumors (GIST).

Cancéropole Grand Sud-Ouest Workshop « Signaling, microenvironment and Targeting ». Toulouse, FRANCE. February 5th-6th, 2024

Irene Pezzati, Sandrine Faure, Pascal de Santa Barbara, Karidia Konate, Eric Vivès, Sébastien Deshayes, Prisca Boisguérin. Targeting the YAP1/TAZ pathway in gastrointestinal stromal tumors (GIST).

9th annual meeting of SFNano (French society of nanomedecine). Montpellier, FRANCE December 4th-6th, 2023

Irene Pezzati, Sandrine Faure, Pascal de Santa Barbara, Karidia Konate, Eric Vivès, Sébastien Deshayes, Prisca Boisguérin. Interfering with the YAP1/TAZ pathway in chemotherapy-resistant gastrointestinal stromal tumors to develop new pharmacological molecules.

Cambridge - Montpellier meeting of PhD students in nanoscience and nanotechnology. Montpellier, FRANCE September 25th, 2023

Multi-protein silencing using WRAP peptide-based nanoparticles to reduce tumor growth. Irene Pezzati, Sandrine Faure, Pascal de Santa Barbara, Sébastien Deshayes, Prisca Boisguérin.

23rd GFPP (Groupe Français des peptides et des protéines) Meeting. Fournols, FRANCE September 17th-21st, 2023

Multi-protein silencing using WRAP peptide-based nanoparticles to reduce tumor growth. Irene Pezzati, Sandrine Faure, Pascal de Santa Barbara, Sébastien Deshayes, Prisca Boisguérin.

2.4. Attendance at conferences

22th Meeting of Doctoral Students in Chemical and Biological Health Sciences. *Montpellier, FRANCE.* June 3rd, 2025

Réunion régionale: Actualités dans la prise en charge des GIST métastatiques. Ecole du cancer de Montpellier, FRANCE. April 4th, 2024

26ème Journées Jeunes Chercheurs (JJC) en cancérologie de la Fondation ARC. Paris, France. November 21st-22nd, 2024

3. Appendix 3: Substantial French summary

Contexte

Les tumeurs stromales gastro-intestinales (GIST) sont des cancers rares, mais représentent la forme la plus courante de tumeurs mésenchymateuses du tube digestif, avec une incidence annuelle mondiale estimée entre 10 et 15 cas par million d'individus. Ces sarcomes dérivent principalement des cellules interstitielles de Cajal ou de leurs précurseurs mésenchymateux. Les GIST se développent majoritairement dans l'estomac et sont causés par des mutations oncogéniques dans les gènes codant pour des récepteurs à activité tyrosine kinase, en majorité KIT (75 à 80% des cas) et, dans une moindre mesure, PDGFRA (10 à 15%). Ces mutations à gain de fonction induisent une activation constitutive des récepteurs en l'absence de leurs ligands spécifiques, responsables d'une croissance et d'une prolifération soutenues.

Pour les GIST localisés à faible risque, le traitement de référence repose sur la résection chirurgicale complète de la tumeur, sans recours à un traitement adjuvant. En revanche, l'imatinib (IM), inhibiteur de tyrosine kinase (TKI), est indiqué pour les GIST à plus haut risque. Il est prescrit en adjuvant après résection complète d'un GIST présentant un risque élevé de récidive. Il est aussi très utilisé en néoadjuvant pour réduire la taille d'une tumeur localement avancée afin de faciliter une résection complète par la suite. L'IM est le traitement de première ligne chez les patients présentant des GIST métastatiques ou inopérables. Pour ces derniers, bien que l'IM ait significativement amélioré le pronostic et offre une grande efficacité initiale, la plupart développent des résistances après 20 à 24 mois. Cela entraîne des rechutes et réduit considérablement les chances de survie. Les TKI de deuxième, troisième ou quatrième ligne, tels que le sunitinib, le régorafénib ou le riprétinib, apportent un bénéfice limité, avec une survie sans progression inférieure à 6 mois et des taux de réponse de moins de 10%.

La résistance aux TKI peut être primaire, lorsque la tumeur est insensible dès le début du traitement, ou secondaire, lorsqu'elle progresse après une réponse initiale. La résistance primaire, observée chez environ 10% des patients, est généralement associée à des mutations spécifiques dans *KIT* ou *PDGFRA* empêchant leur inhibition par l'IM. La résistance secondaire, plus fréquente, est liée à l'acquisition de mutations secondaires, notamment sur le gène *KIT*, ou à l'activation de voies compensatoires telles que PI3K/AKT/mTOR, MAPK/ERK ou JAK/STAT,

permettant aux cellules tumorales d'échapper à l'effet du TKI et de reprendre leur prolifération.

Cette résistance, qui demeure le principal défi dans la prise en charge des patients ayant des GIST avancés et métastatiques, souligne la nécessité de développer de nouvelles approches thérapeutiques.

En clinique, les stratégies innovantes actuelles explorent la combinaison de traitements sous forme de petites molécules (*small molecules*), notamment des inhibiteurs des voies de signalisation clés comme PI3K/AKT/mTOR ou MAPK/ERK. Néanmoins, malgré des résultats encourageants *in vitro*, aucun essai n'a permis de démontrer une translation clinique complète, en raison de la toxicité et de l'inefficacité des inhibiteurs évalués, tant en monothérapie qu'en association avec l'IM. Par ailleurs, d'autres options sont actuellement en cours, ciblant l'homéostasie protéique, l'export nucléaire ou la régulation du cycle cellulaire, toujours dans le but de contourner l'hétérogénéité tumorale et la résistance.

En recherche fondamentale, l'identification de nouvelles cibles moléculaires participe encore aujourd'hui à enrichir la compréhension de la complexité des GIST. Si la plupart des projets se sont concentrés sur l'inhibition directe de KIT et PDGFRA, il apparaît de plus en plus évident que d'autres modulateurs de voies de signalisation contribuent à la croissance tumorale et à l'adaptation thérapeutique de ce sarcome.

Dans ce contexte, notre équipe a mis en évidence le rôle de LIX1 (*Limb expression 1*) comme régulateur de la plasticité cellulaire des GIST et comme acteur de l'adaptation tumorale à l'inhibition de KIT, notamment par la modulation en amont de la voie Hippo. Les coactivateurs de transcription YAP1 (*Yes-associated protein 1*) et TAZ (*Transcriptional co-activator with PDZ-binding motif*), qui sont les principaux effecteurs de cette voie, sont apparus comme des médiateurs potentiels des effets de LIX1. Ces deux protéines sont connues pour leur rôle dans la tumorigenèse de nombreux types de cancers solides. Lorsqu'elles ne sont pas inhibées par les kinases MST1/2 et LATS1/2, YAP1 et TAZ transloquent vers le noyau et interagissent avec des facteurs de transcription tels que TEAD1-4 (*TEA domain family member 1-4*), pour *in fine* activer la transcription de gènes impliqués dans la prolifération, la survie et la migration cellulaire.

Ces observations nous ont conduit à formuler l'hypothèse selon laquelle **YAP1 et TAZ peuvent constituer des cibles thérapeutiques prometteuses pour limiter la progression des GIST et contourner la résistance aux TKI.** Néanmoins, leurs rôles respectifs dans la biologie de ces tumeurs restent encore mal définis, en raison de leur forte homologie structurale et de leurs programmes transcriptionnels largement redondants, qui conduisent souvent à les considérer comme une seule entité fonctionnelle. Mieux caractériser l'implication spécifique de YAP1 et TAZ dans les GIST permettrait à la fois de comprendre les mécanismes moléculaires lors du développement de ce sarcome et d'identifier de nouvelles stratégies thérapeutiques.

Pour explorer expérimentalement ces nouvelles pistes, il est nécessaire de disposer d'outils capables de moduler de manière précise l'expression de ces gènes. De ce fait, l'ARN interférence apparaît comme une approche pertinente. Cette stratégie thérapeutique innovante repose sur l'utilisation de petits ARN interférents (*si*ARN) capables de réduire spécifiquement l'expression de gènes d'intérêt. Si plusieurs siRNA thérapeutiques ont déjà atteint le stade clinique, leur potentiel reste limité par des obstacles liés à la délivrance intracellulaire, en particulier l'échappement endosomal qui limite leur efficacité. Dans ce contexte, les peptides pénétrants de cellules (*CPP*) représentent une alternative prometteuse. Notre équipe a développé les peptides WRAP (*Tryptophan (W)- and arginine (R)-rich amphipathic peptide*) qui se distinguent par leur capacité à s'autoassembler en nanoparticules en contact d'acides nucléiques (siARN, plasmides, mARN). Ces nanoparticules à base de WRAP sont capables d'être internalisées facilement dans les cellules, majoritairement par translocation directe ce qui limite le passage par voies endocytaires. Parmi ces *CPP*, WRAP5, spécialement optimisé pour la délivrance de siARN, combine une efficacité élevée, une faible toxicité et une large applicabilité sur divers modèles cellulaires. Ces caractéristiques en font un outil particulièrement adapté pour explorer de nouvelles approches thérapeutiques, notamment par le ciblage fonctionnel de YAP1 et TAZ dans les GIST.

Objectifs

Cette thèse repose sur l'hypothèse selon laquelle **YAP1 et TAZ contribuent de manière distincte à la tumorigenèse et à la résistance thérapeutique des GIST.** L'objectif principal réside dans l'analyse de leurs contributions individuelles et combinées, en s'appuyant sur une

approche d'ARN interférence et sur l'utilisation d'un système innovant de délivrance intracellulaire, les nanoparticules peptidiques à base de WRAP5.

Le projet s'articule autour de trois axes principaux, chacun correspondant à un chapitre de résultats :

1) Valider l'efficacité des nanoparticules à base de WRAP5 comme vecteurs de siARN dans les GIST ;
2) Déterminer les rôles respectifs de YAP1 et TAZ dans la biologie tumorale des GIST *KIT*-dépendants sensibles à l'IM ;
3) Explorer la contribution de YAP1 et TAZ dans les GIST résistants à l'IM.

L'ensemble de ces objectifs permet non seulement d'éclairer le rôle distinct de YAP1 et TAZ dans les GIST, mais aussi d'ouvrir la voie à de nouvelles stratégies combinatoires pour surmonter la résistance aux TKI.

Stratégie expérimentale et résultats principaux

1) Validation de WRAP5:siARN comme outil de transfection chez les GIST

Le peptide WRAP5, développé par notre équipe comme agent de transfection pour des acides nucléiques, est capable de s'autoassembler en nanoparticules d'une taille moyenne d'environ 100 nm de diamètre en présence de siARN. Ce système de délivrance a déjà fait sa preuve de concept en réduisant l'expression de protéines exogènes ou endogènes dans plusieurs lignées cellulaires. Cependant, le ciblage d'une seule protéine (par exemple un seul acteur du cycle cellulaire comme CDK4 (*Cyclin-dependent kinase 4*) n'entraînait pas d'impact sur le phénotype cellulaire, suggérant la nécessité d'une approche d'inhibition multiple de gènes. Nous avons donc décidé de cibler trois protéines distinctes : CDK4, CD1 (*Cyclin D1*) et MCL-1. Pour cela, nous avons formulé des nanoparticules WRAP5 contenant soit un siARN unique en contrôle, soit un mélange de trois siARN (siMIX) ciblant simultanément ces régulateurs du cycle cellulaire (CDK4 et CD1) et une protéine anti-apoptotique (MCL-1). Dans les cellules GIST-T1 *KIT*-dépendantes et sensibles à l'IM, chaque siARN a induit une diminution d'au moins 60% de sa cible respective, confirmant la robustesse de l'agent de transfection dans ce modèle cellulaire. La microscopie confocale a montré que les trois siARN fluorescents étaient bien co-

internalisés dans la même cellule, et l'optimisation des rapports molaires (notamment le ratio molaire 6/8/6 pour CD1/CDK4/MCL-1) a conduit à une inhibition homogène des trois protéines (~70% de réduction). Sur le plan fonctionnel, seule la condition WRAP5:siMIX a induit une baisse significative de prolifération cellulaire sur le long terme, attestant d'un effet antiprolifératif supérieur à celui obtenu par l'inhibition individuelle des protéines séparément.

Ces résultats démontrent que WRAP5 est un agent de délivrance intracellulaire avec une flexibilité unique pour moduler la combinaison et le ratio des siARN en fonction du profil tumoral. Il constitue un outil puissant pour explorer de manière fonctionnelle des voies oncogéniques complexes. Cette validation dans les GIST, qui a fait l'objet d'une publication, pose ainsi les bases méthodologiques des travaux présentés dans les chapitres suivants, notamment l'étude du rôle de YAP1 et TAZ dans les GIST.

Konate K*, Pezzati I*, et al. (2025) Multiprotein Silencing Using WRAP-Based Nanoparticles: A Proof of Concept. Bioconjugate Chemistry 36(6):1218-1233.
doi: 10.1021/acs.bioconjchem.5c00069.

2) Étude des rôles de YAP1 et TAZ dans la biologie tumorale des GIST

Après validation des nanoparticules à base de WRAP5 comme système de transfection efficace de siRNA pour l'inhibition de protéines cibles dans les GIST, nous avons utilisé cet outil pour mieux définir les rôles de YAP1 et TAZ, les deux effecteurs de la voie Hippo dont l'implication dans le développement des GIST restait mal caractérisée.

Pour ce faire, des siARN spécifiques ciblant YAP1 ou TAZ ont été conçus et encapsulés dans les nanoparticules peptidiques à base de WRAP5. Après traitement des cellules GIST-T1 avec ces nanoparticules, nous avons obtenu une inhibition efficace et spécifique de YAP1 ou de TAZ (60-80 % de réduction protéique) sans effets croisés. Par Western blot, qPCR et immunofluorescence, il a été confirmé que l'inhibition simultanée des deux protéines atteignait des niveaux comparables à ceux de l'inhibition individuelle. Sur le plan fonctionnel, l'extinction de TAZ a entraîné une diminution significative de la prolifération et de la migration dans les cellules GIST-T1 (-30%), alors que l'inhibition de YAP1 seule avait un effet plus restreint. De plus, la combinaison des deux siARN n'apportait pas d'effet synergétique sur l'inhibition des deux protéines.

L'analyse des cibles de la voie Hippo a révélé que TAZ, mais non YAP1, contrôlait fortement l'expression de CYR61 et de CTGF. Le *knockdown* des cibles a démontré une corrélation plus importante entre la baisse de CYR61 et l'effet antiprolifératif observé (-30%). Ces résultats ont été reproduits dans deux autres lignées de GIST *KIT*-dépendantes sensibles à l'IM, les cellules GIST-430 et GIST-882, confirmant le rôle prépondérant de TAZ tout en suggérant une contribution plus faible de YAP1 selon le profil d'expression protéique. Ce travail met clairement en évidence pour la première fois une différence dans le rôle de YAP1 et de TAZ dans les GIST, notamment en identifiant TAZ comme un acteur clé de la prolifération et de la migration tumorales par l'axe TAZ-CYR61.

À partir de données cliniques (ATGsarc), nous avons montré que l'expression élevée de TAZ et de CYR61 était significativement associée à une survie sans progression plus courte et à une incidence métastatique accrue, alors que l'impact pronostique de YAP1 et de CTGF apparaissait plus modeste. Ces observations confirment l'implication de l'axe TAZ-CYR61 dans le développement des GIST.

Ce chapitre ouvre ainsi la voie à de nouvelles stratégies combinatoires utilisant les nanoparticules WRAP5 pour moduler de façon fine les effecteurs de la voie Hippo et compléter les thérapies existantes.

Pezzati I, et al. (2025) Breaking the redundancy: TAZ outperforms YAP1 in GIST progression. bioRxiv doi: 10.1101/2025.09.02.673653
Maintenant soumis à Cell Communication and Signaling

3) Quelle contribution de YAP1 et TAZ dans les GIST résistants à l'IM ?

De manière préliminaire, nous avons entrepris d'explorer le rôle de YAP1 et TAZ dans les GIST résistants à l'IM, un enjeu majeur compte tenu de l'émergence quasi inévitable de sous-clones résistants après un traitement prolongé. Sur un panel de six lignées de GIST, incluant des modèles sensibles (GIST-T1, GIST-430, GIST-882) et résistants à l'IM (GIST-T1/670, GIST-430/654 et GIST-48B), nous avons observé une augmentation globale des niveaux de YAP1 et TAZ dans les lignées acquérant une résistance à l'IM, y compris dans le modèle *KIT*-indépendant GIST-48B. L'analyse du statut de phosphorylation suggère que leur régulation diffère selon le contexte mutationnel et ne se réduit pas à une simple activation/désactivation, soulignant la nécessité d'études complémentaires sur leur localisation subcellulaire. Ces

données confortent l'hypothèse d'une implication de la voie Hippo dans les mécanismes adaptatifs au-delà de la signalisation KIT.

Nous avons ensuite validé la faisabilité du *knockdown* de YAP1 et/ou de TAZ par nanoparticules WRAP5:siRNA dans les lignées résistantes, confirmant que cet outil reste efficace même en contexte d'expression comparative des protéines plus importante. Parallèlement, une cinétique de traitement à l'IM dans les cellules GIST-T1 sensibles a révélé des variations opposées : une augmentation progressive de YAP1 et une diminution de TAZ dès les premières heures de traitement, suggérant une régulation opposée et possiblement des fonctions distinctes dans l'adaptation au traitement. Enfin, un premier test combinant l'inhibition sélective de TAZ et le traitement à l'IM chez les GIST-T1 n'a pas montré de modification de l'IC_{50} dans les conditions explorées, mais laisse envisager qu'une inhibition plus puissante ou prolongée pourrait renforcer l'effet antiprolifératif de l'IM et retarder l'émergence de résistance. Ces résultats préliminaires soutiennent l'idée que TAZ reste un acteur direct de la prolifération tandis que YAP1 pourrait refléter une réponse adaptative ou de survie sous pression thérapeutique. Ils ouvrent la voie à des recherches plus approfondies sur les cibles transcriptionnelles spécifiques de YAP1 et TAZ en contexte de résistance et sur l'optimisation des approches combinatoires WRAP5:siRNA/IM pour améliorer la durabilité de l'inhibition de KIT dans les GIST.

Conclusion et perspectives

En conclusion, cette thèse met en évidence trois points majeurs :

1) Les nanoparticules peptidiques WRAP5:siARN constituent un outil performant et modulable pour délivrer un ou plusieurs siARN dans les GIST, y compris dans des contextes de résistance, ouvrant la voie à des stratégies de *knockdown* ciblé et transposable *in vivo*.

2) L'étude comparative des rôles de YAP1 et TAZ démontre pour la première fois que ces deux effecteurs de la voie Hippo n'ont pas des rôles interchangeables dans les GIST : TAZ apparaît comme le principal moteur de la prolifération et de la migration via l'axe TAZ-CYR61, alors que YAP1 semble jouer un rôle plus limité.

3) Les observations préliminaires dans des modèles résistants à l'IM suggèrent que l'activation de la voie Hippo participe à l'adaptation thérapeutique et qu'il existe une régulation différentielle de YAP1 et TAZ sous pression médicamenteuse.

Ces résultats apportent une dimension nouvelle : plutôt qu'un ciblage simultané des effecteurs de la voie Hippo, une inhibition sélective et ajustée de l'expression de TAZ (et éventuellement de YAP1 selon le contexte) pourrait constituer une stratégie complémentaire aux TKI pour freiner la progression tumorale et retarder l'apparition de résistance. Les nanoparticules à base de WRAP5 constituent un outil adaptable pour tester de telles combinaisons ou pour associer plusieurs siARN à des thérapies conventionnelles.

Les prochaines étapes consisteront à :

- caractériser plus finement les cibles transcriptionnelles spécifiques de YAP1 et TAZ dans les GIST sensibles et résistants à l'IM, par transcriptomique ;
- explorer l'impact de l'inhibition de TAZ (seul ou combiné à YAP1) en modèles précliniques *in vivo*, en particulier dans des xénogreffes de GIST chez la souris ;
- optimiser les peptides WRAP5 pour améliorer le ciblage tumoral des GIST, leur stabilité *in vivo*, et leur profil pharmacocinétique en vue d'applications cliniques ;
- envisager des combinaisons rationnelles avec d'autres agents (TKI de nouvelle génération, inhibiteurs de facteurs de transcription TEAD…).

À terme, l'identification de l'axe TAZ-CYR61 comme cible thérapeutique et la validation d'un système de délivrance adapté pourraient ouvrir la voie à des approches thérapeutiques véritablement personnalisées, combinant inhibition de KIT et modulation sélective de la voie Hippo pour améliorer le contrôle à long terme des GIST avancés et métastatiques.

Targeting the YAP1/TAZ pathway in gastrointestinal stromal tumors (GIST)

Gastrointestinal stromal tumors (GIST) are the most common malignant mesenchymal neoplasms of the digestive tract. Up to 85% harbor gain-of-function mutations in *KIT* or *PDGFRA* genes encoding receptor tyrosine kinases. Most metastatic cases are treated with tyrosine kinase inhibitors, such as first-line Imatinib (IM). Despite the substantial clinical benefits, the emergence of secondary resistance, which is often caused by additional *KIT* mutations, remains a major challenge for *KIT*-mutant GIST patients. This highlights the importance of identifying new therapeutics.

This thesis explores the role of YAP1 (Yes-associated protein 1) and TAZ (Transcriptional co-activator with PDZ-binding motif), downstream effectors of the Hippo pathway, in GIST development and therapy response. Previous work from our team showed the involvement of these proteins in smooth muscle cell plasticity and suggested a link to IM resistance in *KIT*-dependent GIST. However, their specific functions in GIST were unclear.

First, we validated WRAP5, a tryptophan (W)- and arginine (R)-rich amphipathic peptide that self-assembles into nanoparticles in the presence of nucleic acids, as an efficient and non-toxic siRNA delivery system for GIST. Furthermore, WRAP5-based nanoparticles enabled robust and combinatorial silencing of multiple targets in the same cell by encapsulating up to three different siRNA.

We then used WRAP5-based nanoparticles loaded with siRNA against YAP1, TAZ, or with a combination of both in three IM-sensitive GIST cell lines. TAZ silencing strongly reduced cell proliferation and migration, whereas YAP1 knockdown had surprisingly limited effects, with only modest additive inhibition upon dual targeting. CYR61 (cysteine-rich angiogenic inducer 61) and CTGF (connective tissue growth factor) emerged as key downstream drivers, predominantly regulated by TAZ, with CYR61 downregulation particularly related to increased proliferation. Moreover, patient dataset analyses associated high *TAZ* or *CYR61* expression with shorter disease-free survival and higher metastatic potential, highlighting the central TAZ-CYR61 axis.

Finally, in IM-resistant GIST models, YAP1 and TAZ expressions were higher compared to sensitive counterparts. Furthermore, the study demonstrated the potential for the silencing of both proteins through the utilization of WRAP5:siRNA nanoparticles. Preliminary results revealed that these paralogs are subject to differential regulation by IM treatment, and that the combination of IM and siTAZ does not result in a synergistic antiproliferative effect.

In conclusion, this work identifies TAZ as a key regulator of GIST biology, reveals context-dependent functions for YAP1, and establishes WRAP5-mediated siRNA delivery as a promising tool to investigate their therapeutic potential, particularly in IM-resistant GIST.

Keywords: GIST, YAP1, TAZ, siRNA, WRAP5, Imatinib resistance